Vol. 16. No 2, 2014

ISSN 1507-2711

Cena: 25 zł (w tym 5% VAT)

EKSPLOATACJA I NIEZAWODNOŚĆ
MAINTENANCE AND RELIABILITY

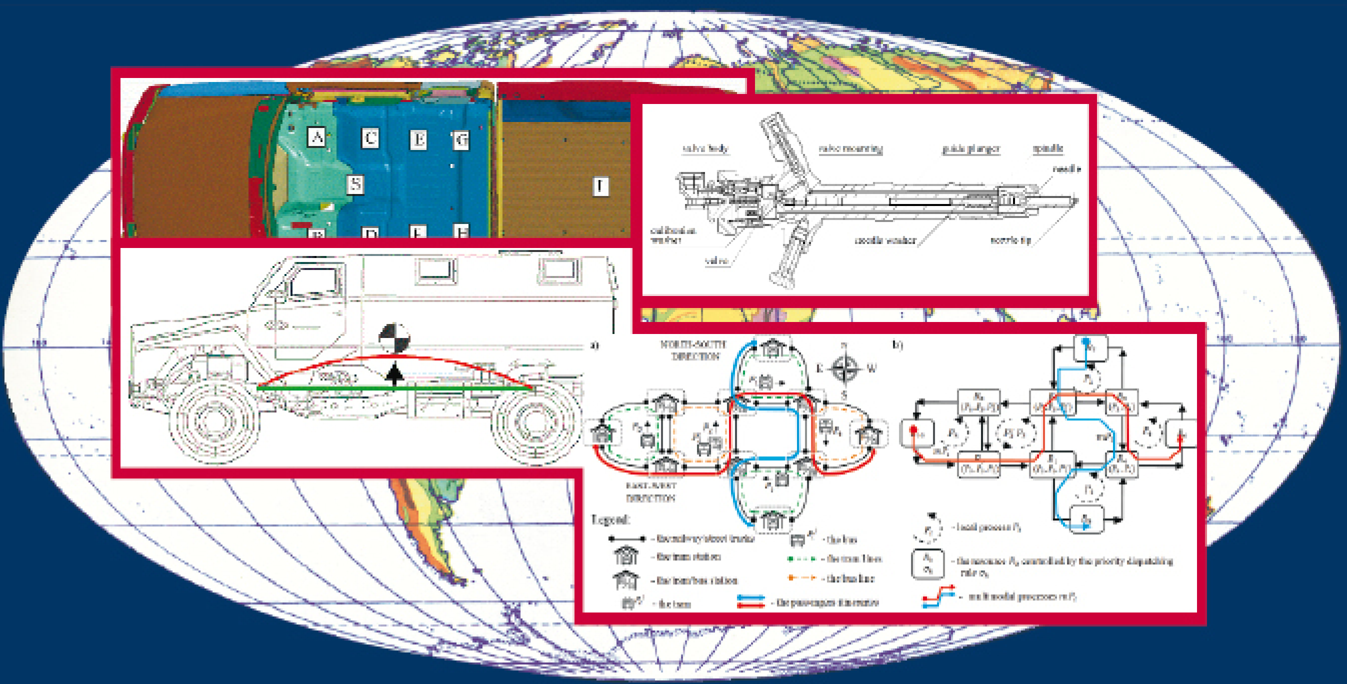

Polskie Naukowo Techniczne Towarzystwo Eksploatacyjne
Warszawa

Polish Maintenance Society
Warsaw

Co-financed by the Minister of Science and Higher Education

The Journal is indexed and abstracted in the Journal Citation Reports (JCR Science Edition), Scopus, Science Citation Index Expanded (SciSearch®) and Index Copernicus International.

The Quarterly appears on the list of journals credited with a high impact factor by the Polish Ministry of Science and Higher Education and is indexed in the Polish Technical Journal Contents database – BAZTECH and the database of the Digital Library Federation.

All the scientific articles have received two positive reviews from independent reviewers.

Our IF is 0.293

Editorial staff:	Dariusz Mazurkiewicz, PhD, DSc (Eng), Associate Professor (Editor-in-Chief, Secretary of the Scientific Board) Tomasz Klepka, PhD, DSc (Eng) (Deputy Editor-in-Chief) Teresa Błachnio-Krolopp, MSc (Eng) (Editorial secretary) Andrzej Koma (Typesetting and text makeup) Krzysztof Olszewski, PhD (Eng) (Webmaster)
Publisher:	Polish Maintenance Society, Warsaw
Scientific patronage:	Polish Academy of Sciences Branch in Lublin
Address for correspondence:	“Eksploatacja i Niezawodność” – Editorial Office 20-618 Lublin, ul. Nadbystrzycka 36, Poland e-mail: office@ein.org.pl http://www.ein.org.pl/
Circulation:	550 copies

Science and Technology

Abstracts IV

HuaWei WANG, Jun GAO

A reliability evaluation study based on competing failures for aircraft engines
Badania dotyczące oceny niezawodności silników lotniczych w oparciu o uszkodzenia konkurujące 171

Bogusław KAROLEWSKI, Piotr LIGOCKI

Modelling of long belt conveyors
Modelowanie długich przenośników taśmowych 179

Aleksandar Đ. BRKIĆ, Taško MANESKI, Dragan IGNJATOVIĆ, Predrag D. JOVANČIĆ, Vesna K. Spasojević BRKIĆ

Diagnostics of bucket wheel excavator discharge boom dynamic performance and its reconstruction
Diagnostyka właściwości dynamicznych wysięgnika zrzutowego koparki kołowej oraz jego przebudowa 188

Radosław CECHOWICZ, Paweł STĄCZEK

Computer supervision of the group of compressors connected in parallel
Komputerowy system nadzorowania zespołu sprężarek pracujących w układzie równoległym 198

David VALIS, Libor ZAK, Ondrej POKORA

Engine residual technical life estimation based on tribo data
Ocena technicznej trwałości resztkowej silnika w oparciu o dane tribologiczne 203

Jerzy CZMOCHOWSKI, Przemysław MOCZKO, Piotr ODYJAS, Damian PIETRUSIAK

Tests of rotary machines vibrations in steady and unsteady states on the basis of large diameter centrifugal fans
Badania drgań maszyn wirnikowych w stanach ustalonych oraz nieustalonych na przykładzie wentylatorów promieniowych dużych średnic 211

Rongxing DUAN, Huilin ZHOU

Diagnosis strategy for micro-computer controlled straight electro-pneumatic braking system using fuzzy set and dynamic fault tree
Wykorzystanie zbiorów rozmytych i dynamicznego drzewa uszkodzeń w strategii diagnostyki elektro-pneumatycznego układu hamulcowego sterowanego za pomocą mikrokomputera 217

Artur ILUK

Method of evaluating the stiffness of a vehicle with respect to the risk of explosion
Metoda oceny sztywności pojazdu pod kątem zagrożenia eksplozją 224

Anna GRINČOVÁ, Daniela MARASOVÁ

Experimental research and mathematical modelling as an effective tool of assessing failure of conveyor belts
Badania eksperymentalne i modelowanie matematyczne jako skuteczne narzędzia oceny uszkodzeń taśm przenośnikowych 229

Roman STRYCZEK, Bogusław PYTLAK

Multi-objective optimization with adjusted PSO method on example of cutting process of hardened 18CrMo4 steel
Optymalizacja wielokryterialna skorygowaną metodą PSO na przykładzie procesu skrawania stali 18CrMo4 w stanie zahartowanym 236

Min-Tsai LAI

Optimal replacement period with repair cost limit and cumulative damage model
Optymalny okres wymiany przy limicie kosztów naprawy i modelu sumowania uszkodzeń 246

Robert PILCH, Jan SZYBKA, Anna TUSZYŃSKA

Application of factoring and time-space simulation methods for assessment of the reliability of water-pipe networks
Zastosowanie metod faktoryzacji oraz symulacjiczasowo-przestrzennej do oceny niezawodności sieci wodociągowych 253

Grzegorz BOCEWICZ

Robustness of Multimodal Transportation Networks
Model oceny odporności multimodalnych sieci transportowych 259

Tomasz STOECK, Tomasz OSIPOWICZ, Karol Franciszek ABRAMEK

Methodology for the repair of Denso Common Rail solenoid injectors
Metodyka naprawy wtryskiwaczy elektromagnetycznych układów zasilania Common Rail Denso 270

Jing LIN, Matthias ASPLUND

Comparison study of heavy haul locomotive wheels' running surfaces wearing
Badania porównawcze zużycia powierzchni bieżnych kół lokomotyw dużej mocy 276

Anna JODEJKO-PIETRUCZUK, Sylwia WERBIŃSKA-WOJCIECHOWSKA

Analysis of maintenance models' parameters estimation for technical systems with delay time
Analiza parametrów modeli obsługiwania systemów technicznych z opóźnieniem czasowym 288

Xinghui ZHANG, Jianshe KANG, Eric BECHHOEFER, Jianmin ZHAO

A new feature extraction method for gear fault diagnosis and prognosis
Nowa metoda diagnozowania i prognozowania uszkodzeń przekładni z wykorzystaniem ekstrakcji cech 295

Andrzej BUCHACZ, Marek PŁACZEK, Andrzej WRÓBEL

Modelling of passive vibration damping using piezoelectric transducers – the mathematical model
Modelowanie pasywnego tłumienia drgań przy użyciu przetworników piezoelektrycznych – model matematyczny 301

Yongmin YANG, Zhimiao LU, Xu LUO, Zhexue GE, Yanling QIAN

Mean failure mass and mean failure repair time: parameters linking reliability, maintainability and supportability
Średnia masa uszkodzenia i średni czas naprawy uszkodzenia: parametryłączące niezawodność, obsługiwalność i utrzymywalność 307

Anna ŻYCZYŃSKA

The heat consumption and heating costs after the insulation of building partitions of building complex supplied by the local oil boiler room
Zużycie ciepła i koszty ogrzewania po dociepleniu przegród budowlanych zespołu budynków zasilanych z lokalnej kotłowni olejowej 313

Cheong Peng AU-YONG, Azlan Shah ALI, Faizah AHMAD

Prediction cost maintenance model of office building based on condition-based maintenance
Predykcyjno-kosztowy model konserwacji budynku biurowego oparty o utrzymanie zależne od bieżącego stanu technicznego (CBM) 319

Paweł KOŁODZIEJ, Marek BORYGA

Frequency analysis of coupling with adjustable torsional flexibility
Analiza częstościowa sprzęgła o regulowanej podatności skrętnej 325

Mariusz WALCZAK, Daniel PIENIAK, Agata M. NIEWCZAS

Effect of recasting on the useful properties CoCrMoW alloy
Wpływ powtórnego przetapiania na właściwości użytkowe stopu CoCrMoW 330

Michał CHŁOPEK, Tomasz DZIK, Marek HRYNIEWICZ

Determining the grip angle in a granulator with a flat matrix
Wyznaczanie kąta chwytu w granulatorze z płaską matrycą 337

Tomasz WALKOWIAK

Simulation based availability assessment of services provided by web applications with realistic repair time
Symulacyjna ocena gotowości usług systemów internetowych z realistycznym modelem czasu odnowy 341

IN MEMORIAM

COL. DR EUGENIUSZ OLEARCZUK, ENG.

On 25 January 2014, Col. Dr Eugeniusz Olearczuk, founding member and honorary member of the Polish Maintenance Society, vice president of the Society in the years 1991-2004, passed away. Dr Eugeniusz Olearczuk, Eng. was born in 1933. He graduated from the Military University of Technology. There, he also defended his doctoral thesis and throughout his working life he delivered lectures and conducted his research. Since 1999, he was lecturer at the Real Estate University in Warsaw. He specialized in the field of maintenance of aviation technology and foundations of maintenance of buildings.

He was author of many books, among others: “Foundations of the theory of operation of technical devices” (in Polish) (WNT, Warsaw 1972), “Operation of aircraft (aspects of the theory)” (in Polish) (MON Publishing, Warsaw 1979), “How is military technology developed” (in Polish) (MON Publishing, Warsaw 1981), “Maintenance of (residential) buildings” (in Polish) (Institute for Sustainable Technologies, Radom 1999), “Maintenance of buildings” (in Polish) COIB Publishing, Warsaw 2005), “The use of buildings” (In Polish) (Issue 1 WSGN Warsaw 2010), “Servicing of buildings” (in Polish) (Issue 3 WSGN Warsaw 2011).

He was member of the Scientific Board of the quarterly “Maintenance and Reliability” and section editor in the PAN quarterly “Scientific Problems of Machines Operation and Maintenance”.

He was organizer of a number of scientific conferences, a respected and kind Colleague. His work will remain in the fond memory of his students and co-workers.

Prof. Andrzej Niewczas

WANG HW, GAO J. **A reliability evaluation study based on competing failures for aircraft engines**. Eksploatacja i Niezawodnosc – Maintenance and Reliability 2014; 16 (2): 171–178.

Aircraft engine is a complex and repairable system, and the diversity of its failure modes increases the difficulty of reliability evaluation. It is necessary to establish a dynamic relationship among data, failure mode and system reliability, to achieve the scientific reliability evaluation for aircraft engines. This paper has used data fusion method to establish reliability evaluation models respectively for performance degradation failures and sudden failures. Furthermore, these two models have been integrated on the basis of competing failures' mechanism. Bayesian model averaging has been used to analyze the impacts of performance degradation failures and sudden failures on aircraft engines' reliability. As a result of above, the goal of an accurate evaluation of the reliability for aircraft engines has been achieved. Example shows the effectiveness of the proposed model.

KAROLEWSKI B, LIGOCKI P. **Modelling of long belt conveyors**. Eksploatacja i Niezawodnosc – Maintenance and Reliability 2014; 16 (2): 179–187.

A mathematical model that allows the analysis of the dynamic states of a belt conveyor was presented. A way of modelling wave phenomena in the tape, changes of mass and resistances to motion and elements of the drive system (motors, frequency converters, couplings, gears and co-operation between the belt and drive pulley) was briefly described. A start up of an exemplary belt conveyor was simulated with the use of obtained formulas. The start-up time histories obtained computationally were compared with measurements. The verified belt conveyor model can be utilized to examine various phenomena and operating states of a belt conveyor.

BRKIĆ AĐ, MANESKI T, IGNJATOVIĆ D, JOVANČIĆ P, SPASOJEVIĆ BRKIĆ VK. **Diagnostics of bucket wheel excavator discharge boom dynamic performance and its reconstruction**. Eksploatacja i Niezawodnosc – Maintenance and Reliability 2014; 16 (2): 188–197.

The paper focuses on an investigation into the possible causes of the bad dynamic performance of bucket wheel excavator C7OOS (BWE) discharge boom in the Kolubara opencast mine, Serbia. A discharge boom load carrying structure model was produced and its static and dynamic calculations were made by the finite element method (FEM). The model was then validated by the experimental method – vibration analysis. The set goals were achieved by the FEM result analysis, which were further confirmed in the experiment. The causes for discharge boom weak performance were established. The main operation problems were found in the inadequate design of the discharge boom tie(s) and the subsequent installation of a steering cabin. Possible discharge boom reconstructions were considered with a view to improving its operation performance. The selection of the reconstruction approach was limited by the technical and financial resources available to the machine users. After the completed reconstruction, the discharge boom improved operation performance was demonstrated in practice.

CECHOWICZ R, STĄCZEK P. **Computer supervision of the group of compressorsconnected in parallel**. Eksploatacja i Niezawodnosc – Maintenance and Reliability 2014; 16 (2): 198–202.

The paper presents the original solution of the control and monitoring system of the compressed air production plant. The plant was supplying the mid–size production system. The developed solution is consistent with the Condition–Based Maintenance approach. Its aim was to integrate the functions of direct control and monitoring of the process to ensure the best possible working conditions of machines (compressors) and to extend the period of their operation. The implementation of the described solution allowed: to eliminate the need for human presence in an environment with very high levels of noise, to improve the quality of the process by stabilising the course of its basic characteristics (variables), to automate the handling of alarm conditions, to increase machines' reliability through their rational use and ensuring proper working conditions, and to document the process. Freeing the operator from the common, repetitive control tasks and equipping him with diagnostic tools enabled him to detect threats (potential failures) sooner and to undertake appropriate corrective actions.

VALIS D, ZAK L, POKORA O. **Engine residual technical life estimation based on tribo data**. Eksploatacja i Niezawodnosc – Maintenance and Reliability 2014; 16 (2): 203–210.

The aim of the paper is to estimate a system technical life. When estimating a residual technical life statistically, a big amount of tribo-diagnostic data is used. This data serves as the initial source of information. It includes the information about particles contained in oil which testify to oil condition as well as system condition. We focus on the particles which we consider to be interesting and valuable. This kind of information has good technical and analytical potential which has not been explored well yet. By modelling the occurrence of particles in oil we expect to find out when a more appropriate moment for performing preventive maintenance might come. The way of

WANG HW, GAO J. **Badania dotyczące oceny niezawodności silników lotniczych w oparciu o uszkodzenia konkurujące**. Eksploatacja i Niezawodnosc – Maintenance and Reliability 2014; 16 (2): 171–178.

Silnik samolotu to złożony system naprawialny, w którym różnorodność przyczyn uszkodzeń zwiększa trudność oceny niezawodności. Dlatego też istnieje konieczność ustalenia dynamicznych związków pomiędzy danymi, przyczynami uszkodzenia i niezawodnością systemu, których znajomość pozwoliłaby przeprowadzać naukową ocenę niezawodności silników lotniczych. W prezentowanej pracy wykorzystano metodę fuzji danych do opracowania modeli oceny niezawodności w zakresie uszkodzeń wynikających z obniżenia charakterystyk oraz uszkodzeń nagłych. Ponadto, opracowane modele zintegrowano na podstawie mechanizmu uszkodzeń konkurujących. Do analizy wpływu dwóch omawianych typów uszkodzeń na niezawodność silników lotniczych wykorzystano procedurę bayesowskiego uśredniania modeli. Dzięki powyższym krokom, osiągnięto założony cel dokładnej oceny niezawodności silników samolotowych. Przykład pokazuje skuteczność proponowanego modelu.

KAROLEWSKI B, LIGOCKI P. **Modelowanie długich przenośników taśmowych**. Eksploatacja i Niezawodnosc – Maintenance and Reliability 2014; 16 (2): 179–187.

Przedstawiono matematyczny model przenośnika taśmowego umożliwiający analizę dynamicznych stanów pracy urządzenia. Skrótowo opisano sposób modelowania zjawisk falowych w taśmie, zmian mas i oporów ruchu oraz elementów układu napędowego czyli silników, przekształtników, sprzęgieł, przekładni i współpracy bębna napędowego z taśmą. Rozwiązując komputerowo uzyskane zależności, symulowano rozruch przykładowego przenośnika. Porównano przebiegi rozruchowe uzyskane obliczeniowo z pomiarowymi. Zweryfikowany model można wykorzystać do badania różnych zjawisk i stanów pracy przenośnika.

BRKIĆ AĐ, MANESKI T, IGNJATOVIĆ D, JOVANČIĆ P, SPASOJEVIĆ BRKIĆ VK. **Diagnostyka właściwości dynamicznych wysięgnika zrzutowego koparki kołowej oraz jego przebudowa**. Eksploatacja i Niezawodnosc – Maintenance and Reliability 2014; 16 (2): 188–197.

W artykule badano możliwe przyczyny złych własności dynamicznych wysięgnika zrzutowego koparki kołowej C7OOS (BWE) pracującej w kopalni odkrywkowej Kolubara w Serbii. Do stworzenia modelu konstrukcji nośnej wysięgnika zrzutowego oraz przeprowadzenia obliczeń statycznych i dynamicznych wykorzystano metodę elementów skończonych (MES). Model został następnie zweryfikowany przy użyciu metody eksperymentalnej – analizy drgań. Wyznaczone cele osiągnięto poprzez analizę wyników MES, które zostały następnie zweryfikowane w badaniach doświadczalnych. Ustalono przyczyny słabego działania wysięgnika. Głównymi problemami eksploatacyjnymi okazały się być nieodpowiednia konstrukcja cięgien wysięgnika oraz montaż kabiny kierowcy. Aby poprawić charakterystyki pracy wysięgnika, rozważono możliwe opcje jego przebudowy. Wybór metody przebudowy ograniczały zasoby techniczne i finansowe użytkownika maszyny. Przebudowa dała poprawę charakterystyk pracy wysięgnika, co wykazano w praktyce.

CECHOWICZ R, STĄCZEK P. **Komputerowy system nadzorowania zespołu sprężarek pracujących w układzie równoległym**. Eksploatacja i Niezawodnosc – Maintenance and Reliability 2014; 16 (2): 198–202.

W pracy przedstawiono własne, wdrożone rozwiązanie problemu automatyzacji sterowania i nadzorowania procesu wytwarzania sprężonego powietrza na potrzeby średniej wielkości systemu produkcyjnego. Opracowane rozwiązanie jest zgodne z podejściem Condition-Based Maintenance. Jego istotą było zintegrowanie funkcji sterowania bezpośredniego oraz nadzorowania przebiegu procesu w celu zapewnienia możliwie najlepszych warunków pracy maszyn i wydłużenia przez to okresu ich eksploatacji. Wdrożenie opisanego rozwiązania pozwoliło na: wyeliminowanie konieczności przebywania ludzi w środowisku o bardzo dużym poziomie hałasu, poprawę jakości procesu poprzez ustabilizowanie przebiegu jego podstawowych charakterystyk (zmiennych), zautomatyzowanie procedur obsługi sytuacji awaryjnych, zwiększenie niezawodności maszyn poprzez ich racjonalne wykorzystanie i zapewnienie prawidłowych warunków pracy, oraz dokumentowanie przebiegu procesu. Uwolnienie operatora od zadań sterowania i wyposażenie go w narzędzia wspomagające diagnostykę procesu spowodowały, że był on w stanie wcześniej wykryć zagrożenia dla przebiegu procesu (potencjalne awarie) i podjąć stosowne działania zaradcze.

VALIS D, ZAK L, POKORA O. **Ocena technicznej trwałości resztkowej silnika w oparciu o dane tribologiczne**. Eksploatacja i Niezawodnosc – Maintenance and Reliability 2014; 16 (2): 203–210.

Celem pracy jest ocena trwałości technicznej układu. W ocenie statystycznej technicznej trwałości resztkowej, wykorzystywane są duże ilości danych tribo-diagnostycznych. Dane te służą jako początkowe źródło informacji. Dostarczają informacji nt. cząsteczek zawartych w oleju, które świadczą o jego bieżącym stanie, jak również o stanie całego układu. Szczególny nacisk położono na cząsteczki, które uznano za godne uwagi i wartościowe. Tego rodzaju informacje mają duży potencjał techniczny i analityczny, który nie został jeszcze wystarczająco zbadany. Modelując występowanie cząsteczek w oleju, spodziewamy się określić najlepszy czas na przeprowadzenie konserwacji zapobiegawczej.

modelling and further estimation is based on the specific characteristics of a regression analysis, fuzzy logic and diffusion processes – namely the Wiener process. Following the modelling results we could, in fact, set the principles of "CBM – Condition Based Maintenance". However, the possibilities are much wider, since we can also plan in service operation and mission. All these steps result in inevitable cost saving which we would like to contribute to.

Sposób modelowania i dalszej oceny oparto o konkretne charakterystyki analizy regresji, logiki rozmytej i procesów dyfuzyjnych-tj.proces Wienera. Śledząc wyniki modelowania możliwe będzie ustalenie reguł utrzymania urządzeń zależnie od ich bieżącego stanu technicznego (condition-based maintenance, CBM). Możliwości są jednak dużo większe, pozwalając także na planowanie eksploatacji rutynowej i zadań. Wszystkie powyższe kroki prowadzą do oszczędności.

CZMOCHOWSKI J, MOCZKO P, ODYJAS P, PIETRUSIAK D. **Tests of rotary machines vibrations in steady and unsteady states on the basis of large diameter centrifugal fans**. Eksploatacja i Niezawodnosc – Maintenance and Reliability 2014; 16 (2): 211–216.

The existence of unsteady states of rotary machines is a common problem. It occurs mainly during the machine start-up and is caused by "passing through" the critical velocity, which activates large scale object vibrations. Moreover, rotary machines vibrations problems are caused by faults such as unbalance, misalignment, bearing defects and others. The paper presents the results of tests of sample centrifugal fans vibrations, both in steady and unsteady states. The recorded time traces of non-stationary vibrations were analyzed with the STFT spectrum. This method allowed to identify main parameters influencing the level of vibrations during the start-up and regular operation of the machine. The tests were performed on four machines, which enabled an additional comparison of operational parameters of the whole flow system.

CZMOCHOWSKI J, MOCZKO P, ODYJAS P, PIETRUSIAK D. **Badania drgań maszyn wirnikowych w stanach ustalonych oraz nieustalonych na przykładzie wentylatorów promieniowych dużych średnic**. Eksploatacja i Niezawodnosc – Maintenance and Reliability 2014; 16 (2): 211–216.

Problem występowania stanów nieustalonych maszyn obrotowych jest powszechnie spotykany. Pojawia się on głównie podczas rozruchu i wywołany jest „przechodzeniem" przez prędkość krytyczną, która wzbudza drgania obiektu w bardzo szerokim zakresie. Ponadto problemy z drganiami maszyn obrotowych wywoływane są przez takie czynniki jak niewyważenie, niewyosiowanie, defekty łożysk i wiele innych. W pracy przedstawiono wyniki badań drgań zarówno w stanach ustalonych jak i nieustalonych przykładowych wentylatorów promieniowych. Za pomocą widm STFT przeanalizowano zarejestrowane przebiegi drgań niestacjonarnych. Dzięki temu możliwe było zidentyfikowanie głównych parametrów mających wpływ na poziom drgań podczas rozruchu oraz pracy normalnej. Badania przeprowadzono na czterech obiektach, co umożliwiło dodatkowe porównanie i wyciągnięcie wniosków odnośnie parametrów eksploatacyjnych całego układu przepływowego.

DUAN R, ZHOU H. **Diagnosis strategy for micro-computer controlled straight electro-pneumatic braking system using fuzzy set and dynamic fault tree**. Eksploatacja i Niezawodnosc – Maintenance and Reliability 2014; 16 (2): 217–223.

In this paper, a new diagnosis strategy for micro-computer controlled straight electro pneumatic braking system is developed to improve the diagnostic efficiency, which makes full use of some reliability theories and fuzzy set techniques. Specifically, it adopts expert elicitation and fuzzy set theory to evaluate the failure rate of the basic events for the braking system, and uses a dynamic fault tree model to capture the dynamic failure mechanisms and calculates some reliability results by mapping a dynamic fault tree into an equivalent Bayesian network (BN). Furthermore, the schemes are proposed to update the diagnostic importance factor (DIF) and the cut sets according to the sensors data. Finally, an efficient diagnostic algorithm is developed based on these reliability results to guide the maintenance crew to diagnose the braking system. The experimental results demonstrate that the proposed method can locate the fault of the braking system with less diagnosis cost.

DUAN R, ZHOU H. **Wykorzystanie zbiorów rozmytych i dynamicznego drzewa uszkodzeń w strategii diagnostyki elektro-pneumatycznego układu hamulcowego sterowanego za pomocą mikrokomputera**. Eksploatacja i Niezawodnosc – Maintenance and Reliability 2014; 16 (2): 217–223.

W niniejszej pracy, opracowano nową strategię diagnostyki elektro-pneumatycznego układu hamulcowego sterowanego za pomocą mikrokomputera Celem badań była poprawa efektywności diagnostycznej. Strategię oparto na wybranych teoriach niezawodności oraz technikach zbiorów rozmytych. W szczególności, strategia wykorzystuje ocenę ekspercką oraz teorię zbiorów rozmytych do określania intensywności uszkodzeń dla podstawowych zdarzeń zachodzących w układzie hamulcowym oraz posługuje się modelem dynamicznego drzewa uszkodzeń aby uchwycić dynamiczne mechanizmy uszkodzeń. Za pomocą przedstawionej strategii oblicza się także wyniki analiz niezawodnościowych poprzez mapowanie dynamicznego drzewa błędów do równoważnej sieci bayesowskiej (BN). Ponadto w artykule zaproponowano schematy służące do aktualizacji czynnika ważności diagnostycznej (DIF) oraz przekrojów niezdatności zgodnie z danymi z czujników. Wreszcie, w oparciu o uzyskane wyniki analiz niezawodnościowych, opracowano wydajny algorytm diagnostyczny, który zawiadamia załogę konserwatorką o konieczności przeprowadzenia diagnostyki układu hamulcowego. Wyniki doświadczeń pokazują, że proponowana metoda pozwala na zlokalizowanie usterki układu hamulcowego przy mniejszych kosztach diagnozy.

ILUK A. **Method of evaluating the stiffness of a vehicle with respect to the risk of explosion**. Eksploatacja i Niezawodnosc – Maintenance and Reliability 2014; 16 (2): 224–228.

This article describes a new method of evaluating the stiffness of structure of a vehicle with respect to its resistance to mine explosion. This method allows for the assessment of the structure of a wide range of tracked and wheeled vehicles in the early stage of the construction process, considering such factors as mass and stiffness of the hull and ground clearance. By applying this method it is possible to assess the risk of lower limb injury for every vehicle occupant, caused by local deformation of the vehicle.

ILUK A. **Metoda oceny sztywności pojazdu pod kątem zagrożenia eksplozją**. Eksploatacja i Niezawodnosc – Maintenance and Reliability 2014; 16 (2): 224–228.

W artykule przedstawiono nową metodę oceny sztywności struktury pojazdu pod kątem odporności na eksplozję miny. Metoda ta umożliwia ocenę konstrukcji szerokiej gamy pojazdów gąsienicowych i kołowych na wczesnym etapie procesu konstruowania pojazdu uwzględniając takie czynniki jak masa i sztywność kadłuba oraz prześwit pod pojazdem. Wynikiem zastosowania metody jest ocena zagrożenia kończyn dolnych wskutek lokalnej deformacji pojazdu dla każdego członka załogi.

GRINČOVÁ A, MARASOVÁ D. **Experimental research and mathematical modelling as an effective tool of assessing failure of conveyor belts**. Eksploatacja i Niezawodnosc – Maintenance and Reliability 2014; 16 (2): 229–235.

One of the main causes of damage is their dynamic stress, which often ends the life-cycle caused end of conveyor belts. Dynamic stress leads to fatigue strength functions in shear loading of fabric conveyor belts. Damage of the conveyor belt can be solved by extensive experimental research in laboratory conditions on complex equipments made just for this purpose. The aim of the study is to determine the relation of power in the conveyor belt to the weight of the material which is falling onto a conveyor belt and to impact level height, which is based on data obtained in the experimental research. The experimental measurements have been performed on a test rig, which was developed at the Institute of Logistics and Transport Industry FBERG of Kosice. Results of mathematical modelling clearly say that proposed regression models describe real behaviour of the conveyor belts in productions during their dynamic stress as a result of the influence of shock and stretching forces very well.

GRINČOVÁ A, MARASOVÁ D. **Experimental research and mathematical modelling as an effective tool of assessing failure of conveyor belts**. Eksploatacja i Niezawodnosc – Maintenance and Reliability 2014; 16 (2): 229–235.

Jedną z głównych przyczyn uszkodzeń taśm przenośnikowych są naprężenia dynamiczne, które często prowadzą do zakończenia cyklu życia taśmy. Naprężenia dynamiczne powodują pojawienie się funkcji wytrzymałości zmęczeniowej w warunkach oddziaływania na taśmę tkaninową obciążenia ścinającego. Problem uszkodzeń taśm przenośnikowych można rozwiązać prowadząc obszerne badania doświadczalne w warunkach laboratoryjnych na skomplikowanych, specjalnie do tego celu stworzonych urządzeniach. Celem prezentowanej pracy było określenie zależności między siłami w taśmie przenośnika a masą materiału spadającego na taśmę oraz wysokością zrzutu, w oparciu o dane z przeprowadzonych badań doświadczalnych. Pomiary eksperymentalne przeprowadzono na stanowisku badawczym zaprojektowanym w Instytucie Logistyki i Przemysłu Transportowego FBERG w Koszycach. Wyniki modelowania matematycznego wyraźnie pokazują, że proponowane modele regresji bardzo dobrze opisują rzeczywiste zachowanie taśm przenośnikowych podczas procesu produkcyjnego, w trakcie którego poddawane są one dynamicznym naprężeniom w wyniku oddziaływaniasiły uderzenia oraz sił rozciągających.

STRYCZEK R, PYTLAK B. **Multi-objective optimization with adjusted PSO method on example of cutting process of hardened 18CrMo4 steel**. Eksploatacja i Niezawodnosc – Maintenance and Reliability 2014; 16 (2): 236–245.

In this paper a Modified Particle Swarm Optimization (PSO) method for multi-objective (MO) problems with a discrete decision space is proposed. In the PSO method the procedure to determine inertia weight, learning factor and social factor is modified. In addition, both an elitism strategy and innovative deceleration mechanism preventing the particles from going beyond the limits of decision space are introduced. The proposed approach has been applied to a series of currently used test functions as well as to optimization problems connected with finish hard turning operation, where the obtained results have been compared with those obtained by means of Genetic Algorithms (GA). The results indicate that the proposed approach is relatively quick, and thus it is highly competitive with other optimization methods. The authors have obtained a very good diversity, convergence and a maximum range of the Pareto front in the criteria space. In order to assess the quality of the generated Pareto set for each of presented examples, a rating has been determined based on the entropy measurement and inverted generational distance (IGD).

LAI M-T. **Optimal replacement period with repair cost limit and cumulative damage model**. Eksploatacja i Niezawodnosc – Maintenance and Reliability 2014; 16 (2): 246–252.

This paper deals with periodical replacement model with single repair cost limit under cumulative damage process. The system is subject to two types of shocks. Type I shock causes damage to the system. The total damage is additive, and it causes a serious failure eventually if the total additive damage exceeds a failure level K. Type II shock causes the system to a minor failure, which can be maintained by minimal repair if the estimated repair cost is smaller than a predetermined repair-cost limit LS or by preventive replacement if the estimated repair cost is larger than LS. The system is also replaced at scheduled time T or at serious failure. The long-term expected cost per unit time is derived using the expected costs as the optimality criterion. The minimum-cost policy is derived, and existence and uniqueness are proved.

PILCH R, SZYBKA J, TUSZYŃSKA A. **Application of factoring and time-space simulation methods for assessment of the reliability of water-pipe networks**. Eksploatacja i Niezawodnosc – Maintenance and Reliability 2014; 16 (2): 253–258.

This article presents a method for determining the reliability of water-pipe networks through the application of factoring algorithms. This is a method based on graph theory and graph reduction, making it possible to calculate the reliability of a system with a specific structure of connections between its elements without determining its reliability structure. The impact of damage to individual pipeline segments on a network's overall reliability was also determined. In water-pipe networks, it is also particularly important to ensure that the appropriate parameters of water are maintained. Values of the water supply conditions index (WSCI) in the entire analysed network and changes resulting from damage to selected pipeline segments were determined by means of time-space simulation. The presented factoring and time-space simulation methods for determining WSCI index values are mutually complementary in the assessment of reliability. They make it possible to improve the credibility of reliability assessment and may be used to conduct rational usage of water-pipe networks.

BOCEWICZ G. **Robustness of Multimodal Transportation Networks**. Eksploatacja i Niezawodnosc – Maintenance and Reliability 2014; 16 (2): 259–269.

This paper describes a declarative approach to modeling a multimodal transportation network (MTN) composed of multiple connecting transport modes, such as bus, tram, light rail, subway and commuter rail, where within each mode, service is provided on separate lines or routes. The considered model of a network of multimodal transportation processes (MTPN) provides a framework to address the needs for transportation networks robustness while taking into account their capacity and demand requirements. Therefore the work focuses on evaluation of the network robustness allowing distinguished multimodal processes to continue in order to accomplish trips following an assumed set of multimodal chains connecting transport modes between origins and destinations. Consequently, a solution to the problem of prototyping robust transits on a given multimodal network is implemented and tested. The conditions that guarantee the network robustness, taking into account disruptions of supply and demand as well as operational control, are provided. The aim of investigations is to provide a tool for evaluating the robustness of a network of multimodal transportation processes as well as different travel modes through a transportation network.

STRYCZEK R, PYTLAK B. **Optymalizacja wielokryterialna skorygowaną metodą PSO na przykładzie procesu skrawania stali 18CrMo4 w stanie zahartowanym**. Eksploatacja i Niezawodnosc – Maintenance and Reliability 2014; 16 (2): 236–245.

W pracy zaproponowano zmodyfikowaną metodę optymalizacji wielocząsteczkowej (PSO) dla problemów optymalizacji wielokryterialnej z dyskretną przestrzenią decyzyjną. W metodzie PSO zmieniono sposób określania momentu bezwładności, współczynnika uczenia oraz współczynnika społecznego. Dodatkowo wprowadzono elitaryzm oraz innowacyjny mechanizm hamowania cząstek chroniący je przed przekraczaniem dopuszczalnych granic przestrzeni decyzyjnej. Zaproponowane podejście zostało zweryfikowane na szeregu aktualnych funkcjach testowych oraz problemie optymalizacji procesu skrawania stali 18CrMo4 w stanie zahartowanym, gdzie porównano je z wynikami uzyskanymi za pomocą algorytmów genetycznych (GA). Uzyskane wyniki wskazują, że zaproponowane podejście jest względnie szybkie i wysoce konkurencyjne w stosunku do innych metod optymalizacji. Autorzy uzyskali bardzo różnorodne, zbieżne i w pełnym zakresie przebiegi frontu Pareto w przestrzeni kryteriów. W celu oceny jakości wygenerowanego zbioru Pareto dla każdego z prezentowanych przykładów wyznaczono ocenę opartą na pomiarze entropii oraz wskaźnika jakości IGD.

LAI M-T. **Optymalny okres wymiany przy limicie kosztów naprawy i modelu sumowania uszkodzeń**. Eksploatacja i Niezawodnosc – Maintenance and Reliability 2014; 16 (2): 246–252.

Niniejszy artykuł dotyczy modelu wymiany okresowej z ograniczeniem kosztów pojedynczej naprawy w ramach procesu sumowania uszkodzeń. Układ podlega dwóm rodzajom zaburzeń. Zaburzenie I typu powoduje uszkodzenie systemu. Uszkodzenie całkowite sumuje się, powodując w końcu poważną awarię jeśli łączna wartość uszkodzeń przekroczy poziom awarii K. Zaburzenie II typu powoduje drobną awarię systemu, która może zostać usunięta dzięki minimalnej naprawie jeśli przewidywany koszt naprawy będzie mniejszy niż zakładany limit kosztów naprawy LS lub na drodze wymiany prewencyjnej, jeżeli przewidywany koszt naprawy będzie większy niż LS. Układ również podlega wymianie w założonym czasie T lub w przypadku poważnej awarii. Długoterminowe przewidywane koszty na jednostkę czasu obliczono z wykorzystaniem przewidywanych kosztów jako kryterium optymalności. Wyprowadzono strategię minimalnych kosztów, udowadniając istnienie i jedyność.

PILCH R, SZYBKA J, TUSZYŃSKA A. **Zastosowanie metod faktoryzacji oraz symulacjiczasowo-przestrzennej do oceny niezawodności sieci wodociągowych**. Eksploatacja i Niezawodnosc – Maintenance and Reliability 2014; 16 (2): 253–258.

W artykule przedstawiono sposób wyznaczenia niezawodności sieci wodociągowych przy wykorzystaniu algorytmu faktoryzacji. Jest to metoda oparta na teorii grafów i ich redukcji, umożliwiająca obliczenie niezawodności układu o określonej strukturze połączeń między elementami ale bez wyznaczania jego struktury niezawodnościowej. Dla wybranej sieci wyznaczono wpływ uszkodzenia poszczególnych odcinków rurociągów na jej niezawodność. W sieciach wodociągowych szczególnie ważne jest zapewnienie odpowiednich parametrów dostarczanej wody. Za pomocą symulacji czasowo-przestrzennej określono wartości wskaźnika warunków poboru wody WWPW w całej analizowanej sieci oraz jego zmiany, w efekcie uszkodzenia wytypowanych odcinków rurociągów. Przedstawione metody faktoryzacji i symulacja czasowo-przestrzenna, do wyznaczenia wartości wskaźnika WWPW, wzajemnie się uzupełniają w ocenie niezawodności. Pozwalają zwiększyć wiarygodność oceny niezawodności i mogą być wykorzystywane w prowadzeniu racjonalnej eksploatacji sieci wodociągowych.

BOCEWICZ G. **Model oceny odporności multimodalnych sieci transportowych**. Eksploatacja i Niezawodnosc – Maintenance and Reliability 2014; 16 (2): 259–269.

Dynamiczny rozwój infrastruktury komunikacji miejskiej obejmującej linie autobusowe, trolejbusowe, tramwajowe, linie metra, kolei podmiejskiej, itp. składające się na tzw. Multimodalne Sieci Transportowe (MST) rodzi wiele nowych problemów. Wśród ważniejszych z nich warto wymienić problemy planowania obsługi ruchu pasażerskiego w sytuacjach związanych z awariami elementów infrastruktury, wypadkami losowymi czy też z obsługą imprez masowych. Wiadomo, że istnienie rozwiązań dopuszczalnych gwarantujących zakładaną przepustowość infrastruktury warunkuje tzw. odporność MST na ww. zakłócenia. W tym kontekście, niniejsza praca przedstawia pewien deterministyczny model multimodalnej sieci transportowej złożonej z połączonych stacjami przesiadkowymi, linii komunikacji miejskiej. Składające się na sieć, pracujące w zamkniętych cyklach, linie komunikacji miejskiej pozwalają obsłuchiwać ruch pasażerski na wybranych kierunkach np. północ-południe. Obsługiwane strumienie pasażerów modelowane są jako tzw. multimodalne procesy transportowe. Wprowadzone miary odporności MST, umożliwiające ocenę rozważanych wariantów infrastruktury, pozwalają na wyznaczenie warunków spełnienie, których gwarantuje dopuszczalną jakość obsługi ruchu pasażerskiego. Umożliwiają, zatem zarówno planowanie obsługi pasażerów na wybranych trasach, jak i kształtowanie struktury rozbudowywanej i/lub modernizowanej sieci komunikacji miejskiej.

STOECK T, OSIPOWICZ T, ABRAMEK KF. **Methodology for the repair of Denso Common Rail solenoid injectors**. Eksploatacja i Niezawodnosc – Maintenance and Reliability 2014; 16 (2): 270–275.

This paper presents the problems of Denso Common Rail solenoid injector verification and repair. Due to conscious policy of the manufacturer who does not offer spare parts or special tooling, their servicing comes down most frequently to external cleaning, internal rinsing by the thermo-chemical method, and testing on test benches. Based on the analysis of failures and malfunctions being most frequently observed, own methodology for the repair process have been presented, specifying the successive stages of disassembly and final assembly. A possibility of effective fuel metering correction has been demonstrated, which is presented on the example of injectors in a 2.2 HDI engine of Citroën Jumper II delivery van.

STOECK T, OSIPOWICZ T, ABRAMEK KF. **Metodyka naprawy wtryskiwaczy elektromagnetycznychukładów zasilania Common Rail Denso**. Eksploatacja i Niezawodnosc – Maintenance and Reliability 2014; 16 (2): 270–275.

W artykule przedstawiono problematykę weryfikacji i naprawy wtryskiwaczy elektromagnetycznych Common Rail firmy Denso. Ze względu na świadomą politykę producenta, który nie oferuje części zamiennych i specjalistycznego oprzyrządowania, ich obsługa sprowadza się najczęściej do czyszczenia zewnętrznego, płukania wewnętrznego metodą termochemiczną oraz testowania na stołach probierczych. W oparciu o analizę najczęściej spotykanych uszkodzeń i niesprawności, zaprezentowano własną metodykę procesu naprawy, z wyszczególnieniem kolejnych etapów demontażu oraz montażu końcowego. Wskazano na możliwość efektywnej korekty dawkowania, którą pokazano na przykładzie wtryskiwaczy silnika 2,2 HDI pojazdu Citroën Jumper II.

LIN J, ASPLUND M. **Comparison Study of Heavy Haul Locomotive Wheels' Running Surfaces Wearing**. Eksploatacja i Niezawodnosc – Maintenance and Reliability 2014; 16 (2): 276–287.

The service life of railway wheels can differ significantly depending on their installed position, operating conditions, re-profiling characteristics, etc. This paper compares the wheels on two selected locomotives on the Iron Ore Line in northern Sweden to explore some of these differences. It proposes integrating reliability assessment data with both degradation data and re-profiling performance data. The following conclusions are drawn. First, by considering an exponential degradation path and given operation condition, the Weibull frailty model can be used to undertake reliability studies; second, among re-profiling work orders, rolling contact fatigue (RCF) is the principal reason; and third, by analysing re-profiling parameters, both the wear rate and the re-profiling loss can be monitored and investigated, a finding which could be applied in optimisation of maintenance activities.

LIN J, ASPLUND M. **Badania porównawcze zużycia powierzchni bieżnych kół lokomotyw dużej mocy**. Eksploatacja i Niezawodnosc – Maintenance and Reliability 2014; 16 (2): 276–287.

Resurs kół pociągu może być znacząco różny w zależności od ich miejsca zamontowania, warunków pracy, charakterystyk związanych z reprofilacją, itp. W artykule, porównano koła dwóch wybranych lokomotyw kursujących na Linii Rud Żelaza w północnej Szwecji, aby zbadać niektóre ze wspomnianych różnic. Zaproponowano możliwość łączenia danych pochodzących z oceny niezawodności z danymi degradacyjnymi oraz danymi z reprofilacji. Przeprowadzone badania pozwalają wyciągnąć następujące wnioski. Po pierwsze, krzywa wykładnicza degradacji oraz zadane warunki pracy można wykorzystać w celu przeprowadzenia badań niezawodności z użyciem modelu Weibulla z efektami losowymi (tzw. "frailty model"); po drugie, główną przyczyną zlecania reprofilacji kół jest zmęczenie toczne (RCF); po trzecie, analiza parametrów reprofilacji pozwala na monitorowanie i badanie zarówno szybkości zużycia kół, jak i ubytku materiału podczas reprofilacji, co może mieć zastosowanie w optymalizacji czynności obsługowych.

JODEJKO-PIETRUCZUK A, WERBIŃSKA-WOJCIECHOWSKA S. **Analysis of maintenance models' parameters estimation for technical systems with delay time**. Eksploatacja i Niezawodnosc – Maintenance and Reliability 2014; 16 (2): 288–294.

In the article authors are interested in BIP performance for three-element system ("k-out-of-n" reliability structure), the maintenance policy which is one of most commonly used in practice. The BIP may be implemented in technical systems when some information about reliability characteristics is known. The basic reliability parameters that have to be specified in such systems are: an estimation of system components' time to failure and some delay time characteristics. In order to determine the effects of possible errors and to specify sufficient accuracy of the estimation, the analysis of system costs was done for various values of the expected delay time, assuming three different probability distributions of the delay time (Weibull, Uniform, and Normal). The modelling process was based on the use of *GNU* Octave software. Test analysis of delay time parameter, assuming different types of probability distributions is the base to conclude: if the form of the distribution has any meaning for economic results of the system, and what kind of consequences may result from improper mean delay time estimation E(h).

JODEJKO-PIETRUCZUK A, WERBIŃSKA-WOJCIECHOWSKA S. **Analiza parametrów modeli obsługiwania systemów technicznych z opóźnieniem czasowym**. Eksploatacja i Niezawodnosc – Maintenance and Reliability 2014; 16 (2): 288–294.

W pracy analizie poddano system trzyelementowy (struktura niezawodnościowa progowa), którego procesy obsługiwania realizowane są zgodnie z założeniami Polityki Przeglądów Blokowych (BIP). Strategia ta może być zastosowana w procesie utrzymania systemów technicznych, gdy znane są pewne jego charakterystyki niezawodnościowe, bazujące m.in. na informacjach o czasach pomiędzy uszkodzeniami elementów systemu. W badaniach skupiono się na trzech rozkładach prawdopodobieństwa tej zmiennej losowej (normalny, Weibull, prostokątny). Model symulacyjny opracowano przy wykorzystaniu oprogramowania *GNU* Octave. Analiza okresu opóźnienia czasowego, przy założeniu różnych postaci rozkładów prawdopodobieństwa tej zmiennej losowej, pozwoliła na ocenę: czy znajomość typu rozkładu prawdopodobieństwa zmiennej losowej h ma istotne znaczenie dla wyników ekonomicznych funkcjonowania systemu, oraz jakie konsekwencje mogą wystąpić w wyniku niewłaściwej estymacji wartości średniej E(h).

ZHANG X, KANG J, BECHHOEFER E, ZHAO J. **A new feature extraction method for gear fault diagnosis and prognosis**. Eksploatacja i Niezawodnosc – Maintenance and Reliability 2014; 16 (2): 295–300.

Robust features are very critical to track the degradation process of a gear. They are key factors for implementing fault diagnosis and prognosis. This has driven the need in research for extracting good features. This paper used a new method, Narrowband Interference Cancellation, to suppress the narrow band component and enhance the impulsive component enabling the gear fault detection easier. This method can improve the signal to noise ratio of impulse train associated with the gear fault frequency. A run-to-failure test is used to demonstrate the method's effectiveness. Based on the time synchronous signal of high speed shaft, Sideband Index is extracted from the signals processed by Narrowband Interference Cancellation. This feature has good degradation trend than traditional Sideband Index extracted from the time synchronous average signal directly. Comparison of features based on different extraction process proves the effectiveness of developed method.

ZHANG X, KANG J, BECHHOEFER E, ZHAO J. **Nowa metoda diagnozowania i prognozowania uszkodzeń przekładni z wykorzystaniem ekstrakcji cech**. Eksploatacja i Niezawodnosc – Maintenance and Reliability 2014; 16 (2): 295–300.

Cechy odporne (robustfeatures) mają krytyczne znaczenie w trakcie śledzenia procesu degradacji przekładni. Stanowią one kluczowy czynnik w procesie diagnozowania i prognozowania uszkodzeń. Fakt ten stwarza w badaniach naukowych potrzebę ekstrakcji pożądanych cech. W niniejszej pracy wykorzystano nową metodę, tzw. metodę eliminacji zakłóceń wąskopasmowych (NarrowbandInterferenceCancellation), za pomocą której można wytłumić składową wąskopasmową, a wzmocnić składową impulsową, co ułatwia wykrywanie uszkodzeń przekładni. Metoda ta pozwala poprawić stosunek sygnału do szumu w szeregu impulsów związanym z częstotliwością charakteryzującą uszkodzenie przekładni. Skuteczność przedstawionej metody można wykazać za pomocą badań typu „pracuj do awarii" (run-to-failure) . Na podstawie synchronicznego sygnału wału wysokoobrotowego, z sygnałów przetwarzanych za pomocą metody eliminacji zakłóceń wąskopasmowych ekstrahuje się wskaźnik wstęgi bocznej (Sideband Index). Cecha ta ma lepszy trend degradacji niż tradycyjny wskaźnik wstęgi bocznej ekstrahowany bezpośrednio z sygnału uśrednionego synchronicznie w czasie. Porównanie cech wyodrębnionych w różnych procesach ekstrakcji dowodzi skuteczności opracowanej metody.

BUCHACZ A, PŁACZEK M, WRÓBEL A. **Modelling of passive vibration damping using piezoelectric transducers – the mathematical model**. Eksploatacja i Niezawodnosc – Maintenance and Reliability 2014; 16 (2): 301–306.

A proposal of mathematical modelling of vibrating piezoelectric transducers using the electrical analogy is presented in this work. The developed mathematical model is used in analysis of vibrating piezoelectric plates with adjoined external passive electric elements and for designating of their characteristics. A substitute electric system of the piezoelectric transducer that is equal to a three-port system was intro-

BUCHACZ A, PŁACZEK M, WRÓBEL A. **Modelowanie pasywnego tłumienia drgań przy użyciu przetworników piezoelektrycznych – model matematyczny**. Eksploatacja i Niezawodnosc – Maintenance and Reliability 2014; 16 (2): 301–306.

W pracy przedstawiono propozycję modelowania matematycznego drgających przetworników piezoelektrycznych poprzez zastosowanie analogii elektrycznej. Opracowany model stosowany jest w analizie oraz wyznaczaniu charakterystyk drgających płytek piezoelektrycznych z dołączonymi, zewnętrznymi, biernymi elementami elektrycznymi. Wprowadzono układ zastępczy przetwornika piezoelektrycznego równoważny trójwrotniduced. A piezoelectric transformer created by connection of two plates was analysed. Substitute systems of both plates were introduced. All mechanical parameters of the analysed system were replaced by equivalent electrical parameters in obtained Mason's model.

YANG Y, LU Z, LUO X, GE Z, QIAN Y. **Mean failure mass and mean failure repair time: parameters linking reliability, maintainability and supportability**. Eksploatacja i Niezawodnosc – Maintenance and Reliability 2014; 16 (2): 307–312.

Up to now, no parameters linking reliability, maintainability and supportability directly are available in reliability engineering. Index such as availability can be used to check the compatibility of those RAM features only after individual index of every characteristic is obtained such as MTBF, MTTR, etc. Thus available methods to balance those three features are not efficient and direct during the product design phase. In this paper, concepts of mean failure mass and mean failure repair time are presented. By investigating the relationship of the failure probability and the mass of a product, a feature linking reliability and supportability is obtained. Similarly, by studying the relationship of the failure probability and the mean time to repair of a product, a feature linking reliability and maintainability is obtained. Based on above definitions, an approach of reliability, maintainability and supportability trade-off during design phase is achieved. Effectiveness of both of the new concepts is demonstrated by an example of balancing the maintainability and supportability of a subsystem of a space station.

ŻYCZYŃSKA A. **The heat consumption and heating costs after the insulation of building partitions of building complex supplied by the local oil boiler room**. Eksploatacja i Niezawodnosc – Maintenance and Reliability 2014; 16 (2): 313–318.

The paper presents the indices of energy consumption obtained in operating conditions as well as the heating costs before and after the insulation of external partitions of eight multiple dwelling buildings supplied by the common heat source which is the local boiler room heated by light fuel oil. The heat distribution to the particular buildings is by the district heating network. In order to determine the average unitary indices of energy consumption aimed at heating of the whole building complex, the analysis of fuel consumption is carried out, with consideration of standard computational conditions. The analysis lasted for four years after the insulation of buildings, from 2008 to 2011; its results are compared to the ones obtained from the analysis conducted before the insulation, in 2006. The investment was realised in 2007. The obtained real energy consumption indices are compared to the current requirements of technical conditions. On the basis of the data referring to the operation of buildings, the decrease in the heat consumption due to the insulation of partitions, the variability of fuel price, and the costs of heat generation are estimated . Moreover, the decrease in the emission of pollutants into the atmosphere is defined, as well as the costs of heat generation, which would be incurred if there was no insulation of partitions, are estimated.

AU-YONG CP, ALI AS, AHMAD F. **Prediction cost maintenance model of office building based on condition-based maintenance**. Eksploatacja i Niezawodnosc – Maintenance and Reliability 2014; 16 (2): 319–324.

Building maintenance costs are continuously increasing as a result of poor maintenance. Consequently, there is an urgent need to develop solutions to reduce the maintenance costs. Various studies demonstrated that the characteristics of condition-based maintenance are directly related to the cost performance. Thus, this paper seeks to establish the relationships between the characteristics of condition-based maintenance and the cost performance. The researcher then developed a regression model for maintenance planning and prediction. The study adopted a mix method approach that includes questionnaire survey, interview, and case study. The findings highlighted the reliability of maintenance data and information as the most significant characteristic of condition-based maintenance. Consequently, the study concluded that the planning and the application of the condition-based maintenance strategy should consider its significant characteristics and make reference to the resulting prediction model. Furthermore, the study recommended measures to improve the significant characteristics and the cost performance in practice.

KOŁODZIEJ P, BORYGA M. **Frequency analysis of coupling with adjustable torsional flexibility**. Eksploatacja i Niezawodnosc – Maintenance and Reliability 2014; 16 (2): 325–329.

The article presents the frequency analysis of a flexible coupling allowing changes of torsional flexibility. The authors derived a relationship for coupling flexibility considering geometric and material parameters. Coupling flexibility change is executed in such a manner that the quotient of extortion frequency and natural frequency of the system is higher than 1.4. Oscillation parameters for selected values of torsional flexibility were calculated for extortion frequencies approximating natural frequencies and after flexibility change.

kowi elektrycznemu. W pracy analizowano połączenia dwóch płytek piezoelektrycznych działających jako transformator piezoelektryczny, wprowadzając układy zastępcze obu przetworników. Przy stosowaniu układów zastępczych w postaci obwodów elektrycznych wszystkie wielkości mechaniczne w otrzymanym układzie Masona zostały zastąpione równoważnymi wielkościami elektrycznymi.

YANG Y, LU Z, LUO X, GE Z, QIAN Y. **Średnia masa uszkodzenia i średni czas naprawy uszkodzenia: parametry łączące niezawodność, obsługiwalność i utrzymywalność**. Eksploatacja i Niezawodnosc – Maintenance and Reliability 2014; 16 (2): 307–312.

Jak dotąd w inżynierii niezawodności nie istniały parametry łączące niezawodność, obsługiwalność i utrzymywalność. Wskaźniki takie jak gotowość mogą być stosowane w celu sprawdzenia zgodności tych cech RAM (Reliability, Availability, Maintainability – Niezawodność, Gotowość, Obsługiwalność) dopiero po uzyskaniu indywidualnego wskaźnika każdej charakterystyki, takich jak MTBF, MTTR, itp. W ten sposób dostępne metody równoważenia owych trzech cech nie są wystarczająco skuteczne i bezpośrednie w fazie projektowania produktu . Niniejszy artykuł przedstawia pojęcia średniej masy uszkodzenia i średniego czasu naprawy uszkodzenia. Badając zależność prawdopodobieństwa uszkodzenia i masy produktu, uzyskuje się cechę łączącą niezawodność i utrzymywalność. Podobnie, badając zależność prawdopodobieństwa uszkodzenia i średniego czasu naprawy produktu, uzyskuje się cechę łączącą niezawodność i obsługiwalność. Na bazie powyższych definicji osiągnięto kompromisowe podejście do niezawodności, obsługiwalności i utrzymywalności podczas fazy projektowania. Skuteczności obu nowych koncepcji dowodzi przykład równoważenia niezawodności i obsługiwalności podsystemu stacji kosmicznej.

ŻYCZYŃSKA A. **Zużycie ciepła i koszty ogrzewania po dociepleniu przegród budowlanych zespołu budynków zasilanych z lokalnej kotłowni olejowej**. Eksploatacja i Niezawodnosc – Maintenance and Reliability 2014; 16 (2): 313–318.

W artykule przedstawiono wskaźniki zużycia energii uzyskane w warunkach eksploatacyjnych i koszty ogrzewania przed i po dociepleniu przegród zewnętrznych grupy ośmiu budynków mieszkalnych wielorodzinnych zasilanych ze wspólnego źródła ciepła. Źródłem ciepła jest kotłownia lokalna opalana olejem opałowym lekkim, dystrybucja ciepła do poszczególnych budynków następuje poprzez osiedlową sieć ciepłowniczą. W celu określenia średnich jednostkowych wskaźników zużycia energii na cele grzewcze dla całego zespołu budynków przeprowadzono analizę zużycia paliwa uwzględniając standardowe warunki obliczeniowe. Analizą objęto okres czterech lat po dociepleniu budynków od 2008–2011 r. i odniesiono do stanu przed dociepleniem z 2006 r., inwestycja była realizowana w 2007 r. Uzyskane rzeczywiste wskaźniki zużycia energii porównano do obecnie obowiązujących wymagań warunków technicznych. Na podstawie danych z eksploatacji budynków przeanalizowano spadek zużycia ciepła z tytułu docieplenia przegród, zmienność cen paliwa i kosztów eksploatacyjnych ogrzewania, określono spadek emisji zanieczyszczeń do atmosfery, oszacowano koszty eksploatacyjne ogrzewania jakie zostałyby poniesione w przypadku braku docieplenia przegród budowlanych.

AU-YONG CP, ALI AS, AHMAD F. **Predykcyjno-kosztowy model konserwacji budynku biurowego oparty o utrzymanie zależne od bieżącego stanu technicznego (CBM)**. Eksploatacja i Niezawodnosc – Maintenance and Reliability 2014; 16 (2): 319–324.

Koszty konserwacji budynków nieustannie rosną ze względu na nieodpowiednią konserwację. Z tej racji, niezbędne jest wypracowanie rozwiązań obniżających koszty konserwacji. Różne badania wykazały, iż charakterystyki utrzymania urządzeń zależnie od ich bieżącego stanu technicznego (condition-based maintenance, CBM) są bezpośrednio powiązane z wydajnością kosztu. Niniejszy artykuł stara się więc ustalić związek pomiędzy charakterystykami utrzymania budynków zależnie od ich bieżącego stanu technicznego a wydajnością kosztu. Następnie opracowano model regresji dla planowania konserwacji jak i predykcji. W badaniach użyto metody mieszanej łączącej badania kwestionariuszowe, wywiad oraz studium przypadku. Rezultaty podkreśliły, iż wiarygodność danych z konserwacji i informacji to najbardziej istotne charakterystyki CBM. W konsekwencji, wnioski z badań sugerują, iż planowanie i wdrożenie strategii utrzymania w zależności od bieżącego stanu technicznego powinno brać pod uwagę jej istotne charakterystyki i odwoływać się do wynikającego z niej modelu predykcji. Ponadto, praca zawiera zalecenia jakimi środkami można w praktyce poprawić istotne charakterystyki i wydajność kosztu.

KOŁODZIEJ P, BORYGA M. **Analiza częstościowa sprzęgła o regulowanej podatności skrętnej**. Eksploatacja i Niezawodnosc – Maintenance and Reliability 2014; 16 (2): 325–329.

W pracy przedstawiono analizę częstościową sprzęgła podatnego umożliwiającego zmianę sztywności skrętnej. Wyprowadzono zależność na sztywność sprzęgła uwzględniając parametry geometryczne i materiałowe. Zmiana sztywności sprzęgła dokonuje się tak aby iloraz częstości wymuszenia i częstości drgań własnych układu był większy od 1,4. Obliczono parametry drgań dla wybranych wartości współczynnika sztywności skrętnej przy częstościach wymuszenia bliskich częstości drgań własnych oraz po zmianie sztywności.

WALCZAK M, PIENIAK D, NIEWCZAS AM. **Effect of recasting on the useful properties CoCrMoW alloy**. Eksploatacja i Niezawodnosc – Maintenance and Reliability 2014; 16 (2): 330–336.

Recasting of the previously cast metal can change the chemical composition of the newly formed material, which ultimately could affect the properties of a dental alloy. The research used a dental alloy CoCrMoW trade name Remanium 2001. Three groups of dental alloy were prepared by mixing 50% fresh alloy to alloy remnants from previous castings. The specimens in the first casting group used 100% fresh alloy and served as control (R1). The second group consisted of equal amounts of fresh alloy and alloy remnants cast only once (R2). The third group contained 50% fresh alloy and alloy cast twice (R3). Microstructural analysis was performed and the chemical composition, XRD studies, hardness, and tribological test and the metal–ceramic bond strength was investigated according to ISO9693 standard. New material should be used in casting, and if previously casted material is used, it should be mixed with new material. The use of the recasting procedure can lower the costs of CoCrMoW castings and can be safely in dentistry.

WALCZAK M, PIENIAK D, NIEWCZAS AM. **Wpływ powtórnego przetapiania na właściwości użytkowe stopu CoCrMoW**. Eksploatacja i Niezawodnosc – Maintenance and Reliability 2014; 16 (2): 330–336.

Przetapianie uprzednio odlanego metalu może spowodować zmianę składu chemicznego nowopowstałego materiału, co w końcowym efekcie może oddziaływać na właściwości użytkowestopu stomatologicznego. Do badań zastosowano stop stomatologiczny CoCrMoW o nazwie handlowej Remanium 2001.Przygotowano 3 grupy stopu stomatologicznego przez zmieszanie 50% fabrycznie nowego stopu ze stopem po poprzednim przetopieniu. Grupę pierwszą odlano w 100% z nowego fabrycznie stopu jako grupę kontrolną (R1). Grupa druga (R2) została odlana z mieszaniny jednakowych ilości nowegostopu oraz stopu odlanego tylko raz.Grupa trzecia (R3) zawierała 50% świeżego stopu oraz stopu odlanego 2 razy.Wykonano analizę mikrostrukturalną oraz składu chemicznego, badania XRD, pomiary twardości, badania tribologiczne oraz badania przyczepności wg ISO 9693.Wykazano, że w odlewaniu należy używać nowego materiału a w przypadku wykorzystania materiału wcześniej używanego należy go wymieszać z materiałem nowym. Wykorzystanie procedury przetapiania może obniżyć koszty odlewów CoCrMoW oraz może być bezpieczne w stomatologii.

CHŁOPEK M, DZIK T, HRYNIEWICZ M. **Determining the grip angle in a granulator with a flat matrix**. Eksploatacja i Niezawodnosc – Maintenance and Reliability 2014; 16 (2): 337–340.

The article addresses the new concept of determining the grip angle in a roll – a flat matrix working arrangement. It was verified experimentally with the exemplary use of composite fuels. For this purpose, a methodology has been developed and the external and internal friction coefficients for several fuel blends have been determined. Knowing them enables one to determine the grip angle which has a significant influence on the efficiency of the granulator. Then, pressure granulation tests with selected blends were carried out. The test results and the calculations are presented in the article. The comparison of the experimental grip angle and the one determined on the basis of a theoretical equation testifies to the correspondence between the theory and the actual physical situation. The determined friction coefficients also determine the selection of an adequate diameter and width of the roller as well as the shape of its working surface. It is of essential importance for ensuring the correct operation of a press with a flat matrix.

CHŁOPEK M, DZIK T, HRYNIEWICZ M. **Wyznaczanie kąta chwytu w granulatorze z płaską matrycą**. Eksploatacja i Niezawodnosc – Maintenance and Reliability 2014; 16 (2): 337–340.

W artykule zwrócono uwagę na nową koncepcję określania kąta chwytu w układzie roboczym rolka - płaska matryca. Poddano ją weryfikacji eksperymentalnej na przykładzie paliw kompozytowych. W tym celu opracowano metodykę i wyznaczono współczynniki tarcia zewnętrznego oraz wewnętrznego kilku mieszanek paliw. Ich znajomość umożliwia określenie kąta chwytu mającego istotny wpływ na wydajność granulatora. Następnie przeprowadzono próby granulacji ciśnieniowej wybranych mieszanek. Wyniki badań oraz obliczeń przedstawiono w artykule. Porównanie doświadczalnego kąta chwytu oraz wyznaczonego z równania teoretycznego świadczy o zbieżności teorii z rzeczywistą sytuacją fizyczną. Wyznaczone współczynniki tarcia determinują również dobór odpowiedniej średnicy i szerokości rolki, a także kształtu jej powierzchni roboczej. Ma to istotne znaczenie dla prawidłowej eksploatacji prasy z płaską matrycą.

WALKOWIAK T. **Simulation based availability assessment of services provided by web applications with realistic repair time**. Eksploatacja i Niezawodnosc – Maintenance and Reliability 2014; 16 (2): 341–346.

Paper presents a numerical method for determining changes of availability of services provided by web applications in time. It takes into account the reliability and functional aspects. The reliability analysis allows determining the probability that the system is operational at a given time. The analysis includes the structure of a computer system, random times to failures (hardware or software – related to security breaches) and the detailed repair time model. The repair time model takes into account working hours of administrators and a time associated with delivering components to exchange. Functional analysis allows the determination of the probability that the user will be served in less than a specified time limit. It is based on modelling the interaction between a user and a server as a sequence of tasks on one or more hosts. It takes into account the variability of workload over a week and web application parameters such as the choreography of service, allocation of tasks on hosts and technical parameters of hosts and tasks. The described method was the basis for development of a Monte-Carlo simulator that allows variability of service availability over a week to be calculated. The paper contains the numerical results of the sample analysis.

WALKOWIAK T. **Symulacyjna ocena gotowości usług systemów internetowych z realistycznym modelem czasu odnowy**. Eksploatacja i Niezawodnosc – Maintenance and Reliability 2014; 16 (2): 341–346.

W artykule przedstawiono metodę numerycznego wyznaczania zmian gotowości usług internetowych w czasie. Bierze ona pod uwagę aspekty niezawodnościowe i funkcjonalne systemu komputerowego świadczącego usługi. Analiza niezawodnościowa pozwala na wyznaczenie prawdopodobieństwa, że system będzie zdatny w danym momencie. Uwzględnia ona strukturę systemu komputerowego, losowe czasy do uszkodzeń (sprzętowych jak i oprogramowania związanych z naruszeniami zabezpieczeń) oraz szczegółowy model odnowy biorący pod uwagę godziny pracy administratorów oraz czas związany z dostarczeniem elementów do wymiany. Analiza funkcjonalna pozwala na wyznaczanie prawdopodobieństwa, że użytkownik zostanie obsłużony w czasie mniejszym niż zadany. Oparta jest ona na modelowaniu procesu realizacji usługi jako sekwencji zadań wykonywanych na jednym lub kilku komputerach. Bierze ona pod uwagę zmienność intensywności napływu użytkowników w ciągu tygodnia oraz parametry takie jak: sekwencję zadań, alokację zadań na komputerach oraz parametry techniczne komputerów i zadań. Opisana metoda była podstawą do stworzenia aplikacji komputerowej wyznaczającej techniką symulacji Monte-Carlo zmienność gotowości systemu w ciągu tygodnia. Artykuł zawiera numeryczne rezultaty przykładowej analizy.

Article citation info:
WANG HW, GAO J. A reliability evaluation study based on competing failures for aircraft engines. Eksploatacja i Niezawodnosc – Maintenance and Reliability 2014; 16 (2): 171–178.

HuaWei WANG
Jun GAO

A RELIABILITY EVALUATION STUDY BASED ON COMPETING FAILURES FOR AIRCRAFT ENGINES

BADANIA DOTYCZĄCE OCENY NIEZAWODNOŚCI SILNIKÓW LOTNICZYCH W OPARCIU O USZKODZENIA KONKURUJĄCE

Aircraft engine is a complex and repairable system, and the diversity of its failure modes increases the difficulty of reliability evaluation. It is necessary to establish a dynamic relationship among data, failure mode and system reliability, to achieve the scientific reliability evaluation for aircraft engines. This paper has used data fusion method to establish reliability evaluation models respectively for performance degradation failures and sudden failures. Furthermore, these two models have been integrated on the basis of competing failures' mechanism. Bayesian model averaging has been used to analyze the impacts of performance degradation failures and sudden failures on aircraft engines' reliability. As a result of above, the goal of an accurate evaluation of the reliability for aircraft engines has been achieved. Example shows the effectiveness of the proposed model.

Keywords*: aircraft engine, reliability evaluation, competing failures, Bayesian model averaging, data fusion.*

Silnik samolotu to złożony system naprawialny, w którym różnorodność przyczyn uszkodzeń zwiększa trudność oceny niezawodności. Dlatego też istnieje konieczność ustalenia dynamicznych związków pomiędzy danymi, przyczynami uszkodzenia i niezawodnością systemu, których znajomość pozwoliłaby przeprowadzać naukową ocenę niezawodności silników lotniczych. W prezentowanej pracy wykorzystano metodę fuzji danych do opracowania modeli oceny niezawodności w zakresie uszkodzeń wynikających z obniżenia charakterystyk oraz uszkodzeń nagłych. Ponadto, opracowane modele zintegrowano na podstawie mechanizmu uszkodzeń konkurujących. Do analizy wpływu dwóch omawianych typów uszkodzeń na niezawodność silników lotniczych wykorzystano procedurę bayesowskiego uśredniania modeli. Dzięki powyższym krokom, osiągnięto założony cel dokładnej oceny niezawodności silników samolotowych. Przykład pokazuje skuteczność proponowanego modelu.

Słowa kluczowe*: silnik lotniczy, ocena niezawodności, uszkodzenia konkurujące, bayesowskie uśrednianie modeli, fuzja danych.*

1. Introduction

The level of the aircraft engines' reliability affects flight safety directly. Estimating the reliability level scientifically and objectively is the foundation of reliability management and decision-making of maintenance for aircrafts. The difficulties of reliability evaluation for aircraft engines lie in two aspects. First, there are less failure data and rich condition monitoring data. Second, there is a problem of competing failures caused by the diversity of failure modes arising from the complexity of the system.

Extracting information about reliability from a large amount of monitoring information is a common concern issue in the current theoretical and engineering field. Researchers in the United States, Britain, Australia and other countries promote using HUMS (health and usage monitoring systems,) to monitor the health and use of engines, structure, etc, which can provide full-time health information and on-line monitoring, in order to make the diagnosis and prediction of the remaining life of the equipment, structure and operation [7]. HP Engine Company has developed an advanced life prediction system for gas turbine engines, which integrates fault prognostics and health management capacity [16] .Volponi [18] used data fusion technology for aircraft engine health management. Niu et al. [10] employed data fusion strategy for improving condition monitoring, health assessment and prognostics. Cobel [6] proposed using data fusion method, which fuses condition monitoring data and fault data effectively, to predict the remaining life, used genetic algorithm to select optimal monitoring parameters, applied GPM (General path model, GPM) to achieve that transform the traditional reliability analysis based on failure time to analysis based on failure process.

For complex systems, the reliability evaluation of single failure mode or single point of failure is an ideal assumption. But in terms of practical situation of aircraft engines, the failure modes are various and multi-failure modes often coexist. The failure modes can be divided into degradation failure and sudden failure only on the basis of major categories of classification. Different failure modes interact with each other, constantly change their forms of expression and mechanism of action in different stages of the running system. It is a problem of competing failures in essence, increasing the complexity of the reliability evaluation. The problem of competing failures has drawn a lot of concern in the field of reliability engineering. Bedford [2] analyzed the characters of reliability evaluation models for various competing failures from a statistical point. Lehmann [9] surveyed some approaches to model the relationship between failure time data and covariate data like internal degradation and external environment models. Bagdonavičius et al [1] made use of the half updating process of the linear degradation model to study the non-parameter estimation method of competing failure model, and to simplify the using decomposition method. Pareek et al. [11] studied the problem of censored data processing for competing failures. Bedford et al. [3] presented a competing risks reliability model for a system that releases signals each time on its condition deteriorates and provided a framework for the determination of the underlying system time from right-censored data. Su et al. [17] regarded the incidence of sudden failure as the function of performance degradation amount, made use of Wiener process to describe the degradation process, and proposed a reliability evaluation model for competing failures. Bocchetti et al. [4] proposed a competing risk model to describe the reliability of the cylinder liners of a marine Diesel engine, in which the wear process is described by through a stochastic process and the failure time due to the thermal cracking is described by the Weibull distribution. Park et al. [12] and Kundu et al. [8] considered the analysis of incomplete data in the presence of competing risks among several groups. Chen et al. [5] developed methods for competing risks when individual events are correlated with clusters. Wang et al. [19] used Bivariate exponential models to analysis of competing risks data involving two correlated risk components. Xing et al. (2010) [20] presented a combinatorial method for the reliability analysis of system subject to competing propagated failures and failure isolation effect. Salinas-Torres et al. (2002) [15] and Polpo et al. (2011) [14] proposed the Bayesian nonparametric estimator of the reliability of a series system under a competing risk scenario. Peng et al. (2011) developed reliability models and preventive maintenance policies for systems subject to multiple Dependent Competing Failure Process (MDCFP) .

For the problem of aircraft engines' competing failures, the information fusion technology will be referenced to the aircraft engines' reliability modeling and the input variables of the reliability model will be determined by information fusion. The impacts of competing failure modes on system reliability will be analyzed through data. This paper will use Bayesian model averaging method to study the data, to select the optimal model, and to propose a reliability evaluation model for aircraft engines based on competing failures.

2. The modeling framework of reliability evaluation for aircraft engines based on competing failures

2.1. The modelling process of reliability evaluation based on competing failures

This paper intends to combine the recent research results concerning reliability evaluation and competing failures based on information fusion, and to propose reliability evaluation methods based on competing failures for aircraft engines. Its characteristics are reflected in the following aspects. First, it takes into account both the characteristics of information and failure mechanism, establishing the reliability evaluation models respectively for the performance degradation and sudden failures. Second, in the case of sudden failures and performance degradation failures coexist, the reliability evaluation model based on competing failures is established. Third, the impacts of different failure modes' mechanism on the reliability are analyzed. The modeling process is shown in Fig.1.

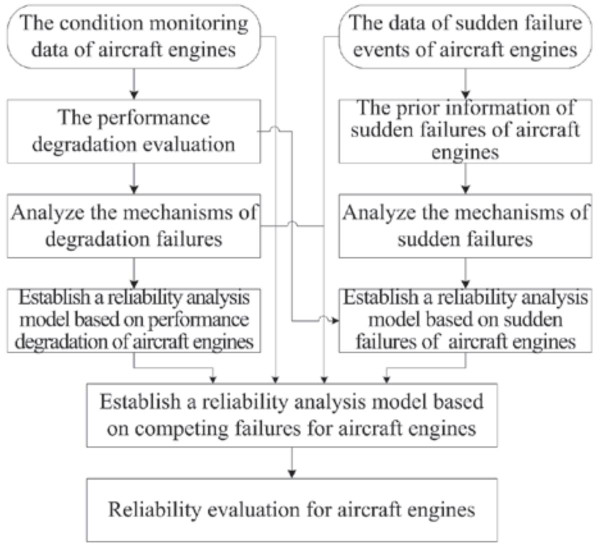

Fig 1. The flow diagram of reliability evaluation for aircraft engines based on competing failures

2.2. The reliability modeling methods of aircraft engines based on competing failures

The reliability modeling methods of aircraft engines based on competing failures include the following three-part.

2.2.1. The reliability evaluation of performance degradation failures for aircraft engines

The performance monitoring of aircraft engines includes three categories, namely, gas path performance monitoring, oil monitoring and vibration monitoring. The engines' performance degradation (or reduced efficiency) will usually be reflected in changes of monitoring parameters. The main monitoring parameters are: the turbine gas temperature (EGT), fuel flow (WF), oil pressure (OP), oil temperature (OT) and the oil consumption rate (OCR), the deviation of the low-pressure rotor vibration value (DLPRV) and high-pressure rotor vibration value deviation (DHPRV) and so on. The excessive EGT, the WF increasing, the larger DLPRV and DHPRV, the higher OCR all can reflect the performance degradation of aircraft engines. Comprehensively using above parameters to reflect the performance degradation of aircraft engines from the multi-dimensional perspective will be more realistic. This paper use Bayesian linear model to fuse above monitoring information, and its advantages are reflected in the following aspects. The Bayesian linear model, which foothold is expectation, reflects the uncertainty in the form of variance. The Bayesian linear model can well represent the randomness of monitoring parameters and performance degradation variables. It can fuse the impacts of various sources of data on the performance degradation, while taking fully into account the correlation between the data to avoid the phenomenon of information overlap. It has a learning function and it can fully fuse the data of different timing points. Noise parameters can be designed to avoid performance degradation's uncertainty caused by the uncertainty of the monitoring data results. It's worthy noting that, the Bayesian linear model can also fuse various types of nonlinear parameters through appropriate transformation.

2.2.2. The reliability evaluation of sudden failures for aircraft engines

The reliability analysis model based on the sudden failures includes two aspects. First, the reliability analysis of sudden failures, which is a reliability analysis problem of typical small-sample because the aircraft engine is high-reliability system and the fault information is rarely collected. The second are the correlation analysis between degradation failures and sudden failures, and quantifying the impacts of degradation failures on sudden failures. The reliability of sudden failures for aircraft engines is achieved by describing the law of its life changes. For the choice of sudden failures' distribution form, the final form is selected mainly through the combination of the failure mechanism analysis, following the fitting of the data validation and uncertainty analysis on the basis of the failure mechanism analysis. Because Weibull distribution model itself can reflect the impacts of the performance degradation on the law of life changes, so it is generally regarded as the main choice. The condition monitoring parameters of aircraft engines can not directly reflect the impacts that they pose on the sudden failures, but the performance degradation of aircraft engines can be extracted from the condition monitoring parameters. And then, the link between sudden failures and performance failures can be established by transforming the performance degradation as the shape parameters of the Weibull distribution appropriately.

Notice the actual situation that there are insufficient or even no failure data, this paper uses Bayesian methods to establish reliability analysis model of sudden failures.

2.2.3. The reliability evaluation of competing failures for aircraft engines

For the two major categories of failures, the research focused on the analysis of the relationship between sudden failures and performance degradation failures. For the mechanisms of the two failures between each other, the competing failures is usually regarded as a series model in the reliability analysis, but the reliability will be underestimated by using this method because a variety of competing causes of failures can not be real-time and simultaneous. If calculating the remaining life or reliability of different failures modes respectively and take the lowest as the reliability of competing failures, the reliability will be overestimated because to some extent the characteristics that a variety of competitive modes coexist in a certain period of time will be ignored. Competing failures needs considering the two failures modes' mechanisms comprehensively, but knowing how to act and change between the two modes can't rely solely on the failures mechanism analysis, the data is the key to understand it. To study the mechanism of two competing failures, this paper will use Bayesian model averaging method. Bayesian model averaging (Bayesian model averaging, BMA) is a probability forecast approach that is proposed recently and is used in multi-mode collection. The forecast probability density function (PDF) of a particular variable in BMA, is a weighted average of a single model forecast probability distribution after deviation correction, and the weight is the corresponding model's posterior probability which represents each model's relative forecast skill in the model training phase. The secondary use of condition monitoring data and event data can be achieved through BMA technology. And this not only solves the problem of reliability analysis based on a single failures mode, but also solves the problem of interaction of multiple failures modes. Based on the data re-learning, the goal of an accurate analysis of civil aircraft system reliability can be achieved.

3. The problem description of competing failures for aircraft engines

The problem description of competing failures for aircraft engines includes three aspects. The first is the process description of performance degradation failures, following the sudden failures description. And the third is competing failure description based on the sudden failures and performance degradation failures.

3.1. Performance degradation failures

Let $y(t)$ be the amount of performance degradation failures at time t and l be the failures threshold. When $y(t) \geq l$, aircraft engines will come up with performance degradation failures. Aircraft engines' performance degradation is irreversible, that is, the performance gradually decreases and the amount of performance degradation is constantly increasing with the use of time. Therefore, the Gamma process can be applied to describe the degradation process. Assume that y_0 is aircraft engines' initial performance, so $w(t) = y(t) - y(t_0)$ represents the accumulated deterioration at time t . Because degradation amount increases monotonically, for any t_i, t_j , if $t_j > t_i$, there must be $w(t_j) - w(t_i) > 0$. Assume that degradation amount $w(t)$ obey $Ga(\mu(t), \lambda)$, its density function can be expressed as follows:

$$f_w(\xi, \alpha(t), \lambda) = \frac{\lambda^{\alpha(t)}}{\Gamma(\alpha(t))} \zeta^{\mu(t)-1} e^{-\lambda\zeta} \tag{1}$$

where, α and λ represent shape parameter and scale parameter respectively; $\Gamma(\alpha) = \int_0^\infty t^{\alpha-1} e^{-t} dt$ is Gamma function.

Generally assume that the scale parameter does not change in a performance monitoring process. Shape parameter changes with the change of the degradation process, because the extent and rate of the performance degradation experience an increasing trend, so we assume that shape parameter is proportional with expected degradation degree and time power, that is:

$$\alpha(t) = kt^v \tag{2}$$

Further, Eq. (2) can be transformed as following:

$$f_w(\xi, \alpha(t), \lambda) = \frac{\lambda^{kt^v}}{\Gamma(kt^v)} \zeta^{kt^v - 1} e^{-\lambda x} I_{(0,\infty)}(\zeta) \tag{3}$$

Based on the theory of system reliability, the reliability for degradation failures can be depicted as following:

$$R(t) = P\{T > t\} \Rightarrow P\{w(t) < \varepsilon\} \tag{4}$$

where, ε is the failure threshold for performance degradation of an aircraft engine.

Then, the reliability evaluation for performance degradation of an aircraft engine can be depicted as following:

$$R(t) = \int_0^\varepsilon f_w(\zeta) d\zeta = \int_0^\varepsilon \frac{\lambda^{kt^v}}{\Gamma(kt^v)} \xi^{kt^v - 1} e^{-\lambda\xi} d\xi \tag{5}$$

3.2. Sudden failures

The Weibull distribution is widely used in engineering fields. Through assigning different values to its parameters, it can fuse the impact of performance degradation on the law of life changes, so to some extent, it can describe the relationship between performance degradation failures and sudden failures.

Assume that the law of life changes for sudden failure of aircraft engines complies with the Weibull distribution, it can be expressed as:

$$f\left(t;\beta,\gamma\right)=\frac{\gamma}{\beta}\left(\frac{t}{\beta}\right)^{\gamma-1}\exp\left[-\left(\frac{t}{\beta}\right)^{\gamma}\right], \text{ if } t>0 \tag{6}$$

Among that, $\beta>0$, $\gamma>0$ represent scale parameter and shape parameter respectively. And γ characterize the performance degradation.

When the shape parameter is known, the sudden failure reliability evaluation can be transformed to estimate scale parameter β. It is assumed that the scale parameter β has a conjugate gamma prior, that is:

$$\pi\left(\beta\middle|c,d\right)=\begin{cases}\dfrac{d^{c}}{\Gamma(c)}\beta^{c-1}e^{-d\beta}, & if \quad \beta>0\\ 0, & if \quad \beta\le 0\end{cases} \tag{7}$$

where c and d are scale parameter' conjugate prior hyper parameters. The values of c and d can be calculated through the acquisition of the scale parameter' prior mean and variance. Further, it can calculate the posterior mean and variance of the scale parameter, to achieve the reliability evaluation of the sudden failure.

More generally, the conditional probability of sudden failure on the amount of degradation can be determined through data learning, in order to analyze the impact of degradation failure on sudden failure. Because the characteristics distribution of degradation amount is a function of time, so the process above can be simplified. Reliability can be calculated by the joint distribution function which based on the sudden failure's conditional probability and probability distribution, the relevant solution can use Monte Carlo simulation method.

The reliability of sudden failure can be expressed as follows:

$$R_s=1-\int_0^{T_s} f\left(t,\beta,r\right)dt \tag{8}$$

3.3. Competing failures

The basic assumptions for competing failure of aircraft engines are as follows.

I There are two random variables X and Y, where Y denote the degradation failure and X denote sudden failure. X and Y are competing failures for causing failure.

II The performance degradation failure is irreversible.

III There is correlation between performance degradation failure and the random variables of sudden failure.

So in the case of sudden failure, the reliability of aircraft engines in competing failures can be expressed as follow:

$$R_c(t)=P(T>t)=P\left(T_g>t,T_s>t\right)=\int_0^{\varepsilon}\exp\left[-\int_0^{t}\lambda_s\left(\tau\middle|y\right)d\tau\right]f_w(y,\alpha,\lambda)dy \tag{9}$$

where $R_c(t)$ is the reliability under the competing failures at time t. Eq. (8) is a problem of high dimensional integral calculation, the calculation itself has no difficulty. However, competing failure is not synchronous, and the data of correlation between competing failure and sudden failure can not be collected. In a certain degree, performance degradation failure and sudden failure can not play a role at the same time; maybe one failure mode plays the main part. Assume that the corresponding reliability evaluation model of the performance degradation failure is M_1, the corresponding reliability evaluation model of the sudden failure is M_2, Eq. (9) for the reliability evaluation model based on the competing failures can be expressed as M_3. For the observational data collected, the expression of the various failure modes can be obtained through the study of observational data.

$$P\left(D\middle|M_1,M_2,M_3\right)=\sum_{k-1}^{3} w_k g_k\left(D\middle|M_k\right) \tag{10}$$

Conditional probability density function $g_k\left(D\middle|M_k\right)$ represents the conditional probability of observed variable D which based on model M_k. w_k represents the posterior probability as the k th model is the best model, and w_k is non-negative and satisfies $\sum_{k=1}^{N} w_k=1$. The expression represents the relative contribution of each model to civil aircraft system reliability evaluation in the model training phase.

4. Reliability evaluation algorithm for aircraft engines

4.1. Reliability evaluation algorithm for performance degradation failures

I Through the fusion of condition monitoring information, the expectation and variance of the degree of aircraft engines' performance degradation can be extracted to calculate the results;

Assume that the monitoring parameters of aircraft engines' performance degradation are expressed by matrix $\mathbf{X}=\left[\mathbf{X}_1,\mathbf{X}_2,\cdots,\mathbf{X}_k\right]$, where k represents monitoring parameters, e is deviation. The relationship between performance degradation and condition monitoring parameters can be expressed by the following stochastic equation:

$$\begin{cases}\mathbf{Y}=\mathbf{X}, +\mathbf{e}\\ \mathbf{e}\sim N\left(0,\sigma^2\right)\end{cases} \tag{11}$$

Among that, $\mathbf{Y}=\begin{bmatrix}y_1\\ y_2\\ \vdots\\ y_n\end{bmatrix}$, $\mathbf{e}=\begin{bmatrix}e_1\\ e_2\\ \vdots\\ e_n\end{bmatrix}$, $\mathbf{e}=\begin{bmatrix}e_1\\ e_2\\ \vdots\\ e_n\end{bmatrix}$.

$\mathbf{e}_i$ is independent between each other and obey the normal distribution $N\left(0,\sigma^2\right)$, and σ^2 is known.

$\boldsymbol{\theta}$ can be calculated through monitoring parameters. The mean is $\boldsymbol{E}(\boldsymbol{\theta})$. And $\boldsymbol{C}(\boldsymbol{\theta})$ is covariance matrix.

For monitoring parameters, generally assume that they are in line with the inverse Gaussian distribution. Through continuous monitoring, the mean and variance are also constantly updating. The mean and covariance matrix can be expressed as follows.

$$\mathbf{E}(\theta|x,y) = \mu_\theta + \mathbf{C}(\theta)X^{\mathrm{T}}\left(\mathbf{XC}(\theta)\mathbf{X}^{\mathrm{T}} + \mathbf{C}_e\right)^{-1}(y - \mathbf{X}\mu_\theta) \quad (12)$$

$$\mathbf{C}(\theta|x,y) = \mathbf{C}(\theta) - \mathbf{C}(\theta)\mathbf{X}^{\mathrm{T}}\left(\mathbf{XC}(\theta)\mathbf{X}^{\mathrm{T}} + C_e\right)^{-1}\mathbf{XC}(\theta) \quad (13)$$

With the increasing observational information, the Eq.(12), (13) can be used repeatedly to update the fusion results of the monitoring information for the performance degradation.

II Making use of the calculations results of mean and variance to calculate the scale parameter λ.

$$E(w(t)) = \frac{kt^v}{\lambda} \quad (14)$$

$$Var(w(t)) = \frac{kt^v}{\lambda^2} \quad (15)$$

Assume that μ_j, σ_j respectively represents the mean and variance of the accumulated degradation collected in the j th time. By the Eq. (14), (15) shows:

$$\hat{\lambda}_j = \frac{\hat{\mu}_j}{\hat{\sigma}_j^2} \quad (16)$$

From Eq. (16), we can know that λ is changing in the different monitoring stages.

III Calculating the parameter k and v of the shape parameter $\alpha(t)$.

$\alpha(t)$ is a time-varying parameter. According to monitoring the information's mean and collecting the monitoring information's time for several times, this model can be linear regressed after calculating the (15)'s logarithm to get $\hat{k}$ and $\hat{v}$.

IV Calculating performance reliability

Put the relevant parameters into the Eq. (5), the performance reliability can be calculated.

4.2. Reliability evaluation algorithm for sudden failures

I Calculating the hyper parameters of scale parameter β's prior distribution

By the Eq. (7), the prior mean and variance of the scale parameter β are:

$$E(\beta) = \frac{c}{d} \quad (17)$$

$$\sigma^2(\beta) = \frac{c}{d^2} \quad (18)$$

The reliability of sudden failure at time t_{R_0} is known, and then β can be expressed as:

$$\beta = \left[\frac{t_{R_0}}{\ln(1/R_0)^{1/r}}\right]^{1/r} \quad (19)$$

Put β's mean and variance into Eq. (17) and (18), the hyper parameters $\hat{c}$ and $\hat{d}$ can be calculated.

II Calculating the posterior mean and variance of the scale parameters

Collect the observational data of sudden failures $\{(t_1,n_1),(t_2,n_2),\cdots,(t_m,n_m)\}$, where t_i represents the happen time of sudden failures, and n_i represents the number of samples of sudden failures. The hyper parameters $\hat{c}$ and $\hat{d}$ are known, and then the posterior mean and variance of the scale parameters can be expressed as follows:

$$E(\beta') = \frac{c + \sum_{i=1}^{m} t_i}{d + \sum_{i=1}^{m} m_i} \quad (20)$$

$$\sigma^2(\beta') = \frac{c + \sum_{i=1}^{m} t_i}{\left(d + \sum_{i=1}^{m} m_i\right)^2} \quad (21)$$

III Calculating the reliability of sudden failures

Put $\hat{\gamma}$ which got by Eq. (11) and $\hat{\beta}$ which got by Eq. (19) into Eq. (8), the reliability of sudden failures can be calculated.

4.3. Reliability evaluation algorithm for competing failures

I Description of the possibility of alternative model

The possibility of the model depends on the fitting function of the predicted values and experimental data for each model. And it can be expressed by deviation function and the measurement error. Assume that the output results of model M_k obey normal distribution, and their expectations can be a simple linear function of the original experimental results $a_k + b_k M_k$, the standard deviation is σ_k. Then, there is $g_k(D|M_k) \sim N(a_k + b_k M_k, \sigma_k^2)$. Among that, a_k and b_k are error correction items, which can be obtained through a simple linear regression.

II The weight calculation of alternative model

For the weight calculation of alternative model, this paper selects expectation maximization (EM) algorithm to accomplish it. The advantages of this method are that it is very effective for the problem of incomplete data, and it is in line with our civil aircraft system data collection, especially in the case of the incomplete observational data and the direct fault collection. In the calculation process, introduce a non-observed variable z. If the k th model is the best prediction in the model collection, set the value of

z as 1, otherwise 0. At any time, as long as there is a value is 1, others are 0. Initializing the weight and variance of each model, the algorithm begins to iterate between the expectation step and the maximum step. Its expression is:

$$z_k^j = \frac{w_k g\left(D \middle| f_k, \sigma_k^{j-1}\right)}{\sum_{l=1}^{N} w_l g\left(D \middle| f_l, \sigma_k^{j-1}\right)} \tag{22}$$

where, j represents the number of iterations. Then, $g\left(D \middle| f_k, \sigma_k^{(j-1)}\right)$ represents the conditional probability distribution of the k th model focusing on observing D. $g\left(D \middle| f_k, \sigma_j^{k-1}\right)$ is normal distribution, the mean is f_k and $\sigma_k^{(j-1)}$ is the variance. In the following maximization step, the BMA weight and variance are updated according to the latest $z_k^{(j)}$ until convergence is reached.

5. Example

Table 1 shows the 35 samples which have repaired and replaced engines. There are six parameters have been monitored, which are DEGT (the deviration exhaust gas tempreture), DWF (the deviration of fuel flow), DOP (the deviation of oil pressure), DHPRS (the deviation of high-pressure rotor speed), DLPRV (the deviation of the low-pressure rotor vibration value) and DHPRV (the deviation of high-pressure rotor vibration value). The engines' TSI (Time since installation) and FH (Fight hour) from the beginning of the monitoring moment can be obtained. The 36th sample is the engine still in the monitoring stage. From the data of table 1, the relationship between the various monitoring parameters can be extracted and be used as the basis of information fusion. Among that, the PDD (Performance degradation degree) is not the data collected directly, but the Gamma distribution shape parameter got by Monte-Carlo simulation method, according to engine remaining wing life, in the case of a given reliability threshold (90%), and in accordance with that its performance degradation meets Gamma random process.

Fuse the information and performance degradation degree according to the monitoring information collected and the algorithm proposed in section 2. The vector fused monitoring parameters is:

$$\hat{\beta} = [-0.0103, 0.1795, 0.0016, 0.0318, 0.0152, -0.0158, 0.0156]^{\mathrm{T}}$$

Table 1. Key performance monitoring parameters for some aircraft engines

NO	DEGT	DWF	DOP	DHPRS	DLPRV	DHPRV	TSI(FH)	PDD
1	7.51	2.54	1.89	-7.27	1.06	0.32	4055	0.1192
2	-4.74	3.52	1.92	-5.16	0.52	0.55	7095	0.0459
3	-0.03	2.03	1.19	-8.33	0.57	0.37	7801	0.0378
4	8.04	5.16	1.69	-7.74	0.24	0.57	3331	0.1176
5	7.77	7.80	2.12	-6.81	0.86	0.46	3832	0.1308
⋮	⋮	⋮	⋮	⋮	⋮	⋮	⋮	⋮
31	22.69	7.58	2.12	-1.07	0.64	0.99	1055	0.2000
32	4.23	4.83	1.96	-58.92	0.17	0.62	3397	0.0996
33	14.28	5.25	1.63	-2.03	0.78	0.94	1422	0.1572
34	11.38	3.14	1.63	4.19	0.23	0.74	1830	0.1465
35	8.24	3.17	2.18	9.78	1.05	0.76	1954	0.1185

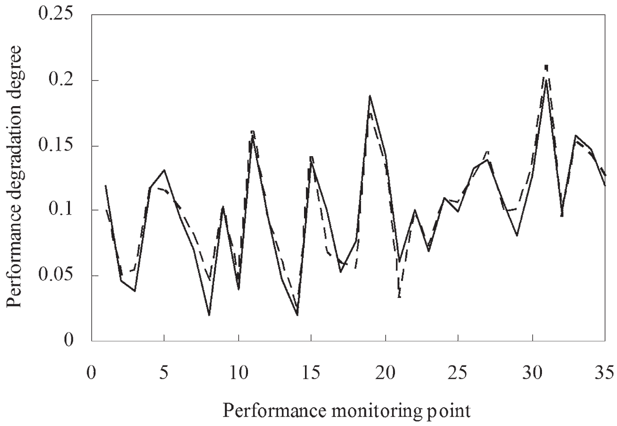

Fig. 2. The difference of performance degradation between real value and predictive value (The solid line shows the real value and the dashed line shows the predictive value)

The estimated values of performance degradation after fusion and the actual degradation values are compared in Figure 2.

According to monitoring information and maintenance information, the prior value of sudden failures can be determined as $E\left(R_{3000}\right) = 0.97$, $\sigma^2\left(R_{3000}\right) = 3.76 \times 10^{-4}$. $E(\beta)$ and $\sigma^2(\beta)$ can be computed by Eq.(19). $\hat{c}$ and $\hat{d}$ can computed by Eq.(17) and Eq.(18). The posterior mean and variance of $\hat{\beta}$ can be computed by Eq. (20) and Eq. (21). Then combining the results of performance degradation evaluation, the reliability of sudden failures can be computed by Eq. (8). Figure 3 shows the changing trend of the probability density function of sudden failures.

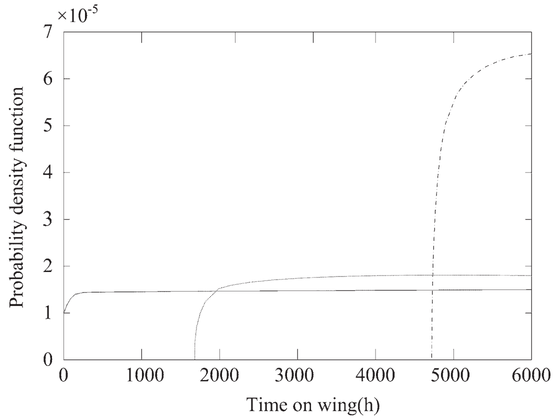

Fig. 3. The changing trend of the probability density function of sudden failures (The solid line shows the firs phase, the dotted line shows the second phase and the dashed line shows last phase)

Table 2 gives one engine's wing time and key monitoring parameters. For the above data, use different models to calculate the results of reliability evaluation. The comparison of each model is shown in Table 3.

For the three alternative models, namely, the reliability evaluation models of sudden failures, the performance degradation failures and competing failures, use Bayesian model averaging to calculate the weights of the three models respectively for three timing points. The calculation process is shown as Eq. (22). Estimate the reliability of aircraft engines, make the results compared with the actual values to calculate the deviation. The results are shown in Table 3.

The following conclusions can be drawn from Table 3. First, BMA can really analyze the mechanism of action between the different failure modes through learning different data. The advantages of the model are that it has higher fore-

Table 2. Key Monitoring parameters and main calculation results for on wing aircraft engines

NO \ Item	TSI (FH)	DEGT	DWF	DOP	DHPRS	DLPRV	DHPRV	$\hat{\beta}$	PDD
1	1707	–2.46	1.23	1.57	–0.12	0.33	0.94	55138	0.0567
2	4740	4.43	3.77	2.30	–2.78	0.52	0.48	46321	0.0832
3	5595	8.24	3.17	2.18	6.53	1.05	0.76	12334	0.1075

Table 3. The comparison of reliability evaluation results using different models

NO \ Item	M_1		M_2		M_3		M		
	$\hat{R}_G$	Deviation	$\hat{R}_S$	Deviation	$\hat{R}_C$	Deviation	Weight	$\hat{R}$	Deviation
1	0.9717	0.12%	0.9749	0.45%	0.9473	-2.39%	0.92	0.9711	0.062%
							0.05		
							0.03		
2	0.9565	0.59%	0.9580	0.75%	0.9163	-3.64%	0.73	0.9506	-0.074%
							0.11		
							0.16		
3	0.9512	2.42%	0.9493	2.21%	0.9030	-2.76%	0.28	0.9252	-0.377%

cast accuracy and it can effectively avoid the reliability overestimate or underestimate. From the prediction results of BMA model, because the existence of both positive deviation and negative deviation, there is no systematic bias from the forecast perspective. Therefore, the results are more credible.

Second, when aircraft engines are in the phase of higher reliability, the factors which lead to failure or affect the reliability are mainly reflected in the failure of performance degradation. From the weight calculation results of BMA, the greater stage of high reliability we are in, the more proportion of share the performance degradation will occupy.

Third, when aircraft engines are in the phase of high reliability, the possibility of sudden failure is generally less than the degradation failure. This is mainly due to the effects of degradation failure degree on the reliability of degradation failure is greater than on the reliability of the sudden failure. As the first two monitoring points shown in Table 3, the reliability of sudden failures is higher than performance degradation failures.

Furthermore, when aircraft engines are in the operational phase of higher reliability, the probability of the occurrence of sudden failure will increase. As the third monitoring point, this is a real moment that two failure modes play a role at the same time, reflecting in the decreased evaluation deviation using traditional reliability evaluation model of competing failure.

6. Conclusions

In this paper, the mechanism of performance degradation and sudden failures of aircraft engines has been analyzed, a reliability evaluation model for competing failures has been proposed, and the traditional model of competing failures has been transformed. This method not only can make full use of condition monitoring information, but also can analyze the mechanism and transforming relationship between performance degradation failures and sudden failures through data learning. The method should be studied further.

***Acknowledgement**: The research work supported by National Natural Science Foundation and Aviation Fund of China (60879001,U1233115) and Qinglan Project.*

References

1. Bagdonavičius V, Bikelis A, Kazakevičius V et al. Analysis of joint multiple failure mode and linear degradation data with renewals. Journal of Statistical Plaaning and Inference, 2007;137(7): 2191–2207.
2. Bedford T. Competing risk modeling in reliability. In Modern statistical and mathematical methods in reliability. Edited by Wilson A, Limnios N, KellyMcNuly S et al.Word Scientific Publisher, New Jersey.
3. Bedford T, Dewan I, Meileijson I. The signal model: A model for competing risks of opportunistic maintenance. European Journal of Operational Research, 2011; 214(3): 665–673.
4. Bocchetti D, Giorgio M, Guida M et al. A competing risk model for the reliability of cylinder lines in marine Diesel engines. Reliability Engineering and System Safety, 2009; 94(8):1299–1307.
5. Chen BE, Lramer JL, Greene MH. Competing risk analysis of correlated failure time data. Biometrics, 2008;64(1):172–179.
6. Cobel JB. Merging data sources to predict remaining useful life-An automated method to identify prognostic parameters. University of Teenessee, Knoxville, 2010.
7. Kenneth P. Measuring the Performance of a HUM System – the Features that Count. Proceeding of Third International Conference on Health and Usage Monitoring – HUMS2003 . DSTO Platforms Sciences Laboratory, Australia 2003, 5–15.
8. Kundu D, Sarhan AM. Analysis of incomplete data in presence of competing risks among several groups. IEEE Transactions on Reliability 2006; 55(2): 262 – 269.
9. Lehmann A. Joint modeling of degradation and failure time data. Journal of Statistical Planning and Inference 2009;139(5): 1693–706.
10. Niu G, Yang BS, Pecht M. Development of an optimized-based maintenance system by data fusion and reliability-centered maintenance. Reliability Engineering and System Safety 2010; 95(7): 786–796.
11. Pareek B, Kundu D, Kumar S. On progressively competing risks data for Weibull distributions. Computational ststistics and data analysis 2009; 53(12–1): 4083–4094.
12. Park C, Kulasekera KB. Parametric inference of incomplete data with competing risks among several groups. IEEE Transactions on Reliability2004; 53(1): 11–21.
13. Peng H, Feng QM, Coit DW. Reliability and maintenance modeling for systems subject to multiple dependent competing failure process. IIE Transactions 2011,43(5): 12–22.
14. Polpo A, Sinha D.Correction in Bayesian nonparametric estimation in a series system or a competing-risk model. Statistics and Probability

Letters 2011; 81(12): 1756–1759.
15. Salinas-Torres V, Pereira C, Tiwari R. Bayesian nonparametric estimation in a series system or a competing risks model. Journal of Nonparametric Statistics 2002; 14(4): 449–458.
16. Suarez EL, Duffy MI, Gamache RN et al. Jet engine life prediction systems integrated with prognostics health management. Proceeding of IEEE Aerospace Conference 2004; 3596–3602.
17. Su C, Zhang Y. System reliability assessment based on Wiener process and competing failure analysis .Journal of Southeast University 2010; 26(4): 554–557.
18. Volponi A. Data fusion for enhanced aircraft engine prognostics and health management—Task 14: Program plan development. Pratt & Whitney Internal Memo 2001, 10.
19. Wang CP, Ghosh M. Bayesian analysis of bivariate competing risks model with covariates. Journal of Statistical Planning and Inference 2003; 115(2–1): 441–459.
20. Xing LD, Levitin G. Combinatorial analysis of systems with competing failures subject to failure isolation and propagation effects. Reliability Engineering and System Safety 2010; 95(11): 1210–1215.

HuaWei WANG
College of Civil Aviation
Nanjing University of Aeronautics and Astronautics
Nanjing, Jiangsu210016, China
E-mail: huaweiwang678@gmail.com

Jun GAO
Department of Management
Shijiazhuang Mechanical Engineering College
Shijiazhuang, Heibei050003, China
E-mail: guaguaguagua@163.com

Article citation info:
KAROLEWSKI B, LIGOCKI P. Modelling of long belt conveyors. Eksploatacja i Niezawodnosc – Maintenance and Reliability 2014; 16 (2): 179–187.

Bogusław KAROLEWSKI
Piotr LIGOCKI

MODELLING OF LONG BELT CONVEYORS

MODELOWANIE DŁUGICH PRZENOŚNIKÓW TAŚMOWYCH*

A mathematical model that allows the analysis of the dynamic states of a belt conveyor was presented. A way of modelling wave phenomena in the tape, changes of mass and resistances to motion and elements of the drive system (motors, frequency converters, couplings, gears and co-operation between the belt and drive pulley) was briefly described. A start up of an exemplary belt conveyor was simulated with the use of obtained formulas. The start-up time histories obtained computationally were compared with measurements. The verified belt conveyor model can be utilized to examine various phenomena and operating states of a belt conveyor.

***Keywords**: belt conveyor, modelling, computer simulation, dynamics, inductive drive.*

Przedstawiono matematyczny model przenośnika taśmowego umożliwiający analizę dynamicznych stanów pracy urządzenia. Skrótowo opisano sposób modelowania zjawisk falowych w taśmie, zmian mas i oporów ruchu oraz elementów układu napędowego czyli silników, przekształtników, sprzęgieł, przekładni i współpracy bębna napędowego z taśmą. Rozwiązując komputerowo uzyskane zależności, symulowano rozruch przykładowego przenośnika. Porównano przebiegi rozruchowe uzyskane obliczeniowo z pomiarowymi. Zweryfikowany model można wykorzystać do badania różnych zjawisk i stanów pracy przenośnika.

***Słowa kluczowe**: przenośnik taśmowy, modelowanie, symulacja komputerowa, dynamika, napęd indukcyjny.*

1. Introduction

Belt conveyors are economical, efficient and are a more and more often used means of transportation. Advancements in belt conveyor technology have provided essentially unlimited adaptability, allowing conveyors to provide solutions for every geographic region and all belts of applications worldwide [1]. During the design and operation of longer and more efficient conveyors, new demanding problems have appeared which did not occur in shorter structures [15]. The start up of a conveyor involves significant variability of belt forces as well as strokes of driving torques and accelerations. The threat of belt damage and other subassemblies exists. Additional problems appear in the case of the curvilinear belt route [3].

Carrying out investigations on real operative installations are difficult and expensive. Moreover, results of measurements can only be utilized in the evaluation of existing objects. On this base it is not possible to determine the effects of potential changes or new solutions. The formulation of coherent mathematical models of belt conveyors which take into account phenomena that occur in dynamic states, considerably expands investigative and design possibilities and gives a chance to predict and solve various questions.

Despite many years of using conveyors, many exploitation problems have not been resolved [14]. Companies exploiting belt conveyors expect high reliability and performance to be ensured. Simulation studies using a mathematical model of the conveyor, made at the stage of design, allows this to be made and they have a significant impact on the subsequent process of exploitation and reliability. Examples of use of the model to determine dynamic waveforms in mechanical elements (speeds, accelerations, forces) is shown for example in [9], and both in mechanical and in electrical forms (currents and torques of motors) in [21, 22].

The initial stages of the development of dynamic modelling of belt conveyors is described in [11]. In the 70's at the University of Hanover, Germany, the model of the tape was divided into two sections, taking into account the viscoelastic properties [2]. Then the model was extended, taking into account a larger number of masses [3].

In the 80's at the University of Newcastle in Australia, a model based on the propagation of stress waves in the tape was built [10]. Also, the U.S. company Conveyor Dynamics built a model that contains the source variable as a function of time, the driving force, taking into account friction and theviscoelastic properties of the tape [31].

In Poland in the 90's theoretical basis for modeling the belt and the whole conveyor was developed at the Technical University of Wroclaw [4, 17, 36, 46], Silesian University of Technology [30] and the Academy of Mining and Metallurgy in Cracow [24].

Comprehensive modelling which takes into account the transverse conveyor belt moving in a vertical direction was dealt with at the Technical University of Delft in the Netherlands [28]. Work allowing the determination of the behavior in the vicinity of the tape's horizontal curves was carried out at the Austrian University of Mining and Metallurgy in Leoben [8]. The company Krupp Fördertechnik and the University of Hanover focused especially on modelling the drive [39, 40]. The created model provides the ability to dynamically calculate the convergence side tape on horizontal curves.

Most of these centers still improve old models [3, 12, 21, 22, 25, 29]. Chinese centers also carry out such work [9].

The use of multiple drives in long conveyors entails new challenges and problems, such as inelastic slip on one of the pulleys and different distribution of power between the drives. Work regarding these issues include [16, 33, 37, 42].

A new theme is to study possible energy savings [23, 26, 38, 44].

Many authors dealing with the behavior of a model study of conveyor belt dynamic states, expanded the model in the desired direction, focusing on the improvement of a particular item of equipment, while ignoring or assuming a simplified description of other phenomena. In a large part of these works motor models were greatly simplified (for example, the course of the motor torque was approximated with two straight sections), which can result in large differences between the

(*) Tekst artykułu w polskiej wersji językowej dostępny w elektronicznym wydaniu kwartalnika na stronie ***www.ein.org.pl***

behavior of the model in relation to the actual device. In none of these works (apart from the works carried out by the authors of this article [17, 18, 20–22]) changes in the parameters of induction motors are not taken into account.

In the study, the results of which can be found in the literature, little attention was given to modelling the mechanical connection of the motor shaft drive drum. Even in many of the advanced models of conveyor there was a simplification assumed, consisting of the treatment of the clutch and mechanical gear as rigid elements. When the flexible coupling was taken into account [30], models of other elements were simplified.

There is no fully comprehensive approach where different elements and events would be described in a similar way. Electricians favor the problem of modeling motors, simplifying the mechanical issues, and the mechanics behave vice versa.

In addition to models arising in scientific centers, there are solutions created by companies designing conveyors, but they do not give details of used dependence.

So work began on the creation of an extensive conveyor model that takes into account:

- ring and squirrel cage motors with parameters changing as a result of displacement of current and core saturation,
- frequency converters and soft-start circuits,
- flexibility of flexible couplings and clutch slip,
- mechanical deflection of gear teeth,
- the possibility of the belt slipping on the drive pulley,
- one-, two- or three pulley drive and indirect drives,
- different models of belt, which can be divided into any number of segments,
- excavated material weight changes as a result of charging and discharging,
- changes of resistance to motion as a function of the mass, velocity and force of the strip,
- components resistance of motion connected with pressing of the belt in idlers or deformation of the belt and excavated material between idler sets and traditionally accepted idlers rolling resistance and slipping of the belt on idlers,
- gradually moving the belt and changing the value of the friction coefficients of static to dynamic,
- impact of belt sag between idler sets and transverse forces in the belt to vibration in the vertical plane.

The presented model was created by combining the well-known mathematical descriptions of various conveyor components, the use of the research results of its subassemblies and taking into account the theoretical analysis. Without detailed research it is difficult to assess which elements have a significant impact on the behavior of the system. Therefore, attempts were made to take into account in the model as much as possible phenomena occurring in the real device. Conveyor components were described in a uniform convention with a similar degree of accuracy. After verification of the model, it is then possible with its use, to study the impact of various phenomena and parameters on the obtained waveforms. These tests can be used to formulate simplified versions of the general model, dedicated to specific, narrowly focused goals.

2. The belt Conveyor Model

The functioning of every conveyor element (represented in fig. 1) is described with the use of a mathematical relationship remaining in a uniform convention to ensure the possibility of complex solving received equations. A block diagram of a drive system model connected with a single motor as well as a block diagram of the overall belt conveyor model is presented in figures 2 and 3.

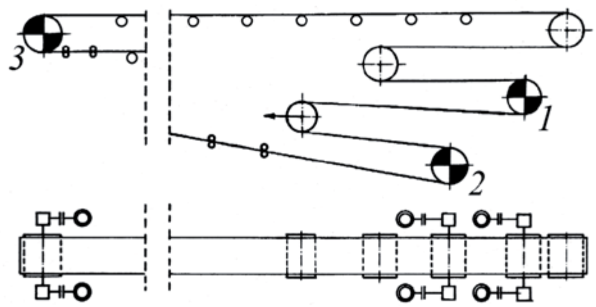

Fig. 1. Belt conveyor system with marked numbers of drive pulleys

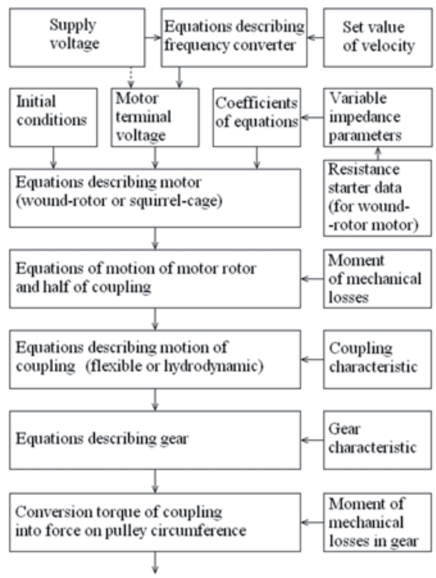

Fig. 2. Block diagram of a single drive system model

2. 1. The belt Model

The most important part of the conveyor is a rubber belt. The belt movement is described by two partial differential equations, of which one represents the equilibrium of the forces acting on the belt and the other the relationship between the stress and elongation of the belt [45]. The models section of the belt may have a different number of elements. The simplest model is elastic. A more powerful model is the two-element model of Kelvin-Voigt, consisting of springs and a damper connected in parallel. The three element model is seen as standard. It is made as a serial connection between the spring and Kelvin-Voigt model. Even more powerful is the four element model.

Each model can be completed with a module with Coulomb friction by taking into account changes in friction. The coefficient of friction that occurs in the formulas on resistances to the motion section of the belt changes from static to dynamic. When a section of the belt starts moving, the ratio decreases from static value μ_s to movement μ_r. Further growth of some components of motion resistances with speed increases must be reflected by calculating these resistances. By taking into consideration the impact of Coulomb friction, from a one-element model, a two-parameter model is achieved, and from a two-element model a three-parameter model is achieved , etc. [28, 31, 46]. Therefore, a distinction between the number of elements and the number of model parameters was introduced.

There were tests carried out which presented how the choice of rheological model of the belt influences the obtained dynamical proc-

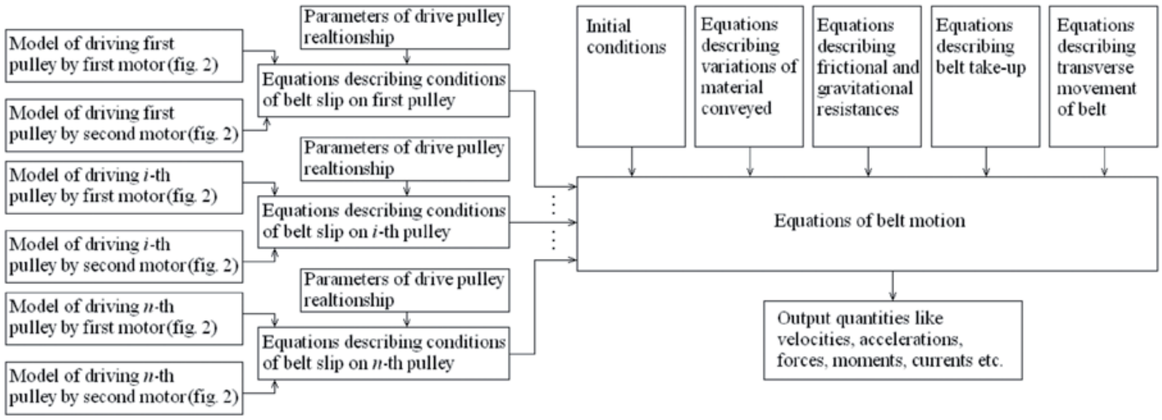

Fig. 3. Block diagram of the mathematical model of a belt conveyor

esses. By using the developed conveyor model, starting waveforms were calculated.

The calculations were made for the conveyor system shown in figure 1, with a length of 3620 meters, equipped with a steel cord belt with a width of 1.8 m and nominal speed 5.24 m/s. The drive consisted of five ring induction motors with a power of 630 kW each and a rated voltage of 6 kV, coupled with three drum drives (two in front and one at the end). The effect of using the 1, 2 and 3-element belt model, which includes changes of friction, making the model to be 2, 3 and 4-parameters, on strength waveforms in the belt which tensions the drum was examined. The results – the top three waveforms in Figure 4 – were compared with the results of measurements carried out by the staff of the Institute POLTEGOR [35] (lower course). Parameters for each model should be selected so that they correspond to the approximation of the same creep curve. Due to this, the dissimilarity between the characteristics are caused by the differences between models, and not by differences in parameter values.

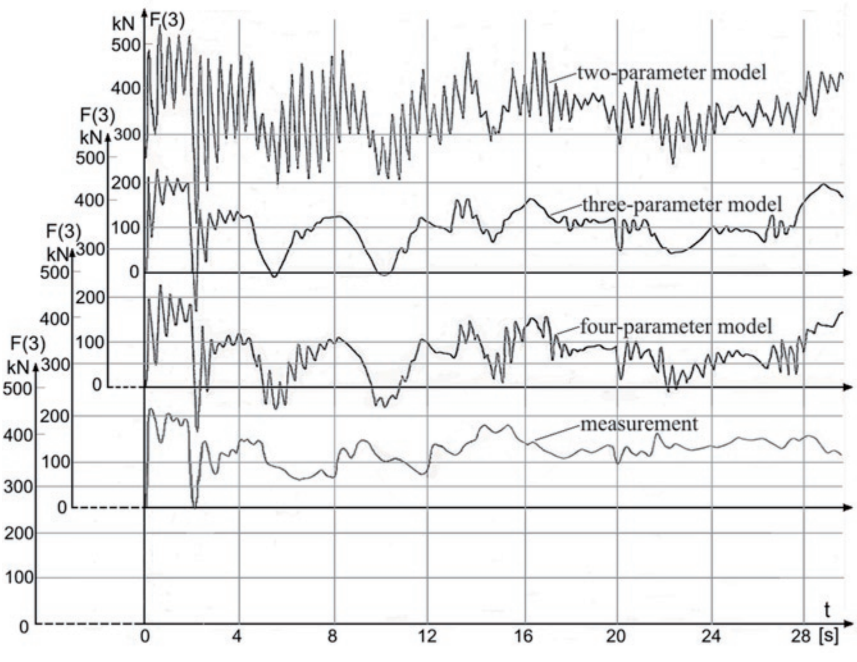

Fig. 4. Comparison of the forces in the belt on the take-up pulley obtained using different models of the belt with the measurement results

Vibration forces obtained with the 2-parameter model possess too large an amplitude and are insufficiently suppressed. The most similar to the measuring results are the results of the application of the three-parameter model (two-elements with variable friction). Some differences are mainly caused by a slightly different frequency of vibration force in calculations and measurements. This may be due to inaccurate estimation of the belt load factor during the measurements. Adding springs to the four parameter model resulted in the generation of additional vibration which did not occur in the measured waveform. A similar effect can be expected in the case of a five-parameter model. Models with greater than 4 parameters are rarely used and have not been studied.

In most tasks it is enough to use the two-element model including a variable friction, that is three-parameters. This model was used in further studies. A high impact on the quality of the results is the appropriate selection of the variables in the model. Parameters of models for transient analysis to be determined in a specific way so as to ensure that approximating the measured waveforms in the time duration of the transient, that is up to periods of tens of seconds. It is possible to use the free vibration tape sample analysis method [45].

2. 2. Mass calculation

In the mass of a particular segment, the influence of idler inertias or non-drive pulleys (converted into equivalent mass), as well as masses of the belt and load, were taken into account.

An exemplary formula which determines the mass of the i-th segment of the upper strand is:

$$m(i) = \left(m_{jt} + m_{jn}(i) + \frac{4 \cdot z_{kg} \cdot J_{kg}}{l_{zg}(i) \cdot D_{kg}^2} \right) \cdot l(i) \quad [\text{kg}] \quad (1)$$

where:

m_{jt} – belt mass per unit length [kg·m^{-1}],
$m_{jn}(i)$ – load mass per unit length on the belt segment between i and $i+1$ point [kg·m^{-1}],
$l(i)$ – length of i-th segment [m],
z_{kg} – number of rolls in each upper idler rolls station,
J_{kg} – roll moment of inertia [kg·m^2],
$l_{zg}(i)$ – idler rolls stations spacing for upper strand [m],
D_{kg} – idler diameter for upper strand [m].

The mass of belt segments on drive pulleys depends on conditions of cooperation between the belt and pulley. If the belt has the same velocity as a pulley's lining, masses of the pulley and other elements which are connected with it in a rigid way (i.e. slow-speed wheels of toothed gear) will also be taken into account in calculations (fig. 5). Masses of further elements of the drive system (following wheels of toothed gear, couplings, motor rotors) are connected in a flexible way. Their motion is described by applying other equations. If the belt starts to slip on the pulley's lining, the motion of the pulley and part of the gear should also be described by applying a separate equation.

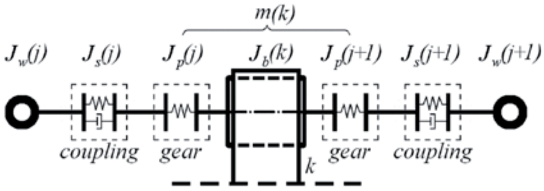

Fig. 5. Drive system connected with k-th drive pulley: m(i) – mass of segment on drive pulley, moments of inertia of: $J_w(j)$- j-th motor rotor, $J_s(j)$- j-th coupling, $J_p(j)$- j-th gear, $J_b(k)$- k-th drive pulley

The load level of the upper strand can change. The model enables the simulation of conveyor start-up with a belt that is unloaded (empty), fully loaded or loaded in a specified degree. There is a possibility to simulate the start-up of a conveyor included in a sequence of conveyors, that is preceded by an earlier conveyor which drops a load onto the conveyor (fig. 6).

Dropping a load from the belt on the head station causes the emptying of the following belt segments (area $n_{pz} – n_{pl}$), whereas the feeding conveyor fills the terminal segments from loading point n_{pl}. Variability of the mass and load distribution along the carry strand are functions of the belts' velocities of both the examined and feeding conveyor. Differences of moments of switching on of the conveyors and duration of each start-up were taken into account.

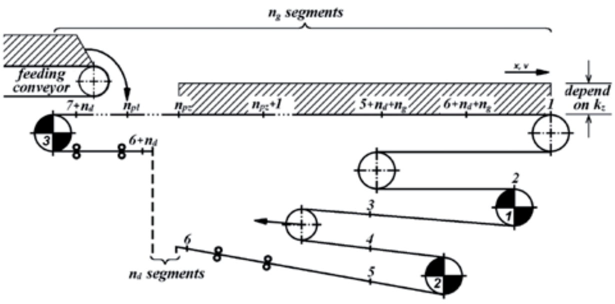

Fig. 6. Scheme of load distribution on the conveyor belt

2. 3. Resistance of motion variability

The motion of the belt is opposed by motion resistances W. Both passive resistances involving friction forces and active gradient resistance connected with downhill or uphill haulage were taken into consideration. A method of elementary resistances [43] and its modifications [4, 5, 6, 7] are used in the model with the aim of determining friction resistances. The resistance of motion components such as resistance of the idler bearing rolls rotation W_{tk} [27] and resistance of belt slipping on idlers surface W_{st} [43] are taken into account. Moreover, the trampling resistance [13], that is compounded of indentation rolling resistance W_{tt} [4, 41], flexing belt resistance W_{pt} and flexing material resistance W_{du} is taken into account:

$$W = f(W_{tk}, W_{st}, W_{tt}, W_{pt}, W_{du}) \text{ [N]} \tag{2}$$

and:

$$W_{tk} = f(m, v, T),$$
$$W_{st} = f(m, v),$$
$$W_{tt} = f(m),$$
$$W_{pt} = f(m, v, F),$$
$$W_{du} = f(m, v, F).$$

where: m – mass on given belt segment [kg],
v – belt velocity [m·s^{-1}],
T – ambient temperature [^{o}C],
F – belt force [N].

Example calculations were performed for the conveyor with the parameters given in section 2.1.

Dynamical changes of values of particular components of primary motion resistances of the belt during start-up were determined. Examinations for two variants according to the used way of motion resistances modelling were performed:

– variant I – using method of elementary resistances,
– variant II – using method of calculation of the components of a belt conveyor flexure resistance.

Courses of the actual values of particular components of primary resistances of motion of the whole belt for variant I during a period of start-up which last for 60 s, are presented in fig. 7.

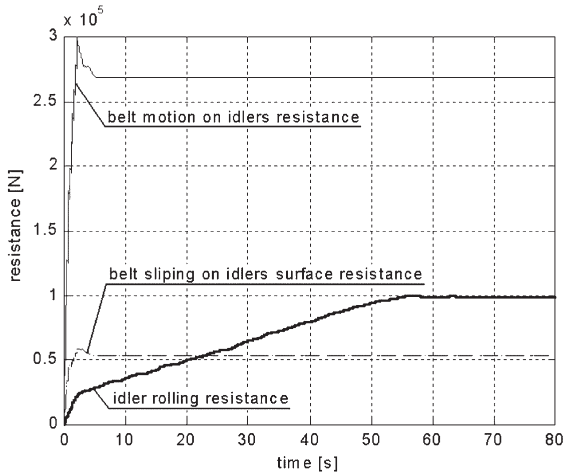

Fig. 7. Courses of actual values of particular components of belt primary motion resistances during start-up determined by the method of elementary resistances

At the beginning of start-up all the resistances increase from zero in connection with the gradual start of the moving of subsequent segments of the flexible belt. The further slow increase of idler rolling resistances results from their dependence on belt velocity. Belt slipping and motion resistances have the highest values at the moment when the whole belt starts moving. When the belt velocity increases, friction factors decrease from static to dynamic value and therefore both these resistances have lower values. The belt slipping on idler surface resistances and belt motion on idler resistances depend on the quality of conformance and the parameters of the belt which are invariable during the start-up period. Futhermore, they depend on the stage of belt loading which is only variable on short segments of the conveyor. Therefore in further parts of start-up, after the first several-seconds of the period of changes, these resistances only changed insignificantly.

In fig. 8 courses of changes of primary motion resistance components achieved in variant II which means taking into consideration the resistances dependence on belt tension are presented.

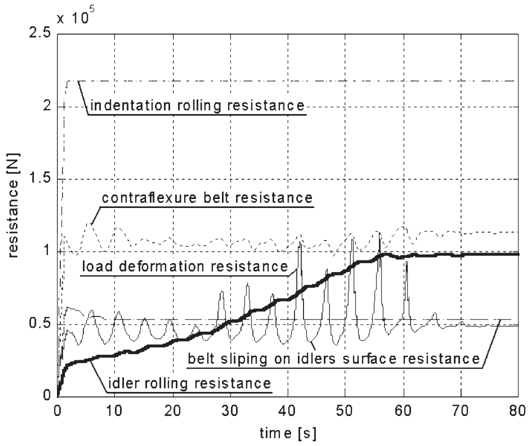

Fig. 8. Courses of actual values of particular components of belt primary motion resistances during start-up determined by method of calculation of the components of a belt conveyor flexure resistance

In calculations using the method of calculation of the components of a belt conveyor flexure resistance two analogical components occur like in the method of elementary resistances. They are idler rolling resistance and belt slipping on idlers surface resistance. For both variants the same formulas describing these two components were applied. Therefore both shapes of courses as well as values of these two components in both variants are very similar, which is visible in fig. 6 and 7. Strictly speaking, slight vibration appeared in the idlers rolling resistance. Small differences are also connected with a tiny extension of starting time in variant II.

Belt motion on idler resistance that is presented in variant I was replaced by flexure resistance in variant II shattered into three differential components. Except in the period of initial increase, indentation rolling resistance (fig. 8) is in fact invariable. However, in courses of contraflexure belt resistances and even more of load deformation resistances, oscillations connected with dependence of these resistances on belt tension occur.

The courses of sum of belt primary motion resistances for both variants are presented in fig. 9.

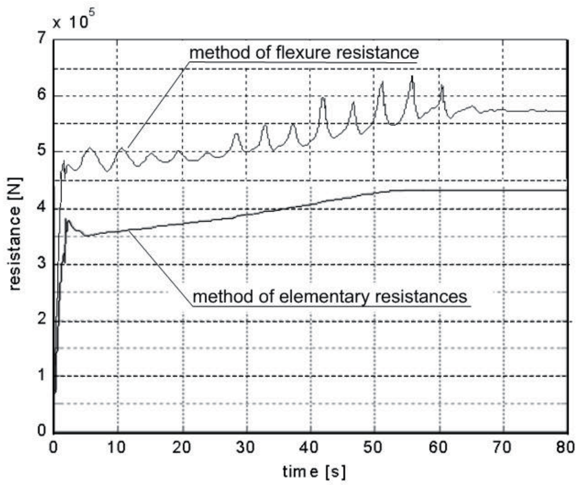

Fig. 9. Courses of sum of belt primary motion resistances during start-up calculated for both methods

At the beginning of start-up the value of sum of resistances increases suddenly in connection with the gradual start in the movement of following belt segments. This phenomenon is partly compensated by higher values of static resistances during transition from static to dynamic friction at the moment of the start in the movement of following segments. In the further part of the course, the resistance increases, together with a velocity, until the belt achieves a steady velocity.

Values of resistances corresponding to particular phases of motion in variant II are much higher than in variant I. This explains the fact, that when used in the model of the conveyor method of elementary resistances, underrate values of currents drawn by the motors are obtained [20]. In further studies, the method of the components of a flexure resistance was used.

2. 4. Model of the belt sag

Except for longitudinal oscillations, transverse displacement of the belt as belt sag between adjacent idler stations is taken into account in the model. Examination of the belt sag effect is aimed at preventing the appearance of the belt lifting above idlers within concave curves in a vertical plane during dynamic states (fig. 10). Curves along the conveyors route are applied in order to limit ground works costs.

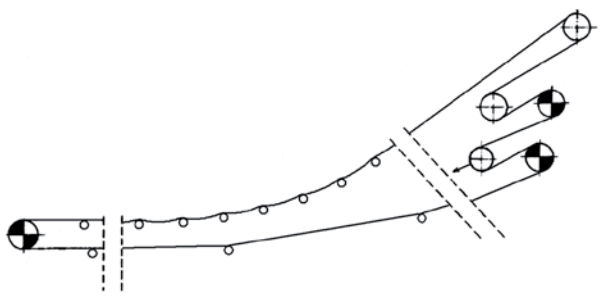

Fig. 10. Model of belt sags between idlers within conveyor route concave curves in a vertical plane

Based on the catenary equation, belt sag f is expressed as follows:

$$f = \frac{l_z^2 \cdot G}{8F} \text{ [m]} \tag{3}$$

where: l_z – length between adjacent idler stations [m],
F – horizontal component of force acting on a belt segment between idler stations [N],
G – weight per unit of belt and load [N·m^{-1}].

2. 5. Model of conveyors drive

In the conveyor belt model, circuit models of driving induction motors, both wound-rotor and squirrel-cage, were utilised.

The form of flux equations is as follows:

$$\frac{d}{dt}\psi_{s1} = u_{l1} - \frac{R_l + R_s}{L_l + L_{sz}'}\psi_{s1} + \frac{R_l + R_s}{L_z}[\cos\vartheta_e \cdot \psi_{r1} + \cos(\vartheta_e + 120°)\cdot\psi_{r2} + \cos)\vartheta_e - 120°)\cdot\psi_{r3}] \text{ [V]}$$

$$\frac{d}{dt}\psi_{s2} = u_{l2} - \frac{R_l + R_s}{L_l + L_{sz}'}\psi_{s2} + \frac{R_l + R_s}{L_z}[\cos(\vartheta_e - 120°)\cdot\psi_{r1} + \cos\vartheta_e \cdot \psi_{r2} + \cos(\vartheta_e + 120°)\cdot\psi_{r3}] \text{ [V]}$$

$$\psi_{s3} = -\psi_{s1} - \psi_{s2} \text{ [Wb]} \tag{4}$$

$$\frac{d}{dt}\psi_{r1} = \frac{R_r}{L_z}[\cos\vartheta_e \cdot \psi_{s1} + \cos(\vartheta_e - 120°)\cdot\psi_{s2} + \cos(\vartheta_e + 120°)\cdot\psi_{s3}] - \frac{R_r(L_l + L_{sz})}{L_{rz}(L_l + L_{sz}')}\cdot\psi_{r1} \text{ [V]}$$

$$\frac{d}{dt}\psi_{r2} = \frac{R_r}{L_z}[\cos(\vartheta_e + 120°)\cdot\psi_{s1} + \cos\vartheta_e \cdot \psi_{s2} + \cos(\vartheta_e - 120°)\cdot\psi_{s3}] - \frac{R_r(L_l + L_{sz})}{L_{rz}(L_l + L_{sz}')}\cdot\psi_{r2} \text{ [V]}$$

$$\psi_{r3} = -\psi_{r1} - \psi_{r2} \text{ [Wb]}$$

current equations:

$$i_{s1} = \frac{1}{L_l + L_{sz}'}\psi_{s1} - \frac{1}{L_z}[\cos\vartheta_e \cdot \psi_{r1} + \cos(\vartheta_e + 120°)\cdot\psi_{r2} + \cos(\vartheta_e - 120°)\cdot\psi_{r3}] \text{ [A]}$$

$$i_{s2} = \frac{1}{L_l + L_{sz}'}\psi_{s2} - \frac{1}{L_z}[\cos(\vartheta_e - 120°)\cdot\psi_{r1} + \cos\vartheta_e \cdot \psi_{r2} + \cos(\vartheta_e + 120°)\cdot\psi_{r3}] \text{ [A]}$$

$$i_{s3} = -i_{s1} - i_{s2} \text{ [A]} \tag{5}$$

$$i_{r1} = -\frac{1}{L_z}[\cos\vartheta_e \cdot \psi_{s1} + \cos(\vartheta_e - 120°)\cdot\psi_{s2} + \cos(\vartheta_e + 120°)\cdot\psi_{s3}] + \frac{L_l + L_{sz}}{L_{rz}(L_l + L_{sz}')}\cdot\psi_{r1}$$

$$i_{r2} = -\frac{1}{L_z}[\cos(\vartheta_e + 120°)\cdot\psi_{s1} + \cos\vartheta_e \cdot \psi_{s2} + \cos(\vartheta_e - 120°)\cdot\psi_{s3}] + \frac{L_l + L_{sz}}{L_{rz}(L_l + L_{sz}')}\cdot\psi_{r2}$$

$$i_{r3} = -i_{r1} - i_{r2} \text{ [A]}$$

The following electromagnetic moment formula and equation of motion was assumed

$$T_e = -\frac{2}{3} p \cdot L_M[(i_{s1}\cdot i_{r1} + i_{s2}\cdot i_{r2} + i_{s3}\cdot i_{r3})\cdot\sin\vartheta_e + (i_{s1}\cdot i_{r2} + i_{s2}\cdot i_{r3} + i_{s3}\cdot i_{r1})\cdot\sin(\vartheta_e + 120°)$$
$$+ (i_{s1}\cdot i_{r3} + i_{s2}\cdot i_{r1} + i_{s3}\cdot i_{r2})\cdot\sin(\vartheta_e - 120°)] \text{ [N}\cdot\text{m]}$$

$$\frac{d\Omega_e}{dt} = \frac{p}{J}(T_e - T_m) \text{ [rad·s-2]} \tag{6}$$

$$\frac{d\vartheta_e}{dt} = \Omega_e \text{ [rad·s-1]} \tag{7}$$

where:

- $\psi_{s1}, \psi_{s2}, \psi_{s3}$ – actual values of stator fluxes [Wb],
- $\psi_{r1}, \psi_{r2}, \psi_{r3}$ – actual values of rotor fluxes converted into stator [Wb],
- i_{s1}, i_{s2}, i_{s3} – actual values of stator currents [A],
- i_{r1}, i_{r2}, i_{r3} – actual values of rotor currents converted into stator [A],
- u_{l1}, u_{l2} – actual values of the supplying line phase voltages [V],
- R_s, R_r – stator and rotor resistances converted to the stator side [Ω],
- R_l, L_l – resistance and inductance of the motor supplying line [Ω], [H],
- L_z, L_{sz}' – substitute inductance and stator transient induc tance [H],
- ϑ_e, Ω_e – „electrical" angle between axes of the first st tor and rotor phase in the modelled motor with pole pairs number of $p = 1$ and „electrical" value of rotor 's angular velocity [rad], [rad·s^{-1}],
- T_e – electromagnetic torque acting on the motor's rotor with pole pairs number of p [N·m],
- T_m – sum of motor mechanical losses torque and the torque transferred via coupling connected with the motor [N·m],
- J – inertia of spinning masses connected rigidly with the rotor [kg·m^2],
- t – time [s].

The variability of motor parameters caused by current displacement and saturation was taken into account. Each drive in the program was modelled independently.

2. 6. Modelling of frequency converters and soft start equipment

Squirrel cage motors can be supplied by frequency converters. A model of frequency converter with bipolar pulse-width modulation with the assistance of carrying a signal was applied [32]. Each of the conveyor squirrel-cage driving motors may be supplied via a frequency converter with a scalar control of velocity, according to the principle of control that assumes stabilization of voltage amplitude with stator flux [34]. There is a possibility to assume an arbitrary shape of the start-up ramp in the program.

The model takes into account the possibility of supplying drive motors with soft-start devices. To this end, during the simulation ignition time of the suitable thyristor in each half-period of voltage was determined, thus changing the value of the effective voltage.

2. 7. Modelling of driving torque transmission systems

Elasticity of gears, flexibility of flexible couplings and slip of hydrodynamic couplings are taken into account [18]. Characteristics of each flexible coupling is approximated as:

$$T_c = a\Delta\phi + b\Delta\phi^3 + \tau_s(a + 3b\Delta\phi^2)\frac{d\Delta\phi}{dt} \text{ [N·m]} \tag{8}$$

where:
- T_c – moment transmitted via coupling [N·m],
- $\Delta\varphi$ – torsional angle measured between coupling's elements [rad],
- a, b – factors which determine participation of linear and nonlinear term of an equation in couplings characteristics [N·m ·rad^{-1}], [N·m ·rad^{-3}]
- τ_s – delay time, i.e. time-constant of torsional angle growing after step change of torsional moment [s].

2. 8. Belt slip of drive pulley

The driving force that is delivered to the drive pulley is transmitted to the belt by means of the friction effect [19, 46]. If the force winding on drive pulley is too high in relation to the value of the force winding off drive pulley, the belt will be too weakly pressed against the pulley and a belt slip will appear. The occurrence of inelastic belt slip phenomena is undesirable. One should then choose preliminary values of belt forces or use the starting torque control to prevent the belt slip. The conveyors model involves the belt slip effect and it permits the determination of velocity difference between the belt and the pulley.

The maximal value of the force which can be transmitted from a drive pulley to the belt is determined as [19]:

$$PD(k) = F(i+1)\cdot(e^{\mu\cdot\alpha} - 1) + W(i) + m(i)\cdot\frac{dv(i)}{dt} \text{ [N]} \tag{9}$$

where:
- $PD(k)$ – driving force which can be transmitted to the belt without belt slip [N],
- $F(i+1)$ – force in the belt winded off the drive pulley [N],
- μ – factor of friction between the belt and the drive pulley,
- α – pulleys wrapping angle [rad].

If the force on the circumference of the drive pulley is smaller than the maximal force, which the pulley can transmit to the belt, then all the force, produced by driving motors and transferred to the pulley's circumference, will be transmitted to the belt. If the abovementioned condition isn't fulfilled then the force transmitted to the belt via the drive pulley will only be equal to the maximum force possible to transfer. It is expressed by the following equations:

$$P_b = \begin{cases} PS & \text{for } PS \le PD \text{ and } v_{poś} = 0, \\ PD & \text{in other cases} \end{cases} \text{ [N]}$$
$$v_{poś} = v_b - v(i), \quad [\text{m}\cdot\text{s}^{-1}] \tag{10}$$
$$\frac{d}{dt}v_{poś}\cdot l(i)\cdot[m(i) - m_{jt}] = PS - P_b \text{ [N]}$$

where: P_b – driving force transmitted to the belt via drive pulleys [N],
PD – maximal force possible to transmit to the belt by drive pulley [N],
PS – force on the circumference of the drive pulley, originated from driving motors [N],
$v(i)$ – belt velocity in point of winding on the pulley [$m\cdot s^{-1}$],
v_b – linear velocity of points on pulleys circumference [$m\cdot s^{-1}$],
v_{pos} – rubbing speed between belt and drive pulley [$m\cdot s^{-1}$].

A surplus of driving moment accelerates the drive pulley. The belt slip then appears between the pulley and the belt. When the surplus of driving moment fades, the belt catches up with the pulley and the belt slip disappears.

3. Measuring verification

Simulation program was developed to solve the model. The program enables the simulation of diverse operating conditions of a conveyor and the investigation of the influence of particular phenomena on obtained courses of forces, moments, velocities, accelerations, voltages, currents and powers absorbed by driving motors.

The measuring verification was performed by matching selected computational and measured time histories. The measurement was made on a 3620 meter long conveyor described in section 2.1 [35]. The conveyor was driven by five wound-rotor motors, 630 kW each, connected with three drive pulleys. The take up device was operated periodically, ensuring 228 kN of belt pretension.

Analysis was carried out for start up time courses of belt forces at points near the take-up pulley, velocities at points near the first head drive pulley and for a current of one of the driving motors for cases when the belt is loaded at 33% (fig. 11, 12 and 13) and 75% (fig. 14 and 15) of nominal value. Computational time histories are slightly different than results of measurement but the character of changes is similar which reflects the correctness of the model. Maximal differences between instantaneous values from computations and measurement for forces do not exceed 30% of the measured value. Differences for currents do not exceed 27% of the rated current of motor (75 A). Velocities differ no more than about 7% of steady velocity. The maximal differences are often achieved once, after the appearance of a step in the course of given quantity. In most parts of the start-up period differences are much smaller. Bearing in mind how many elements and phenomena influence results, the obtained accuracy of computations seems to be satisfactory.

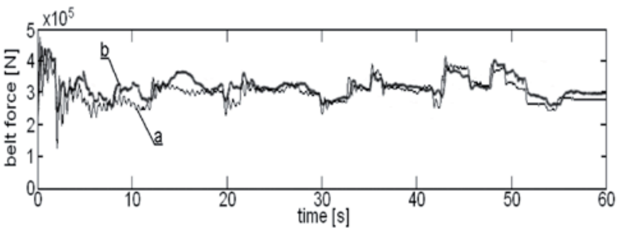

Fig. 11. Time histories of belt forces on take-up pulley (33% of belt load): a) computation, b) measurement

4. Summary

The conveyor model is a universal tool which can be utilised to optimize conveyor operation, check new solutions or to verify a project. Tests performed during the design of the conveyor allows parameters to be properly chosen. This has an important impact on the exploitation and reliability of the work of the device.The simulation program based on the model can be applied to determine the ways of controlling driving systems which ensure limitation of critical mechanical quantities in the system's elements, especially values of the belt forces in dynamic states. The model enables the examination of, among others, the influence of drive location, time of start of particular motors, kind of motors' selection, way of control of frequency converters for squirrel-cage motors or selection of resistance starters and program of start-up control for wound-rotor motors. The criterion of start-up control assessment is to achieve the shortest possible start-up duration with assurance of not exceeding the specified belt forces level. The control of steady work should ensure such a belt velocity control that will maintain the nominal level of belt load, regardless of the value of the fed material stream.

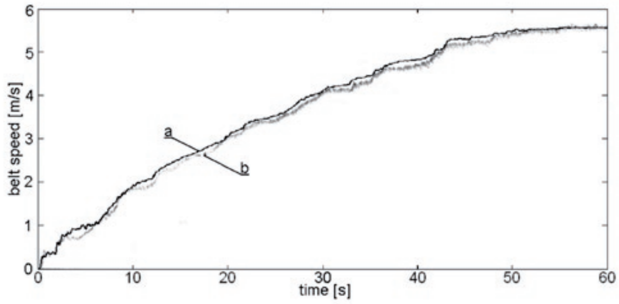

Fig. 12. Time histories of belt velocities near head station(33% of belt load): a) computation, b) measurement

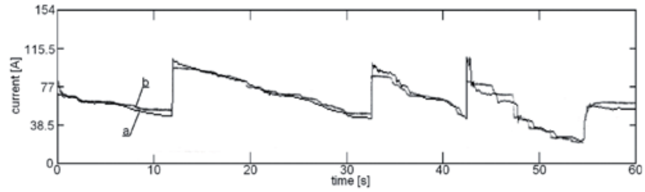

Fig. 13. Time histories of starting current of motor driven pulley No 2 (33% of belt load): a) computation, b) measurement

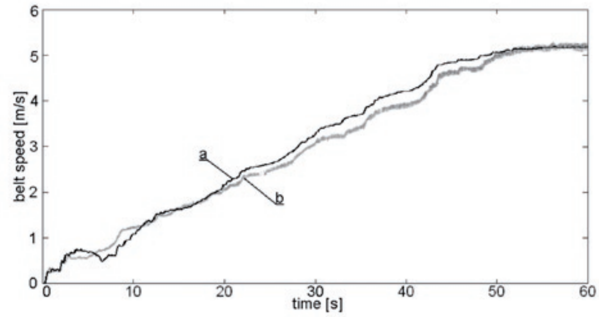

Fig. 14. Time histories of belt velocities near head station (75% of belt load): a) computation, b) measurement

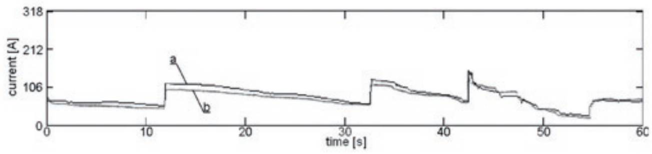

Fig. 15. Time histories of starting current of motor driven pulley No 2 (75% of belt load): a) computation, b) measurement

References

1. Continental Group of Companies, Advantages Offered by Belt Conveyor Technology. Bulk Solids Handling 2001, Vol. 21; 2: 183–187.
2. Funke H. Zum dynamischen Verhalten von Förderbandanlagen beim Anfahren und Stillsetzen unter Berücksichtigung der Bewegungswiderstände. Ph.D. Dissertation 1973, Hannover University of Technology, Germany.
3. Funke H, Hartmann K, Lauhoff H. Design and Operating Performance of a Long-Distance Belt Conveyor System with Horizontal Curves and Simultaneous Material Transport in the Upped and Lower Strands. Bulk Solids Handling 2000, Vol. 20; 1: 45–55.
4. Gładysiewicz L. Die Ermittlungsmethode des Eindruckrollwiderstandes zwischen Fördergurt und Tragrolle. Wrocław: Prace Naukowe Instytutu Górnictwa Politechniki Wrocławskiej 1983; 42: 58–70.
5. Gładysiewicz L. Metoda wyznaczania oporów głównych przenośnika taśmowego ze szczególnym uwzględnieniem właściwości taśmy. Prace Naukowe Centralnego Programu Badań Naukowych 02.05., Praca habilitacyjna 1990, Warszawa: Wydawnictwo Politechniki Warszawskiej.
6. Gładysiewicz L. Metoda obliczeń składowych oporu falowania przenośnika taśmowego. Górnictwo Odkrywkowe 1993; 2: 30–42.
7. Gładysiewicz L, Król R, Bukowski J. Eksperymentalne badania oporów ruchu przenośnika taśmowego (Tests of Belt conveyor resistance to motion). Eksploatacja i Niezawodnosc – Maintenance and Reliability 2011; 3: 17–25.
8. Grimmer KJ, Kessler F. The Design of Belt Conveyors With Horizontal Curves. Bulk Solids Handling 1992, Vol. 12: 4: 557–563.
9. Guangbu Li, Ruqiong Li. Belt Conveyor Modelling and Performance Simulation Based on AMESim. Materials of Second International Conference on Information and Computing Science 2009: 304–307.
10. Harrison A. Criteria for Minimizing Transient Stresses in Conveyor Belts. Transactions Institute Engine Australia, Mechanical Engineering 1983, Vol. 8; 3: 129–134.
11. Harrison A. Belt Conveyor Research 1980-2000. Bulk Solids Handling 2001, Vol. 21; 2: 159–164.
12. Harrison A. Non-linear Belt Transient Analysis by Numerical Simulation. Bulk Solids Handling 2008;4: 242–247.
13. Jonkers CO. The indentation rolling resistance of belt conveyors. Fördern und Heben1980, Vol.30; 4: 313–317.
14. Kacprzak M, Kulinowski P, Wędrychowicz D. Informatyczny system zarządzania procesem eksploatacji górniczych przenośników taśmowych (Computerized information system used for management of mining belt conveyors operations). Eksploatacja i Niezawodnosc – Maintenance and Reliability 2011; 2: 81–93.
15. Kahrger R, Dilefeld M, Pohl M. Henderson 2000 – A World Class Conveying System. Bulk Solids Handling 2000, Vol. 20; 3: 319–322.
16. Karanth B, Ramakoteswara RK, Parameswaran MA. A Systematic Approach to the Experimental Investigation on Two Pulley Conveyor Belt Drive. Bulk Solids Handling 1995,Vol. 15; 4: 579–586.
17. Karolewski B. Modelowanie zjawisk dynamicznych w przenośnikach taśmowych. Wrocław: Prace Naukowe Instytutu Energoelektryki Politechniki Wrocławskiej, Praca habilitacyjna 1985; 63.
18. Karolewski B. An Investigation of Various Conveyor Belt Drive Systems Using a Mathematical Model. Bulk Solids Handling 1986, Vol. 6; 2: 349-354.
19. Karolewski B. Modell der Durchhaenge zwischen den Förderbandtragrollensaetzen und des Schlupfes auf der Antriebstrommel. Deutsche Hebe- und Fördertechnik 1992; 5: 46–50.
20. Karolewski B, Ligocki P. Modelowanie przenośnika taśmowego. Górnictwo Odkrywkowe 2004; 1: 41–45.
21. Karolewski B, Ligocki P. Modelowanie dynamiki przenośników taśmowych z silnikami indukcyjnymi klatkowymi. Przegląd Elektrotechniczny 2009; 3: 56–58.
22. Karolewski B, Ligocki P. Wpływ sposobu rozruchu na obciążenia wybranych elementów przenośnika taśmowego. Przegląd Górniczy 2010; 1-2: 33–37.
23. Kasztelewicz Z, Szymański J. Metoda energooszczędnego sterowania napędem przenośnika o regulowanej prędkości taśmy w kopalniach węgla brunatnego (Energy saving control method of electrical drives in coveyor belts with regulated speed in surface brown coal mine). Archives of Mining Sciences 2008; 53: 319–329.
24. Kulinowski P, Jabłoński R. Computer – Aided Analysis of Dynamics of Belt Conveyor With Automatic Follow-Up Device Stretching the Belt. 1-st International Conference on Information Technologies in the Minerals Industry, 1997.
25. Kulinowski P. Analiza dynamiki rozruchu przenośników taśmowych z uwzględnieniem charakterystyk sprzęgieł hydrokinetycznych. Transport Przemysłowy 2004; 1: 25–29.
26. Lauhoff H. Speed Control on Belt Conveyors – Does it Really Save Energy? Bulk Solids Handling 2005; 25(6): 368–377.
27. Lodewijks G. The Rolling Resistance of Conveyor Belts. Bulk Solids Handling 1995, Vol. 15; 1: 15–22.
28. Lodewijks G. Dynamics of Belt Systems. Delft University of Technology, The Netherlands, Ph.D. thesis 1996, Universitettsdrukkerij.
29. Lodewijks G. Two Decades Dynamics of Belt Conveyor Systems. Bulk Solids Handling 2002, Vol. 22; 2: 124–132.
30. Markusik S. Dynamika rozruchu przenośników taśmowych z napędem jedno- lub dwubębnowym czołowym. Gliwice: Zeszyty Naukowe Politechniki Śląskiej 1982; 711.
31. Nordell LK, Ciozda ZP. Transient belt stresses during starting and stopping: Elastic response simulated by finite element methods. Bulk Solids Handling 1984, Vol. 4; 1: 99–104.
32. Nowacki Z. Modulacja szerokości impulsów w napędach przekształtnikowych prądu przemiennego. Warszawa: PWN 1991.
33. Nuttal A, J, G, LodewkijS G. Dynamics of Multiple Drive Belt Conveyor Systems. Particle & Particle Systems Characterization 2007; 24: 365–369
34. Orłowska-Kowalska T. Bezczujnikowe układy napędowe z silnikami indukcyjnymi. Wrocław: Oficyna Wydawnicza Politechniki Wrocławskiej 2003.
35. Palczak Cz. i inni, Pomiary wybranych wielkości przenośnika 15.02 po okresie docierania pod obciążeniem. Prace Programu Rządowego PR8/1.2-89/R1, Wrocław: COBPGO Poltegor 1983.
36. Pieńkowski K. Modelling and digital simulation of the multimotor electromechanical system of long belt conveyors. Modelling, Simulation and Control, 1985, Vol. B5; 1: 43–63.
37. Qing He, Hong Li. Review of Dynamic Modelling and Simulation of Large Scale Belt Conveyor System, International Conference on

Intelligent Computing and Information Systems ICICIS 2011, Part 1, CCIS 134: 167–172.
38. Reicks A, V. Conveyor Models as Quantitative Platforms for Belt Conveyor Energy Options. Bulk Solids Europe 2012; 10.
39. Schulz G. Further Results in the Analysis of Dynamics Characteristics of Belt Conveyors. Bulk Solids Handling 1993; 13(4): 705–710.
40. Schulz G. Comparison of Drives for Long Belt Conveyors. Bulk Solids Handling 1995; 15(2): 247–251.
41. Spaans C. The Calculation of the Main Resistance of Belt Conveyors. Bulk Solids Handling 1991; 11(4) 15–22.
42. Sur S. Dual Drives for Belt Conveyors. Bulk Solids Handling, August 1987; 7(4): 509–514.
43. Ścięgosz W. Obliczenia podstawowe przenośników taśmowych. Wrocław: Zeszyty Problemowe COBPGO POLTEGOR 1972; 43.
44. Zhang S, Xia X. Modelling and Energy Efficiency Optimization of Belt Conveyors. Applied Energy 2011; (88)9: 3061–3071.
45. Żur T. Viscoelastic Properties of Conveyor Belts. Bulk Solids Handling 1986; 6(3): 553–560.
46. Żur T, Hardygóra M. Przenośniki taśmowe w górnictwie. Katowice: Wyd. Śląsk 1996.

Bogusław KAROLEWSKI
Faculty of Electrical Engineering
Institute of Electrical Machines, Drives and Measurements
Wrocław University of Technology
Wybrzeże Wyspiańskiego 27, 50-370 Wrocław, Poland
E-mail: boguslaw.karolewski@pwr.wroc.pl

Piotr LIGOCKI
MT PROJEKT, s.c,
ul. Jeżowska 14, 54-049 Wrocław, Poland
E-mail: piotr.ligocki@mtprojekt.pl

Article citation info:
BRKIĆ A Đ, MANESKI T, IGNJATOVIĆ D, JOVANČIĆ P, SPASOJEVIĆ BRKIĆ V K. Diagnostics of bucket wheel excavator discharge boom dynamic performance and its reconstruction. Eksploatacja i Niezawodnosc – Maintenance and Reliability 2014; 16 (2): 188–197.

Aleksandar Đ. BRKIĆ
Taško MANESKI
Dragan IGNJATOVIĆ
Predrag D. JOVANČIĆ
Vesna K. SPASOJEVIĆ BRKIĆ

DIAGNOSTICS OF BUCKET WHEEL EXCAVATOR DISCHARGE BOOM DYNAMIC PERFORMANCE AND ITS RECONSTRUCTION

DIAGNOSTYKA WŁAŚCIWOŚCI DYNAMICZNYCH WYSIĘGNIKA ZRZUTOWEGO KOPARKI KOŁOWEJ ORAZ JEGO PRZEBUDOWA

The paper focuses on an investigation into the possible causes of the bad dynamic performance of bucket wheel excavator C7OOS (BWE) discharge boom in the Kolubara opencast mine, Serbia. A discharge boom load carrying structure model was produced and its static and dynamic calculations were made by the finite element method (FEM). The model was then validated by the experimental method – vibration analysis. The set goals were achieved by the FEM result analysis, which were further confirmed in the experiment. The causes for discharge boom weak performance were established. The main operation problems were found in the inadequate design of the discharge boom tie(s) and the subsequent installation of a steering cabin. Possible discharge boom reconstructions were considered with a view to improving its operation performance. The selection of the reconstruction approach was limited by the technical and financial resources available to the machine users. After the completed reconstruction, the discharge boom improved operation performance was demonstrated in practice.

Keywords: *Discharge boom, bucket wheel excavator, dynamic performance, vibration analysis.*

W artykule badano możliwe przyczyny złych własności dynamicznych wysięgnika zrzutowego koparki kołowej C7OOS (BWE) pracującej w kopalni odkrywkowej Kolubara w Serbii. Do stworzenia modelu konstrukcji nośnej wysięgnika zrzutowego oraz przeprowadzenia obliczeń statycznych i dynamicznych wykorzystano metodę elementów skończonych (MES). Model został następnie zweryfikowany przy użyciu metody eksperymentalnej – analizy drgań. Wyznaczone cele osiągnięto poprzez analizę wyników MES, które zostały następnie zweryfikowane w badaniach doświadczalnych. Ustalono przyczyny słabego działania wysięgnika. Głównymi problemami eksploatacyjnymi okazały się być nieodpowiednia konstrukcja cięgien wysięgnika oraz montaż kabiny kierowcy. Aby poprawić charakterystyki pracy wysięgnika, rozważono możliwe opcje jego przebudowy. Wybór metody przebudowy ograniczały zasoby techniczne i finansowe użytkownika maszyny. Przebudowa dała poprawę charakterystyk pracy wysięgnika, co wykazano w praktyce.

Słowa kluczowe: *Wysięgnik zrzutowy, koparka kołowa, właściwości dynamiczne, analiza drgań.*

1. Introduction

In terms of energy balance, open cast mines have the largest share in electrical power production in Serbia. The increasing price of electrical power compounded by the increasing social dependence on energy sources demand the close monitoring of machines and equipment in opencast mining operations, their regular maintenance, increased availability and efficiency. To achieve these goals – the maintenance of complex excavation, belt conveyor and dumping conveyor systems in opencast mines – ever greater significance is given to the diagnostics of the condition and performance of drive groups, steel constructions of excavation and transport machinery. The basic task of the condition analysis of each load carrying structure is to determine as accurately as possible its deformations, stress distribution and oscillation frequency. Carrying structures with bad dynamic behaviour can lead to undesirable occurrences in belt conveyor and dumping conveyor operations, such as: excessive construction deformations, entry into resonant oscillations, large dynamic response, the appearance of fatigue, the breakdown of connections between construction parts, long periods needed for construction oscillations to die out and similar [2, 3, 8, 16]. When modernizing the structure of the machine or modifying its operating parameters, it is necessary to establish the impact of changes on the behaviour of the machine undergoing modernization [17]. As a result a need arose to precisely determine the dynamic characteristics of the machine, which would help to establish its resonance range or to plan its modernization [4].

Such analyses are inherent in the design process of new belt conveyors and dumping conveyors and the correction and reconstruction of the existent ones. These machines operate in arduous conditions which additionally aggravates their operation performance. An engineer is expected to use accurate and quickly calculation methods to ensure reliable and cost effective construction. This can be achieved by using modern CAD/FEM calculation methods and calculation validation by means of experimental methods on the produced construction [18]. Nevertheless, Rusinski and others in [18, 19] point out some of the reasons leading to the breakdown of load carrying structures (faults in design, technology and operation). Faults in design are caused by the use of simplified calculation methods, the neglect of load influence and the existence of residual stresses, as well as the influence of construction element fits. Faults in technology occur in construction production and the most common causes are the use of inappropriate materials and the inappropriate production of joints. Faults in operation occur due to overloads, which may result from improper use or unforeseen circumstances. All of these can lead to weak static and dynamic performance of load carrying structures in ore excavation, conveyance and dumping machines.

Detecting the causes of weak performance and the breakdown of load carrying structure parts in the machines which make up the EBD system (excavator, belt conveyor, and dumping conveyor) is the subject of numerous studies, particularly in the light of some large scale accidents. In their research Rusinski and others [13, 14] analyse the causes of the breakdown of the dumping conveyor's steerable carriage in an opencast lignite mine during work in winter conditions. Using FEM analysis and the experimental (chemical analysis) method it was established that the accident was caused by faults in design and production, due to the use of the undercarriage half shafts systems. In paper [1] the structural failure of the bucket wheel stacker reclaimer was analysed by the computer structure analysis method and experimental methods of microstructure characterization. The conclusion of this research was that the main cause for breakdown was a high concentration of stress in the welded connection of the load carrying structure elements (tubular tie-rod and flange) combined with cleavage crack propagation in the direction of lower fracture toughness. In research [6] the causes of the failure of the stacker-cum-reclaimer in an ore handling plant in India were analysed by visual methods, metallographic studies, and finite element and experimental methods of establishing stress distribution on construction elements. The research conclusion was that the accident was due to faults in the operational conditions. Paper [7] deals with an evaluation of measuring of vibrations on a bucket wheel excavator (BWE) SchRs 1320 during mining and while analyzing its dynamical properties several measurements were made.

This paper analyses the bad static and dynamic performance of the BWE C700S O&K discharge boom in the opencast mine in Kolubara, Serbia. The static and dynamic FEM calculations of the discharge boom load carrying structure were made thus describing the physical problem and operation performance, which, in turn, allows the construction performance diagnostics. The analysis entails computer calculation by the FEM method. On the basis of the calculation results the cause of the weak performance of the discharge boom was established and several solutions for its reconstruction were offered. The selected manner of reconstruction was demonstrated and the reasons for the decision given. The validity of the FEM calculation was demonstrated on the reconstructed BWE discharge boom by experimental methods and its improved static and dynamic performance were then tested.

2. Methods

2.1. FEM analysis theoretical principles

Discharge boom weak dynamic performance is a common occurrence during the excavator operation. The discharge boom of the observed excavator C700S in figure 1, in the opencast mine in Kolubara, Serbia, was reported to have entered resonant conditions, with the oscillation amplitude reaching up to 600 mm. To find out the cause of this malfunction it is necessary to perform a detailed calculation. A dynamic performance analysis is very important for the evaluation of the selection parameters and the subsequent decision, especially in the case of constructions such as the discharge boom of a dumping conveyor system, whose operational performance and integrity depend largely on its dynamic characteristics.

Fig. 1 Discharge boom of C700S excavator in the Kolubara open cast mine

The static, dynamic and heat analysis of load carrying structures is most commonly performed by FEM (the Finite Element Method) [9, 10, 11, 12]. The basic static and dynamic (with damping) equations in matrix form and the global coordinate system can be expressed as follows (1), (2):

$$[K]\{\delta\}=\{F\} \tag{1}$$

$$[M]\{\ddot{\delta}(t)\}+[B]\{\dot{\delta}(t)\}+[K]\{\delta(t)\}=\{F(t)\} \tag{2}$$

In the above given expressions [M], [B], and [K] stand for the mass matrix, the damping matrix and the stiffness matrix, $\{\delta(t)\},\{\dot{\delta}(t)\}, and \{\ddot{\delta}(t)\}$ stands for the displacement, velocity and node acceleration vectors, $\{F(t)\}$ the dynamic load vector, and t – time.

The program used for the static and dynamic analysis of discharge boom performance was package KOMIPS [9] based on the FEM application, developed at the Faculty of Mechanical Engineering in Belgrade. For all kinds of final elements and the global node the equivalent stress is calculated according to the Huber-Hencky-Mises hypothesis. With the application of this program we will perform the discharge boom modelling and static and dynamic calculation, and determine the real model node movements and stress distribution on the construction model elements. On the basis of the obtained results we will define the causes of discharge boom weak performance and improve it through the direct modification of the model. Direct modification implies changes in the construction's design parameters (mass and stiffness of certain construction parts). In addition to the aforementioned, the KOMIPS program package also supports specific calculations of construction elements which allow the determination of the membrane and bending stress distribution, the deformation energy distribution and the kinetic and potential energy distribution per model element. The said distributions are expressed in percentages per element, or selected element groups, or graphically in the form of lines of equal potentials and energies per model. The energy deformation distribution per construction part defines their sensitivity to modification.

The equation of the deformation energy balance and external force work (3) is obtained by multiplying the basic static equation (1) by the transposed displacement vector.

$$\{\delta\}^T[K]\{\delta\}=\{\delta\}^T\{F\}\equiv 2E_d \tag{3}$$

The deformation energy of the final element ed is expressed in the form below (4):

$$e_d = \frac{1}{2}\{\delta_{sr}\}_e^T \left[\overline{k_{rs}}\right]_e \{\delta_{sr}\}_e \tag{4}$$

In the equation, (4) $\left[\overline{k_{rs}}\right]_e$ stands for the global matrix of stiffness of a given element, and $\{\delta_{sr}\}_e$ is the corresponding global displacement vector. The kinetic and potential energy distribution on the main modes of the vibrations per construction element allows an even more precise analysis of their performance. The equation of the potential and kinetic energy balance [12] is obtained by multiplying the basic dynamic equation without the damping effect by the eigenvectors transposed matrix [11]. The kinetic e_k^r and potential e_p^r energy of the finite element e and the whole system Er on the r main mode of the vibrations can be expressed by the equation below (5):

$$\begin{aligned} e_k^r &= \omega_r^2 \{\mu_{sr}\}_e^T [m]_e \{\mu_{sr}\}_e \\ e_p^r &= \{\mu_{sr}\}_e^T \left[\overline{k_{rs}}\right]_e \{\mu_{sr}\}_e \\ E^r &= E_k^r = E_p^r = \omega_r^2 \{\mu_r\}^T [M]\{\mu_r\} = \{\mu_r\}^T [K]\{\mu_r\} \end{aligned} \tag{5}$$

In the equations (5), ω_r stands for r eigenvalue (circular frequency of free undamped oscillations), $\{\mu_r\}$ stands for r eigenvector, and $\{\mu_{sr}\}$ stands for the corresponding r eigenvector of the finite element.

2.2. Modelling

Figure 1 shows the excavator discharge boom at the beginning of operation as it was designed and produced. After a certain time, the user installed a steering cabin on the discharge boom, as shown in figure 2. As already said, the dynamic performance of the discharge boom in operation became very bad (large deformations, large vibration amplitudes which took a long time to decay, construction vibrations). To find out the cause of the described performance of the discharge boom it is necessary to carry out calculations with the reduced model and to draw appropriate conclusions, which then need to be verified by calculations on a discharge boom spatial model.

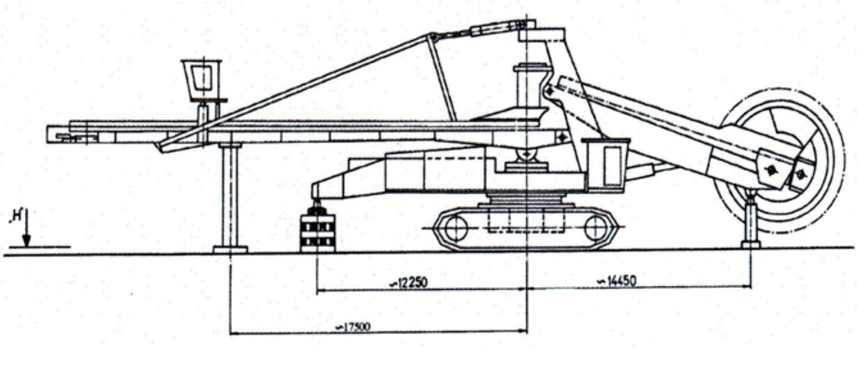

Fig. 2. The discharge boom of the C700S excavator with a steering cabin

The reduced model for the static and dynamic calculation of the discharge boom load carrying structure shown in figure 3 presents a plane model obtained by the reduction of the spatial linear model of the discharge boom structure. The calculation plane model will be used for the analysis of the discharge boom performance in the plane.

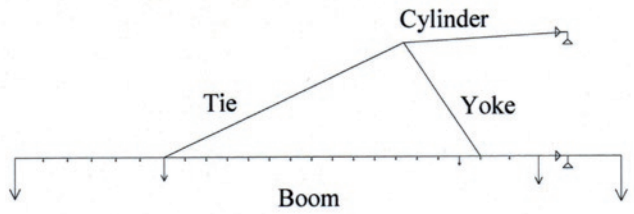

Fig. 3. Discharge boom reduced plane model

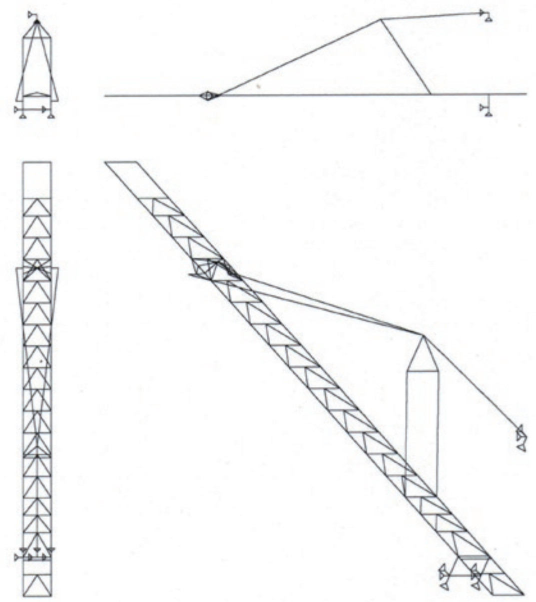

Fig. 4. Spatial model of discharge boom

The load acting on the model comprises the discharge boom weight itself, the load weight, the belt weight, the drive station weight, and the cabin weight [16]. The discharge boom supports on the excavator are modelled as two joints. The hydro cylinder is modelled by the linear element with a joint connection at both its ends. The yoke is also jointly connected to the discharge boom carrier and the connection point between the cylinder and tie. The reduced plane model comprises 25 linear elements of beam type which perform the discretization of the boom carrier construction, and three linear truss elements (tie, yoke and cylinder).

The results of the FEM calculation of the static and dynamic performance obtained from the boom construction reduced model need to be verified and confirmed on a more realistic and precise model which will demonstrate the real construction performance in operation more faithfully. The new model represents a spatial-linear model of the discharge boom. The number of nodes in the spatial model is 364, and the number of linear finite elements of beam and truss type 438. The discharge boom new spatial model is shown in figure 4. The methods of connecting the boom to the excavator, the yoke and hydro cylinder to the boom structure, and how the load acts on the model are the same as in the reduced model.

2.3. Results and discussion

2.3.1. Static and dynamic calculation of the reduced plane model

The deformed structure of the discharge boom plane model is shown in figure 5.

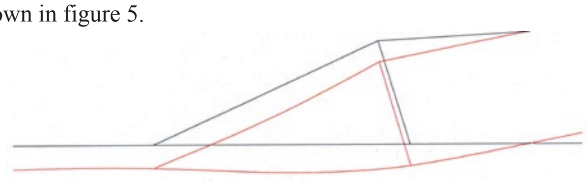

Fig. 5. Plane model deformation

Table 1. Load distribution and deformation energy distribution per element group

Model element	Axial force [kN]	Bending moment [kNmm]	Deformation energy [%]
Carrier	350/450	535000	72.2: cantilever=9.6, 1/3L= 3.5, 2/3L=17.6, 3/3L=41.5
Tie	380	-	16.8
Cylinder	450	-	10.5
Yoke	180	-	0.5

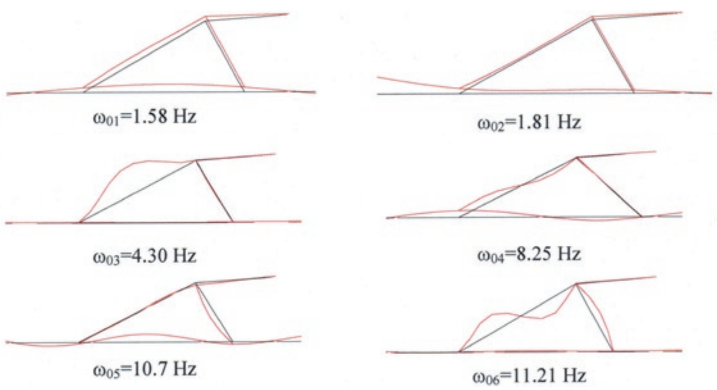

Fig. 6. Main modes of plane model vibrations

Table 2. Potential and kinetic energy distribution in the first two modes of vibrations

Model elements	Potential / kinetic energy distribution for the first two modes of vibrations [%]	
	ω_{01}=1.58 Hz	ω_{02}=1.81 Hz
Carrier	80 / 35	90 / 16
Tie	12 / 3	6 / 1
Cylinder	8 / 0	4 / 0
Yoke	0 / 0	0 / 0
External masses	0 / 62	0 / 73

The maximum deformation of the model points on the boom left end amounts to 104 mm. For a more precise definition of the discharge boom static performance and optimization elements it is necessary to analyse the load and energy deformation distribution per model element as shown in table 1.

An analysis of the static calculation results leads to the following conclusions about model performance:

- The boom deformation between the joint support of the boom structure and the yoke is significant due to the inaccurate positioning of the yoke connection.
- Additional deformation of the left boom cantilever is caused by the installed steering cabin.
- The axial force in the tie and hydro cylinder is considerable, while insignificant in the yoke.
- The bending moment of the boom carrier is large in the connection point between the boom structure and the yoke.
- The deformation energy distribution on the boom structure is dominant over the other elements (72.2% goes to the boom structure element group), while within the boom structure itself it is dominant between the joint and the yoke.

The first dynamic calculation is made for free undamped vibrations. The first six main modes of vibrations are shown in figure 6. They also demonstrate the boom deformation mode in resonance (overlapping) with actuation. The first two main modes represent the vibration of the discharge boom, the third represents the vibration of the tie, the fourth is the joint vibration of the tie and the discharge boom, the fifth is that of the boom and the yoke, while the sixth is the vibration of the tie and the yoke. In this case, the first three main modes of vibrations are sufficient for dynamic performance analysis.

After the calculation of free undamped oscillation, a dynamic calculation of forced damped oscillations in the frequency domain was made; these can produce the frequency characteristics of the structure. This is how we obtain the structure performance for simulated combinations of actuation and response; the simplest way to express this is through dynamic amplification in the observed frequency domain. The discharge boom frequency characteristics for vertical actuation acting on the connection point between the tie, yoke and hydro cylinder and the vertical response on the left end of the boom carrier are shown in figure 7.

An example of discharge boom time response for displacement and stress in the selected connection point between the tie, yoke and hydro cylinder is shown in figure 8.

By analysing the results of dynamic calculation the following conclusions about model performance can be made:

- The first two eigenfrequencies are very low, very close to each other and they overlap with static deformation.
- The factor of dynamic amplification with 5% damping equals around 38 for the first and 30 for the second modes of vibrations, which are rather significant values. The dynamic stability system diagram also shows a high imaginary part of characteristics; i.e. high system instability.
- The potential energy distribution on the boom structure is dominant in relation to other elements, while kinetic energy distribution is dominant on the external load (external masses) and on the boom structure elements.

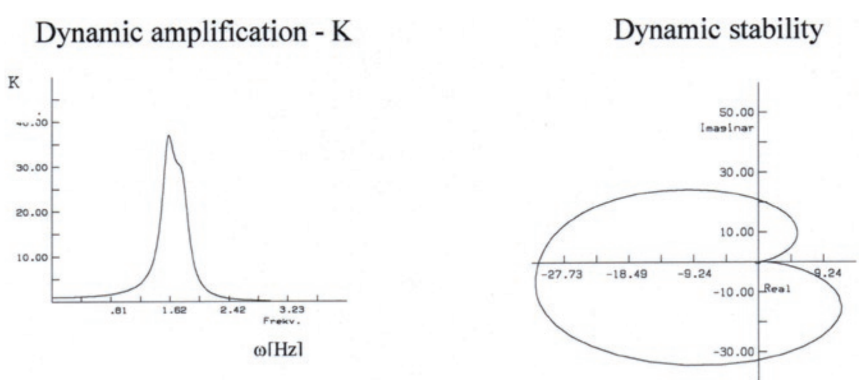

Fig. 7. Discharge boom frequency characteristics

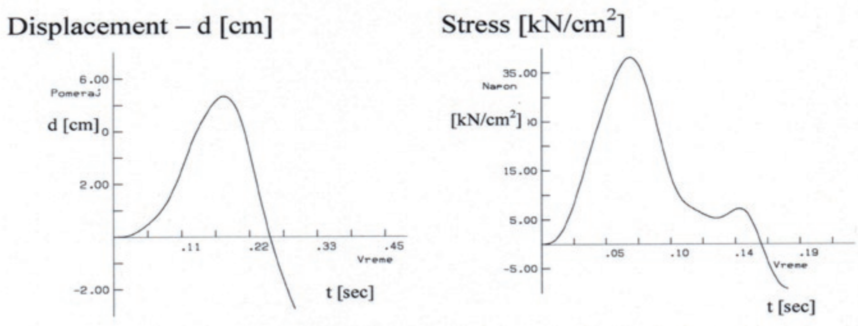

Fig. 8. Time response of discharge boom

calculation), whereby the second is insignificantly larger than the corresponding one in the plane model. Smaller values of dynamic amplification factor can be noted, as well as reduced system dynamic instability in relation to the corresponding values of the plane model. These results were also expected due to greater accuracy in the distribution of mass and stiffness in the spatial model.

The dynamic calculation carried out on the discharge boom spatial model completely confirms its bad performance. The actuation to the discharge boom comes from the bucket wheel on the bucket wheel excavator. The bucket wheel turns with 6 RPM. Since there are 12 buckets on the bucket wheel, it follows that the bucket wheelcauses the actuation frequency of 1.2 Hz. The actuation frequency is close to the first eigen frequency. The dynamic calculation results for the spatial model are more accurate and show the more favourable behaviour of the boom than the plane model. Due to the simpler determination of the structural parameters the modification influences its dynamic behaviour. We will analyse the plane model below.

2.3.2. Dynamic Calculation of the Discharge Boom Spatial Model

The results of the reduced plane model calculation were verified by means of the dynamic calculation of the more realistic and precise discharge boom structure spatial model. The dynamic calculations of the first eight main modes of vibrations are shown in figure 9. As expected, due to a more accurate stiffness and mass distribution, a change in frequencies and modes of vibrations occurred compared to those of the plane model. New modes of vibrations (6, 7 and 8) appeared as a result of the spatial model due to the introduction of 3 added degrees of freedom of nodes. The first three modes of vibrations are largely identical whereby the first two main modes swapped places. The fifth and ninth eigenvalues of the spatial model correspond to the fourth and fifth of the plane model.

The forced damped response of the spatial model in the frequency domain for vertical actuation acting on the connection point between the tie, yoke and hydro cylinder and the vertical response on the left end of the boom structure are shown in figure 10.

Based on the performed dynamic calculations of the spatial model we can conclude that the first two eigen values of the spatial model are very close (the conclusion of the plane model confirmed by dynamic

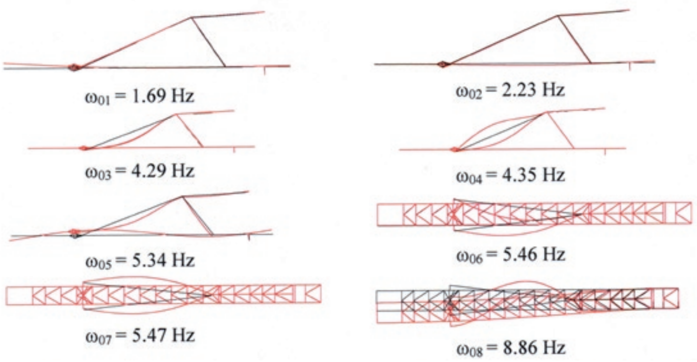

Fig. 9. Main modes of vibrations of the spatial model

2.4. Reanalysis of boom discharge construction performance and its reconstruction

Reanalysis or structural dynamic modification presents a set of methods which can improve the dynamic performance of the discharge boom structure. The dynamic response of the system is primarily characterized by relevant eigenvalues and main modes of vibrations. Dynamic characteristic modification entails changes to the relevant structural parameters in order to achieve the desired dynamic performance in the changed eigenfrequencies and main modes of vibrations.

The dynamic calculation results of the discharge boom plane model define the parameters for model optimization; i.e. the boom reconstruction method for the improved dynamic performance of its load carrying structure. The main course of dynamic model optimization is an increase in the value of the eigenfrequencies, as well as an increase in their value difference.

On the basis of the above said we will consider the following modification models which may lead to an improvement in the dynamic performance of the discharge boom:

- boom model without the subsequent installation of a steering cabin;
- boom model with increased stiffness on the bending boom carrier by introducing additional ties;
- boom model with a changed connection point between the yoke and boom cantilever.

To determine which dynamic model satisfies these demands to the highest extent, it is necessary to perform static and dynamic calculations of different model variants. The analysed discharge boom modified models have XYij markings, with the following meanings:

- X = S – static calculation;
- X = D – dynamic calculation;
- Y = A - model with a subsequently installed steering cabin;
- Y = B - model without a subsequently installed steering cabin;
- i = 0 – the existing model;
- i = 1 – model modified with the addition of two new ties;
- i = 2 – model modified with the addition of two new ties and their infill;
- j = 0 – the existing model;

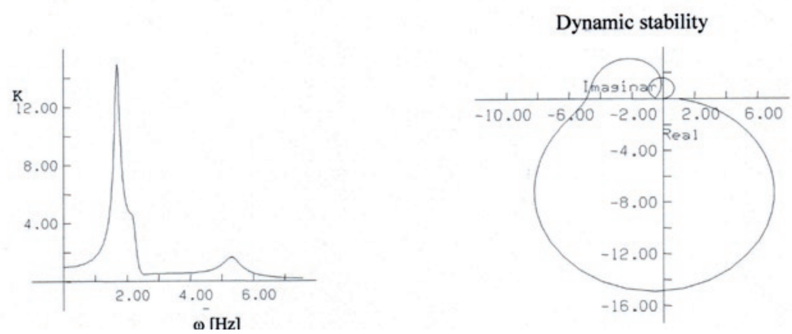

Fig. 10. Frequency characteristics of the discharge boom spatial model

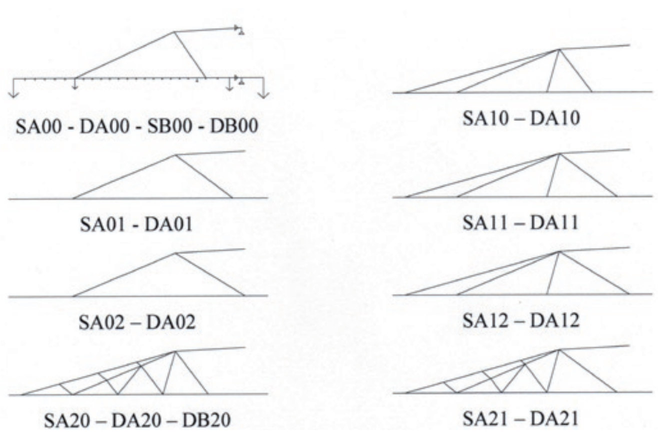

Fig. 11. Variants of analysed modified models of discharge boom

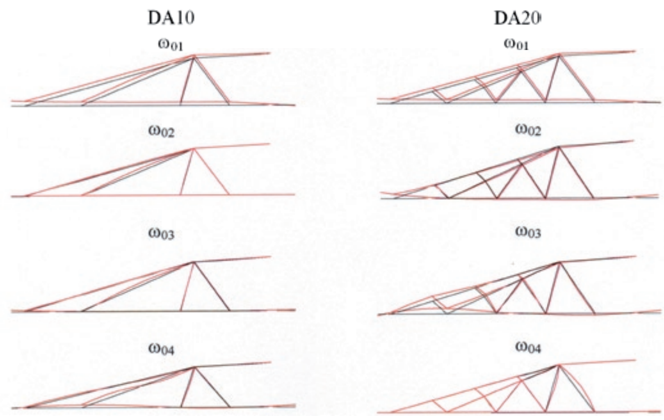

Fig. 13. Main modes of vibrations of the modified model with additional ties and infills

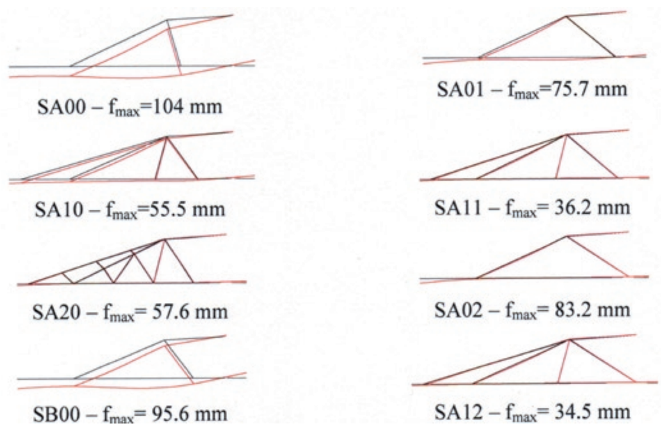

Fig. 12. Deformations of discharge boom modified models

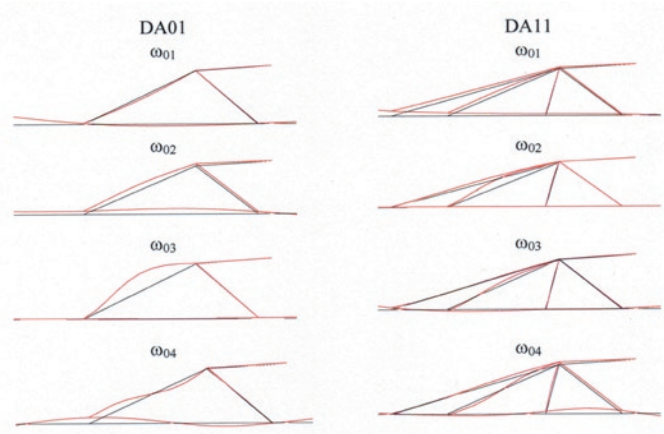

Fig. 14. Main vibration modes in the modified model with changed yoke-boom connection position

– j = 1 – model modified by moving the connection between the yoke and boom structure to the middle distance from the joint rest;
– j = 2 – model modified by moving the connection between the yoke and boom structure to the boom structure joint support.

Table 3. The values of axial force in [kN] per element group of discharge boom modified models

Model elements	SA00	SA10	SA20	SA01	SA11	SA02	SA12	SB00
Carrier	350	280	280	300	250	280	260	260
Tie	380	110	120	330	120	310	130	280
Cylinder	450	450	470	450	450	450	450	330
Yoke	180	300	320	190	240	200	230	130
Additional tie	-	180	200	-	140	-	140	-
Additional infill	-	-	0	-	-	-	-	-

Table 4. Deformation energy [kNcm] distribution per element group in the discharge boom modified models

Model elements	SA00	SA10	SA20	SA01	SA11	SA02	SA12
Beam	72.2	59.3	60.4	49.2	21.3	41.8	15.3
Tie	16.8	3.4	2.6	26.8	8.3	28.5	10.2
Cylinder	10.5	23.0	22.9	22.3	48.1	27.1	51.9
Yoke	0.5	3.3	3.4	1.7	5.6	2.6	6
Additional tie	-	11.0	10.7	-	16.7	-	16.5
Additional infill	-	-	0	-	-	-	-
Σ E_d [kNcm]	1418	647	709	669	310	551	287

The variants of the analysed modified models are shown in figure 11.

An analysis of the values of the modified model deformations enables the following conclusions:

- the steering cabin increases the deformation of the left boom cantilever;
- the introduction of new ties drastically reduces the deformation of all boom structure elements;
- the optimum position of the yoke-boom structure connection is between its current position and the boom structure joint support in the case of the model without ties, and at the joint-support in the case of the model modified with two new ties;
- the introduction of a tie infill insignificantly increases boom structure deformation, but it should have a positive influence on discharge boom dynamic performance.

Models SA12 and SA11 demonstrate the best performance as regards deformation values. Bearing in mind the difficulties involved in boom reconstruction by changing the yoke-boom structure connection point, the boom reconstruction according to modified models SA10 and SA20 is both technically and economically the most effective.

Axial force distribution on the boom structure for the considered model variants is given in Table 3. The optimum solution in view of this criterion is again model SA12 or SA11. The proposed solution (SA10 and SA20) has increased force in the yoke which does not pose a technical problem. The steering cabin contributes to the increase in axial force.

The deformation energy distribution in percentages per element of the analysed models is shown in Table 4. The total deformation energy is minimal on models SA12 and SA11. The deformation energy was transposed from the boom structure elements to the cylinder.

Keeping the steering cabin, and the current position of the yoke, the effect of additional ties (DA10) and their infills (DA20) on boom dynamic behaviour in the first four modes of vibrations is shown in figure 13. Analysing the given results we can conclude that the introduction of the addition of new ties and their infills favourably influences the dynamic behaviour of the basic model.

Table 5. Values of circular frequencies of free undamped vibrations [Hz] in the modified models

ω	DA00	DA10	DA20	DA01	DA11	DB00	DB10	DB20
ω_{01}	1.58	2.03	2.23	1.62	3.04	1.61	2.10	2.58
ω_{02}	1.81	2.38	4.64	2.33	3.92	3.22	4.11	6.94
ω_{03}	4.30	4.19	9.43	3.08	6.03	8.52	4.65	12.27
ω_{04}	8.25	4.74	13.16	7.11	7.83	9.31	8.93	13.31
ω_{05}	10.7	5.86	17.67	9.93	11.1	10.97	11.42	18.46
ω_{06}	11.21	8.30	21.77	11.05	14.53	12.20	13.81	21.98
ω_{07}	13.56	10.85	22.82	18.37	21.85	13.56	15.30	25.50
ω_{08}	18.43	11.98	24.16	20.55	22.24	19.83	20.30	28.22
ω_{09}	23.09	13.85	24.57	24.07	25.85	23.46	23.34	30.21
ω_{010}	24.53	15.02	26.57	25.60	26.48	28.15	23.62	31.81

The effect of the changed yoke-boom structure connection position (DA01) and the addition of new ties without infills (DA11) on discharge boom dynamic behaviour in the first four modes of vibrations is shown in figure 14. Analysing the given results we can conclude that only moving the connection between the yoke and boom structure insufficiently influences the improvement of the dynamic behaviour of the basic model, making it necessary to introduce the addition of new ties.

The values of the first ten circular frequencies in the considered model are shown in Table.5.

Based on the calculation results of free undamped vibration we can conclude that the introduction of new ties is fully justified. The presence of additional mass (steering cabin) has an adverse effect on discharge boom dynamic performance. The most advisable position for the yoke-boom structure connection is in the joint support. In the case of all the modified models there is an increase in the vibration frequency values, as well as their distance, which removes the basic cause of discharge boom weak performance. The dynamic behaviour of the modified model without a steering cabin and with additional new ties (DB10), and their infill (DB20), in the first four vibration modes is shown in figure 15.

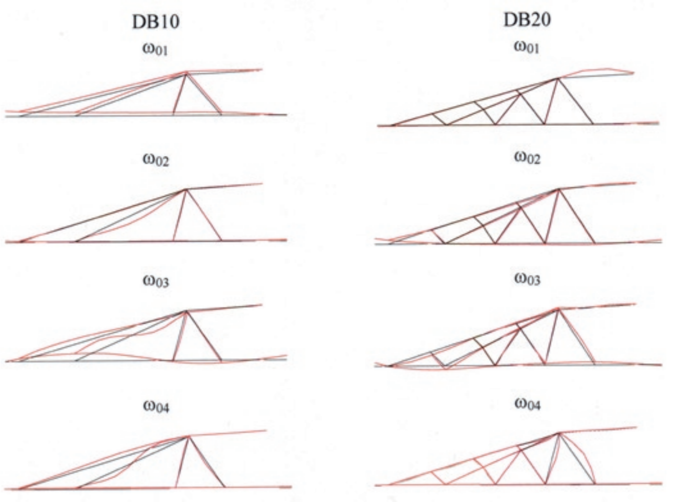

Fig. 15. Main modes of vibrations without a cabin and additional ties

The potential and kinetic energy distribution in the main modes of vibrations leads to the same conclusions as deformation energy distribution. The improved model variants have reduced energy in the boom structure and increased energy in the hydro cylinder.

The results of forced damped vibration calculations in the frequency domain which can produce the frequency characteristics of the modified models are shown in figure 16. Vertical actuation acts on the cylinder-tie-yoke connection point, while the vertical response is observed on the boom structure left end.

The frequency characteristics indicate the weak performance of the model with additional mass (steering cabin) on the boom structure left end, as well as the model without ties. Weak performance is observable in the high factor of dynamic amplification, the large imaginary part of characteristics, the low vibration frequencies and their short distances.

The demonstrated procedure for static and discharge boom dynamic performance analysis allows a highly ef-

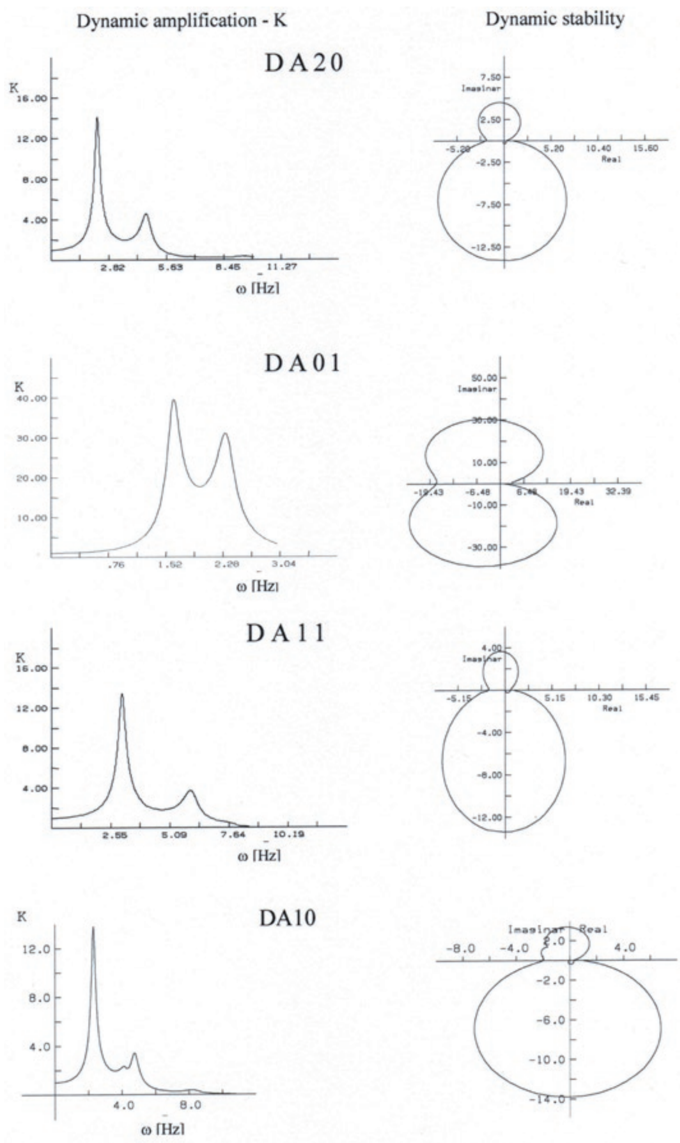

Fig. 16. Frequency characteristics of the discharge boom construction modified models

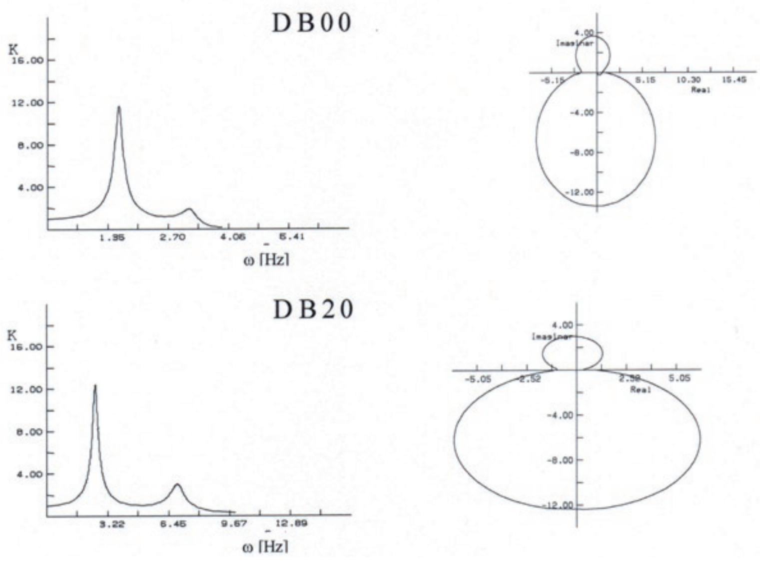

Fig. 16. Frequency characteristics of the discharge boom construction modified models (continued)

Fig. 17. Reconstructed BWE C700S discharge boom on the Kolubara open-cast mine

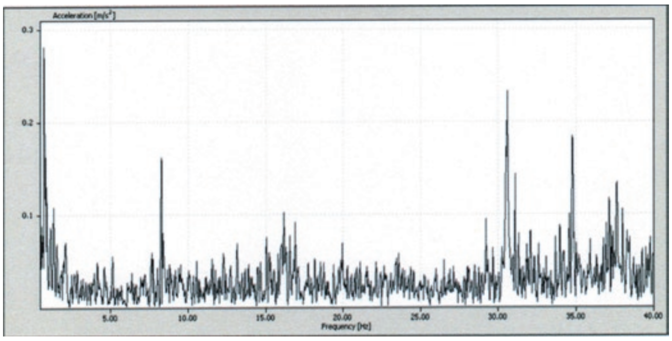

Fig. 18. Acceleration of additional tie-boom structure connection points in the vertical direction

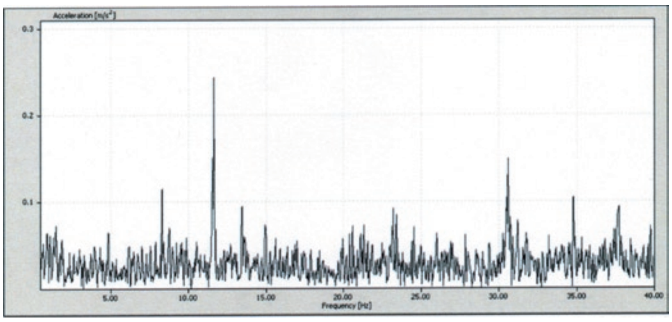

Fig. 19. Acceleration of additional tie and boom structure connection point in the lateral direction

ficient and quality assessment of construction exploitation performance, the detection of poor performance cause, the degree of impact of the construction's dynamic parameter on exploitation performance and allows for decision making on the selection of a reconstruction solution. The limitations present in the solution selection lie in the staff, and both the technical and financial capacities of the excavator users for the implementation of the optimal solution. According to all of the above, the selected solution for the discharge boom reconstruction comprises the following improvements on the present one: the steering cabin is removed (a camera is attached instead), two new ties without infills are added, while the yoke-boom structure connection remains in the same position (modified models SB10 and DB10).

The reconstructed BWE discharge boom is shown in figure 17. The performed reconstruction of the discharge boom solves the basic cause of previous poor performance.

Dynamic parameter values were experimentally determined for the reconstructed boom so as to describe its behaviour in operation. Location of the measuring sensors and directions in which accelerations will be measured is very important[15]. Accelerometer placement is shown on the fig.17. Selected place has the most inconvenient boom`s dynamic behaviour. Carrying structure vibrations were measured from the position of the last added tie-boom structure connection in the vertical direction and in two horizontal directions (axis and lateral). Vibration measurement was performed with equipment consisting of a three-component acceleration gauge sensor, an analogue-digital converter and USB computer communication. The software package supports the analysis of the time and frequency acceleration signal. The frequency signal was received by the application of the FFT analysis. Figures 18 and 19 show the measured accelerations within the frequency domain.

The performed experimental measurement is aimed at establishing the presence of local or global structure response close to the actuation frequency, and the verification of the FEM calculation model. The eigenfrequencies of FEM model DB10 given in table 5 largely overlap with the measurements shown in figure 18, hence the conclusion that

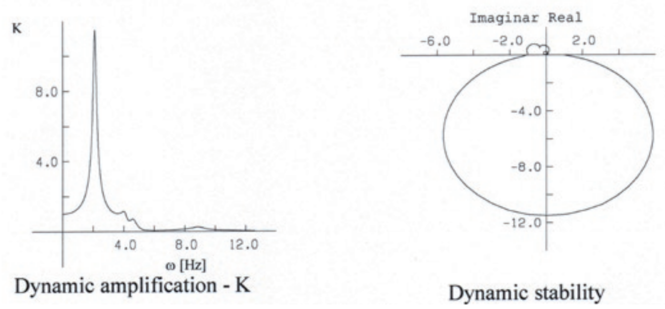

Fig. 20. Frequency characteristics of DB10 plane model of reconstructed discharge boom

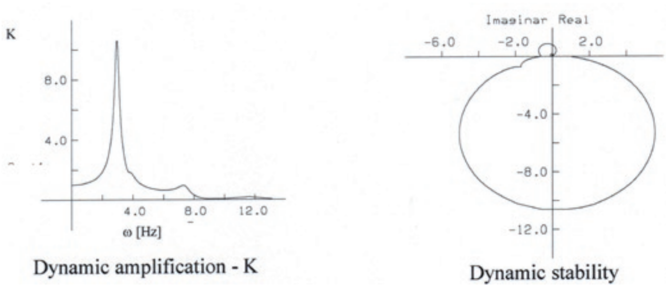

Fig. 21. Frequency characteristics of DB10 spatial model of reconstructed discharge boom

the FEM calculation model is validated. We also conclude that the measured acceleration values of the additional tie connection point on the boom structure in the vertical and lateral direction are within the limits of permissible values for this type of construction as prescribed in [5]. All of the above serves to prove that the dynamic behaviour of BWE C700S operation performance is significantly improved after the implemented reconstruction. This conclusion is further confirmed by the results of dynamic calculations of forced damped vibrations in the frequency domain of model DB10 according to which the boom reconstruction was carried out. The frequency characteristics of the reconstructed boom plane model are shown in figure 20, while figure 21 shows those for the reconstructed boom spatial model.

The numerical calculation of the spatial model show higher values of eigenfrequencies compared to those of the plane model. The experimental measurements were carried out on the BWE C700S reconstructed discharge boom in operating conditions. Although calculations were not done on the whole BWE model, the results of the measurements are in correlation with the calculation results on the discharge boom model. Correlation is related to the identification of the presence of the boom vibration close to its eigenfrequencies. The spatial model gives more accurate results, but for the investigation in this paper the plane model was accurate enough.

3. Conclusion

The diagnostics of the load carrying construction condition shown in this paper are performed by the FEM and experimental method in order to detect the cause of the BWE C700S discharge boom operation problem in the Kolubara opencast mine, Serbia. The cause of the exploitation problem was established – insufficient stiffness of the boom ties as defined in the design, as well as the subsequently attached steering cabin which does not form part of the original design. Numerical analysis (FEM) showed that the deformation energy distribution was dominant in the elements of the boom structure(72%), that the boom deformations were very high (104 mm), that the first two vibration frequencies were very low and at high proximity, and that the dynamic performance factors for the first two vibrations were considerable, all of which contribute to weak boom operation performance and point to possible courses of action in boom redesign. The paper analysed the dynamic performance of several possible dynamic behaviour improvement models.The selected model is optimal when taking into account the technical, financial and staffing capacities of the user for the reconstruction implementation. The boom reconstruction was implemented by removing the steering cabin and introducing two new boom ties.

The BWE discharge boom dynamic behaviour improvement was verified by the experimental method on the reconstructed boom. The experiment results prove a good match with the FEM analysis results, which validate the numerical model. The major advantages of the reconstructed discharge boom over the original comprise the following:

(1) Maximum boom deformation is reduced from 104 mm to 51.5 mm.
(2) The first two eigenfrequencies are increased as is their distance as shown in table 5.
(3) A more even deformation energy distribution on the construction elements is achieved.
(4) The dynamic amplification factor for the first vibration mode is reduced from 38 to 12, and a significantly higher system dynamic stability is secured due to a considerable reduction in the imaginary part of characteristics (figure 20).
(5) All accelerations of structure modes are reduced within the limits of permissible values [5] (up to 2 m/s^2).

The application of the described diagnostics methodology of load carrying structure performance is justified and necessary in the engineering analysis of exploitation problems since it produces good results and is cost effective.

Acknowledgement:
This work is partially supported by the Ministry of Education and Science of Serbia grants nos. TR35040, TR35030 and E!6761.

References

1. Araujo LS, De Almeida LH, Batista EM. Analysis of a Bucketwheel Stacker Reclaimer Structural Failure, Proceedings of the conference Materials science & technology, Charles R. Morin Memorial symposium on failure analysis and prevention, 2009, Pittsburg, Proceedings on CD, http://www.matscitech.org.
2. Arsić M, Bošnjak S, Zrnić N, Sedmak A, and Gnjatović N. Bucket wheel failure caused by residual stresses in welded joints. Engineering Failure Analysis 2011; 18: 700-712.
3. Bošnjak SM, Arsić MA, Zrnić NĐ, Rakin MP, Pantelić MP. Bucket wheel excavator: Integrity assessment of the bucket wheel boom tie-rod welded joint. Engineering Failure Analysis 2011; 18: 212-222.
4. Bošnjak SM, Zrnić ND. Dynamics, failures, redesigning and enviromentally friendly technologies in surface mining systems. Archives of Civil and Mechanical Engineering 2012; 12: 348-359.
5. DIN 22261-1 and DIN 22261-2, Excavators, spreaders and auxiliary equipment in opencast lignite mines. Part 1: construction, commissioning and monitoring, Part 2: calculation principles, Berlin: German Institute for Standardization, 1998.
6. Ghosal S, Misra D, Saha TK, Chakravorty D, and Chaudhuri B. Failure Analysis of Stacker-cum-Reclaimer in Ore Handling Plant. J Fail. Anal. And Preven.2008; 8: 564-571.
7. Gottvald J. Analysis of vibrations of bucket wheel excavators Schrs1320 during mining process. FME Transactions 2012; 40: 165-170.
8. Jovančić PD, Ignjatović D, Tanasijević M, Maneski T. Load-bearing steel structure diagnostics on bucket wheel excavator, for the purpose of failure prevention. Engineering Failure Analysis 2011; 18: 1203-1211.
9. Maneski T. Monography computer modelling and structures calculation (in Serbian), 1st ed., Belgrade: Faculty of Mechanical Engineering, 1998.
10. Maneski T, Ignjatović D. Repair and reconstruction of bucket wheel excavators. Structural Integrity and Life 2004; 1: 9-28.
11. Maneski T, Ignjatović D. Structural performance diagnostics. Structural Integrity and Life 2004; 1: 3-7.
12. Markowski T, Mucha J, Witkowski W. FEM analysis of clinching joint machine's C-frame rigidity. Eksploatacja i Niezawodnosc – Maintenance and Reliability 2013; 15 (1): 51-57.
13. Rusinski E, Czmochowski J, and Moczko P. Failure reason investigations of dumping conveyor breakdown. J. of Achievements in Materials and Manufacturing Engineering 2007; 23: 75-78.
14. Rusinski E, Czmochowski J, Moczko P. Investigations of causes of dumping conveyor breakdown. J. of Achievements in Materials and Manufacturing Engineering 2007; 24: 267-274.

15. Rusinski E, Czmochowski J, Pietrusiak D. Problems of steel construction modal models identification. Eksploatacja i Niezawodnosc-Maintenance and Reliability 2012; 14 (1): 54-61.
16. Rusinski E, Czmochowski J, Iluk A, Kowalczyk M. An analysis of the causes of a BWE counterweight boom support fracture. Engineering Failure Analysis2010; 17: 179-191.
17. Rusinski E, Dragan S, Moczko P, Pietrusiak D. Implementation of experimental method of determining modal characteristics of surfface mining machinery in the modernization of the excavating unit. Archives of Civil and Mechanical Engineering 2012; 12 (4): 471-476.
18. Rusinski E, Moczko P, Czmochowski J. Numerical and experimental analysis of a mine's loader boom crack. Automation in Construction 2008; 17: 271-277.
19. Rusinski E, Moczko P, Kaczynski. Structural modifications of excavator's bucket wheel by the use of numerical methods. Solid State phenomena 2010; 165: 330-335.

Aleksandar Đ. BRKIĆ
Innovation Center, University of Belgrade
Faculty of Mechanical Engineering
KraljiceMarije 16, 11120 Belgrade 35, Serbia
E-mail: abrkic@mas.bg.ac.rs

Taško MANESKI
Department of Strength of Constructions
University of Belgrade
Faculty of Mechanical Engineering
KraljiceMarije 16, 11120 Belgrade 35, Serbia
E-mail: tmaneski@mas.bg.ac.rs

Dragan IGNJATOVIĆ
Predrag D. JOVANČIĆ
Department of Mining Machinery
University of Belgrade
Faculty of Mining and Geology
Đušina 7, 11120 Belgrade 35, Serbia
E-mails: dragan.ignjatovic@rgf.bg.ac, predrag.jovancic@rgf.bg.ac

Vesna K. Spasojević BRKIĆ
Industrial Engineering Department
University of Belgrade
Faculty of Mechanical Engineering
KraljiceMarije 16, 11120 Belgrade 35, Serbia
E-mail: vspasojevic@mas.bg.ac.rs

Article citation info:
CECHOWICZ R, STĄCZEK P. Computer supervision of the group of compressorsconnected in parallel. Eksploatacja i Niezawodnosc – Maintenance and Reliability 2014; 16 (2): 198–202.

Radosław CECHOWICZ
Paweł STĄCZEK

COMPUTER SUPERVISION OF THE GROUP OF COMPRESSORS CONNECTED IN PARALLEL

KOMPUTEROWY SYSTEM NADZOROWANIA ZESPOŁU SPRĘŻAREK PRACUJĄCYCH W UKŁADZIE RÓWNOLEGŁYM*

The paper presents the original solution of the control and monitoring system of the compressed air production plant. The plant was supplying the mid–size production system. The developed solution is consistent with the Condition–Based Maintenance approach. Its aim was to integrate the functions of direct control and monitoring of the process to ensure the best possible working conditions of machines (compressors) and to extend the period of their operation. The implementation of the described solution allowed: to eliminate the need for human presence in an environment with very high levels of noise, to improve the quality of the process by stabilising the course of its basic characteristics (variables), to automate the handling of alarm conditions, to increase machines' reliability through their rational use and ensuring proper working conditions, and to document the process. Freeing the operator from the common, repetitive control tasks and equipping him with diagnostic tools enabled him to detect threats (potential failures) sooner and to undertake appropriate corrective actions.

Keywords: *monitoring, diagnosis, operation of compressors, Statistical Process Control, Condition Based Maintenance.*

W pracy przedstawiono własne, wdrożone rozwiązanie problemu automatyzacji sterowania i nadzorowania procesu wytwarzania sprężonego powietrza na potrzeby średniej wielkości systemu produkcyjnego. Opracowane rozwiązanie jest zgodne z podejściem Condition-Based Maintenance. Jego istotą było zintegrowanie funkcji sterowania bezpośredniego oraz nadzorowania przebiegu procesu w celu zapewnienia możliwie najlepszych warunków pracy maszyn i wydłużenia przez to okresu ich eksploatacji. Wdrożenie opisanego rozwiązania pozwoliło na: wyeliminowanie konieczności przebywania ludzi w środowisku o bardzo dużym poziomie hałasu, poprawę jakości procesu poprzez ustabilizowanie przebiegu jego podstawowych charakterystyk (zmiennych), zautomatyzowanie procedur obsługi sytuacji awaryjnych, zwiększenie niezawodności maszyn poprzez ich racjonalne wykorzystanie i zapewnienie prawidłowych warunków pracy, oraz dokumentowanie przebiegu procesu. Uwolnienie operatora od zadań sterowania i wyposażenie go w narzędzia wspomagające diagnostykę procesu spowodowały, że był on w stanie wcześniej wykryć zagrożenia dla przebiegu procesu (potencjalne awarie) i podjąć stosowne działania zaradcze.

Słowa kluczowe: *nadzorowanie, diagnostyka, eksploatacja sprężarek, statystyczne sterowanie procesem.*

1. Introduction

The paper describes the compressed air plant control and monitoring system that is based on the idea of Condition–Based Maintenance (CBM), i.e. performing maintenance and repair only when the need for such actions results directly from machine observation, and not when it is imposed by the maintenance schedule. The idea of CBM is growing in popularity as evidenced in works [6] and [8] where the most common solutions and diagnostic methods were summarised.

Three main components should be taken into consideration to successfully implement the CBM strategy: acquisition of data containing information about the status of the monitored devices, processing of the obtained information (data), and decision–making mechanism. The precise diagnosis is essential in CBM systems as it is used as a basis for decisions on maintenance and repair actions [11].

Potential benefits of CBM approach are twofold: firstly, service operations are performed when there is a real need for them (good parts are not replaced just because their planned operation time has expired), secondly, the danger of machine failure due to premature part wear is eliminated. The properly implemented CBM system makes possible to reduce the maintenance costs of the machines and increase the overall performance of a manufacturing system by eliminating the downtime associated with equipment failures.

One of the methods to monitor the state of the process that can be used in CBM is using control charts, which are well known part of a broader strategy of statistical process control (SPC). The main purpose of the control charts is to detect and signal deviations from the natural variability of the process (of selected quality characteristics). This approach has been used, for example, in [5]. Control charts, proposed by Shewhart [10], were used for the first time in the automotive industry to evaluate the quality of the production batch.

The compressed air plant, for which the described method was developed, was composed of four reciprocating compressors working in parallel, and supplying the factory distribution network. There were various devices and machines (receivers) connected to the compressed air distribution network in the factory. They had different air consumption characteristics (cargo handling systems, transport devices, auxiliary devices, and hand tools). The demand for air during the manufacturing system operation was characterised by high dynamics. For this reason, the development of a static plan of compressor operations was a difficult task. The production of compressed air had to be controlled and monitored continuously by the operator who, having

(*) Tekst artykułu w polskiej wersji językowej dostępny w elektronicznym wydaniu kwartalnika na stronie ***www.ein.org.pl***

access only to the current readings of measurement devices, had to make decisions about switching on or off the compressors and had to carry out maintenance work according to the maintenance plan. Due to the time–consuming nature of these operations and the considerable number of measurement points, the evaluation of technical condition of the compressors was made occasionally, a few times a day. Therefore, it could happen that the machines worked temporarily under adverse conditions (e.g. overload), which was one of the causes of their failures and downtime. This, in turn, led to problems with the receivers connected to the air distribution network.

To improve this situation, it was decided to automate the control and diagnosing of the process of production of compressed air. Additional prerequisites to automate the process were: the need to improve the working conditions of the operator, the need to stabilise the pressure in the compressed air distribution network, the requirement for an automatic documenting of the manufacturing processes [9].

2. Control of the compressed air plant

A system for automated control and monitoring of the compressed air plant was developed and implemented. In this system, the values of the basic variables of the process were monitored continuously and control algorithms guaranteed correct operation conditions for each of the machines, as well as uniform loading of all compressors. A detailed description of the control algorithms for individual machines and the entire plant was given in the works [2] and [3].

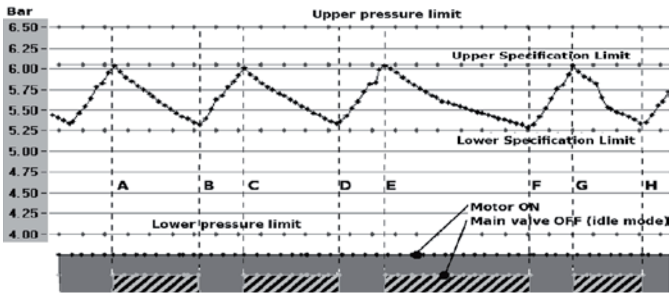

Fig. 1. Time chart for pressure in the network and the status of the compressor with low compressed air demand

In Fig. 1 the recorded pressure waveform in the air distribution network is shown. The recording was done during the time of low air consumption (low load of the compressed air plant). At that time, it was enough to use just one compressor to satisfy the demand. The motor driving the reciprocating compressor was working all the time, and the air was pumped only during the periods of B–C, D–E and F–G. In the remaining time (intervals A–B, C–D, E–F and G–H) the compressor inlet valves were deliberately opened (idle mode).

The duration of each interval of quasi-periodic waveform resulted from the rate of pressure rise or fall, that is from the air flow rate to the receivers. The main objective of the automatic control system was to maintain the pressure in the air distribution network within the tolerance limits 5.25..6.05bar (LSL..USL). In Fig. 1, the alarm limits are also marked. There is a sudden drop in the air pressure, shown in Fig. 1, in the period G–H. This drop was caused by a temporary increase in air demand. The system responded to it with the shortening of the idle time of the compressor.

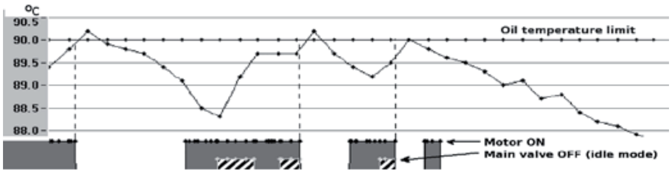

Fig. 2. Temporal switching off the compressor motor caused by exceeding the maximum temperature of the oil

The process data record shown in Fig. 2 documents the oil temperature alarm event and switching off the compressor motor that followed. Such situations did occur when the compressor was working for long time during the summer heat. The compressor (precisely, the motor) was turned off each time when the predicted oil temperature value went beyond the set limit of 90°C (three events are marked in the graph). After the temperature went below the limit, the compressor was switched on again (automatically, by the control system).

The pressure drop shown in Fig. 3 is the result of thermal overload of one of the compressors. In the segment A–B the machine was working correctly. In the time B–C there was an increased demand for compressed air, which resulted in an increase in the switching frequency of the compressor. At the end of this time (in the moment C) the oil temperature went beyond the limit. The compressor was automatically switched off and then, after the oil temperature went below the limit, switched on again. Since the increased demand for compressed air continued throughout the time C–D, the following emergency shut–downs resulted in the gradual decrease of air pressure in the network. Eventually, the pressure went down to a very low level and reached the lower limit, activating an alarm and alerting the technical staff about the situation. When the alarm was signalled, some of the pneumatic devices were switched off by the users, which reduced the demand (at the end of the time C–D). From that moment on, the air pressure remained within tolerance limits. During the time shown in Fig. 3 only one compressor was working (other machines were switched off permanently by the factory personnel).

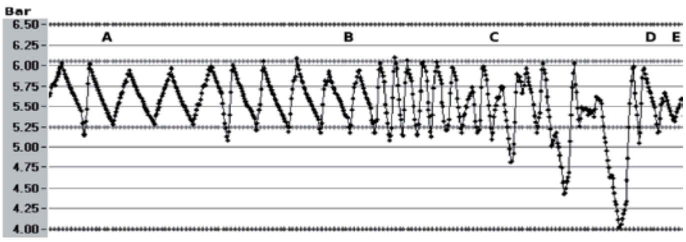

Fig. 3. Compressed air pressure fluctuations caused by the thermal overload of one of the compressors

3. Monitoring and diagnostics

The values of the main variables of the compressed air manufacturing process were recorded and presented on the operator screen in the form of readings (numeric values) and time graphs (similar to these shown in Fig. 1..3). The following analogue variables were monitored for the diagnostic purposes:

a) air temperature at the outlet of each compressor,
b) oil temperature in the sump,
c) oil pressure in the compressor lubrication system,
d) air pressure in the distribution network.

Additionally, signals from the oil temperature and oil pressure limit switches were recorded.

The work [2] describes the method used for the quality evaluation of the process of the production of compressed air and the obtained results. The process capability index [7], calculated for air pressure p in the distribution network, was c_{pk}=0.578 during typical work conditions (typical demand for compressed air). The relatively low value of the capability index means, that statistically during approximately 7% of the working time the pressure p was outside the tolerance limits. It results from the properties of the control algorithm used, and the properties of the actuators – the compressors. The momentary output of the compressor resembled a discrete signal (each of the four machines could be in one of the three states: active, idle, or standby). Furthermore, there were technological limits imposed on the control system such as maximum number of motor starting events per hour and maximum continuous operating time. These conditions meant that the nature of the changes in the air pressure at the output (in the distribution network) was quasi–periodic and the extreme values of the pressure p in one cycle often went outside tolerance limits – Fig. 4.

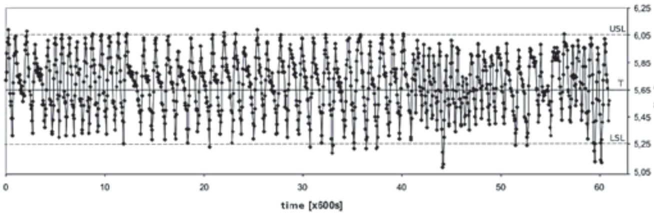

Fig. 4. The air pressure in the distribution network during the normal work of the compressed air plant (typical demand for air)

If the process correctness were evaluated only on the basis of the actual value of the pressure p in the network, it would result in frequent generation of unjustified alarms caused by typical fluctuations of the process variable. It was therefore decided to monitor the average value of the pressure p calculated over a suitably selected range (window) of time.

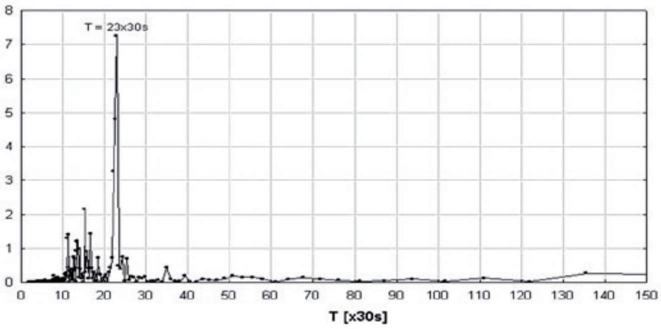

Fig. 5. The frequency spectrum of the signal of the air pressure in the distribution network

The frequency analysis of the monitored quality characteristics p (Fig. 5.) under typical production conditions (Fig. 4.) indicated the existence of a dominant oscillation frequency equal to:

$$f_1 = \frac{1}{23 \cdot 30s} = 0.0014Hz \tag{1}$$

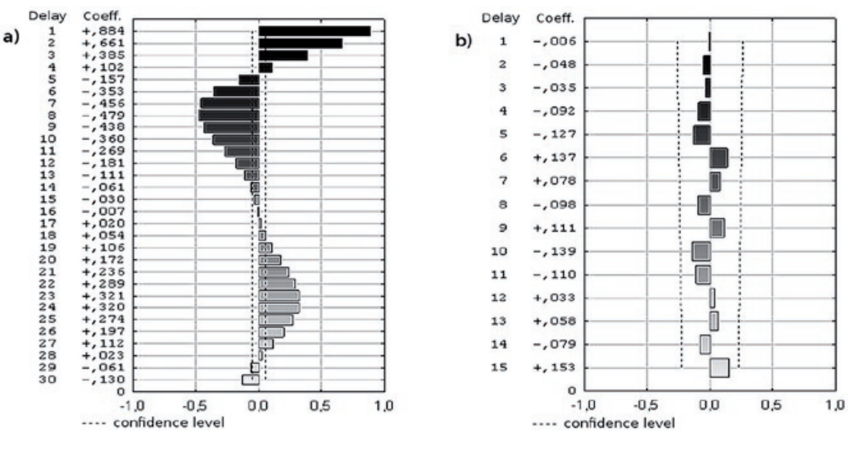

Fig. 6. Autocorrelation coefficients of the air pressure time-series: a) for raw data (variable p, the interval between successive measurements 30s), b) for the average of the subsequent 23 measurements (variable p_{23})

where the period of 30s is a constant interval between successive measurements of the value of variable p. Quasi-periodic nature of the pressure fluctuations p is also confirmed by the results of autocorrelation analysis (Fig. 6), where the ratio of the autocorrelation function for the shift of N_1=23 observations reaches the local extreme.

For the purpose of detecting irregularities in the course of the compressed air production, a new variable p_{23} was created. Variable p_{23} was the arithmetic mean value of 23 consecutive measurements of p. Variable p_{23} calculated for the normal work conditions (the source data taken from Fig. 4) shows no deviations from the normal distribution (Fig. 7). Also, the time-series of the newly created variable does not show the existence of autocorrelation, which was verified by performing the appropriate statistical test [1] (Fig. 6b). It was therefore justified to use standard control charts *X/R* [7] to monitor the course of the compressed air manufacturing process with the quality characteristics p_{23}.

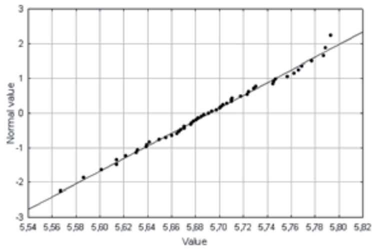

Fig. 7. Normality test for the p_{23} variable being the arithmetic average of 23 consecutive observations of the variable p

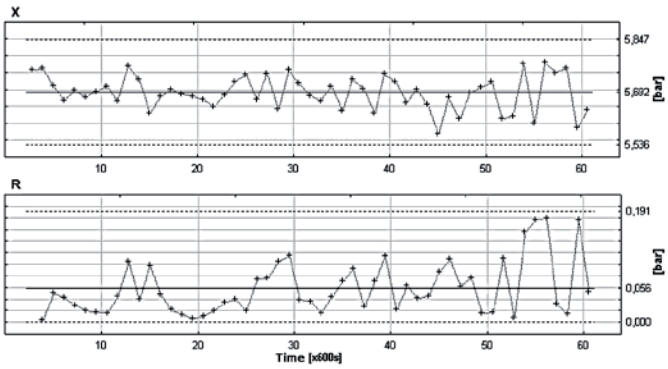

Fig. 8. Control charts X/R for the variable p_{23} during the normal process run (source data from Fig. 4), the sample size n=1

X/R charts for the variable p_{23} made for the normal work of the compressed air plant (from measurements shown in Fig. 4) are shown in Fig. 8. Sample size for the card was set to n=1 to reduce the time delay to detect and signal the disturbance of the process, which may be as long as: N_1*n*30s=11.5minutes.
The central line of the *X* control chart for pressure variable p_{23} is equal to the average of the process assumed to be under control (Fig. 4.). The small eccentricity of the process:

$$\hat{p}_{23} - T = 5.692 - 5.650 = 0.042 = 0.05(USL - LSL) \tag{2}$$

results from the properties of the compressor control algorithm and was accepted in terms of technological requirements. The control limits *LCL*, *UCL* were calculated from the standard deviation of the variable p_{23} (for the same period) which equalled σ_{23}=0.052bar. The statistics of *X/R* that are shown in Fig. 8 confirm the absence of significant deviations from the typical variability in the quality characteristics p_{23}.

The course of air pressure *p* changes in the distribution network during high air demand fluctuations in amplitude and in frequency was shown in Fig. 9. At the beginning of this period, during a small load of the system (for about 30 minutes), only one compressor was working. At the end of this period (about 30th minute), the air demand

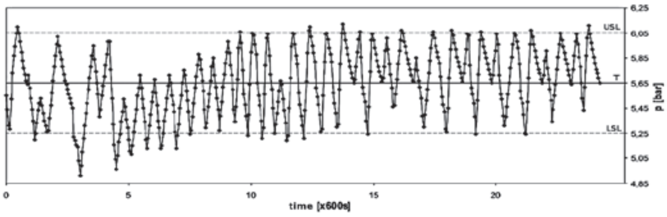

Fig. 9. The air pressure in the distribution network during the time of high demand fluctuations (disturbances)

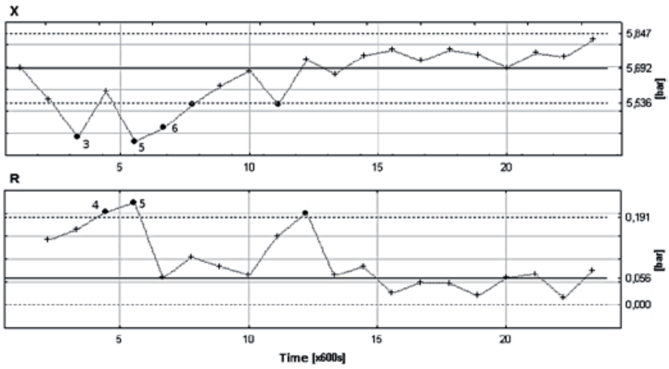

Fig. 10. Control charts X/R for the variable p_{23} at the time of process disturbances (source data from Fig. 10), sample size n=1

increased rapidly, which can be seen in the chart as a steep drop in the network pressure curve. The load in network was, at that moment, so large that one compressor could not supply enough air, so the control system automatically turned on the second machine. From the 35th minute on, the average pressure in the network was increasing. There was, however, a significant, highly dynamical and random "noise" (typical air consumption pattern for the devices performing handling and material displacement operations). It was not until the 80th minute when the network pressure *p* was within tolerance limits.

Control charts *X/R* (*n*=1) for the variable p_{23} made from the data shown in Fig. 9 are presented in Fig. 10. The points on the *X* chart (samples No. 3, 5, and 6) and on the *R* chart (samples No. 4, and 5), clearly indicate the disturbances in the process (insufficient air production). In this situation, the computer control system generates an alarm to notify the operator that the system cannot meet the demand with just two working compressors (the two remaining compressors were switched off permanently). If these conditions lasted for a longer time, a thermal overload might occur (as the one shown in Fig. 3), which would then result in the shutdown of the compressors and a total halt in the compressed air production. Thanks to the alarm generated by the *X/R* charts, the operator could manage the situation before critical alarm occurred and react appropriately by allowing another compressor to work or by reducing the load in the network.

4. Summary

Based on experience of the operators and analysis of the data from nearly two years of operation of compressors with a modernised control and supervision system, three most common causes of compressor downtime were identified:

a) high oil temperature and compressor output air temperature,
b) high air humidity,
c) breakdown (disconnection) of the measurement device or limit switch.

The number of machine malfunctions caused by factors a) and b), was significantly reduced through the use of control charts, whose task was to detect deviations from the natural variability of the process as early as possible. Thanks to the quick diagnosis and applied countermeasures, the compressors were not overloaded and, as a result, were not shut down.

Interference caused by factors from group c) was random and occurred sporadically. As there was no possibility to diagnose the state of the measurement and limit switch circuits, the control and monitoring system did not signal the possibility of failure caused by the events from this group. A similar approach to the assessment of a single compressor was presented in the work [4].

The tangible result of the implementation of the computer control and monitoring system was a significant reduction in the numbers of failures in the compressed air plant. The operator of the system, equipped with diagnostic tools (control charts), could accurately predict the possibility of failure in the majority of cases before they emerged.

Another significant outcome from the implementation of the system was the possibility to control the compressed air network load (compressed air consumption) by the production management personnel. Thanks to the information from the monitoring system, it was possible to plan production operations so as not to cause high and long–term load of compressors, which was the most common cause of emergency production stops.

References

1. Box GEP, Jenkins GM. Analiza szeregów czasowych. PWN, Warszawa, 1971.
2. Cechowicz R, Stączek P. Autonomous Control of Compressed Air Plant. Advances in Manufacturing Science and Technology 2010, 2(34), 71-81, Rzeszów.
3. Cechowicz R, Stączek P. Automatyzacja Procesu Produkcji Sprężonego Powietrza. IM Inżynieria Maszyn R. 11, z. 1 (2006), 112-119.
4. Chen R, Yao W. Experimental Investigation on Reciprocating Air Compressor Performance. Advanced Materials Research 2012; 230-232: 1269-1273.
5. Gupta S, Maiti J, Kumar R, Kumar U. A control chart guided maintenance policy selection, International Journal of Mining, Reclamation and Environment 2009; 23(3): 216-226.
6. Jardine A, Lin D, Banjevic D. A review on machinery diagnostics and prognostics implementing condition–based maintenance, Mechanical Systems and Signal Processing 2006; 20(7): 1483-1510.
7. Montgomery DC. Introduction to Statistical Quality Control. Willey, 1997.

8. Prajapati A, Bechtel J, Ganesan S. Condition based maintenance: a survey. Journal of Quality in Maintenance Engineering 2012; 18(4): 384-400.
9. Rembold U, Nnaji BO, Storr A. Computer Integrated Manufacturing and Engineering, Addison–Weseley, 1993.
10. Shewhart WA. Economic Control of Quality of Manufactured Product. Macmillan And Co. Ltd, London, 1931.
11. Zhang Z, Zhou Y, Sun Y, Ma L. Condition–based maintenance optimisation without a predetermined strategy structure for a two–component series system. Eksploatacja i Niezawodnosc – Maintenance and Reliability 2012; 14(2): 120-129.

Radosław CECHOWICZ
Paweł STĄCZEK
Faculty of Mechanical Engineering
Lublin University of Technology
Nadbystrzycka 36, 20–816 Lublin, Poland
E–mail: wm.ka@pollub.pl

Article citation info:
VALIS D, ZAK L, POKORA O. Engine residual technical life estimation based on tribo data. Eksploatacja i Niezawodnosc – Maintenance and Reliability 2014; 16 (2): 203–210.

David VALIS
Libor ZAK
Ondrej POKORA

ENGINE RESIDUAL TECHNICAL LIFE ESTIMATION BASED ON TRIBO DATA

OCENA TECHNICZNEJ TRWAŁOŚCI RESZTKOWEJ SILNIKA W OPARCIU O DANE TRIBOLOGICZNE

The aim of the paper is to estimate a system technical life. When estimating a residual technical life statistically, a big amount of tribo-diagnostic data is used. This data serves as the initial source of information. It includes the information about particles contained in oil which testify to oil condition as well as system condition. We focus on the particles which we consider to be interesting and valuable. This kind of information has good technical and analytical potential which has not been explored well yet. By modelling the occurrence of particles in oil we expect to find out when a more appropriate moment for performing preventive maintenance might come. The way of modelling and further estimation is based on the specific characteristics of a regression analysis, fuzzy logic and diffusion processes – namely the Wiener process. Following the modelling results we could, in fact, set the principles of "CBM – Condition Based Maintenance". However, the possibilities are much wider, since we can also plan in service operation and mission. All these steps result in inevitable cost saving which we would like to contribute to.

Keywords: *Field data assessment, off-line diagnostics, first hitting time, residual life, maintenance optimization.*

Celem pracy jest ocena trwałości technicznej układu. W ocenie statystycznej technicznej trwałości resztkowej, wykorzystywane są duże ilości danych tribo-diagnostycznych. Dane te służą jako początkowe źródło informacji. Dostarczają informacji nt. cząsteczek zawartych w oleju, które świadczą o jego bieżącym stanie, jak również o stanie całego układu. Szczególny nacisk położono na cząsteczki, które uznano za godne uwagi i wartościowe. Tego rodzaju informacje mają duży potencjał techniczny i analityczny, który nie został jeszcze wystarczająco zbadany. Modelując występowanie cząsteczek w oleju, spodziewamy się określić najlepszy czas na przeprowadzenie konserwacji zapobiegawczej. Sposób modelowania i dalszej oceny oparto o konkretne charakterystyki analizy regresji, logiki rozmytej i procesów dyfuzyjnych-tj.proces Wienera. Śledząc wyniki modelowania możliwe będzie ustalenie reguł utrzymania urządzeń zależnie od ich bieżącego stanu technicznego (condition-based maintenance, CBM). Możliwości są jednak dużo większe, pozwalając także na planowanie eksploatacji rutynowej i zadań. Wszystkie powyższe kroki prowadzą do oszczędności.

Słowa kluczowe: *analiza danych terenowych, diagnostyka off-line, czas pierwszego przejścia, trwałość resztkowa, optymalizacja eksploatacji.*

1. Introduction – motivation

Reliability, safety and availability of complex and time dynamic systems – like mechatronic, communication, space and smart systems – has attracted more and more attention in recent years – see, e.g. [17]. Systems – we would like to present – work in various and mostly adverse operating conditions due to their applications. Therefore it is hardly possible to analyse the reliability of an individual system using prior complex reliability tests, historical pieces of information of other similar systems or using expert judgement. Dependability characteristics are surely of our interest as we are concerned of system reliability and an availability level. However, the reliability and availability level of systems under our observation is highly concerned by designers plus engineers for condition monitoring and maintenance decisions. Based on practical development in this area it emerges that condition-based maintenance has become an attractive research area in past decades – see, e.g. [18–24]. Moreover, for the equipment under our observation there is no actual link, prescription and firm threshold for fixed time maintenance intervals specified in standards – both global (IEC, ISO) and/or specific ones, like, e.g. MIL-STD, STANAGs, etc. The majority of maintenance procedures – specifically the PM intervals – are based on historical observations, similar products´ experience or expert decisions. The firm prescriptions on the fixed time PM intervals on the other hand would be obsolete and very rigid in terms of current technical needs. Based on the information previously introduced, reliability analysis, evaluation and predictive methods for reliability assessment need to take into accountactual, recent and real-time/on-line system conditions during operation. Real-time reliability and availability assessment may act as vital role in condition-based maintenance which may help to form further maintenance and optimisation decisions – some examples see, e.g. [12]. In real processing of data mining there is important need to have also practical applicability of proposed theoretical models and ideas emerging from modelling. We can find some works on tackling the problems of condition-based maintenance in many aspects. For example in [14] there is a problem of predicting the real-time conditional reliability of an individual tool after its performance data was obtained. In [2] there is proposed an on-line reliability estimation method of an individual component based on degradation signals in which the performance was modelled. Products with exponential degradation paths were studied, e.g. in [8], while degradation signal modelling based on exponential smoothing was modelled, e.g. in [3] and [19] – namely the degradation measures with finite duration impulses. In [20] there is considered the existence of multivariate performance measures, while the proposal forthe approach which combines degradation process monitoring with environmental variation is presented in [13].

At present there is a tendency to change the format of technical maintenance. Preventive maintenance (PM) at fixed intervals has been abandoned and condition based maintenance has been introduced instead. This trend might be followed only on condition that high-quality data on system condition is available. In technical literature, e.g. [2, 3, 8, 14], there are different ways of using direct and indirect diagnostic data. There are introduced the possibilities of vibrodiagnostics, thermal radiation, and also tribo-diagnostics there. As for the vibrodiagnostics and the thermal radiation, they frequently appear in existing publications and scientific papers. Regarding the tribodiagnostic data, it has been assessed mainly empirically, restrictedly and by specialists.

During the operation of the observed technical equipment in previous years, a lot of tribodiagnostic data were obtained. The truth is that these data have not been used efficiently. The authors of this article identified the potential of these data and applied it in further analysis. The operation data we possess are firmly given by order to collect observations on diagnostics in course of in-service operation – we speak about tribo-diagnostic data. These data are obtained thanks to parts syntactic methods (Atomic Emission Spectrometry – AES) and morphology observation (Laser Net Finder – LNF). From these data we are about to present these indicators which are really of use in terms of presenting the system real deterioration. No such previous observations and assessment of operating object were conducted. Previous works – see, e.g. [33] – do not speak very deeply about some technical observations and tribo-data as to special big systems like diesel locomotives, mine lorries and war ships. No such extensive investigation has been conducted on medium lorries and common off-road vehicles. What we know for sure is the fact that the tribo data have real potential of presenting system condition. It is probably the most accurate way of determining system state using non-direct diagnostics. Therefore we hope that based on our analytical principles – presented here – real optimisation steps in preventive maintenance planning, costing and mission planning will be allowed/possible to be performed.

There were a few reasons for starting this research. The main reason was obviously to find the way of saving costs during the phase of operation and maintenance of the observed technical equipment. It is rather clear that both the operation and the maintenance have the potential to save costs. The question is how the potential might be identified and used further. The technical literature currently available shows us that the condition based maintenance is a right alternative. However, to introduce this type of maintenance, a certain amount of high-quality data as inputs should be available.

Another reason for assessing and searching for RUL (Residual Useful Life) was to find a lot more adequate model than the ones introduced earlier. The previous models are based on a regression analysis and fuzzy logic which has the potential to support regression models. What we are trying to do in the paper, is to present a new view on the same issue which is supposed to either support the conclusions or disprove them.

2. State-of-the-art and literature survey

Some work in the field of oil data assessment has already been conducted, see, e.g. [10]. In this paper we introduced some fundamental data correlation and characteristics.

In the most recent literature publications a lot of space is devoted to a condition based maintenance. Therefore we have chosen the latest sources dealing with Mean Residual Life (MRL) estimation based on data mining, modelling and other approaches. Deterioration and degradation are other areas we are particularly interested in. For example the work [10] presents the modelling of residual life (MRL – mean residual life) using Proportional Hazards model (PH model) in case of indirect condition monitoring, i.e. the equipment state is not deterministically known. The other work [23] presents possibilities of modelling Remaining Useful Life (RUL) using either a model based approach or a data-driven approach. In [7] we suggested the approach based on a mathematical model for degradation-based signals from a population of components. In work [11] there are methods of estimating the parameters of condition monitored equipment whose failure rate follows the Cox's time-dependent Proportional Hazards Model. The work [28] presents principles of a non-linear model to estimate the remaining useful life of a system based on monitored degradation signals. Approach looking for balance between costs and preventive periodic maintenance is presented e.g. in [21].

A diffusion process with a non-linear drift coefficient with a constant threshold was transformed to a linear model with a variable threshold to characterize the dynamics and nonlinearity of the degradation process (this new diffusion process contrasts sharply with existing models that use a linear drift, and also with models that use a linear drift based on transformed data that were originally nonlinear). The estimation of remaining useful life, an analytical approximation to the distribution of the first hitting time of the diffusion process crossing a threshold level is obtained in a closed form. An effort to estimate the permanent system deterioration is made in [16]. Therefore the level of true degradation determines the appropriate maintenance actions which are to be carried out. It is another approach to modelling the degradation process by segregating it into manifested (temporary) degradation and true (permanent) degradation – equipment degradation. The estimation of true degradation (with the use of quantitative data + imprecise and vague knowledge) is carried out using fuzzy sets and fuzzy inference system (FIS) on the observed condition indicators and process information. The case study presents steel rolling mill equipment – bearings – degradation. In [9]we focused on the development of a prognostic model to estimate MRL (Mean Residual Life) of Rail Wagon Bearings within certain confidence intervals. This work is concerned with the prognosis of mechanical rotating components. It is about the construction of a survival curve from censored data derived from a nonparametric method introduced by Kaplan and Meier. In the work there is also a construction of the degradation curve using Proportional Hazard Models introduced by COX with censored data used for estimating the survival function.

Our paper, however, is also aimed at looking for the RUL of the equipment, but not in the first instance. We would like to get an optimising coefficient for hard time PM as well as tools for mission planning. For that reason we will use a multivariate function approach when determining an optimal threshold for diagnostic indicators. The paper presents two main approaches to the data assessment. The first one is based on a regression analysis and supported by FIS (Fuzzy Inference System). The FIS is a tool which serves either to accept or reject our decisions when selecting a regression course model. The regression approach shall indicate a possible way of determining the ERL (Estimated Residual Life). The second approach introduces another way based on a diffusion process, namely the Wiener process. This should help with determining the expected distribution of FHT (First Hitting Time) which actually represents the RUL distribution.

3. Objects of diagnostics, oil field data and methods of oil assessment

The assumed objects of diagnostics are in our case heavy tracked vehicle engines. These engines have not been ready yet in terms of design to use an ON-LINE diagnostic system. In practice similar possibilities of other applications have already been existing. It results from the information stated above that we are still supposed to use an OFF-LINE engine diagnostics system when sampling lubrication fluid at certain intervals, and using known and optimised special tribodiagnostic methods [34]. In our case we use the results and information from atomic emission spectrometry. Following this analysis we can obtain the information about the presence of the individual elements of a specific kind and the amount of elements. When evaluating data, the information is transformed many times and provides only estimated reality which might be different from reality itself. If the vagueness in classes distribution is not given by a stochastic character of measured characteristics, but by the fact that the exact line among states classes does not exists, it will be later on good to apply a fuzzy set theory and adequate multi-criteria fuzzy logic. However, we cannot identify the real origin of the respective elements – e.g. as results of fatigue, cutting or sliding. Therefore in our further research we try to identify where these elements might come from. We base our assumptions on the idea to increase the potential for maintenance optimisation inputs and cost benefit analysis inputs. We can perform a good analysis as we have a statistically significant set of data. Taking into account the amount of data, the results are believed to be valuable and statistically reliable. We concentrate on Fe particles contents and their presence in the engine of a heavy tracked vehicle.

4. Application of the regression approach

In this part we present the outcomes of regression functions utilization to describe the data forming and course development. We concentrate only on Fe particles and one vehicle engine type, namely a heavy off-road tracked vehicle. In some previous works, see, e.g. [15 and 34] several outcomes have already been presented. Therefore our results here are based only on the most likely regression courses.

Consequently, the dependencies such as a linear, parabolic and base function – a square root plus confidence intervals in all instances will be applied. This will be supported by FIS. The data used for the analysis are listed in Table 1.

Table 1. Input data of Fe particles

Sample / Mh	Fe particles (ppm)	Sample / Mh	Fe particles (ppm)
1/0	17.57	7/46	15.84
2/8	20.88	8/57	16.41
3/11	15.77	9/64	23.15
4/22	19.58	10/72	23.94
5/26	20.53	11/84	20.86
6/35	12.73	12/95	17.59

In view of their random character, a random vector $X = (X_1,\ldots,X_k)$ represents independent variables and a dependent variable is represented by a random variable Y.

When describing and examining the dependence of Y on X, we use a regression analysis, and this dependence is expressed by the following regression function:

$$y = \varphi(\mathbf{x}, \boldsymbol{\beta}) = E(Y|\mathbf{X} = \mathbf{x}), \qquad (1)$$

where $\mathbf{x} = (x_1,\ldots,x_k)$ is vector of numerical variables, y is a dependent variable, $\boldsymbol{\beta} = (\beta_1,\ldots,\beta_m)$ is vector of regression coefficients β_j.

For our data we will look for a regression function in a linear form and we will apply a linear regression model:

$$y = \sum_{j=1}^{m} \beta_j f_j(\mathbf{x}), \qquad (2)$$

where $f_j(\mathbf{x})$ are well-known functions where $\beta_1,\ldots,\beta_m$ are not involved.

For the data we will select gradually the following regression functions for individual item:

- $m=2, f_1(x)=1, f_2(x)=x$, regression function: $y=\beta_1+\beta_2 x$
- $m=3, f_1(x)=1, f_2(x)=x, f_3(x)=x_2$, regression function: $y=\beta_1+\beta_2 x+\beta_3 x^2$
- $m=2, f_1(x)=1, f_2(x)=x^{1/2}$, regression function: $y=\beta_1+\beta_2 x^{1/2}$

The coefficient of determination (R^2) will show its suitability for approximation / data spacing with a relevant regression function. With the coefficient getting bigger, the regression analysis reflects the assessed data better. The form of the coefficient of determination calculation is as follows:

$$R^2 = 1 - \frac{S^*_{\min}}{\sum_{i=1}^{n} y_i^2 - n(\bar{y})^2}, \text{ where } S^*_{\min} = \sum_{i=1}^{n}\left(y_i - \sum_{j=1}^{m} b_j f_{ji}\right)^2. \qquad (3)$$

The outcomes from the regression analysis for group of vehicles of the same type are presented below in figures 1–3.

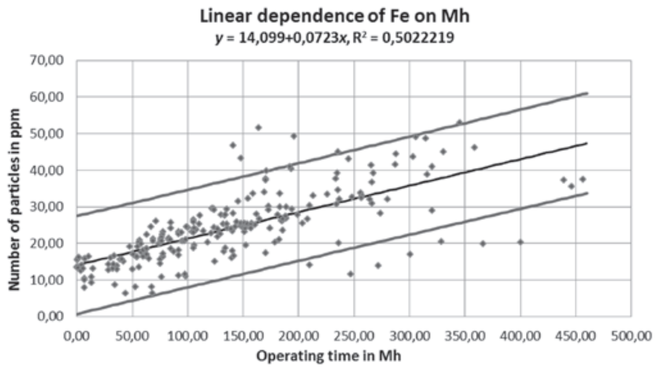

Fig. 1. Linear dependence of Fe particles course (for individual vehicle) on operating time in Mh

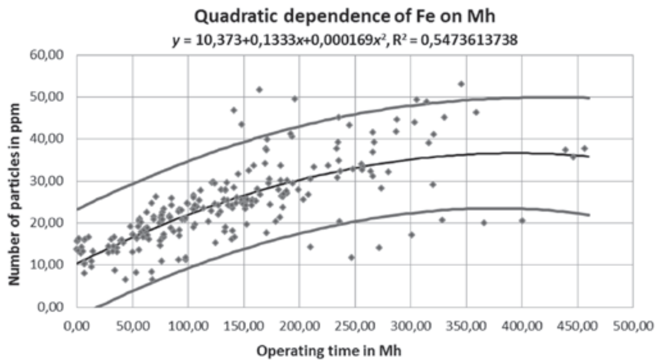

Fig. 2. Quadratic dependence of Fe particles course (for individual vehicle) on operating time in Mh

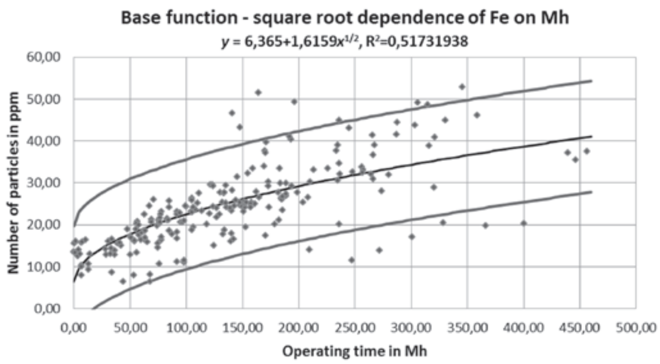

Fig. 3. First base function dependence of Fe particles course (for individual vehicle) on operating time in Mh

5. Utilisation Of Fuzzy Inference System (FIS) to support and to compare with Regression Approach

A Fuzzy Inference System (FIS) is based on the terms a fuzzy *set* and a fuzzy *relation* which were introduced by Lotfi A. Zadeh in 1965. The fuzzy set is one of possible generalizations of the term set. The fuzzy set is a pair ($\mathbf{U}$, μ_A) where $\mathbf{U}$ is a universal set and μ_A: $\mathbf{U} \rightarrow \langle 0,1 \rangle$ is a membership function assigning the elements from U to a fuzzy set A. The membership is marked with $\mu_A(x)$.

Nowadays one of the most widely used applications is a Fuzzy Inference System – FIS (once used as a "fuzzy regulator" term). Two basic types of the FIS are used, and they are Mamdami and Sugeno [22 and 31]. Each FIS consists of input and output variables and FIS rules. For each FIS we specify:

– the number of input and output variables,
– for each input and output the number of predefined values (linguistics values) in the form of fuzzy sets,
– FIS rules described by predefined values.

We do not often expect a fuzzy set to be the FIS output, but we wish to get a single value $z_0 \in Z$, i.e. we want to defuzzify the FIS output. The centroid method is one of the most frequently used defuzzication methods. The FIS specified this way is called *Mamdani* FIS [22].

If we do not know how the process works (i.e. the FIS rules cannot be set), but the sufficient amount of input and output data is available, we can use the modification of Mamdani-FIS Sugeno (Takagi-Sugeno FIS) [22 and 31].

When looking for FIS correlation between output values and input ones as for an unknown process, the method used a lot more frequently is the Sugeno FIS method which is in fact a Mamdani FIS modification. In order to find a relevant FIS, we use the data that serves as a background for the input and output values of the process. In most cases these values are a subset of real numbers, and therefore the inputs and outputs are in a numerical form. The input variables are similar to Mamdani FIS. The output variables Z_j are in constant or linear forms.

$$Z_j = \alpha_j \text{ or } Z_j = \alpha_j + \beta_{1,j}x_1 + \beta_{2,j}x_2 + \ldots + \beta_{n,j}x_n, \quad (4)$$

where α_j, $\beta_{i,j}$ $i = 1, 2, \ldots, n$, $j = 1, 2, \ldots, k$ are suitable constants, k is the number of rules in the FIS model, and n-tuple ($x_1, x_2, \ldots, x_n$) consists of n input variables to the FIS (model). Sugeno FIS output is the value of weighted average Z_j where the weight is obtained by comparing the input ($x_1, x_2, \ldots, x_n$) with predefined input values [22 and 31].

To find a suitable Sugeno FIS, which describes the selected data, it is appropriate to divide the data into tuning and checking data. We find the FIS that corresponds to the tuning data best. The tuning part of data is divided into smaller parts, and predefined input (output) values and the rules describing relationship between relevant inputs and outputs are assigned to each part. There are two basic ways of dividing the data:

– dividing the area (which includes turning data) into smaller parts. A fuzzy set is assigned to each part, and their combination is used for creating rules.
– applying clustering methods to find clusters in data. One rule is made for each cluster.

After selecting the number of fuzzy sets (linguistics values) and rules, we search for appropriate parameters (α_j, $\beta_{i,j}$) using output variables Z_j. These parameters were found through a neural network. The tuning itself results in setting parameters for the FIS to describe assigned tuning data as well as possible. The accuracy is verified by calculating the output values from the test data by the FIS, and then they will be compared with the original output of the test data. The design, tuning and selection of the FIS were performed in MATLAB (Version 5.3) – FuzzyToolbox.

The FIS is applied here in order to support our regression courses and principles. When looking for a correlation between data, fuzzy model results and regression results, we concentrated on quadratic and first base function courses only.Following the results of the regression analysis, we decided in favour ofthese two models, since they have higher R^2 coefficient of determination and therefore the most suitable correlation and inference. We also choose a more strict condition in the form of a mean value of the observed object (vehicles group). The outcomes are presented in Figures 4 and 5.

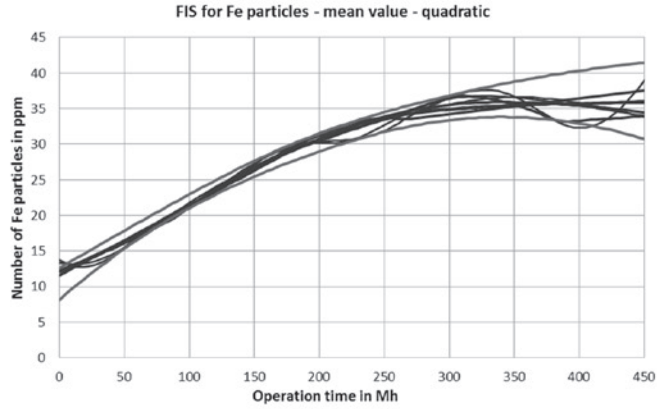

Fig. 4. Comparison of quadratic Fe course and fuzzy model

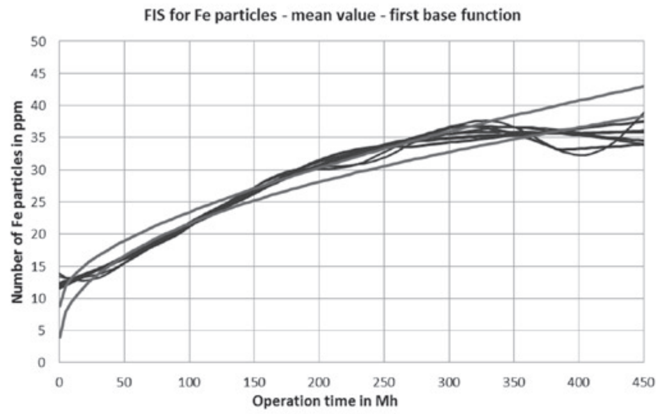

Fig. 5. Comparison of first base function Fe course and fuzzy model

It is remarkable that the expected regression courses of Fe – quadratic and first base – suit also the FIS.

6. Estimation of RUL based on a regression function

It is worthy of attention that a Fe particles generation based on oil field data might have a linear, a quadratic and a base functions course. This correlation and inference outcomes are based on the analysis performed above while using a regression and fuzzy approach. The linear course seems to be the best inference for this particular vehicle engine type. Therefore we take into consideration the linear dependence course. Moreover, we have available data obtained from a similar engine laboratory life test. Such test simulated real engine operation and was performed as an accelerated test until the engine was destroyed. These data and the engine serve as a reference item for a further analysis and comparison. Therefore we decided to try to estimate the residual life based on the reference engine and all the outcomes presented above. We believe that the capability to "read the diagnostic data" might help with mission planning, maintenance optimisation, or, e.g. in a cost benefit analysis. Some sources of inspiration can be found, for example, in [1, 4, 5, 16, 25, 26, 27, 29, 30, 32, 35]. The interval estimation of residual life was made on the basis of the Fe particles analysis and the results of the accelerated life test. Its value is rated on a scale of 220 Mh to 257 Mh. It results from the set interval and the real value declared for oil change that in practice the oil is changed when its durability is higher than 50%.In Figure 6 there is a graphical presentation of the RUL estimation.

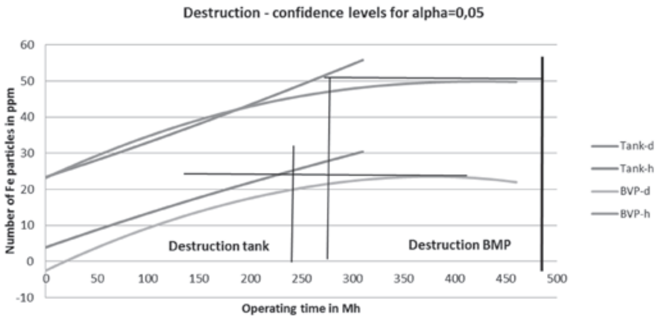

Fig. 6. RUL estimation based on regression

7. Utilization of the Wiener process

As it has been mentioned before, the data are available in a big amount – it is a statistically important set. The data is collected at intervals and under conditions determined by a methodology which includes:

- homogenous time intervals given by technical equipment mileage,
- oil temperature and right oil mixing,
- the same place of sample collection,
- the same way of performing the tribo analysis after the sampling.

When applying the Wiener process, we use some outcomes from a regression analysis. These regression outcomes are re-calculated into a usable form. The example of the data form is in Table 2.

Table 2. Input data of Fe particles – example

Sample / Mh	Fe particles (ppm)	Standard deviation mean value	Standard deviation individual value
1/0.15	13.71158	0	4.753368309
2/0.30	13.72016	0.001014608	4.753368417
3/0.45	13.73055	0.002029216	4.753368742
4/0.60	13.74004	0.003043824	4.753369284
5/0.75	13.74953	0.004058431	4.753370042
6/0.90	13.75902	0.005073039	4.753371016

We assume that the case we observe is a stochastic process with time dependence. The generation of Fe particles is time dependant. Therefore the application of a diffusion process seems to be perfectly adequate. Due to the normal distribution of a random variable and its application capabilities, the Brownian motion might be used universally. The application of the Brownian motion can be found in many areas. The Brownian motion is usually modelled with differential equations. We select one specific example of diffusion processes and that is the Wiener process [37]. The rules of the general Wiener process might be specified as follows. A real stochastic process $\{W(t)\ t\in\langle 0; +\infty)\}$ in a probability space (Ω, A, P) will be called the *Brownian motion* or the *Wiener process* if the following applies:

1. $W(0) = 0$,
2. $W(t) - W(s)$ has $N(0, t - s)$ distribution for $t > s \geq 0$,
3. For arbitrary $0 < t_1 < t_2 < \cdots < t_n$ increments $W(t_1)$, $W(t_2) - W(t_1)$, $W(t_3) - W(t_2)$, . . . , $W(t_n) - W(t_{n-1})$, $W(t)$ trajectories are mutually independent random variables and continuous almost everywhere.

Next, it applies that:

1. $E[W(t)] = 0$ for $t \geq 0$
1. Var $[W\hat{\ }2(t)] = t$ for $t \geq 0$

The Wiener process represents one possible form of diffusion processes. It is actually the integral of what in practical applications is called a white noise. The Wiener process with a drift will be used in our application. The initial mean value (drift) is β_1 and standard deviations for each time increment have been previously calculated – see Table I. For our model we apply the Wiener process with a drift given by a stochastic differential equation:

$$dY(t) = \mu \cdot dt + \frac{\sigma \cdot dW(t)}{\sqrt{(t)}} \tag{4}$$

where dW(t) is increment of the Wiener process and dt is increment of time, σ is a standard deviation (either of an individual or a mean value), μ is a mean value, t is an instant of time, process initial value $Y(0) = \beta_1$. Time increment for modelling was 0.15 Mh. When modelling and simulating, we apply the course of an individual and a mean value, as shown in Fig. 7 and 8. The critical value of particles amount is 50.

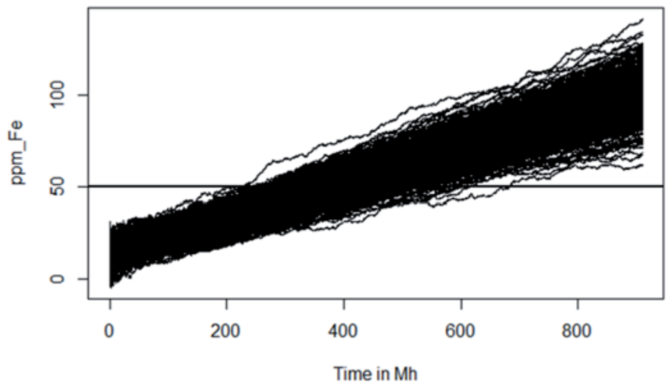

Fig. 7. Course of Wiener process simulation for an individual value

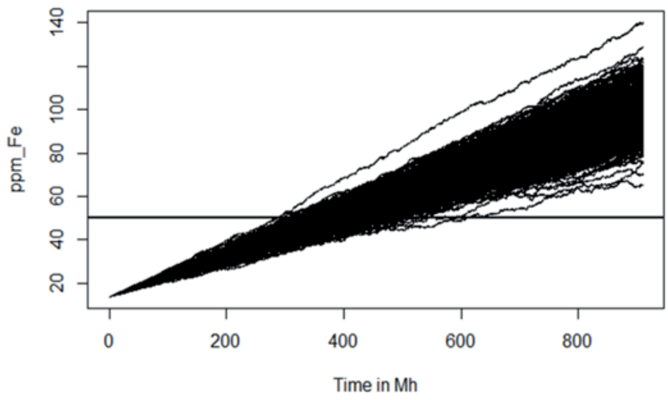

Fig. 8. Course of Wiener process simulation for mean value

We take into account the 95% interval of trajectories which achieve a critical value 50. The vertical line 200 shows a determined interval of PM. These intervals are for an individual and a mean value and are put in Figure 9 and Figure 10.

In order to determine the First Hitting Time (FHT) distribution of an individual and a mean value, we set histograms and performed tests for a presumed type of distribution. The expected types of probability density distribution such as Gamma (full/firm line), LogNorm (dashed line – overcovered by IGD), Inverse Gaussian (IGD) – dotted

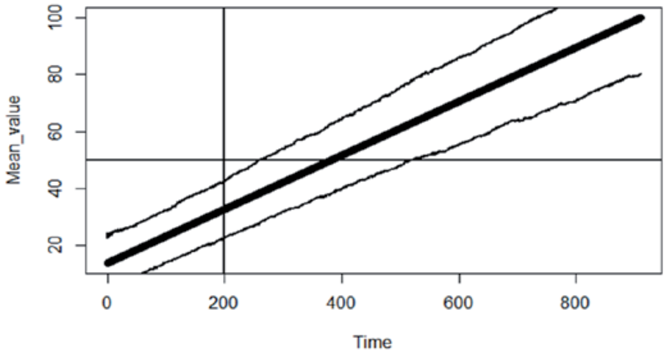

Fig. 9. Confidence interval thresholds – 95% for an individual value

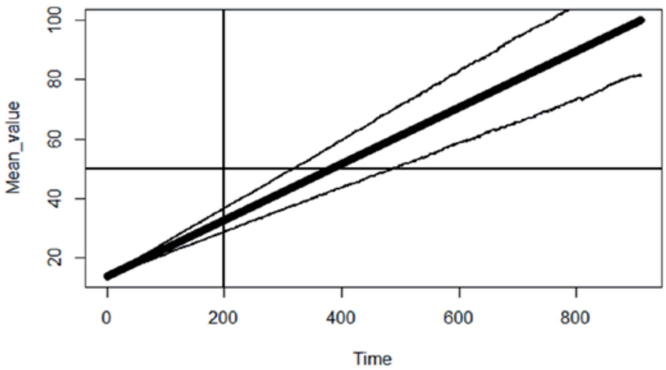

Fig. 10. Confidence interval thresholds – 95% for a mean value

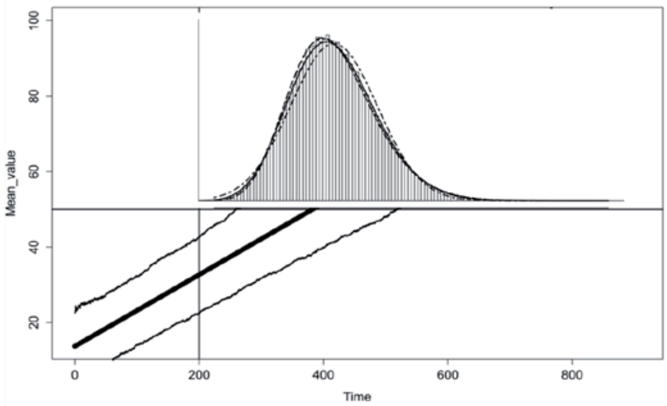

Fig. 11. Course of FHT pdf for an individual value

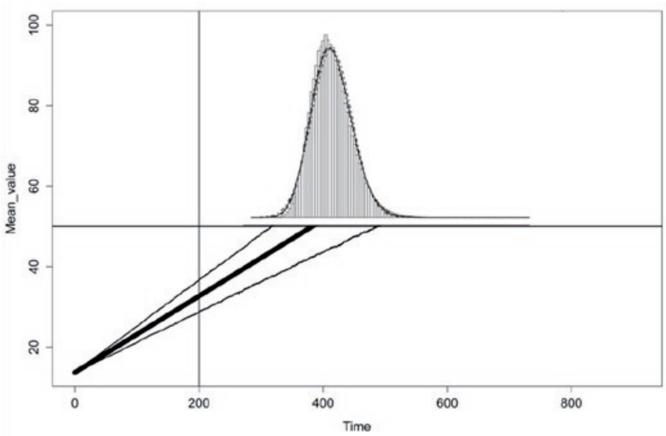

Fig. 12. Course of FHT pdf for a mean value

line), Normal (dash and dotted line) or Weibull's were not proved. The courses of these tested distributions are shown in Fig. 7 and Fig. 8. We expect then to obtain the FHT distribution only in the form of an empiric distribution function.

8. Estimation of RUL based on the Wiener process

The tested values reached for the individual value the following limits: a minimum value = 134 Mh, a lower confidence interval 2.5% = 265 Mh, an upper confidence interval 97.5% = 524 Mh, a mean value = 382 Mh, median = 378 Mh, maximum = 887 Mh.

As to the mean value, the following limits were achieved: a minimum value = 258 Mh, a lower confidence interval 2.5% = 315 Mh, an upper confidence interval 97.5% = 480 Mh, a mean value = 385 Mh, Median = 381 Mh, Maximum = 746 Mh.

It follows from the results stated above that the mean value is more or less the same, but the lower threshold of confidence intervals is not. However, the lower confidence intervals are interesting for us in order to determine the possible beginning of the PM interval. But if we used the mean value, it would be sufficiently far from the original/fixed PM interval. On the basis of the results we could work with a conservative version and set a new PM interval using the lowest value of a lower threshold of a confidence interval. This would be 265 Mh (an individual value). If we were for a benevolent alternative, we could rely on the mean value and set the PM interval at 380 Mh (more or less the same for both the individual and the mean value).

When planning a mission, we could work with versions that if common operating conditions were observed, a vehicle could be operated with one oil filling theoretically up to the upper confidence limit 97,5%. Considering conservative or benevolent versions, it would be 480 Mh, or 520 Mh.

9. Discussion

Since we have worked with two approaches to one problem, it is always interesting to compare the results. As we can see, the obtained values of RUL estimations do not differ when working with conservative estimations. The procedure based on the Wiener process, however, is somewhat clearer and brings better analytical results. The form of RUL estimation is better to determine. It is also much easier to introduce other forms of a particle production course, not only the linear one. Following this assumption – applying a quadric, or a base function course, we can develop our further procedure and research. Assessing available oil data, however, has a lot greater potential.

10.Conclusion

In this article we have introduced possible approaches to modelling indirect diagnostic measures. Our intention was to introduce a coherent research form when dealing with indirect oil diagnostic data and analyze it with different approaches / ways. Owing to the different approaches, we were able to present quantitative RUL values which are in view of PHM or CBM very important.

The achieved results complement the set of approaches to the indirect observation of a technical condition. Following the conclusions of modelling with the Wiener process, the results of previous approaches might be completed when searching for:

- optimum interval PM,
- recommended/allowed time for mission completion,
- optimizing dependencies of life cycle cost analyzing.

The approach introduced above opens the possibilities of analyzing other essential diagnostic indicators. The setting of the time derived from the histogram and pdf course should be as accurate as possible and undistorted.

In our further analysis we are going to develop the Wiener approach even more and complement it with other approaches like ARIMA or ARMA methods.

***Acknowledgement**: This paper has been prepared with the great support of the project for the institutional development of K-202 University of Defenceand with support of the project of Ministry of Defence of the Czech Republic – BOPROS nr. OFVTUV2013002.*

Bibliography

1. Bartlett LM, Hurdle EE, Kelly EM, Intergrated System Fault Diagnostics Utilising Diagraph and Fault Tree-based Approaches 2009; Reliability Engineering and System Safety, 9(94), 1371-1380.
2. Chinnam RB, On-line reliability estimation for individual components using statistical degradation signal models. Quality and Reliability Engineering International 2002; 18, 53-73.
3. Chinnam RB. On-line reliability estimation of individual components, using degradation signals. IEEE Transactions on Reliability 1999; 4(48), 403-412.
4. Cornak S. Selected Problems of Drivers Microclimate. Proc. International Conference Transport Means 2009; Kaunas: University of Kaunas, 124-127.
5. Cornak S, Skolil J. The Selected Aspects of Life Fluids Evaluation. Proc. International Conference on Military Technologies, ICMT 2009, Brno: UO, 39-45.
6. Edleston OSST, Bartlett LM. A Tabu search algorithm applied to the staffing roster problem of Leicestershire police force. Journal of the Operational Research Society 2012; 4(63), 489-496.
7. Gebraeel N, Pan J. Prognostic Degradation Models for Computing and Updating Residual Life Distributions in a Time-Varying Environment. IEEE Transaction on Reliability 2008; 4(57), 539-550.
8. Gebrael NZ, Lawley MA, Li R, Ryan JK, Residual-life distribution from component degradation signals: A Bayesian approach 2005; IIE Transactions, 37, 543-557.
9. Ghasemi A, Hodkiewicz MR. Estimating Mean Residual Life for a Case Study of Rail Wagon Bearings. IEEE Transaction on Reliability 2012; 3(61), 719-730.
10. Ghasemi A, Soumaya SY, Ouali MS. Evaluating the Reliability Function and the Mean Residual Life for Equipment With Unobservable States. IEEE Transaction on Reliability 2010; 2(59), 426-439.
11. Ghasemi A, Yacout S, Ouali MS. Parameter Estimation Methods for Condition-Based Maintenance With Indirect Observations. IEEE Transaction on Reliability 2010, 2(59), 426-439.
12. Jardine AKS, Lin D, Banjevic D. A review on machinery diagnostics and prognostics implementing condition-based maintenance 2006. Mechanical Systems and Signal Processing, 7(20), 1483-1510.
13. Kharoufeh JP, Cox SM. Stochastic models for degradation-based reliability. IIE Transactions 2005; 37, 533-542.
14. Kim YS, Kolarik WJ. Real-time condition reliability prediction from on-line tool performance data. International Journal of Production Research 1992; 8(30), 1831-1844.
15. Koucky M, Valis D. Suitable approach for non-traditional determination of system health and prognostics. Zeszyty naukowe 2011; 1(159), 123-134.
16. Kumar EV, Chaturvedi SK, True degradation estimation of industrial equipment with fuzzy sets: a case study. Proceedings of the Institution of Mechanical Engineers Part O – Journal of Risk and Reliability 2009; 2(223), 167-179.
17. Labeau PE, Smidts C, Swaminathan S. Dynamic reliability: Towards an integrated platform for probabilistic risk assessment. Reliability Engineering and System Safety 2010; 3 (68), 219-254.
18. Li W, Pham H, An inspection-maintenance model for systems with multiple competing processes. IEEE Transactions on Reliability 2005; 2(54), 318-327.
19. Lu H, Kolarik WJ, Lu SS. Real-time performance reliability prediction. IEEE Transactions on Reliability 2001; 4(50), 353-357.
20. Lu S, Lu H, Kolarik WJ. Multivariate performance reliability prediction in real-time. Reliability Engineering and System Safety 2001; 72, 39-45.
21. Maillart LM, Pollock SM. Cost-optimal condition-monitoring for predictive maintenance of 2-phase systems. IEEE Transactions on Reliability 2002; 3(51), 322-330.
22. Mamdani EH, Applications of fuzzy logic to approximate reasoning using linguistic synthesis. IEEE Transactions on Computers, 12(26), 1182-1191.
23. Medjaher K, Tobon-Mejia DA, Zerhouni N. Remaining Useful Life Estimation of Critical Components With Application to Rearing. IEEE Transaction on Reliability 2012; 2(61), 292-302.
24. Park KS. Condition-based predictive maintenance by multiple logistic function. IEEE Transactions on Reliability 1993; 4(42), 556-560.
25. Rak J, Pietrucha K. Risk in drinking water quality control. Przemysl Chemiczny 2008; 5(87), 554-556.
26. Revie M, Bedford T, Walls L. Supporting Reliability Decisions During Defence Procurement Using a Bayes Linear Methodology. IEEE Transactions on Engineering Management 2011; 4(58), 662-673.
27. Shafti F, Bedford T, Deleris LA, Hosnins JRM, Shen H, Walls L. Service operation classification for risk management. IBM Journal of Research and Development 2010; 3(54), 662-673.
28. Si XS, Wang W, HuCh H, Zhou DH, Pecht MG. Remaining Useful Life Estimation Based on a Nonlinear Diffusion Degradation Process. IEEE Transaction on Reliability 2012; 1(61), 50-67.
29. Stodola J, Stodola P. Mechanical System Wear and Degradation Process Modelling. Transactions of Famena 2010; 4(34), 19-32.

30. Stodola P, Jamrichova Z, Stodola J. Modelling of Erosion Effects on Coating of Military Vehicles Components. Transactions of Famena 2012; 3(36), 33-44.
31. Sugeno M. Industrial applications of fuzzy control. Elsevier Science Pub. Co., 1985.
32. Titrou A, Bedford T, Walls L. Bayes geometric scaling model for common cause failure rates.Reliability Engineering and System Safety 2010; 2(95), 70-76.
33. Toms LA, Toms AM. Machinery Oil Analysis - a Guide for Maintenance Managers, Supervisors and Technicians. Society of Tribologists and Lubrication Engineers 2008.
34. Vališ D, Koucký M, Žák L. On approaches for non-direct determination of system deterioration. Eksploatacja i Niezawodnosc – Maintenance and Reliability 2012; 1(14), 33-41.
35. Valis D, Vintr Z, Koucky M. Contribution to highly reliable items' reliability assessment. Reliability, Risk and Safety: Theory and Applications, Proceedings of the European Safety and Reliability Conference, ESREL 2009; Prague, Czech Republic, 2010; 1-3: 1321-1326.
36. Yang SK. A condition based failure-prediction and processing-scheme for preventive maintenance. IEEE Transactions on Reliability 2003; 3(52), 373-383.

David VALIS
Department of Combat and Special Vehicles
Faculty of Military Technologies
University of Defence
Kounicova 65, 662 10 Brno, Czech Republic
E-mail: david.valis@unob.cz

Libor ZAK
Department of Applied Mathematics
Faculty of Mechanical Engineering
Brno University of Technology
Technicka 2896/2, 616 69 Brno, Czech Republic
E-mail: zak.l@fme.vutbr.cz

Ondrej POKORA
Department of Mathematics and Statistics
Faculty of Natural Sciences
Masaryk University
Kotlarska 267/2, 611 37 Brno, Czech Republic
E-mail: pokora@math.muni.cz

Article citation info:
CZMOCHOWSKI J, MOCZKO P, ODYJAS P, PIETRUSIAK D. Tests of rotary machines vibrations in steady and unsteady states on the basis of large diameter centrifugal fans. Eksploatacja i Niezawodnosc – Maintenance and Reliability 2014; 16 (2): 211–216.

Jerzy CZMOCHOWSKI
Przemysław MOCZKO
Piotr ODYJAS
Damian PIETRUSIAK

TESTS OF ROTARY MACHINES VIBRATIONS IN STEADY AND UNSTEADY STATES ON THE BASIS OF LARGE DIAMETER CENTRIFUGAL FANS

BADANIA DRGAŃ MASZYN WIRNIKOWYCH W STANACH USTALONYCH ORAZ NIEUSTALONYCH NA PRZYKŁADZIE WENTYLATORÓW PROMIENIOWYCH DUŻYCH ŚREDNIC*

The existence of unsteady states of rotary machines is a common problem. It occurs mainly during the machine start-up and is caused by "passing through" the critical velocity, which activates large scale object vibrations. Moreover, rotary machines vibrations problems are caused by faults such as unbalance, misalignment, bearing defects and others. The paper presents the results of tests of sample centrifugal fans vibrations, both in steady and unsteady states. The recorded time traces of non-stationary vibrations were analyzed with the STFT spectrum. This method allowed to identify main parameters influencing the level of vibrations during the start-up and regular operation of the machine. The tests were performed on four machines, which enabled an additional comparison of operational parameters of the whole flow system.

Keywords: *rotary machines, unsteady states, vibrations.*

Problem występowania stanów nieustalonych maszyn obrotowych jest powszechnie spotykany. Pojawia się on głównie podczas rozruchu i wywołany jest „przechodzeniem" przez prędkość krytyczną, która wzbudza drgania obiektu w bardzo szerokim zakresie. Ponadto problemy z drganiami maszyn obrotowych wywoływane są przez takie czynniki jak niewyważenie, niewyosiowanie, defekty łożysk i wiele innych. W pracy przedstawiono wyniki badań drgań zarówno w stanach ustalonych jak i nieustalonych przykładowych wentylatorów promieniowych. Za pomocą widm STFT przeanalizowano zarejestrowane przebiegi drgań niestacjonarnych. Dzięki temu możliwe było zidentyfikowanie głównych parametrów mających wpływ na poziom drgań podczas rozruchu oraz pracy normalnej. Badania przeprowadzono na czterech obiektach, co umożliwiło dodatkowe porównanie i wyciągnięcie wniosków odnośnie parametrów eksploatacyjnych całego układu przepływowego.

Słowa kluczowe: *maszyny obrotowe, stany nieustalone, drgania.*

1. Introduction

Vibrations in steady and unsteady states [18] occur in almost all cases of rotary machines operation. In the first case, vibrations occur during the nominal operation of the machine and, generally, if the technical condition of the machine is good, do not constitute a significant operational problem. The other type of vibrations occurs during the start-up and braking of a supercritical machine. If the rotary machine is set in motion properly and under control, vibrations occurring during the operation are not a significant risk. It is important to smoothly and quickly "pass through" critical velocities of the rotary machine. The critical velocity matching resonance frequency might become a cause of damage of the machine, if the start-up is not performed properly. Rotation of the elements with the critical velocity provides high energy of excitation in wide spectrum. This causes resonance vibrations of the system. It has to be noted that the critical velocity of the rotor, often matching the frequency of its natural vibrations, is not the only resonance area in which the fan may operate. In the case of more complex machines, the frequency of natural vibrations of particular elements, e.g. a casing has to be taken into account. Additionally, in the case of fan rotors, it has to be remembered that the excitation frequency equals the rotary frequency of the shaft but also the blade passing frequency, which is the product of the number of blades and a rotary velocity of the shaft [16]. Moreover, numerous flow effects cause dangerous vibrations of fan elements in other frequency ranges [7, 8, 25].

The level of excitation energy is also influenced by significant assembly and operating factors such as static and dynamic balancing of rotary elements, alignment of connections, bearings condition, electromagnetic interference and others [3, 6, 8, 9].

Proper operation of fans, particularly those of huge power and large diameters, not only decreases operating costs but also increases the safety of work. Their proper operation ensures constant air exchange and suction of dangerous gases in the mine pits, which along with safety systems [14, 15] protects pit mine workers. In the paper the results of vibrations tests of centrifugal fans responsible for ventilation of the mine are presented. Flow regulation of this type of fans is based on the fan airflow-pressure curve, where areas of unstable operation are located, which is unfavorable for the object. Tests performed during the machine operation allow to obtain key information for proper operation of the machine. Such tests are significant due to general lack of information regarding the subject of this type of machine behavior in the industry and because of the fact that the previous research was performed at a smaller scale in the laboratory

(*) Tekst artykułu w polskiej wersji językowej dostępny w elektronicznym wydaniu kwartalnika na stronie ***www.ein.org.pl***

[7, 25]. The analysis and interpretation of the results were granted as well. The goal of the tests was to verify correctness of the flow system operation parameters and analyze possibility to increase the system functionality and efficiency, which was related to the fact that the systems were designed in 1970's.

2. The analysis of vibrations in diagnostics of the rotary machines

Machine vibrations are an important diagnostic symptom. It concerns a large number of machines operating in different conditions and industrial, civil and military applications [4, 12]. The analysis of vibration signals allows to verify the condition of the machine and is performed in order to verify damages of elements such as toothed wheels, bearings, rotary machines parts [1, 11, 17, 22]. However, verification of turbomachines vibrations may be frequently more difficult than single machine elements, due to a larger number of factors influencing the recorded vibration signal. These can include phenomena resulting from the flow of the medium and related pressure pulsation. The problem of an influence of the flow phenomena on the flow machine vibrations and noise emitted was discussed in numerous publications, e.g. [2, 7, 13, 22, 23, 25].

Among numerous methods of vibrations analysis for diagnostic purposes [5, 10, 17, 21, 22] those based on the Fourier's analysis [10, 21, 24] are widely applied. This method allows transition from the time to frequency domain and is based on the concept according to which each signal may be presented as the sum of different amplitudes and frequencies sinusoidal signals [21, 24]. Because of the commonly applied digital record of the signal, in practice the Fourier's analysis results in application of the Discrete Fourier Transform (DFT) [21]:

$$G(k) = \frac{1}{N}\sum_{n=0}^{N-1} g(n)\exp(-j2\pi kn/N) \cdot \quad (1)$$

The algorithm enabling quick calculation of DFT is so called Fast Fourier Transform (FFT) [21]. The trace of vibrations amplitude in the frequency function achieved through this method allows to specify characteristic frequencies occurring during the machine operation.

In the case of rotary machines in which the states of unsteady operation occur, characteristic frequencies change in time, especially during the operation in the aforementioned states. In this case application of the Fourier Transform, in which integration takes place during the whole period of time, is not sufficient to recognize frequency changes over time. Due to that fact, in the vibrations analysis, it is reasonable to apply Short Time Fourier Transform (STFT), which is based on the Fourier's analysis performed within the narrow time frame displaced according to the agreed parameters of length, resolution or overlapping of frames. This method allows to observe relation of frequency and time and recognize transition states of the machine operation. The relation defining the STFT method is presented as follows [21]:

$$S(f,\tau) = \int_{-\infty}^{\infty} x(t)\varpi(t-\tau)\exp(-j2\pi ft)dt \ , \quad (2)$$

where $\varpi(t)$ corresponds to the time frame displaced during data acquisition.

Due to numerous advantages in diagnostics of the rotary machines the analysis of data presented in the paper was performed in accordance with the STFT method.

3. Tested objects

The main ventilation system of a mine, which is the subject of the test, uses centrifugal fans denoted in Poland as WPK - 5,35, which in connection with the fan stations enable the mine ventilation. In the figure 1 the WPK-5.35 fan is presented.

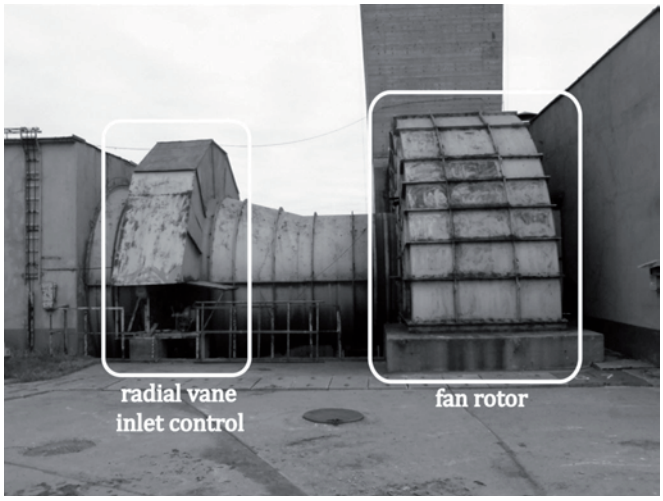

Fig. 1. Centrifugal fan WPK – 5.35

Vibrations of casings, channels, inlet vanes and air shutters noticed during fans operation negatively influence the working conditions. In order to precisely specify the level and cause of vibrations the tests were performed during the start-up of each fan at the station. Additionally, the tests were performed during the opening of the inlet vanes (figure 2), in order to determine the influence of different flow effects occurring during that process on the level of fan vibrations.

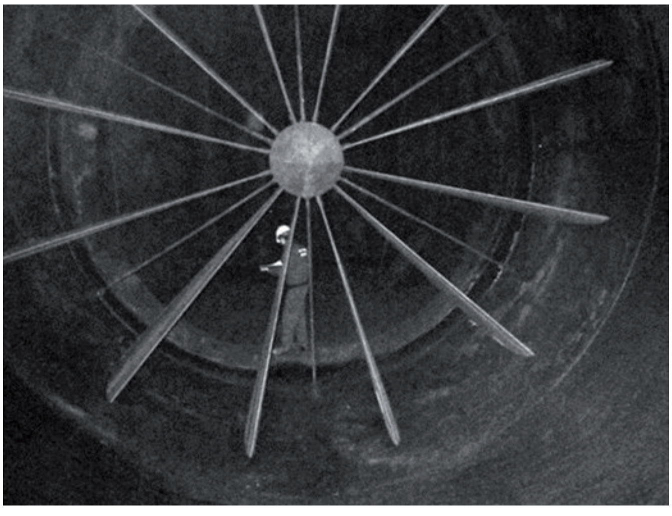

Fig. 2. Radial vane inlet control of the fan

4. Experimental tests

The goal of the tests was to record the vibrations velocity level in the ventilation systems during unsteady (start-up, opening of the inlet vanes) and steady states (regular operation). The tests were performed on the casings and intake channels of the fans and on the bearings housing of the rotors shafts. The identical arrangements of sensors, which is presented in the figures 3 and 4, were applied to all fans. Four WPK-5.35 ventilators, which cooperate within two different types of fan stations, were selected.

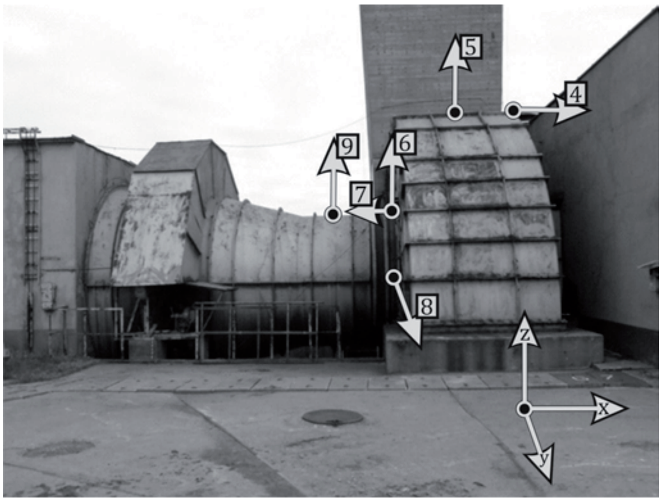

Fig. 3. Arrangement of measuring sensors on the fan casing

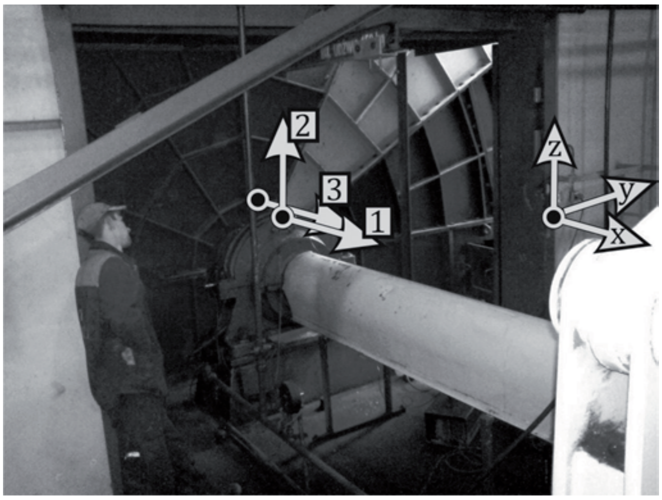

Fig. 4. Arrangement of measuring sensors on the fan casing

Sensors in the measuring channel 1 and 2 were placed on the housing of the shaft bearing located closer to the rotor. The sensors on the other seven channels were placed directly on the rotors casings and the intakes channels. A detailed description of directions and arrangement of sensors on particular channels is presented in the table 1. Setting directions of the sensors are in compliance with the coordinate system presented in the figures 3 and 4.

Table 1. Arrangement of measuring points

Channel no.	Direction	Location
1.	X	shaft bearing housing
2.	Z	shaft bearing housing
3.	X	fan casing
4.	X	fan casing
5.	Z	fan casing
6.	Z	fan casing
7.	X	fan casing
8.	Y	fan casing
9.	Z	fan casing

In the figure 5 the sensor on the channels no. 2 and 3 is presented. In the figure 6 the whole measuring system during the acquisition process is presented.

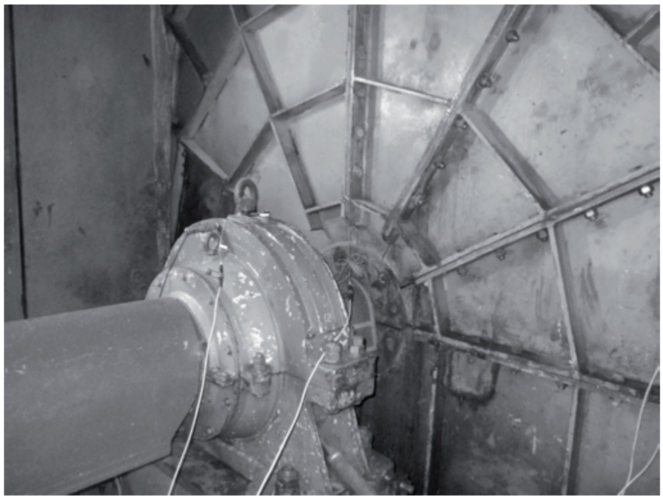

Fig. 5. Sensors on channels 2 and 3

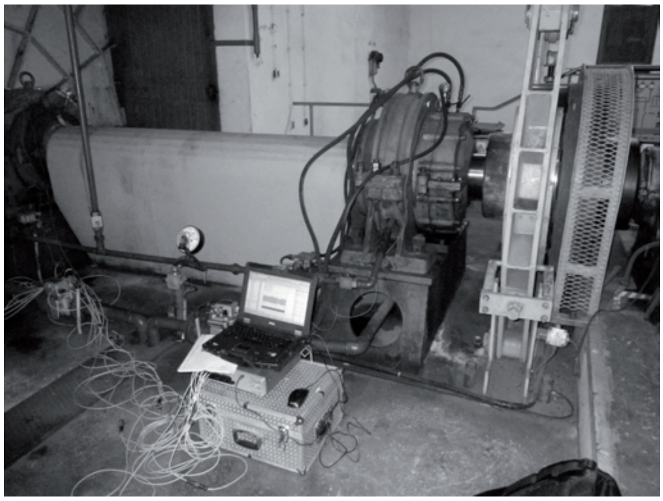

Fig. 6. Sensors installation and data acquisition

5. Tests results

Figures 7–10 present selected STFT diagrams recorded on the selected fan. Characteristic changes of frequency in particular phases of the fan operation are presented in the figure 7.

The change of the blade passing frequency, which increases during the start-up, is easily noticed. Less clear, but also noticeable, are vibrations coming from the start-up system. Their frequency decreases to 50 Hz when the fan operates with its nominal revolutions. Particular attention should be paid to the stage in which the fan achieves the nominal revolutions (375 rpm [19]) but the inlet vanes have not yet been opened. It is clearly recognized that this is an unfavorable moment for the system as it causes strong activation of vibrations in the whole range. After opening of the inlet vanes, the stable operation of the fan and related characteristic frequencies of vibrations are recognized. In all figures presenting spectrum vibrations recorded by sensors located on the casing (figure 7-9) the aforementioned blade frequency of the rotor amounting to about 50Hz is clearly noticed. Its harmonic 100 Hz and 150 Hz are observed as well. A detailed interpretation of vibrations visible on the STFT diagrams will be possible after performing numerical, experimental or operational modal analysis. As a result, mode shapes and frequencies of natural vibra-

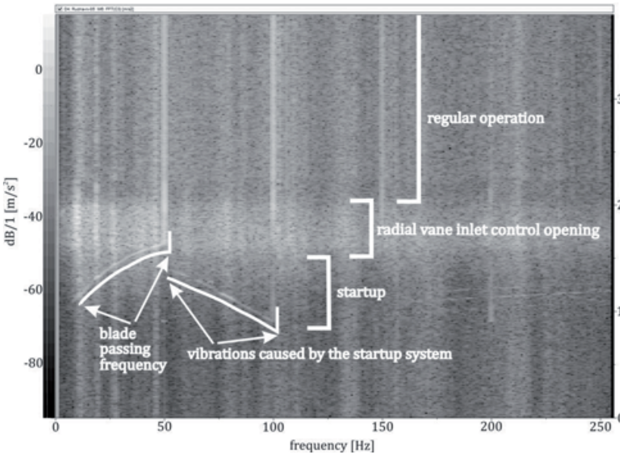

Fig. 7. W3 fan start-up – channel 3 (direction x, fan casing)

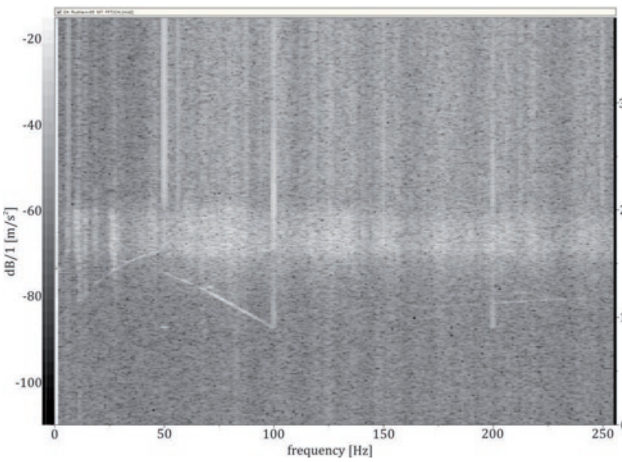

Fig. 8. W3 fan start-up – channel 4 (direction x, fan casing)

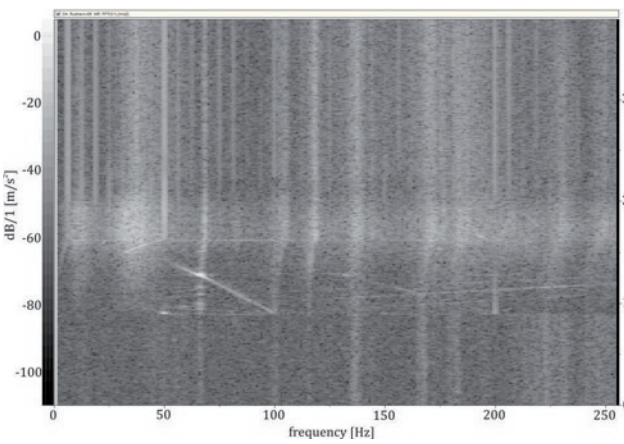

Fig. 9. W3 fan start-up – channel 5 (direction x, fan casing)

tions will be specified and it will be possible to identify them on the presented diagrams.

The results obtained from the sensors recording bearing vibrations (in the figure 10 the spectrum of vibrations into the x direction is presented), tightly correlate with the fan casing vibrations, yet the level of acceleration is significantly lower. However, a significant difference in spectrums during the start-up and operation of the fan is noticed. During the start-up, the sensors located on the bearing do not record changes of blade velocity (vibrations are induced by the flow and influence only the fan casing). It is observable only after reaching the nominal velocity, when the flow pulsations are strong enough to influence the whole system. Also, a frequency not recorded on the fan

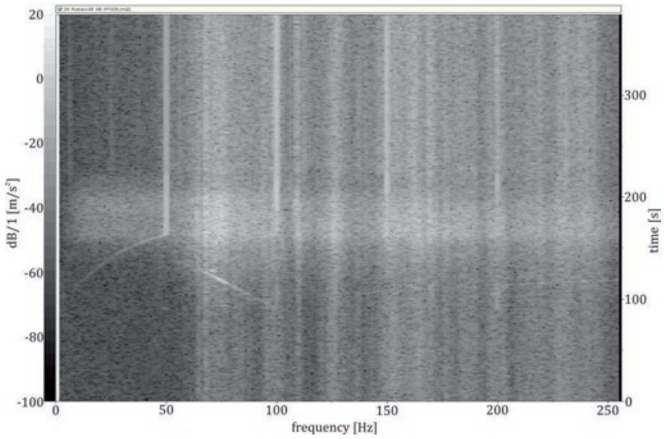

Fig. 10. W3 fan start-up – channel 1 (direction x, bearing housing)

casing amounting to about 6.25 Hz occurs. This corresponds with the rotary frequency and vibrations are induced by an unbalance of the shaft and rotor.

In the case of other fans, vibrations spectrums are similar. What distinguishes particular fans is a difference between duration of the start-up and opening of the inlet vanes. In the first case the start-up of the fan proceeded efficiently and it is difficult to notice on the STFT spectrum changing blade and start-up frequencies, as they after a while decline in the vibrations of the whole system caused by still unopened inlet vanes. The list of the vibrations levels is presented in the table 2.

In the table the levels of maximum vibrations and root mean square (RMS) of vibrations for an unsteady state (start-up and opening of the inlet vanes) and for a steady state (operation with a nominal rotary velocity and open inlet vanes) are presented. In order to verify in which case (on which fan) the situation is the least favorable, the vibrations levels in particular channels are compared. The color font of the values indicates the maximum value of vibrations velocity or RMS in a particular channel (in the particular measuring point) recorded in an unsteady state among all tested fans. The values in the color boxes indicate respectively the maximum value of vibrations velocity or RMS in the particular channel (in the particular measuring point) recorded in a steady state among all tested fans.

6. Summary and conclusions

Tests presented in the paper were performed in the real operation conditions. These allowed to specify characteristic frequencies and levels of forced vibrations of large sizes, power and efficiency centrifugal fan elements.

The vibrations analysis performed with the use of the Short Time Fourier Transform presented changes in the level and frequency of vibrations which correspond with particular phases of fans start-up sequences. As a result strong transient states in the process of operation of tested objects were identified. By verification of the received vibration spectrum characteristics, primary excitation frequencies were distinguished: rotary frequency of the rotor, blade passing frequency and their harmonic frequencies. Excitation in the wide frequency band noticed during opening of the inlet vanes results from the operation of the fan the region of instability (located on the left side from peak pressure point on fan airflow-pressure curve).

Apart from identifying of operation conditions of the fans for its different states it was also possible to compare characteristic parameters and make conclusions on the technical conditions of the objects tested and potential correction operations.

On the basis of tests performed, a huge discrepancy of vibrations level on particular fans was noticed. The highest level both in the steady and unsteady state is related to the W1 fan. It has the most

Table 2. List of parameters measured in particular rotors for all measured channel

Fan	Channel direction	1 x	2 z	3 x	4 x	5 z	6 z	7 x	8 y	9 z
W3	Unsteady state RMS [m/s^2]	0.208	0.114	1.440	0.100	1.590	**1.321**	0.632	0.341	0.622
	Unsteady state MAX[m/s^2]	2.826	9.279	**13.361**	0.915	13.015	9.259	5.015	1.535	9.744
	Steady state RMS [m/s^2]	0.131	0.171	0.987	0.093	1.479	2.138	0.630	0.490	0.670
	Steady state MAX[m/s^2]	0.527	9.288	3.787	0.396	9.968	10.837	2.463	1.763	10.287
W4	Unsteady state RMS [m/s^2]	0.155	0.120	1.323	0.192	**2.411**	0.787	1.024	0.329	**0.707**
	Unsteady state MAX [m/s^2]	1.488	9.252	12.349	**1.816**	**17.564**	9.287	**7.592**	**4.190**	9.497
	Steady state RMS [m/s^2]	0.099	0.152	0.848	0.175	2.181	0.789	0.894	0.356	0.768
	Steady state MAX [m/s^2]	0.406	9.319	3.692	0.874	10.539	9.272	3.290	1.276	10.144
W1	Unsteady state RMS [m/s^2]	**0.290**	**0.152**	1.218	**0.257**	1.801	1.298	**1.394**	**0.775**	**0.777**
	Unsteady state MAX [m/s^2]	3.149	9.308	7.919	1.327	13.261	9.297	**7.410**	2.518	9.547
	Steady state RMS [m/s^2]	0.184	0.196	0.752	0.228	0.989	1.505	1.056	0.886	0.774
	Steady state MAX [m/s^2]	0.688	9.299	2.627	0.699	10.313	11.695	3.518	2.400	9.958
W2	Unsteady state RMS [m/s^2]	0.210	0.132	**1.665**	0.141	1.910	0.346	0.829	0.296	0.441
	Unsteady state MAX [m/s^2]	**4.008**	9.281	**13.425**	1.107	16.413	9.422	5.851	1.710	9.572
	Steady state RMS [m/s^2]	0.141	0.281	0.566	0.078	0.954	0.401	0.505	0.155	0.473
	Steady state MAX [m/s^2]	0.721	9.386	2.111	0.538	10.760	9.259	1.890	0.857	9.737

maximum values of the RMS. This indicates a general high level of vibrations.

Similar situation occurs in the case of the W4 fan at the station. However, a significant difference is the fact that the largest number of extreme values is recognized for the maximum acceleration levels. This indicates that instantaneous accelerations of a high value occur.

Vibrations levels of the other two fans are significantly lower compared to the abovementioned.

The observed results confirm occurrence of diverse and inappropriate (too long) duration of fans start-ups. The occurrence of vibrations is also caused by the following factors: unnecessary keeping fans in motion while the radial vane inlet control is unopened, inappropriate unbalance of the rotary systems or inappropriate regulation of inlet vanes.

Also, a discrepancy between the vibration levels of particular fan casings is noticed. It may be however specified that in the channel 3 and 7 the vibrations levels the mostly deviating from the average in a given channel are observed. This proves that huge excitation of the fan casing into the axis direction in the middle area of the casing occurs. It is attributable to the fact that these are the most vulnerable areas of the casing, which vibrate with a large amplitude. In all cases it was possible to identify characteristic vibration frequencies correlated with the enforcement and the other potentially being the natural vibrations activated by operation of the rotor.

Such characteristic behaviors of fan rotor casings may prove the phenomenon of beat effect. The analysis of particular processes of acceleration allowed to find in some channels characteristic amplitude fluctuation, which confirms accuracy of this thesis. Therefore, there is probability of casings operation in the state comparable to resonance vibrations. This may cause the increase of the vibrations amplitude and generate casing damages. This fact may be finally confirmed after specifying the frequency and mode of the natural vibrations of fan casings either during the operation or with numerical or experimental methods [24]. After confirmation of this thesis it will be possible to implement construction changes in order to relocate the natural frequency of casings into the higher range.

Tests presented in the paper allow to identify operation conditions of complex mechanical-flow systems such as turbomachines. Operation of this type of machines is connected with numerous problems, which mainly result in different type of vibrations of particular elements or the whole group. The proper interpretation of reasons for their occurrence allows to make quick modifications in order to increase durability, decrease possibility of failure or allow further safe operations. In the case of huge power turbomachines, which were subject of the tests, the scale of these objects draws particular attention to the observed irregularities, whose symptoms are the increased levels of vibrations. In the case of this type of objects it is worth to consider installation of systems of periodical or constant monitoring of vibrations, recognized not only in the bearing support of the power transmission system, as it is right now, but also in the areas whose vibrations allow the early identification of potential problems. These areas are e.g. inlet vanes, fan casings etc. Additionally, it is accurate to monitor the flow parameters such as fan pressure ratio, flow machine efficiency and correlate them with the vibration signals. Such an attitude allows to fully identify phenomena occurring in different states of the machine operation and interpret them correctly. The next step should be to verify the influence of tested phenomena on the condition of the object. Numerical methods (FEM, BEM, FDM), which allow to perform simulations reflecting real (measured) operating conditions and predict its influence on the technical condition of the object, may be here applied.

***Acknowledgement**: Research co-financed by the European Union within the European Social Fund*

Bibliography

1. Al-Badour F, Sunar M, Cheded L. Vibration analysis of rotating machinery using time-frequency analysis and wavelet techniques. Mechanical Systems and Signal Processing 2011; 25: 2083-2101.
2. Baumgartner M, Kameier F, Hourmouziadis J. Non-Engine Blade Vibration in a High Pressure Compressor. ISABE-Twelfth International Symposium on Airbreathing Engines. Melbourne, Australia, September 10-15, 1995.
3. Białas K. Mechanical and electrical elements in reduction of vibrations. Journal Of Vibroengineerig 2012; 14: 123-128.
4. Bošnjak S, Zrnić N, Dragović B. Dynamic Response of Mobile Elevating Work Platform under Wind Excitation Strojniški Vestnik – Journal of Mechanical Engineering 2009; 55: 104-113.
5. Buchacz A, Płaczek M. Development of Mathematical Model of a Mechatronic System. Solid State Phenomena 2010; 164: 319-322.
6. Cory W. T. W. Fans&Ventilation – A Practical Guide, Elsevier, 2005.
7. Datong Qi, Yijun Mao, Xiaoliang Liu, Minjian Yuan. Experimental study on the noise reduction of an industrial forward-curved blades centrifugal fan. Applied Acoustics 2009; 70: 1041-1050.
8. Fortuna S. Wentylatory: podstawy teoretyczne, zagadnienia konstrukcyjno-eksploatacyjne i zastosowanie. Kraków: TECHWENT, 1999.
9. Gryboś R. Dynamika maszyn wirnikowych. Warszawa: Wydawnictwo Naukowe PWN, 1994.
10. He L. Fourier methods for turbomachinery applications. Progress in Aerospace Sciences 2010; 46: 329-341.
11. Jalan A. Kr, Mohanty A. R. Model based fault diagnosis of rotor-bearing system for misalignment and unbalance under steady-state condition. Journal of Sound and Vibration 2009; 327, 604-622.
12. Jamroziak K, Kosobudzki M. Determining the torsional natural frequency of underframe of off-road vehicle with use of the procedure of operational modal analysis. Journal of Vibroengineering 2012; 14: 472-476.
13. Kameier F. Rotating blade flow instability as a source of noise in axial turbomachines. Journal of Sound and Vibration 1997; 5: 833-853.
14. Karliński J, Ptak M, Działak P. Simulation tests of roll-over protection structure. Archives of Civil and Mechanical Engineering 2012; 13: 232-244.
15. Karliński J, Rusiński E, Smolnicki T. Protective structures for construction and mining machine operators. Automation in Construction 2008; 17: 232-244.
16. Kuczewski S. Wentylatory. Warszawa: WNT, 1978.
17. Łazarz B, Wojnar G, Czech P. Wykrywanie wczesnych faz uszkodzeń kół zębatych w warunkach eksploatacyjnych. Eksploatacja i Niezawodnosc – Maintenance and Reliability 2011; 1: 68-77.
18. Parszewski Z. Drgania i dynamika maszyn. Warszawa: WNT, 1982.
19. Pawiński J, Roszkowski J, Strzemiński J. Przewietrzanie kopalń. Katowice: Śląskie Wydawnictwo Techniczne, 1995.
20. Radkowski S. Use of vibroacoustical signal in detecting early stages of failures. Eksploatacja i Niezawodnosc – Maintenance and Reliability 2007; 3: 11-18.
21. Randall R. B., Vibration-based Condition Monitoring, A John Wiley and Sons, Ltd., 2011.
22. Rao A. Rama, Dutta BK. Vibration analysis for detecting failure of compressor blade. Engineering Failure Analysis 2012; 25: 211,218.
23. Sarkar S, Bijl H. Nonlinear aeroelastic behavior of an oscillating airfoil during stall-induced vibration. Journal of Fluids and Structures 2008; 24: 757-777.
24. Uhl T. Komputerowo wspomagana identyfikacja modeli konstrukcji mechanicznych. Warszawa: WNT, 1997.
25. Wolfram D. Carolus T. Experimental and numerical investigation of the unsteady flow field and tone generation in an isolated centrifugal fan impeller. Journal of Sound and Vibration 2010; 329: 4380-4397.

Jerzy CZMOCHOWSKI
Przemysław MOCZKO
Piotr ODYJAS
Damian PIETRUSIAK
Department of Machine Design and Research
Wroclaw University of Technology
Lukasiewicza 7/9, 50-371 Wroclaw, Poland
E-mails: jerzy.czmochowski@pwr.wroc.pl,
przemyslaw.moczko@pwr.wroc.pl
piotr.odyjas@pwr.wroc.pl
damian.pietrusiak@pwr.wroc.pl

Article citation info:
DUAN R, ZHOU H. Diagnosis strategy for micro-computer controlled straight electro-pneumatic braking system using fuzzy set and dynamic fault tree. Eksploatacja i Niezawodnosc – Maintenance and Reliability 2014; 16 (2): 217–223.

Rongxing DUAN
Huilin ZHOU

DIAGNOSIS STRATEGY FOR MICRO-COMPUTER CONTROLLED STRAIGHT ELECTRO-PNEUMATIC BRAKING SYSTEM USING FUZZY SET AND DYNAMIC FAULT TREE

WYKORZYSTANIE ZBIORÓW ROZMYTYCH I DYNAMICZNEGO DRZEWA USZKODZEŃ W STRATEGII DIAGNOSTYKI ELEKTRO-PNEUMATYCZNEGO UKŁADU HAMULCOWEGO STEROWANEGO ZA POMOCĄ MIKROKOMPUTERA

In this paper, a new diagnosis strategy for micro-computer controlled straight electro pneumatic braking system is developed to improve the diagnostic efficiency, which makes full use of some reliability theories and fuzzy set techniques. Specifically, it adopts expert elicitation and fuzzy set theory to evaluate the failure rate of the basic events for the braking system, and uses a dynamic fault tree model to capture the dynamic failure mechanisms and calculates some reliability results by mapping a dynamic fault tree into an equivalent Bayesian network (BN). Furthermore, the schemes are proposed to update the diagnostic importance factor (DIF) and the cut sets according to the sensors data. Finally, an efficient diagnostic algorithm is developed based on these reliability results to guide the maintenance crew to diagnose the braking system. The experimental results demonstrate that the proposed method can locate the fault of the braking system with less diagnosis cost.

Keywords: *Diagnosis strategy, Fuzzy set, Dynamic fault tree, Expected diagnosis cost.*

W niniejszej pracy, opracowano nową strategię diagnostyki elektro-pneumatycznego układu hamulcowego sterowanego za pomocą mikrokomputera Celem badań była poprawa efektywności diagnostycznej. Strategię oparto na wybranych teoriach niezawodności oraz technikach zbiorów rozmytych. W szczególności, strategia wykorzystuje ocenę ekspercką oraz teorię zbiorów rozmytych do określania intensywności uszkodzeń dla podstawowych zdarzeń zachodzących w układzie hamulcowym oraz posługuje się modelem dynamicznego drzewa uszkodzeń aby uchwycić dynamiczne mechanizmy uszkodzeń. Za pomocą przedstawionej strategii oblicza się także wyniki analiz niezawodnościowych poprzez mapowanie dynamicznego drzewa błędów do równoważnej sieci bayesowskiej (BN). Ponadto w artykule zaproponowano schematy służące do aktualizacji czynnika ważności diagnostycznej (DIF) oraz przekrojów niezdatności zgodnie z danymi z czujników. Wreszcie, w oparciu o uzyskane wyniki analiz niezawodnościowych, opracowano wydajny algorytm diagnostyczny, który zawiadamia załogę konserwatorką o konieczności przeprowadzenia diagnostyki układu hamulcowego. Wyniki doświadczeń pokazują, że proponowana metoda pozwala na zlokalizowanie usterki układu hamulcowego przy mniejszych kosztach diagnozy.

Słowa kluczowe: *Strategia diagnostyki, zbiór rozmyty, dynamiczne drzewo błędów, przewidywany koszt diagnozowania*

1. Introduction

The micro-computer controlled straight electro-pneumatic braking system is a key system to ensure the safe operation of urban rail transit. Its performance has been greatly improved with wide application of high technology. On the other hand, its complexity of technology and structure increasing significantly raise challenges in system diagnosis and maintenance. These challenges are displayed as follows: (1) lack of sufficient fault data. Fault data integrity has significant influence on the system diagnosis efficiency. However, it is very difficult to obtain mass fault samples which need lots of case studies in practice due to some reasons. One reason is imprecise knowledge in early stage of new product design. The other reason is the changes of the environmental conditions which may cause that the historical fault data can not represent the future failure behaviours. (2) Failure dependency of components. The micro-computer controlled straight electro-pneumatic braking system adopts many redundancy units and fault tolerance techniques to improve its reliability. So the behaviours of components in the system and their interactions, such as failure priority, sequentially dependent failures, functional dependent failures, and dynamic redundancy management, should be taken into consideration. (3) High level of uncertainty. The micro-computer controlled straight electropneumatic braking system is usually operated in a dynamic environment and is greatly affected by the technical, human and operational malfunctions that may lead to hazardous incidents. Aiming at these issues, many efficient diagnosis methods have been proposed. Assaf et al. proposed a fault tree based approach to determine the diagnosis order of components using DIF, which can, to some extent alleviate fault data acquisition bottleneck [1, 17]. However, this method determines the diagnostic sequence only by components' DIF, and usually causes minimal cut sets with a smaller DIF to be checked first, thereby influencing the diagnosis result. Tao et al. presented an improved method for system fault diagnosis which makes the overall consideration of components' DIF and minimal cut sets' DIF [22]. However, these diagnosis methods are based the static fault tree which cannot model dynamic fault behaviours. For this purpose, Duan et al. proposed a hybrid diagnosis method using dynamic fault tree and discrete-time BN [15]. In many cases, when a system fails, additional evidence is observed too, which may be collected from sensors. Hence, Assaf et al. put forward a method to incorporate evidence data from sensors into the diagnostic process to further improve the diagnosis efficiency [2]. But, the solution for dynamic fault tree was based on Markov model which is ineffective in handing larger dynamic fault tree and modelling power capabilities. What's more, it cannot incorporate the evidence information into the reasoning and can't update the components' posterior failure probability based on the evidence data from sensors, which affects the diagnostic accuracy. In the application of fault tree analysis mentioned above, the failure probability of basic events must be known. In addition, the failure rates of the system components are considered as crisp values. However, in practice, the failure rates of the system components are imprecise, deficient or vague in the system modelling. To overcome these difficulties and limitations in fault tree analysis, Fuzzy fault tree has been proposed, which employs fuzzy set and possibility theory, and deals with ambiguous, qualitatively incomplete, ill-defined and inaccurate information [3, 5, 12]. However, these approaches use the static fault tree to model the system fault behaviours and can not handle the challenge (2).So fuzzy dynamic fault tree (FDFT) analysis has been introduced [10], which takes into account not only the combination of failure events but also the order in which they occur. But the solution for FDFT is Markov chains (MC) based approach, which has the infamous state space explosion problem and can not incorporate sensors data into diagnosis process. Usually, BN is one of the most efficient models in the uncertain knowledge and reasoning field. It has been used to locate the system fault in many fields [4, 13]. However, the construction of BN model usually needs lots of fault data, which are very difficulty to obtain in reality. Motivated by the problems mentioned above, this paper presents a diagnosis strategy for micro-computer controlled straight electro-pneumatic braking system based on fuzzy set and dynamic fault tree. It pays special attention to meeting above three challenges. We adopt expert elicitation and fuzzy set theory to deal with insufficient fault data and uncertainty problem by treating failure rate as fuzzy numbers. Furthermore, we use a dynamic fault tree model to capture the dynamic behaviours of the braking system failure mechanisms and calculate some reliability results by mapping a dynamic fault tree into an equivalent BN in order to avoid the infamous state space explosion problem. In addition, we present a new method to incorporate sensors data into the system diagnosis to optimize the diagnosis process. The objective of this paper is to present an efficient diagnosis strategy for micro-computer controlled straight electro-pneumatic braking system using fuzzy set and dynamic fault tree. The rest sections of this paper are organized as follows: Section 2 provides a brief introduction on the braking system and its dynamic fault tree model. In section 3 describes estimation of failure rate for the basic events. Section 4 presents a novel diagnosis strategy which makes use of the qualitative structure, quantitative information and sensors data. The outcomes of the research and future research recommendations are presented in the final section.

2. Dynamic fault tree of braking system

The micro-computer controlled straight electro-pneumatic braking system has been the first choice braking system for urban rail transit, which has the advantages of the swift response, flexible operation, combined application with electric braking and anti-slip control. It is an electro-mechanic control system, and achieves its function by the coordination of electrical circuit part and air circuit part. Specifically, it includes power unit for braking system, service braking instruction processing unit, service braking control unit, emergency braking instruction processing unit, air supply unit and braking execution unit. The service braking instruction processing unit includes braking controller, logic controller and braking instruction line, which generates the service braking signals and transmits them into the braking control unit of every vehicle; service braking control unit receives service braking signals, calculates service braking force and detects braking system state. It consists of microcomputer brake control unit (MBCU) and several valves; Four modules (empty weight valves, under compaction switch, emergency braking button and emergency braking switch) form the emergency braking instruction processing unit which generates the emergency braking signals and transmits them into the emergency braking control unit; air supply unit offers air for braking system and thus a train is actuated to brake by braking execution unit. High coupling degree together with complicated logic relationships exists in these modules. Lots of current research about the micro-computer controlled straight electro-pneumatic braking system has focused on its reliability analysis using a reliability block diagram [14] or static fault tree [21]. It attempts to find out the weakest part of the system and then presents some reasonable solutions to improve its reliability. Fig. 1 shows a dynamic fault tree for service braking failure of a micro-computer controlled straight electro-pneumatic braking system. Any one of braking control failure, air supply unit failure, braking control output failure and braking execution unit failure will result in service braking failure. The failure events and different components of the braking system are represented by different symbols which are presented in Table 1.

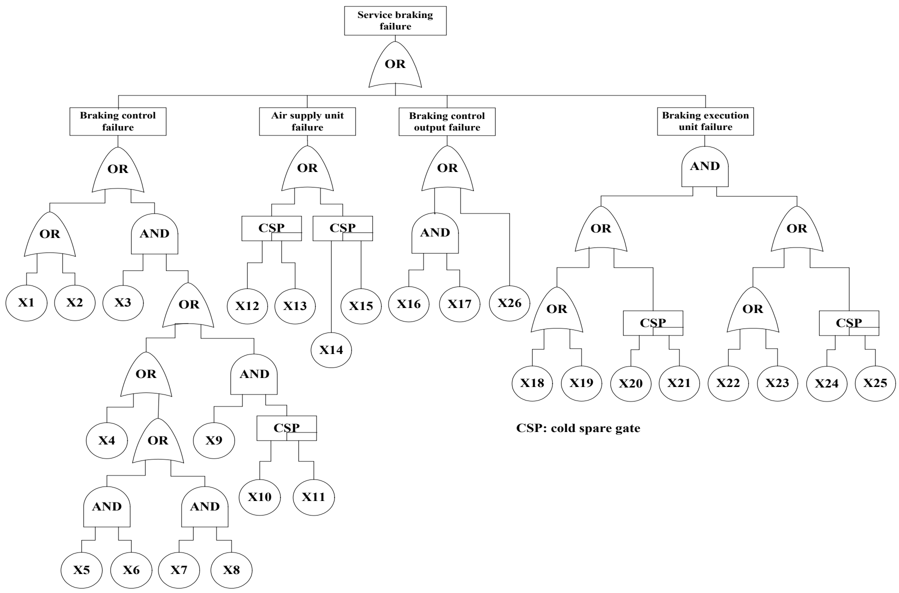

Fig. 1. A dynamic fault tree for service braking failure of braking system

3. Estimation of failure rates for braking system

In order to evaluate the reliability result for the braking system, failure rates of the basic events must be known. However, it is very difficult to estimate a precise failure rate due to insufficient data, or vague characteristic of the events, especially for the new equipments. In this study, the expert elicitation through several interviews and questionnaires and fuzzy set theory are used to determine the failure rates of the basic events.

3.1. Experts evaluation

Experts are selected from different fields, such as design, installation, operation, maintenance and management of the braking system, to judge failure rates of the basic events. They evaluate them in quali-

Table 1. The basic events of the braking system

Node symbol	Description	Node symbol	Description
X1	Microcomputer brake control unit	X14	Air cylinder 1
X2	EP brake valve	X15	Air cylinder 2
X3	Brake line failure	X16	Large membrane
X4	Power board of pulse width modulation	X17	Small membrane
X5	Digital input board	X18	High pressure oil seal ring 1
X6	Input/output board	X19	Low pressure oil seal ring 1
X7	Modulation board	X20	Left clamp 1
X8	Digital output board	X21	Left clamp 2
X9	Pulse width modulation line	X22	High pressure oil seal ring 1
X10	Multifunction Vehicle Bus 1 failure	X23	Low pressure oil seal ring 2
X11	Multifunction Vehicle Bus 2 failure	X24	Right clamp 1
X12	Compactor 1 failure	X25	Right clamp 2
X13	Compactor 2 failure	X26	Relay valve

tative natural languages based on their experiences and knowledge about the braking system. The granularity of the set of linguistic values usually used in engineering fields is from four to seven terms. In the paper, the component failure rates are defined by seven linguistic values, i.e. very high, high, reasonably high, medium, reasonably low, low and very low.

3.2. Converting linguistic terms to fuzzy numbers

After experts' evaluation, a numerical approximation method is used to systematically map linguistic terms into triangular fuzzy numbers. Each predefined linguistic value has a corresponding mathematical representation. The shapes of the membership functions to mathematically represent linguistic variables in engineering systems are shown in Fig. 2. To eliminate the bias coming from an expert, eleven experts are asked to justify how likely a basic event will fail in the system under investigation. So, it is necessary to aggregate their opinions into a single one. There are many methods to combine fuzzy numbers. A popular approach is the linear opinion pool [7]:

$$M_i = \sum_{j=1}^{n} \omega_j A_{ij}, \quad i = 1,2,3,\ldots,m \tag{1}$$

where m is the number of basic events; A_{ij} is the linguistic expression of a basic event i given by expert j; n is the number of the experts; ω_{ij} is a weighting factor of the expert j and M_i represents combined fuzzy number of the basic event i.

Usually, an α-cut addition followed by the arithmetic averaging operation is used for aggregating more membership functions of fuzzy numbers of different types. The membership function of the total fuzzy numbers from n experts' opinion can be computed as follows:

$$f(z) = \max_{z=x_1+x_2+,\ldots,+x_n} \left[\omega_1 f_1(x) \wedge \omega_2 f_2(x) \wedge \ldots \wedge \omega_n f_n(x))\right] \tag{2}$$

where $f_n(x)$ is the membership function of a fuzzy number from expert n and $f(z)$ is the membership function of the total fuzzy numbers.

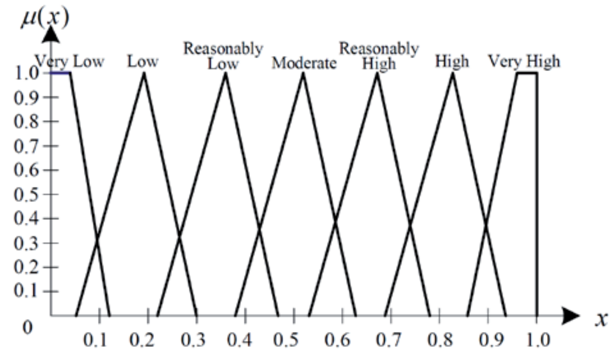

Fig. 2. Fuzzy numbers used for representing liguistic value

3.3. Calculating fuzzy fault rates of the basic events

Obviously, the final ratings of the basic events are also fuzzy numbers and cannot be used for fault tree analysis because they are not crisp values. So, fuzzy number must be converted to a crisp score, named as fuzzy possibility score (*FPS*) which represents the most possibility that an expert believes occurring of a basic event. This step is usually called defuzzification. There are several defuzzification techniques [8]: area defuzzification technique, the left and right fuzzy ranking defuzzification technique, the centroid defuzzification technique, the area between the centroid point and the original point defuzzification technique, and the centroid based Euclidean distance defuzzification technique. In this paper, an area defuzzification technique is used to map the fuzzy numbers into *FPS*. If (a, b, c; 1) is a normal triangular-fuzzy number, then its area defuzzification technique is as follows:

$$FPS = \frac{(2a+2b)^2 + (b+c)(2b-3a-c) - 2b(3b+c) - 4ab}{18(a-c)} \tag{3}$$

The event fuzzy possibility score is then converted into the corresponding fuzzy failure rate (*FFR*), which is similar to the failure rate. Based on the logarithmic function proposed by Onisawa [18], which utilizes the concept of error possibility and likely fault rate, the fuzzy failure rate can be obtained by the following equation (4).

Table 2. The FPS and FFR of basic events

Basic events	Fuzzy numbers			FPS	FFR
	a	b	c		
X1	0.1498	0.2499	0.4094	6.98e-2	3.5e-6
X2	0.1991	0.2201	0.3584	5.88e-2	1.6e-6
X3,X9, X10,X11	0.1101	0.2099	0.2572	5.04e-2	7.6e-7
X4	0.0996	0.2005	0.1999	4.44e-2	4.1e-7
X5	0.1802	0.3403	0.9097	9.61e-2	1.4e-5
X6	0.1151	0.2148	0.2844	5.33e-2	1.0e-6
X7	0.1397	0.2301	0.8426	9.07e-2	1.1e-5
X8	0.1698	0.3204	0.5534	8.63e-2	8.9e-6
X12,X13	0.1651	0.3103	0.5744	8.58e-2	8.7e-6
X14,X15	0.1549	0.2801	0.5688	8.16e-2	7.1e-6
X16,X17	0.1131	0.2128	0.2224	4.93e-2	6.8e-7
X18,X19,X22,X23	0.1851	0.6502	0.9716	1.31e-1	4.8e-5
X20,X21,X24,X25	0.1801	0.5499	0.9526	1.24e-1	3.8e-5
X26	0.1599	0.3002	0.5666	8.37e-2	7.8e-6

Table 2 shows the fuzzy failure rates of the basic events for the braking system.

$$FFR = \begin{cases} \dfrac{1}{10^{\left[\frac{1-FPS}{FPS}\right]^{\frac{1}{3}} \times 2.301}}, & FPS \neq 0 \\ 0, & FPS = 0 \end{cases} \quad (4)$$

4. Diagnosis strategy

4.1. Calculating reliability data

After the dynamic fault tree is constructed and all basic events have their corresponding fault rates, reliability results of the braking system can be calculated. We use the zero-suppressed binary decision diagram (ZBDD) to generate all minimal cut sets (*MCS*) [19]. Firstly, it converts the dynamic fault tree into the static fault tree by separating logic constraints and timing constraints. Secondly, this algorithm generates the minimal cut sets of the resulting static fault tree using some set operations as follows:

$$\begin{aligned} &S_c = S_1 \cap S_2, D_1 = S_1 - S_c, D_2 = S_2 - S_c \\ &U = D_1 \cup D_2, P = D_1 * D_2, D_3 = U - P \end{aligned} \quad (5)$$

where $S_1$and S_2 are the input of *MCS-AND* and *MCS-OR*. S_c, D, U, and P respectively represent set intersection, set difference, set union, and set product.

The *MCS* generation algorithm is executed recursively during the depth-first left-most traversal of a fault tree. It first generates the *MCS* of the inputs of a connection gate, and then performs a serial of set operations to combine the *MCS* of the inputs into the *MCS* of the output of the connection gate. Finally, it expands each minimal cut set to minimal cut sequences by considering the timing constraints. For convenience, we define the sum of all minimal cut sets as the characteristic function of the system. The characteristic function of the braking system is

$$\begin{aligned} F = {} & X1 + X26 + X2 + X12X13 + X18X23 + X19X24X25 \\ & + X18X24X25 + X19X23 + X19X22 + X23X20X21 \\ & + X14X15 + X3X5X6 + X3X4 + X3X7X8 + X22X20X21 \\ & + X18X22 + X16X17 + X3X9X10X11 + X24X20X21X25 \end{aligned} \quad (6)$$

Quantitative analysis for dynamic fault tree is used to calculate the importance parameters. DIF is the corner stone of our methodology and provides an accurate measure of components' relevance from a diagnosis perspective. The DIF is defined conceptually as the probability that an event has occurred given the top event has also occurred.

$$DIF_{MCS_n} = P(MCS_n|S), DIF_C = P(C|S) \quad (7)$$

MCS_n: n^{th} minimal cut sets, *C:* a component in system *S*

In order to avoid infamous state space explosion problem we calculate the DIF by mapping a fault tree into an equivalent discrete-time BN (DTBN). In addition, DTBN can deal with the evidence data and update the DIF after receiving them. We divide the mission time into n+1intervals. Each node variable has a finite number n+1 of states. The n first states divide the time interval [0, T] (T is the mission time) into n equal intervals, and the last state n+1 represents the time interval [T,∞]. Random variables X is in state n+1 means that the corresponding basic component or gate output did not fail during the mission time [6]. In the paper, we use n=2 to balance the accuracy and computational complexity. Assume mission time 2000, we convert the dynamic fault tree in Fig. 1 to the BN using the approach in [6,11] and enter the evidence that the braking system has failed:

$$\begin{aligned} &P(Top = state2) = 0 \\ &P(Top = state1) = 0.5 \\ &P(Top = state0) = 0.5 \end{aligned} \quad (8)$$

Solving the BN using the inference algorithm gives the results of some importance factors in Table 3 and Table 4.

Table 3. DIF of components for the braking system

Components	Components' DIF	Components	Components' DIF
X18,X19	3.24e-1	X6,X7	7.01e-3
X22,X23	3.24e-1	X21,X25	4.79e-3
X26	2.87e-1	X6	2.01e-3
X1	1.25e-1	X3	1.55e-3
X20,X24	7.64e-2	X9,X10	1.52e-3
X2	5.74e-2	X16,X17	1.39e-3
X5	2.71e-2	X13	1.34e-3
X7	2.17e-2	X15	8.74e-4
X8	1.77e-2	X4	8.19e-4
X14	1.47e-2	X11	5.78e-7

4.2. Updating reliability data according to sensors information

When the braking system fails, sometimes additional evidence from diagnostic sensors is observed too, and this may be used to optimize the system diagnosis. However, the performance of a diagnostic system highly depends upon the number and location of sensors. According to the optimal sensors placement in [16] and Table 3, X18 and X19 will be the best location of sensors. If sensors detect the failure of X18 and X19, we can adopt the evidence to reduce the number of the diagnosed minimal cut sets using algorithm 1. The cut sets under evidence (*CUE*) is the set of all essential minimal cut sets obtained after evidence eliminates some cut sets. The following *CUE* function is generated:

$$\begin{aligned} F_{CUE} = {} & X1 + X2 + X22 + X23 + X26 + X24X25 \\ & + X14X15 + X16X17 + X12X13 + X3X4 \\ & + X3X7X8 + X3X5X6 + X3X9X10X11 \end{aligned} \quad (9)$$

Since a failure sensor can lead to a faulty diagnosis progress, we introduce the DIF of sensor to take this situation into account. The DIF for a sensor with respect to the system is measured by the same way the DIF of the components:

$$DIF_{Sensor} = P(Sensor|S) = q_{Sensor} / Q_S \quad (10)$$

where q_{Sensor} and Q_S represent the unreliability of sensor and the system, respectively.

Assume sensors have a fixed probability of failure of 10^{-6}; the DIF of the sensor is 1.79×10^{-5}. The updated *CUE* function is as follows:

Table 4. DIF of minmal cut sets for the braking system

MCS	MCS' DIF	MCS	MCS' DIF
X26	2.78e-1	X19 X24 X25	2.25e-3
X18 X22	1.50e-1	X12 X13	1.34e-3
X18 X23	1.50e-1	X14 X15	8.74e-4
X19 X22	1.50e-1	X3 X4	1.17e-4
X19 X23	1.50e-1	X20 X21 X24 X25	3.37e-5
X1	1.25e-1	X16 X17	3.32e-5
X2	5.74e-2	X3 X4	2.17e-5
X23 X20 X21	2.25e-3	X7 X8 X3	1.32e-5
X18 X24 X25	2.25e-3	X3 X5 X6	1.50e-6
X22 X20 X21	2.25e-3	X3 X9 X10 X11	2.40e-11

$$\begin{aligned} F'_{CUE} &= X1 + X2 + X22 + X23 + X26 + X24X25 \\ &+ X14X15 + X16X17 + X12X13 + X3X4 \\ &+ X3X7X8 + X3X5X6 + X3X9X10X11 + Sensor \end{aligned} \tag{11}$$

In addition, we add the sensors evidence nodes to the BN from the dynamic fault tree and set the conditional probability, which can be used to update the DIF of the components and *CUE*. The DIF of the *CUE* can be calculated using equation (12).

$$DIF_{CUE} = \frac{P(CUE, E, S)}{P(S) DIF_E} \tag{12}$$

S: system, *E*: variables with given evidence.

Now we input the evidence defined as equation (13) to the BN and update the DIF of components and CUE using the inference algorithm. Table 5 and 6 shows the diagnostic data with sensors data.

$$\begin{aligned} &P(X18 = state2) = 0 \\ &P(X18 = state1) = P(X18 = state0) = 0.5 \\ &P(X19 = state2) = 0 \\ &P(X19 = state1) = P(X19 = state0) = 0.5 \end{aligned} \tag{13}$$

Algorithm 1 GetCUE(*F*, *E*, *v*)

```
Input:
  F: the characteristic function
  E: evidence information function
  v: if occurred, v=1, otherwise v=0
Output: CUE
    F_CUE=0
    if (v=0) {E=ITE(E,0,1)}
    for (∀product ∈ E )
      { tempF=F
      for (∀component ∈ product ) {
        if ( (∃product ∈ F) = component )
            { tempF=F_component=0 }
        else { tempF=F_component=1 }
      }
      F_CUE=ITE(F_CUE, 0, tempF)
    }
    return (F_CUE)
```

Table 5. The updated DIF of components for the braking system

Components	Components' DIF	Components	Components' DIF
X22,X23	4.65e-1	X14	1.41e-2
X26	7.86e-2	X25	6.93e-3
X24	7.84e-2	X6	1.99e-3
X20	7.32e-2	X3	1.55e-3
X1	3.54e-2	X9,X10	1.52e-3
X5	2.76e-2	X16,X17,X21	1.37e-3
X7	2.17e-2	X4	8.01e-4
X8	1.76e-2	X13	3.81e-4
X12	1.75e-2	X15	2.47e-4
X2	1.62e-2	X11	5.78e-7

Table 6. The updated DIF of CUE for the braking system

CUE	CUE's DIF	CUE	CUE's DIF
X22	4.65e-1	X14 X15	2.47e-3
X23	4.65e-1	Sensor	1.79e-5
X26	7.86e-2	X16 X17	9.33e-6
X1	3.54e-2	X3 X4	6.11e-6
X2	1.62e-2	X3 X7 X8	1.54e-6
X24 X25	6.93e-3	X3 X5 X6	2.22e-7
X12 X13	3.78e-4	X3 X9 X10 X11	3.53e-12

4.3. Diagnosis strategy

As *CUE* represents minimal sets of component failures under evidence that can cause a system failure, we should diagnose it one by one to find the root reason of the braking system failure. Only when we finish diagnosing a *CUE* can we do next. The order by which *CUE* are checked depends on its DIF ordering, while the order of components in the same *CUE* is determined by their DIF. The *CUE* with larger DIF is checked first. Accordingly, components with larger DIF in a *CUE* are checked first. This assures a reduced number of system checks while fixing the braking system. Based on quantitative and qualitative data obtained from reliability analysis after incorporating evidence, the diagnostic strategy is as follows:

Step1. Sort all *CUE* and select the *CUE* with highest DIF value.
Step2. Check the component *C* with highest DIF in the *CUE*.
Step3. Split the *CUE* into those with *C* and those without.

a) If *C* failed test we take the set of *CUE* that include *C*
- Select the *CUE* untested with highest DIF value.
- And recursively repeat Step2 - Step3.

b) If C has not failed test we take the other set of *CUE*
- Select the *CUE* untested with highest DIF value.
- And recursively repeat Step2 - Step3.

The diagnosis strategy can easily be described in the graphical diagnostic decision tree (DDT). It provides us with a map that allows us to recognize the failing components. It is a directed acyclic graph composed of circular nodes and arcs linking parent nodes to child nodes. A node represents a component being tested. Arcs point to the next component to be tested; right arcs point to components within the same cutest as the parent node, and left arcs point to components which are not in the same cutest as the parent node. Moreover, when diagnostician reaches a node and tests the component at the node, the test either fails or passes. If the test fails then the right arc is traversed indicating the need to repair the tested component in the parent node. If a test passes then the left arc is traversed indicating that the cut sets which include the tested component in the parent node have not failed. Once the order of components is determined, we can generate the DDT of the braking system shown in Fig.3.

Average diagnostic cost is often used to evaluate the fault diagnosis method. The diagnostic cost is lower; the method is better. As we all know, the output of fault diagnosis method is the DDT, we can evaluate it with the help of several decision tree evaluation measures. Traditional evaluation measures have the mean depth of the tree [20], which calculates the expected number of tests needed to isolate a fault, and the expected cost function [9], which takes into account the testing cost of a path as a weighting factor. But these measures only consider the test cost and the failure probability of components, and neglect system qualitative structure and the importance factors of each component. Also, they only diagnose one fault at a time and are not capable of detecting multiple faults by a single tree traversal. Based on these evaluation mechanisms, we introduce expected diagnostic cost (EDC) which incorporates the qualitative (structure) and quantitative (reliability analysis) into one measure for predicting diagnosis cost [16]. This evaluation index takes both diagnosis accuracy and diagnosis cost into consideration, also considers the relationship between component failure and system failure, and can evaluate the diagnosis algorithm objectively. EDC can be computed by:

$$EDC = \frac{\sum_{i=1}^{n} qcutset_i cp_i}{Q_S} \qquad (14)$$

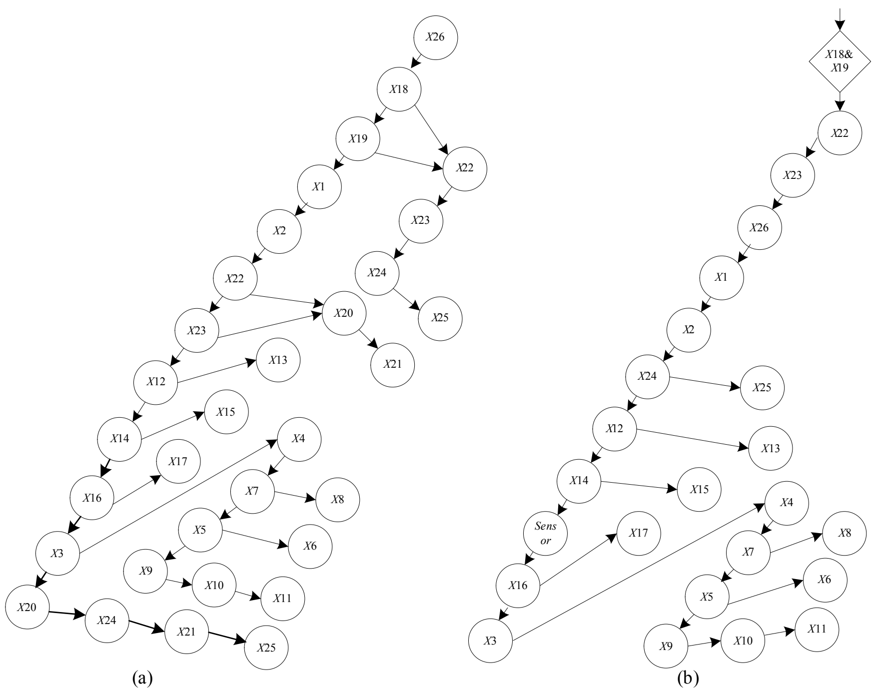

Fig. 3. DDT for service braking failure of braking system, (a) DDT without evidence from sensors; (b) DDT with evidence from sensors

where Q_s is the unreliability of the system, cp_i is the sum of all test costs from the top node to the cutset's leaf node, qcutseti is the unreliability of cut sequences.

For convenience, assuming all components have a unit test cost and their test cost is independent, the diagnostic cost of different algorithms using equation (14) is shown in Table 7, which indicates the proposed approach is more efficient than others. Furthermore, the curve in Fig. 4 depicts the effect of sensors' reliability on EDC of the braking system. So we should choose the sensors with higher reliability to detect the components in order to decrease the diagnosis cost of the braking system.

Table 7. The comparison among three diagnosis methods

Diagnosis methods	*EDC*
Diagnosis method without sensors	3.562
Diagnosis method with sensors data by Assaf and Dugan [2]	2.586
Diagnosis method in the paper	1.918

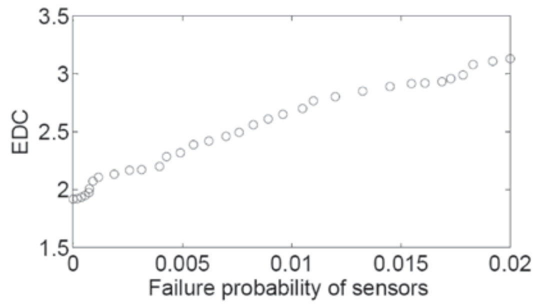

Fig. 4. The relation curves of EDC and failure probability of sensors

5. Conclusion

In this work, we have discussed the use of fuzzy set theory, dynamic fault tree and BN to diagnose the micro-computer controlled straight electro-pneumatic braking system. Specifically, it has emphasized three important issues that arise in engineering diagnostic applications, namely the challenges of insufficient fault data, uncertainty and failure dependency of components. In terms of the challenge of insufficient fault data and uncertainty, we adopt expert elicitation and fuzzy set theory to evaluate the failure rates of the basic events for the braking system; In terms of the challenge of failure dependency, we use a dynamic fault tree to model the dynamic behavior of system failure mechanisms and calculate some reliability results by mapping a dynamic fault tree into an equivalent BN in order to avoid the state space explosion problem. Furthermore, we incorporate sensors data into fault diagnosis, cope with the sensors reliability and propose the schemes on how to update DIF and the cut sets. In addition, an efficient diagnostic decision algorithm is developed based on these results to optimize system diagnosis. The experimental results demonstrate its efficiency. The proposed method makes use of the advantages of the dynamic fault tree for modeling, fuzzy set theory for handling the uncertainty and BN for inference ability, which is especially suitable for the complex system diagnosis.

In the future work, we will focus on the dynamic fault tree model optimization and take the test cost, sensitive analysis and other attributes into the diagnosis strategy.

Acknowledgement*:*
The research work was supported in part by National Natural Science Foundation of China (61062009, 61074139) and the Science and Technology Foundation of Department of Education in Jiangxi Province (GJJ12146).

References

1. Assaf T, Dugan JB. Design for diagnosis using a diagnostic evaluation measure. IEEE Instrumentation and Measurement Magazine 2006; 9(4):37-43.
2. Assaf T, Dugan JB. Diagnosis based on reliability analysis using monitors and sensors. Reliability Engineering and System Safety 2008; 93(4): 509-521.
3. Ayhan Mentes, Ismail H. Helvacioglu. An application of fuzzy fault tree analysis for spread mooring systems. Ocean Engineering 2011; 38: 285–294.
4. Doguc O, Ramirez-Marquez JE. Using Bayesian approach for sensitivity analysis and fault diagnosis in complex systems. Journal of Integrated Design and Process Science 2009; 3(1): 33-48.
5. E Jafarian, Rezvani MA. Application of fuzzy fault tree analysis for evaluation of railway safety risks. Proceedings of the Institution of Mechanical Engineers, Part F: Journal of Rail and Rapid Transit 2012; 226: 14-25.
6. Boudali H, Dugan JB. Discrete-time Bayesian network reliability modeling and analysis framework. Reliability Engineering and System Safety 2005; 87: 337-349.
7. Huang D, Chen T, Wang MJJ. A fuzzy set approach for event tree analysis. Fuzzy Sets and Systems 2001; 118 (1): 153–165.
8. Julwan Hendry Purba, Jie Lu, Guangquan Zhang, Da Ruan. An Area Defuzzification Technique to Assess Nuclear Event Reliability Data from Failure Possibilities. International Journal of Computational Intelligence and Applications 2012; 11(4): 1250022-1-16.
9. Koutsoukos X, Zhao F, Haussecker H, Reich J, Cheung P. Fault modeling for monitoring and diagnosis of sensor-rich hybrid systems. Proceedings of the 40th IEEE conference on decision and control 2001; 793-801.
10. Li YF, Huang HZ, Liu Y, Xiao, Li HQ. A new fault tree analysis method: fuzzy dynamic fault tree analysis. Eksploatacja i Niezawodnosc – Maintenance and Reliability 2012; 14 (3): 208-214.
11. Li YF, Mi J, Huang HZ, Xiao NC, Zhu SP. System reliability modeling and assessment for solar array drive assembly based on Bayesian networks. Eksploatacja i Niezawodnosc - Maintenance and Reliability 2013; 15 (2): 117–122.
12. Manjit Verma, Amit Kumar. Fuzzy fault tree approach for analysing the fuzzy reliability of a gas power plant. International Journal of Reliability and Safety 2012; 6(4): 354-370.
13. Mansour MM, Wahab MAA, Soliman WM. Bayesian networks for fault diagnosis of a large power station and its transmission lines. Electric Power Components and Systems 2012; 40(8): 845-863.
14. Mengling Wu. Discussion of the Reliability Model of the Micro-computer Controlled Straight Electro-pneumatic Braking System. Rolling Stock 2006; 44(3): 20-23.
15. Rongxing Duan, Guochun Wan, Decun Dong. Intelligent Fault Diagnosis Method Based on Dynamic Fault Tree Analysis. Journal of Computational Information Systems 2010; 6(3): 949-957.
16. Rongxing Duan, Dongxiu Ou, Huilin Zhou, Optimal Sensor Placement for Fault Diagnosis based on diagnosis cost specifications. Journal of Computational Information Systems 2011; 7(9): 3253-3260.
17. Shaoxu Ni, Yufang Zhang, Xiaofeng Liang. Intelligent Fault Diagnosis Method Based on Fault Tree. Journal of Shanghai Jiaotong University 2008; 42(8):1372-1386.
18. Takehisa Onisawa. An approach to human reliability in man-machine systems using error possibility. Fuzzy Sets and System 1988; 27 (2) 87-103.
19. Tang, Zhihua, Dugan, Joanne Bechta. Minimal cut set sequence generation for dynamic fault trees. Proceedings of annual reliability and maintainability symposium on product quality and integrity 2004; 207-213.
20. Tong DW, Jolly CH, Zalondek KC. Diagnostic tree design with model-based reasoning. Proceedings of IEEE automatic testing conference 1989; 161-167.
21. Wu Mengling, Wang Xiaoyan, Yan Kaijun. Analysis by FMEA and FTA Method of Micro-computer Controlled Directacting Electro-pneumatic Braking System. Electric Drive for Locomotives 2008; 1: 32-36.
22. Yongjian Tao, Decun Dong, Peng Ren. An improved method for system fault diagnosis using fault tree analysis. Journal of Harbin Institute of Technology 2010; 42(8): 143-147.

Rongxing DUAN
Huilin ZHOU
School of Information Engineering
Nanchang University
Xuefu Rd., 999 Jiangxi, China
E-mail: duanrongxing@ncu.edu.cn

Article citation info:
ILUK A. Method of evaluating the stiffness of a vehicle with respect to the risk of explosion. Eksploatacja i Niezawodnosc – Maintenance and Reliability 2014; 16 (2): 224–228.

Artur ILUK

METHOD OF EVALUATING THE STIFFNESS OF A VEHICLE WITH RESPECT TO THE RISK OF EXPLOSION

METODA OCENY SZTYWNOŚCI POJAZDU POD KĄTEM ZAGROŻENIA EKSPLOZJĄ*

This article describes a new method of evaluating the stiffness of structure of a vehicle with respect to its resistance to mine explosion. This method allows for the assessment of the structure of a wide range of tracked and wheeled vehicles in the early stage of the construction process, considering such factors as mass and stiffness of the hull and ground clearance. By applying this method it is possible to assess the risk of lower limb injury for every vehicle occupant, caused by local deformation of the vehicle.

Keywords: *military vehicles, risk of explosion, IED, stiffness of structure.*

W artykule przedstawiono nową metodę oceny sztywności struktury pojazdu pod kątem odporności na eksplozję miny. Metoda ta umożliwia ocenę konstrukcji szerokiej gamy pojazdów gąsienicowych i kołowych na wczesnym etapie procesu konstruowania pojazdu uwzględniając takie czynniki jak masa i sztywność kadłuba oraz prześwit pod pojazdem. Wynikiem zastosowania metody jest ocena zagrożenia kończyn dolnych wskutek lokalnej deformacji pojazdu dla każdego członka załogi.

Słowa kluczowe: *pojazdy wojskowe, zagrożenie eksplozją, IED, sztywność struktury.*

1. Introduction

The use of military vehicles in areas where landmine or Improvised Explosive Devices (IEDs) are used is highly hazardous to military vehicle occupants. The task of evaluating the resistance of such vehicles to explosions is complex and is often possible only after the vehicle has been constructed [2]. This problem is particularly important in relation to military vehicles; however, in the era of terrorist threat, there is often a need to analyze the safety of civilian vehicles in this respect.

Occupant safety should be evaluated on many aspects related to different types of threats [11]. The most dangerous and difficult to combat are threats related to injury of lower limbs [8] and spine [3, 7].

$$I = \int_0^t p \, dt \tag{1}$$

where t is the time of the pressure impulse and p – the instantaneous average value of pressure of gases acting on the loaded surface.

The energy transmitted to the structure can be regarded as two energy streams. One of them is dissipated through permanent deformation of the structure; the second is transmitted to the structure as kinetic energy. The kinetic energy may, in turn, be divided into the energy of elastic deformations, which are excited by wave impact in the form of vibrations consistently with its natural frequencies, and into global structure motion. The latter is understood as the change in the velocity vector of the vehicle's center of gravity in relation to the environment, resulting from the explosion.

The diagram in figure 2 depicts the phases of blast energy transmission. The high-frequency vibrations excited in the first stage by the wave impact propagate at the speed of sound in the entire structure, which can lead to temporary damages of less resistant elements. Due to the high velocity of the elastic wave, this stage is very short, in the range of several milliseconds.

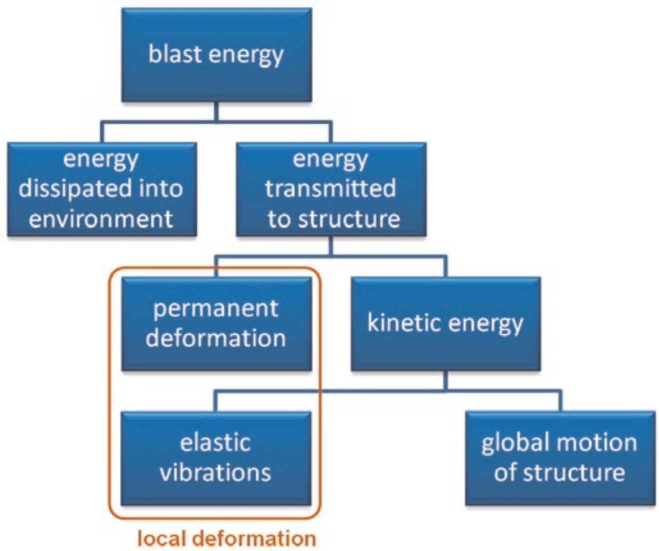

Fig. 1. Diagram depicting the process of transmitting blast energy to the vehicle structure

The diagram in figure 2 depicts the phases of blast energy transmission. The high-frequency vibrations excited in the first stage by the wave impact propagate at the speed of sound in the entire structure, which can lead to temporary damages of less resistant elements. Due to the high velocity of the elastic wave, this stage is very short, in the range of several milliseconds.

In the second stage, local deformation occurs in the lower part of the vehicle, which includes permanent deformations and elastic vibrations, whose proportions depend on the strength of the structure. Permanent deformations dominate in vehicles of low structural strength, whereas elastic deformations may dominate in vehicles structurally resistant to explosion under the vehicle.

(*) Tekst artykułu w polskiej wersji językowej dostępny w elektronicznym wydaniu kwartalnika na stronie ***www.ein.org.pl***

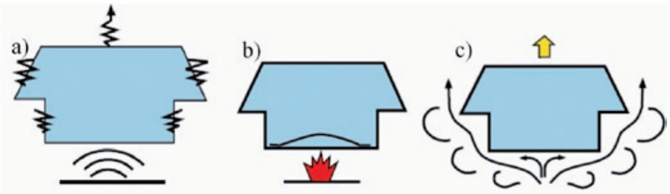

Fig. 2. Load to vehicle caused by landmine explosion: a) propagation of elastic waves, b) local deformation of structure, c) global vehicle motion [6]

In the third stage of explosion the whole structure accelerates. This stage is longer than the second stage due to significantly larger inertia of the whole vehicle than the inertia of the vehicle floorplate. It should be noted that the global motion of the structure caused by the explosion can overlap the motion of the structure prior to the explosion, e.g. the advance velocity of a vehicle which is moving when the landmine explodes. If the advance velocity is significant, the vertical height of the vehicle leaping over an exploding explosive charge may be so high that the pressure impulse distributes over a larger area of the floorplate. In terms of safety, such a phenomenon is advantageous as it decreases the concentration of energy and local deformation. This effect intensifies with the increase in burial depth of the explosive charge, which lengthens the time of energy transmission. In the case of surface detonation, or detonation of shallow buried explosives, the transmission of energy to the hull is too short for the velocity of the vehicle to impact the blast load to the structure surface.

The threat to lower limbs is related to the second stage, i.e. the local deformation of the structure. The load to lower limbs is a result of the vertical motion of the floorplate, in which case the key parameters related to the threat of lower limb injury are the vertical velocity and maximum deflection. Figure 3 shows an example graph of the vertical velocity of the floorplate during explosion.

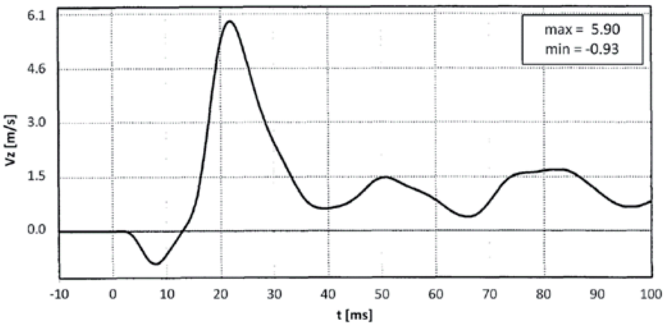

Fig. 3. Example graph of the vertical velocity of the floorplate during explosion. [1]

The figure shows a large increase in the floorplate velocity in the initial stage of loading, which is a result of the plastic and elastic deformation of the vehicle floor (second stage in figure 2). This is followed by a series of elastic vibrations of the floor near average velocity, which correspond to the global vertical velocity of the vehicle (third stage, figure 2).

The basic parameters which determine the deflection of the floorplate are the load mass, distance between the charge and the floor of the vehicle, mass of vehicle and the stiffness of vehicle structure. Whereas the mass of the vehicle has significant influence on the global motion of the vehicle (figure 2c), the stiffness in connection with the mass determines the degree of local deformation to the structure (figure 2b). The diagram in figure 4 shows the relation between mass, stiffness and threat of injury to lower limbs.

By using an additional deflectors under the vehicle it is possible to decrease the local deformation, but this also decreases the distance to the explosive charge. This is exceptionally disadvantageous in vehicles with low ground clearance.

	low mass	high mass
low stiffness	high global velocity high local deformations (HMMWV)	low global velocity high local deformations (heavy tracked vehicle)
high stiffness	high global velocity low local deformations (armored wheeled vehicle)	low global velocity low local deformations (MRAP)

decrease in threat of injury

Fig. 4. Relation between mass, stiffness of vehicle and threat of injury to lower limbs

The assessment of the level of threat of injury to lower limbs is possible by performing costly tests on firing grounds using anthropomorphic manikins [12]. The biomechanical criterion in such a case is the maximum axial force in the lower leg Similar tests can be performed by simulation, however such calculations are complex and are not suitable for evaluating the vehicle in the design stage [4]. Full simulation of the threat of injury requires the modeling of the detonation process of an explosive charge buried in the ground, the propagation of the shock wave with the products of detonation and soil ejected into the air. Figure 5 shows an example simulation of a detonation of a 10 kg TNT charge buried in the ground at a depth of 100 mm using the MM-ALE method.

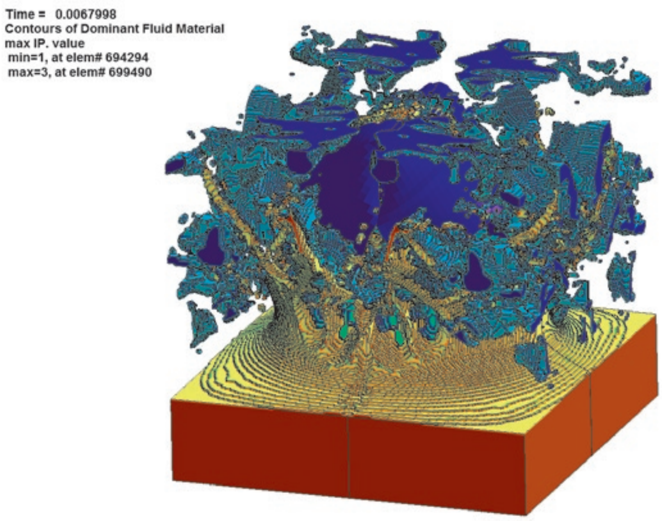

Fig. 5. Simulation of an explosion of an explosive buried in the ground using the MM-ALE method

In the existing literature there is no method for assessing the local deformation in a vehicle as a result of landmine of IED explosion under the vehicle, without performing a full simulation of the explosion. Such a method, which takes into consideration the key safety-related parameters of the whole system, including the detonating explosive and the structure of the vehicle, would allow for a preliminary analysis of the vehicle with respect to such events.

3. Method

The local deformation of the vehicle floorplate is determined by the mass of the vehicle and the stiffness of the floorplate in vertical direction. The maximum force acting statically on the vehicle floor at a given point is limited to the force which lifts one or two wheels off the ground. Therefore, maximum force may be exerted by pressing on the floor directly under the vehicle's center of gravity, which is illustrated in the diagram in figure 6. This point is also considered the most dangerous point of detonation under a vehicle[12].

The surface subject to the action of products of detonation and the soil ejected by the explosion is frequently located at some distance from the feet of the passenger. This could be due to a double floor, elastic mats which separate the feet from the vehicle floor or additional shields under the floor of the vehicle.

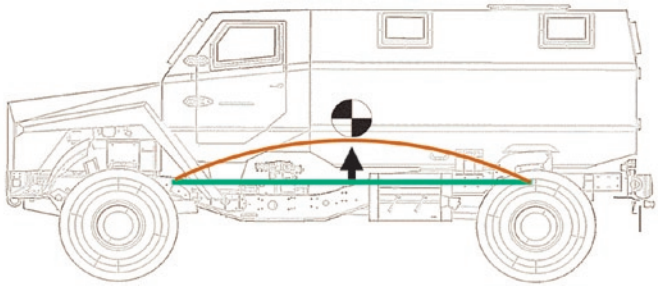

Fig. 6. Local deformation to the floorplate of the vehicle caused by explosion

As the direction of wave incidence on the surface deviates from the perpendicular direction, the pressure and pressure impulse decrease. The relation between the impulse of incident pressure I_s, impulse of reflected pressure I_r, and the angle of wave incidence θ can be defined as the formula described in [9]:

$$I_{r\theta} = I_r \cos^2(\theta) + I_s(1+\cos(\theta) - 2\cos^2(\theta)) \qquad (2)$$

The impulse of reflected pressure I_r exerted on the vehicle floor can be defined using the equation described in [5], which is based on experimental surface tests of detonations of explosive charges. The value of the impulse is determined by the scaled distance Z expressed by the Hopkinson-Cranz formula:

$$Z = \frac{R}{W^{1/3}} \qquad (3)$$

which relates the distance from the center of the explosive device R [m] with the mass of the explosive W [kg]. The relationship between the value of the impulse of incident and reflected pressure and the scaled distance may be expressed by the formula:

$$I_{s,r} = \exp(A + B\ln(Z) + C\ln(Z)^2 + D\ln(Z)^3 + E\ln(Z)^4) W^{1/3} \qquad (4)$$

where Z is expressed in [m/kg$^{1/3}$], whereas I_s, I_r in [Pa s]. The values of parameters A, B, C, D and E for the impulse of incident pressure I_s are given in [10]. The values of reflected pressure I_r were calculated on the basis of the formula in [5]. The numerical values of parameters are presented in table 1.

*Table 1. Values of parameters describing the impulse of incident pressure **I_s** and reflected pressure **I_r** as a function of scaled distance **Z** [10]*

	A	*B*	*C*	*D*	*E*	Remarks
I_s	5.522	1.117	0.6	-0.292	-0.087	for *Z* in the range 0.2÷0.96
I_s	5.466	-0.308	-1.464	1.362	-0.432	for *Z* in the range 0.96÷23.8
I_r	6.775	-1.346	0.102	-0.0112	0	for *Z* in the range 0.2÷100

Let us define the measurement of threat of lower limb injury as parameter S, which is proportional to the ratio of vertical deflection Δh of the surface loaded with shock wave pressure and the initial distance h of that surface from the feet of the passenger. The proportionality factor is the pressure impulse of reflected wave $I_{r\theta}$, which includes the inclination of the surface loaded with pressure in relation to the direction of wave incidence.

$$S = I_{r\theta} \frac{\Delta h}{h} \qquad (5)$$

This parameter enables the assessment of threat of injury resulting from local deformation of vehicle floor for different classes of vehicles without the necessity to perform full simulations of the explosion. It includes such factors as ground clearance, mass of the explosive charge, geometry and stiffness of the vehicle floor and the initial distance between the feet and the impact point of the shock wave.

An attempt to statically deflect the vehicle floorplate in selected points causes elastic or elastic and plastic deformation of the vehicle structure. In order to measure the static deflection Δh it is necessary to adopt a measurement base connected to the vehicle. Due to the fact that the threat of feet injury is related to the motion of the floor relative to the vehicle , the nearest points with high stiffness in vertical direction, e.g. the lower parts of the vehicle's side walls, should be used as the base for measuring the deflection. Figure 7 presents a diagram of the measurement method.

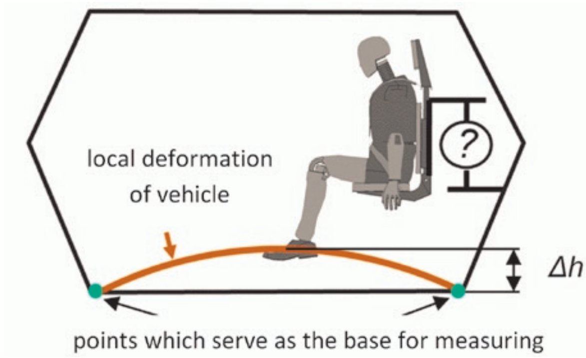

Fig. 7. Method of static measurement of the vehicle floor deflection

4. Results

The measurement of static deflection may be performed on a real vehicle or using a numerical model. Figure 8 presents an example measurement of the vertical stiffness of the floor of a Ford F250 vehicle. The static deflection in this case is 132 mm and the plastic deformation of the floorplate is significant.

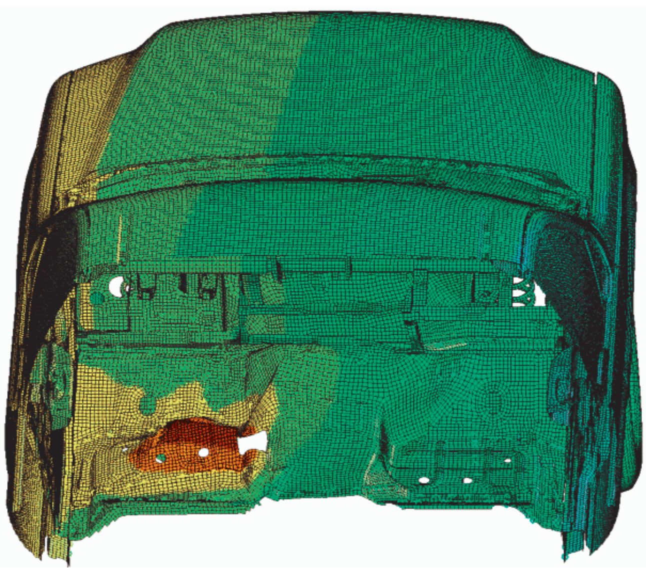

Fig. 8. Local static deformation of Ford F250 vehicle under the driver's feet, maximum static deflection (marked red) equal to 132 mm, large plastic deformations

Fig. 9. Analyzed vehicles

Table 2. Results of calculations for selected vehicles

vehicle type	pickup	tracked	wheeled	wheeled with deflector
M [Mg]	2.6	33	12.5	12.5
Δh [mm]	132	7	3	11
h_s [mm]	25	175	170	520
R [m]	0.65	0.57	1.17	0.82
W [kg]	0.5	6	10	10
Z [m/kg$^{1/3}$]	0.65	0.31	0.54	0.38
Θ [degrees]	0	0	17	17
S [Pa s]	**4735**	**332**	**68**	**139**

The values of parameter S were calculated for several vehicles. Calculations were performed for a pickup-type vehicle (Ford F250), a tracked vehicle with a mass of 33 Mg and an armored wheeled vehicle with a mass of 12.5 Mg both with and without an additional deflector under the chassis frame. Figure 9 depicts the analyzed vehicles. The results of calculations and the basic parameters of vehicles are presented in table 2.

Calculations were performed for different masses of explosive charge. Results indicate that a detonation of a 0.5 kg TNT explosive charge under a pickup vehicle is much more dangerous than the detonation of 10 kg under a mine-resistant wheeled vehicle. A tracked vehicle, due to its large mass and flat floor with relatively low stiffness, is less resistant to detonation of 6 kg TNT than a significantly lighter wheeled vehicle with a much higher ground clearance. The value of parameter S for a wheeled vehicle with an additional V-shaped deflector is higher, because it receives a higher pressure impulse and the deflector has lower stiffness. These factors are so unfavorable that they are not compensated by the significantly larger distance between the loaded surface and the passenger's feet.

Figure 10 illustrates how the change in the ground clearance impacts the value of parameter S. One can observe that the impact of ground clearance is significant, especially in the range below 0.5 m characteristic of tracked vehicles.

Figure 11 illustrates how the distance between the feet and the impact point of the wave influence the value of parameter S. One can see that in the neighborhood of 170 mm the change in the distance h has significant influence on the threat of lower limb injury.

The presented method enables the evaluation of the threat caused by local deformation at different locations within the same vehicle, e.g. threat to individual passengers. To this end, the abovementioned method should be used to measure the local stiffness of floor under the

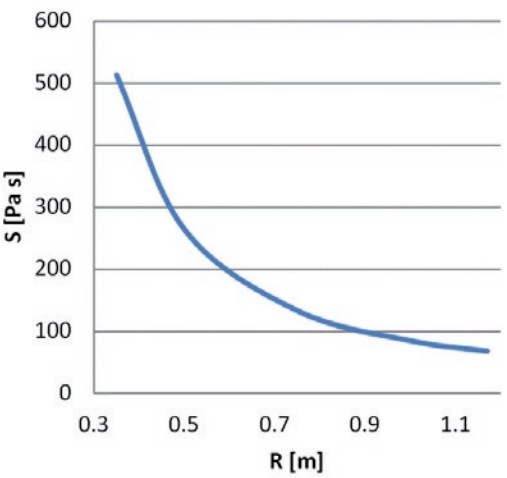

Fig. 10. Influence of ground clearance R of wheeled vehicle on the value of parameter S for a charge of 10 kg TNT and inclination angle of 17 degrees

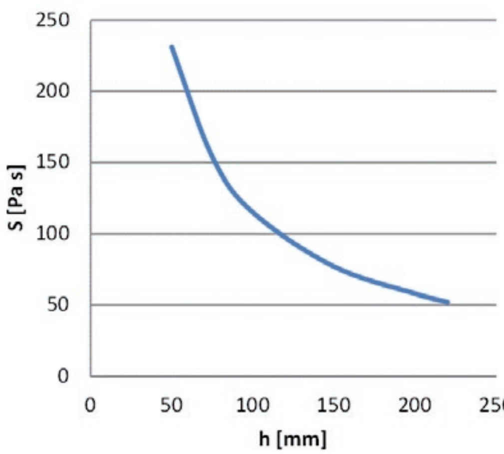

Fig. 11. The influence of the distance h between feet and the impact point of the wave on the value of parameter S for wheeled vehicle, charge of 10 kg TNT and inclination angle of 17 degrees

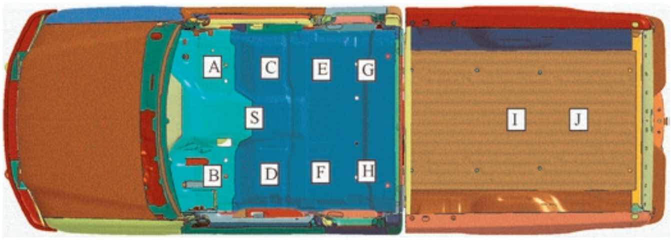

Fig. 12. Location of measurement points for local deflection of floor, Ford F250

Table 3. Values of parameter **S** for detonation of 500 g TNT charge under Ford F250 vehicle, location of points in parentheses as depicted in figure 12

left side [mm]	center [mm]	right side [mm]	description
4735 (B)	-	2475 (A)	feet in front
	4232 (S)		center of vehicle mass
2116 (D)	-	1721 (C)	seats in front
2690 (F)	-	3192 (E)	feet in back
1542 (H)	-	1470 (G)	seats in back
-	1112 (I)	-	bed
-	1040 (J)	-	bed

feet of individual occupants. Figure 12 presents an example of such analysis performed at different points for the Ford F250 vehicle. Table 3 presents the values of parameter *S* for detonation of 500 g of TNT, calculated on the basis of stiffness measurements in selected points.

Local deflection, and thus the level of threat of injury, is significantly different at different points of the vehicle. Despite the fact that the largest loading force occurs under the center of gravity, higher deflection values were recorded under the driver's feet, where there are gaps in the floorplate, which consequently reduce its stiffness. Figure 8 shows the distribution of deformations for this case.

This example illustrates the capability of the method of assessing the vehicle structure with respect to its resistance to local deformation resulting from an explosion under the vehicle. This assessment may apply not only to the vehicle as a whole, but also to selected areas of the structure.

5. Conclusion

The presented method enables the assessment of stiffness of a projected or existing structure with respect to its resistance to local deformation caused by explosion under the vehicle. In order to compare the resistance of different vehicles, the parameter *S* may be used, which, to a certain extent, defines the threat of lower limb injury. In the case of other methods, it is necessary to perform full analyses with explosion simulation or exceptionally costly tests on firing grounds. The possibility to assess structures in the early stage of design offers the opportunity to increase structural resistance of vehicles to explosion. An additional advantage is the possibility to assess the resistance of the vehicle at any point, which allows for the estimation of threat of lower limb injury for each vehicle occupant individually.

In its current form, the method allows only for the comparison of the level of threat between different vehicles or between individual structural solutions for the body and deflectors. To assess the threat directly, it is necessary to analyze the entire vehicle-occupant system with the use of biomechanical criteria.

Bibliography

1. Alem NM, Strawn GD. Evaluation of an Energy Absorbing Truck Seat for Increased Protection from Landmine Blasts, USA Army Research Laboratory, Report no. 96-06, 1996.
2. Iluk A. Metody numeryczne w procesie konstruowania terenowego pojazdu minoodpornego. Górnictwo Odkrywkowe 2010; 51: 320–324.
3. Iluk A. Selected aspects of the control of the human body motion in the vehicle subjected to the blast load. IRCOBI Conference Proceedings 2012; 391–404.
4. Iluk A. Wybrane aspekty kształtowania odporności przeciwminowej terenowego pojazdu opancerzonego. Zeszyty Naukowe - Wyższa Szkoła Oficerska Wojsk Lądowych im. gen. T. Kościuszki 2010; 42; 109–120.
5. Kingery CN. Airblast Parameters verses Distance for Hemispherical TNT Surface Burst, Armament Research and Development Center, Report no. 1344, 1999
6. Ogorkiewicz RM. Shaping up for the Fight: Vehicle Designs Take on Challenge of Mine Warfare. Jane's International Defence Review 2009.
7. Ragel B, Allred D, Brevard S, Davis R, Frank E. Spine: Fractures of the Thoracolumbar Spine Sustained by Soldiers in Vehicles Attacked by Improvised Explosive Devices. Spine 2009; 34:2400–2405.
8. Ramasamy A, Masouros S, Newell N. In-vehicle extremity injuries from improvised explosive devices: current and future foci. Philosophical transactions of the Royal Society of London. Series B, Biological sciences 2011; 366:160–70.
9. Randers-Pehrson G. Airblast Loading Model for DYNA2D and DYNA3D, USA Army Research Laboratory, Technical Report no. 1310, 1997.
10. Swisdak M. Simplified Kingery airblast calculations, Naval Surface Warfare Center, Twenty-Sixth DOD Explosives Safety Seminar, 1994.
11. Valis D, Vintr Z, Malach J. Selected aspects of physical structures vulnerability – state-of-the-art. Eksploatacja i Niezawodnosc – Maintenance and Reliability 2012; 14:189–194.
12. North Atlantic Treaty Organization, AEP-55: Procedures for Evaluating the Protection Level of Logistic and Light Armoured Vehicles, Volume 2 Edition 1, 2006.

Artur ILUK
Wrocław University of Technology
Institute of Machine Construction and Operation
ul. Łukasiewicza 7/9
50-371 Wrocław, Poland
e-mail: artur.iluk@pwr.wroc.pl

Article citation info:
GRINČOVÁ A, MARASOVÁ D. Experimental research and mathematical modelling as an effective tool of assessing failure of conveyor belts. Eksploatacja i Niezawodnosc – Maintenance and Reliability 2014; 16 (2): 229–235.

Anna GRINČOVÁ
Daniela MARASOVÁ

EXPERIMENTAL RESEARCH AND MATHEMATICAL MODELLING AS AN EFFECTIVE TOOL OF ASSESSING FAILURE OF CONVEYOR BELTS

BADANIA EKSPERYMENTALNE I MODELOWANIE MATEMATYCZNE JAKO SKUTECZNE NARZĘDZIA OCENY USZKODZEŃ TAŚM PRZENOŚNIKOWYCH

One of the main causes of damage is their dynamic stress, which often ends the life-cycle caused end of conveyor belts. Dynamic stress leads to fatigue strength functions in shear loading of fabric conveyor belts. Damage of the conveyor belt can be solved by extensive experimental research in laboratory conditions on complex equipments made just for this purpose. The aim of the study is to determine the relation of power in the conveyor belt to the weight of the material which is falling onto a conveyor belt and to impact level height, which is based on data obtained in the experimental research. The experimental measurements have been performed on a test rig, which was developed at the Institute of Logistics and Transport Industry FBERG of Kosice. Results of mathematical modelling clearly say that proposed regression models describe real behaviour of the conveyor belts in productions during their dynamic stress as a result of the influence of shock and stretching forces very well.

Keywords: *experimental research, modelling, conveyor belt, conveyor belt stenting.*

Jedną z głównych przyczyn uszkodzeń taśm przenośnikowych są naprężenia dynamiczne, które często prowadzą do zakończenia cyklu życia taśmy. Naprężenia dynamiczne powodują pojawienie się funkcji wytrzymałości zmęczeniowej w warunkach oddziaływania na taśmę tkaninową obciążenia ścinającego. Problem uszkodzeń taśm przenośnikowych można rozwiązać prowadząc obszerne badania doświadczalne w warunkach laboratoryjnych na skomplikowanych, specjalnie do tego celu stworzonych urządzeniach. Celem prezentowanej pracy było określenie zależności między siłami w taśmie przenośnika a masą materiału spadającego na taśmę oraz wysokością zrzutu, w oparciu o dane z przeprowadzonych badań doświadczalnych. Pomiary eksperymentalne przeprowadzono na stanowisku badawczym zaprojektowanym w Instytucie Logistyki i Przemysłu Transportowego FBERG w Koszycach. Wyniki modelowania matematycznego wyraźnie pokazują, że proponowane modele regresji bardzo dobrze opisują rzeczywiste zachowanie taśm przenośnikowych podczas procesu produkcyjnego, w trakcie którego poddawane są one dynamicznym naprężeniom w wyniku oddziaływaniasiły uderzenia oraz sił rozciągających.

Słowa kluczowe:*badania eksperymentalne, modelowanie, taśma przenośnika, stentowanie taśmy przenośnika.*

1. Introduction

Belt transport is a high performance transport system which has a wide application in praxis. The conveyor belts represent the most productive, and thus even the most economical transport device with a high transport performance and ecologic harmlessness. By Kulinowski [17] for belt conveyors, the transport task can be defined as a process whose purpose is to transport the set quantity of handled material within a defined time between the set loading and offloading locations.

From the point of belt conveyor operation the most important construction element is the conveyor belt. Conveyor belt is a closed element, which orbits around the end of drums and also it forms the support and traction element of conveyor belt. Rope belt conveyors are the only exceptions where the belt is only a load bearing element and the rope has a tow function. According to Zur, belt conveyor is a limited range, continuously moving transport facility that carries material on the belt surface, between two belts or inside a belt [28]. According to Marasová [20] conveyor belt carries resistances arising from the movement and serves for transportation of material, loads or people.

During the operation, conveyor belt is influenced by many different stresses, which cause the process of damaging and wearing the belt. Wearing of conveyor belts depends on many factors, but mainly on the operating conditions in which the conveyor belt is working and on the kind of transported material [15, 20, 26, 27]. The operating experience shows that the most critical point, where 66 to 80% of all the damages of conveyor belt arise is the place of feeding, so called dunes. A point impact load, which is one of the main reasons of damaging of conveyor belt is formed at dunes. This point load arises from sharp-edged pieces conveyed material on the conveyor belt. If the energy of impact is greater than the ability of supports and a conveyor belt to absorb this energy, conveyor belt gets damaged mainly in its upper cover layer in the form of transverse and longitudinal grooves, injections and punctures.

The theoretical knowledge, experimental measurements and operating experience shows that the speed and the way of damaging the conveyor belt at the places of dunes depend mainly on itself design of belt and on character of design elements, from which the belt is made. It also depends on the power situation in belt, exactly in the part, where the action of point-forces begins and on the stiffness of the supporting elements of the belt.

Among the functional features of conveyor belts the importance also lies in the tensile strength and resistance of conveyor belts to deflection which is classified as conveyor belt ability to absorb impact energy waist emerging at the impact of the material on the belt, i.e. to absorb the energy shock through deformation work of the conveyor belt without its damaging. In theory, the authors effort is focused on the creation of mathematical models to describe the characteristics of the conveyor belt. Mathematical apparatus for determining optimum reliability and durability of conveyor belts using the theory of recovery was described in the works [24, 25]. The issue of damaging conveyor belts is concerned in many works [9, 10, 22, 23].

The models of punctures rubber-textile conveyor belts have been marginally addressed in the works [2, 3, 4, 5, 13, 14]. Nowadays a significant attention is devoted to mathematical modelling using finite element method [16, 18, 19]. Research of damaged conveyor belts can be implemented at two levels: directly during the operation of conveyor belts, or through special test equipment .Aldrich et al. [1] were realising research of conveyor belts damaging in praxis by using of machine vision and kernel methods. In contrast to it, Fiset and Dussault [11], Ballhaus [6, 7] and Flebbe [12] have analysed the causes of conveyor belts damage in laboratory conditions.

Experimental research in laboratory conditions provides considerable information about the properties of materials. Therefore, the impact tests on laboratory instruments have become a common testing method. In these tests there are forces acting on the sample measured during impact in most cases continually during the test period. Results contain complete information of absorbed energy and deformation of the sample. Currently there are no established uniform criteria for assessing the resistance of conveyor belts against punctures. There are numbers of experimental machines and equipment on which tests on resistance of conveyor belts to deflation were performed.

2. Methodology of experimental research

During operational measurements either directly during operation of a conveyor belt or during measuring of effects of tested samples it is possible to determine force effect on to the individual construction parts of the conveyor belt, such as roller table. However, during operational measurements it is not possible to determine any external load arising, which caused these force effects. And that is why the experimental measurements begin on experimental equipment, where it is able to exactly determine weight of impact load, impact height and forces acting on the belt at the moment of load impact.

A test rig for puncturing tests of conveyor belts was designed and constructed at the Institute of Logistics and Transport Industry in Košice several years ago. According to the gained experiences a laboratory was created later on. It serves to simulation and modelling of structural parts of conveyor equipment including conveyor belts and modern experiment equipment for testing conveyor belts from the point of their resistance to puncturing [20].

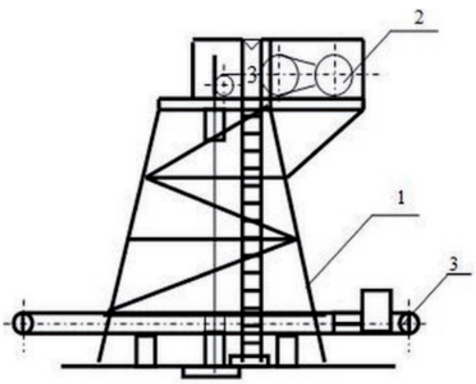

Fig. 1. Side view of the existing structure of test equipment 1 – Tower (mast), 2 – reel device of ram, 3 – belt conveyor

The original device (Fig.1) was upgraded later on (Fig.2). For testing rig a concrete foundation with a grill for attaching the tower, control room for operating the machine and test rig itself were built for the testing rig in advance.

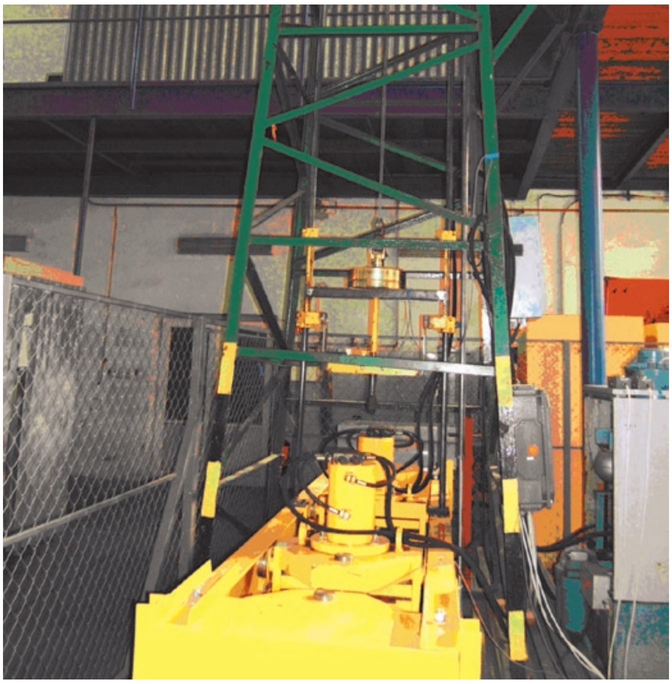

Fig. 2. View of innovated test rig

The test rig is equipped with a hydraulic system for clamping strip samples (Fig.3) and other hydraulic system for tensioning the sample during the test. Hydraulics provide the better clamping and tensioning strip samples and thus allows to obtain relevant test results. The design of the test equipment is based on the current requirements resulting from the present research, as well as from the requirements of the manufacturer of conveyor belts in Slovakia.

Fig. 3. Test table with hydraulic rig

During the realization of the experiment the following parameters can change:

- *weight of the ram* – in the range from 50 kg to 100 kg (simulation of different density of the transported material)
- *ram head* – a spherical shape (Fig.4), pyramid and cone (simulation of different types of impact material)
- *the amount of impact ram* – up to 2.6 meters (simulating the impact of different heights at belt conveyor)
- *type of conveyor belt* (simulation of different operating conditions for which different types of conveyor belts are intended).

Fig. 4. Globular head ram

3. Result and discussion

3.1. Material and realization of the experiment

The research was conducted in order to determine the actual values of impact and tension forces simulating operational conditions and comparing them with those obtained by regression models. Experimental measurements have been performed on a test rig shown in Figure 2.

The objects of experimental tests were steel cord conveyor belts STEELBELT type (Fig. 5) produced in the Slovak Republic.

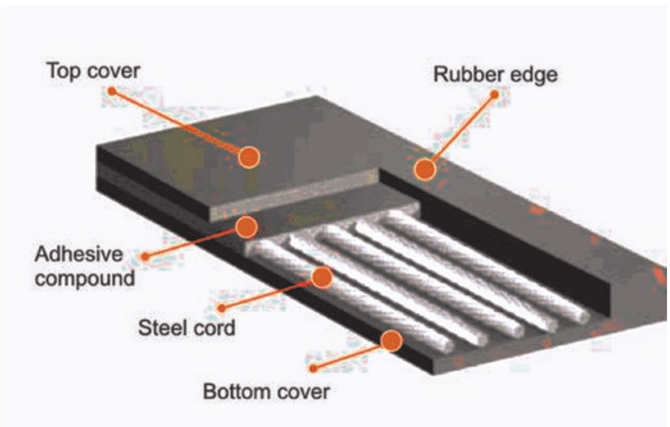

Fig. 5. Cord conveyor belt

Conveyor belts STEELBELT (Fig.5) are suitable to transport material over long axial distances in difficult working conditions. Low elongation under load and their excellent ability to adapt to the conveyor trough due to low transverse stiffness make them suitable for their use mainly in demanding conditions [21].

The skeleton is composed of high-strength steel reinforcing cords laid one plane and coated in rubber core, which provides a perfect blend of top and bottom coating. This hardback ensures optimal functional ability and high durability. Shift cords by selected spacing can be achieved by different strength council. Coatings protect the frame of the conveyor belt against external climatic environmental influences and mechanical damage. Coatings come into contact with the conveyor rollers and drums and protect the skeleton from the adverse effects of abrasion.

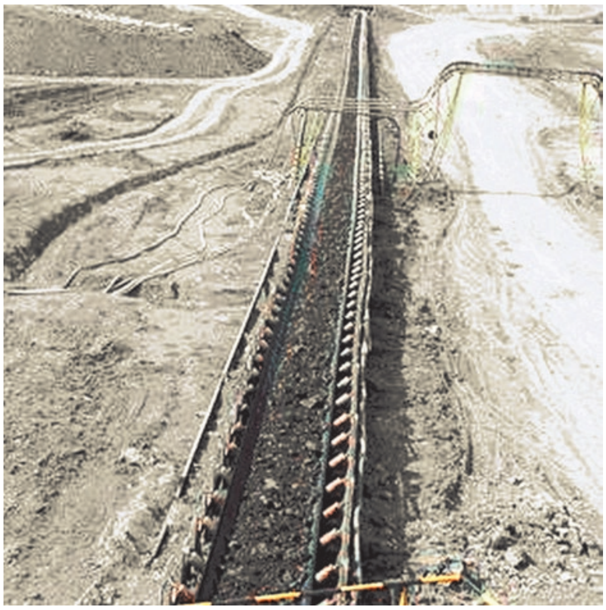

Fig.6. Conveyor belts STEELBELT in use

Ram head with spherical shape and two types of steel cord conveyor belts were used during testing: conveyor belt type ST 1250 with strength 1250 $N.mm^{-1}$ and conveyor belt type ST 2500 with the strength 2500 $N.mm^{-1}$.

The procedure for experiment is as follows:

1. A specimen with a length from 1.2 m to 1.4 m and a width from 0.4 meters to 0.6 meters is cut out from the conveyor belt.
2. The specimen of the conveyor belt is fastened into hydraulic jaws on both sides.
3. It is stretched by the force equal to 1/10 of strength of the belt set by the manufacturer by using hydraulic equipment.
4. The drop-hammer of the relevant weight is lifted by a pulley block to the required height, from which it is released by free fall onto the conveyor belt. During which values of the tension and impact force in kN units are recorded during the whole measurement by two tens-meter sensors.

Evaluation of tests in case of puncture detection consists in a visual inspection of conveyor belt. Meanwhile, it is also determined at what size of tensile force F_S and impact force F_I the puncture of a belt i.e. damage of a belt was caused from the recording of measured data (Fig.7).

3.2. Analysis and design of experiment regression model

Evaluation of the results of the process of damaging the conveyor belt by puncturings is based on long-term follow-up and subsequent statistical evaluation of measured data. In modelling the process of

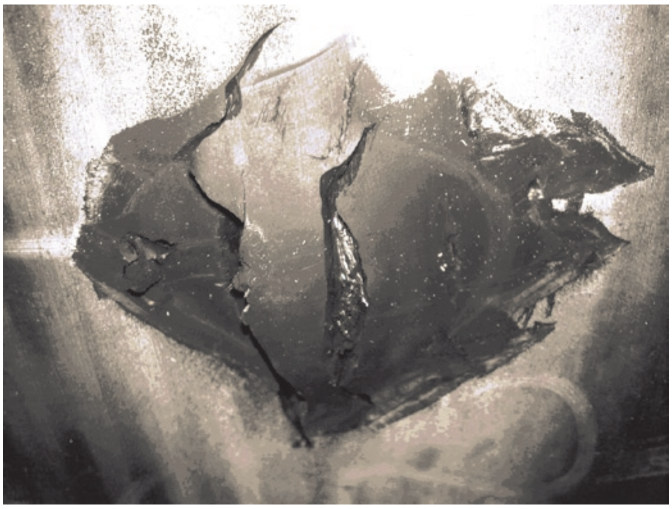

Fig. 7. Damage of a conveyor belt in a way of an impact break

degradation, we used basic statistical methods and multiple regression analysis. To estimate the coefficients of the selected regression model we used the method of least squares. Determining of the close dependence among quantitative variables was considered by a correlation analysis.

The relationship between variable y and several independent variables x_j, $j = 1, 2, \ldots, k$ can be expressed by the multiple linear regression model in the form:

$$y = \beta_0 + \beta_1 x_1 + \beta_2 x_2 + \beta_3 x_3 + \beta_4 x_4 + \beta_5 x_5 + \ldots \beta_k x_k + \varepsilon \,, \qquad (1)$$

where:

β_0 and β_j for $j = 1, 2, \ldots, k$ – parameters of regression model,

ε – random error [8].

Point estimate of the multiple linear regression model is the regression function:

$$Y = b_0 + b_1 x_1 + b_2 x_2 + b_3 x_3 + b_4 x_4 + b_5 x_5 + \ldots + b_k x_k \,, \qquad (2)$$

where:

Y – theoretical, estimated value of the dependent variable,

b_0 – the estimated parameter β_0.

The parameters of the regression model are estimated using the method of least squares to which it applies:

$$\sum_{i=1}^{n} (y_i - Y_i)^2 = \sum_{i=1}^{n} e_i^2 \to \min. \qquad (3)$$

where: $e_i = y_i - Y_i$.

The aim of the experiment is to determine the dependence of impact force F_I, respectively tension force F_S from independent variables *Weight of the ram* (m) and *The amount of impact ram* (h) . The best results showed a regression model, which is originated from the regression function in the form:

$$y = \beta_0 + \beta_1 x_1 + \beta_2 x_2 + \beta_3 x_3 + \varepsilon \,, \qquad (4)$$

where variables x_i, $i = 1,2,3$ we chosen in the following way:

$x_1 = m, x_2 = h, x_3 = m \cdot h$ and $y = F_I$, resp. $y = F_S$.

Adjusted regression model has the form:

$$Y = b_0 + b_1 \cdot m + b_2 \cdot h + b_3 \cdot m \cdot h. \qquad (5)$$

The method of least squares as a method of estimating parameters of a regression model is very sensitive to the presence of extreme outlying points in the sample. Therefore, at the beginning of the regression analysis, we assessed the quality of the data for outlying and extreme values. Values considered as outliers were excluded from the field. Outlying values were mainly those values, which are beginning to show damage to the conveyor belt, respectively there has been a breakdown of the conveyor belt.

To verify the statistical significance of the regression model we **use the F – test the statistical significance of the model**. The null and alternative hypotheses are: H_0 *: regression model is not statistically significant* against H_1 *: regression model is statistically significant*.

The test statistics is computed using the form:

$$F = \frac{(n-k-1) \cdot \sum_{i=1}^{n} (Y_i - \overline{y})^2}{k \cdot \sum_{i=1}^{n} (y_i - Y_i)^2} \,, \qquad (6)$$

where:

y_i – i^{th} observed value of dependent variable,

Y_i – i^{th} estimated value of dependent variable using the regression model,

$\overline{y}$ – mean of the dependent variable,

k – number of independent variables,

n – number of observations.

If the null hypothesis is true, the test statistics F is an observed value of an F distributed random variable with k and $(n-k-1)$ degrees of freedom. The null hypothesis is rejected at the level of significance α, if $F > F_{1-\alpha}(k; n-k-1)$. In case of rejection of the null hypothesis at least one explanatory variable has a statistically significant effect on the test explained variable.

Statistical significance of the regression model parameters will be verified by testing **the statistical significance of regression parameters** β_j. The null and alternative hypotheses are: H_0 *: parameter of regression model is not statistically significant* against H_1 *: parameter of regression model is statistically significant.* The test statistics computed using the form:

$$t = \frac{b_j}{s_{b_j}} \,, \qquad (7)$$

where b_j is the point estimate of the parameter β_j and s_{b_j} is the estimated standard error. We reject the null hypothesis at the level of significance α, if $|t| > t_{1-\frac{\alpha}{2}}(n-k-1)$.

In hypothesis testing acceptance or rejection of the null hypothesis can be carried also by decision rule for a p-value. If p-value is less than the level of significance α, the null hypothesis is rejected. If p-value is greater than the level of significance α, the null hypothesis is accepted.

Conveyor belt type *ST 1250*

Point estimate a linear regression model that captures the dependence of impact force from selected independent variables has the form:

$$F_I = -1.2873 + 0.0588m - 0.7945h + 0.1313m \cdot h \ . \tag{8}$$

To check the statistical significance of the model, we used the F – test of the statistical significance of the model. Because $p - value << \alpha$, we assume that the proposed regression model is statistically significant. Statistical significance of each parameter regression model has been verified through a test of statistical significance of the regression parameter. The results show that all of the parameters appear to be statistically significant (Table 1).

Table 1. Estimates of the parameters of a regression model for conveyor belt type ST 1250

Parameter	The point estimate	The lower limit of 95% of the estimate	The upper limit of 95% of the estimate	p-value	Statistical significance of the parameter
b_0	–1.2873	–1.9506	–0.6241	0,0004 <α	significant
b_1 (m)	0.0588	0.0490	0.0687	9,94.10^{-14}<α	significant
b_2 (h)	–0.7945	-1.3303	–0.2584	0,0049<α	significant
b_3 (m.h)	1.1313	0.1225	0.1401	1,1.10^{-25}<α	significant

Multiple index value determination is $I^2 = 0.9981$, which means that 99.81% of the variability of the variable F_I can be explained by the influence of the variables *Weight of the ram*, *The amount of impact ram* and their interaction.

Analogically, we obtain regression models for tensioning force. Model has the form:

$$F_S = 22.5681 + 0.2407m + 4.8752h + 0.1929m \cdot h \ . \tag{9}$$

The obtained model and parameters of the model are statistically significant. Multiple index value determination is $I^2 = 0.9827$, which means that 98.27% of the variability of the F_S can be explained by the influence of the variables *Weight of the ram*, *The amount of impact ram* and their interaction.

Conveyor belt type *ST 2500*

Parameters of the regression model for conveyor belt type ST 2500 and the value of the index determination for the impact and tension force are shown in Table 2.

Table 2. Point estimates of the regression model for conveyor belt type ST 2500

Force	Point estimates of regression model	Index determination
F_I	$F_I = -1.5635 + 0.0687m - 1.3970h + 0.1341m \cdot h$	0.9987
F_S	$F_S = 44.6561 + 0.2153m + 7.3865h + 0.1004m \cdot h$	0.9860

Graphical representation of the measured (empirical) values and calculated (theoretical) values of impact force and tension force to the belt ST 2500 is on Figure 8.

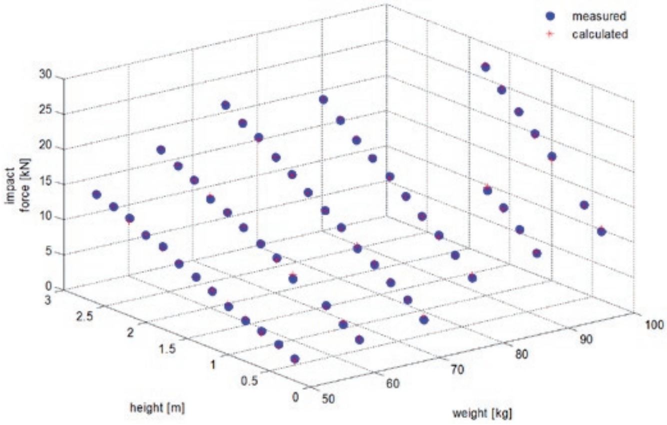

Fig.8. Measured and calculated values of impact force –conveyor belt type ST 2500

3.3. Evaluation of the experiment

Two types of steel cord conveyor belts were considered during modelling and experimental research: conveyor-type ST 1250 with strength 1250 N.mm^{-1} a conveyor belt type ST 2500 with strength 2500 N.mm^{-1}. From measurements, which have been performed on a test rig and ram with spherical tip the following conclusion has resulted:

- cross section of the conveyor belt type ST 1250 appears at a ram of weight:

  $m = 60\ kg$ at its impact from the height $h = 2.2\ m$,

  $m = 70\ kg$ at its impact from the height $h = 1.8\ m$,

  $m = 80\ kg$ at its impact from the height $h = 1.6\ m$,

  $m = 90\ kg$ at its impact from the height $h = 1.4\ m$,

- cross section of the conveyor belt type ST 2500 appears at a ram of weight:

  $m = 80\ kg$ at its impact from the height $h = 2.2\ m$,

  $m = 90\ kg$ at its impact from the height $h = 2.0\ m$,

  $m = 100\ kg$ at its impact from the height $h = 1.8\ m$.

In both cases is can be concluded that size of the energy needed to breakdown of the conveyor belt can be compared with a potential energy of the load impacting the conveyor belt.

Potential energy [J], where the acceleration due to gravity, in the case of the conveyor belt ST 1250 is in the range $\langle 1\,236, 1\,295 \rangle$ J of the conveyor belt in the case of ST 2500 is in the range $\langle 1\,727, 1\,766 \rangle$ J. These values are roughly threshold energy at which it is possible to breakdown the conveyor belt.

The mentioned values are only approximate because the values were measured with difference by weight and the amount of impact. The conveyor belt might have been punctured at the levels that were outside the scope of measurement. Due to a more accurate estimate of limiting energy causing puncturing the conveyor belt, it will be necessary to carry out measurements with smaller differentiate weight or maybe with higher impact.

4. Conclusion

Experimental tests provide not only the information about a process of degradation but even data necessary for their subsequent use in mathematical modelling.

One of the special methods was carried out in the experimental research-the method for determining the resistance to deflection. That method was used because puncturing on conveyor belts often occurs during the transport of a material with large fragmentation, and thus decreases their tensile strength, which is the most important parameter of the conveyor belt in terms of reliability.

On the basis of the facts mentioned above, the important fact is that for a subsequent evaluation of measured data it is able:

- to use a created mathematical model directly without checking other models,
- based on the model created with specific coefficients to determine sizes interpolation of shock, respectively tension forces even for other impact heights and ram weights,

through the methodology used within solution of problems to provide manufacturer with an ability, to set technical parameters of types conveyor belts put out by them for technical praxis, taking operation conditions into account.

Both experimental research and modelling of conveyor belts are important for producers as well as for users of conveyor belts. Users are free to reconsider the way of choice of type and construction of their conveyor belt. Determination of impact energy threshold, at which the breakdown appears, thus destroying DP has practical significance for the user. He can directly set impact height in the place of dunes and regulate the maximum weight load with shredders in the operation and thus not to achieve or exceeded the size of the marginal impact energy. Manufactures got an opportunity to try new design and develop new and more resistant structures of conveyor belts.

***Acknowledgement**: The work presented in this paper was supported by the Project* VEGA *1/0922/12.*

References

1. Aldrich C, Jemwa G.T, van Dyk J.C, Keyser M.J, van Heerden J.H.P. Online analysis of Coal on a Conveyor Belt by use of Machine Vision and Kernel Methods. International Journal of Coal Preparation and Utilization 2010; 30: 331–348.
2. Andrejiova M. Attestation of assumptions about random error of the regression model 2011. Creative Mathematics and Informatics 2011; 20(1): 4–7
3. Andrejiova M, Pavliskova A. Analysis of regression model of functional dependency in impact force from height and weight of ram for conveyor belt. Annals of Faculty Engineering Hunedoara: international journal of engineering 2010; 8(3): 267–270.
4. Andrejiova M, Pavliskova A. Lineárny regresný model závislosti životnosti dopravného pásu od jeho niektorých parametrov. Transport & Logistics 2010; 7: 234–238.
5. Andrejiova M, Marasova D. Multiple regression model of functional dependency in impact force from height and weight of ram for conveyor belt. Cuprum: Czasopismo naukowo-techniczne górnictwa rud 2010; 3: 5–14.
6. Ballhaus H. Stress and Wear of Conveyor Belts by Loading Point Impact. Bulk Solids Handlings 1983; 3(1): 347–353.
7. Ballhaus H. Die Impulskräfte beim Aufprall grobstückingen Gutes auf den Fördergut. Braumkohle 1980; 32: 184–18.
8. Draper NR, Smith H. Applied regression analysis. John Wiley and Sons 1998.
9. Fedorko G, Molnar V, Zivcak J, Dovica M, Husakova N. Failure analysis of textile rubber conveyor belt damaged by dynamic wear. Engineering Failure Analysis 2013; 28: 103–114.
10. Fedorko G, Molnar V, Ivanco V, Dovica M, Husakova N. Simulation of Interaction of a Pipe Conveyor Belt with Moulding Rolls. Procedia Engineering, 2012; 48: 129–134.
11. Fiset M, Dussault D. Laboratory simulation of the wear process of belt conveyor rollers. Wear 1993; 164: 1012–1015.
12. Flebbe H. Untersuchung von Fördergurten auf ihre dynamische Festigkeit. Braumkohle 1982; 34: 186–19.
13. Grincova A, Hlubikova A, Kresak J. Metodika skúšania dopravných pásov pri prieraze. Doprava a logistika 2008; 5: 209–213.
14. Grincova A, Berezny S, Marasova D. Tvorba regresného modelu na základe experimentálnych skúšok dopravných pásov proti prierazu. Acta Montanistica 2009; 14: 113–120.
15. Hardygora M, Golosinska G. Effect of the belt and loading station design on impact resistance of steel cord conveyor belts. Bulk Solids Handling 1986. 6: 561–566.
16. Hatala J, Maras M. Application of the method finite elements by numerical modeling stress-strain state in conveyor belts, Acta Montanistica Slovaca 1997;. 2: 101–108.
17. Kulinowski P. Simulation studies as the part of an integrated design process dealing with belt conveyor operation. Eksplotacja i Niezawodnosc – Maintenance and Reliability 2013; 15(1): 83–88.
18. Lodewijks G. On the application of beam elements in finite element models of belt conveyors part I. Bulk Solids Handling 1994; 14: 729–737.
19. Lodewijks G. On the application of beam elements in Finite Element models of belt conveyors, Part II. Bulk Solids Handling 1995; 15: 571–591.
20. Marasová D. et al. Pásová doprava. Technická univerzita Košice, 2006.
21. Matador Conveyor Belt. [online], 2013. http: http://www.matador.sk
22. Mazurkiewicz D. Analysis of the ageing impact on the strength of the adhesive sealed joints of conveyor belts. Journal of Materials Processing Technology 2008; 208: 477–485.
23. Mazurkiewicz D. Test of extendability and strength of adhesive-sealed joints in the context of developing a computer system for monitoring the condition of belt joints during conveyor operation. Eksplotacja i Niezawodnosc – Maintenance and Reliability 2010; 3: 34–39.
24. Pavliskova A, Jadronova M. Application of mathematical model of operating costsfor calculating conveyor belts Life. Manufacturing Engineering 2006; 5: 61–6.
25. Pavliskova A, Andrejiova M. Comparison of model life of conveyor belts with selected statistical methods. Transport & Logistics 2009; 9: 421–425.
26. Sinay J, Kopas M, Tomkova M. Belt conveyors and technical risks. MEP 01, Faculty of mining and geology, Beograd 2001: 155–157.
27. Tomaskova M, Kopas M, Perhac P. Analýza rizík pri prevádzke pásových dopravníkov pomocou komplexnej metódy posúdenia. Transport & Logistics 2006; 4.

28. Żur T. Belt conveyors in mining. Poland: Śląsk Publishers, Katowice 1979.

Anna GRINČOVÁ
Department of Mathematics and Theoretical Informatics
Faculty of Electrical Engineering and Informatics
Technical University of Kosice
Nemcovej 32, 042 00 Kosice, Slovak Republic
E-mail: anna.grincova@tuke.sk

Daniela MARASOVÁ
Logistics Institute of Industry and Transport
Faculty of Mining, Ecology, Process Control and Geotechnologies
Technical University of Kosice
Park Komenského 14, 043 84 Kosice, Slovak Republic
E-mail: daniela.marasova@tuke.sk

Article citation info:
STRYCZEK R, PYTLAK B. Multi-objective optimization with adjusted PSO method on example of cutting process of hardened 18CrMo4 steel. Eksploatacja i Niezawodnosc – Maintenance and Reliability 2014; 16 (2): 236–245.

Roman STRYCZEK
Bogusław PYTLAK

MULTI-OBJECTIVE OPTIMIZATION WITH ADJUSTED PSO METHOD ON EXAMPLE OF CUTTING PROCESS OF HARDENED 18CrMo4 STEEL

OPTYMALIZACJA WIELOKRYTERIALNA SKORYGOWANĄ METODĄ PSO NA PRZYKŁADZIE PROCESU SKRAWANIA STALI 18CrMo4 W STANIE ZAHARTOWANYM*

In this paper a Modified Particle Swarm Optimization (PSO) method for multi-objective (MO) problems with a discrete decision space is proposed. In the PSO method the procedure to determine inertia weight, learning factor and social factor is modified. In addition, both an elitism strategy and innovative deceleration mechanism preventing the particles from going beyond the limits of decision space are introduced. The proposed approach has been applied to a series of currently used test functions as well as to optimization problems connected with finish hard turning operation, where the obtained results have been compared with those obtained by means of Genetic Algorithms (GA). The results indicate that the proposed approach is relatively quick, and thus it is highly competitive with other optimization methods. The authors have obtained a very good diversity, convergence and a maximum range of the Pareto front in the criteria space. In order to assess the quality of the generated Pareto set for each of presented examples, a rating has been determined based on the entropy measurement and inverted generational distance (IGD).

Keywords: *hard turning, particle swarm optimization (PSO) method, evolutionary computations, multi-objective optimization, entropy.*

W pracy zaproponowano zmodyfikowaną metodę optymalizacji wielocząsteczkowej (PSO) dla problemów optymalizacji wielokryterialnej z dyskretną przestrzenią decyzyjną. W metodzie PSO zmieniono sposób określania momentu bezwładności, współczynnika uczenia oraz współczynnika społecznego. Dodatkowo wprowadzono elitaryzm oraz innowacyjny mechanizm hamowania cząstek chroniący je przed przekraczaniem dopuszczalnych granic przestrzeni decyzyjnej. Zaproponowane podejście zostało zweryfikowane na szeregu aktualnych funkcjach testowych oraz problemie optymalizacji procesu skrawania stali 18CrMo4 w stanie zahartowanym, gdzie porównano je z wynikami uzyskanymi za pomocą algorytmów genetycznych (GA). Uzyskane wyniki wskazują, że zaproponowane podejście jest względnie szybkie i wysoce konkurencyjne w stosunku do innych metod optymalizacji. Autorzy uzyskali bardzo różnorodne, zbieżne i w pełnym zakresie przebiegi frontu Pareto w przestrzeni kryteriów. W celu oceny jakości wygenerowanego zbioru Pareto dla każdego z prezentowanych przykładów wyznaczono ocenę opartą na pomiarze entropii oraz wskaźnika jakości IGD.

Słowa kluczowe: *toczenie na twardo, metoda optymalizacji wielocząsteczkowej (PSO), obliczenia ewolucyjne, optymalizacja wielokryterialna, entropia.*

1. Introduction

The search of optimal decision poses a problematic issue from the perspective of many, often conflicting criteria. Usually, the search results in a large set of solutions. Typical methods of single criterion optimization usually give one solution in a single run of the calculation process, and therefore such methods are useless in multi-objective optimization. In order to obtain many solutions in a single run of calculation process the unconventional methods must be employed. However, only a few of these make it possible to obtain an evenly distributed, coherent and complete set of solutions.

Nowadays, the most popular of these methods are based on evolutionary techniques; Genetic Algorithms (GA) in particular. Generally, these techniques are based on metaheuristics, improving the current situation of an individual in the population, increasing its chances of survival and/or enabling it to inherit the genetic code. The Particle Swarm Optimization (PSO) method is one of those techniques. It has become widely accepted, since it's introduction in 1995 [11] and is used in many fields [19].

PSO has also become the major alternative for GA in the area of multi-objective optimization. The comparison to genetic algorithm and ant colony optimization algorithm indicates that PSO is more effective than the others because of its faster convergence rate [14]. The number of publications describing the use of PSO has grown exponentially for the last few years [20]. The success of this method results from its intuitive nature, the algorithm which is easy to use for programming, and the fact that it is liable to modification, which makes it an excellent tool for experimental research. Reyes-Sierra and Coello Coello [25] have provided a complete taxonomy of existing MOPSOs' algorithms. They studied the main features of MOPSOs such as: the existence of an external archive for non-dominated solutions, the election strategy of non-dominated solutions as the leaders guiding the swarm, the neighbourhood topology, and the existence or non-existence of a mutation operator. During the past few years, several efficient multi-objective variants of PSO have been proposed. Interesting proposals for improving the original PSO algorithm appear every year [21]. More than thirty different Multi-Objective Particle Swarm Opti-

(*) Tekst artykułu w polskiej wersji językowej dostępny w elektronicznym wydaniu kwartalnika na stronie ***www.ein.org.pl***

mizers (MOPSOs) have been described in the literature [5]. New approaches are still being put forward, some focusing on the successful and improved results achieved by the basic algorithm MOPSO [16]. Zhang et al. [28] proposed a new multi-swarm cooperative multi-objective particle swarm optimization algorithm. To better its performance, several improved techniques such as the Pareto dominance-based species technique, the escape strategy of mature species, and the local MOPSO algorithm have also been introduced. The proposed algorithm can produce solution sets that are highly competitive as far as the convergence, diversity, and distribution are concerned. Kaveh, and Laknejadi [10] proposed a hybrid method which is a combination of the particle swarm method and a recently developed algorithm charge system search (CSS). Combining the proposed method with a mutation operator and particle redistribution strategy strengthens the search ability of the proposed algorithm. Magnus and Pedersen [15] suggest a table of PSO parameters which may be used by a researcher in the first place when optimizing new problems. Chakraborty et al. [3] present an analysis of the general Pareto-based MOPSO and find conditions on its most important control parameters (the inertia factor and acceleration coefficients) that govern the convergence behaviour of the algorithm to the optimal Pareto front in the objective function space. Many multi-objective optimization problems in real world engineering applications involve discrete and/or discontinuous parameters [7].

We think that the three following features have a significant impact on the efficiency of MOPSO: the control method of approach and the attempts to exceed the limits of decision space by the particles, consideration of continuous or discrete decision space, and control of the movement speed of particles.

A quality assessment of the Pareto front generated during the multi-objective optimization is not easy [1]. There are many different approaches here and their wider description can be found in the work [29]. In order to compare effectiveness of various approaches, special tests have been developed. Usually, this assessment includes three aspects: convergence meant as the minimum distance between adjacent solutions on the Pareto front, diversification understood as a uniform distribution of the solutions in criteria space, and a maximum range of Pareto front in the criteria space. A suitably chosen metric of decision space has a crucial meaning for the correct assessment in reference to the first and the second aspect. De Carvalho and Pozo [4] performed an empirical analysis of measure by means of three quality indicators (generational distance, inverted generational distance and spacing) to examine how the many-objective technique named control of dominance area of solutions (CDAS) affects the convergence and diversity of MOPSO algorithms. Also Pradhan and Panda [22] used some performance metrics, such as: set coverage metric, generational distance, maximum Pareto-optimal front error, spacing and spread.

One of the main issues dealt with by the researchers seeking effective, intelligent methods for multi-objective optimization is how to obtain a complete and coherent set of Pareto solutions. A current quality assessment of the Pareto front may serve as a determinant of its proper shape. The Entropy-based Multi-Objective Genetic Algorithm (E-MOGA) method, which strongly improves the convergence and uniformity of the Pareto front in comparison to the Multi-Objective Genetic Algorithm (MOGA), can serve as an example here. To assess the quality of solutions, the approach described in this work also uses two forms of entropy: external and internal, as well as inverted generational distance (IGD). This approach does not modify the method of entropy calculation, but it makes the comparison of different tests possible. Our research confirms the following conclusion: "a solution set with a higher entropy is spread more evenly throughout the feasible region and provides a better coverage of the space" [8].

In practical problems the decision space is limited by technical capabilities. The limit values are often optimal. Therefore, the proposed PSO algorithm approach has a built-in mechanism of the particle deceleration, in order to prevent them from exceeding the limits of decision space by its better penetration of the values near the boundary. In industry the decision maker consider the most often a discrete decision space. In design, he is usually able to analyse only a very limited number of solutions [6]. A continuous decision space is only relevant for theoretical consideration. Therefore, the proposed approach takes into account the position change of a particle in one direction only as a multiple of some fixed discrete value.

The speed control of particles movement is one of the main, but little explored parameter influencing the efficiency of the PSO algorithm. Nebro et al. [17] have proposed a new MOPSO algorithm which includes a velocity constriction mechanism. In our approach, as described below, heuristics strategy has also been used for the particles' speed control.

2. Methodology

Let us imagine N-dimensional, discrete space of decision-making, in which each point of the space is represented by a vector $\mathbf{x}$. Each component x_i of the vector $\mathbf{x}$ has the specified range of variation ΔL_i, corresponding to the interval $[L_i^-, L_i^+]$, and a constant step of discretization d_i in the range of the variation. The discrete area of decision-making is dictated with the practical reasons in mind, because in reality, the designer determines the precision of the settings. Realization of the PSO method in discrete space somewhat complicates the algorithm. On the other hand, it eliminates oversized concentrations of solutions in a certain areas of the Pareto front, which tend to elongate the calculation process. Due to the fact that individual ranges of the variation can differ from one another considerably, which results in differences d_i, it was assumed that d_i creates a new unit for the given dimension. This assumption establishes an appropriate metric to calculate the distance between the points in the decision space and at the same time enables the quality assessment of the generated Pareto set, by measuring the entropy.

Formally, the multi criteria optimization problem can be expressed in the following way: we require a vector $\mathbf{x}^*=[x_1^*, x_2^*, ..., x_N^*]^T$, which satisfies:
K inequality constraints

$$g_k(\mathbf{x}) \geq 0 \quad \text{for} \quad k=1, 2, ..., K \tag{1}$$

and M equality constraints

$$h_m(\mathbf{x}) = 0 \quad \text{for} \quad m=1, 2, ..., M \quad \text{and} \quad M<N \tag{2}$$

and optimizes the vector of the objective function $\mathbf{f}(\mathbf{x})=[f_1(\mathbf{x}), f_2(\mathbf{x}), ..., f_l(\mathbf{x})]^T$, where $\mathbf{x}=[x_1, x_2, ..., x_N]^T$ is the vector of decision variables.

The PSO method is often subjected to various modifications. One of the questions that researchers ask themselves is: how should the social factor in the generation of successive positions of the particle be taken into account? In case of a single criterion optimization, one can choose the movement in the direction of the best located neighbour in a specified surrounding of the analyzed particle, or the movement towards the best individual from the whole population. In case of multiobjective optimization, one can additionally select a movement toward the Pareto front. In this paper a few variant approaches were tested. The best results were achieved when the movement toward the nearest located solution on the Pareto front had been chosen.

In the canonical version of PSO, a particle is associated with the position attribute, the velocity attribute and the individual experience attribute. The position of a particle is always updated in every step using the equation (3)

$$x_i = x_i^0 + v_i \tag{3}$$

and the velocity is updated in the following way:

$$v_i = w \cdot v_i^0 + c_1 \cdot r_1 \cdot \left(x_i^{bp} - x_i \right) + c_2 \cdot r_2 \cdot \left(x_i^{gb} - x_i \right) \tag{4}$$

where: x_i^0 – i-th component of the position vector in the previous step, v_i^0 – i-th component of the velocity vector in the previous step, w – inertia weight, c_1, c_2 – acceleration coefficients, r_1; $r_2 \in [0,1]$ are random values, x_i^{pb} – best particle position, x_i^{gb} – best global position.

In multi-objective algorithms, a set containing a representation of all non-dominated solutions (leaders) is maintained.

The general structure of code of the proposed algorithm is shown as follows:

```
BEGIN
        Initialize Swarm
        Initialize Particles_Best
        Initialize Leaders_archive
        FOR t=1 to Number_of_Iteration
                FOR p=1 to Population_Size
                        Find_Leader_p
                        Move_Particle_p
                        Evaluate_new_position_of_Particle_p
                        Update_Particle_Best_p
                        IF new_Leader=TRUE
                                Update_Leaders_Archive
                        ENDIF
                NEXT p
        NEXT t
        Output_Leaders_Archive
END
```

where, t denotes the generation index, p denotes particle index.

The proposed approach to determination of the Pareto front with the PSO method consists of the following steps:

Step 1. Generating of the initial population of particles. For each particle p=1, 2, …, N_{pop} The components of the decision variables vector of $\mathbf{x}_p$ and the initial speed vector $\mathbf{v}_p$ for i-the dimension of the decision space are generated randomly:

$$\left.\begin{aligned} x_{ip} &= L_i^- + d_i \cdot \text{round}\left(\text{”}\, L_i \cdot \text{rand}(\,)\right) \\ v_{ip} &= 2 \cdot \text{rand}(\,) - 1 \end{aligned}\right\} \quad \text{for} \quad i=1, 2, \ldots, N \tag{5}$$

Meanwhile, the position of the particle in the criteria space (fitness space) is calculated $best_p=[f_1(\mathbf{x}_p), f_2(\mathbf{x}_p), ..., f_l(\mathbf{x}_p)]^T$, and analysis regarding the location of the solution against the Pareto front is performed. The location generated in this step is stored as the $best_p$, which means the best position of the particle p achieved up to now. The Initial Pareto front is determined during this step.

Step 2. Accomplishment of successive iterations during which the particles are moving in the decision space. During the next iterations, the course of the Pareto front is being constantly modified if necessary.

What follows for each particle p is:

Step 2.1. Calculation of the distance d_p^f (Fig. 1) of the particle p from the current Pareto Set (from the current leader for the particle p):

$$d_p^f = \min\left(d_1^f, d_2^f, ..., d_{L_p}^f \right) \tag{6}$$

where:

$$d_l^f = \sqrt{\sum_{i=1}^{N} \left(\frac{x_i - x_i^f}{d_i} \right)^2} \quad \text{for} \quad l=1, 2, ..., L_p \tag{7}$$

where: x_i – current location of the particle in the i-dimension, x_i^f – the location of the nearest point on the forehead of Pareto (leader) in the i-dimension.

Step 2.2. Determining coefficients w, c_1, c_2, (Fig. 2) that are used for calculation of velocity components of particle p motion. The coefficient w is actually the weight, and it is taken into account when considering the current direction of particle motion. In case of the coefficient w, its value is set as a reference value and is determined at constant level equal to 0.5. The coefficient c_1 decides how closely the particle will try to return to its the best position. It was assumed that in the first phase of iterations this coefficient will play a decisive role, guaranteeing penetration of the decision space by the particle near its current location. In the final phase of iterations this coefficient reaches the value of 0, because the main task in this phase is to direct all particles near to the Pareto front. The coefficient c_2 takes into account the social impact of the particle, enabling it to choose the direction of the particle's movement toward better located particles, especially those on the Pareto front. In the proposed approach, the partial components of particle movement associated with the coefficient c_2 point at the shortest way toward the Pareto set. In the first iteration cycles the social impact is ignored, allowing the particle to move in random directions and thus better penetrate its environment. In the second phase, the social coefficient becomes decisive. In the presented approach the oscillation of the coefficient c_2 value, was used so as to enable a particle to temporarily abandon the close surrounding of the Pareto set. Therefore the particle can leave the Pareto set and penetrate the area near to the Pareto set better, and consequently its further movement in the right direction is possible. To determine current values of the coefficients, the following formulas were adopted:

$$w = 0.5 = const \tag{8}$$

$$c_1 = 1 - \frac{1}{e^{-20q/\left(N_q - 0.5\right)}} \tag{9}$$

$$c_2 = \frac{0.5 + 0.5 \cdot \cos\left(34.5q/N_q\right)}{1 + e^{-10q/\left(N_q - 0.5\right)}} \tag{10}$$

where: q – number of successive iteration, N_q – number of all iterations.

Step 2.3. Determining the particle deviation d_p^b from its the best position. It is calculated from the formula:

$$d_p^b = \sqrt{\sum_{i=1}^{N} \left(\frac{x_i - x_i^b}{d_i} \right)^2} \tag{11}$$

where: x_i^b – i-th component of the best position of particle so far.

Step 2.4. Determining directional vector components for the best particle position so far:

$$p_i^b = r_1 \cdot \frac{x_i^b - x_i}{d_p^b} \quad \text{for} \quad i=1, 2, \ldots, N \tag{12}$$

where: r_1=rand( ) – random number, the same for all components.

Step 2.5. Determining directional vector components of the particle p for the Pareto set (leader):

$$p_i^f = r_2 \cdot \frac{x_i^f - x_i}{d_p^f} \quad \text{for} \quad i=1, 2, \ldots, N \tag{13}$$

where: r_2=rand( ) – random number, the same for all components.

Step 2.6. Calculating the elements of movement speed vector:

$$v_i = w \cdot v_i^0 + c_1 \cdot p_i^b + c_2 \cdot p_i^f \quad \text{for} \quad i=1, 2, \ldots, N \tag{14}$$

where: v_i^0 – i-th component of the speed vector in the previous step.

Step 2.7. The normalization of the movement speed vector components:

$$v_i^n = \frac{v_i}{\sum_{i=1}^{N} v_i^2} \quad \text{for} \quad i=1, 2, \ldots, N \tag{15}$$

Step 2.8. Correction of the particle speed resulting from the possibility of exceeding of the permitted movement area. The speed correction is carried out by the inhibition mechanism of the particle according to the following formulas:

$$dv_i = a_i \cdot v_i^n \cdot \text{abs}\left(x_i - \frac{L_i^+ + L_i^-}{2} - \text{sgn}\left(v_i^n\right) \cdot \frac{L_i^+ - L_i^-}{2} \right) \tag{16}$$

where: a_i – coefficient of movement speed of the particle. This coefficient should be chosen in such a way to guarantee similar mobility of the particles in all directions. The coefficient value is chosen from the range of (0,1].

Step 2.9. Calculation of new components of particle position:

$$x_i' = d_i \cdot \text{round}\left(\frac{x_i - dv_i}{d_i} \right) \quad \text{for} \quad i=1, 2, \ldots, N \tag{17}$$

Step 2.10. Generation of a new location of the particle in the criteria space. In case when the criteria are not within the assumed constraints, the next part of this step is omitted. Checking whether the new position of the particle in the modified metric is the best position so far. If the current particle position is located on the Pareto front, such position is added to the Pareto set and all the solutions which are predominated by the new solution are removed.

Step 2.11. In case of failure to achieve desired number of iterations, return to step 2.1.

The term "entropy" appears in many areas of science and is associated with the assessment of disorder or arrangement. Individual entropy treated as the amount of information (Hartley 1928) can be determined by the formula: $h_i=-\ln(p_i)$, where p_i – the probability of an event. Absolute entropy of n events is the weighted arithmetic average of the amount of information received with the occurrence of individual events, where the probability of these events constitute the weights $H=-\sum(p_i \cdot \ln(p_i))$ (Shannon 1948). In turn, relative entropy H_r is expressed by the formula $H_r=H/\ln(n)$.

In the paper the two different definitions of entropy are used: external and internal. The external entropy is measured by means of assessing how close a given set is to the reference set of solutions. In this case, as the reference set we chose the ideal Pareto set, i.e. the complete set of solutions possible to be achieved in a given discrete space of the decision. To meet this requirement the authors calculated the reference Pareto set. The generated Pareto set was used as the set comparable with the calculated set. However, by the internal entropy we mean the measure of entropy defined on the generated Pareto set, taking into account mutual distances of particular solutions from their nearest neighbours in this set. In practice, we have a possibility of calculating only the internal entropy. The objective of this work is to show, however, that when the internal entropy reaches a sufficiently high level, the external entropy reaches a satisfactory level, too.

Assess the external entropy one should define the elements' interaction function s from the set S with the element f from the set F. It was assumed, that this function (Fig. 3) is expressed by the formula:

$$I_f = \max_s \left(e^{-b \cdot \left(r_{f \to s}\right)^2} \right) \tag{18}$$

where: $r_{f\to s}$ is the distance between the element f and the element s measured in the assumed metric decision space, b – coefficient controlling the range of impact, in conducted tests was established as 1.

In practice, it is sufficient to find the distance $r_{f\to s}$ from the current Pareto set in the decision space for each solution f belonging to ideal Pareto front F.

$$r_{r \to s} = \min\left(\sqrt{\sum_{i=1}^{N} \left(\frac{x_i^s - x_i^f}{d_i} \right)^2} \right) \tag{19}$$

where: $f \in F$, $s \in S$.

To be able to compare different experiments' results, it is preferable to normalize values of the influence function, to have their sum equal 1. As a result, the maximum entropy can amount to 1:

$$I_f^n = \frac{I_f}{\sum_f I_f} \tag{20}$$

Hence, the quality assessment of current Pareto front in the form of external entropy is:

$$H^e = \frac{-\sum_f I_f^n \cdot \ln\left(I_f^n\right)}{\ln\left(n_f\right)} \tag{21}$$

where: n_f – the power of the set F.

As mentioned above, an ideal Pareto front remains unknown in the course of practical calculations. Hence, actual evaluation of the quality of the Pareto front should be determined by the measure of the internal entropy H^i. The Agglomeration method was used for the calculation of the H^i. In the first step, a randomly chosen solution from the set S *is* moved to initially empty set S'. In the following steps, the next solutions $s \in S$ (which are located in the nearest distance to the set S' in the decision space) are moved to the set S'. Figure 4 illustrates the method of calculating mutual distances in the decision space. At the same time, the distance D_s of a transferred solution to the set S' is written on the stack during each step.

The influence function of the solution s onto neighbouring solutions takes the form:

$$I_s = e^{-b\left(D_s - 1\right)^2} \tag{22}$$

where: it was assumed that b=1.

After normalization:

$$I_s^n = \frac{I_s}{\sum_s I_s} \tag{23}$$

Internal entropy of the set S is calculated by the formula:

$$H^i = \frac{-\sum_{s-1} I_s^n \cdot \ln\left(I_s^n\right)}{\ln\left(n_s - 1\right)} \tag{24}$$

where: n_s – the power of the set S.

For example, the value of internal entropy for the sequence of 0-1-2-4-5 (Fig. 4).

where: $I_{0\to1}=I_{0\to2}=1$, $I_{2\to4}=0.135$, $I_{4\to5}=0.035$, 0-1-2-4-5 chain length is 2.17, $I^n_{0\to1}=I^n_{0\to2}=0.46$, $I^n_{2\to4}=0.062$, $I^n_{4\to5}=0.016$, is:

H^i=–(0.46ln(0.46)+0.46ln(0.46)+0.062ln(0.062)+0.016(ln(0.016))/ln(4)=0.694

Additionally, the inverted generational distance (IGD) is used in assessing the performance of the algorithms in our experimental studies.

3. Experiments and results

3.1. Test functions

The modified particle swarm optimization method proposed here for the multi-objective problems has been applied to the solve several currently used test functions.

The first of the test problems was presented in the paper [13]. The objective functions for the particular criteria of the optimization were described by the formulas:

$$\begin{aligned} f_1 &= x_1 + \frac{2}{|J_1|}\sum_{j\in J_1}\left(x_j - \sin\left(6\pi x_1 + \frac{j\pi}{n}\right)\right)^2 \to \min \\ f_2 &= 1 - \sqrt{x_1} + \frac{2}{|J_2|}\sum_{j\in J_2}\left(x_j - \sin\left(6\pi x_1 + \frac{j\pi}{n}\right)\right)^2 \to \min \end{aligned} \tag{25}$$

where: $J_1=\{j\,|\,j$ is odd and $2\le j\le n\}$ and $J_2=\{j\,|\,j$ is even and $2\le j\le n\}$, and the decision space $\Omega=[0,1]\times[-1,1]^{n-1}$ and n=3.

After 500 iterations 251 solutions were found and they are presented in the Figures 5 and 6. Additionally, the Figure 7 shows a graph of entropy values, power of Pareto set and IGD (Inverted Generational Distance) in the function of iteration.

The second test problem was also presented in the paper [13]. The objective functions for the particular optimization criteria were expressed by the formulas:

$$\begin{aligned} f_1 &= x_1 + \frac{2}{|J_1|}\sum_{j\in J_1}\left(x_j - \left(0.3x_1^2\cos\left(24\pi x_1 + \frac{4j\pi}{n}\right) + 0.6x_1\right)\cdot\cos\left(6\pi x_1 + \frac{j\pi}{n}\right)\right)^2 \to \min \\ f_2 &= 1 - \sqrt{x_1} + \frac{2}{|J_2|}\sum_{j\in J_2}\left(x_j - \left(0.3x_1^2\cos\left(24\pi x_1 + \frac{4j\pi}{n}\right) + 0.6x_1\right)\cdot\sin\left(6\pi x_1 + \frac{j\pi}{n}\right)\right)^2 \to \min \end{aligned} \tag{26}$$

where: $J_1=\{j\,|\,j$ is odd and $2\le j\le n\}$ and $J_2=\{j\,|\,j$ is even and $2\le j\le n\}$, and the decision space $\Omega=[0,1]\times[-1,1]^{n-1}$ and n=3.

500 iterations found 204 solutions, which are presented in the Figures 8 and 9 for $d_1=d_2=d_3=0.01$. There were 491 solutions for $d_1=d_2=d_3=0.002$ and they are presented in the Figures 10 and 11. Additionally, the Figures 12 and 13 show a graph of entropy values, power of the Pareto set and IGD in the function of iteration for values of $d_1=d_2=d_3=0.01$ and 0.002 accordingly.

The third test problem was presented in the work [27]. The objective functions for the particular optimization criteria were described by the formulas:

$$\begin{aligned} f_1 &= x_1 \to \min \\ f_2 &= g(x)\left[1 - \sqrt{\frac{f_1(x)}{g(x)}} - \frac{f_1(x)}{g(x)}\sin\left(10\pi x_1\right)\right] \to \min \\ g(x) &= 1 + \frac{9\left(\sum_{i=2}^{n} x_i\right)}{(n-1)} \end{aligned} \tag{27}$$

where: $x=(x_1, \ldots, x_n)^T\in[0,1]^n$ and n=3.

After 500 iterations we found 134 solutions, which are presented in Figures 14 and 15. Additionally, the Figure 16 shows a graph of the entropy values, power of the Pareto set and IGD in the function of iteration.

As shown in the above figures, the modified particle swarm optimization algorithm has generated better sets of Pareto solutions (PSO solutions) than those presented in the publications cited above and in the works [13, 27]. For comparison, in the above figures, an ideal Pareto set is presented (all solutions). The analysis of Pareto solution sets shows that the PSO method can find the most solutions from the ideal Pareto set in a very short time period (after 500 iterations).

3. 2. Multi-criteria optimization of hard turning operation of hardened 18CrMo4 steel

In the next step, a modified particle swarm optimization algorithm for multi-objective optimization problems has been used for solving the problems of multi-objective optimization in finish hard turning of hardened steel. The obtained experimental results were compared with the results from the work by [24], where GA with Modified Distance Method (MDM) [18] were used to solve the problem of multi-objective optimization of hard turning operation.

Technological progress in the area of cutting materials has made it possible to machine hardened materials with use of cutting tools with specified contour and angles of the edge. However, this operation is relatively rare in industry, due to the very high cost of tools made of cubical boron nitride (CBN) and the necessity to use the machine tools with appropriately high rigidity. Therefore, this operation should be performed with the optimal values of cutting parameters and many optimization criteria should be taken into account [9]. This will increase profitability and the number of industrial applications.

Hard finish turning operation of hardened (58HRC) 18CrMo4 steel machined with the use of CBN tools with Wiper geometry was subjected to optimization. 18CrMo4 steel (C – 0.18%, Mn – 0.32%, Si – 0.31%, P – 0.012%, S – 0.003%, Cr – 1.02%, Ni – 0.14%, Cu – 0.28%, Ti – 0.071%) is used for toothed elements. The research included: the effect of cutting speed v_c=100–200 m/min, feed f=0.1–0.3 mm/rev, depth of cut a_p=0.1–0.2 mm, and length of cutting distance L on: unit production cost K_j, time per unit t_j, resultant cutting force F and selected parameters of the surface roughness: R_a, R_z and R_{max} [24]. The research was carried out with respect to the machined surface mating with sealing rings (Radial shaft seal), where the following parameters are recommended: R_a=0.2–0.8 µm, R_z=1–4 µm i $R_{max}\le$6.3 µm [12]. On the basis of experimental research results formulas [24] were developed for:

– unit production cost K_j,

$$K_j = \frac{1.25\pi}{v_c f}\left(0.35 + \frac{v_c^{1.672184} f^{0.036654} a_p^{0.072133}}{423.326}\right) + 0.56 \tag{28}$$

– time per unit t_j,

$$t_j = \frac{1.25\pi}{v_c f}\left(1 + \frac{v_c^{1.672184} f^{0.036654} a_p^{0.072133}}{85219.833}\right) + 1.6 \tag{29}$$

– resultant cutting force F,

$$F = \sqrt{\begin{aligned}&\left(993.402604 \cdot v_c^{-0.200600} \cdot f^{0.623620} \cdot a_p^{0.660314} \cdot L^{0.158012}\right)^2 + \\ &\left(320.402695 \cdot v_c^{-0.213734} \cdot f^{0.293166} \cdot a_p^{0.373255} \cdot L^{0.240112}\right)^2 + \\ &\left(814.912603 \cdot v_c^{-0.388726} \cdot f^{0.386365} \cdot a_p^{1.502916} \cdot L^{0.285235}\right)^2\end{aligned}} \tag{30}$$

– arithmetical mean of roughness profile ordinates R_a,

$$\begin{aligned}R_a = {} & 0.634065 - 0.004599 v_c - 1.221571 f - 1.125925 a_p + 0.000010 v_c^2 + \\ & 2.265811 f^2 + 0.007205 v_c \cdot f + 0.007658 v_c \cdot a_p + 0.0000001 v_c \cdot L + \\ & 6.020526 f \cdot a_p - 0.039339 v_c \cdot f \cdot a_p\end{aligned} \tag{31}$$

– average, maximal height of roughness from 5 elementary sectors R_z,

$$\begin{aligned}R_z = {} & 2.678195 - 0.015906 v_c - 3.961551 f - 4.844458 a_p + 0.000027 v_c^2 + \\ & 3.816645 f^2 + 0.046635 v_c \cdot f + 0.033541 v_c \cdot a_p + 28.458806 f \cdot a_p + \\ & 0.001495 a_p \cdot L - 0.243340 v_c \cdot f \cdot a_p - 0.008445 f \cdot a_p \cdot L + \\ & 0.000049 v_c \cdot f \cdot a_p \cdot L\end{aligned} \tag{32}$$

– maximum height of roughness R_{max},

$$\begin{aligned}R_{max} = {} & 2.775193 - 0.016948 v_c - 2.123522 f + 0.000042 v_c^2 + 5.430604 f^2 + \\ & 0.028112 v_c \cdot f - 0.058322 v_c \cdot f \cdot a_p + 0.000008 v_c \cdot a_p \cdot L\end{aligned} \tag{33}$$

In the equations (30)-(33), cutting distance L is present apart from cutting parameters. The value L was derived from the dependency VB_C=g(v_c, f, a_p, L)=0.2 mm, and was inserted into the above specified equations as the constant [23].

As a result of the optimization performed with the use of the modified PSO method for multi-objective optimization problems, after 50 iterations a set of non-dominated solutions was obtained as having 197 solutions and it is presented in Figure 17. For comparison, the set of non-dominated solutions obtained with the help of GA with MDM is presented as well (Fig. 18). Here the result of performed optimization was a Pareto set consisting of 106 non-dominated solutions.

As can be seen, the PSO method has detected much more solutions, and such solutions are better than the ones generated with the help of GA with MDM (Fig. 19). This confirms supremacy of the PSO over the AG and the opinion expressed in the work [2, 26], where the authors compared the PSO method with the ACO, TS, SA, MA, GA methods. In each case of turning and milling operations, the PSO has proved to be the best for selecting the optimal cutting method.

Figure 19 shows the entropy graph and the power of the Pareto set in the function of iteration.

4. Conclusions

In this article, only a discrete space of particle movement is considered. In practice, we always define the location in a particular dimension with a specific, rational accuracy. As has been confirmed by experimental studies, the decision space discretization is essential. The method proved effective only after discretization. The conducted in the work research show that such an approach is correct.

A great number of experiments has been conducted for both constant and variable in time coefficients w, c_1 and c_2. For the particle inertia coefficient determined as the base coefficient (hence its constant value), experiments have been conducted in order to adjust the remaining two coefficients correctly. Obviously, these formulas are heuristic. They cannot be treated as universal. Nevertheless, we think that introduction of oscillation and the reduction of chaos (randomness) in successive iterations has a positive effect on efficiency of the method. This has been confirmed by the conducted experiments.

The evaluation of determined Pareto front quality is executed by the measurment of internal entropy. As pointed out by the performed tests, internal entropy at levels greater than 0.9 corresponds to the external entropy on a very similar level. Because the external entropy for multidimensional multi-objective optimization problems is not known, we can refer to the level of the internal entropy, not only as an assessment degree of the generated Pareto front, but also as a criterion for interrupting the calculation when the internal entropy exceeds a certain, satisfactory level. The external and internal entropy show significant changes during the calculations, in contrast to the parameter of IGD, which stabilizes quickly. The only negative phenomenon here is a longer time needed for computation, when the number of solutions on the Pareto front increases. Hence, we should choose appropriate steps of discretization of the d_i in order to avoid this problem.

Further research connected with the proposed method should tend towards the determination of the parameter a_i at the appropriate level. It has a very large impact on the mobility of particles, which should take the referred average interval. It seems that suitable values are very closely linked to the specific character of the problems being solved. Therefore, it is difficult to determine these values a priori. Instead, one should develop a mechanism of its adaptive selection during calculations. Another important factor for the effectiveness of the PSO method is a suitable choice of ranges in the decision space. In the work this issue has not been studied deeply. Nevertheless, on the base of the tests performed one can conclude that the appropriate narrowing of the decision space to the range corresponding to the position of particles on the Pareto front is very beneficial. When evaluating the obtained tests' results, we can draw the conclusion that the developed modified PSO method is highly competitive when compared to the previous proposals of the PSO, and should find numerous practical applications.

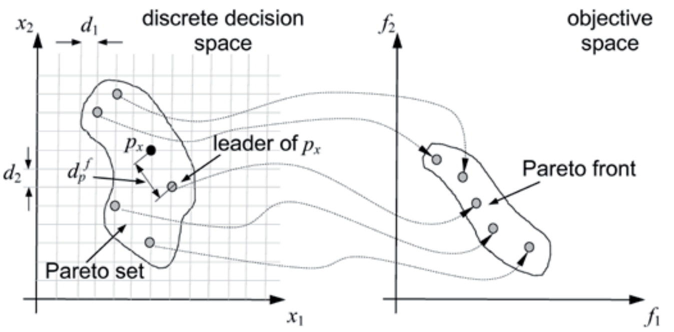

Fig. 1. Leader of particle in discrete decision space

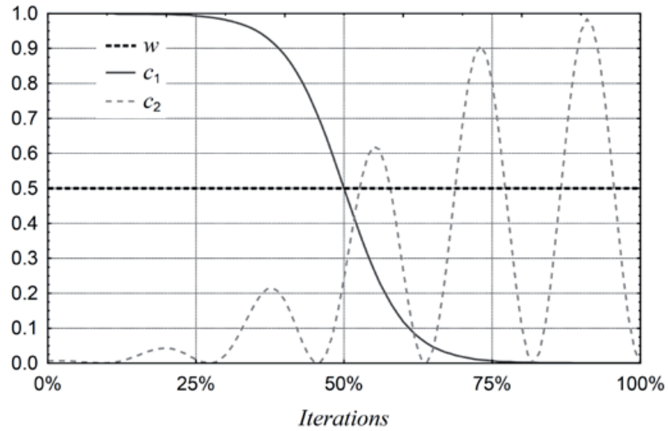

Fig. 2. Changes of w, c_1, c_2 coefficients value during calculations

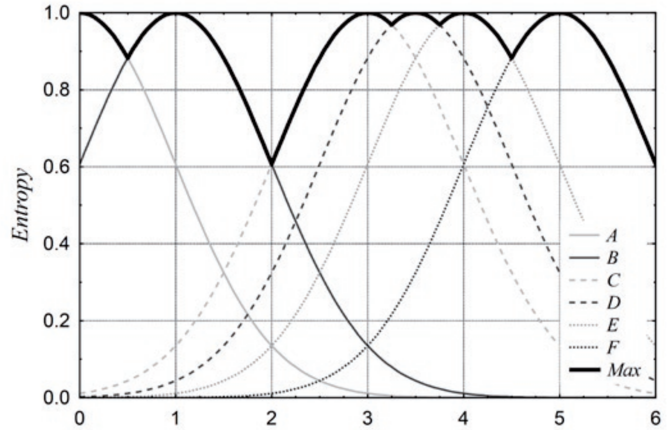

Fig. 3. Determination of the influence function value

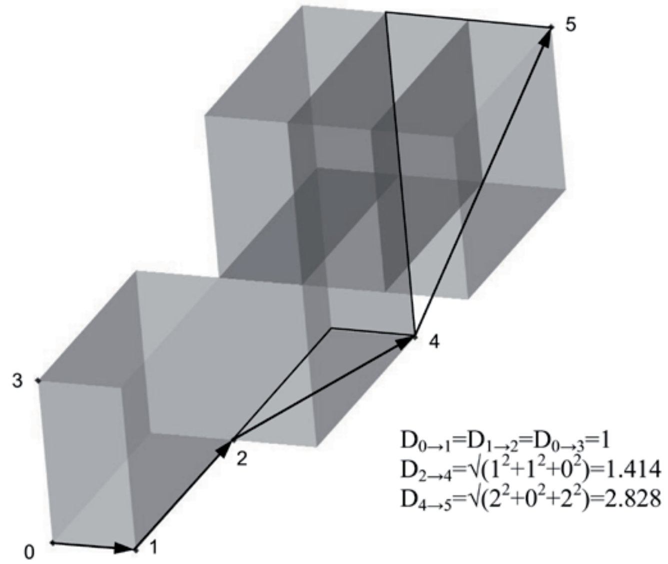

Fig. 4. Determination of the distance in 3-dimensional decision space

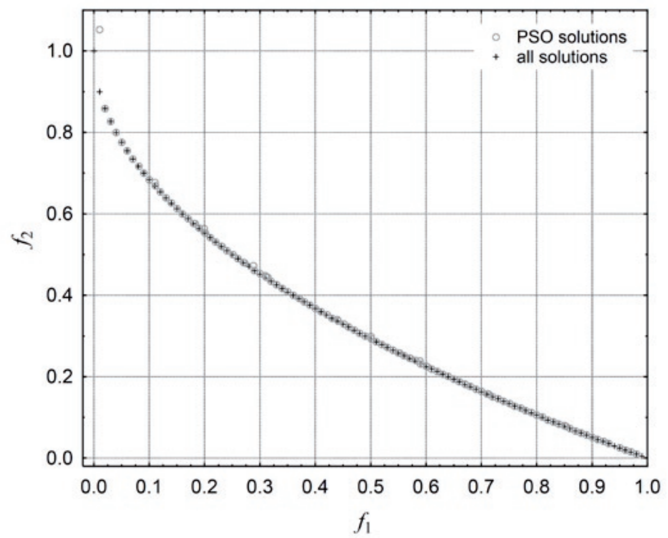

Fig. 5. Set of Pareto-optimal solutions for the first test problem generated for the parameters: N_{pop}=200, N_q=500, a=const=0.2, d_1=d_2=d_3=0.01

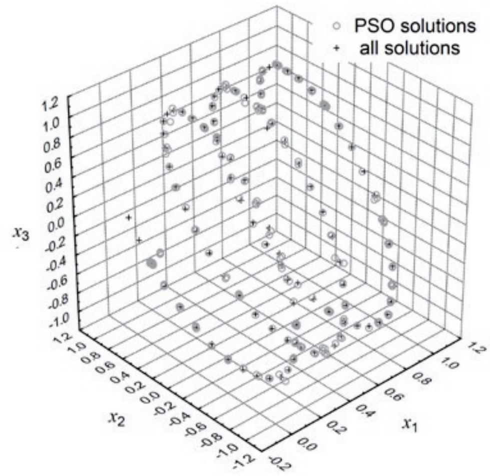

Fig. 6. Set of Pareto-optimal solutions for the first test problem in the decision space for the parameters: N_{pop}=200, N_q=500, a=const=0.2, d_1=d_2=d_3=0.01

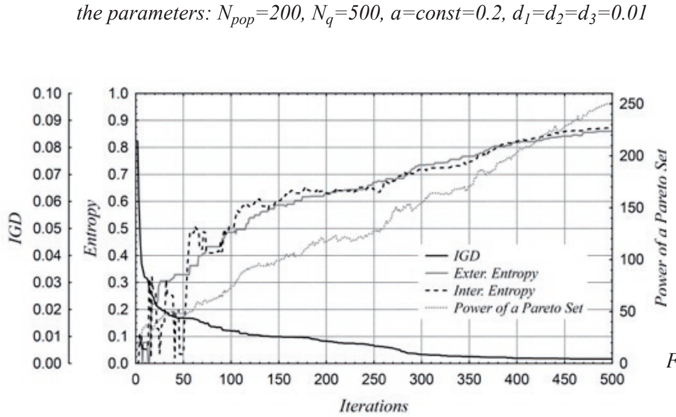

Fig. 7. Values of external and internal entropy, power of Pareto set and IGD in the function of iteration for the first test problem for the parameters: N_{pop}=200, N_q=500, a=const=0.2, d_1=d_2=d_3=0.01

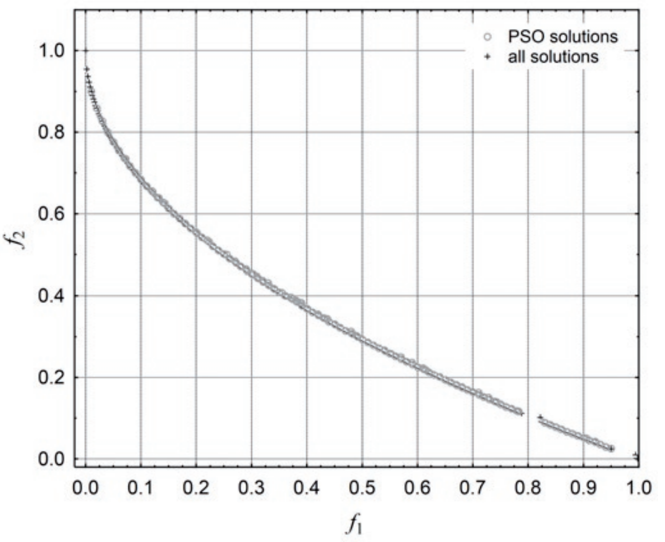

Fig. 8. Set of Pareto-optimal solutions for the second test problem generated for the parameters: N_{pop}=200, N_q=500, a=const=0.2, d_1=d_2=d_3=0.01

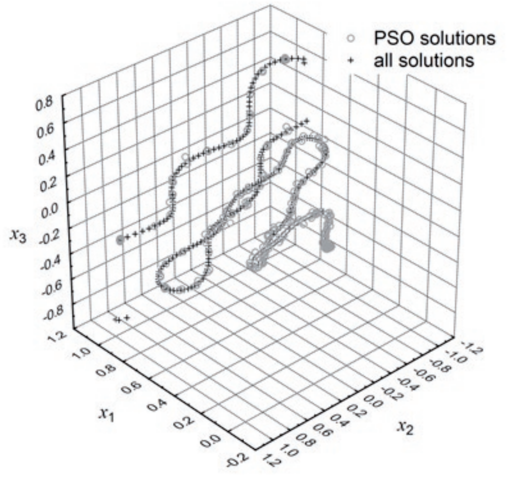

Fig. 9. Set of Pareto-optimal solutions for the second test problem in the decision space for the parameters: N_{pop}=200, N_q=500, a=const=0.2, d_1=d_2=d_3=0.01

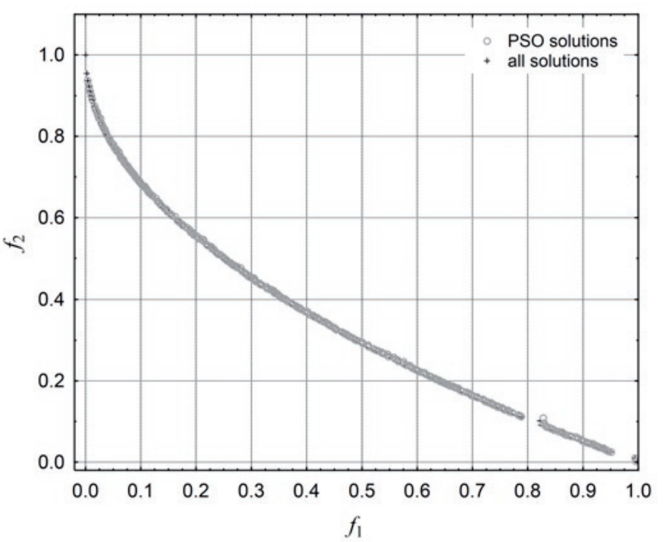

Fig. 10. Set of Pareto-optimal solutions for the second test problem generated for the parameters: N_{pop}=200, N_q=500, a=const=0.2, d_1=d_2=d_3=0.002

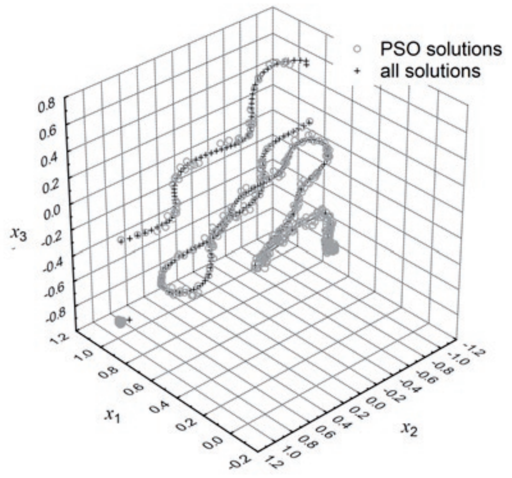

Fig. 11. Set of Pareto-optimal solutions for the second test problem in the decision space for the parameters: N_{pop}=200, N_q=500, a=const=0.2, d_1=d_2=d_3=0.00

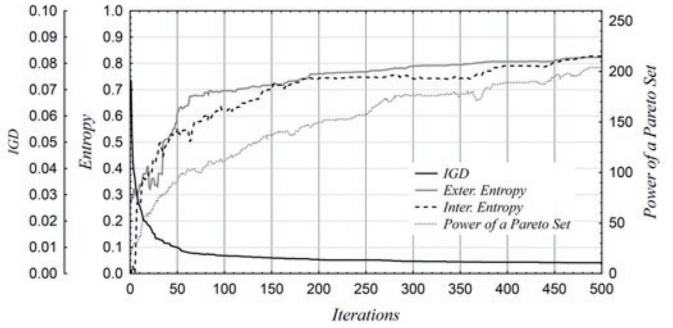

Fig. 12. Values of external and internal entropy, power of Pareto set and IGD in the function of iteration for the second test problem for the parameters: N_{pop}=200, N_q=500, a=const=0.2, d_1=d_2=d_3=0.01

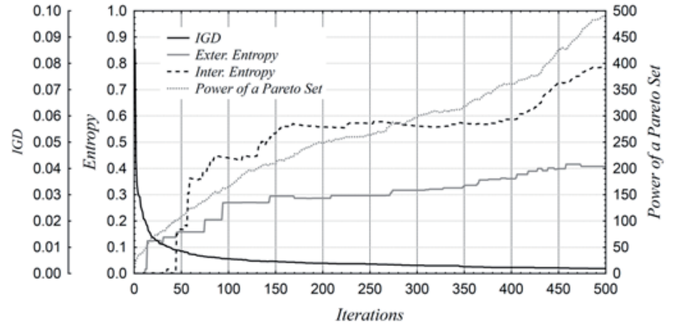

Fig. 13. Values of external and internal entropy, power of Pareto set and IGD in the function of iteration for the second test problem for the parameters: N_{pop}=200, N_q=500, a=const=0.2, d_1=d_2=d_3=0.002

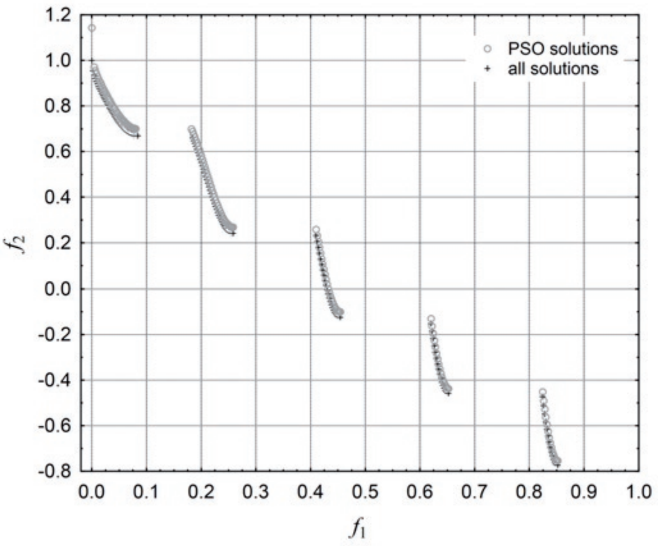

Fig. 14. Set of Pareto-optimal solutions for the third test problem generated for the parameters: N_{pop}=200, N_q=500, a=const=0.2, d_1=d_2=d_3=0.002

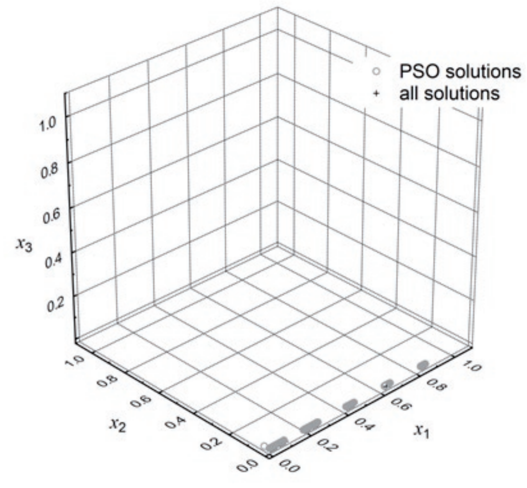

Fig. 15. Set of Pareto-optimal solutions for the third test problem in the decision space for the parameters: N_{pop}=200, N_q=500, a=const=0.2, d_1=d_2=d_3=0.002

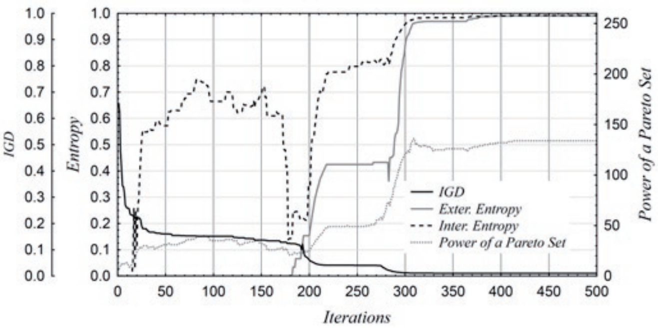

Fig. 16. Values of external and internal entropy values, power of Pareto set and IGD in the function of iteration for the third test problem for the parameters: N_{pop}=200, N_q=500, a=const=0.2, d_1=d_2=d_3=0.002

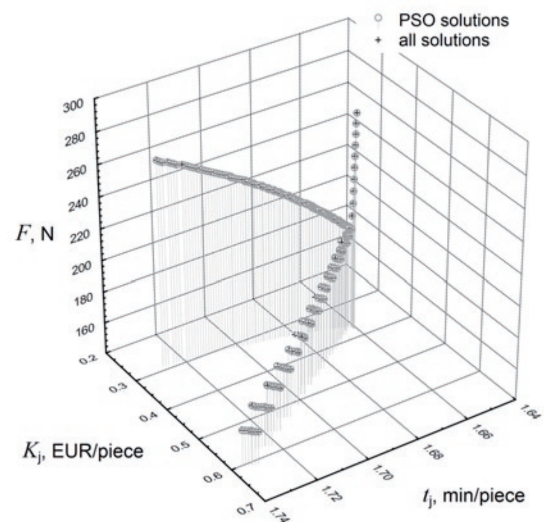

Fig. 17. Set of Pareto-optimal solutions generated with help of the PSO method for the parameters: N_{pop}=200, N_q=50, a=const=0.8, d_1=1, d_2=d_3=0.01

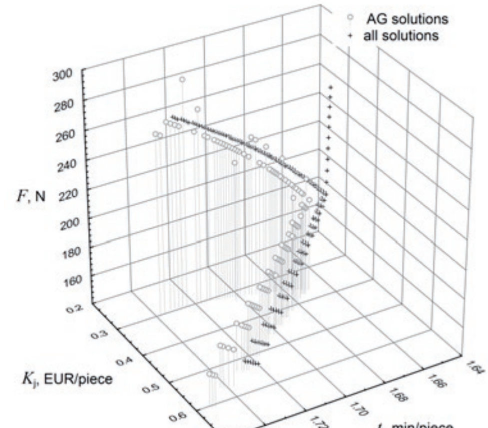

Fig. 18. Set of Pareto-optimal solutions generated with help of the genetic algorithms [24]

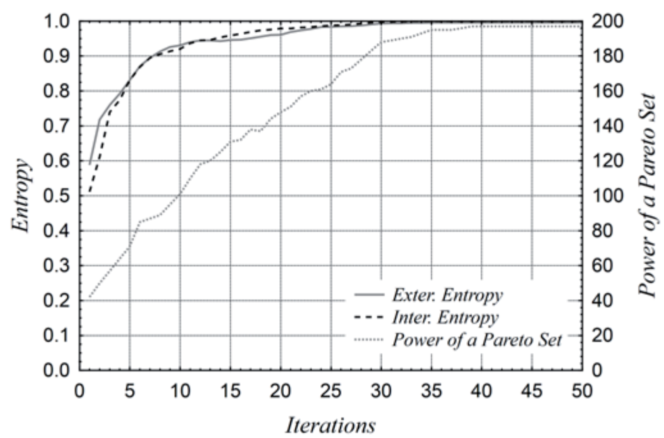

Fig. 19. Values of external and internal entropy, and power of the Pareto set in the function of iteration

References

1. Aleti A. Quality Assessment of Multiobjective Optimisation Algorithms in Component Deployment. Proceedings of ESEC/FSE Doctoral Symposium, Amsterdam 2009.
2. Baskar N, Asokan P, Saravanan R, Prabhaharan G. Optimization of Machining Parameters for Milling Operations Using Non-conventional Methods. International Journal of Advanced Manufacturing Technology 2005; 25: 1078-1088.
3. Chakraborty PD, Gourab GR, Ajith A. On convergence of the multi-objective particle swarm optimizers. Information Sciences 2011; 181: 1411-1425.
4. De Carvalh AB, Pozo A. Measuring the convergence and diversity of CDAS Multi-Objective Particle Swarm Optimization Algorithms: A study of many-objective problems. Neurocomputing 2012; 75: 43-51.
5. Durillo JJ, García-Nieto J, Nebro AJ, Coello Coello CA, Luna F, Alba E. Multi-Objective Particle Swarm Optimizers: An Experimental Comparison. Proceedings of the 5th International Conference EMO, Lectures in Computer Science 2009; 5467: 495-509.
6. Erfani T, Utyuzhnikov SV. Directed Search Domain: A Method for Even Generation of Pareto Frontier in Multiobjective Optimization. Journal of Engineering Optimization 2011; 43: 1-18.
7. Fasting J. Multi-objective optimization: Elitism in discrete and highly discontinuous decision spaces. University of Skövde, DV722A – Thesis Project in Informatics 2011.
8. Farhang-Mehr A, Azram S. Entropy-based multi-objective genetic algorithm for design optimization. Structural and Multidisciplinary Optimization 2002; 24: 351-361.
9. Karpat Y, Özel T. Multi-objective optimization for turning processes using neural network modeling and dynamic-neighborhood particle swarm optimization. International Journal of Advanced Manufacturing Technology 2007; 35: 234-247.
10. Kaveh A, Laknejadi K. A novel hybrid charge system search and particle swarm optimization method for multi-objective optimization. Expert Systems with Applications 2011; 38: 15475-15488.
11. Kennedy J, Eberhart R. Particle Swarm Optimization. Proceedings of IEEE International Conference on Neural Networks 1995; 4: 1942-1948.
12. Kunstfeld T, Haas W. Shaft surface manufacturing methods for rotary shaft lip seals. Sealing Technology 2005; 7: 5-9 .
13. Li H, Zhang Q. Multiobjective Optimization Problems with Complicated Pareto Sets, MOEA/D and NSGAII. IEEE Trans. Evolutionary Computations 2009; 13: 284-302.
14. Liu LL, Zhao GP, Young SS, Young YJ. Integrating theory of constraints and particle swarm optimization in order planning and scheduling for machine tool production. The international Journal of Advances Manufacturing Technology 2011; 57: 285-296.
15. Magnus E, Pedersen H. Good Parameters for Particle Swarm Optimization. Hvass Laboratories Technical Report no. HL1001 2011.
16. Moslemi H, Zandieh M. Comparisons of some improving strategies on MOPSO for multi-objective (r, Q) inventory system. Expert Systems with Applications 2011; 38: 12051-12057.
17. Nebro AJ, Durillo JJ, García-Nieto J, Coello Coello C A, Luna F, Alba E. SMPSO: A New PSO-based Metaheuristic for Multi-objective Optimization. IEEE Symposium on Computational Intelligence in Multicriteria Decision-Making 2009; 66-73.
18. Osyczka A, Kundu S. A modified distance method for multicriteria optimization using genetic algorithms. Computers & Industrial Engineering 1996; 30: 871-882.
19. Poli R. An Analysis of Publications on Particle Swarm Optimization Applications. Technical Report CSM-469. Department of Computer Science, University of Essex 2007.
20. Poli R. Analysis of the Publications on the Applications of Particle Swarm Optimization. Journal of Artificial Evolution and Applications 2008; 2008.
21. Poli R, Kennedy J, Blackwell T. Particle Swarm Optimization. An Overview. Swarm Intelligence 2007; 1: 33-57.
22. Pradhan PM, Panda G. Solving multiobjective problems using cat swarm optimization. Expert Systems with Applications 2012; 39: 2956-2964.
23. Pytlak B. The influence of cutting parameters on the tool wear and cutting forces during turning of hardened 18HGT steel. Advances in Manufacturing Science and Technology 2007; 31: 37-53.
24. Pytlak B. Multicriteria optimization of hard turning operation of the hardened 18HGT steel. The International Journal of Advanced Manufacturing Technology 2010; 49: 305-312.
25. Reyes-Sierra M, Coello Coello C A. Multi-Objective Particle Swarm Optimizers: A Survey of the State-of-the-Art. International Journal of Computational Intelligence Research 2006; 2: 287-308.
26. Saravanan R, Siva Sankar R, Asokan P, Vijayakumar K, Prabhaharan G. Optimization of cutting conditions during continues finished profile machining using non-traditional techniques. International Journal of Advanced Manufacturing Technology 2005; 26: 30-40.
27. Zhang Q, Li H. MOEA/D: A Multiobjective Evolutionary Algorithm Based on Decomposition. IEEE Transactions on Evolutionary Computation 2007; 11: 712-731.
28. Zhang Y, Gong DW, Ding ZH. Handling multi-objective optimization problems with a multi-swarm cooperative particle swarm optimizer. Expert Systems with Applications 2011; 38: 13933-13941.
29. Zitzler E, Knowles J, Thiele L. Quality Assessment of Pareto Set Approximations. In Branke J, Deb K, Miettinen K, Slowinski R. editors, Multiobjective Optimization: Interactive and Evolutionary Approaches 2008; 373-404.

Roman STRYCZEK
Bogusław PYTLAK
Department of Manufacturing Technology and Automation
University of Bielsko-Biala,
43–309 Bielsko-Biała, ul. Willowa 2, Poland
E-mails: rstryczek@ath.bielsko.pl, bpytlak@ath.bielsko.pl

Article citation info:
LAI M-T. Optimal replacement period with repair cost limit and cumulative damage model. Eksploatacja i Niezawodnosc – Maintenance and Reliability 2014; 16 (2): 246–252.

Min-Tsai LAI

OPTIMAL REPLACEMENT PERIOD WITH REPAIR COST LIMIT AND CUMULATIVE DAMAGE MODEL

OPTYMALNY OKRES WYMIANY PRZY LIMICIE KOSZTÓW NAPRAWY I MODELU SUMOWANIA USZKODZEŃ

This paper deals with periodical replacement model with single repair cost limit under cumulative damage process. The system is subject to two types of shocks. Type I shock causes damage to the system. The total damage is additive, and it causes a serious failure eventually if the total additive damage exceeds a failure level K. Type II shock causes the system to a minor failure, which can be maintained by minimal repair if the estimated repair cost is smaller than a predetermined repair-cost limit L_S or by preventive replacement if the estimated repair cost is larger than L_S. The system is also replaced at scheduled time T or at serious failure. The long-term expected cost per unit time is derived using the expected costs as the optimality criterion. The minimum-cost policy is derived, and existence and uniqueness are proved.

Keywords: *periodical replacement model, cumulative damage model, repair cost limit, minimal repair.*

Niniejszy artykuł dotyczy modelu wymiany okresowej z ograniczeniem kosztów pojedynczej naprawy w ramach procesu sumowania uszkodzeń. Układ podlega dwóm rodzajom zaburzeń. Zaburzenie I typu powoduje uszkodzenie systemu. Uszkodzenie całkowite sumuje się, powodując w końcu poważną awarię jeśli łączna wartość uszkodzeń przekroczy poziom awarii K. Zaburzenie II typu powoduje drobną awarię systemu, która może zostać usunięta dzięki minimalnej naprawie jeśli przewidywany koszt naprawy będzie mniejszy niż zakładany limit kosztów naprawy L_S lub na drodze wymiany prewencyjnej, jeżeli przewidywany koszt naprawy będzie większy niż L_S. Układ również podlega wymianie w założonym czasie T lub w przypadku poważnej awarii. Długoterminowe przewidywane koszty na jednostkę czasu obliczono z wykorzystaniem przewidywanych kosztów jako kryterium optymalności. Wyprowadzono strategię minimalnych kosztów, udowadniając istnienie i jedyność.

Słowa kluczowe: *Model wymiany okresowej, model sumowania uszkodzeń, limit kosztów naprawy, naprawa minimalna.*

1. Introduction

Preventing unexpected failure of the system during production process is very important because the production loss from system failure is very expensive, sometimes is very dangerous. In such situation, it is wise to replace the system before failure. Therefore, preventive maintenance (PM) models with regard to deteriorating systems have widely attracted the attention of several researchers and practitioners.

The system suffers external shocks, and then these shocks can incur damage to the system. Lai *et al.* (2006) divided shock models into five categories depending on the effect of shock damage to the system: (1) Cumulative damage model; (2) Instantaneous failure model; (3) Increasing operating cost model; (4) Increasing failure rate model; and (5) δ-shock model. On cumulative damage model, the system is subjected to shocks and suffers some amount of damage such as wear, fatigue, crack growth, creep, and dielectric at each shock. The total damage due to shocks is additive, and the system can fail when the total damage exceeds a failure level. The reliabiity properties and preventive maintennace policies for variuos damage models were summarized sufficiently in Nakagawa (2007).

In cumulative damage model, many researchers have used the optimum control-limit policy where a system is replaced when the total damage exceeds a threshold level (Nagakawa (1976)). On the other hand, the replacement models where a system is replaced at a planned time T were proposed in Taylor (1975), Mizuno (1986), and Perry (2000). Furthermore, the replacement models where a system is replaced at shock *N* were proposed in Nagakawa (1984).

Nakagawa and Kijima (1989) applied the periodical replacement policy with minimal repair at failure to a cumulative damage model and obtained the optimal values T^*, N^*, and Z^*, individually. Kijima and Nakagawa (1991) considered a cumulative damage shock model with imperfect PM policy. Satow and Nakagawa (1997) presented a modified cumulative damage model and considered a system suffers two kinds of damage. They proposed three replacement policies as following: the system can be replaced before failure at time *T*, at shock *N* or at damage level *k*, where *k* is less than failure level *K*. The optimal values T^*, N^*, and k^* which minimize the expected cost rates of three replacement policies are obtained individually. Satow *et al.* (2000) continued the work of Satow and Nakagawa (1997). The system is preventively replaced when the cumulative damage exceeds a threshold *k*. The optimal value k^* which minimizes the expected cost is obtained.

Qian *et al.* (1999) presented an extended cumulative damage model with two kinds of shocks: one is failure shock and the other is damage shock at which it suffers only damage. The system is replaced at scheduled time *T* or at failure. Qian *et al.* (2003) considered an extended cumulative damage model with maintenance at each shock and minimal repair at each failure. The optimal values T^* and N^* which minimize the expected cost are obtained. Qian *et al.* (2005) considered a cumulative damage model, where the system undergoes the PM at a certain time *T* or the total damage exceeds a managerial level *k*. The optimal values T^* and k^* are obtained simultaneously.

Ito and Nakagawa (2011) considered three cumulative damage models: (1) a unit is subjected to shocks and suffers some damage due to shocks. (2) The amount of damage due to shocks is measured only at periodic time. (3) The amount of damage increases linearly with the time. The unit fails when the total damage has exceeded a failure level K. The optimal T^* for Models 1 & 3 and N^* for Model 2 are obtained. Recently, Nakagawa (2007) summarized a large amount of preventive maintenance optimization problems for cumulative damage model.

In PM models with minimal repair, Drinkwater and Hastings (1967) introduced firstly the concept of repair cost limit. When a unit fails, repair cost is estimated and minimal repair is then executed in case the estimated cost is less than a predetermined limit; otherwise, the unit is replaced. PM models with repair-cost limit policy have been discussed in several articles. Several extensions of these policies have been proposed in Kapur *et al.* (1983), Park (1985), Bai and Yun (1986), Kapur and Garg (1989), and Yun and Bai (1987, 1988). Dohi *et al.* (2000) applied the TTT method to determine the optimal repair-time limit, in which it wants to minimize the long-run expected cost per unit time in the steady state case. Continuously, Dohi *et al.* (2003) discussed it to minimize the expected total discounted over an infinite time horizon.

In this paper, we consider a periodical replacement policy incorporating with the concept of repair cost limit under a cumulative damage model. The outline of this paper is as follows. In Section 2, the problem is defined. The long-term expected cost per unit time $A(T,L_s)$ and the conditions characterising the optimal period T^* are derived in Section 3. Finally, a numerical example and conclusions are presented in Sections 4 and 5, respectively.

2. Problem Definition

A system subjected to external shocks is considered and these shocks are supposed to occur randomly at a non-homogeneous Poisson process with an intensity function $\lambda(t)$. These shocks can be divided into two types: type I shock and type II shock. A shock whenever occurs is type I and type II with probailities p $(0<p\le 1)$ and $q=(1-p)$, respectively. Thus, we can know that the occurrences of type I and type II shocks are according to two non-homogeneous Poisson processes $\{N_1(t),t\ge 0\}$ and $\{N_2(t),t\ge 0\}$ with intensity rates $p\lambda(t)$ and $q\lambda(t)$, respectively. The effects of two types of shock to the system are described as follows:

Type I shocks cause the damage to the system and these damages are additive. When a type I shock occurs, an amount X_i of damage due to this shock has a probability distribution $H_i(x)=P(X_i\le x)$ and a finite mean μ_x, $i=1,2,3,\ldots$. Then the accumulated damage to the j-th type I shock after the installation $\mathrm{W}_j=\sum_{i=1}^{j}\mathrm{X}_i$ has a distribution function:

$$P(W_j\le w)=H^{(j)}(w)=\begin{cases}1 & j=0\\ H_1*H_2*\cdots*H_j(w), & j=1,2,3,\cdots\end{cases}, \quad (1)$$

where the "*" mark is denoted the *Stieltjes* convolution, i.e., $a*b(t)\equiv\int_0^t b(t-u)da(u)$ for any function $a(t)$ and $b(t)$. The probabiliity that the number of type I shocks occurred in $[0,t)$ equals to j is given by.

$$P(N_1(t)=j)=\frac{(m_1(t))^j\exp(-m_1(t))}{j!}=P_{1j}(t), \quad (2)$$

where $m_1(t)=\int_0^t p\lambda(x)dx$ denote the mean number of type-I shocks occurred in $[0,t)$.

If the accumulated damage exceeds a failure level K, then a serious failure occurs and the system must be replaced by a new one. The probability that a serious failure occurs at *j-th* type I shock is $H^{(j-1)}(K)-H^{(j)}(K)$. Let random variable Z denote the occurrence time of the first serious failure, so the survival function of Z is given by

$$\overline{F_z}(t)=P(Z>t)=P(W_{N_1(t)}<K)=\sum_{j=0}^{\infty}P(N_1(t)=j,W_j<K)=\sum_{j=0}^{\infty}P_{1j}(t)H^{(j)}(K) \quad (3)$$

and the density function of Z is $f_z(t)=p\lambda(t)\sum_{j=0}^{\infty}\left(H^{(j)}(t)-H^{(j+1)}(t)\right)P_{1,j}(t)$.

A type II shock whenever occurs makes the system into minor failure, and such a failure can be corrected by minimal repair. Hence, the probability that the number of minor failures occurred in $[0,t)$ equals to j is given by:

$$P(N_2(t)=j)=\frac{(m_2(t))^j\exp(-m_2(t))}{j!}=P_{2j}(t) \quad (4)$$

where $m_2(t)=\int_0^t q\lambda(x)dx$ denote the mean number of minor failures during $[0,t)$.

When a minor failure occurs, the repair cost due to this failure is evaluated. We assume that the repair cost Y_i due to *i-th* minor failure are nonnegative *i.i.d.* random variables with a probability distribution $G(y)=P(Y_i\le y)$, $i=1,2,3,\ldots$ .If Y_i is smaller than a predetermined limit L_S, then the system is corrected by minimal repair. Otherwise, the system is replaced. Thus, $\delta=P(Y_i>L_s)$ is the probability of the system's preventive replacement at the minor failure occurement. We let μ_y be the mean of random variable Y_i truncated at L_S. Let random variable U denote the time of replacement due to minor failure has the following distribution:

$$\overline{F_u}(t)=P(U>t)=\sum_{j=0}^{\infty}P(N_2(t)=j)\times P(Y_1<L_s,Y_2<L_s,\ldots,Y_j<L_s)=\exp(-\delta m_2(t)) \quad (5)$$

and the density function of U is $f_u(t)=\delta q\lambda(t)\exp(-\delta m_2(t))$.

Except the system replacement at a serious failure or at one minor failure in case that the corresponding repair cost is larger than L_S, the system is also preventively replaced at a scheduled time T. In summary, the system is replaced at scheduled time T, or at a time of one minor failure where the repair cost exceeds a pre-determined limit L_S, or at serious failure. The probabilities for these three cases will be computed as follows.

First, if all repair cost for minor failures occurred before T are less than L_S and the accumulted damage due to type I shocks up to time T is less than failure level K, i.e., $\min(Z,U,T)=T$, preventive replacement is executed at scheduled time T. Thus, the probability that the system will be replaced preventively at scheduled time T is given by:

$$P\left(\min(Z,U) > T\right) = P\left(Z > T\right) \times P\left(U > T\right) = e\exp\left(-\delta m_2(T)\right) \sum_{j=0}^{\infty} P_{1j}(T) H^{(j)}(K) . (6)$$

Second, if $\min(Z,U,T) = U$, the system will be replaced preventively at some one minor failure that the corresponding repair cost is the first time larger than limit L_S. Thus, the probability that the system will be replaced preventively at one minor failure is derived as follows:

$$P\left(U < T, U < Z\right) = \int_0^T P(Z > t) f_u(t) dt = \sum_{j=0}^{\infty} H^{(j)}(K) \int_0^T P_{1j}(t) \exp\left(-\delta m_2(t)\right) \delta q \lambda(t) dt \quad (7)$$

Finally, if $\min(Z,U,T) = Z$, the system will be replaced at a serious failure. Thus, the probability of a failure replacement is given by:

$$\begin{aligned} P(Z < T, Z < U) &= \int_0^T P(U > t) \sum_{j=1}^{\infty} P(W_{j-1} < K \le W_j) P(S_{1j} \in (t, t + \Delta t)) \\ &= \sum_{j=0}^{\infty} \left(H^{(j)}(K) - H^{(j+1)}(K)\right) \int_0^T \exp\left(-\delta m_2(t)\right) P_{1j}(t) p \lambda(t) dt \end{aligned} \quad (8)$$

Moreover, the following assumptions are required:

(a1) The system is monitored continuously, and all failures are detected immediately.

(a2) Repairs and replacements are completed instantaneously.

(a3) The steady state case is considered.

Moreover, the replacement that is executed at scheduled time T or at the occurrence of one minor failure where the repair cost exceeds limit L_S is called preventive replacement of cost C_0 . While replacement executed at serious failure is called failure replacement of cost $C_1 (C_1 > C_0)$. Under a fixed limit L_S, this problem is to find an optimal T^* to minimize the long-term expected cost per unit time $A(T, L_s)$ in the steady state case.

3. Long-term expected cost per unit time

A replacement cycle is actually a time interval between the installation of the system and the first replacement or a time interval between consecutive replacements. Therefore, the successive replacement cycles will constitute a renewal process. Let $\overline{R}(T, L_s)$ and $\overline{Z}(T, L_S)$ denote the mean length of a replacement cycle and the expected total cost incurred during a replacement cycle, respectively. By using renewal-reward theorem, we can see that the long-term expected cost per unit time in the steady state case is given by (Ross (1983)):

$$A(T, L_s) = \frac{\overline{R}(T, L_s)}{\overline{Z}(T, L_s)} . \quad (9)$$

Under the defined preventive maintenance policy, the expected length of a replacement cycle $\overline{Z}(T, L_S)$ is given by:

$$\overline{Z}(T, L_S) = \int_0^{\infty} P(\min(T, Z, U) > t) dt = \sum_{j=0}^{\infty} H^{(j)}(K) \int_0^T P_{1j}(t) \exp(-\delta m_2(t)) dt \quad (10)$$

If the system is replaced at scheduled time T, then the number of minor failures during $\left[0, T\right]$ will be $N_2(T)$. If the system is replaced at time U, then the number of minor failures during $[0,U]$ will be $N_2(U)$. And, if the system is replaced at the first serious failure, then the number of minor failures during $[0,Z]$ will be $N_2(Z)$. Therefore, the expected number of minor failures until replacement is:

$$\begin{aligned} E\left(N_2(\min(T, Z, U))\right) &= H^{(j)}(K) P_{1j}(T) e\exp\left(-\delta m_2(T)\right) E(N_2(T)) + \sum_{j=0}^{\infty} H^{(j)}(K) \int_0^T P_{1j}(t) f_u(t) E(N_2(t)) dt \\ &+ \sum_{j=0}^{\infty} \left(H^{(j)}(K) - H^{(j+1)}(K)\right) \int_0^T P_{1,j}(t) p \lambda(t) \exp\left(-\delta m_2(t)\right) E(N_2(t)) dt \\ &= \sum_{j=0}^{\infty} H^{(j)}(K) \int_0^T P_{1j}(t) \exp\left(-\delta m_2(t)\right) q \lambda(t) dt \end{aligned}$$

Furthermore, the expected total cost $\overline{R}(T, L_s)$ during a replacement cycle can be dervied dervied as follows:

$$\begin{aligned} \overline{R}(T, L_s) &= C_0 \sum_{j=0}^{\infty} H^{(j)}(K) P_{1j}(T) e\exp\left(-\delta m_2(T)\right) + C_0 \sum_{j=0}^{\infty} H^{(j)}(K) \int_0^T P_{1j}(t) \exp\left(-\delta m_2(t)\right) \delta q \lambda(t) dt \\ &+ C_1 \sum_{j=0}^{\infty} \left(H^{(j)}(K) - H^{(j+1)}(K)\right) \int_0^T \exp\left(-\delta m_2(t)\right) P_{1j}(t) p \lambda(t) dt + \mu_y E\left(N_2(\min(T, Z, U))\right) \\ &= C_0 + (C_1 - C_0) \sum_{j=0}^{\infty} \left(H^{(j)}(K) - H^{(j+1)}(K)\right) \int_0^T \exp\left(-\delta m_2(t)\right) P_{1j}(t) p \lambda(t) dt \\ &+ \mu_y \sum_{j=0}^{\infty} H^{(j)}(K) \int_0^T P_{1j}(t) \exp\left(-\delta m_2(t)\right) q \lambda(t) dt \end{aligned} \quad (11)$$

Combining (10) and (11), the long-term expected cost per unit time $A(T, L_s)$ is obtained as follows:

$$A(T,L_s)=\frac{\left[\begin{array}{l} C_0+(C_1-C_0)\sum_{j=0}^{\infty}\left(H^{(j)}(K)-H^{(j+1)}(K)\right)\int_0^T \exp\left(-\delta m_2(t)\right)P_{1j}(t)p\lambda(t)dt \\ \qquad\qquad +\mu_y\sum_{j=0}^{\infty}H^{(j)}(K)\int_0^T P_{1j}(t)\exp\left(-\delta m_2(t)\right)q\lambda(t)dt \end{array}\right]}{\left(\sum_{j=0}^{\infty}H^{(j)}(K)\int_0^T P_{1j}(t)\exp(-\delta m_2(t))dt\right)} \tag{12}$$

A necessary condition that a finite T* minimizes $A(T,L_s)$ under a fixed L_S can be obtained by differentiating $A(T,L_s)$ with respect to T and setting it equal to zero. If we let $\frac{dA(T,L_S)}{dT}$ equal to zero, we have:

$$\begin{aligned} &(C_1-C_0)\left[\begin{array}{l}\sum_{j=0}^{\infty}H^{(j+1)}(K)\int_0^T \exp\left(-\delta m_2(t)\right)P_{1j}(t)p\lambda(t)dt \\ \qquad -D(T)p\lambda(T)\sum_{j=0}^{\infty}H^{(j)}(K)\int_0^T \exp(-\delta m_2(t))P_{1j}(t)dt\end{array}\right] \\ &+\left[p(C_1-C_0)+q\mu_y\right]\times\left(\sum_{j=0}^{\infty}H^{(j)}(K)\int_0^T \exp(-\delta m_2(t))P_{1j}(t)\left[\lambda(T)-\lambda(t)\right]dt\right)=C_0 \end{aligned} \tag{13}$$

where $D(T)=\sum_{j=0}^{\infty}H^{(j+1)}(K)P_{1j}(T)\Big/\sum_{j=0}^{\infty}H^{(j)}(K)P_{1j}(T)$. So, equation (13) will be rewritten as:

$$\begin{aligned} &(C_1-C_0)\left[\sum_{j=0}^{\infty}H^{(j+1)}(K)\int_0^T \exp\left(-\delta m_2(t)\right)P_{1j}(t)p\lambda(t)dt-D(T)p\lambda(T)\overline{Z}(T,L_s)\right] \\ &+\left((C_1-C_0)+\frac{q\mu_y}{p}\right)\times\left[\begin{array}{l}p\lambda(T)\overline{Z}(T,L_S) \\ \qquad -\sum_{j=0}^{\infty}H^{(j)}(K)\int_0^T \exp(-\delta m_2(t))P_{1j}(t)p\lambda(t)dt\end{array}\right]=C_0 \end{aligned} \tag{14}$$

For simplification, let $U(T)$ denote the left-hand side of (14).

Theorem 1: If $\lambda(t)$ is an increasing function of t and $\lim_{T\to\infty}U(T)>C_0$, there are at least one finite optimal T*, $0\le T^*<\infty$ such that $A(T^*,L_S)<A(T,L_S)$ for all T. And, if $\lambda(t)$ is strictly increasing and $U'(T)>0$ for all T, then $U(T)$ is a strictly increasing function of T and the optimal T* is also unique. Furthermore, if $\lim_{T\to\infty}U(T)>C_0$ is not satisfied, then T* is infinite.

Proof: Here, $U(0)\equiv\lim_{T\to 0}U(T)=0$ and

$$\begin{aligned} U(\infty)=\lim_{T\to\infty}U(T)=\lim_{T\to\infty}&\left(\begin{array}{l}(C_1-C_0)\left[\begin{array}{l}\left(\sum_{j=0}^{\infty}H^{(j+1)}(K)\int_0^T P_{1j}(t)\exp(-\delta m_2(t))p\lambda(t)dt\right) \\ \qquad -D(T)p\lambda(T)\left(\sum_{j=0}^{\infty}H^{(j)}(K)\int_0^T P_{1j}(t)\exp(-\delta m_2(t))dt\right)\end{array}\right] \\ \quad +\left(p(C_1-C_0)+q\mu_y\right)\left(\sum_{j=0}^{\infty}H^{(j)}(K)\int_0^T P_{1j}(t)\exp(-\delta m_2(t))\left(\lambda(T)-\lambda(t)\right)dt\right)\end{array}\right) \\ =\left((C_1-C_0)-\frac{\mu_y}{\delta}\right)\left(\frac{\delta q}{\delta q+p}\right)\sum_{j=0}^{\infty}H^{(j)}(K)\left(\frac{p}{\delta q+p}\right)^j+(C_1-C_0)p\lambda(\infty)\left(1-D(\infty)+\frac{q\mu_y}{p}\right) \end{aligned} \tag{15}$$

where $\lim_{T\to\infty}\int_0^T \exp(-\delta m_2(t))P_{1j}(t)p\lambda(t)dt = \left(\frac{p}{\delta q+p}\right)^{j+1}$. Since $U(0)=0<C_0$, and if $\lim_{T\to\infty}U(T)>C_0$, then there exist at least one finite optimal T^* such that $U(T^*)=c_0$, i.e., T^* satisfies (14). Such a T^* is a candidate which minimizes $A(T,L_S)$. Furthermore, if $\lambda(t)$ is strictly increasing and

$$U'(T)=(C_1-C_0-1)\times\left(\sum_{j=0}^{\infty}H^{(j+1)}(K)P_{1j}(T)\exp(-\delta m_2(T))p\lambda(T)\right)$$
$$-\left[D'(T)p\lambda(T)+D(T)p\lambda'(T)\right]\times\overline{Z}(T,L_s)>0$$

then $U(T)$ is a strictly increasing function of t, and hence, the optimal T^* is also unique. And, the resulting optimal long-term expected cost per unit time will be:

$$A(T^*,L_S)=U(T^*)$$

Conversely, if $U'(T)>0$ and $U(\infty)<C_0$ or $U'(T)\le 0$, then T^* is infinite.
In our model, we can have the following special cases:

Case 1. If $L_s\to\infty$, then $A(T,L_S)$ will be reduced simply to

$$A(T,\infty)=\frac{\left[\begin{array}{r}C_0+(C_1-C_0)\sum_{j=0}^{\infty}\left(H^{(j)}(K)-H^{(j+1)}(K)\right)\int_0^T\exp(-m_2(t))P_{1j}(t)p\lambda(t)dt\\ +\mu_y\sum_{j=0}^{\infty}H^{(j)}(K)\int_0^T P_{1j}(t)\exp(-m_2(t))q\lambda(t)dt\end{array}\right]}{\sum_{j=0}^{\infty}H^{(j)}(K)\int_0^T P_{1j}(t)\exp(-m_2(t))dt}$$

This is reduced to a periodical replacement policy with minimal repair at minor failure and with replacement at serious failure.

Case 2. If $L_S\to\infty$ and $p=1$, then $\delta=1$. $A(T,L_S)$ will be reduced to

$$A(T,\infty)=\left[C_0+(C_1-C_0)\sum_{j=0}^{\infty}\left(H^{(j)}(K)-H^{(j+1)}(K)\right)\int_0^T\lambda(t)P_{1j}(t)dt\right]\Bigg/\sum_{j=0}^{\infty}H^{(j)}(K)\int_0^T P_{1j}(t)dt$$

which is the same as in Zuckerman (1980) and model 1 in Ito and Nakagawa (2011).

4. Numerical Example

In this numerical example, we consider that external shocks occur randomly at a non-homogeneous Poisson process with an intensity function $\lambda(t)=\lambda t^{\beta-1},\ \lambda>0,\ \beta>0$. We assume that the shape parameter is set at $\beta=2$, and that $\lambda(t)=\lambda t$ is an increasing function of t. Suppose that the amount of damage X_i due to the *i-th* type I shock has an exponential distribution with finite mean $\mu_x=12$, $i=1,2,3,\ldots$. And, the failure level *K* of this system is set to be 100. So, the convolution $H^{(j)}(100)$ is computed as follows:

$$H^{(j)}(100)=\int_0^{100}\frac{1}{\Gamma(j)\mu_x}\left(\frac{x}{\mu_x}\right)^{j-1}e^{-\frac{x}{\mu_x}}dx=\int_0^{100/\mu_x}\frac{y^{j-1}e^{-y}}{(j-1)!}dy$$

Preventive and failure replacements occur at cost of $C_0=1000$ and $C_1=1500$, respectively, while the cost of consecutive minimal repairs are *i.i.d.* normal distribution with finite mean $\mu_y=50$ and standard deviation $\sigma_y=10$. If th predetermined limit L_S is set to be 62.82, so

$$\delta=P(Y_i>62.82)=P\left(\frac{Y_i-\mu_y}{\sigma_y}>\frac{62.82-50}{10}\right)=0.1\,.$$

Since $\lambda(t)=\lambda t$ is increasing in *t*, so $\lambda(\infty)\to\infty$, furthermore,

$$\sum_{j=0}^{\infty}H^{(j)}(100)\left(\frac{p}{\delta q+p}\right)^j=1+\sum_{j=1}^{\infty}\left(\int_0^{100/12}\frac{1}{(j-1)!}(y)^{j-1}e^{-y}dy\right)\times\left(\frac{p}{\delta q+p}\right)^j$$
$$=1+\left(\frac{p}{\delta q}\right)\times\left(1-e^{-\left(\frac{25\delta q}{3(\delta q+p)}\right)}\right)$$

tends to a fixed number and $D(\infty)\to 1$, then $U(\infty)\to\infty$, as $t\to\infty$. That means that $\lim_{T\to\infty}U(T)>C_0$. According to the conditions of ***Theorem 1***, we can see that the optimal T^* will be finite and unique.

We use Mathematical software "MAPLE" to compute $A(T,L_S)$ under different combinations of parameters *λ*, *p* and *δ*. In order to understand the effects on T^* and $A(T^*,L_S)$ from different parameters, we consider two cases:
Case 1: *p*=0.9, 0.8, 0.7, 0.6, 0.5 and *λ*=1.0, 1.5, 2.0, 2.5, 3.0, *δ*=0.1.
Case 2: *δ*=0.1, 0.15, 0.2, 0.25, 0.3, *p*=0.7, *λ*=2.

The results of cases 1 and 2 are showed in Tables 1 and 2, respectively. From tables, 1 and 2, we have the following conclusions:

(1) When *λ* is greater, it is shown that the optimal preventive period T^* decreases but the minimum long-term expected cost per unit time $A(T^*,L_S)$ increases. The greater *λ* implies that the failures of the system occurred easily, so the optimal T^* must be shorter to prevent the occurrence of random failures.
(2) When *p* is smaller (and $(1-p)$ is greater), we can see that the optimal preventive period T^* increases but the minimum $A(T^*,L_S)$ is firstly decreasing and then increasing. The smaller *p* implies that the probability of replacing the system at serious failure is smaller, so the optimal T^* can be longer.
(3) When *δ* is greater, it will be shown that the optimal preventive period T^* and the minimum long-term expected cost per unit time $A(T^*,L_S)$ increase simultaneously. The greater *δ* implies that the possibility of replacing of the system from serious failure is reduced slightly, so the optimal T^* can be extended slightly.

Table 1. Optimal T^* and $A(T^*, L_S)$ at different values of λ and p.

	p=0.9		*p*=0.8		*p*=0.7		*p*=0.6		*p*=0.5	
λ	T^*	$A(T^*, L_S)$	T^*	$A(T^*, L_S)$	T^*	$A(T^*, L_S)$	T^*	$A(T^*, L_S)$	T^*	$A(T^*, L_S)$
1.0	4.14	324.4449148	4.36	322.9600534	4.62	322.1957584	4.93	322.4162087	5.31	324.0059950
1.5	3.38	397.3623157	3.56	395.5436502	3.78	394.6077033	4.03	394.8774576	4.34	396.8248869
2.0	2.95	458.8561575	3.09	456.7344917	3.27	455.6532650	3.49	455.9652071	3.75	458.2141217
2.5	2.62	512.9920485	2.76	510.6440824	2.92	509.4369527	3.12	509.7845672	3.36	512.2985146
3.0	2.39	561.9551858	2.52	559.3825379	2.67	558.0590004	2.85	558.4410978	3.07	561.1954111

Table 2. Optimal T^* and $A(T^*, L_S)$ at different values of δ.

	δ=0.1		δ=0.15		δ=0.20		δ=0.25		δ=0.30	
λ	T^*	$A(T^*, L_S)$	T^*	$A(T^*, L_S)$	T^*	$A(T^*, L_S)$	T^*	$A(T^*, L_S)$	T^*	$A(T^*, L_S)$
2.0	3.27	455.6532650	3.3	467.2935446	3.32	479.1248321	3.35	491.1283410	3.38	503.2854405

5. Conclusions

In this paper, a periodical replacement policy with repair-cost limit under cumulative damage model is introduced, in which we derived the long-term expected cost per unit time $A(T, L_S)$ by incorporating costs due to replacement and minimal repair. This research verifies that under some specific conditions, the optimal period T^* to minimize $A(T, L_S)$ will be finite and unique. This work can be extended to consider multi-unit system or include the concept of imperfect repair.

Acknowledgement: *This research was supported by the National Science Council of Taiwan, under Grant No. NSC 99-2410-H-218 -016.*

References

1. Bai DS, Yun WY. An age replacement policy with minimal repair cost limit. IEEE Transaction on Reliability 1986; R-35: 401-403.
2. Dohi T, Kaio N, Osaki O. A graphical method to repair-cost limit replacement policies with imperfect repair. Mathematical and Computer Modelling 2000; 31:99-106.
3. Dohi T, Kaio N, Osaki O. A new graphical method to estimate the repair-time limit with incomplete repair and discounting. Computers & Mathematics with Applications 2003; 46: 999-1007.
4. Drinkwater RW, Hastings NAJ. An economic replacement model. Operations research 1967; 18: 121-131.
5. Ito K, Nakagawa T. Comparison of Three Cumulative Damage Models. Quality Technology and Quantitative Management 2011; 8(1): 57-66.
6. Kapur PK, Garg RB. Optimal number of minimal repairs before replacement with repair cost limit. Reliability Engineering and System Safety 1989; 26: 39-46.
7. Kapur PK, Garg RB, Butani NL. Some replacement policies with minimal repairs and repair cost limit. International Journal of System Science 1983; 20: 267-273.
8. Kijima M, Nakagawa T. A cumulative damage shock model with imperfect preventive maintenance. Naval Research Logistics 1991; 38(2): 145-156.
9. Lai, M.T. Shih, W. and Tang, K.Y. Economic discrete replacement policy subject to increasing failure rate shock model. The International Journal of Advanced Manufacturing Technology 2006; 27(11-12): 1242-1247.
10. Mizuno, N. Generalized mathematical programming for optimal replacement in a Semi-Markov shock model. Operations Research 1986; 34: 790-795.
11. Nakagawa T. On a replacement problem of a cumulative damage model. Operations Research 1976; 27(4): 895-900.
12. Nakagawa T. A summary of discrete replacement policies. European Journal of Operations Research 1984; 17: 382-392.
13. Nakagawa T. Shock and Damage Models in Reliability Theory. London: Springer- Verlag, 2007.
14. Nakagawa T, Kijima M. Replacement policies for a cumulative damage model. IEEE Transaction on Reliability 1989; 38(3): 581-584.
15. Park KS. Pseudo dynamic cost limits replacement model under minimal repair. Microelectronics Reliability 1985; 25: 573-579.
16. Perry D. Control limit policies in a replacement model with additive phase-type distributed damage and linear restoration. Operations Research Letters 2000; 27: 127-134.
17. Qian C, Nakamura S, Nakagawa T. Cumulative damage model with two kinds of shocks and its application to the backup policy. Journal of the Operations Research Society of Japan 1999; 42:501-511.
18. Qian C, Nakamura S, Nakagawa T. Replacement and minimal repair policies for a cumulative damage model with maintenance. Computers

& Mathematics with Applications 2003; 46(7): 1111-1118.
19. Qian CH, Ito K, Nakagawa T. Optimal preventive maintenance policies for a shock model with given damage level. Journal of Quality in Maintenance Engineering 2005; 11(3): 216 - 227.
20. Ross SM. Stochastic Processes. New York: John Wiley & Sons, 1983.
21. Satow T, Nakagawa T. Three replacement models with two kinds of damage. Microelectronics Reliability 1997; 37(6): 909-913.
22. Satow T, Teramoto K, Nakagawa T. Optimal replacement policy for a cumulative damage model with time deterioration. Mathematical and Computer Modelling 2000; 31(10-12): 313-319.
23. Taylor HM. Optimal replacement under additive damage and other failure models. Naval Research Logistics 1975; 22(1):1-18.
24. Yun WY, Bai DS. Cost limit replacement policy under imperfect repair. Reliability Engineering 1987; 19: 23-28.
25. Yun WY, Bai DS. Repair cost limit replacement policy under imperfect inspection. Reliability Engineering and System Safety 1988; 23:59-64.
26. Zuckerman D. A note on the optimal replacement time of damaged devices. Naval Research Logistics Quarterly 1980; 27(3):521-524.

Min-Tsai LAI
Department of Business Administration
Southern Taiwan University of Science and Technology
No.1, Nan-Tai street, Yung-Kung Dist. 710, Tainan City
Taiwan, R.O.C.
E-mail: lai1962@mail.stust.edu.tw

Article citation info:
PILCH R, SZYBKA J, TUSZYŃSKA A. Application of factoring and time-space simulation methods for assessment of the reliability of water-pipe networks. Eksploatacja i Niezawodnosc – Maintenance and Reliability 2014; 16 (2): 253–258.

Robert PILCH
Jan SZYBKA
Anna TUSZYŃSKA

APPLICATION OF FACTORING AND TIME-SPACE SIMULATION METHODS FOR ASSESSMENT OF THE RELIABILITY OF WATER-PIPE NETWORKS

ZASTOSOWANIE METOD FAKTORYZACJI ORAZ SYMULACJICZASOWO-PRZESTRZENNEJ DO OCENY NIEZAWODNOŚCI SIECI WODOCIĄGOWYCH*

This article presents a method for determining the reliability of water-pipe networks through the application of factoring algorithms. This is a method based on graph theory and graph reduction, making it possible to calculate the reliability of a system with a specific structure of connections between its elements without determining its reliability structure. The impact of damage to individual pipeline segments on a network's overall reliability was also determined. In water-pipe networks, it is also particularly important to ensure that the appropriate parameters of water are maintained. Values of the water supply conditions index (WSCI) in the entire analysed network and changes resulting from damage to selected pipeline segments were determined by means of time-space simulation. The presented factoring and time-space simulation methods for determining WSCI index values are mutually complementary in the assessment of reliability. They make it possible to improve the credibility of reliability assessment and may be used to conduct rational usage of water-pipe networks.

***Keywords**: reliability of network systems, water-pipe network, factoring algorithm, time-space simulation.*

W artykule przedstawiono sposób wyznaczenia niezawodności sieci wodociągowych przy wykorzystaniu algorytmu faktoryzacji. Jest to metoda oparta na teorii grafów i ich redukcji, umożliwiająca obliczenie niezawodności układu o określonej strukturze połączeń między elementami ale bez wyznaczania jego struktury niezawodnościowej. Dla wybranej sieci wyznaczono wpływ uszkodzenia poszczególnych odcinków rurociągów na jej niezawodność. W sieciach wodociągowych szczególnie ważne jest zapewnienie odpowiednich parametrów dostarczanej wody. Za pomocą symulacji czasowo-przestrzennej określono wartości wskaźnika warunków poboru wody WWPW w całej analizowanej sieci oraz jego zmiany, w efekcie uszkodzenia wytypowanych odcinków rurociągów. Przedstawione metody faktoryzacji i symulacja czasowo-przestrzenna, do wyznaczenia wartości wskaźnika WWPW, wzajemnie się uzupełniają w ocenie niezawodności. Pozwalają zwiększyć wiarygodność oceny niezawodności i mogą być wykorzystywane w prowadzeniu racjonalnej eksploatacji sieci wodociągowych.

***Słowa kluczowe**: niezawodność układów sieciowych, sieć wodociągowa, algorytm faktoryzacji, symulacja czasowo-przestrzenna.*

1. Introduction

Reliability in a descriptive sense can be defined as the measure of trust that we have in a person or technical object that interests us. The development of reliability theory over the last decade or so has led to the elaboration of many methods of reliability assessment applied to solving a wide range of problems [1, 6, 7, 11]. The presented solutions pertain to both assessment of reliability and the risk of using water-pipe networks and methods of searching for optimal solutions for the implementation of economically justified redundancy in network structures [1, 7, 11, 14, 18]. Another significant aspect is the provision of supply of sufficient amounts of water, which must also fulfil qualitative requirements, to end users [6, 13]. Since the 1980s, the subject of water line and sewage system reliability has been undertaken in parallel by the Cracow University of Technology and the Warsaw University of Technology in Poland [15]. A series of interesting solutions have been found, which have been successfully implemented in practice for the control of water supply to users [2, 3].

This article presents the application of the factoring method for estimation of the reliability of water lines as a critical part of infrastructure, for the purpose of indicating locations in the network that, if damaged, pose a threat to supplying users with water. For such points in the network, the Water Supply Conditions Index (WSCI) was determined [3]. This index is significant in the assessment of water supply. Analysis of obtained results was also conducted to indicate segments that would significantly impact network reliability if damaged.

Analysis was conducted on a selected part of the water-pipe network being used under actual conditions.

2. Characteristics of a selected water-pipe network

The analyzed network consists of a transit system, water main, and distribution pipelines with diameters ranging from 100 [mm] – 400 [mm]. In this work, terminals and pipelines with diameters of less than 100 [mm] were omitted, as they do not have a significant impact on the functioning and reliability of the system as a whole.

Most pipelines form closed rings; however, the presence of branched endings justifies the classification of this network both as a ring and branched network. A large number of closed rings has a positive influence on the reliability of the operation of this network,

(*) Tekst artykułu w polskiej wersji językowej dostępny w elektronicznym wydaniu kwartalnika na stronie ***www.ein.org.pl***

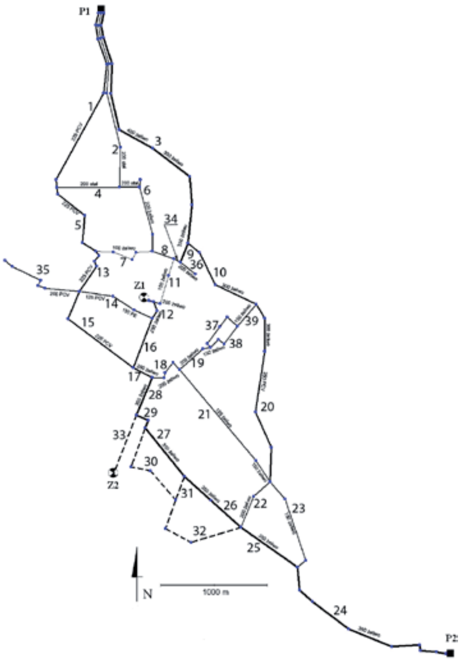

Fig. 1. Structure of water-pipe network connections

because in the case of failure of one pipeline water can be supplied to a consumer via a different route. The elements with the greatest influence on the functioning of the entire system are pumping plants, along with delivery lines and reservoirs. A supply source system comprising pumping plants is advantageous here, as their location on opposite sides of this extended network results in better functioning of the system, equalisation of pressure, and a high level of reliability.

The network supplies water to approximately 40 000 residents with an average demand for water amounting to about 10 000 [m^3] daily. Users are located at heights fluctuating within the range of 283,5–320 [m] above sea level. The highest areas are in the downtown area, around the existing Z1 reservoir, and in the southwestern part of the city in the vicinity of the Z2 reservoir.

The north pumping plant (P1) is situated at a height of 293 [m] above sea level and operates in the pressure range of 4,2 [MPa] – 6,1 [MPa]. Water is supplied to the city through three transit pipelines running in parallel, with diameters of 200 [mm], 225 [mm] and 400 [mm]. In the case of failure of one of the pipelines, the two remaining pipelines take on the burden of water supply to the city. The south pumping plant (P2) is situated 6 metres higher, and so its pumping parameters are lower: 3,5 [MPa] – 5,1 [MPa]. From the P2 pumping plant, water is supplied to the city by only one transit pipeline. Thus, there is a danger that in the case of failure of this pipeline, pumping plant P2 will be put completely out of operation, which may cause insufficient pressure in the network and a decrease in comfortable water consumption for users. In such a situation, consumers situated at the greatest heights may be deprived of water from the network. The location of the Z1 reservoir in the downtown area is also advantageous because it additionally supplies areas with a greater population density and greater demand located farther from the pumping plant, and thus also stabilises pressure. Unfortunately, its ability to accumulate water in the event of failure is severely limited by its small capacity (550 [m^3]).

This network was built in the 1970s and is made mostly of cast iron, polyvinyl chloride, and several steel segments. Thus the main causes of failure are leaks in connections of cast iron pipelines and material defects in plastic pipelines.

3. Applied methods of reliability analysis of the water-pipe network

The connection structure of the water-pipe network shown in fig. 1 is complex from the perspective of reliability. The factoring algorithm was used to determine the reliability of the presented network. This is a method based on graph theory and graph reduction, making it possible to determine network reliability under the following basic assumptions [4, 9, 10, 16, 17]:

– the analyzed network represents an undirected graph:

$$G=(V,E) \tag{1}$$

where:

V – set of graph peaks – nodes in the network (connection of more than 2 pipelines or a recipient connection point): $V=(v_1, v_2,\ldots,v_n)$,

E – set of graph edges – connections (pipelines) in the network: $E=(e_1, e_2,\ldots,e_m)$,

– it is accepted that graph peaks, or nodes in the network, are always in a serviceable state,
– the probabilities of individual connections being damaged in the network are to be assumed or determined by using e.g. statistical methods and data on malfunctions gathered for the given network or for networks exploited under similar conditions,
– any incidents of damage are independent from one another.

Network reliability is defined as the probability of the existence of at least one serviceable connection between all nodes of set K in the network ($2\le|K|\le|V|$). This makes it possible to determine various measures of network reliability depending on the number of nodes contained in set K. When K=2, reliability is the probability of the existence of a connection between two nodes, e.g.: source – reception point or inlet – outlet. When K=V, reliability is the probability of the existence of a connection between all nodes of set V. In a water-pipe network, this can be interpreted as the probability that water supply is available for all nodes in set K, and thus, for all users.

Determination of a dependency making it possible to calculate reliability is done by way of the appropriate reduction of the network, represented by an undirected graph, according to the following notation [4, 8, 9, 17]:

$$R(G_K)=R_{ei}\cdot R(G_K|e_i\ serviceable)+(1-R_{ei})\cdot R(G_K|e_i\ unserviceable) \tag{2}$$

$$R(G_K)=R_{ei}\cdot R(G_{K'}*e_i)+(1-R_{ei})\cdot R(G_K-e_i) \tag{3}$$

where:

$G_{K'}*e_i=(V-u-v+w,E-e_i)$ – graph reduction when connection e_i is serviceable; peaks at the ends of connection e_i are subtracted from the set of peaks (V), a peak resulting from their connection is added in their place, and the reduced connection e_i is removed from connection set (E),

$$K'=\begin{cases} K & if\ u,v\notin K \\ K-u-v+w & if\ u\in K\ lub\ v\in K, \end{cases}$$

$G_K-e_i=(V,E-e_i)$ – graph reduction when connection e_i is unserviceable; the peak set (V) is unchanged and connection e_i is removed from the connection set.

Figure 2 demonstrates the method to reduce and obtain a dependency for calculation of the measure of network reliability sought. Depending on the number of nodes in set K, system reduction is carried out according to the method presented in figure 2. The method from fig. 2a is applied only when all nodes are included in set *K*. The method from fig. 2b, presented here for K=2, is analogous for all cases where $K<V$.

The application of the presented method enables the reduction and

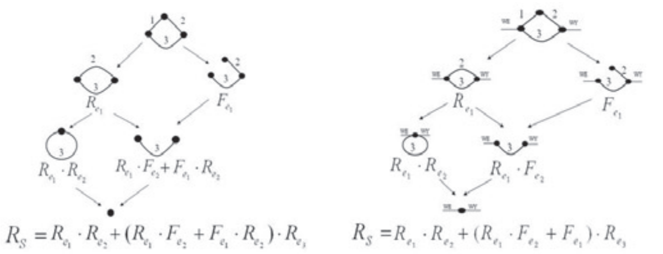

Fig. 2. Method of system reduction according to the factoring algorithm: a) K=V, b) K=2

determination of the reliability of a network system of any degree of complexity. However, the problem becomes significantly more complicated as the number of connections in the network increases, because the reduction procedure is more time-consuming and the form of the final dependency is extensive [4, 10, 16, 18]. Figure 3 shows a fragment of reduction for a simple system where, for 7 connections, the final dependency is already extensive [10]. For more complex systems, such as the water-pipe network analysed here, it is necessary to use a computer program.

Fig. 3. Fragment of system reduction with seven connections for a case where K=V [9]

Besides providing water to recipients through undamaged pipelines, it is particularly important to ensure the required parameter values of supplied water in a water-pipe network. This concerns both hydraulic parameters and those of chemical composition. In this paper, aspects related to the chemical composition of water will not be taken into consideration. As for hydraulic parameters, it is most important to ensure the required pressure values for all consumers and their ability to receive necessary amounts of water at any time [2, 3, 13].

Because the factoring algorithm does not account for the above aspects in its analysis, the 'ISYDW' program, developed at the Cracow University of Technology, was used to calculate hydraulic parameters of water supply to consumers [2,3]. The computational model applied in this program accounts for the following, among other things:

- the structure of connections in the network,
- the diameters and lengths of all pipelines,
- flow resistance and resultant losses of pressure,
- altitudes of users in the network and the corresponding required pressures,
- variable outputs of network supply sources,
- capacities of reservoirs cooperating with the network,
- volume of water demand of consumers in the network.

The program carries out a simulation of network operation, and the execution of calculations makes it possible to observe changes of hydraulic parameters at individual points in the network over a selected time interval, the method in which the network functions, and changes in these parameters in the event of failure of pipelines, reservoirs, or network supply sources. The determined values for hydraulic parameters in the network are then compared to the required values. A convenient method of assessing the degree to which required parameter values are fulfilled is to observe the Water Supply Conditions Index (WSCI). This index defines the degree to which the capability to supply water to consumers is reduced. It is defined as the quotient of the volume of water consumption and the volume of demand. Full user comfort is defined as a WSCI of 1; when this value falls below 1, users do not receive water with the appropriate parameters (pressure in the network is lower than the required pressure, and the user cannot receive the required amount of water). For an individual node in the network, this value is determined according to the following dependency [2, 3]:

$$WSCI = \frac{ZU}{ZP} \le 1 \tag{4}$$

where:
ZU – value of water consumption,
ZP – value of water demand, which is known.

The *ZU* value is determined according to the dependency:

$$ZU = ZP \cdot \left(\frac{h}{h_{min}} \right)^{0,5} \tag{5}$$

where:
h – pressure in the node at a given moment in time,
h_{min} – minimum pressure in a given node providing full comfort of water consumption.

Depending on pressure value h in the node, the following situations are possible:

- if $h= h_{min}$ then $ZU=ZP$ and $WSCI=1$,
- if $h= 0$ then $ZU=0$ and $WSCI=0$,
- if $0<h< h_{min}$ then $0<ZU<ZP$ and $0<WSCI<1$.

The value of the index for the entire network is the quotient of the sum of consumption values for all nodes and the sum of the demand values for all nodes at a given moment in time.

4. Results of calculations

Due to the labour demand related to reduction of the graph representing the network analyzed in this paper, reliability calculations were carried out using a computer programme developed at the AGH Technical University [12].

The nodes in the network consist of all branches, connection points of the network with supply sources and user connection points. For the presented water-pipe network, all 28 nodes were included in set *K*. In this case, a state of network serviceability is every situation in which water transfer to every node in the network is possible, and calculated reliability is the probability of such a situation.

Network reliability, determined as the probability of the existence of a connection between all nodes, with changes dependent on the probability of connections remaining in a serviceable state, is presented on fig. 4.

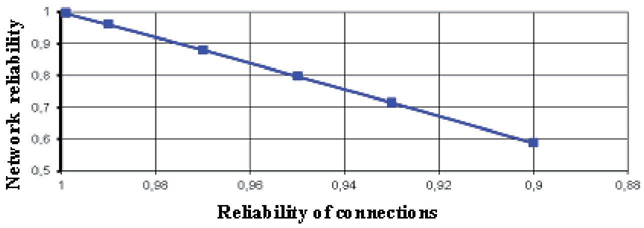

Fig. 4. Network reliability as a dependency of the probability of serviceability of its connections

The main goal of analysis is to determine the impact of damage to individual connections in the network on its reliability. To simplify the calculations presented further on in the paper, only one of the values from figure 4 was taken as a point of reference. This is a case in which the value of the probability of connections remaining in a serviceable state is expressed as $R_p = 0{,}99$, according to literature data elaborated on the basis of many years of study of water-pipe networks [5,15]. Network reliability, determined as the probability of existence of a connection between all nodes, is then equal to $R_s = 0{,}95997$.

The determined values of network reliability in the event of damage to a given connection, as well as the impact of connection damage on network reliability expressed as a percentage, are shown in figures 5 and 6. The zero value of reliability in fig. 5 signifies that damage to a given connection causes a state of network unserviceability in terms of the accepted assumptions. There is no way water can be transferred to the node at the end of this connection. In the case where a supply source is located at the end of the damaged connection, it cannot supply water to the network. These connections (24, 33, 35, 36) can be seen as critical from the perspective of the reliability of the analyzed network.

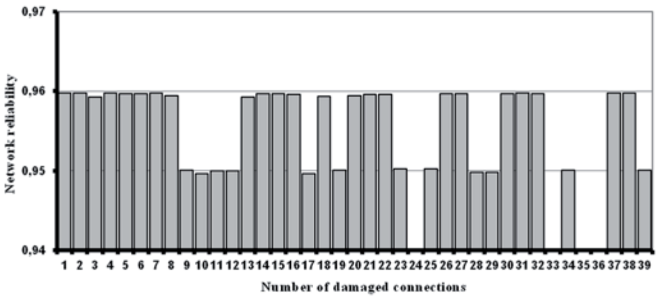

Fig. 5. Network reliability in the event of damaged connections

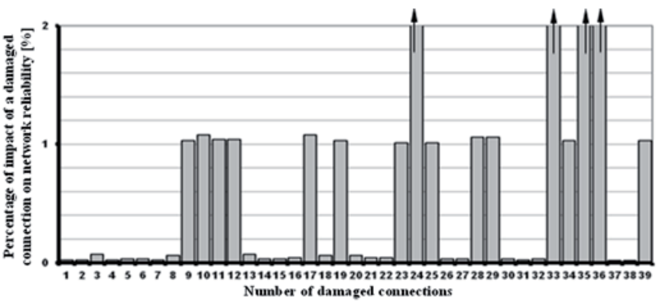

Fig. 6. Percentage of impact of a damaged connection on network reliability

It can also be seen that if certain connections in the ring structures are damaged, this will not cause a state of network unserviceability; however, such damage has a decidedly larger influence on the reliability of the network as a whole. Such critical connections are: 9, 10, 11, 12, 17, 19, 23, 25, 28, 29, 34, 39. Thus, it turns out that from the perspective of maintaining the cohesion of the network structure and the capability of supplying water to all nodes in the network, the serviceability of these connections is also of great significance.

Next, assuming damaged connections in the network, a simulation of network functioning was carried out in the ISYDYW program and WSCI index values were determined. Each time-space simulation was carried out for a full day. Based on information from the use of actual networks, it was assumed that the time to repair a damaged connection would not exceed 1 day [2,3].

When reservoirs and pumping plants are operating correctly, the WSCI index for the entire network is equal to 1. Temporary disengagement of a reservoir does not cause a reduction in comfortable water consumption, whereas total planned closing of a reservoir at peak hours causes a reduction of the WSCI value to 0,9 for several nodes. This means that the small number of consumers supplied from these nodes and residing at the highest altitudes may be affected by insufficient pressure. If reservoir closing is unplanned, then the entire western part of the city is subject to slight inconvenience (WSCI = 0,9), and in the vicinity of several nodes, this inconvenience is significantly greater (at peak hours WSCI = 0,3 – 0,4).

Failure of a 200 [mm] or 225 [mm] transit pipeline (connection 1, 2) from pumping plant P1 does not have a significant impact on WSCI. However, failure of the 400 [mm] pipeline (connection 3) at peak hours causes a drop in WSCI value in several nodes on the west side of the city to 0,9, and, at the most disadvantageous point, to 0,7. However, the effects of disconnection of this pipeline can be minimised by increasing the output of pumping plant P2.

In the case of total shutdown of pumping plant P1 at the most disadvantageous time of day, the WSCI index in the eastern part of the network reaches a value of approximately 0,85; in the western part 0,15 – 0,55.

The most difficult situation occurs when pumping plant P2 is shut down (damage to connection 24). Pressure drops throughout the city, and in the eastern part, the greatest values of the WSCI index are in the range of 0,8 – 0,9 and fall to 0,5 at peak hours. However, in the western part of the city, WSCI fluctuates in the range of 0,15 – 0,55. This means that the water supply needs of only 50% of consumers are met. The course of changes of the mean WSCI index determined for the entire network during a given day is shown in figure 7. It is clearly visible that in the hours from 3 pm to 11 pm, water supply conditions will deteriorate significantly.

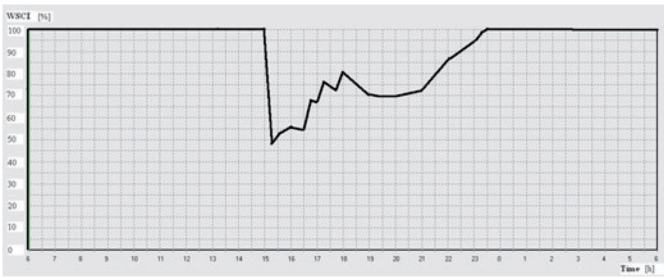

Fig. 7. Change in mean WSCI if connection 24 is damaged

Based on the calculations, it can be stated that the most significant connections in the analyzed network are designated by the numbers: 17, 24, 25, 28, 33. Damage to these connections significantly aggravates water supply conditions at certain points in the network and in large areas of the network.

A list of the most important connections indicated by reliability analysis and time-space simulation has been presented in table 1. Connections of the greatest significance have been marked with the "**X**" symbol.

The results obtained in both methods show a certain convergence. It can, however, be seen that not all connections indicated in the reliability analysis are significant from the perspective of time-space

Table 1. Most important connections in the network indicated by both computing methods

Damaged connection no.	Influence on structural reliability	Influence on water supply conditions to recipients (WSCI)	Minimum mean WSCI value during the day calculated for the entire network	Minimum WSCI value during the day for the worst point in the network
9	x		≅1	0,98
10	x		≅1	0,98
11	x		≅1	0,98
12	x		≅1	0,96
17	x	**X**	0,97	0,37
19	x		≅1	0,98
23	x		≅1	0,98
24	X	X	0,48	**0,13**
25	x	**X**	0,86	**0,13**
28	x	**X**	0,91	**0,13**
29	x		≅1	0,98
33	X	X	0,56	**0,13**
34	x		≅1	0,98
35	**X**		≅1	0,98
36	**X**		≅1	0,98
39	x		≅1	0,98

simulation and have a weaker influence on the determined value of the WSCI index.

Differences mainly result from different approaches to the problem in the two methods. Reliability analysis determines whether water can be transferred to all points in the network with connections being damaged within a certain probability. The most important connections are determined in terms of the fulfilment of this condition.

In time-space analysis, certain quantities not taken into consideration in reliability analysis were accounted for. These include both the diameters and lengths of individual pipelines as well as loss of flow and variable outputs of supply sources. The obtained results make it possible to determine whether, and to what degree, required hydraulic parameters of water will be supplied to consumers.

It can thus be said that the methods are complementary, and in the final assessment of network reliability, connections indicated as significant in both methods should be given special consideration. The critical connections indicated in both methods (17, 24, 25, 28, 33, 35, 36) are the most important from the perspective of structural reliabiltiy as well as the ability to ensure required water supply conditions for consumers in the network. This constitutes a direct guideline for undertaking necessary inspection and technical activities in order to ensure their correct functioning.

In the case under consideration, the following can be recommended:

- impose strict inspection of: construction work, and particularly of performance of excavations and other work involving heavy machinery performed in the area of critical pipeline segments,
- in the case of water main pipelines (24, 25), the construction of a backup should be considered (as in the case of pumping plant P1), particularly if further development of the existing network is planned and in light of the fact that segment 24 is the only connection between pumping plant P2 and the network.

5. Conclusions

The presented factoring and time-space methods used to determine the values of the WSCI index are mutually complementary in the assessment of reliability and can be used to conduct rational usage of water-pipe networks.

Running a time-space simulation in order to determine WSCI index values and to assess structural reliability of the water-pipe network leads to the identification of critical pipeline segments, which, if damaged, could cause the greatest inconvenience to water users. Ensuring the appropriate supervision and technical inspection for these parts of the network is a significant element of usage strategy, because water supply systems are one of the most critical parts of the infrastructure, of particular significance to the functioning of the country and its citizens. Accordingly, ensuring their safe and reliable operation is a particularly important matter.

References

1. Agrawal ML, Gupta R, Bhave PR. Reliability – based strenghting and expansion of water distribution networks. Journal of Water Resources Planning and Management 2007; 133(6): 531–541.
2. Knapik K. Czasowo-przestrzenna symulacja działania systemu dystrybucji wody. Monografia. Kraków: Wydawnictwo Politechniki Krakowskiej, 1989.
3. Knapik K. Dynamiczne modele w badaniach sieci wodociągowych. Monografia. Kraków: Wydawnictwo Politechniki Krakowskiej, 2000.
4. Koide T, Shinmori S, Ishii H. Efficient computation of network reliability importance on K-terminal reliability. International Journal of Reliability, Quality and Safety Engineering 2005; 12(3): 213–226.

5. Kwietniewski M, Roman M, Kłoss-Trębaczkiewicz H. Niezawodność wodociągów i kanalizacji. Warszawa: Arkady, 1993.
6. Levallois P, Grondin J, Gingras S. Evaluation of consumer attitudes on taste and tap water alternatives in Quebec. Water Science and Technology 1999; 40: 135–139.
7. Lukas A, Mayr E, Ruhri M, Katmair H. Failure Experience Improvement System (FEIS) for water supply systems. Journal of Hydroinformatics 2012; 14.3: 646–658.
8. Madeyski L, Mazur Z. Pesymistyczna złożoność obliczeniowa algorytmu faktoryzacji Fact. ZEM 1998; 33(3): 391–404.
9. Page LB, Perry JE. A practical implementation of the factoring theorem for network reliability. IEEE Trans. Reliability 1988; 37: 259–267.
10. Pilch R. Factorisation algorithm-based on method used for the calculation of network system's reliability. Scientific Problems of Machines Operation and Maintenance 2011; 4(168): 45–57.
11. Pilch R, Szybka J, Broniec Z. Determining of hot water-pipe exploitation time on the basis of limiting states. Eksploatacja i Niezawodnosc – Maintenance and Reliability 2012; 14(3): 203–207.
12. Sułek P. Ocena niezawodności układów sieciowych metodą faktoryzacji. Praca dyplomowa. Kraków: WIMiR, AGH, 2011.
13. Suribabu CR, Neelakantan TR. Balancing reservoir based approach for solution to pressure deficient water distribution networks. International Journal of Civil and Structural Engineering 2011; 2(2): 639–647.
14. Torii AJ, Lopez RH. Reliability analysis of water distribution networks using the adaptive response surface approach. Journal of Hydraulic Engineering 2012; 138(3): 227–236.
15. Wieczysty A. Niezawodność miejskich systemów zaopatrzenia w wodę. Monografia. Kraków: Wydawnictwo Politechniki Krakowskiej, 1993.
16. Won J-M, Karray F. A greedy algorithm for faster feasibility evaluation of all-terminal-reliable networks. IEEE Transactions on Systems, Man & Cybernetics 2011; 41(6): 1600–1611.
17. Wood RK. Factoring algorithms for computing K–terminal network reliability. IEEE Trans. Reliability 1986; (R-35): 269–278.
18. Yazdani A, Jeffrey P. Applying network theory to quantify the redundancy and structural robustness of water distribution systems. Journal of Water Resources Planning and Management 2012: 138(2): 153–161.

Robert PILCH
Jan SZYBKA
AGH University of Science and Technology
Faculty of Mechanical Engineering and Robotics
Department of Machine Design and Technology
Al. A. Mickiewicza 30, 30-059 Kraków, Poland
E-mails: pilch@agh.edu.pl; szybja@agh.edu.pl

Anna TUSZYŃSKA,
Cracow University of Technology
Faculty of Environmental Engineering
Institute of Water Supply and Environmental Protection
Ul. Warszawska 24, 31-155 Kraków, Poland

Article citation info:
BOCEWICZ G. Robustness of Multimodal Transportation Networks. Eksploatacja i Niezawodnosc – Maintenance and Reliability 2014; 16 (2): 259–269.

Grzegorz BOCEWICZ

ROBUSTNESS OF MULTIMODAL TRANSPORTATION NETWORKS

MODEL OCENY ODPORNOŚCI MULTIMODALNYCH SIECI TRANSPORTOWYCH*

This paper describes a declarative approach to modeling a multimodal transportation network (MTN) composed of multiple connecting transport modes, such as bus, tram, light rail, subway and commuter rail, where within each mode, service is provided on separate lines or routes. The considered model of a network of multimodal transportation processes (MTPN) provides a framework to address the needs for transportation networks robustness while taking into account their capacity and demand requirements. Therefore the work focuses on evaluation of the network robustness allowing distinguished multimodal processes to continue in order to accomplish trips following an assumed set of multimodal chains connecting transport modes between origins and destinations. Consequently, a solution to the problem of prototyping robust transits on a given multimodal network is implemented and tested. The conditions that guarantee the network robustness, taking into account disruptions of supply and demand as well as operational control, are provided. The aim of investigations is to provide a tool for evaluating the robustness of a network of multimodal transportation processes as well as different travel modes through a transportation network.

***Keywords**: multimodal networks, transportation systems, cyclic scheduling, robustness, multimodal processes, state space, cyclic steady state.*

Dynamiczny rozwój infrastruktury komunikacji miejskiej obejmującej linie autobusowe, trolejbusowe, tramwajowe, linie metra, kolei podmiejskiej, itp. składające się na tzw. Multimodalne Sieci Transportowe (MST) rodzi wiele nowych problemów. Wśród ważniejszych z nich warto wymienić problemy planowania obsługi ruchu pasażerskiego w sytuacjach związanych z awariami elementów infrastruktury, wypadkami losowymi czy też z obsługą imprez masowych. Wiadomo, że istnienie rozwiązań dopuszczalnych gwarantujących zakładaną przepustowość infrastruktury warunkuje tzw. odporność MST na ww. zakłócenia. W tym kontekście, niniejsza praca przedstawia pewien deterministyczny model multimodalnej sieci transportowej złożonej z połączonych stacjami przesiadkowymi, linii komunikacji miejskiej. Składające się na sieć, pracujące w zamkniętych cyklach, linie komunikacji miejskiej pozwalają obsłuchiwać ruch pasażerski na wybranych kierunkach np. północ-południe. Obsługiwane strumienie pasażerów modelowane są jako tzw. multimodalne procesy transportowe. Wprowadzone miary odporności MST, umożliwiające ocenę rozważanych wariantów infrastruktury, pozwalają na wyznaczenie warunków spełnienie, których gwarantuje dopuszczalną jakość obsługi ruchu pasażerskiego. Umożliwiają, zatem zarówno planowanie obsługi pasażerów na wybranych trasach, jak i kształtowanie struktury rozbudowywanej i/lub modernizowanej sieci komunikacji miejskiej.

***Słowa kluczowe**: sieci multimodalne, systemy transportowe, harmonogramowanie cykliczne, odporność na zakłócenia, procesy multimodalne, przestrzeń stanów, cykliczne przebiegi ustalone.*

1. Introduction

Multimodal route planning that aims to find an optimal route between the source and the target of a trip while utilizing several transportation modes including different passenger/cargo transportation systems, e.g. ship, airline, AGV systems, train and subway networks, are of significant and fast growing importance [9, 11, 14, 16, 20]. Multimodal transportation process (MTP), i.e. a set of transport modes which provide connection from the origin to the destination, executed in a multimodal transportation network (MTN) can be seen as passengers and/or goods flow transferred between different modes to reach their destination [5].

MTPs planning problems, i.e. taking into account MTPs routing and scheduling can be found in different application domains (such as manufacturing, intercity fright transportation supply chains, multimodal passenger transport network combining several unimodal networks as well as data and supply media flows, e.g., cloud computing, oil pipeline and overhead power line networks**)** [1, 3, 5, 6, 8, 15, 16]. The problems concerning multimodal routing of freight flows and scheduling of multimodal transportation processes (MTPN) scheduling, are NP-hard [7, 12].

The local transportation processes serviced by different transportation modes, while executed along unimodal networks (lines), are usually cyclic. Hence, MTPs supported by them also have the periodic character. That means that the periodicity of MTPN depends on periodicity of unimodal (local) processes executed in MTN. Of course, the MTPN throughput is maximized by the minimization of its cycle time.

Apart from such typically used objectives as the maximization of a user's (e.g. a passenger) benefits and/or the minimization of a provider's (e.g. public transport service bureau) costs, the present paper discusses the importance of a network structure in assuring a robust network. In other words, a network structure design, that is efficient at handling traffic in normal conditions and provides spare capacity in exceptional situations, is of our main interest.

Therefore, the considered problem can be seen as a problem of robust MTPN designing where the assumed demand objectives are satisfied. That is, assuming each line is serviced by a set of stream-like moving transportation means (vehicles) and operation times required for travelling between subsequent stations as well as semaphores ensuring vehicles mutual exclusion on shared stations are given, the main question concerns MTPN timetabling, for instance guaranteeing the shortest time of passengers' itinerary following a given direction. MTN capacity determines a maximum traffic flow obtainable with

(*) Tekst artykułu w polskiej wersji językowej dostępny w elektronicznym wydaniu kwartalnika na stronie ***www.ein.org.pl***

use of all available lines and roads. In turn, a network demand reflects its users' perspective, i.e. MTPs encompassing traveling passengers itineraries and conditions, taking into account factors such as the quality of transport options available and their prices. Depending on different supply and demand as well as operation control disruptions the MTPN timetabling and, consequently, the time of the passengers trip, following different itineraries, may dramatically differ. In that context, special attention is devoted to disruptions causing MTPNs' deadlock occurrence while threatening MTP by congestions arise.

The declarative models employing the constraint programming techniques implemented in modern platforms such as OzMozart, ILOG, [2, 3, 4] seems to be well suited to cope with MTPs planning problems. Since a problem of robust MTPNs design remains still open, the sufficient conditions guaranteeing the assumed level of MTN's robustness are of primary importance. Therefore, constraints stating the sought conditions can be formulated in terms of MTPN declarative model as well.

To the best of our knowledge, there is no research paper on cyclic scheduling of MTPs subjected to assumed robustness of MTPN modelled in terms of SCCPs. The existing approach to solving the SCCPs scheduling problem is based upon the simulation models, e.g. the Petri nets [17], the algebraic models [18] upon the (max,+) algebra or the artificial intelligent methods [10]. The SCCP driven models, assuming a unique process execution along each cyclic route while allowing to take into account the stream-like flow of local cyclic processes, e.g. buses servicing a given city line, studied in [5], do not take into account the MTP robustness factor. Therefore, this work can be seen as a continuation of our former investigations conducted in [2, 3, 4, 5, 19]. In that context, our paper provides contribution to a time and/or distance robust path-finding problem [13, 14] within the environment of multimodal transportation network as well as its possible implementation in the route advisory systems solving the Multi-Criteria, Multi-Modal Shortest Path Problem [9].

The rest of the paper is organized as follows. We start by introducing a concept of multimodal transportation network (MTN) and then provide its representation in terms of a system of concurrently flowing cyclic processes (SCCP) encompassing a network of multimodal transportation processes (MTPN) while allowing for multimodal transportation processes (MTPs) modeling. The MTPN robustness issues in different contexts of supply and demand as well as operation control disruptions (disruptions leading to the deadlocks) are discussed.

Next, we present the formulation of the problem of robust MTPN designing where network's capacity and demand objectives are simultaneously taken into account. Afterwards, we discuss the implications of adopting different robustness measures and following from them network robustness conditions. Then, we discuss and compare the results obtained through the model for an arbitrarily chosen set of MTPs. In the final section, we briefly summarize our results and provide some concluding results.

2. Multimodal Transportation Network

Multimodal Transportation Network (MTN) concerning the organization of city traffic and the network of public transportation can be modelled with focus on the network of city serviced lines and/or routes. Subway or tram lines as well as bus routes form cycles interconnected via common shared interchange stations or closely situated (short walk-distance) transportation mode specific stations. The means of transportation servicing a particular line mode can be seen in turn as transportation processes enabling passengers to move along their destination route.

2.1. Structure of Multimodal Processes Network

The MTPN seen as a network of vehicles periodically circulating along cyclic routes (see Fig. 1a) can be modeled in terms of Systems of Concurrently flowing Cyclic Processes (SCCP) shown in Fig. 1b). Vehicles are used for the transport of passengers following two directions: north-south (blue line – mP_1) and east-west (red line – mP_2). These routes, setting the courses of multimodal processes, are composed of fragments of the local mode transportation lines (trams and busses). In the considered case, there are six means of transportation: trams (P_1, P_3, P_5) and busses (P_2, P_2' , P_4).

The SCCP is assumed to include two types of processes:

– *local processes* (representing modes of transport – P_1, P_2, P_3, P_4, P_5), whose operations are cyclically repeated along the set routes (sequences of successively visiting stations). For the system from Fig. 1b), the line linking stations R_1, R_2, R_8, R_9 provide two buses that can be modeled by two streams, P_2 and P_2', respectively. The routes of local processes are defined as follows: p_1=(R_7, R_2, R_3), p_2=p_2'=(R_1, R_2, R_8, R_9), p_3= (R_1, R_5, R_4), p_4= (R_3, R_4, R_6), p_5= (R_8, R_{10}, R_9).
  The i-th operation (executed on resource R_k) of the local process P_j (or its stream) is denoted by $o_{i,j}$ and $t_{i,j}$ denotes the time of its execution.

– *multimodal processes* (mP_1, mP_2) representing streams of passengers. Operations of the multimodal processes are implemented cyclically along routes being compositions of fragments of routes of local processes representing resources used for transporting materials along a given route. For the system from Fig. 1b), the routes of multimodal processes (i.e. itineraries of passenger streams) are defined as follows:

mP_1=((R_{10}, R_9),(R_9, R_1, R_2),(R_2, R_3),(R_3, R_4, R_6)), mP_2=((R_7, R_2, R_3),(R_3, R_4,),(R_4, R_1, R_5)).

Similarly as before the i-th operation of the multimodal process, mP_j is denoted by $mo_{i,j}$ and $mt_{i,j}$ denotes the time of its execution.

Process operation are implemented on two kinds of resources: local resources (each of them is used by only one process of a given kind – R_5, R_6, R_7, R_{10}) and shared resources (each of them is used by more than one process of a given kind: R_1–R_4, R_8, R_9).

The local processes use resources that are shared in the mutual exclusion mode, i.e. in a given moment only one local process operation of a given kind can be implemented on a resource (in other words one station can be occupied by only one transportation mode).

The access to shared resources of local processes, is given in the sequence determined by the dispatching rules Θ. It is assumed that $\Theta=\{\sigma_1,\ldots,\sigma_k,\ldots,\sigma_{lk}\}$, where σ_k – is the sequence whose elements determine the order in which the processes (or their streams) are provided with access to the resource R_k. In case of the system from Fig. 1b), the access to shared resources is determined by the following rules:

$$\sigma_1=(P_2,P_3,P_2'),\ \sigma_2=(P_1,P_2,P_2'),\ \sigma_3=(P_1,P_4),\ \sigma_4=(P_3,P_4),\ \sigma_8=(P_5,P_2,P_2'),\ \sigma_9=(P_5,P_2,P_2').$$

The subsequent operation starts right after the current operation is completed, providing that the resource indispensible to its implementation is available. While waiting for the busy resource, the process does not release the resource which was assigned for implementing the previous operation [4]. Moreover, an assumption is made that processes are of non-expropriation nature, and the times and sequence of operations performed by the processes do not depend on external interferences.

The parameters described above constitute the structure of SCCP that determines its behavior. Formally, the structure of SCCP is defined as the following tuple [4]:

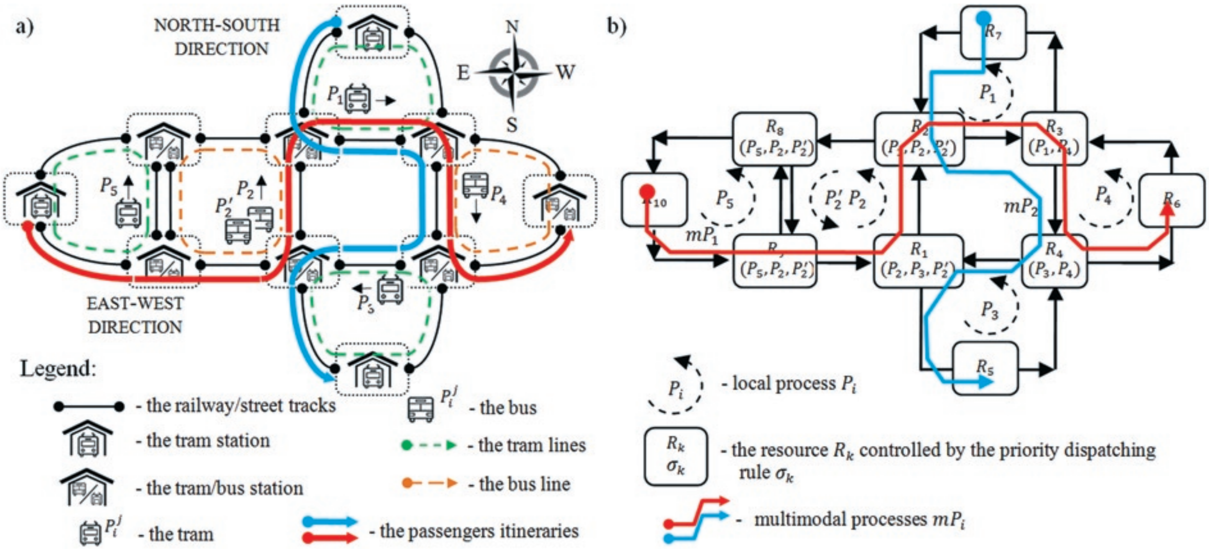

Fig. 1. An example of MTPN a) and corresponding SCCP model b)

$$SC=((R,SL),SM)\ , \tag{1}$$

where: $R=\{R_k \mid k=1,...,lk\}$ – set of resources,

$SL=(P,U,O,T,\Theta)$ – structure of local processes, where:

$P=\{P_i \mid i=1\ldots ln\}$ – set of local processes (streams), P_i – i-th process,

$U=\{p_i=(p_{i,1},\ldots,p_{i,j},\ldots,p_{i,lr(i)}) \mid i=1\ldots ln\}$ – set of routes of local processes, p_i – i-th route, $p(i,j)\in R$ – resource required for implementing j-th operation of the process P_i,

$O=\{O_i=(o_{i,1},..,o_{i,j},...,o_{i,lr(i)}) \mid i=1\ldots ln\}$ – set of sequences of operations, $o_{i,j}$ – j-th operation of the process P_i,

$T=\{T_i=(t_{i,1},\ldots,t_{i,j},\ldots,t_{i,lr(i)})) \mid i=1\ldots ln\}$ – set of sequences of operation performance times , $t_{i,j}$ – time of performing an operation $o^h_{i,j}$,

$\Theta=\{\sigma_k=(s_{k,1},...,s_{k,d},...,s_{k,lh}) \mid k=1\ldots lk\}$ – set of dispatching rules, σ_k – dispatching rule for the resource R_k, $s_{k,d}$ – local process, lh– length of the rule σ_k,

$SM=(mP,mU,mO,mT)$ – structure of multimodal processes, where:

$mP=\{mP_i \mid i=1\ldots lw\}$ – set of multimodal processes mP_i, lw- number of the processes

$mU=\{mp_i=(mp_{i,1},\ldots,mp_{i,j},\ldots,mp_{i,lm(i)}) \mid i=1\ldots lw\}$ – set of routes of multimodal processes, mp_i – i-th route,

$mO=\{mO^h_i=(mo_{i,1},...,mo_{i,j},...,mo_{i,lm(i)}) \mid i=1\ldots lw\}$ – set of sequences of operations, $mo_{i,j}$ – j-th operation of the process mP_i,

$mT=\{mT_i=(mt_{i,1},\ldots,mt_{i,j},\ldots,mt_{i,lm(i)}) \mid i=1\ldots lw\}$ – set of sequences of operation times, $mt_{i,j}$ – time of operation performance $mo_{i,j}$.

2.2. Behavior of Multimodal Processes Network

In the systems of concurrent cyclic processes, the behavior is usually presented [2, 3, 4], as schedules determining the moments of initiating all the operations implemented within them. Fig. 2b) provides an example of such a schedule that determines the way of implementing the processes of SC structure from Fig. 2a).

The presented schedule is an example of the cyclic behavior, i.e. the successive states of the processes are reachable within the constant period (the operations of local and multimodal processes are repeated within the period α=7 time units [t.u.]).

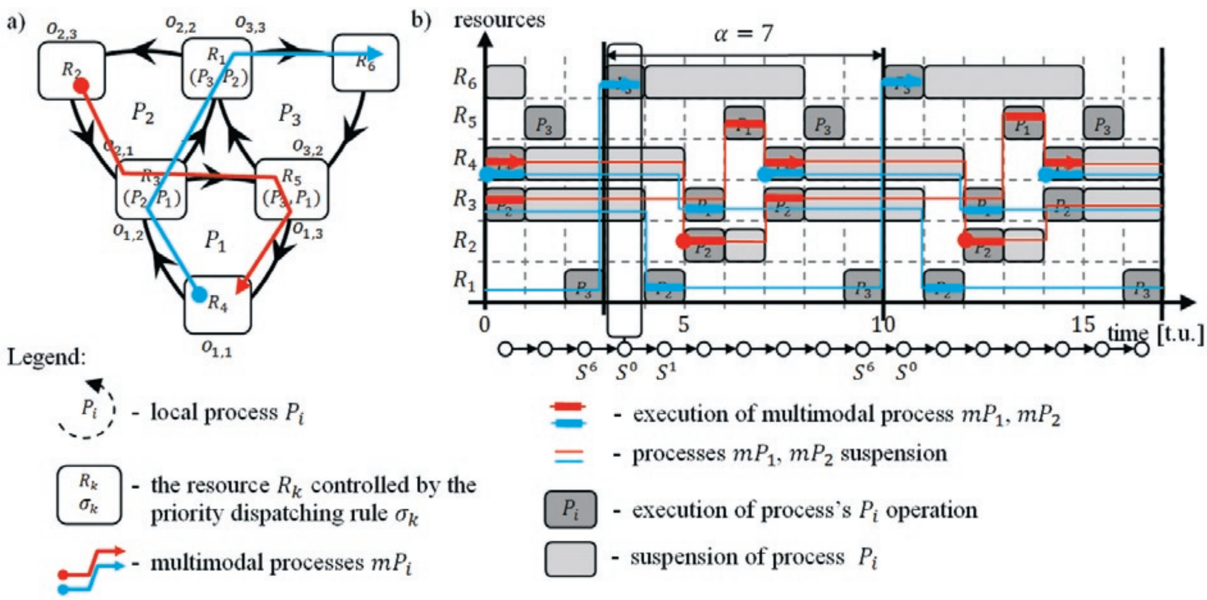

Fig. 2. Example of SCCP structure a) and the corresponding cyclic schedule b)

In this approach, each behavior can be represented by a sequence of successive states (subsequent allocations of processes, as well successively changing, according to the rules Θ of access rights). In case of the schedule from Fig. 2b), it is a sequence of 7 states $S^0, S^1, \ldots, S^6$. Formally, the SCCP state is defined as follows [4]:

$$S^r=(Sl^r,\, mS^r\,), \tag{2}$$

where Sl^r means the r^{th} state of local processes:

$$Sl^r=(A^r, Z^r, Q^r),$$

$A^r=(a_1^r,a_2^r,\ldots,a_k^r,\ldots,a_{lk}^r)$ – allocation of local processes in the r-th state, $a_k^r \in P\cup\{\Delta\}$; $a_k^r=P_i$ – **allocation** meaning that the resource R_k occupied by the process P_i, and $a_k^r=\Delta$ – means that the resource R_k is unoccupied.

$Z^r=(z_1^r,z_2^r,\ldots,z_k^r,\ldots,z_m^r)$ – sequence of semaphores of the r-th state, $z_k^r \in P$ – **semaphore** determining the process (an element of rule σ_k), which has an access to the resource R_k next in the sequence, i.e. $z_k^r=P_i$ means that process P_i is the next to access the resource R_k.

$Q^r=(q_1^r,q_2^r,\ldots,q_k^r,\ldots,q_m^r)$ – **sequence of semaphore indexes** of the r-th state, q_k^r – **index** determining the position of the semaphore value z_k^r in the dispatching rule σ_k, $q_k^r \in \mathbb{N}$. For example, if a semaphore z_2^r indicates the process P_1: $z_2^r=P_1$ which is the second element of the dispatching rule σ_2, then $q_2^r=2$.

mS^r – means the r-th state of multimodal processes:

$$mS^r=\left(mA_1^r,\ldots,mA_i^r,\ldots,mA_l^r\right),$$

$mA_i^r=\left(ma_{i,1}{}^r, ma_{i,2}{}^r,\ldots,ma_{i,k}{}^r,\ldots,ma_{i,m}{}^r\right)$ – sequence of allocations of a multimodal process mP_i in the r-th state, $ma_{i,k}{}^r \in \{mP_i,\Delta\}$, $ma_{i,k}{}^r=mP_i$ – allocation means that the resource R_k is occupied by the process mP_i, and $ma_k^r=\Delta$ – means that the resource R_k is unoccupied.

Behaviors of the system characterized by various sequences of subsequently reachable states $S^r(2)$ can be illustrated in a graphical form as the state space $\mathcal{P}$. Fig. 3a) shows an example illustrating this possibility for the system from Fig. 2a). If we take the graph-theoretical interpretation of the space $\mathcal{P}$, the diagraph corresponding to it is represented by the pair $\mathcal{P}=(\mathbb{S},\mathbb{E})$, where $\mathbb{S}$ means a set of admissible SCCP states [4], $\mathbb{E}\subseteq\mathbb{S}\times\mathbb{S}$ means a set of arcs representing transitions between SCCP states (transitions take place according to the function $S^f=\delta(S^e)$ described in [4].

Cyclic behaviors of SCCP are connected with the presence of cycles (e.g. cycle in digraph G_1) in the space $\mathcal{P}$. A sequence of states being part of a cycle is called as a **cyclic steady state**.

Formally, the cyclic steady state is the sequence $D_C=\left(S^{d_1},\ldots,S^{d_i},S^{d_{i+1}},\ldots,S^{d_{ld}}\right)$ of various admissible states $S^{d_i},S^{d_{i+1}}\in\mathbb{S}$, in which each pair of states satisfies the expression $S^{d_{i+1}}=\delta\left(S^{d_i}\right)$, $i=1\ldots(ld-1)$ and $S^{d_1}=\delta^{lp}\left(S^{d_{ld}}\right)$.

The states of space $\mathcal{P}$ leading to the shared cyclic steady state D_C constitute a coherent digraph called **Whirlpool** $W(D_C)$ (Fig. 3b).

$$W\left(D_C\right)=G\left(D_C\right)\dot{\cup}\left(\dot{\bigcup_{\forall D_T\in DT\left(D_C\right)}}G\left(D_T\right)\right) \tag{3}$$

where: $G(D_C)$ – digraph consisting of cyclic steady state D_C,

$G(D_T)$ – digraph consisting of sequence of states D_T leading to the cyclic steady state D_C, $D_T\in DT(D_C)$, where: $DT(D_C)$ – set of all sequences of states leading to D_C,

$G_1 \dot{\cup} G_2$ – sum of digraphs $G_1=(V_1,V_1)$ and $G_2=(V_2,E_2)$:

$$G_1\dot{\cup}G_2=(V_1\cup V_2, E_1\cup E_2),$$

$$\dot{\bigcup}_{G_i\in G^*}G_i=G_1\dot{\cup}G_2\dot{\cup}\ldots\dot{\cup}G_a,\ for\ G^*=\{G_1,G_2,\ldots,G_a\}$$

An example of a whirlpool is presented in Fig. 3b). It shows clearly that the initiation of process implementation of any state belonging to this whirlpool consequently results in cyclic state D_C.

It must be emphasized that not all digraphs of the state space $\mathcal{P}$ result in a cyclic steady states D_C. Some states lead to deadlock states S^* (marked with the symbol $\otimes$), which means system interruption caused by a closed-loop resource request occurrence.

An example of a deadlock caused by a closed-loop resource request is illustrated in Fig. 3a). In the state S^*, the process P_2 waits for releasing the resource R_3 by the process P_1, the process P_1 waits for releasing the resource R_5 by the process P_3 and the process P_3 waits for the access to resource R_1. The access to resource R_5 is possible only for the process P_2; yet, it cannot reach the resource as it is

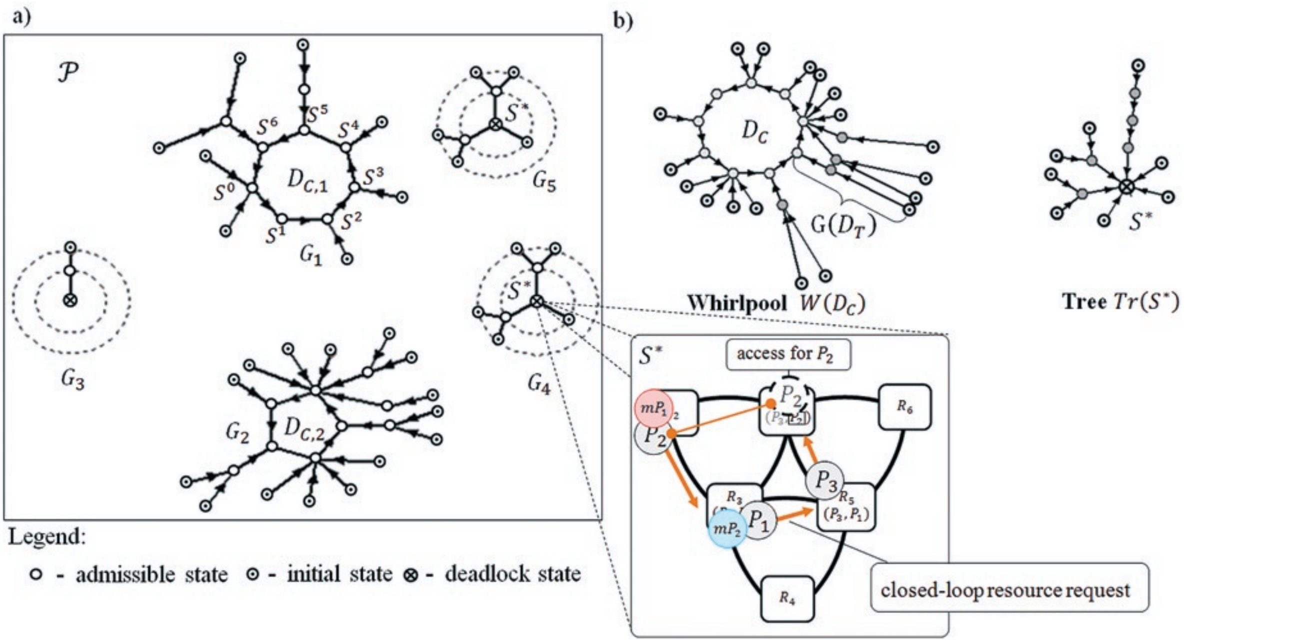

Fig. 3. The states space $\mathcal{P}$ determined by structure from Fig 2a), and the basic components of $\mathcal{P}$ b)

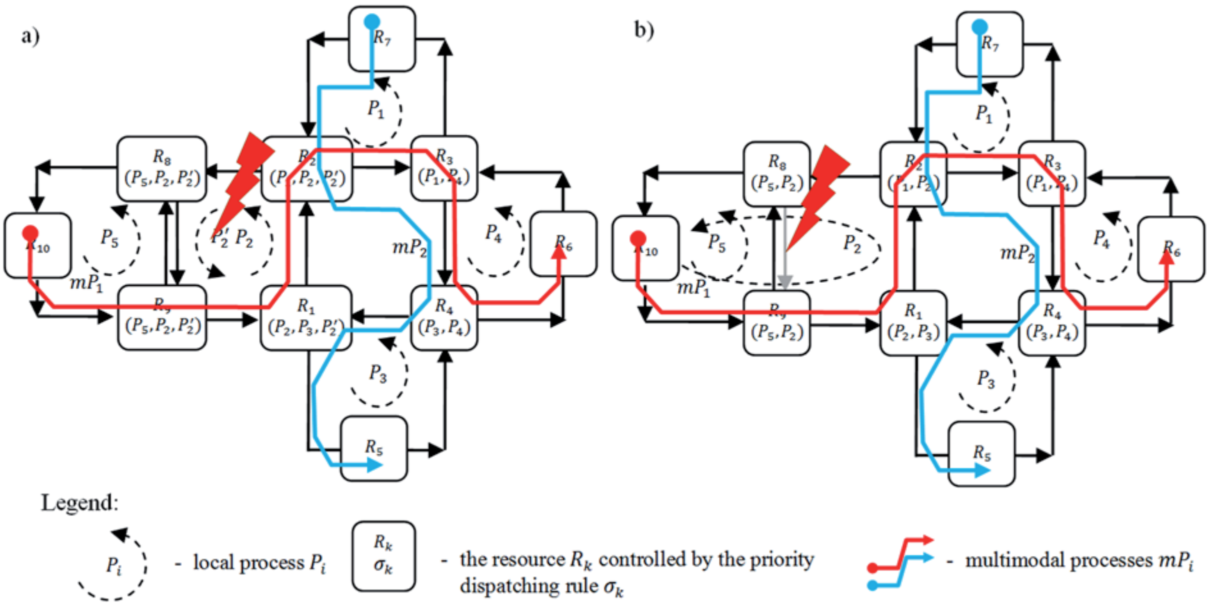

Fig. 4. Example of structural disruption in system from Fig. 1, stream failure P_2' a) , connection failure $R_8 - R_9$ b)

blocked by P_1. In practice, we face such situations when buses (trams) queue up in the order of service different that that required in a given station. In the considered case, bus P_2 is the last in the queue though it is the first to be served. As a result, such deadlocks stop the work of the system.

States causing deadlocks constitute the other type of behavior digraphs: **Tree** (Fig. 3b):

$$Tr\left(S^*\right) = \left(\dot{\bigcup_{\forall D_T \in DT\left(S^*\right)}} G\left(D_T\right) \right), \tag{4}$$

where: $G(D_T)$ – a digraph consisting of sequence of states D_T leading to the deadlock state S^*, $DT \in DT(S^*)$; $DT(S^*)$ – a set of all sequences of states leading to the deadlock state S^*.

Whirlpools and trees are the two basic components of the state space $\mathcal{P}$. Whirlpools make it possible to estimate the presence of cyclic steady states (determining the collision-free and deadlock-free transport of passengers in MTN). Trees enable determining dangerous states that lead to deadlocks (e.g. traffic congestions).

2.3. Disruptions in Supply and Demand

Determining the state spaces is the subjects of numerous investigations [2, 3, 4]. One of the properties of the considered SCCPs is the fact that once obtained behavior (cyclic steady state D_C that guarantees meeting the requirements of a user, deadlock S^*) does not change

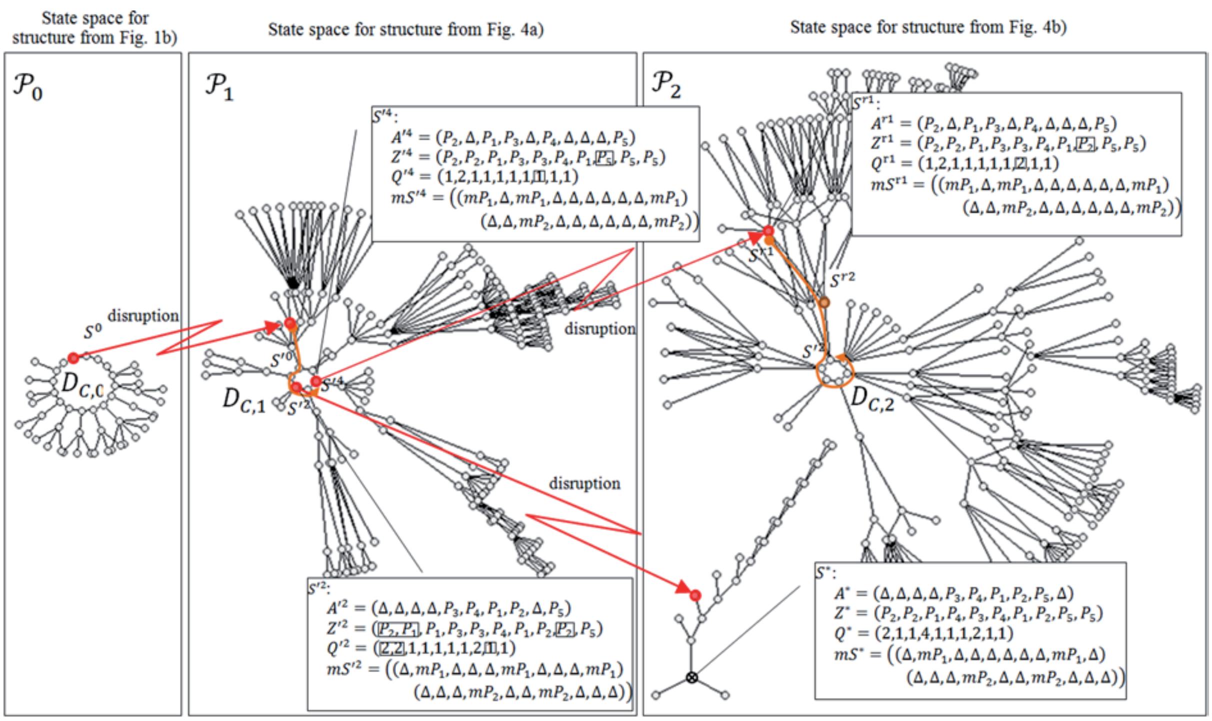

Fig. 5. The change of the state space generated by Fig. 4 while cussed by structural disruptions

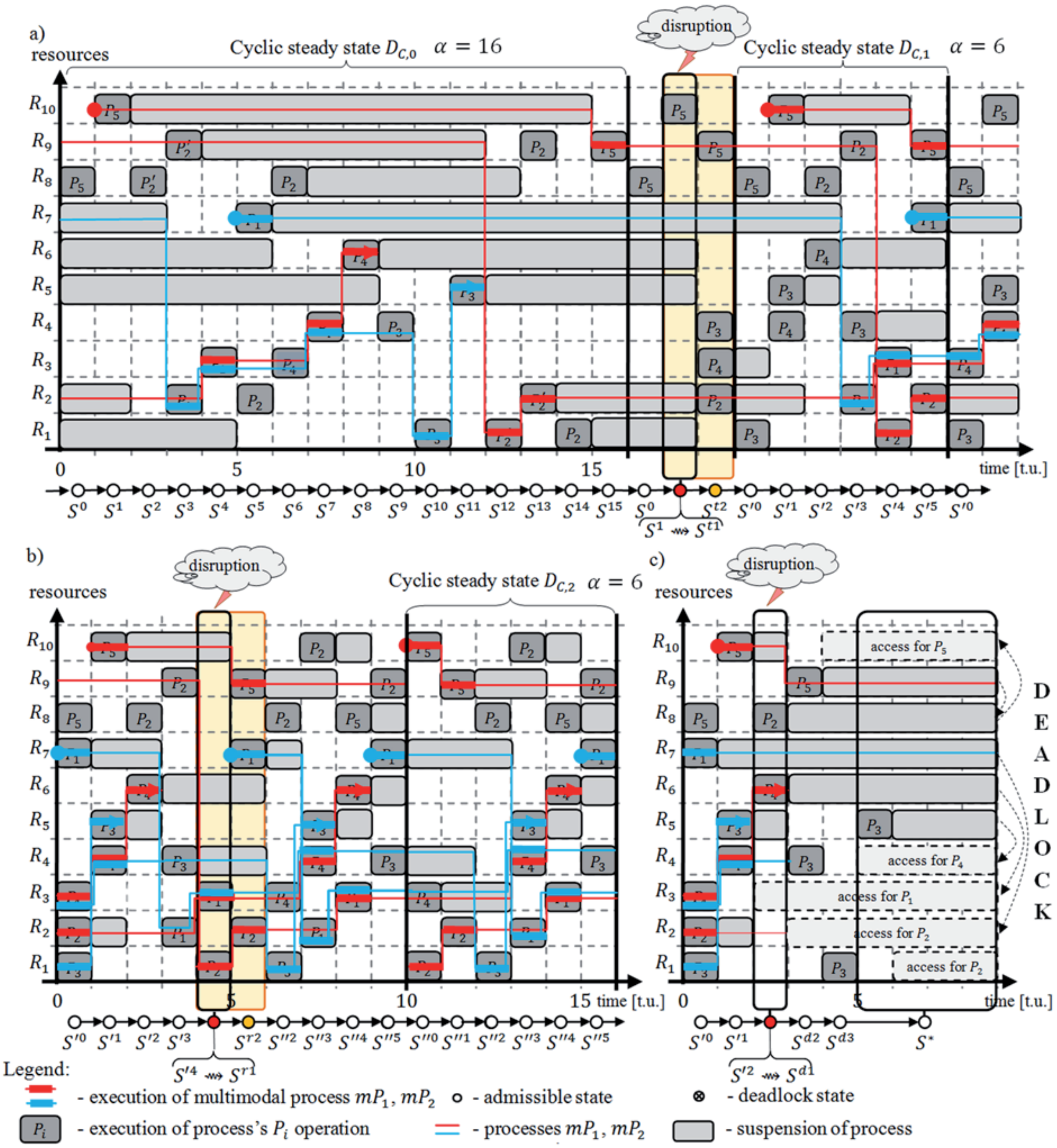

Fig. 6. Schedules illustrating changes of SCCP behavior caused by structural disruptions: leading to the cyclic steady state – disruption from Fig 4a) a), leading to the cyclic steady state – disruption from Fig 4b) b), leading to the deadlock c)

until the work conditions of the system are changed (e.g. change in the parameters of structure *SC*). An alteration in conditions of this kind may be caused by a number of external disruptions. Among disruptions in supply and demand, two types of disruptions can be distinguished:

- structural disruption: disruptions related to changes in the structure *SC* including, among others, addition or removal of a process (e.g. a new bus) – see Fig. 4a), changes in process routes caused by failures of transport lines (the railway/street tracks) – see Fig. 4b), resources failure (the tram/bus stations), etc.
- behavioral malfunction: disruptions related to changes in the way processes are implemented (disruptions of the system state S^r) including:
  - delays in the course of operation implementation (changes in duration of operation $t_{i,j}$). SCCPs systems subjected to this kind of disruptions have the ability to return to cyclic steady states unaided [5],
  - disruption in operation control resulting in changes in the current access rights to the shared resources (changes in values of semaphores $Z^r$and indexes Q^r related to them). Such disruptions include failures of traffic lights, railway signal, etc.

Examples of structural damages are presented in Fig. 4. We are considering a situation when the removal of stream P_2' (line P_2' bus broke down) – see Fig. 4a), and next there was a failure in the connection between resources R_8 and R_9 – see Fig. 4b). Consequently, the route of the local process P_2 was changed into $p_2=(R_1,R_2,R_8,R_{10},R_9)$; in practice it means that bus P_2, changed its itinerary. When such a series of disturbances occurs the question arises whether it is possible to maintain the cyclic behavior of the system.

Figure 5 shows state spaces $\mathcal{P}_0$, $\mathcal{P}_1$, $\mathcal{P}_2$ generated by the structures of SCCP affected by subsequent failures. In case of the first failure,

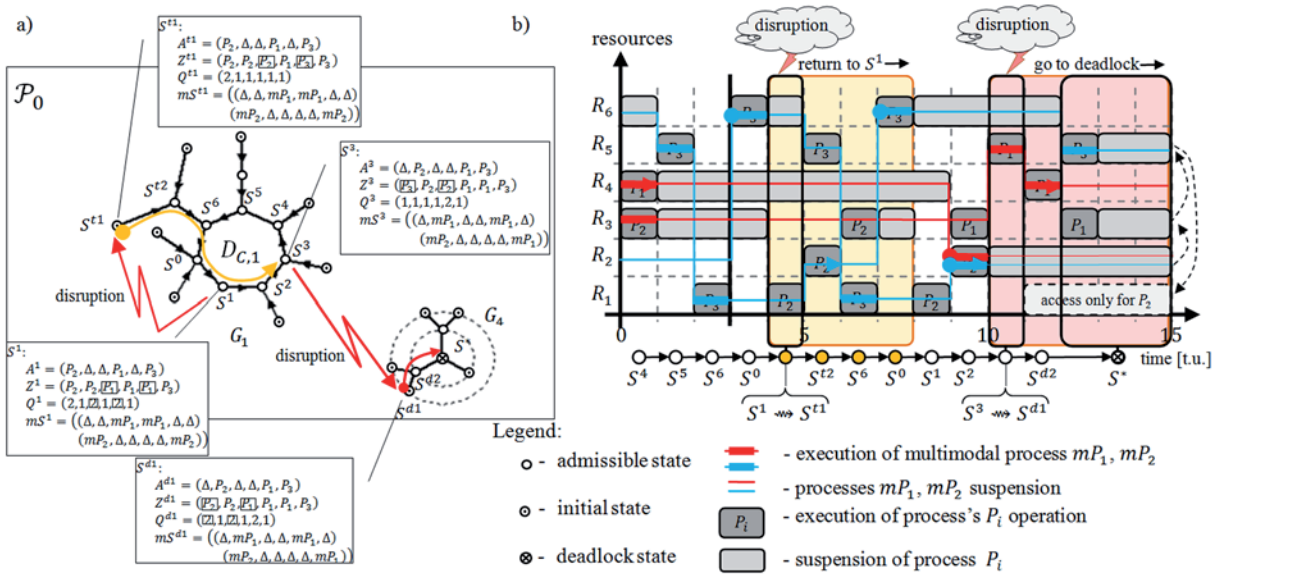

Fig. 7. The state space $\mathcal{P}_0$ generated by the system from Fig. 2 due to disruptions in operation control a), Gantt's diagram illustrating the changes in a system behavior b)

changing the state space from $\mathcal{P}_0$ to $\mathcal{P}_1$results in the transition of the system from the state S^0 to S^{r1}, which leads to cyclic steady state $D_{C,1}$. Generally, disruptions of this kind (removing processes) lead back to the cyclic steady state; these disruptions were subjected to investigations described in [5].

In case of the next disruption (removal of the connection $R_8 - R_9$), the behavior of the system is not that obvious. Figure 5 presents two possible scenarios for the further behavior of the system, depending on the state in which the disruption occurred. The occurrence of a disruption is equivalent to changing the state space to $\mathcal{P}_2$, where the state S^4 passes to the state S^{r1}, and the state S^2 passes to the state S^{d1} (as a result of changing the itinerary of the process P_2, some values of semaphores and indexes change – they are marked with a frame $\square$).

It is clear that the occurrence of a disruption in the state S^4 results in disturbances in the behavior of the system manifested by the states (i.e. S^{r1}, S^{r2}) leading to a new cyclic steady state $D_{C,2}$. On the other hand, the disruption in the state S^2 (see Fig. 6c) results in states leading to the deadlock S^*. Schedules illustrating the described-above transitions are presented in Fig. 6.

As the described example shows, the occurrence of the structural disruption in SCCP causes a change of states and, consequently, the current state of the system. Further behavior of the system depends on the fact whether the newly obtained state is a part of a whirlpool (leading to a cycle, as S^{r1}) or a tree (leading to a deadlock, as S^{d1}).

2.4. Disruptions in Operation Control

A change in the structure *SC* caused by the occurence of structural disruption leads to the change in the state space (e.g. a change from $\mathcal{P}_0$ to $\mathcal{P}_1$ and $\mathcal{P}_1$ to $\mathcal{P}_2$). However, such situations do not happen in case of behavioral malfunction, and especially in case of disruptions in operation control. Disruptions of this kind do not lead to the physical damage of the structure (connection failure, removal of a process, etc.) and, consequently, they do not cause changes in the space state. It means that the change of the current state space, resulting from a disruption, occurs in the same space.

An example illustrating a situation of this kind is shown in Fig. 7. The considered disruption is of the operation control type. Its idea is to change the current access rights to resources (by changing semaphores Z^1 and corresponding indexes Q^1). For example, the disruption in the state S^1 consists of changing the access rights to the resource R_3 (from $\mathcal{P}_1$ to $\mathcal{P}_2$) and R_5 (from $\mathcal{P}_1$ to $\mathcal{P}_3$). The change of this kind results in a transition of the system into the state S^{t1} which, subsequently (through the states S^{t1} and S^6) can return to the cyclic steady state $D_{C,1}$. In practice, such a disruption may mean a signaling system failure in the stations R_3 and R_5, which results in the change of servicing order of trams and buses in these stations. Another example, this time leading to deadlock (see Fig. 7), is the disruption in the state S^3.

Similarly as in case of structural damages, the system's ability to return to cyclic steady state after the disruption of operation control depends on the system's ability to pass to the state included in the whirlpool.

3. Problem formulation

The existence of states leading to cyclic steady state, among states resulting from a disruption, proves the system's ability to self-organize. The system's robustness results from this ability. It is assumed that the robustness is expressed as:

$$Rob(dist) = \frac{NC(dist)}{NT(dist)} \tag{5}$$

where:

$Rob(dist)$ – robustness of SCCP to disruption dist; $Rob(dist) \in [0,1]$;
$Rob(dist) = 0$ – means the lack of robustness, i.e. disruption dist will always lead to a deadlock,
$Rob(dist) = 1$ – means full robustness to disruption *dist*, regardless of the disruption state, the system always returns to the cyclic steady state,

$\mathcal{P}_{dist}$ – state space imposed by disruption *dist*,

$NC(dist)$ – number of states leading to cyclic steady states contained in $\mathcal{P}_{dist}$,

$NT(dist)$ – number of states contained in $\mathcal{P}_{dist}$, $NT(dist)=|\mathbb{S}_{dist}|$.

According to (5), in all the cases discussed so far, the system's robustness to disruption *dist* should be regarded as the ratio of the number of whirlpool's states to states of the space $\mathcal{P}_{dist}$. The value, obtained in this way, determines the natural robustness (denoted as Rob_0 (*dist*) determined by the structure of the system *SC*(1).

Owing to the fact that in many cases occurring in practice [2, 3, 4] the state space $\mathcal{P}_{dist}$ includes mainly digraphs of the tree type, the value Rob_0 (*dist*) does not exceed 0.5. That means, that over 50% of possible disruptions lead to stoppage of the system (deadlocks).

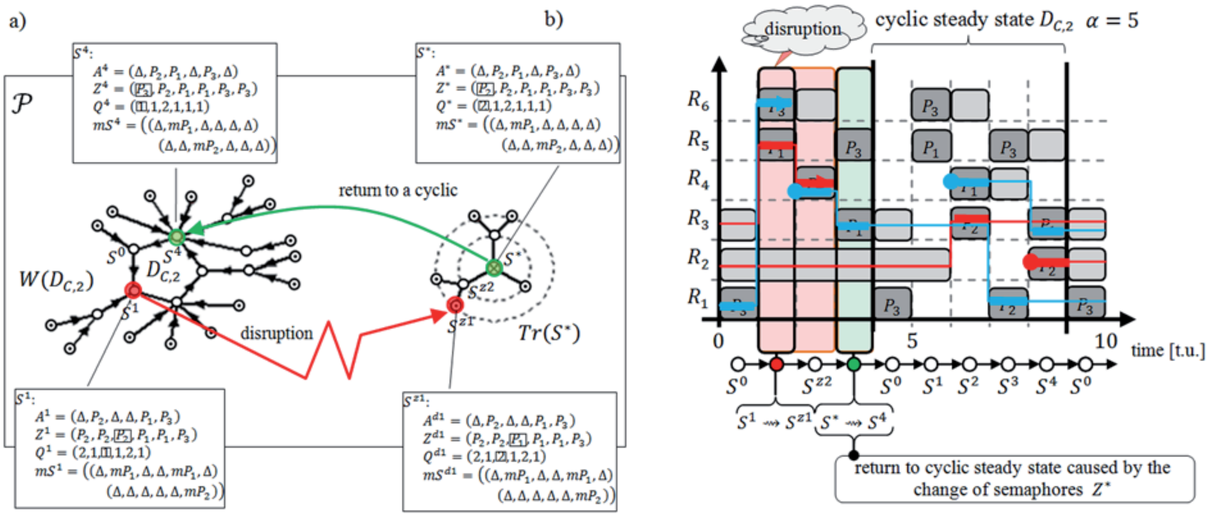

Fig. 8. An example of a return to cyclic steady state in the state space from Fig. 3

Therefore, investigations are carried out aiming at MTN structure design robustness of which is higher than Rob_0 (*dist*). In general case the robustness of a MTN depends on its structural features (such as redundancy, density, and so on) and on control mechanism employed in course of synchronization of concurrently executed flows. In that context, the present work attempts to determine these conditions for disruptions in operation control. Within this approach, the considered problem takes the following form:

There is a given MTN network modelled by SCCP with the structure SC (1). The robustness of the system Rob_0 (dist) to disruptions in operation control is known. The answer to the following question is sought: Are there any conditions (e.g. determining the methods of controlling the system) guaranteeing Rob(dist)>Rob_0 (dist)?

4. Robustness Conditions

In our further considerations, let's make an assumption that we are constraining to disruptions in operation control (e.g. disruptions in signaling – see Fig. 7). According to the previously made annotation (see point 2.4), it means that, as a result of a disruption, the state space does not change: $\mathcal{P}_{dist}=\mathcal{P}$.

In such a space, only states belonging to whirlpools make it possible to return to cyclic steady state. (see Fig. 7). It means that the increase in robustness (5) comes down to determining whether it is possible to reach cyclic steady states from states that do not belong to whirlpools. In other words, it is crucial to answer the following question: Is the transition between structures of the whirlpool type and the tree type possible in space $\mathcal{P}$ (Fig. 8a)?

As Fig. 8a) shows, that this kind of transition depend on the existence of a state that is, at the same time, an element of both the tree and the whirlpool. However, the presence of such states in space $\mathcal{P}$ is not acceptable [3]. Transitions of this kind may occur only as a result of modification of elements (semaphores and indexes) of the proper states (e.g. S^* and S^4). For this purpose, the properties referring to states possessing the same allocation are used.

Figure 8b) shows the implementation of process operations of the system from Fig. 2 caused by the disruption in state S^{z1} (the disruption consists in change of access rights to the resource R_3). As a result of the disruption, the system passes to the state S^{z1}, which leads to a deadlock (state S^*). It is noticeable that the allocation of local processes of state S^* is identical as the allocation in the state S^4: $A^*=A^4$. In practice, it means that in the state S^* means of transport (buses and trams) are in the same stations as in the state S^4. Hence, the deadlock is caused by improper assignment of access rights to resources (signaling that controls the order of service in stations). It means that it is enough to change the access rights to resources and the system will return to cyclic steady state. In the considered case, such a change comes down to changing semaphores from Z^* to Z^4 (on the resource R_1 the access P_2 is changed into the access for P_3).

The example above shows that in certain situations (e.g. concerning structures of the tree type) it is possible to return to cyclic steady state as a result of changing current values of semaphores (signaling). However, a condition must be fulfilled that the states, between which the transition happens, are characterized by the same allocation of processes. This observation leads to the following property:

Property 1

If in the space $\mathcal{P}$ there are two states $S^a \in V_{Tr}(S^*)$, $S^b \in V_W(D_{C,2})$ (where: $V_{Tr}(S^*)$ –set of states belonging to the tree $Tr(S^*)$ (4), $V_W(D_{C,2})$ – set of states belonging to the whirlpool $W(D_{C,2})$ (3)) possessing the same allocation of local processes $A^a=A^b$, then the whirlpool $W(D_{C,2})$ (and, consequently, cyclic steady state $D_{C,2}$) is reachable from the tree $Tr(S^*)$.

□

The presence of states that make it possible to return to cyclic steady state increases the system's robustness to *disruptions in operation control*. The evaluation of the presence of such states (as well as determining their number) requires searching through the states of $\mathcal{P}$ in order to identify the same allocation of processes. In the situation when the cyclic steady state $D_{C,1}$ (being a part of the whirlpool $W(D_{C,1})$ and the tree $Tr(S^*)$ are known, determining the states possessing the same allocation comes down to searching through all the admissible pairs of states, i.e. elements of the set $V_W(D_{C,1}) \times V_{Tr}(S^*)$. The proper algorithm has the following form:

Algorithm 1

function StatesCoAll $\left(W(D_{C,1})=\left(V_W(D_{C,1}),E_W(D_{C,1})\right), Tr\left(S^*\right)=\left(V_{Tr}(S^*),E_{Tr}(S^*)\right)\right)$

```
AC ← ∅
forall S^a ∈ V_Tr(S*)
  forall S^b ∈ V_W(D_C,1)
    if A^a = A^b then AC ← AC ∪ (S^a, S^b)
    end
  end
end
return AC
end
```

where: $W(D_{C,1})=(V_W(D_{C,1}),E_W(D_{C,1}))$, $Tr(S^*)=V_{Tr}(S^*)$, $E_{Tr}(S^*))$ – input data: whirlpool related to cyclic steady state $D_{C,1}$, and the tree leadig to the deadlock S^*,

AC – set of pairs (S^a,S^b) of states possessing the same allocation.

The result of Algorithm 1 is the set AC of pairs of states (S^a,S^b) possessing the same allocation: $AC \subseteq V_W(D_{C,1}) \times V_{Tr}(S^*)$. If we assume, for simplicity reasons, that the considered digraphs ($W(D_{C,1})$, $Tr(S^*)$) have the same number of states (determined by ld), the computational complexity of the proposed Algorithm 1 is estimated by the quadratic function $f(ld)=\mathcal{O}(ld^2)$.

The presented algorithm makes it possible to estimate the reachability of only two selected digraphs $W(D_{C,1})$, $Tr(S^*) \in DG$ (DG – set of digraphs of the space $\mathcal{P}$). Investigating the reachability between all the digraphs of the set DG comes down to evaluating the reachability of each pair of this set. The computational complexity of a procedure of this kind amounts to: $f(ld,dg)=\frac{1}{2}(dg^2-dg)\cdot ld^2 (dg=|DG|)$.

Owing to the polynomial character of the computational complexity function, the problem of evaluating the reachability of whirlpools seen as subspaces of $\mathcal{P}$ is easy to handle.

It must be emphasized that all states of the set AC make it possible to return to the cyclic steady state as a result of changes in the values of semaphores. Therefore, using these states in the process of returning the system to the cyclic steady state enhances the system's robustness to the existing disruptions:

$$Rob(dist)=\frac{|VW|+|AC|+|AD|}{NT(dist)} \tag{6}$$

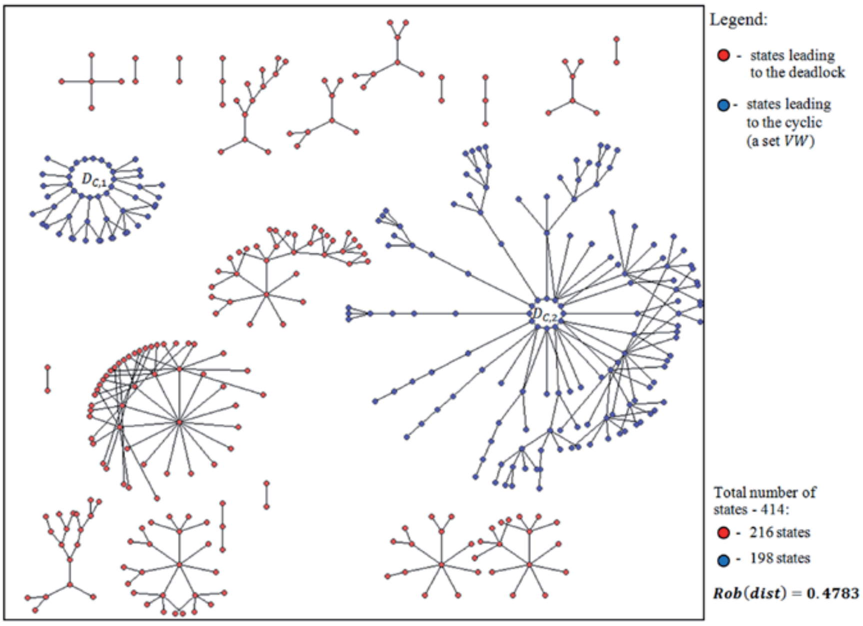

Fig. 9. State space of the system from Fig. 1

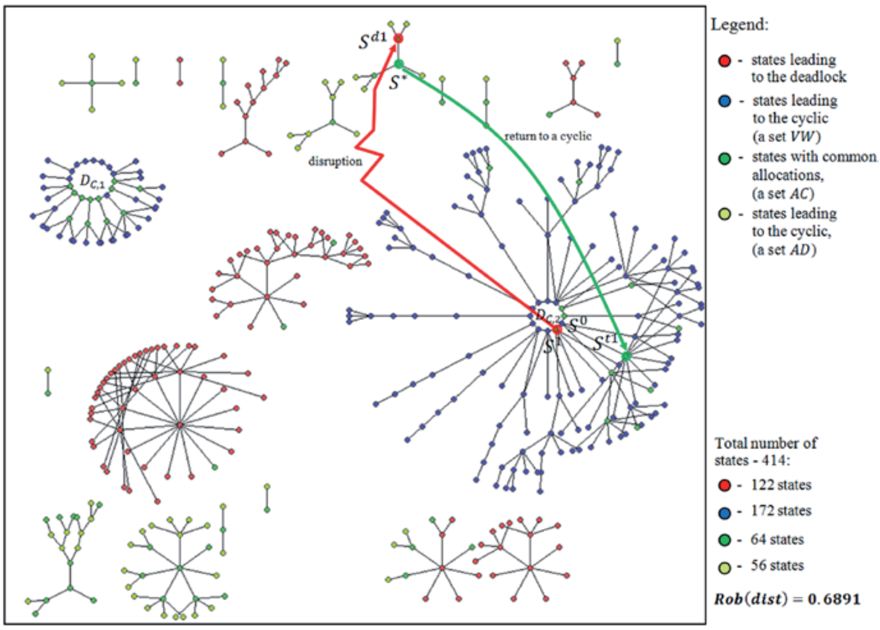

Fig. 10. State space of the system from Fig. 1 with highlighted states possessing the same allocation (set AC) and states leading to them (set AD)

where: VW – set of states constituting whirlpools of the state $\mathcal{P}$, AC - set of states possessing the same allocations, AD – set of states leading to the states of the set AC.

Contrary to (5), with the expression (6), the states that make it possible to return to cyclic steady state include not only states of the set VW, but also states with the same allocation (set AC) and all the states leading to them (set AD).

5. Numerical Example

The developed approach to determining states possessing the same allocation was used to evaluate the robustness of the system from Fig. 1 to disruptions in operation control. For this purpose, the state space $\mathcal{P}$ (see Fig. 9) was determined with use of the method presented in [3]. The space $\mathcal{P}$ includes 414 states, out which 198 states are elements of whirlpools (in the space there are two whirlpools leading to two cyclic steady states). The robustness (5) of such systems to disruptions in operation control (disruptions which do not lead to changes in state space) amounts to $Rob(dist)=0.4783$. In practice, it means that over a half of disruptions (if we assume that all disruption are equally probable) lead to the stoppage of the system (deadlock).

The robustness of the system can be enhanced by taking into account states possessing the same allocation in the process of returning to cyclic steady state. These states were determined on the basis of algorithm 1. Figure 10 shows the space $\mathcal{P}$ of the system from Fig. 1 along with states with the same allocation (set AC) and states leading to them (set AD). Owing to the knowledge about these states it is possible to return to the cyclic steady state even when the system passes to a state belonging to a tree. An example of such a transition is presented in Fig. 10 – the transition between the states S^1, S^{d1}, S^*, S^{r1}, S^0. By taking into consideration states of the sets AC and AD the robustness of the system (6) can be increased to the value $Rob(dist)=0.6891$.

6. Conclusions

The article has discussed the major disruptions in the labor of systems with cyclic multimodal processes and focused mainly on disruptions in operation control. In order to evaluate the robustness of NTN to this kind of disruptions the measure $Rob(dist)$ has been introduced: it determines the system's ability to return to the cyclic steady state.

In order to enhance the robustness of NTN, an approach based on a property which states that the return to the cyclic steady state is possible from states possessing the same allocation, is proposed.

In this case, the return is possible as a result of change in access rights (semaphores) to the shared resources. The analyzed example shows that owing to the fact that these states are classified as the so-called "safe" states the robustness of system can be increased by as much as 44% (the value $Rob(dist)$ has risen from z 0.4783 up to 0.6891).

The proposed algorithm of determining states possessing the same allocation is characterized by polynomial computational complexity. Therefore, it is possible to use this approach in networks with a scale that is met in practice.

The use of the proposed conditions (Property 1) is restrained to disruptions in operation control. That is why, further investigations will focus on an attempt to expand the developed conditions to the area of disruptions including, among others, the structural disruption.

References

1. Bielli M, Boulmakoul A, Mouncif H. Object modeling and path computation for multimodal travel systems. European Journal of Operational Research 2006; 175(3): 1705-1730.
2. Bocewicz G. Reachability of multimodal processes cyclic steady states space. Environmental Issues in Automotive Industry, series: EcoProduction, Golińska P (Eds.): Springer Heidelberg, 2014: 129-162.
3. Bocewicz G, Banaszak Z. Declarative approach to cyclic scheduling of multimodal processes. EcoProduction and Logistics, Emerging Trends and Business Practices, series: EcoProduction, Golińska P (Eds.): Springer Heidelberg, 2013: 203-238.
4. Bocewicz G, Banaszak Z. Declarative approach to cyclic steady states space refinement: periodic processes scheduling. International Journal of Advanced Manufacturing Technology 2013; 67(1-4): 137-155.
5. Bocewicz G, Banaszak Z, Nielsen I. Robustness of multimodal processes itineraries. Proceedings of IFAC Conference on Manufacturing Modeling, Management and Control. Saint Petersburg 2013: 2092-2097.
6. Boyac B, Geroliminis N. Estimation of the network capacity for multimodal urban systems. Procedia - Social and Behavioral Sciences, 6th International Symposium on Highway Capacity and Quality of Service 2011; 16: 803-813.
7. Chiraphadhanakul V. Routing and scheduling models for robust allocation of slack. M.Sc. theses in Trasnportationa and Operational research, Massachusets Institute of technology, 2010.
8. Coronado Mondragon A E, Coronado Mondrago E S, Coronado Mondragon C E, Mung'au F, Estimating the performance of intelligent transport systems wireless services for multimodal logistics applications. Expert Systems with Applications 2012; 39(4): 3939-3949.
9. Guo Z. Transfers and path choice in urban public transport system. Ph.D. theses, Massachusetts Institute of Technology, 2008.
10. Heo S-K, Lee K-H, Lee H-K, Lee I-B, Park J H. A new algorithm for cyclic scheduling and design of multipurpose batch plants. Industrial & Engineering Chemistry Research 2003; 42(4): 836-846.
11. Hu Z-H. A container multimodal transportation scheduling approach based on immune affinity model for emergency relief. Expert Systems with Applications 2011; 38(3): 2632-2639.
12. Levner E, Kats V, Alcaide D, Pablo L, Cheng T C E. Complexity of cyclic scheduling problems: a state-of-the-art survey. Computers & Industrial Engineering 2010; 59(2): 352-361.
13. Li M. Robustness Analysis for Road Networks A framework with combined DTA models. Ph.D. theses, Delft University of Technology, 2008.
14. Liu L. Data model and algorithms for multimodal route planning with transportation networks. Ph.D. theses, Technische Universität München, 2010.
15. Ortúzar J D, Willumsen L G. Modelling transport. 3rd Edition John Wiley & Sons, West Sussex, England, 2002.
16. Petersen H L. Decision support for planning of multimodal transportation with multiple objectives. Ph.D. theses, Dept. of Transport, Technical University of Denmark, Kongens Lyngby, 2009.

17. Song J-S, Lee T-E. Petri net modeling and scheduling for cyclic job shops with blocking. In: Computers & Industrial Engineering 1998; 34(2): 281-295
18. Von Kampmeyer T. Cyclic scheduling problems. Ph.D. theses, Fachbereich Mathematik/Informatik, Universität Osnabrück, 2006.
19. Wang B, Yang H, Zhang Z-H. Research on the train operation plan of the Beijing-Tianjin intercity railway based on periodic train diagrams. Tiedao Xuebao/Journal of the China Railway Society 2007; 29(2): 8-13.
20. Zografos K G, Androutsopoulos K N. Algorithms for itinerary planning in multimodal transportation Networks, IEEE Trans. on Intelligent Transportation Systems 2008; 9(1): 175-184.

Grzegorz BOCEWICZ
Department of Electronics and Computer Science
Koszalin University of Technology,
Sniadeckich 2, 75-453 Koszalin, Poland,
E-mail: bocewicz@ie.tu.koszalin.pl

Article citation info:
STOECK T, OSIPOWICZ T, ABRAMEK KF. Methodology for the repair of Denso Common Rail solenoid injectors. Eksploatacja i Niezawodnosc – Maintenance and Reliability 2014; 16 (2): 270–275.

Tomasz STOECK
Tomasz OSIPOWICZ
Karol Franciszek ABRAMEK

METHODOLOGY FOR THE REPAIR OF DENSO COMMON RAIL SOLENOID INJECTORS

METODYKA NAPRAWY WTRYSKIWACZY ELEKTROMAGNETYCZNYCH UKŁADÓW ZASILANIA COMMON RAIL DENSO*

This paper presents the problems of Denso Common Rail solenoid injector verification and repair. Due to conscious policy of the manufacturer who does not offer spare parts or special tooling, their servicing comes down most frequently to external cleaning, internal rinsing by the thermo-chemical method, and testing on test benches. Based on the analysis of failures and malfunctions being most frequently observed, own methodology for the repair process have been presented, specifying the successive stages of disassembly and final assembly. A possibility of effective fuel metering correction has been demonstrated, which is presented on the example of injectors in a 2.2 HDI engine of Citroën Jumper II delivery van.

Keywords: *compression-ignition engine, injectors, repair, adjustment.*

W artykule przedstawiono problematykę weryfikacji i naprawy wtryskiwaczy elektromagnetycznych Common Rail firmy Denso. Ze względu na świadomą politykę producenta, który nie oferuje części zamiennych i specjalistycznego oprzyrządowania, ich obsługa sprowadza się najczęściej do czyszczenia zewnętrznego, płukania wewnętrznego metodą termochemiczną oraz testowania na stołach probierczych. W oparciu o analizę najczęściej spotykanych uszkodzeń i niesprawności, zaprezentowano własną metodykę procesu naprawy, z wyszczególnieniem kolejnych etapów demontażu oraz montażu końcowego. Wskazano na możliwość efektywnej korekty dawkowania, którą pokazano na przykładzie wtryskiwaczy silnika 2,2 HDI pojazdu Citroën Jumper II.

Słowa kluczowe: *silnik o zapłonie samoczynnym, wtryskiwacze, naprawa, regulacja.*

1. Introduction

The Common Rail injectors are the most sensitive, i.e. damageable, elements of the fuel delivery system of modern car engines [7, 8, 10]. This is chiefly due to exceptionally difficult operation conditions which may include, among others, high pressure and temperature, ballistic phenomena, turbulent fluid flow, etc. Defects appear as a result of the normal wear of needle and nozzle assemblies and actuators, occurring usually after the time of longer operation or use of considerable intensity. There are also defects being induced by erosion and cavitation, in particular in the vicinity of nozzle holes and control valve seat [1, 5, 6, 9, 12, 13]. In some cases, however, hugely accelerated processes take place, leading to premature damages. Failure wear, being also called pathological wear, may occur due to the use of fuels with inappropriate physicochemical properties (viscosity, density, water and sulphur content) and those being contaminated, for example, with the filings from faulty high-pressure pump [2, 5, 6, 7, 9, 12]. The external damages, resulting from the improper assembly and disassembly of injectors being performed inconsistently with the recommendations of manufacturer or without specialist tools, e.g. slide tampers, hydraulic instruments, bench vices, repair kits, torque wrenches, etc., are a separate group.

2. Research objective

The Denso solenoid injectors are characterised by the design and the principle of operation being similar to the Bosch first-generation products which have been comprehensively discussed in the literature [2, 3, 8, 10]. Therefore, the verification of respective parts is similar, focusing in particular on evaluation of the wear of: needle, nozzle tip, guide plunger, control unit (valve, body, mounting). Figure 1 also presents the elements which are taken into account when injector adjustment is needed, i.e. pressure spindle (full load fuel charge) and calibration and needle washers (pilot fuel charge and idle run fuel charge, respectively).

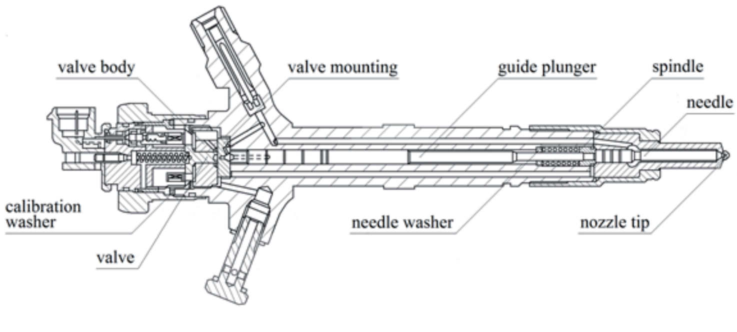

Fig. 1. A diagram showing Denso solenoid injector

The principal objective of this study was to provide a cognitive, factual evaluation of the repairability of Denso injectors, considering the given assumptions, i.e. lack of access to spare parts and necessity to determine guidelines for respective disassembly and assembly stages. These processes required an adapter to be prepared for unscrewing and screwing a nozzle nut which, due to wrench sizes, is not

(*) Tekst artykułu w polskiej wersji językowej dostępny w elektronicznym wydaniu kwartalnika na stronie ***www.ein.org.pl***

provided with the tooling being used when servicing injectors made by other manufactures. The second objective, of an utilitarian nature, was to make an attempt to determine a method for the correction of fuel charge, the value of which was not within acceptable limits during the tests being performed.

3. Test object and test bed

The test object were Denso solenoid injectors which had been removed from a 2.2 HDI (*High Pressure Direct Injection*) engine of Citroën Jumper II delivery van with the mileage of 148 thousand km. It is a four-cylinder, 16-valve compression-ignition engine with a maximum power of 88 kW, with Common Rail direct fuel injection system. The repair of injectors was conducted on laboratory stands at VASCO Co. Ltd in Mierzyn near Szczecin, co-operating with the Department of Automotive Engineering of the West Pomeranian University of Technology (ZUT) in Szczecin. The following tests were used in this process:

- test benches (Diesel Bench CRU 2 Zapp, Diesel Tech DS2 Zapp),
- FL150/70 microscope with a camera for recording digital images on a PC-class computer,
- MIC-40700 LCR meter,
- Flexbar IP54 digital micrometer,
- ultrasonic cleaners (Elma Elmasonic S 10 H, Carbon Tech Ultrasonic Bath S15/C2),
- GRS Tools POWER HONE diamond grinder,
- vices and injector disassembly and assembly kits,
- torque wrenches.

4. Test scope and methodology

Tests were conducted according to an own methodology adopted which included three successive implementation stages (Fig. 2).

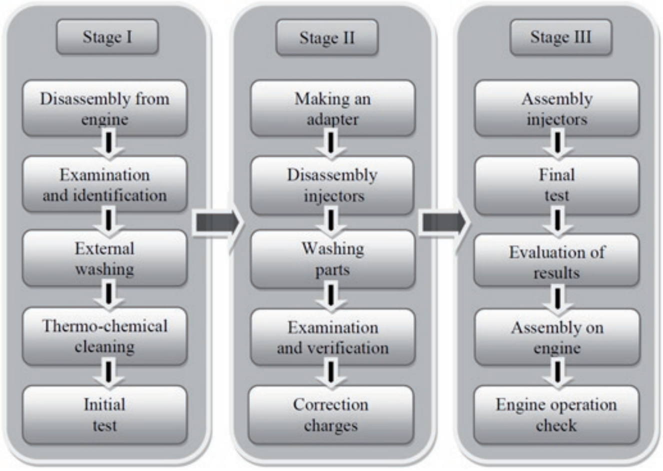

Fig. 2. Methodology for the repair of injectors being analysed

The steps included in respective stages match the standard Bosch procedures. The basic difference is the third step of repair introduced by the manufacturer, basing on the equipment and instrumentation dedicated solely for own products. A distinctive feature of the current technology in operation is earlier adjustment of injectors in order to obtain correct results on a test bench. The methodology being pre-

Table 1. Examples of the most frequent external damages of Denso injectors

Type of part	Type of defect	Possible causes
Main body	Cracking	Incorrect assembly on or disassembly from engine (too strong tightening of the mounting yoke, no lubricant, wrong tools selected)
	Deformation of shape	Incorrect assembly on or disassembly from engine; grinding of the surface is required to aid injector mounting
	Contamination, coking	Long-term operation of engine; fuelling with poor quality fuels or those with high level of vegetable component; combustion of lubricating oil due to scavenge phenomena
High pressure connector	Deformation of shape	Incorrect assembly on or disassembly from engine (tightening the injection pipe nut with too high torque, strong impact)
	Thread damage	
Control solenoid valve	Damages to plastic housing	Incorrect assembly on or disassembly from engine
	Damage to nut	Incorrect assembly or disassembly (tightening with too high torque, wrong tools selected)
	Damage to electrical connection	Incorrect assembly or disassembly of feeder cable plug
	Damage to overflow pipe and connector	Incorrect assembly or disassembly
Nozzle	Nozzle tip damage	Overheating; unauthorised cleaning
	Contamination, coking	Long-term operation of engine; fuelling with poor quality fuels or those with high level of vegetable component; combustion of lubricating oil due to scavenge phenomena
	Nozzle tip burning	Long-term and intensive operation of engine, fuelling with poor quality fuels
	Deformation of holes	Long-term operation of engine; fuelling with poor quality fuels; high combustion temperatures; erosion and cavitation processes

Table 2. Preset test parameters when measuring injector delivery rate

Type of fuel charge	Injection Pressure [MPa]	Injection time [μs]	Set value of injection fuel charge [mg/skok]	Set value of return fuel charge [mg/skok]
Full load	160	910	47,74 ± 6,93	32,90 ± 32,90
Emission (half-load)	80	720	18,28 ± 4,20	25,00 ± 25,00
Idle run	25	710	3,90 ± 1,84	15,00 ± 15,00
Pilot	80	320	1,84 ± 1,22	15,00 ± 15,00

sented is a classic approach based on the long-standing workshop and laboratory practice but being possible to use in a much broader scope. It assumes a correction of fuel charges only after the results of initial test stage have been obtained. Furthermore, successive stages may be modified as required, enabling the repair of solenoid injectors of different types and manufactures. In the case of the Denso products, it was necessary to make an adapter for nozzle nut.

4.1. Stage I

First of all, the injectors were prepared to initial test. After their removal from the engine, the injectors were evaluated by visual assessment and completeness check of components. Examples of external damages, detectable in this stage, are summarised in Table 1. Next, theirs were identified, reading the numbers on the main body and entering them into the memory of test benches in order to carry out the measuring stage.

The washing of injectors in ultrasonic cleaners was carried out so that control solenoid valves were not immersed in the cleaning fluid. This is because the plastic housing may soften and insulation may be damaged. Duration of this process did not exceed 30 min. Next, the injectors were dried and purged with compressed air.

The procedure of initial test was started checking the solenoid coil resistance and inductance and its fault to frame. This testing should be treated as a supplementary (additional) one because inspection of injectors on test benches includes within its scope basic electrical measurements. It should also be noted that defects of the element under discussion in Denso products have been occasionally encountered during several years of practice, which does not find confirmation in

Table 3. Examples of the most frequent internal damages of Denso injectors

Type of part	Type of defect	Possible causes
Control valve unit	Scratching or deformation of valve seat	Too large half-ball travel; poor fuel quality and fuel contamination; improper filtration; presence of solids (faulty pump); erosion and cavitation processes
	Scratching of valve spindle surface	Poor fuel quality (lubricating ability) and fuel contamination; improper filtration; presence of solids (faulty pump)
	Damages to the surface of valve body and mounting	Poor fuel quality and fuel contamination; improper filtration; presence of solids (faulty pump); erosion and cavitation processes
	Corrosion of the surface of valve body and mounting	Poor fuel quality (sulphur and water)
Guide plunger	Surface scratching or seizure	Poor fuel quality (lubricating ability) and fuel contamination; improper filtration; presence of solids (faulty pump)
	Surface corrosion	Poor fuel quality (sulphur and water)
Nozzle	Seat deformation	Poor fuel quality and fuel contamination; improper filtration; presence of solids (faulty pump)
	Worsening of the needle and nozzle assembly cooperation	Abrasive wear as a result of natural processes
	Surface scratching or seizure	Poor fuel quality (lubricating ability) and fuel contamination; improper filtration; presence of solids (faulty pump)
	Pressure face corroding	Poor fuel quality (sulphur and water)
	Contact zone overheating	Long-term and intensive operation of engine; too high temperature of operation
Needle	Worsening of the needle and nozzle assembly cooperation	Abrasive wear as a result of natural processes
	Damage to needle cone	Poor fuel quality (lubricating ability) and fuel contamination; improper filtration; presence of solids (faulty pump)
	Surface scratching or seizure	
	Surface corroding	Poor fuel quality (sulphur and water)
	Contact zone overheating	Long-term and intensive operation of engine; too high temperature of operation

the assessment being presented in the paper by Kuszewski and Ustrzycki [11].

In injector measurements made on testers, the following initial tests were carried out:

- electrical test „eRLC" (*Resistance, Inductance, Capacitance*), except the capacitance being checked for the products with piezoelectric elements,
- leakage test „LKT" (Static Leak Test),
- nozzle opening pressure test „NOP" (*Nozzle Opening Pressure*),
- volume test „iVM" (*Injector Volume Metering*) for respective fuel charges, the parameters of which are summarised in Table 2.

4.2. Stage II

To unscrew nozzle nuts, a special adapter was made, using a 30 mm hexagonal iron (Fig. 3). This was a necessary condition to carry out disassembly because adapters for injectors of other manufacturers have different dimensions.

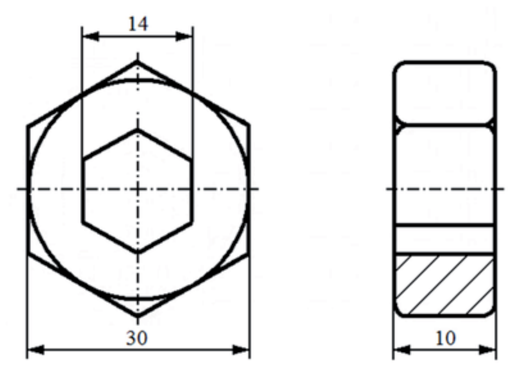

Fig. 3. An adapter enabling nozzle nut to be unscrewed

When unscrewing the nut, a torque of 150 Nm should not be exceeded because the sealing surface may be permanently damaged and the pins locating nozzle position against a fuel feed hole may be shorn. After this step, an access to the following elements was gained: needle, lower spring, needle washer, spindle ,and guide plunger. It should be noted that any resistance occurring when removing the latter from the main body is evidence of permanent seizure and impossibility to repair the injector.

Before disassembling the upper part, scribing markings were made, locating the original position of control solenoid valve against a high pressure connector. The unscrewing of nut enabled the following elements to be removed: valve shim and spring washer, upper spring, and half-ball valve. Access to the body and mounting, co-operating with the latter, required a special triple-bit wrench to be applied.

All parts, except solenoid valve, were rinsed in ultrasonic cleaners and then dried and purged with compressed air. Their evaluation and verification was done by the visual method (organoleptic assessment), as well as at high magnification of laboratory microscope. A summary of the most frequent internal defects, detectable in this stage, is presented in Table 3. Possible correction of fuel charges should take place after last stage, before assembling the injectors and carrying out the main tests.

4.3. Stage III

In the first instance, upper parts of the injectors were assembled, preserving the reverse order to disassembly. The tightening torque for the valve body should not exceed 75 Nm. The mounting of half-ball is important so that its flat surface is outside the seat. It must also be remembered that the original position of solenoid valve coil against a high pressure connector is to be preserved. Threads for solenoid valve and nozzle nuts should be lubricated with white mineral oil and their tightening should be done with torques amounting to 10–15 Nm and 45 Nm.

Inspection of the injectors on test benches was carried out in a similar way to that for the initial test. Owing to that, a comparison of the test results from before and after the repair was possible. Next, the injectors were assembled on the engine, the operation of which was assessed during a test drive.

5. Results and discussion

Evaluation of the injectors did not show any external defects or missing components. After the preparation stage, initial tests were performed, the results of which are summarised in Table 4 and Figures 4 and 5. Electrical measurements excluded a failure solenoid coils, while no fault to frame in them was found in the supplementary test (outside test bench) These findings were consistent with the guidelines being presented by other authors [8, 9]. In the leakage tests, no fuel leaks on injector tips were found, while fuel overflow delivery rates were minimal. Also the nozzle opening pressure was positively evaluated. Any failures in this respect would induce an immediate termination of the test stage, disqualifying a given injector from further tests.

Table 4. Results of the initial tests for the Denso injectors being analysed

Injector number	Electrical test „eRLC"		Leakage test „LKT" [MPa]	Nozzle opening pressure test „NOP" [MPa]
	Coil resistance [Ω]	Coil inductance [μH]		
1	0,54	181	81,80	16,00
2	0,72	184	82,70	18,50
3	0,55	179	90,30	15,50
4	0,72	179	86,80	16,00

The analysis of fuel delivery rate in the „iVM" test showed that idle run fuel charges for injector 2 and 4 were too small, amounting to 1.78 mg/stroke and 1.94 mg/stroke, respectively. The results pointed to the worsening of the needle and nozzle assembly co-operation, which became apparent only when setting low pressure on a tester. Malfunction of this type is one of the most frequently detectable defects, being also encountered in the products of other manufacturers, but it is usually observed in the injectors of engines with a relatively low operational mileage. In such cases, a change in the initial stress of lower spring is required, which reduces the lift of needle at low pressure and in consequence the charge of injected fuel. The correction of fuel charge is conducted by reducing needle washer thickness.

The process of disassembly was carried out for all products being analysed, mainly to wash and carefully verify their components. It can, however, be simplified in the situation when only idle run fuel charge adjustment is assumed, which requires the nozzle itself to be unscrewed and taken to pieces. Due to the fact that needle washer replacement is not possible, its butting face was ground off on a GRS Tools POWER HONE grinder. An assumption was made, like in the case of Bosch injectors, that thickness reduction by 0.1 mm would allow obtaining an increase in fuel delivery rate by about 1,5 mg/stroke. The size of fuel charges in the products being positively evaluated was also taken into account i order to obtain relatively similar injection parameters. Therefore, the thickness of needle washers in injectors 2 and 4 was reduced from 1.33 mm to 1.27 mm. Before assembling, evaluation of all parts was made in a microscopic examination, focusing in particular on the needle and nozzle assembly and actuators. No internal damages were detected.

The findings of main tests show that adjustment of the injectors being repaired produced advantageous results (Figs 6 and 7). An increase in idle run fuel charges by a predicted value of 0.75 and

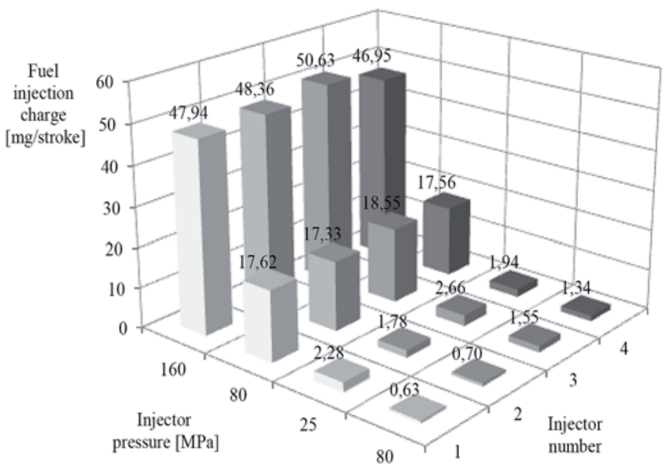

Fig. 4. Results for injected fuel delivery rate according to injection pressure obtained from the initial test for the injectors being analysed

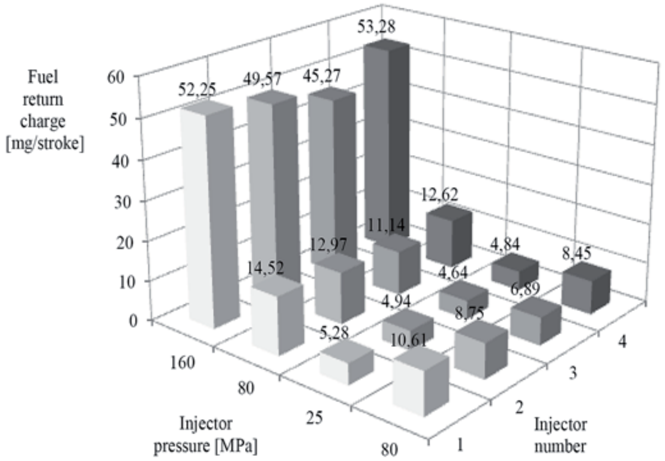

Fig. 5. Results for fuel return charge according to injection pressure obtained from the initial test for the injectors being analysed

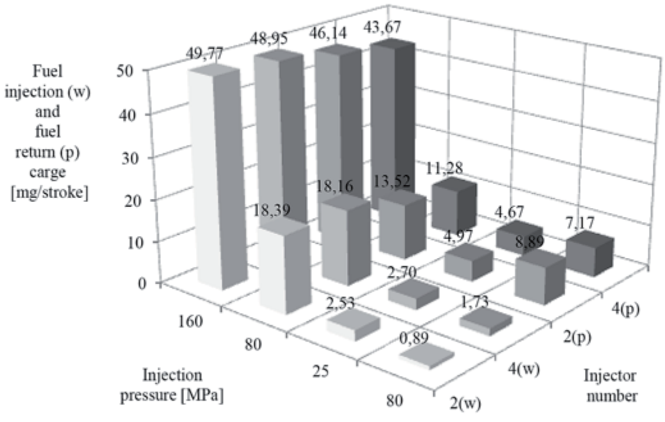

Fig. 6. Results for fuel injection and fuel return charge according to injection pressure obtained from the initial test for the analysed injectors after repair

0.76 mg/stroke. This means an improvement in the co-operation of needle and nozzle assembles because needles in both products stopped to be blocked when setting low pressure. As a result, more fuel will go to given cylinders of the drive unit, while the rotational speed will not be lowered.

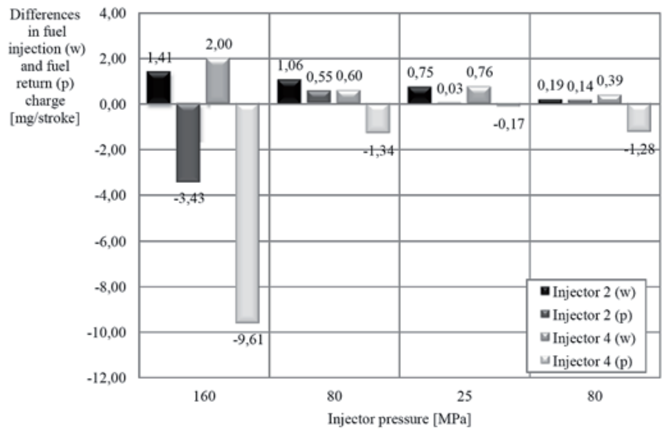

Fig. 7. Differences in fuel injection and fuel return charge according to injection pressure in the injectors being repaired

An intermediate effect on other fuel delivery rates was observed, in particular reduction of the fuel amount on most overflows. In injector 2, this effect occurred only with the full load, while for other fuel charges (emission, idle run and pilot fuel charges) the increase was negligibly small. In this respect, the repair process should be also positively assessed because excessive amount of fuel on the return might manifest in difficulties in starting the engine, its spontaneous stoppage, and observable loss of power at different load ranges. In the products being analysed, these problems should not be found. The test results being obtained on test benches and the verification of parts, in which other causes were excluded, e.g. damages to valve unit, loss of internal leak-tightness, nozzle hole plugging, is evidence of this.

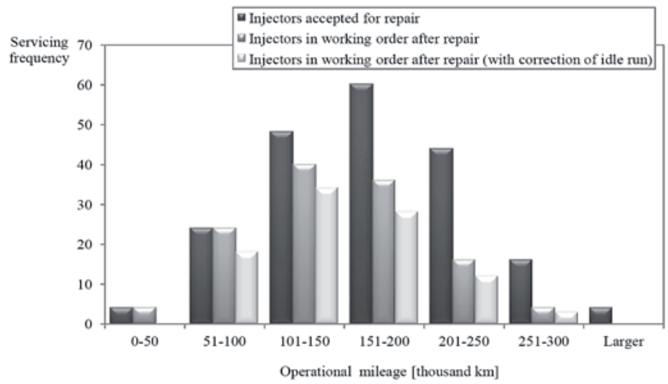

Fig. 8. Histogram of Denso solenoid injector repairs

Figure 8 presents the histogram of Denso solenoid injector repairs in VASCO Co. Ltd which were performed in the time period of October 2012 – February 2013. The data referring to the products being acknowledged operational represent the unimodal distribution, being characterised by a moderate right-side asymmetry. The obtained results indicate a high efficiency of this process with mileage to 200 thousand km but in most cases a correction of idle run fuel charge was necessary. Considerably less observations are grouped within the ranges being found at the end of the series. This is because the repairs become groundless with no spare parts, while the cleaning itself and adjustment brought selective benefits only. As a consequence, it was decided to limit acceptance of the injectors from motor-car engines with high operational mileage for repair.

6. Conclusions

The results of own study show that the repair of Denso Common Rail injectors may be conducted but its efficient depends on many factors. A crucial issue is the initial condition, and more specifically the type of malfunction being found, which - with lack of spare parts - may exclude a given product. This refers in particular to the needle and nozzle assembly and actuators, including control valve unit and guide plunger. The workshop practice shows that application of the substitute parts being found on the market is not is not indicated because, in respect of their quality, they decidedly fall behind the original elements, leading to accelerated (pathological) wear. A relatively numerous group is also external damages, developing frequently when disassembling or assembling the injectors which is performed without the tooling required or not observing the servicing procedures.

The proposed procedure methodology specifies the scope of activities to which attention should be paid during the repair process. Also, an adapter of own design has been presented, the making of which allowed disassembling the nozzle unit. The obtained results have broaden the scope of Denso solenoid injector servicing, which is usually reduced to external washing, internal cleaning and testing on test benches. However, it is noteworthy that, out of consideration for the aforesaid limitations, correction of respective fuel charges is possible for motor-car engines with a relatively low mileage, so for those with no serious internal damages.

References

1. Asi O. Failure of a diesel engine injector nozzle by cavitation damage. Engineering Failure Analysis 2006; 13: 1126-1133.
2. Bosch Robert GmbH. Diesel-Engine Management. Plochingen: Automotive Aftermarket Division; 2004.
3. Bosch Robert GmbH. Zasobnikowe układy wtryskowe Common Rail. Warszawa: WKiŁ; 2009.
4. Cisek J, Mruk A, Szczypiński-Sala W. Wpływ biopaliw (FAME) na właściwości eksploatacyjne rozpylaczy paliwa silnika z zapłonem samoczynnym. Mechanika. Czasopismo Techniczne - Technical Transactions 2012; 8: 233-244.
5. Dernotte J, Hespel C, Foucher F, Houille S, Mounad'm-Rousselle C. Influence of physical fuel properties on the injection rate in a Diesel injector. Fuel 2012; 96: 153-160
6. Galle J, Verhelst S, Sierens R, Goyos L, Castaneda R, Verhaege M, Vervaeke L, Bastiaen M. Failure of fuel injectors in a medium speed diesel engine operating on bio-oil. Biomass and Bio-energy 2012; 40: 27-35.
7. Gładysek J, Gładysek M. Ocena stanu wtryskiwaczy common rail. Auto Moto Service 2009; 9: 22-24.
8. Günther H. Układy wtryskowe Common Rail w praktyce warsztatowej: budowa, sprawdzanie, diagnostyka. Warszawa: WKiŁ; 2010.
9. Idzior M, Borowczyk T, Karpiuk W, Stobnicki P. Możliwości badania stanu technicznego nowoczesnych wtryskiwaczy silników o zapłonie samoczynnym. Logistyka 2011; 3: 933-942.
10. Knefel T. Ocena techniczna wtryskiwaczy Common Rail na podstawie doświadczalnych badań przelewów. Eksploatacja i Niezawodnosc - Maintenance and Reliability 2012; 1: 42-53.
11. Kuszewski H, Ustrzycki A. Metodyka diagnozowania wtryskiwaczy układu Common Rail z wykorzystaniem stołu probierczego EPS 815. X Słupskie Forum Motoryzacji. Innowacje w motoryzacji a ochrona środowiska. Starostwo Powiatowe w Słupsku; 2007: 243-252.
12. Olszowski S. Badanie przyczyn przybywania oleju w silnikach nowej generacji o zapłonie samoczynnym. Transcomp - XIV international conference. Computer systems aide science, industry and transport 2010; 6: 2581- 2588.
13. Salvador FJ, Romero JV, Rosello MD, Martinez-Lopez J. Validation of a code for modeling cavitation phenomena in Diesel injector nozzles. Mathematical and Computer Modelling 2010; 52: 1123-1132.

Tomasz STOECK
Tomasz OSIPOWICZ
Karol Franciszek ABRAMEK
West Pomeranian University of Technology
The Department of Automotive Engineering
Piastów 19 St., 70-310 Szczecin, Poland
E-mails: tstoeck@wp.pl, tosipowicz@zut.edu.pl, kabramek@zut.edu.pl

Article citation info:
LIN J, ASPLUND M. Comparison Study of Heavy Haul Locomotive Wheels' Running Surfaces Wearing. Eksploatacja i Niezawodnosc – Maintenance and Reliability 2014; 16 (2): 276–287.

Jing LIN
Matthias ASPLUND

COMPARISON STUDY OF HEAVY HAUL LOCOMOTIVE WHEELS' RUNNING SURFACES WEARING

BADANIA PORÓWNAWCZE ZUŻYCIA POWIERZCHNI BIEŻNYCH KÓŁ LOKOMOTYW DUŻEJ MOCY

The service life of railway wheels can differ significantly depending on their installed position, operating conditions, re-profiling characteristics, etc. This paper compares the wheels on two selected locomotives on the Iron Ore Line in northern Sweden to explore some of these differences. It proposes integrating reliability assessment data with both degradation data and re-profiling performance data. The following conclusions are drawn. First, by considering an exponential degradation path and given operation condition, the Weibull frailty model can be used to undertake reliability studies; second, among re-profiling work orders, rolling contact fatigue (RCF) is the principal reason; and third, by analysing re-profiling parameters, both the wear rate and the re-profiling loss can be monitored and investigated, a finding which could be applied in optimisation of maintenance activities.

Keywords*: reliability analysis; locomotive wheels; frailty; re-profiling; wear; Markov Chain Monte Carlo.*

Resurs kół pociągu może być znacząco różny w zależności od ich miejsca zamontowania, warunków pracy, charakterystyk związanych z reprofilacją, itp. W artykule, porównano koła dwóch wybranych lokomotyw kursujących na Linii Rud Żelaza w północnej Szwecji, aby zbadać niektóre ze wspomnianych różnic. Zaproponowano możliwość łączenia danych pochodzących z oceny niezawodności z danymi degradacyjnymi oraz danymi z reprofilacji. Przeprowadzone badania pozwalają wyciągnąć następujące wnioski. Po pierwsze, krzywa wykładnicza degradacji oraz zadane warunki pracy można wykorzystać w celu przeprowadzenia badań niezawodności z użyciem modelu Weibulla z efektami losowymi (tzw. "frailty model"); po drugie, główną przyczyną zlecania reprofilacji kół jest zmęczenie toczne (RCF); po trzecie, analiza parametrów reprofilacji pozwala na monitorowanie i badanie zarówno szybkości zużycia kół, jak i ubytku materiału podczas reprofilacji, co może mieć zastosowanie w optymalizacji czynności obsługowych.

Słowa kluczowe*:analiza niezawodności; koła lokomotywy; efekty losowe; reprofilacja; zużycie; markowowska metoda Monte Carlo.*

1. Introduction

The service life of different railway wheels can vary greatly. Take a Swedish railway company, for example. For the wheels of its 26 locomotives, statistics show that from 2010 to 2011, the longest mean time between re-profiling was around 59 000 kilometres and the shortest was about 31 000 kilometres. The large difference can be attributed to the non-heterogeneous nature of the wheels; each differs according to its installed position, operating conditions, re-profiling characteristics, etc. [6, 7, 14, 17, 23].

One common preventive maintenance strategy (used in our study) is re-profiling wheels after they run a certain distance. Re-profiling reduces the wheel's diameter; once the diameter is reduced to a pre-specified length, the wheel is replaced by a new one. Seeking to optimise this maintenance strategy, researchers have examined wheel degradation data to determine wheel reliability and failure distribution [6, 7, 23]. However, most studies cannot solve the combined problem of small data samples and incomplete datasets while simultaneously considering the influence of several covariates [14].

In addition, most reliability studies are implemented under the assumption that individual lifetimes are independent and identically distributed (i.i.d). In reality, sometimes Cox proportional hazard (CPH) models cannot be used because of the dependence of data within a group. For instance, because they have the same operating conditions, the wheels mounted on a particular bogie may be dependent. Modelling dependence in multivariate survival data has received considerable attention, especially in cases where the datasets comprise inter-related subjects of the same group [1, 20]. A key development in modelling such data is to consider frailty models, in which the data are conditionally independent. When frailties are considered, the dependence within subgroups can be considered an unknown and unobservable risk factor (or explanatory variable) of the hazard function. In this paper, we consider a gamma shared frailty, first discussed by Clayton [4] and Oakes [16] and later developed by Sahu et al. [20], to explore the unobserved covariates' influence on the wheels on the same bogie. We also adopt the Weibull hazard model to determine the distribution of the wheels' lifetime; the validity of this model has been established by Lin et al. [14].

Besides the degradation analysis, re-profiling information is a key source of data to evaluate the wheels' performance. As Fröhling and Hettasch [8] note, the "loss of material during re-profiling because of hollow or flange wear" is a significant element in the integrated data processing of the wheel-rail interface management. Even so, related studies remain limited.

To fill this gap in the literature, this paper compares the wheels on two selected locomotives on the Iron Ore Line in northern Sweden, taking an integrated data approach to reliability assessment by considering both degradation data and re-profiling data.

The remainder of the paper is organised as follows. Section 2 describes the background of the comparison study, by introducing the Iron Ore Line, as well as the degradation data and re-profiling parameters for the locomotive wheels being studied, along with their operating conditions. Section 3 presents the degradation analysis using a Weibull frailty model; the analysis considers the wheels' location in the bogies and their operating conditions as covariates and uses Markov Chain Monte Carlo (MCMC) methods. Sections 4 to 6 comprise the comparison study; the three sections compare the re-profiling work orders, the specified re-profiling parameters (the wheel diameters, the flange thickness, the radial run-out, and the lateral run-out), and the wear rate of the wheels, respectively. Each section is accompanied by a discussion. Section 7 offers conclusions and makes suggestions for future study.

2. Study Background

This section gives background information on the Iron Ore Line. It also introduces the degradation data and the re-profiling parameters for the locomotive wheels being studied, along with their operating conditions.

Fig. 1. Geographical location of Iron Ore Line (Malmbanan)

2.1. Iron Ore Line (Malmbanan)

The Iron Ore Line (Malmbanan) is the only existing heavy haul line in Europe; it stretches 473 kilometres and has been in operation since 1903. As Fig. 1 shows, it is mainly used to transport iron ore and pellets from the mines in Kiruna (also Malmberget, close to Kiruna, in Sweden) to Narvik Harbour (Norway) in the northwest and Luleå Harbour (Sweden) in the southeast. The track section on the Swedish side is owned by the Swedish government and managed by Trafikverket (Swedish Transport Administration), while the iron ore freight trains are owned and managed by the freight operator (a Swedish company). Each freight train consists of two IORE metric tonnes with axle loads of 30 tonnes. The trains operate in harsh conditions, including snow in the winter and extreme temperatures ranging from - 40 °C to + 25 °C. Because carrying iron ore results in high axle loads and there is a high demand for a constant flow of ore/pellets, the track and wagons must be monitored and maintained on a regular basis. The condition of the locomotive wheel profile is one of the most important aspects to consider.

2.2. Degradation data and re-profiling parameters

We use the degradation data from two selected heavy haul cargo locomotives (denoted as locomotive 1 and locomotive 2), collected from October 2010 to January 2012. The selection criteria are discussed in Section 2.3. Each locomotive is studied separately, and $n = 2$. For each locomotive, see Fig.2, there are two bogies (incl., Bogie I, Bogie II); and each bogie contains six wheels. The installed position of a wheel on a particular locomotive is specified by the bogie number (I, II-number of bogies on the locomotive), a wheel-set number (1, 2, 3-number of wheel-sets for each bogie, shown as "Axel" in Fig.2) and

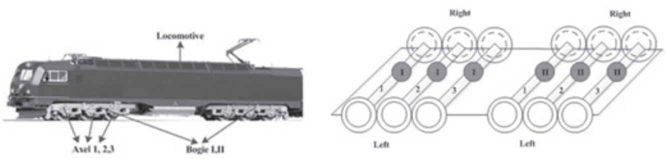

Fig. 2. Wheel positions specified in this study

the position of the wheel-set (right or left) where each wheel is mounted. For instance, the abbreviation I1H represents the wheel installed in the first bogie, the first wheel-set and the right side.

The diameter of a new locomotive wheel in this study is about 1250 mm. Following the current maintenance strategy, a wheel's diameter is measured after it runs a certain distance. If it is reduced to 1150 mm, the wheel set is replaced by a new one. Otherwise, it is re-profiled (see Fig.3). Therefore, a threshold level for failure, denoted as y_0 , is defined as 100 mm (y_0 = 1250 mm – 1150 mm). The wheel's failure condition is assumed to be reached if the diameter reaches y_0 . The dataset includes the diameters of all locomotive wheels at a given inspection time, the total running distances corresponding to their "mean time between re-profiling", and the wheels' bill of material (BOM) data, from which we can determine their positions.

The type of measurement tool is SIEMENS SINUMERIK (see

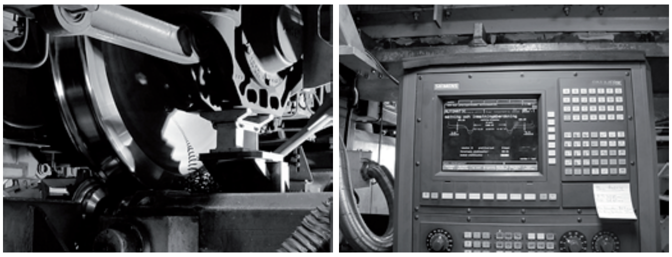

Fig. 3. One locomotive wheel under re-profiling and the measurement tool

Fig.3). During the re-profiling process, the re-profiling parameters include but are not limited to: 1) the diameters of the wheels; 2) the flange thickness; 3) the radial run-out; 4) the lateral run-out.

2.3. Comparison of the operating conditions

In this study, both locomotive 1 and locomotive 2 are operating on the Iron Ore Line (Malmbanan). In Fig.4, the horizontal axle represents the different working intervals; "Nrv-Kmb" represents the route from Narvik to Kiruna, while "Kmb-Nrv" represents the route from Kiruna to Narvik. Those intervals make up the whole Iron Ore Line (Malmbanan). The longitudinal axle of Fig. 4 (a) represents the proportion (%) of operating in each working interval (%); the longitudinal axle of Fig. 4 (b) represents the running distances (kilometers) in those intervals. For instance, the first blue bars (around 35% in (a) and about 40000 kilometres in (b)) represent that, locomotive 1 has been operated around 40000 kilometres in the interval between "Nrv" and "Kmb". And these 40000 kilometres are almost 35% of locomotive 1's total running distances.

As seen in Fig.4, during the period in question (from October 2010 to January 2012), the total running distance for locomotive 1 is 101035 kilometres and for locomotive 2, 81302 kilometres. About 70% of the locomotives' workload is between Narvik and Kiruna. There is no substantial difference between the running routes, but it seems that locomotive 1 works harder than locomotive 2, because the former runs 24% farther. As there is not a big difference between the topographies, we assume that the only difference in operating conditions is the total running distance.

3. Degradation analyses with the Weibull frailty model

In this section, we propose the Weibull frailty model for analysing the wheels' degradation data, using a MCMC computation scheme.

Before continuing, it should be pointed that Lin et al. [5] have used the Bayesian Exponential Regression Model, Bayesian Weibull Regression Model (easily transferred to an Extreme-Value Regression Model) and Bayesian Lognormal Regression Model, separately, to analyze the lifetime of locomotive wheels using degradation data and taking into account the position of the wheel. Their results show

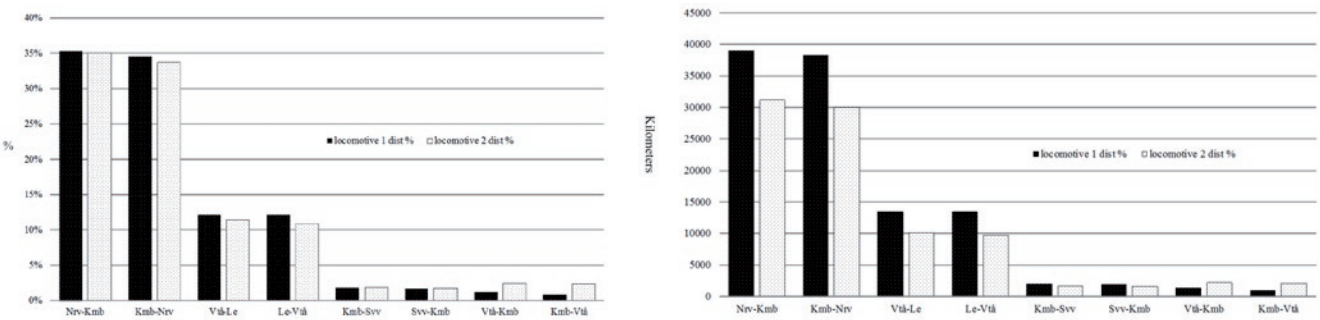

Fig. 4. Comparison of the operating conditions for locomotive 1 and locomotive 2

that "the performance of the Weibull Regression Model is close to the Log-normal Regression Model, which could also be a suitable choice under specified situations." As the Weibull Regression Model is more acceptable to engineers and the differences between the Weibull Regression and Lognormal Regression Models are quite small, we choose the former model in this comparative study.

3.1. Weibull frailty model

Most reliability studies are implemented under the assumption that individual lifetimes are independent and identically distributed (i.i.d). In reality, at times, Cox proportional hazard (CPH) models cannot be used because of the dependence of data within a group. For instance, because they have the same operating conditions, the wheels mounted on a particular bogie may be dependent. Modelling dependence in multivariate survival data has received considerable attention, especially in cases where the datasets comprise inter-related subjects of the same group [1, 20]. A key development in modelling such data is to consider frailty models, in which the data are conditionally independent.

Frailty models were first considered by Clayton [4] and Oakes [16] to handle multivariate survival data. In their models, the event times are conditionally independent according to a given frailty factor, which is an individual random effect. As discussed by Sahu et al.[20], the models formulate different variabilities and come from two distinct sources. The first source is natural variability, which is explained by the hazard function; the second is variability common to individuals of the same group or variability common to several events of an individual, which is explained by the frailty factor.

Assume the hazard function for the j^{th} individual in the i^{th} group is:

$$h_{ij}(t) = h_0(t)\exp(\mu_i + \mathbf{x}'_{\mathbf{ij}}\beta) . \tag{1}$$

In equation (1), μ_i represents the frailty parameter for the i^{th} group. If $\omega_i = \exp(\mu_i)$, the equation can also be written as:

$$h_{ij}(t) = h_0(t)\omega_i \exp(\mathbf{x}'_{\mathbf{ij}}\beta) . \tag{2}$$

Equation (1) is an additive frailty model, and equation (2) is a multiplicative frailty model. In both equations, μ_i and ω_i are shared by the individuals in the same group, and they are thus referred to as shared-frailty models and actually are extensions of the CPH model.

To this point, discussions of frailty models have focused on the forms of 1) the baseline hazard function and 2) the frailty's distribution. Representative studies related to the former include the gamma process for the accumulated hazard function [3, 21], Weibull baseline hazard rate [20], and the piecewise constant hazard rate [1] which is adopted in this paper due to its flexibility. Some researchers have examined finite mean frailty distributions, including gamma distribution [2, 4], lognormal distribution [15], and the like; others have studied non-parameter methods, including the inverse Gaussion frailty distribution [11], the power variance function for frailty [5], the positive stable frailty distribution [10, 19], the Dirichlet process frailty model [19] and the Levy process frailty model [9]. In this paper, we consider the gamma shared frailty model, the most popular model for frailty.

From equation (2), suppose the frailty parameters ω_i are independent and identically distributed (i.i.d) for each group and follow a gamma distribution, denoted by $Ga(\kappa^{-1},\kappa^{-1})$. Therefore, the probability density function can be written as:

$$f(\omega_i) = \frac{(\kappa^{-1})^{\kappa^{-1}}}{\Gamma(\kappa^{-1})} \cdot \omega_i^{\kappa^{-1}-1} \exp(-\kappa^{-1}\omega_i) . \tag{3}$$

In equation (3), the mean value of ω_i is 1, where κ is the unknown variance of ω_i s. Greater values of κ signify a closer positive relationship between the subjects of the same group as well as greater heterogeneity among groups. Furthermore, as ω_i >1, the failures for the individuals in the corresponding group will appear earlier than if ω_i =1; in other words, as ω_i <1, the predicted lifetimes will be greater than those found in the independent models.

Suppose $\boldsymbol{\omega} = (\omega_1, \omega_2, \cdots, \omega_n)'$; then:

$$\pi(\boldsymbol{\omega}|\kappa) \propto \prod_{i=1}^{n} \omega_i^{\kappa^{-1}-1} \exp(-\kappa^{-1}\omega_i) . \tag{4}$$

Denote the j^{th} individual in the i^{th} group as having lifetime $\mathbf{t_{ij}} = (t_{11}, t_{12}, \cdots, t_{nm_1})'$, where $i = 1,\cdots,n$ and $j = 1,\cdots,m_i$. Suppose the j^{th} individual in the i^{th} group has a 2-parameter Weibull distribution $W(\alpha,\gamma)$, where $\alpha > 0$ and $\gamma > 0$. Then, the p.d.f. is $f(t_{ij}|\alpha,\gamma) = \alpha\gamma t_{ij}^{\alpha-1}\exp(-\gamma t_{ij}^{\alpha})$, and the c.d.f. $F(t_{ij}|\alpha,\gamma)$ and the reliability function $R(t_{ij}|\alpha,\gamma)$ are $F(t_{ij}|\alpha,\gamma) = 1-\exp(\gamma t_{ij}^{\alpha}) = 1 - R(t_{ij}|\alpha,\gamma)$. Meanwhile, the hazard rate function can be written as:

$$h_0(t_{ij}|\alpha,\gamma) = \gamma\alpha t_{ij}^{\alpha-1} . \tag{5}$$

Based on the above discussions (equation (2), (3), and (5)), the Weibull frailty model with gamma shared frailties can be written as

$$h(t_{ij}\left|\mathbf{x_{ij}},\omega_i\right.) = \gamma\,\alpha\,\omega_i t_{ij}^{\alpha-1}\exp(\mathbf{x_{ij}^{'}}\boldsymbol{\beta})\,. \tag{6}$$

In equation (6), $\omega_i \sim Ga(\kappa^{-1},\kappa^{-1})$.

In reliability analyses, the lifetime data are usually incomplete, and only a portion of the individual lifetimes are known. Right-censored data are often called Type I censoring, and the corresponding likelihood construction problem has been extensively studied in the literature [12, 13]. Suppose the j^{th} individual in the i^{th} group has lifetime T_{ij} and censoring time L_{ij}. The observed lifetime $t_{ij} = \min(T_{ij}, L_{ij})$; therefore, the exact lifetime T_{ij} will be observed only if $T_{ij} \le L_{ij}$. In addition, the lifetime data involving right censoring can be represented by n pairs of random variables (t_{ij},υ_{ij}), where $\upsilon_{ij} = 1$ if $T_{ij} \le L_{ij}$ and $\upsilon_{ij} = 1$ if $T_{ij} > L_{ij}$. This means that υ_{ij} indicates whether lifetime T_{ij} is censored or not. The likelihood function is deduced as:

$$L(t) = \prod_{i=1}^{n}\prod_{j=1}^{m_i}[f(t_{ij})]^{\upsilon_{ij}} R(t_{ij})^{1-\upsilon_{ij}}\,. \tag{7}$$

If we denote $\lambda_{ij} = \exp(\mathbf{x_{ij}^{'}}\boldsymbol{\beta} + \log\gamma + \log\omega_i)$, equation (6) becomes $h(t_{ij}\left|\lambda_{ij},\alpha\right.) = \lambda_{ij}\alpha t_{ij}^{\alpha-1}$, the Weibull regression model with a gamma frailty $W(\alpha,\lambda_{ij})$.

If we denote the model's dataset as $D = (n,\omega,\mathbf{t},\mathbf{X},\upsilon)$, following equation (7), the complete likelihood function $L(\boldsymbol{\beta},\gamma,\alpha\left|D\right.)$ for the individuals in the i^{th} group can be written as:

$$L(\boldsymbol{\beta},\gamma,\alpha\left|D\right.) \propto (\gamma\alpha t_{ij}^{\alpha-1}\omega_i\exp(\mathbf{x_{ij}^{'}}\boldsymbol{\beta}))^{\sum_{i=1}^{n}\sum_{j=1}^{m_i}\upsilon_{ij}}\exp(-\sum_{i=1}^{n}\sum_{j=1}^{m_i}\gamma t_{ij}^{\alpha}\exp(\mathbf{x_{ij}^{'}}\boldsymbol{\beta})\omega_i)\,. \tag{8}$$

Let $\pi(\cdot)$ denote the prior or posterior distributions for the parameters. Then, the joint posterior distribution $\pi(\omega_i\left|\boldsymbol{\beta},\alpha,\gamma,D\right.)$ for gamma frailties ω_i can be written as:

$$\begin{aligned}
\pi(\omega_i\left|\boldsymbol{\beta},\alpha,\gamma,D\right.) &\propto L(\boldsymbol{\beta},\gamma,\alpha\left|D\right.)\times\pi(\boldsymbol{\omega}\left|\kappa\right.)\\
&\propto (\gamma\alpha t_{ij}^{\alpha-1}\omega_i\exp(\mathbf{x_{ij}^{'}}\boldsymbol{\beta}))^{\sum_{i=1}^{n}\sum_{j=1}^{m_i}\upsilon_{ij}}\exp(-\sum_{i=1}^{n}\sum_{j=1}^{m_i}\gamma t_{ij}^{\alpha}\exp(\mathbf{x_{ij}^{'}}\boldsymbol{\beta})\omega_i)\times\prod_{i=1}^{n}\omega_i^{\kappa^{-1}-1}\exp(-\kappa^{-1}\omega_i)\\
&\propto \omega_i^{\kappa^{-1}+\sum_{j=1}^{m_i}\upsilon_{ij}-1}\exp\{-(\kappa^{-1}+\gamma\sum_{j=1}^{m_i}t_{ij}^{\alpha}\exp(\mathbf{x_{ij}^{'}}\boldsymbol{\beta}))\omega_i\}\\
&\sim Ga\{\kappa^{-1}+\sum_{j=1}^{m_i}\upsilon_{ij},\kappa^{-1}+\gamma\sum_{j=1}^{m_i}t_{ij}^{\alpha}\exp(\mathbf{x_{ij}^{'}}\boldsymbol{\beta})\}
\end{aligned} \tag{9}$$

Equation (9) shows that the full conditional density of each ω_i is a gamma distribution. Suppose γ has a gamma prior distribution, denoted by $\gamma \sim Ga(\rho_1,\rho_2)$. The full conditional density of γ is:

$$\begin{aligned}
\pi(\gamma\left|\boldsymbol{\beta},\alpha,\omega,D\right.) &\propto L(\boldsymbol{\beta},\gamma,\alpha\left|D\right.)\times\pi(\gamma\left|\rho_1,\rho_2\right.)\\
&\propto (\gamma\alpha t_{ij}^{\alpha-1}\omega_i\exp(\mathbf{x_{ij}^{'}}\boldsymbol{\beta}))^{\sum_{i=1}^{n}\sum_{j=1}^{m_i}\upsilon_{ij}}\exp(-\sum_{i=1}^{n}\sum_{j=1}^{m_i}\gamma t_{ij}^{\alpha}\exp(\mathbf{x_{ij}^{'}}\boldsymbol{\beta})\omega_i)\times\prod_{i=1}^{n}\gamma^{\rho_1-1}\exp(-\rho_2\gamma)\\
&\propto \gamma^{\rho_1+\sum_{i=1}^{n}\sum_{j=1}^{m_i}\upsilon_{ij}-1}\exp\{-(\rho_2+\sum_{i=1}^{n}\sum_{m=1}^{n_i}t_{ij}^{\alpha}\exp(\mathbf{x_{ij}^{'}}\boldsymbol{\beta})\omega_i)\gamma\}\\
&\sim Ga\{\rho_1+\sum_{i=1}^{n}\sum_{j=1}^{m_i}\upsilon_{ij},\rho_2+\sum_{i=1}^{n}\sum_{m=1}^{n_i}t_{ij}^{\alpha}\exp(\mathbf{x_{ij}^{'}}\boldsymbol{\beta})\omega_i\}
\end{aligned} \tag{10}$$

Equation (10) also shows that the full conditional density of γ is a gamma distribution. The full conditional density of $\boldsymbol{\beta}$ and α can be given by:

$$\pi(\boldsymbol{\beta}\left|\eta,\omega,\gamma,D\right.) \propto \exp\{\boldsymbol{\beta}^{'}\sum_{i=1}^{n}\sum_{j=1}^{m_i}\upsilon_{ij}x_{ij} - \gamma\sum_{i=1}^{n}\sum_{m=1}^{n_i}t_{ij}^{\alpha}\exp(\mathbf{x_{ij}^{'}}\boldsymbol{\beta})\omega_i\}\times\pi(\boldsymbol{\beta}) \tag{11}$$

$$\pi(\alpha\left|\boldsymbol{\beta},\gamma,\omega,D\right.) \propto (\prod_{i=1}^{n}\prod_{j=1}^{m_i}t_{ij}^{\upsilon_{ij}})^{\alpha-1}\alpha^{\sum_{i=1}^{n}\sum_{j=1}^{m_i}\upsilon_{ij}}\exp\{-\gamma\sum_{i=1}^{n}\sum_{m=1}^{n_i}t_{ij}^{\alpha}\exp(\mathbf{x_{ij}^{'}}\boldsymbol{\beta})\omega_i\}\times\pi(\alpha)\,. \tag{12}$$

3.2. Comparison study of degradation analyses

3.2.1. Degradation path and lifetime data

From the dataset, we obtain 5 to 6 measurements of the diameter of each wheel during its lifetime (in the period October 2010 to January 2012). By connecting these measurements, we can determine a degradation trend. In their analyses of train wheels, most studies (e.g., [6], [7], [14]) assume a linear degradation path. In this study, the corresponding running distance (kilometres) is recognized as the lifetime. The degradation data of the wheels are tested with ReliaSoft Weibull++. The statistics of Ranks and MSE under different assumption of degradation path are compared, including Linear degradation path, Exponential degradation path, Power degradation path, Logarithmic degradation path, Gompertz degradation path, and Lloyd-Lipow degradation path. The results show that, an exponential degradation path is a better choice for the studied locomotive wheels. Meanwhile, the second choice is Linear degradation, and the third one is Power degradation. In Table 1, we list the lifetimes as their degradation reach to the threshold level (equal to 100mm).

Table.1. Statistics on degradation path and lifetime data

Locomotive	Bogie	Lifetime**	Locomotive 2	Bogie	Lifetime**
1	I	*159.00	2	I	205.47
1	I	*162.04	2	I	205.49
1	I	*159.04	2	I	207.51
1	I	*159.32	2	I	207.82
1	I	152.22	2	I	211.24
1	I	151.13	2	I	211.22
1	II	163.84	2	II	203.45
1	II	163.87	2	II	203.32
1	II	157.84	2	II	203.44
1	II	157.75	2	II	204.08
1	II	159.05	2	II	203.17
1	II	159.53	2	II	203.17

** Right-censored data; ** $\times 10^3$ kilometres*

Note: some lifetime data are right-censored (denoted by the asterisk in Table.1 However, we know the real lifetimes will exceed the predicted lifetimes.

Following the above discussion, a wheel's failure condition is assumed to be reached if the diameter reaches y_0. We adopt the linear path for all wheels and set $y_0 = y$. The lifetimes for these wheels are now easily determined and are shown in the "Lifetime" columns of Table 1. These lifetimes are the input of the Weibull frailty model, as discussed in Section 3.

3.2.2. Parameter Configuration

Following the discussion in 3.2.1, vague prior distributions are adopted in this paper as:

- Gamma frailty prior: $\omega_i \sim Ga\,(0.1, 0.1)$;
- Normal prior distribution: $\beta_0 \sim N\,(0.0, 0.001)$;
- Normal prior distribution: $\beta_1 \sim N\,(0.0, 0.001)$;
- Gamma prior distribution: $\alpha \sim Ga\,(0.1, 0.1)$;
- Gamma prior distribution: $\gamma \sim Ga\,(0.1, 0.1)$.

At this point, the MCMC calculations are implemented using the software WinBUGS [2]. We use a burn-in of 10,001 samples, along with an additional 10,000 Gibbs samples.

3.2.3. Results

Following the convergence diagnostics (incl., checking dynamic traces in Markov chains, time series, and comparing the Monte Carlo (MC) error with Standard Deviation (SD); see [22]), we consider the following posterior distribution summaries (see Table 3): the parameters' posterior distribution mean, SD, MC error, and the 95% highest posterior distribution density (HPD) interval.

In Table 2, $\beta_1 < 0$ means that the wheels mounted in the first bogie (as $x = 1$) have a shorter lifetime than those in the second (as $x = 2$). However, the influence could possibly be reduced as more data are obtained in the future, because the 95% HPD interval includes a 0 point. In addition, the heterogeneity of the wheels on the two locomotives is significant. Nevertheless, $\omega_1 < 1$ suggests that the predictive lifetimes for the wheels mounted on the first locomotive are shorter when the frailties are considered; however, $\omega_2 > 1$ indicates the opposite conclusion.

Table 2. Posterior distribution summaries

Parameter	mean	SD	MC error	95% HPD Interval
β_0	-0.2836	31.36	0.3449	(-60.69,61.4)
β_1	-0.1593	31.62	0.3085	(-63.2,62.71)
α	1.035	3.329	0.03368	(2.449E-16,10.36)
γ	0.9726	3.101	0.02904	(1.683E-15,9.277)
ω_1	0.9763	3.045	0.02924	(1.738E-16,9.595)
ω_2	1.029	3.261	0.0337	(9.718E-16,10.21)

By considering the random effects resulting from the natural variability (explained by covariates) and the unobserved random effects within the same group (explained by frailties), we can determine other reliability characteristics of lifetime distribution. The statistics on reliability $R(t)$ for the two wheels mounted in different bogies are:

- $h(t_1) = 0.97 \times 1.035 \times 0.9763 \times t_1^{0.035} \exp(-0.2836 + (-0.1593x))$
- $h(t_2) = 0.97 \times 1.035 \times 1.029 \times t_2^{0.035} \exp(-0.2836 + (-0.1593x))$

3.3. Discussion

The above results can be applied to maintenance optimisation, including lifetime prediction and replacement, preventative maintenance, and re-profiling. More specifically, determining reliability characteristics distributed over the wheels' lifetime could be used to optimise replacement strategies and to support related predictions for spares inventory. With respect to preventative maintenance, the wheels installed in different bogies should be given more attention during maintenance. Especially when the wheels are re-profiled, they should be checked starting with the bogies to avoid duplication of efforts. Last but not least, as the operating environments are similar for the two locomotives considered here, the frailties between bogies could be caused by the locomotives themselves, the status of the bogies or spring systems, and human influences (including maintenance policies and the lathe operator).

4. Comparison study on re-profiling work orders

This section compares the work orders for wheel re-profiling by date (denoted as "by date" in Fig.5) and the corresponding bogies' total number of kilometres in operation (denoted as "by kilometres" in Fig.6), separately.

In Fig.6, the work order statistics for re-profiling are listed by date. The number of the bar represents the type of work order reported in the system. For instance, number 1 means the reason for re-profiling is a high flange; number 3 represents the RCF problem; number 7 means the re-profiling is due to the dimension difference between wheels in a bogie; number 9 denotes a thick flange. The work orders have 14 categories for re-profiling: high flange, thin flange, RCF, unbalanced wheel, QR measurements, out-of-round wheel, dimension difference in between wheels in same bogie, vibrations, thick flange, cracks, remarks from measurement of the wheel by Miniprof, other defects, to plant for re-profiling, and hollowware. These categories are determined by the operator and are listed in Appendix A. Take Fig.5 (a) for example. By April 2010, the wheels of Locomotive 1 have been re-profiled 12. Eight times it was related to category 3 (RCF problem), and four times it was in category 7 (the dimension difference between wheels in a bogie).

In Fig.5 and Fig.6, the figures on the left side provide the statistics for locomotive 1, while those on the right are for locomotive 2. Note that in Fig.6, the work order statistics on re-profiling are listed by the corresponding bogies' total number of kilometres in operation on the reported date. In Fig.6(b), the wheels have run 87721 kilometres and been re-profiled 16 times, 12 times due to category 1 (high flange) and 4 times due to category 9 (thick flange).

It should be pointed out that since October 2010, new wheels have been mounted on both locomotives. However, the selected work orders are from the beginning of 2010; therefore, more re-profiling has been done on locomotive 1.

For locomotive 1, there are two failure modes: RCF and dimensional differences for wheels in the same bogie. The number of re-profiling work orders due to RCF is 64; the number due to dimensional differences for wheels in the same bogie is 8. Locomotive 2 shows three failure modes, high flange, RCF and thick flange. Again, the dominant failure mode is RCF with 38 re-profilings, followed by high flange with 12 re-profilings and thin flange with 4; see Fig. 5(b). Figs. 5(c) and (d) show the amount of material removed at each re-profiling for all wheels. Even here, the RCF failure dominates with more material lost in re-profiling. Figs. 5(e) and (f) show the mean cut deep for each re-profiling. The RCF failure mode has deeper cuts than other modes; the high flange failure mode has the smallest mean cut depth.

Fig. 6 shows the same information but uses the global traveling distance in kilometres (km). It should be pointed out that for Locomo-

Fig. 6. Work order statistics on re-profiling by kilometre

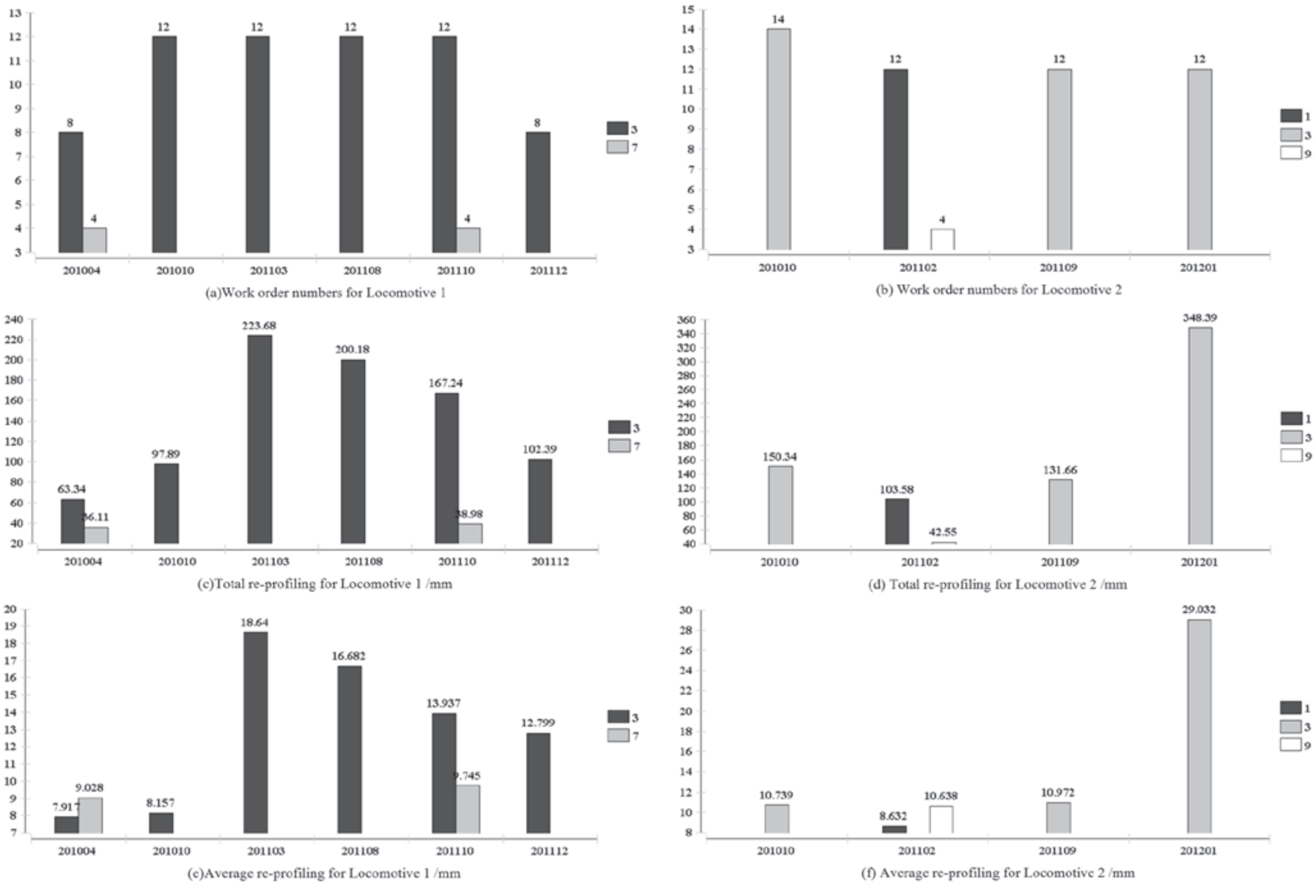

Fig. 5. Work order statistics on re-profiling by date

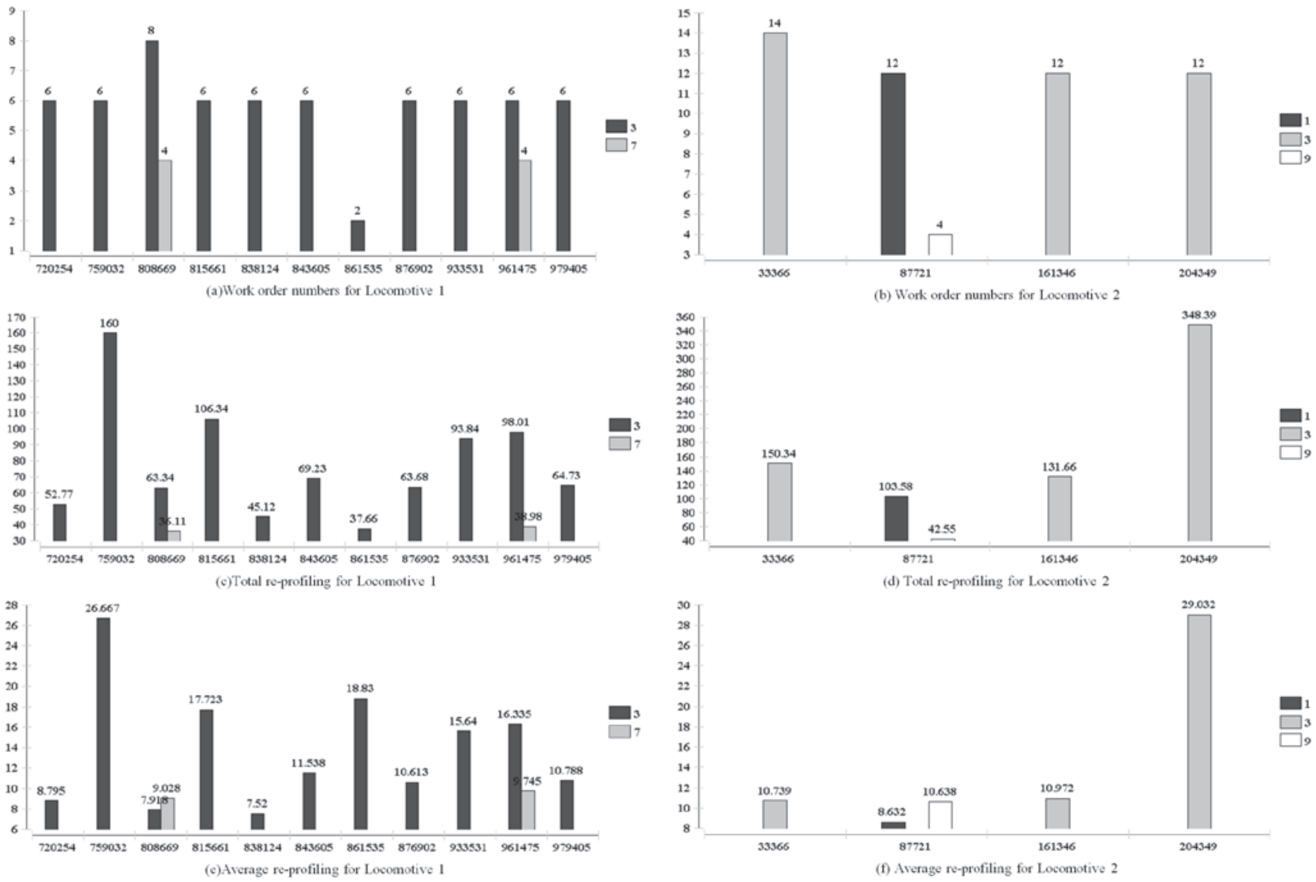

Fig. 6. Work order statistics on re-profiling by kilometre

tive 1, Fig. 6 has more bars on the left hand side because the wheel-sets have been changed and the recorded kilometres are different.

Generally speaking, RCF is the main type of work order for both locomotives. What should also be pointed out is that in the work order statistics, natural wear and the amount of re-profiling are considered simultaneously. Yet the trends in the amount of re-profiling are different. For instance, for locomotive 1, there is a decreasing trend for new wheels, while locomotive 2 shows an increasing trend.

During this investigation, we discovered a number of problems in the work orders. For example, some reported data cannot be recognised (e.g., some wheels are apparently re-profiled twice on one date; some reported wheel diameters after re-profiling are even larger than before re-profiling).

We suggest applying related KPIs to monitor the re-profiling work and the wheel performance in the future.

5. Comparison study on re-profiling parameters

In this section, we compare the re-profiling parameters (the statistics before and after each re-profiling), including the diameter of the wheel (denoted as Rd), the flange thickness (denoted as Sd), the radial runout (denoted as Rr), and the axial runout (denoted as Rx).

5.1. Assessment of re-profiling parameters (Rd)

Starting in this section, we only include statistics by re-profiling date. In addition, due to the similarities of the wheels installed in the same bogie, we only list statistics for the chosen wheel within each bogie. The upper line represents the statistics obtained before re-profiling; the lower line represents statistics after re-profiling. Fig. 7 shows, the y-axle is the wheel diameter and the x-axle is the re-profiling date. For locomotive 1, the graphs start with the last re-profiling of an old wheel; step two is the first re-profiling with new wheels.

The wheels installed in the same bogie show similar trends in the before and after re-profiling statistics (denoted as Δ Rd). Δ Rd is decreasing for locomotive 1 and increasing for locomotive 2.

5.2. Assessment of re-profiling parameter (Sd)

Fig. 8 shows the statistics of the Sd for the selected wheels. Locomotive 1 is represented on the left hand side, with locomotive 2 on the right. For both, the flange thickness increases during winter and decreases in summer; this phenomenon is especially pronounced for locomotive 1 and the first bogie and first wheel-set. A reasonable explanation for this phenomenon (changes in flange thickness in winter and summer) is that, in winter time, the wheel treads have more wear compared with in the summer. Therefore, as the measurements are taken, the positions (from the wheel treads) where to measure the flange thickness are lower than in the summer. Considering the

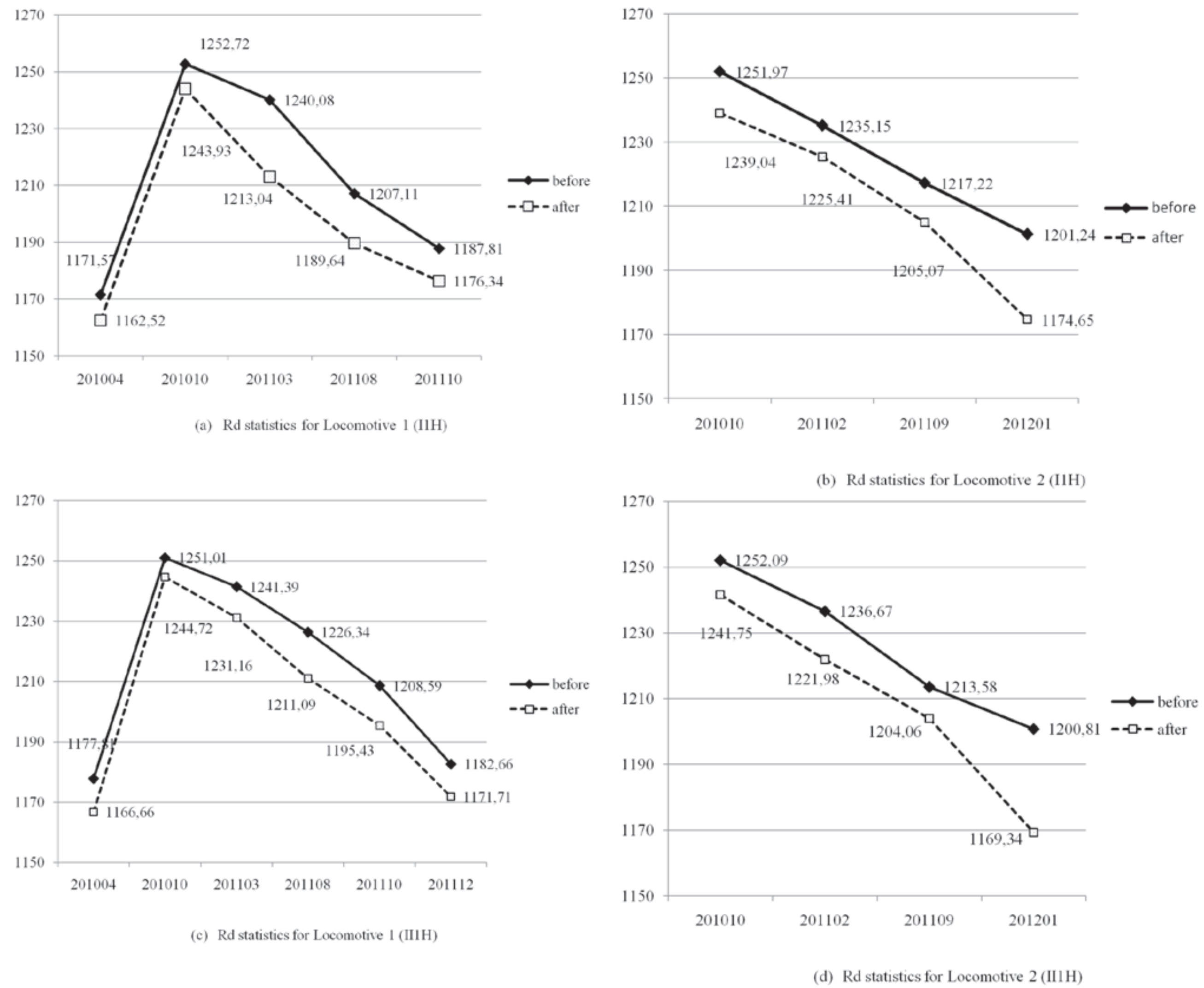

(a) Rd statistics for Locomotive 1 (I1H)

(b) Rd statistics for Locomotive 2 (I1H)

(c) Rd statistics for Locomotive 1 (II1H)

(d) Rd statistics for Locomotive 2 (II1H)

Fig. 7. Rd statistics by date (before and after re-profiling): one example (I1H & II1H)

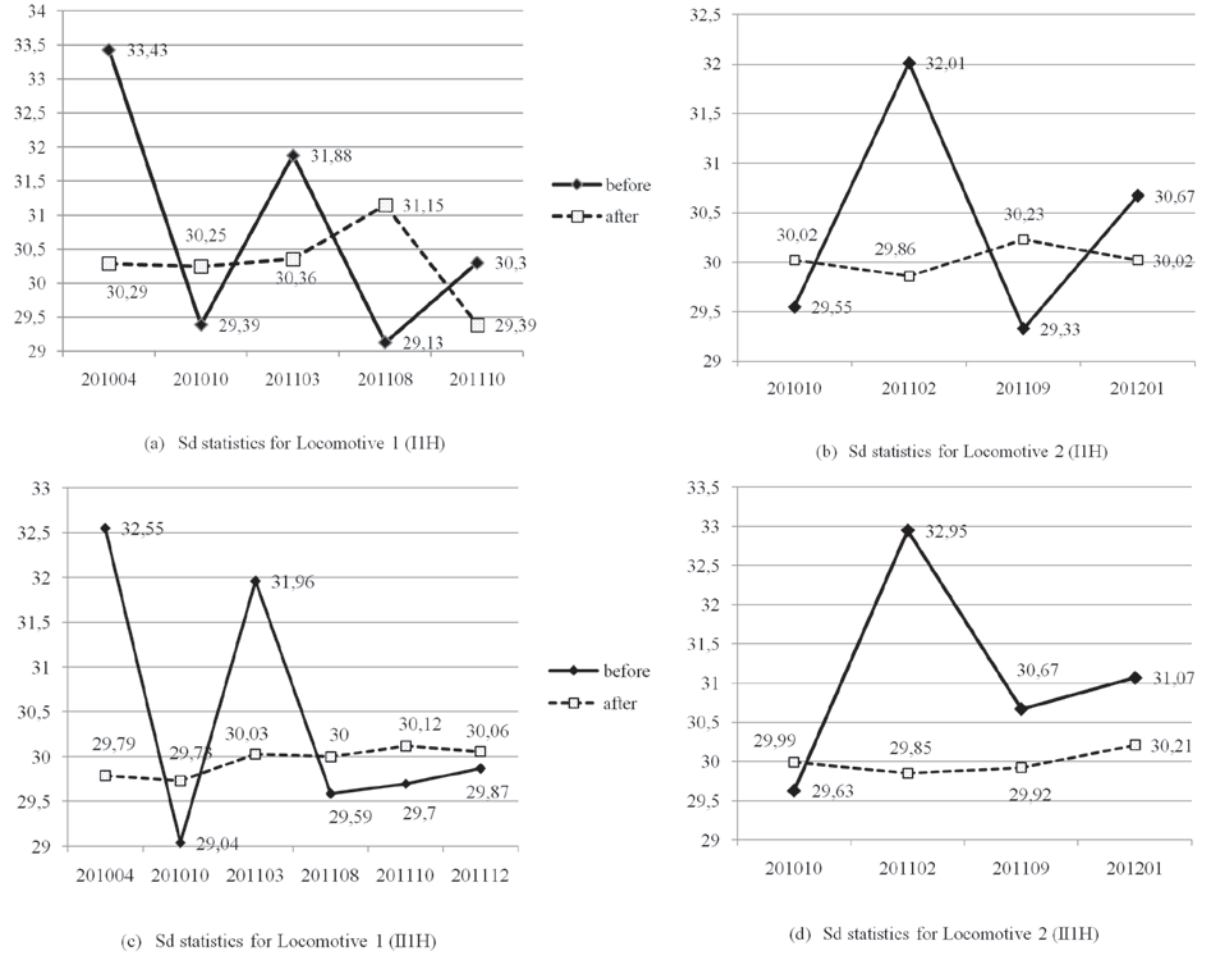

Fig. 8. Sd statistics by date (before and after re-profiling): one example (I1H & II1H)

wheels' geometry, it leads to the increasing of the flange thickness during wither and decrease in summer time.

Like the Rd statistics, the Sd statistics for the wheels installed in the same bogie are quite similar. The "after" statistics are stable. The "before" statistics are gradually becoming stable, which means the gap (denoted as Δ Sd) is decreasing.

Note that if we check the before and after statistics in different seasons, we see that the flange thickness decreases in summer and increases in winter; see Fig. 8 (a).

5.3 Assessment of re-profiling parameter (ΔRd, ΔSd, ΔRr, ΔRx)

In this section, we simultaneously consider the gaps of the four parameters discussed above: ΔRd, ΔSd, ΔRr, and ΔRx.

As discussed above, the statistics for the wheels installed in the same bogie are quite similar. Among these four parameters, the changing of ΔRd is the most obvious one, with ΔSd coming second. The changing of ΔRr and ΔRx are random and the amount is quite small compared to the first two parameters. Therefore, we suggest applying the first two parameters to monitor the wheels' re-profiling performance in the future.

6. Comparison of wear rate

In this section, we compare the wheels' wear rates, shown in Tables 3 to 6. Table 3 shows locomotive 1, bogie 1 and the first wheel-set on the right side; Table 4 shows locomotive 1, bogie 2 and the first wheel-set on the right side; see Fig. 2 for the position of the bogies and wheel-sets. The number of re-profiling work orders is different between bogies: bogie 1 has 4 and bogie 2 has 5. The reason for the difference may be that bogie 1 was changed after the fourth re-profiling. The re-profiling at times 1 to 4 was done at the same time for both bogies, extending over 12 months.

As for locomotive 1, Table 3 shows that it has been running for 123.351 km; the mean distance between re-profiling is 41.117 km. The distance after the last re-profiling for bogie 2 was only 17.930 km, less than half of the average distance for re-profiling numbers 1 to 4; see Table 4. Tables 3 and 4 also show the diameter of the wheel before and after re-profiling and the amount of material removed at each re-profiling. The mean amount of material removed during re-profiling for bogie 1 is 16.193 mm and for bogie 2, 11.176 mm. Remarkably, the amount of re-profiling for bogie 2, step 2 is 27.04 mm, much more than the others; as noted above, the mean is 16.193 mm. If we compare natural wear with artificial wear, the former is between 15 mm and 20% of the total wear. In addition, the total wear rate for locomotive 2, bogie 1, is 0.619 mm/1000 km; for bogie 2, it is 0.393 mm/1000km.

As mentioned, locomotive 1 and locomotive 2 have the same operating conditions (see Fig. 4 for the comparison), but the figures in Tables 5 and 6 show different results. Table 5 shows locomotive 2, the first bogie, the first wheel-set, and the right hand side wheel; Table 6 shows the second bogie, the first wheel-set, and the right hand side wheel. This locomotive has been re-profiled 4 times in 15 months; the mean distance between re-profiling is 56.990 km. The mean amount of material removed for re-profiling for bogie 1 is 15.10 mm; for bogie 2 it is 16.51 mm. The last re-profiling for the first bogie removed 26.59 mm and for the second bogie 31.47 mm. Finally, the total wear rate for locomotive 2, bogie 1, is 0.452 mm/1000 km and for bogie 2, 0.484 mm/1000km

Explanatory comments for Tables 3, 4, 5, 6 include the following:

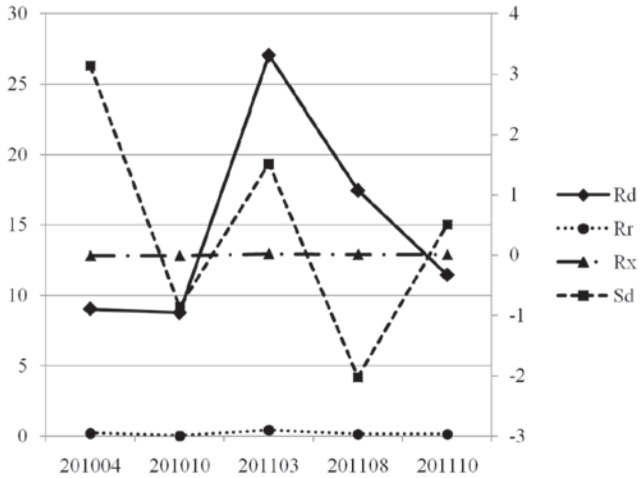

(a) Gap statistics for Locomotive 1 (I1H)

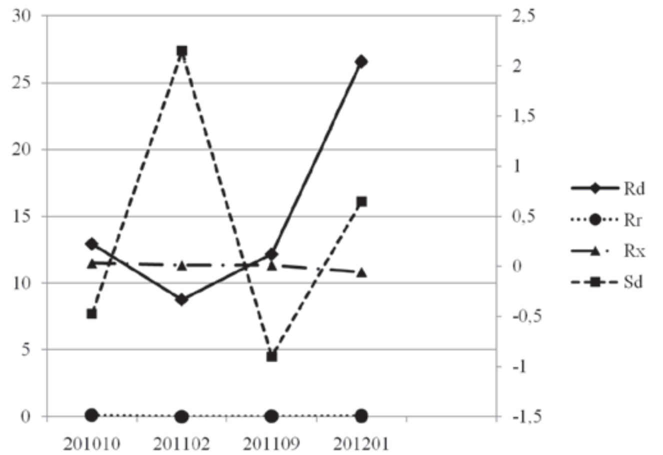

(b) Gap statistics for Locomotive 2 (I1H)

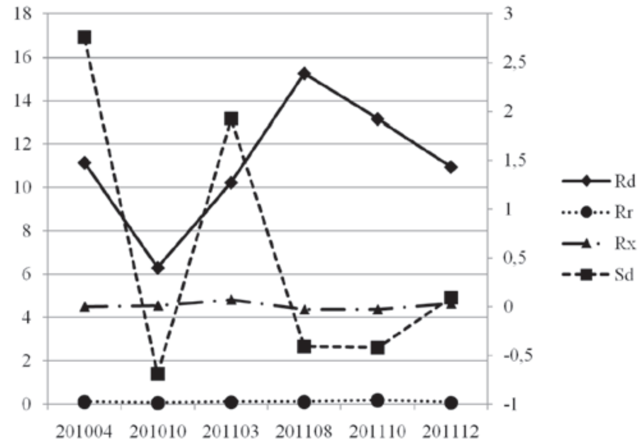

a. Gap statistics for Locomotive 1 (II1H)

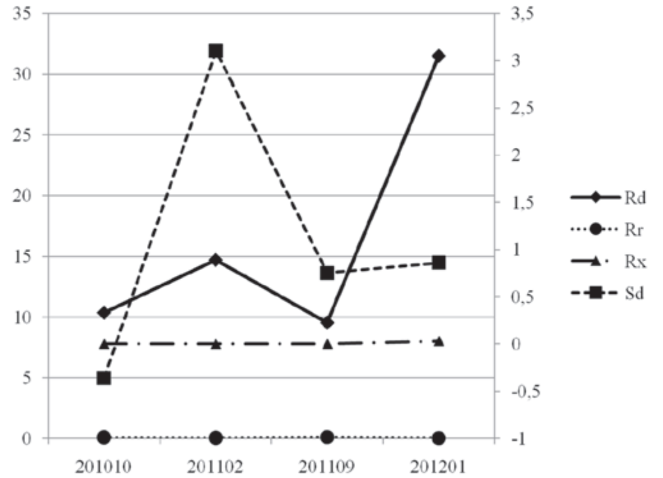

b. Gap statistics for Locomotive 2 (II1H)

Fig. 9 Gap statistics by date (before and after re-profiling): one example (I1H & II1H)*

*) *Note: To make it more clearly, we adopted two axis here (left and right). For Rd and Rr, we adopted the axis on the left side; while for Rx and Sd, we adopted the axis on the righ side.*

Table 3. Statistics for wear rate: an example (locomotive 1, I1H)

Locomotive	1	Position	I1H		Total/Average
Number of re-profiling	1	2	3	4	4 times
Re-profiling date	201010	201103	201108	201110	12 months
Reported kilometres /1000km	720.254	759.032	815.661	843.605	/
Absolute kilometres /1000km	0	38.778	56.629	27.944	123.351
Diameters (before)/mm	1252.72	1240.08	1207.11	1187.81	/
Diameters (after)/mm	1243.93	1213.04	1189.64	1176.34	/
Re-profiling Amount/mm	8.79	27.04	17.47	11.47	64.77
Natural Wear/mm	0	3.85	5.93	1.83	11.61
Total Wear/mm	8.79	30.89	23.4	13.3	76.38
Re-profiling Amount %	1	0.875	0.747	0.862	0.848
Natural Wear %	0	0.125	0.253	0.138	0.152
WearRate_re-profiling	/	0.697	0.308	0.41	0.525
WearRate_Natural	/	0.099	0.105	0.065	0.094
WearRate_Total	/	0.797	0.413	0.476	0.619

Table 4. Statistics for wear rate: an example (locomotive 1, II1H)

Locomotive	2	Position	II1H			Total/Average
Number of re-profiling	1	2	3	4	5	5 times
Re-profiling date	201010	201103	201108	201110	201112	14 months
Reported kilometres /1000km	838.124	876.902	933.531	961.475	979.405	/
Absolute kilometres /1000km	0	38.778	56.629	27.944	17.93	141.281
Diameters (before)/mm	1251.01	1241.39	1226.34	1208.59	1182.66	/
Diameters (after)/mm	1244.72	1231.16	1211.09	1195.43	1171.71	/
Re-profiling Amount/mm	6.29	10.23	15.25	13.16	10.95	44.93
Natural Wear/mm	0	3.33	4.82	2.5	12.77	10.65
Total Wear/mm	6.29	13.56	20.07	15.66	23.72	55.58
Re-profiling Amount %	1	0.754	0.76	0.84	0.462	0.808
Natural Wear %	0	0.246	0.24	0.16	0.538	0.192
WearRate_re-profiling	/	0.264	0.269	0.471	0.611	0.318
WearRate_Natural	/	0.086	0.085	0.089	0.712	0.075
WearRate_Total	/	0.35	0.354	0.56	1.323	0.393

Table 5. Statistics for wear rate: an example (locomotive 2, I1H)

Locomotive	2	Position	11H		Total/Average
Number of re-profiling	1	2	3	4	4 times
Re-profiling date	201010	201102	201109	201201	15 months
Reported kilometres /1000km	33.366	87.721	161.346	204.349	/
Absolute kilometres /1000km	0	54.355	73.625	43.003	170.983
Diameters (before)/mm	1251.97	1234.15	1217.22	1201.24	/
Diameters (after)/mm	1239.04	1225.41	1205.07	1174.65	/
Re-profiling Amount/mm	12.93	8.74	12.15	26.59	60.41
Natural Wear/mm	0	4.89	8.19	3.83	16.91
Total Wear/mm	12.93	13.63	20.34	30.42	77.32
Re-profiling Amount %	1	0.641	0.597	0.874	0.781
Natural Wear %	0	0.359	0.403	0.126	0.219
WearRate_re-profiling	/	0.161	0.165	0.618	0.353
WearRate_Natural	/	0.09	0.111	0.089	0.099
WearRate_Total	/	0.251	0.276	0.707	0.452

Table 6. Statistics for wear rate: an example (locomotive 2, II1H)

Locomotive	2	Position	II1H		Total/Average
Number	1	2	3	4	4 times
Date	201010	201102	201109	201201	15 months
Reported kilometres /1000km	33.366	87.721	161.346	204.349	/
Absolute kilometres /1000km	0	54.355	73.625	43.003	170.983
Diameters (before)/mm	1252.09	1236.67	1213.58	1200.81	/
Diameters (after)/mm	1241.75	1221.98	1204.06	1169.34	/
re-profiling Amount/mm	10.34	14.69	9.52	31.47	66.02
Natural Wear/mm	0	5.08	8.4	3.25	16.73
Total Wear/mm	10.34	19.77	17.92	34.72	82.75
re-profiling Amount %	1	0.743	0.531	0.906	0.798
Natural Wear %	0	0.257	0.469	0.094	0.202
WearSpeed_re-profiling	/	0.27	0.129	0.732	0.386
WearSpeed_Natural	/	0.093	0.114	0.076	0.098
WearSpeed_Total	/	0.364	0.243	0.807	0.484

Table 7. Statistics for total wear rates

	WearRate_total											
	11H	11V	12H	12V	13H	13V	21H	21V	22H	22V	23H	23V
Locomotive 1	0.619	0.607	0.614	0.605	0.542	0.533	0.393	0.404	0.467	0.467	0.467	0.472
Locomotive 2	0.452	0.439	0.448	0.448	0.449	0.448	0.484	0.482	0.568	0.575	0.487	0.476

- Absolute kilometres = the current reported kilometres – the previous reported kilometres;
- Re-profiling Amount = Diameters (before) - Diameters (after);
- Natural Wear = the previous Diameters (after) – the current Diameters (before);
- Total Wear = Re-profiling Amount + Natural Wear;
- Re-profiling Amount % = Re-profiling Amount / Total Wear;
- Natural Wear % = Natural Wear/ Total Wear;
- WearRate_Reprofiling = Re-profiling Amount / Absolute kilometres;
- WearRate_Natural = Natural Wear / Absolute kilometres;
- WearRate_Total = Total Wear / Absolute kilometres;
- Average of the total wear rate = the average of WearRate_Total.

In addition, by comparing the interval of the re-profiling date, we can simply divide each re-profiling episode into seasons (for instance, the summer and warmer times, the winter and cooler times).

In Table 7, we list the statistics for the WearRate_total of all the wheels for the two locomotives. The mean wear rates are 0.516 mm/1000km for locomotive 1 and 0.480 mm/1000km for locomotive 2; in other words, locomotive 1 has a 75% higher wear rate. Wheel-sets 1, 2 and 5 have 11.6 % higher wear rate than wheel-sets 3, 4 and 6.

By comparing the above parameters of the wheels installed in different positions on the locomotives, we can reach the following additional conclusions:

- the average wear rate of the wheels on locomotive 1 is greater than for locomotive 2;
- the natural wear is about 10% ~ 25 % of the total wear; the re-profiling is about 75 %~ 90% of the total;
- the natural wear in winter time is slower than in summer;
- the re-profiling rate in winter is larger than in summer;
- the wheels installed on the second wheel-set in the second bogie have an abnormal higher wear rate compared to the wheels installed in the same bogie but on the other wheel-set; this requires more attention;
- The wheels installed in the same bogie perform similarly.

7. Conclusions

In this paper, the Weibull frailty model is used to analyse the wheels' degradation. The gamma shared frailties $\boldsymbol{\omega}_i$ are used to explore the influence of unobserved covariates within the same locomotive. By introducing covariate $\mathbf{x}_i$'s linear function $\mathbf{x}_i'\beta$, we can take into account the influence of the bogie in which a wheel is installed. The proposed framework can deal with small and incomplete datasets; it can also simultaneously consider the influence of various covariates. The MCMC technique is used to integrate high-dimensional probability distributions to make inferences and predictions about model parameters. Finally, we compare the statistics on re-profiling work orders, the performance of re-profiling parameters (denoted as ΔRd, ΔSd, ΔRr, ΔRx), and wear rates.

The results show the following for the two locomotives: 1) with the specified installation position and operating conditions, the Weibull frailty model is a useful tool to determine wheel reliability by considering an exponential degradation path; 2) rolling contact fatigue (RCF) is the main type of re-profiling work order; 3) the re-profiling parameters can be applied to monitor both the wear rate and the re-profiling loss; 4) the total wear of the wheels can be determined by investigating natural wear and/or loss of wheel diameter through re-profiling loss, but these are different in different locomotives and under different operating conditions; 5) the bogie in which a wheel is installed is a key factor in assessing the wheel's reliability.

Finally, the approach discussed in this paper can be applied to cargo train wheels or to other technical problems (e.g. other industries, other components).

We suggest the following additional research:

- The covariates considered here are limited to the positions of the locomotive wheels; more covariates must be considered. For example, the braking forces and the curving forces should also be considered.
- We have chosen vague prior distributions for the case study. Other prior distributions, including both informative and non-informative prior distributions, should be studied.
- One of our research focuses in the future is to analyse the relationship between re-profiling interval and material removal on the lathe, together with other influencing factors such as the flange wear, wheel diameter, position on the bogie, and other possible covariates mentioned above.
- In subsequent research, we plan to use our results to optimise maintenance strategies and the related LCC (Life Cycle Cost) problem considering maintenance costs, particularly with respect to different maintenance inspection levels and inspection periods (long, medium and short term).

Acknowledgements

The authors would like to thank Luleå Railway Research Centre (Järnvägstekniskt Centrum, Sweden) and Swedish Transport Administration (Trafikverket) for initiating the research study and providing financial support. The authors would also like to thank Thomas Nordmark, Ove Salmonsson and Hans-Erik Fredriksson at LKAB for their support and their discussions of the locomotive wheels. And we would like to thank the editor and anonymous referees for their constructive comments.

References

1. Aslanidou H, Dey DK, Sinha D. Bayesian analysis of multivariate survival data using Monte Carlo methods. Canadian Journal of Statistics. 1998; 26: 33-48
2. Clayton DG, Cuzick J. Multivatiate Generalizations of the Proportional Hazards Model (with Discussion). Journal of the Royal Statistical Society A. 1985, 148: 82-117.
3. Clayton DG. A Monte Carlo method for Bayesian inference in frailty models. Biometrics. 1991, 47:467-485.
4. Clayton DG. A Model for Association in Bivariate Life Tales and its Application in Epi-demiological Studies of Familial Tendency in Chronic Disease Incidence. Biometicka. 1978; 65: 141-151

5. Crowder M. A multivariate distribution with Weibull connections. Journal of the Royal Statistical Society B. 1989, 51: 93-107.
6. Freitas MA, Colosimo EA, and Santos dos TR et al.. Reliability assessment using degradation models: Bayesian and classical approaches. Pesquisa Operacional. 2010; 30 (1):195-219
7. Freitas MA, Colosimo EA, and Santos dos TR et al.. Using Degradation Data to Assess Reliability: A Case Study on Train Wheel Degradation. Journal of Quality and Reliability Engineering International. 2009; 25: 607-629
8. Fröhling RD, Hettasch G. Wheel-rail interface management: a rolling stock perspective. Proceedings of the Institution of Mechanical Engineers. 2010; 224: 491-497
9. Hakon K G, Odd O A, Nilslid H. Frailty models based on levy processes. Advances in Applied Probability. 2003, 35: 532-550.
10. Hougaard P. Frailty models for survival data. Lifetime Data Analysis.1995, 1:255-273.
11. Hougaard P. Survival models for heterogeneous populations derived from stable distributions. Biometrika. 1986, 73: 387-396.
12. Klein JP, Moeschberger ML. Survival Analysis: Techniques for Censored and Truncated Data. Springer-Verlag New York, Inc.1997, p.55.
13. Lawless JF. Statistical Models and Methods for Lifetime Data. John Wiley and Sons.1982, p. 31.
14. Lin J, Asplund M, Parida A. Reliability Analysis for Degradation of Locomotive Wheels using Parametric Bayesian Approach. Quality and Reliability Engineering International. 2013. DOI: 10.1002/qre.1518.
15. McGilchrist C A, Aisbett C W. Regression with Frailty in Survival Analysis. Biometrics. 1991, 47:461-466.
16. Oakes D. A model for association in bivariate survival data. Journal of Royal Statistics Society B. 1982; 44:414-422
17. Palo M, Schunnesson H, Kumar U, et al.. Rolling stock condition monitoring using wheel/rail forces. Journal of Insight-Non-Destructive Testing and Condition Monitoring. 2012; 54 (8): 451-455
18. Pennell M L, Dunson D B. Bayesian Semi parametric Dynamic Frailty Models for Multiple Event Time Data. Biometrika. 2006, 62:1044-1052.
19. Qiou Z, Ravishanker N, Dey D K. Multivariate survival analysis with positive frailties. Biometrika. 1999, 55: 637-644.
20. Sahu SK, Dey DK, and Aslanidou H et al. A Weibull regression model with gamma frailties for multivariate survival data. Lifetime Data Analysis. 1997; 3:123-137
21. Sinha D. Semiparameteric Bayesian analysis of multiple event time data. Journal of the American Statistical Association. 1993, 88: 979-983.
22. Spiegelhalter DJ et al. Bayesian measures of model complexity and fit. Journal of Royal Statist. Society Series B. 2002; 64(3):583-639.
23. Yang C, Letourneau S. Learning to Predict Train Wheel Failures. In: The 11 ACM SIGKDD International Conference on Knowledge Discovery and Data Mining (KDD 2005). Chicago, Illinois, USA. August 21-22, 2005.

Appendix A

Table A.1 work order's categories

Code	Description	Code	Description	Code	Description
1	High flange	6	Out-of-round wheel	11	Measurements on the wheel, Miniprof
2	Thin flange	7	Dimension difference in between wheels in bogie	12	Other defect, pressure defect
3	RCF	8	Vibrations	13	Empty, no code
4	Unbalanced wheel	9	Thick flanges	14	Plant to be re-profiled
5	QR measurements	10	Cracks	15	Double flanges

Jing LIN
Division of Operation and Maintenance Engineering, Luleå University of Technology, 97187, Luleå, Sweden
Luleå Railway Research Centre, 97187, Luleå, Sweden
E-mail: janet.lin@ltu.se

Matthias ASPLUND
Division of Operation and Maintenance Engineering, Luleå University of Technology, 97187, Luleå, Sweden
Luleå Railway Research Centre, 97187, Luleå, Sweden
Swedish Transport Administration, 97102, Luleå, Sweden

Article citation info:
JODEJKO-PIETRUCZUK A, WERBIŃSKA-WOJCIECHOWSKA S. Analysis of maintenance models' parameters estimation for technical systems with delay time. Eksploatacja i Niezawodnosc – Maintenance and Reliability 2014; 16 (2): 288–294.

Anna JODEJKO-PIETRUCZUK
Sylwia WERBIŃSKA-WOJCIECHOWSKA

ANALYSIS OF MAINTENANCE MODELS' PARAMETERS ESTIMATION FOR TECHNICAL SYSTEMS WITH DELAY TIME

ANALIZA PARAMETRÓW MODELI OBSŁUGIWANIA SYSTEMÓW TECHNICZNYCH Z OPÓŹNIENIEM CZASOWYM*

In the article authors are interested in BIP performance for three-element system ("k-out-of-n" reliability structure), the maintenance policy which is one of most commonly used in practice. The BIP may be implemented in technical systems when some information about reliability characteristics is known. The basic reliability parameters that have to be specified in such systems are: an estimation of system components' time to failure and some delay time characteristics. In order to determine the effects of possible errors and to specify sufficient accuracy of the estimation, the analysis of system costs was done for various values of the expected delay time, assuming three different probability distributions of the delay time (Weibull, Uniform, and Normal). The modelling process was based on the use of GNU Octave software. Test analysis of delay time parameter, assuming different types of probability distributions is the base to conclude: if the form of the distribution has any meaning for economic results of the system, and what kind of consequences may result from improper mean delay time estimation E(h).

Keywords: *delay-time, maintenance model, parameters estimation methods.*

W pracy analizie poddano system trzyelementowy (struktura niezawodnościowa progowa), którego procesy obsługiwania realizowane są zgodnie z założeniami Polityki Przeglądów Blokowych (BIP). Strategia ta może być zastosowana w procesie utrzymania systemów technicznych, gdy znane są pewne jego charakterystyki niezawodnościowe, bazujące m.in. na informacjach o czasach pomiędzy uszkodzeniami elementów systemu. W badaniach skupiono się na trzech rozkładach prawdopodobieństwa tej zmiennej losowej (normalny, Weibull, prostokątny). Model symulacyjny opracowano przy wykorzystaniu oprogramowania GNU Octave. Analiza okresu opóźnienia czasowego, przy założeniu różnych postaci rozkładów prawdopodobieństwa tej zmiennej losowej, pozwoliła na ocenę: czy znajomość typu rozkładu prawdopodobieństwa zmiennej losowej h ma istotne znaczenie dla wyników ekonomicznych funkcjonowania systemu, oraz jakie konsekwencje mogą wystąpić w wyniku niewłaściwej estymacji wartości średniej E(h).

Słowa kluczowe: *opóźnienie czasowe, model obsługiwania, metody estymacji parametrów.*

1. Introduction

In the case of complex systems, in which an important issue is a problem of modeling the relationship between two separate subsystems that have an impact on the overall system availability, a lot of works draw attention to the delay times occurrence during operational processes performance [8].

In the year 1976 Christer (following [16]) proposed the delay-time (DT) concept, used to this day in the renewal theory in order to optimize the technical system downtime due to not detected failures occurrence (e.g. [9, 10, 14, 16, 20]). The basic idea rests on an observation that a failure does not usually occur suddenly, but is preceded by a detectable fault for some time prior to actual failure, called a delay time and is denoted by *h* (Fig. 1) [8, 12]. This research area has been widely studied in the literature, e.g. in [2, 3, 6, 7, 8, 12, 13, 24, 25, 26, 27, 28], where reviews of delay-time models from the application point of view are provided, and in [22, 23, 25, 32] which focus on the possibilities of DT models use for multi-unit systems maintenance performance.

The correctness of maintenance model selection for technical systems with time delay is directly dependent on the accuracy of model parameters estimation process. Generally, there is no possibility to measure directly either the delay time associated with a defect, or the initial point *u*. There can be proven a possibility to estimate the delay time for a set of specific faults and failures, and from this deduce the location of the initial point and estimate the delay-time and initial-point distributions [12, 25].

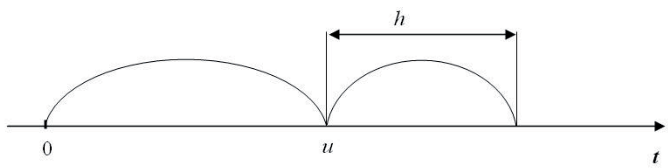

Fig. 1. Delay-time concept [15]

There are two methods to estimate delay-time *h* and initial point *u* parameters in the literature. When the operating data are available and reliable, it is possible to estimate the model parameters using the maximum likelihood method (e.g. [30]). Otherwise, there is applied a subjective estimation of parameters based on expert opinion (e.g. [29]). One of the first works in which authors have developed and investigated the method of subjective opinion of experts use in the parameter *h* estimation process are [10, 14, 15, 16, 20]. These works regarded to maintenance processes performed in civil engineering [10], industrial systems [16], manufacturing [15, 20] and transport maintenance [14].

(*) Tekst artykułu w polskiej wersji językowej dostępny w elektronicznym wydaniu kwartalnika na stronie ***www.ein.org.pl***

In the next paper [13], authors continued their research on the delay time models parameter estimation issues. The authors presented an overview of the literature in the study area and discussed the revision delay-time models. Moreover, they investigated the issue of biased estimates determination in the analysed research area. This issue was later continued in [12], where e.g. the parameter estimation methods criteria used in maintenance decision processes have been analyzed. A literature review of the fields of subjective probability and the experts' opinions application in maintenance decision-making processes performance with the use of DT concept was presented in [7, 29].

In the next works, authors presented the implementation of subjective method of delay time parameters estimation in maintenance issues of industrial systems [19], manufacturing systems [1], and city bus transport companies [21].

On the other hand, for the first time, authors in [5] used an objective method in the process of delay time parameters estimation for the repairable object performance. Model parameters were estimated using maximum likelihood method and Akaike Information Criterion (AIC). The proposed model was developed in [4], where the authors investigated a technical system consisting of multiple components.

In the next work [17] authors considered a multi-element system, in which inspection actions are carried out systematically at time T and at failure. The issue of an objective estimation of the model parameters for complex system were analyzed e.g. in [18].

The problem of model parameters estimation, when there are available only data about the moments of failure occurrence (lack of information about system maintenance process performance), was analyzed in [11]. In other work [31], there is presented an example of time between maintenance actions performance for a manufacturing company.

Particularly noteworthy is the work [30], in which authors developed a model of delay time parameter estimation using both estimation methods.

Literature studies show that the problem of the proper estimation of the parameters of the random variable delay time h is extremely important and there are developed methods for continuous improvement of these estimates. In practice, there is not always the possibility of a correct and accurate approximation of all the delay time parameters for maintained system. In many cases, the available data allow only for estimation of the expected value and standard deviation of the delay time variable. Following this, there can be asked a question about possible consequences of incorrect estimation of the model parameters and the legitimacy of estimation improvement process performance. Therefore, the aim of this article is to assess:

- consequences - economic and reliability ones - which should be taken into account for maintained system, if only selected parameters of delay time will be possible to estimate in practice,
- the necessary delay time parameters estimation accuracy, allowing the selection of the correct time between inspection actions performance in multi-component system.

Achievement of such defined objectives has been performed by carrying out a simulation analysis of a technical system operation process with implementation of different delay time characteristics. The system is maintained according to Block Inspection Policy - BIP. Research results analysis allowed assessing the influence of selected delay time parameters changes on the obtained system maintenance costs and availability ratio. This process enables to assess the consequences connected with parameters under- and overestimation or with absence of delay time parameter data. Moreover, there is a possibility to define the influence of such consequences on performance outputs of multi-unit system, maintained according to BIP strategy. The article bases on simulation studies implementation because of the lack of analytical models development which could be used to define maintenance costs and system availability, depending on the multi-unit system characteristics and BIP strategy requirements and conditions.

In the next Sections, there are discussed the main assumptions used in BIP model, used simulation algorithm, and there are presented the obtained research results.

2. Block Inspection Policy Model

The study investigates system comprised of *3* identical elements, in a *k-out-of-n* reliability structure, working independently under the same conditions. The used maintenance policy is a BIP which assumes that the diagnosis operations of the state of a system are carried out at regular intervals of T time units. This maintenance strategy can be used in the maintenance process of technical system, where some of its reliability characteristics are known, based on e.g. the information about the time between failures of system components. It is assumed, that the system components are independent, as well as the first signs of forthcoming failures (defects occurrence). The inspections are assumed to be perfect. Thus, any component's defect, which occurred in the system till the moment of inspection, will be identified. All elements with identified defects will be replaced within the inspection period. The performance of the investigated system being illustrated in Fig. 2 is also defined by the additional assumptions:

- maintenance actions restores system to as good as new condition,
- failures of the system are identified immediately, and repairs or replacements are made as soon as possible,
- system incurs costs of: new elements, when they are replaced, inspection costs, and some additional, consequence costs, when system fails,
- elements' lifetime, repair time, replacement time and the length of the delay time before element's failure are random and their probability distributions are known.

The performance of the chosen system is modeled with the use of simulation processes. The modeling process was based on the use of *GNU* Octave software. The list of tested system parameters, which were used in the simulation models, is given in Table 1. The scheme of the simulation algorithm is given in Fig. 3.

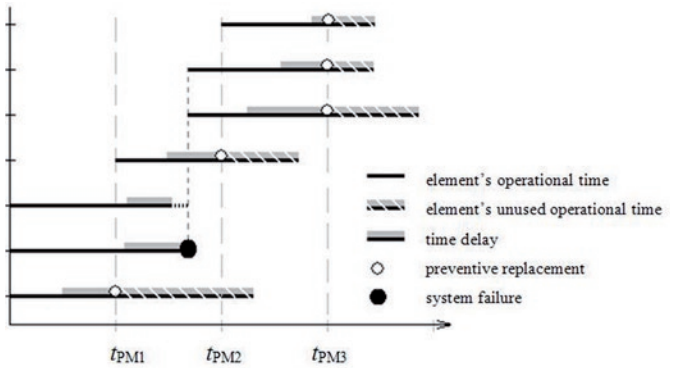

Fig. 2. Idea of the Block Inspection Policy for investigated system

The research analysis regards to the assessment of delay time parameters influence on the investigated system economic results. As a result, there is a necessity to define the expected costs per unit of operating time of the system resulting from BI maintenance policy performance $C_{BI}(T)$:

$$C_{BI}(T) = CE_{BI}(T) + CC_{BI}(T) + CI_{BI}(T) \tag{1}$$

where: C_{BI} – the expected cost resulting from *BI* maintenance policy performance, T – the period between two consecutive inspection actions performance, CE_{BI} – the expected costs of new elements per unit time for *BI* maintenance policy, CC_{BI} – the expected cost of the con-

Table1. Modelled system parameters

Symbol	Description	Tested values
n	Number of system elements	3
k	Minimal number of up-stated elements keeping the system in upstate	1,3
c_e	The cost of new element	1
c_i	The cost of an inspection	1
c_c	The cost of a system failure	10 000
T_i	The time required for inspection	0
T	Constant time between maintenance actions performance	–
$F(t=u+h)$	C.d.f. of elements' lifetime	$F(t)=1-e^{-(\frac{t}{100})^{3,5}}$
$G_r(t)$	C.d.f. of single elements' repair time (resulting from a system failure)	$G_r(t)=1-e^{-(\frac{t}{100})^{2,3}}$
$G_p(t)$	C.d.f of single element's replacement time (resulting from preventive replacement)	$G_p(t)=1-e^{-(\frac{t}{10})^{2,3}}$
		$f_h(h)=\frac{\alpha}{\beta^{\alpha_h}}h^{\alpha_h-1}e^{-(\frac{h}{\beta_h})^{\alpha h}}$
$f_h(h)$	C.d.f. of elements' delay time	$f_h(h)=\begin{cases}\frac{1}{b-a}, & \text{if } a\le h\le b\\ 0, & \text{if } h\le a \text{ or } b\le h\end{cases}$
		$f_h(h)=\frac{1}{\sqrt{2\pi\sigma}}e^{-\left(\frac{(h-\mu)^2}{2\sigma^2}\right)}$

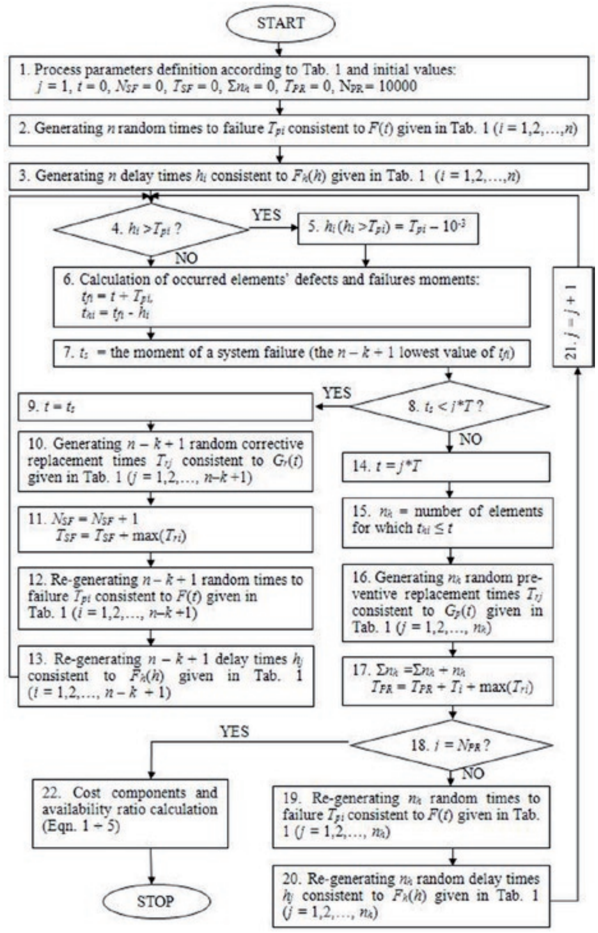

Fig. 3. Simulation algorithm

sequences resulting from a system failure for *BI* maintenance policy, CI_{BI} – the expected costs of performed inspections.

The expected costs of new elements per unit time can be obtained from the following formula:

$$CE_{BI}(T)=\frac{[(n-k+1)\cdot N_{SF}(T)+\sum n_{PR}(T)]\cdot c_e}{OT} \tag{2}$$

where: n – number of elements of the system, k – minimal number of up-stated elements for having system in an operational state, N_{SF} – the number of system failures during assumed time horizon, Σn_{PR} – the expected number of elements that were preventively replaced after inspection, c_e – the cost of new element, OT – the operating time of the system.

Moreover, the expected cost of the consequences resulting from a system failure for the investigated maintenance policy can be calculated from the following formula:

$$CC_{BI}(T)=\frac{N_{SF}(T)\cdot c_c}{OT} \tag{3}$$

where: c_c – the cost of the consequence resulting from a system failure occurrence.

There is also a necessity to define the expected costs of performed inspections:

$$CI_{BI}(T)=\frac{N_{PR}(T)\cdot c_i}{OT} \tag{4}$$

where: N_{PR} – the number of preventive replacements of system elements, c_i – the cost of an inspection performance.

The next step is connected with availability analysis. Thus, the availability ratio is calculated with the use of the following formula:

$$A_{BI}(T)=\frac{OT(T)}{OT(T)+T_{PR}(T)+T_{SF}(T)} \tag{5}$$

where: T_{PR} – the expected time of preventive replacements of system elements, T_{SF} – the expected time of corrective replacements of system elements.

3. Estimation of delay time parameter *h* – analysis of obtained simulation results

While performing the simulation analysis, it was assumed that there are tested three systems, built and operated in the same way and differing only in the area of delay time characteristics of its components. It was assumed, that the systems delay time differs in the form of the probability distribution of the variable *h* (Weibull, rectangular, normal distributions), but the expected value of the variable is the same (E (*h*) = 35). Analysis of the delay time period, assuming the different forms of probability distributions of variable *h*, allows assessing:

- if the form of the probability distribution of the random variable *h is important for* system performance in terms of obtained economic and availability results, and hence - if the knowledge of the form of its probability distribution function is necessary for the proper selection of time between inspections *T*,

- what kind of the economical and reliability consequences can arise in a maintained system in the case of incorrect estimation of parameters describing the variable *h*.

The Figures 4 – 9 show the economic results and availability ratio level of three-element system performing according to BIP policy depending on the expected value E(*h*), the length of the period *T*, and the type of the probability distribution of the random variable *h*. Moreover, the presented analysis results refer to the technical system performing in two extreme reliability structures "*1-out-of-3*" (parallel reliability structure – bright markers) and "*3-out-of-3*" (serial reliability structure - dark markers).

For all the three investigated cases, the obtained economic results are very similar regardless of the type of the probability distribution of the variable *h*. Both parameters: the time between maintenance action performance (*T*) and the expected value of time delay (E(*h*)) have a significant impact on the level of expected maintenance costs. However, obtained results rather do not depend on the type of the probability distribution of the variable *h*. Areas of maintenance costs for both systems, performing in serial and parallel reliability structures, have the same characteristics, e.g. for the cases of the longest delay time (E(*h*) = *MTTF* = 100) maintenance costs for serial system range 0–200 depending on the desired length of time between inspections *T*, but independently of the type of the probability distribution of the elements delay time *h* (Fig. 4, 6, 8). Exactly the same effect can be observed for the other tested values of E(*h*) in both system's reliability structures – the same maintenance costs boundaries, as well as the same curvature of the maintenance cost surfaces. This fact leads to the conclusion that the optimization process of BIP policy parameters for the analysed system requires no knowledge about the type of the probability distribution of the random variable *h*. Hence, the wrong assumption of the type of probability distribution of the random delay time *h* does not cause significant differences in the system maintenance cost assessment. A similar effect can be observed in the analysis of system availability ratio level (Fig. 5, 7, 9).

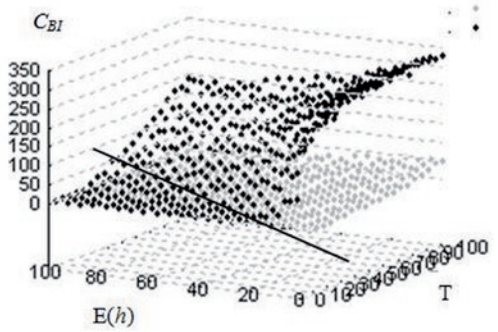

Fig. 4. The expected costs C_{BI} when probability distribution of delay time variable is Weibull distribution

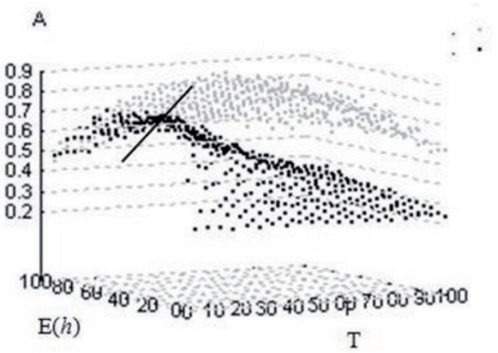

Fig. 5. System availability ratio (A) when probability distribution of delay time variable is Weibull distribution

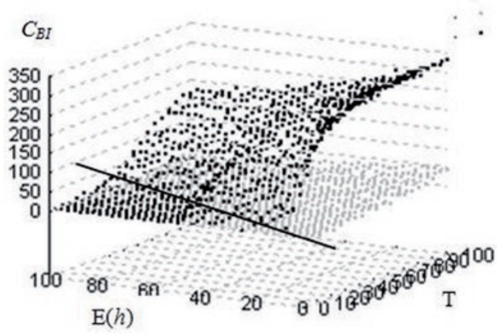

Fig. 6. The expected costs C_{BI} when probability distribution of delay time variable is rectangular distribution

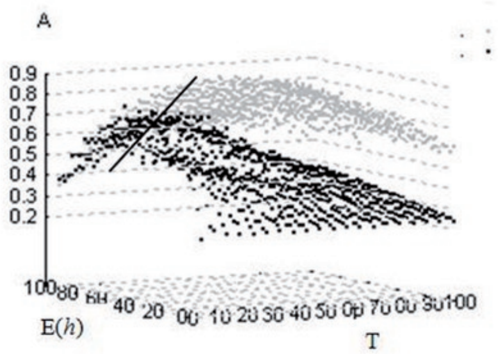

Fig. 7. System availability ratio (A) when probability distribution of delay time variable is rectangular distribution

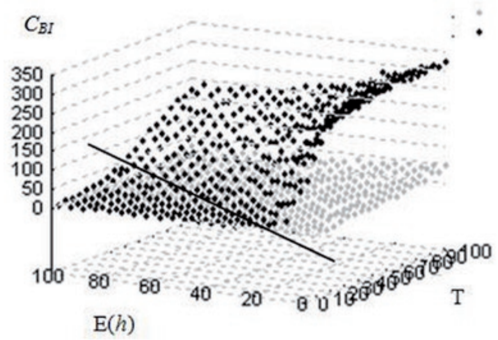

Fig. 8. The expected costs C_{BI} when probability distribution of delay time variable is normal distribution

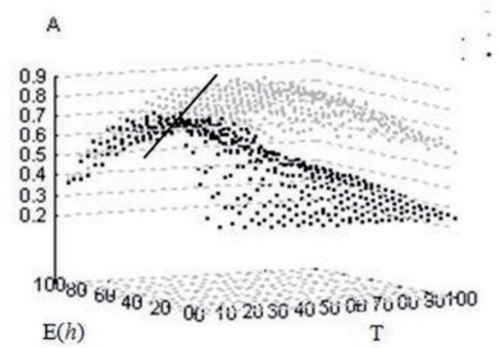

Fig. 9. System availability ratio (A) when probability distribution of delay time variable is normal distribution

The research works [22, 23], which investigate the BIP policy in multi-unit systems performance implementation, determine the relationship between time *T* and the expected value of the variable *h* in systems with serial reliability structure, which is obtained for the lowest maintenance cost and highest system availability:

$$\frac{E(h)}{T} \approx 2 \tag{6}$$

This relationship is shown in the Figures 4 – 9 as an additional line, near which are the best solutions for the economic and availability criteria and analysed expected values E(h). Expression (6) and the results presented in the Figures show that "nearly optimal" period between inspections of the series system performed according to BIP strategy should be determined on the basis of information about the expected value of the delay time.

In order to confirm the fact that the type of the probability distribution of the random variable h has no significant effect on the obtained economical results of BIP use, the relationship described by equation (6) was subjected to further analysis (Figures 10 – 15). For this purpose, all maintenance cost results and system availability ratios, obtained during the simulation experiments are shown in the form of the relationship E(h)/T. The ratio of E(h)/$T \approx 0$ means systems in which:

- the expected value of the elements delay time is very low (short time of defect occurrence before failure),
- the time between inspections T is very overestimated in the relation to the length of the expected elements delay time (wrongly defined time T).

As it can be seen, in both the investigated cases the system economical results, as well as the availability ratio level are very unfavorable. With the increase of the relation E(h)/T, the economic results seem to improve (maintenance costs decrease), there is also observable an increasing system's availability ratio level. The expected maintenance costs of system C_{BI} reaches a minimum at the values of the E(h)/$T \approx 2$ for technical system performing in series reliability structure. The optimal values of costs C_{BI} for the system operating in parallel reliability structure are observed for the smaller value of the relationship E(h)/T, regardless of the type of the probability distribution of the random variable h. In the case, where E(h)/$T >> 2$, maintenance costs are still low what is connected with the "safe" maintenance variant including frequent system elements inspections performance. However, the availability ratio decreases due to the existence of unnecessary, redundant maintenance actions performance. The discussed analysis results are the same for all the studied probability distributions characterizing the elements delay times.

To sum up, the obtained results (Figures 10 – 15) confirm the conclusions reached in the works [22, 23] and lead to the conclusion that the optimal length of time between every inspections performance T can be determined even when we do not have complete information about the form of the probability distribution of the random variable h. The basic parameter of BIP model, which must be evaluated as precisely as possible, is the expected value of the delay time E(h). This is due to its significant impact on all of the system analysed results. On the other hand, for the system in which the random variable h is

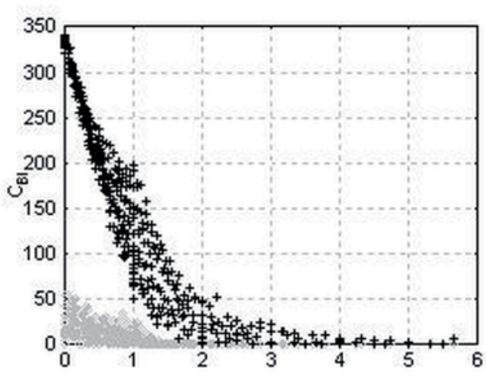

Fig. 10. The expected costs C_{BI} when probability distribution of delay time variable is Weibull distribution

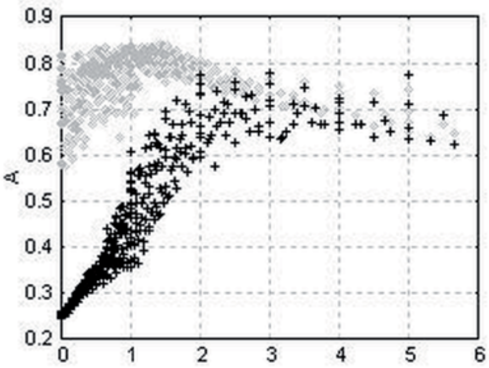

Fig. 11. System availability ratio (A) when probability distribution of delay time variable is Weibull distribution

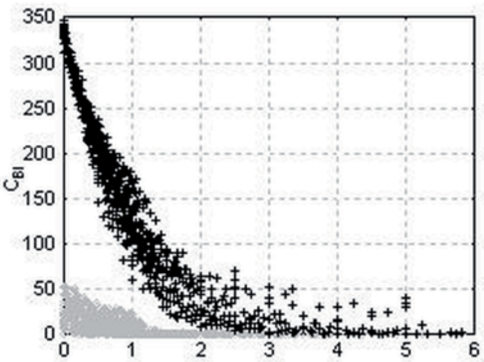

Fig. 12. The expected costs C_{BI} when probability distribution of delay time variable is rectangular distribution

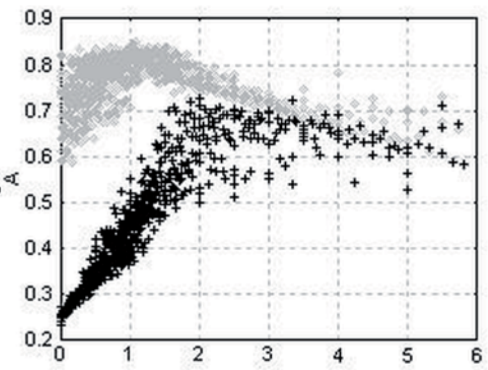

Fig. 13. System availability ratio (A) when probability distribution of delay time variable is rectangular distribution

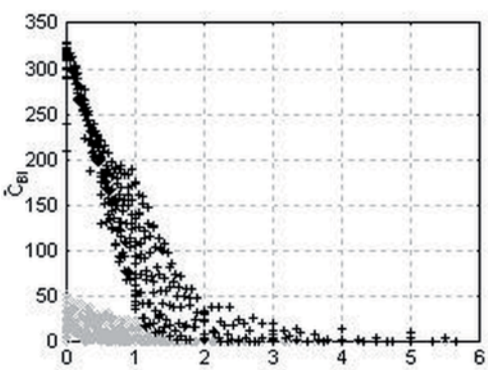

Fig. 14. The expected costs C_{BI} when probability distribution of delay time variable is normal distribution

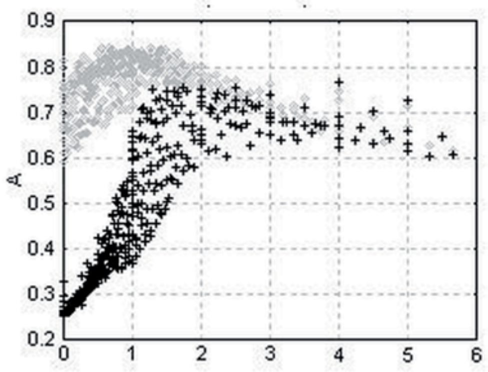

Fig. 15. System availability ratio (A) when probability distribution of delay time variable is normal distribution

described by the rectangular probability distribution, one can detect an economic results variability in the area of their obtained minimum point (Figures 12, 13, E(h)/$T \approx 2$). Unlike the results obtained for other types of probability distributions of the random variable h, even for the relation E(h)/$T > 3$ there are cases where the costs $C_{BI} > 30$. These results confirm that greater dispersion of the values of the variable h (and hence its less predictability) reduces the effectiveness of the BIP strategy implementation. It also means, that if there is a practical possibility, there should be estimated the standard deviation of the random variable – delay time. The exemplary results, obtained for different values of variation coefficient (v) and identical expected value delay time (E(h) = 35) for two probability distributions of the variable h: rectangular and Weibull ones, are presented in the Fig. 16 – 17. These results give us the possibility to conclude, that:

- despite various forms of the probability distributions of random variable h, the economical results are very similar for a similar range of variation coefficient v and time period T,
- when $v = 0$, the system components should be inspected when T = E(h),
- the increasing variation coefficient of the variable h causes, that the "optimum" time between inspections T should be reduced in relation to the expression (6),
- in order to choose the best period between inspections T, one should try to estimate the variability range of the delay time real values, such as the variation coefficient.

The results shown in the Figures 4 – 17 are the basis for the response to the second question defined in the initial part of the chapter relating to the potential consequences of improper estimation of the parameters of the variable h. The consequences level (e.g. financial ones) depends on the level of committed error. Basic observations of obtained results indicate, that the bad estimation of the parameter

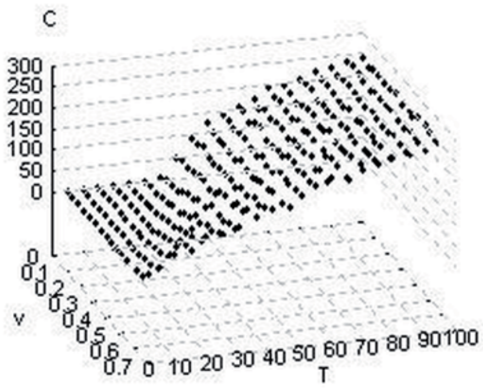

Fig. 16. The expected costs C_{BI} for various values of variation coefficient (v) of delay time parameter when probability distribution of delay time variable is rectangular distribution

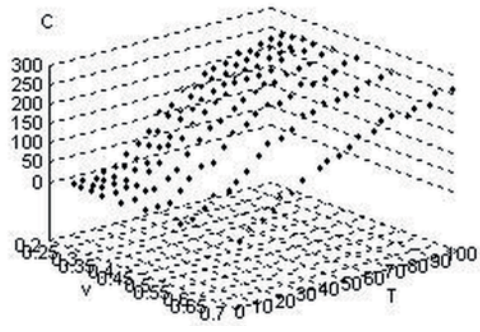

Fig. 17. The expected costs C_{BI} for various values of variation coefficient (v) of delay time parameter when probability distribution of delay time variable is Weibull distribution

E(h) value causes a significant difference between the value of estimated time between inspections T and the value obtained from equation (6). As a result, it can impair the efficiency of the results of BIP strategy implementation. This effect is particularly easy to observe when the expected value of the variable h is overvalued relative to its actual value. Following this, the selected time between inspections T (too long) will cause, that the ratio satisfies the following inequality: E(h)/$T < 2$. Thus, this can cause significant financial and reliability consequences.

4. Summary

The obtained research results of the BIP model analysis allow obtaining a preliminary answer to the question of how the level of delay time parameter estimation may affect the performance of the technical system. The analysis involved observation of the impact of the expected value of the variable h and the forms of the three selected probability distributions of this random variable on the performance level of multi-element technical system in "*k-out-of-n*" reliability structure. There were also analysed certain rules of BIP policy implementation, defined by the authors in [22, 23].

On the basis of this carried out research study, it can be concluded that:

- the main parameter that must be estimated as accurately as it is possible, based on the available statistical data, is the expected duration of the delay time; this parameter unequivocally influences the analyzed cost and reliability results,
- the knowledge about the form of probability distribution of random variable h is important only from the point of view of its dispersion and need not be estimated on the basis of statistical data,
- when there is a possibility to estimate the dispersion of random variable h results, it should be assessed to properly define the time between inspections T,
- there should be conducted further research to determine type of influence of the variation coefficient on optimization formula, described in equation (6).

In the article, authors continue their research related to the DT modelling for multi-unit systems developed in [22, 23, 25, 32]. The next step of our research analysis should be connected with its complementation for assumption of a constant mean value and standard deviation of a variable h. Moreover, authors focus on definition of the DT models implementation possibilities for real technical systems performance optimization (e.g. imperfect maintenance assumption). This will allow defining the basic principles of preventive maintenance policy selection process from the point of view of the person who manages the operational processes of technical system.

References

1. Akbarov A, Christer AH, Wang W. Problem identification in maintenance modeling: a case study. International Journal of Production Research 2008; 46(4): 1031-1046.
2. Alzubaidi HJ. Maintenance modelling of a major hospital complex. PhD thesis. Salford: University of Salford, 1993.
3. Baker RD, Christer AH. Review of delay-time OR modelling of engineering aspects of maintenance. European Journal of Operational Research 1994; 73: 407-422.
4. Baker RD, Wang W. Developing and testing the delay-time model. Journal of the Operational Research Society 1993; 44: 361-374.
5. Baker RD, Wang W. Estimating the delay-time distribution of faults in repairable machinery from failure data. IMA Journal of Mathematics Applied in Business & Industry 1992; 3: 259-281.
6. Choi K-M. Semi-Markov and Delay Time Models of Maintenance. PhD thesis. Salford: University of Salford, 1997.
7. Christer AH. A Review of Delay Time Analysis for Modelling Plant Maintenance. in: Stochastic Models in Reliability and Maintenance, Osaki S. (ed.), Springer, 2002.
8. Christer AH. Developments in delay time analysis for modelling plant maintenance. Journal of the Operational Research Society 1999; 50: 1120-1137.
9. Christer AH. Delay-time model of reliability of equipment subject to inspection monitoring. Journal of the Operational Research Society 1987; 38, (4): 329-334.
10. Christer AH. Modelling inspection policies for building maintenance. Journal of the Operational Research Society 1982; 33: 723-732.
11. Christer AH, Lee C, Wang W. A data deficiency based parameter estimating problem and case study in delay time PM modelling. International Journal of Production Economics 2000; 67: 63-76.
12. Christer AH, Redmond DF. Revising models of maintenance and inspection. International Journal of Production Economics 1992; 24: 227-234.
13. Christer AH, Redmond DF. A recent mathematical development in maintenance theory. IMA Journal of Mathematics Applied in Business and Industry 1990; 2: 97-108.
14. Christer AH, Waller WM. An operational research approach to planned maintenance: modelling P.M. for a vehicle fleet. Journal of the Operational Research Society 1984; 35(11): 967-984.
15. Christer AH, Waller WM. Reducing production downtime using delay-time analysis. Journal of the Operational Research Society 1984; 35(6): 499-512.
16. Christer AH, Waller WM. Delay Time Models of Industrial Inspection Maintenance Problems. Journal of the Operational Research Society 1984; 35(5): 401-406.
17. Christer AH, Wang W. A delay-time-based maintenance model of a multi-component system. IMA Journal of Mathematics Applied in Business & Industry 1995; 6: 205-222.
18. Christer AH, Wang W, Baker R, Sharp J. Modelling maintenance practice of production plant using delay-time concept. IMA Journal of Mathematics Applied in Business and Industry 1995; 6: 67- 84.
19. Christer AH, Wang W, Sharp J, Baker R. A case study of modelling preventive maintenance of production plant using subjective data. Journal of the Operational Research Society 1998; 49: 210-219.
20. Christer AH, Whitelaw J. An operational research approach to breakdown maintenance: problem recognition. Journal of the Operational Research Society 1983; 34(11): 1041-1052.
21. Desa MI, Christer AH. Modelling in the absence of data: a case study of fleet maintenance in a developing country. Journal of the Operational Research Society 2001; 52(3): 247-260.
22. Jodejko-Pietruczuk A, Werbińska-Wojciechowska S. Economical effectiveness of Delay Time approach using in Time-Based maintenance modelling. Proc. of PSAM 11 & ESREL 2012 Conference, 25-29 June 2012, Helsinki, Finland.
23. Jodejko-Pietruczuk A, Werbińska-Wojciechowska S. Analysis of Block-Inspection Policy parameters from economical and availability point of view. Proc. of PSAM 11 & ESREL 2012 Conference, 25-29 June 2012, Helsinki, Finland.
24. Lee Ch. Applications of Delay Time Theory to Maintenance Practice of Complex Plant. PhD thesis. Salford: University of Salford, 1999.
25. Nowakowski T, Werbińska-Wojciechowska S. Developments of time dependencies modeling concepts. Proc. of the European Safety and Reliability Conference, ESREL 2011, Troyes, France, 18-22 September 2011: 832-838.
26. Redmond DF. Delay Time Analysis in Maintenance. PhD thesis. Salford: University of Salford, 1997.
27. Wang W. An overview of the recent advances in delay-time-based maintenance modelling. Reliability Engineering and System Safety 2012; 106: 165-178.
28. Wang H. A survey of maintenance policies of deteriorating systems. European Journal of Operational Research 2002; 139: 469-489.
29. Wang W. Subjective estimation of delay-time distribution in maintenance modelling. European Journal of Operational Research 1997; 99: 511-529.
30. Wang W, Jia X. An empirical Bayesian based approach to delay time inspection model parameters estimation using both subjective and objective data. Quality and Reliability Engineering International 2007; 23: 95-105.
31. Wen-yuan LV, Wang W. Modelling preventive maintenance of production plant given estimated PM data and actual failure times. Proc. of International Conference on Management Science and Engineering ICMSE'06, Lille, 2006.
32. Werbińska-Wojciechowska S. Problems of logistics systems modelling with the use of DTA approach. Logistics and Transport 2012; 2: 63-74.

Anna JODEJKO-PIETRUCZUK
Sylwia WERBIŃSKA-WOJCIECHOWSKA
Mechanical Engineering Faculty
Wrocław University of Technology
Wybrzeże Wyspiańskiego 27, 50-370, Wrocław, Poland
E-mail: sylwia.werbinska@pwr.wroc.pl

Article citation info:
ZHANG X, KANG J, BECHHOEFER E, ZHAO J. A new feature extraction method for gear fault diagnosis and prognosis. Eksploatacja i Niezawodnosc – Maintenance and Reliability 2014; 16 (2): 295–300.

Xinghui ZHANG
Jianshe KANG
Eric BECHHOEFER
Jianmin ZHAO

A NEW FEATURE EXTRACTION METHOD FOR GEAR FAULT DIAGNOSIS AND PROGNOSIS

NOWA METODA DIAGNOZOWANIA I PROGNOZOWANIA USZKODZEŃ PRZEKŁADNI Z WYKORZYSTANIEM EKSTRAKCJI CECH

Robust features are very critical to track the degradation process of a gear. They are key factors for implementing fault diagnosis and prognosis. This has driven the need in research for extracting good features. This paper used a new method, Narrowband Interference Cancellation, to suppress the narrow band component and enhance the impulsive component enabling the gear fault detection easier. This method can improve the signal to noise ratio of impulse train associated with the gear fault frequency. A run-to-failure test is used to demonstrate the method's effectiveness. Based on the time synchronous signal of high speed shaft, Sideband Index is extracted from the signals processed by Narrowband Interference Cancellation. This feature has good degradation trend than traditional Sideband Index extracted from the time synchronous average signal directly. Comparison of features based on different extraction process proves the effectiveness of developed method.

Keywords: *Narrowband Interference Cancellation, degradation, fault diagnosis, fault prognosis, sideband index.*

Cechy odporne (robustfeatures) mają krytyczne znaczenie w trakcie śledzenia procesu degradacji przekładni. Stanowią one kluczowy czynnik w procesie diagnozowania i prognozowania uszkodzeń. Fakt ten stwarza w badaniach naukowych potrzebę ekstrakcji pożądanych cech. W niniejszej pracy wykorzystano nową metodę, tzw. metodę eliminacji zakłóceń wąskopasmowych (NarrowbandInterferenceCancellation), za pomocą której można wytłumić składową wąskopasmową, a wzmocnić składową impulsową, co ułatwia wykrywanie uszkodzeń przekładni. Metoda ta pozwala poprawić stosunek sygnału do szumu w szeregu impulsów związanym z częstotliwością charakteryzującą uszkodzenie przekładni. Skuteczność przedstawionej metody można wykazać za pomocą badań typu „pracuj do awarii" (run-to-failure) . Na podstawie synchronicznego sygnału wału wysokoobrotowego, z sygnałów przetwarzanych za pomocą metody eliminacji zakłóceń wąskopasmowych ekstrahuje się wskaźnik wstęgi bocznej (Sideband Index). Cecha ta ma lepszy trend degradacji niż tradycyjny wskaźnik wstęgi bocznej ekstrahowany bezpośrednio z sygnału uśrednionego synchronicznie w czasie. Porównanie cech wyodrębnionych w różnych procesach ekstrakcji dowodzi skuteczności opracowanej metody.

Słowa kluczowe: *Eliminacja zakłóceń wąskopasmowych, degradacja, diagnoza uszkodzeń, prognozowanie uszkodzeń, wskaźnik wstęgi bocznej.*

1. Introduction

Gears are critical elements in complex machinery, such as helicopter, wind turbine etc. Gear faults misdetection will increase the overall cost of customer or even lead to disaster. Condition based maintenance (CBM) [7] and Prognostics and Health Management (PHM) [5] are developed for supplement the traditional maintenance methods of capital equipment. Most operations and maintenance (O&M) organization are using fault diagnosis and prognosis to improve logistics support of high value equipment. As we know, extracting good features are key steps for effective fault diagnosis and prognosis. For vibration signals based gear fault diagnosis, there are time domain analysis, frequency domain analysis and time-frequency domain analysis. Some statistical features extracted from time domain signals can detect abnormal of gear effectively [10]. However, these techniques are limited in their ability to provide actionable information as to the location of the fault in the gearbox. Frequency domain analysis is difficult for gear faults involving soft/broken teeth as the FFT is not sensitive to impact events.

For many industries (wind farms for example), the investment in the infrastructure to support on-line analysis has not been made and the hardware is unavailable to record vibration signals of every inspection. That is, the cost benefic ratio of on-line equipment is not great enough to convince O&M organization to invest. The goal of this study is to develop robust analysis techniques such that the business case for implementing on-line analysis is made.

As noted, frequency analysis alone has limited effectiveness for some types of faults that occur on gears. Therefore, other time frequency analysis techniques are needed to allow development of condition indicators sensitive to impact/soft tooth/broken tooth faults. For the normal case, statistics of these condition indicators are calculated. Then if condition indicators exceed the predefined thresholds, this denotes the system abnormal. Additional frequency spectrum analysis can be implemented to the raw vibration signal recorded provide more actionable information: e.g. the fault locations in the gearbox. When the operating conditions are un-stationary, time-frequency analysis can be used to fix the fault location and severity.

For the whole degradation process of gear, we expect to detect fault as early as possible and extract effective features that have good deterioration trend. In real world condition, a fault signature is small relative to the vibration signals. The impulsive signals produced by incipient faults are immersed in quasi-stationary signal with far greater energy (e.g. gear mesh, shaft rates) which are noise in the fault detection process. Additionally, because acceleration is the second derivative of displacement, the problem is especially difficult on low speed shaft encountered on wind turbines (main shaft rate of 0.15 to 0.25 Hz for large machines).

In practice, for statistical features extracted from time domain signals or frequency domain analysis, it is very difficult to detect incipient fault of gears of low speed shaft. Wang and Wong [11] developed an autoregressive (AR) model based filtering technique to enhance the gear fault diagnosis. Then, Endo and Randall [6] proposed the use of the minimum entropy deconvolution (MED) technique to enhance the ability of the existing AR model based filtering technique to detect gear faults. AR model can filter the gear meshing waveforms out and only retain the impulsive signal produced by faults, allowing earlier fault detection. The MED searches for an optimum set of filter coefficients that recover the output signal with the maximum value of kurtosis. Therefore, it can enhance the gear fault impulses enabling the fault detection easily (assuming that there are no other impulsive sources, such as a bearing fault).

A limitation of the AR-MED method is the preference of the MED algorithm to deconvolve only a single impulse or a selection of impulses, as opposed to the desired periodic impulses repeating at the period of the fault. Inspired by the MED deconvolution technique, McDonald et al. [9] proposed an improved novel deconvolution norm, Correlated Kurtosis, which takes advantage of the periodicity of the faults and requires no AR model stage prior to deconvolution. Zhang et al. [12] developed a new condition indicator tracking the gear degradation under un-stationary condition based on the AR filtering. In the signals of gear faults, there is a number of narrow band tones and broad noise which mask the desired impulsive signal produced by gear faults. If one can find an effective method that can remove the narrow band tones out, the impulsive signal will be easily detected. Recently, Bechhoefer [2] developed a new method called Narrowband Interference Cancellation (NIC) to enhance the gear fault detection. This method can filter the narrow band signals out. So, the impulsive signals are enhanced.

Based on the work of Bechhoefer, this paper proposes a new feature, which can track the gear degradation effectively. Time synchronous (TS) technology is used to compensate the varying rotation speed. Then, NIC is implemented to filter the narrow band signal out. Finally, sideband index mentioned in [1] is extracted from post-NIC signals. The results demonstrate that this condition indicator is more robust than others.

2. Narrowband Interference Cancellation

We can categorize gears faults in two basic categories: wear (scuffing, micro-pitting) or breakage (soft tooth/broken tooth/crack tooth, etc). The second fault mode is of great interest because it can cause catastrophic fault of a gearbox. These types of faults are characterized by generated an impulse signals with the relative characteristic frequencies. The vibration signals collected from machines contain gear mesh, shaft rotation, bearing vibration and random noise, along with the impulsive signal of interest. The quasi-stationary signals produced by gear and shaft are narrowband, while the impulse signals generated by gear faults are in a wideband. Usually, the gear fault signals are very weak compared to the gear mesh tones and shaft rotation. Therefore, if we can cancel these narrowband signals, the gear faults will be detected easily. This phenomenology can be modeled as:

$$x(n) = s(n)+y(n)+v(n) \tag{1}$$

where

$s(n)$ is the signal of interest,

$y(n)$ is the signal associated with gear mesh, shafts rotation, e.g. interference,

$v(n)$ is random noise.

The interference signal is usually large compared to the signal of interest. It is necessary to remove the interfering signal $y(n)$ from $x(n)$ while preserving the signal of interest $s(n)$. Since the measured signal $x(n)$ and the interference signal $y(n)$ are correlated, one can estimate the interference using an optimal linear estimator:

$$\hat{y}(n) = \mathbf{c}_0^H \mathbf{x}\left(n-D\right) \tag{2}$$

$$\mathbf{R}\mathbf{c}_0 = \mathbf{d} \tag{3}$$

$$\mathbf{R} = E\{\mathbf{x}(n\text{-}D)\mathbf{x}^H(n\text{-}D)\} \tag{4}$$

$$\mathbf{d} = E\{\mathbf{x}(n\text{-}D)y^*(n)\} \tag{5}$$

where D is an integer delay operator. If D=1, then Eq. (2) is the LS forward linear predictor. If $\hat{y}(n) = y(n)$, the output of the filter is $x(n)$- $\hat{y}(n)$ = $s(n)+v(n)$. This means we can completely remove the interference and only the desired signal and noise remains. In practice, signal $y(n)$ is not available. To overcome this obstacle, we can use a minimum means square error D-step forward linear predictor, such that:

$$e^{\mathrm{f}}(n) = x(n)+\mathbf{a}^H\mathbf{x}(n\text{-}D) \tag{6}$$

$$\mathbf{R}\mathbf{a} = \text{-}\mathbf{r}^{\mathrm{f}} \tag{7}$$

where:

$$\mathbf{r}^{\mathrm{f}} = E\{\mathbf{x}(n\text{-}D)x^*(n)\} \tag{8}$$

For this modeling, the components of the observed signal have the following properties:

- The signal of interest $s(n)$, the interference signal $y(n)$, and the noise signal $v(n)$ are mutually uncorrelated.
- The noise signal $v(n)$ is white.
- The signal of interest $s(n)$ is wideband and has a short correlation length (e.g. its impulsive).
- The interference signal $y(n)$ has a long correlation length: its autocorrelation length takes significant values over the range $0 \leq |l| \leq M$, for $M>D$.

In practice, the second and third properties mean that the desired signal and the noise are approximately uncorrelated after a certain small lag. These are precisely the properties exploited by the canceller to separate the narrowband interference from the desired signal and the background noise.

According to the first assumption, we have:

$$E\{x(n\text{-}k)y^*(n)\}=E\{y(n\text{-}k)y^*(n)\}=r_y(k) \tag{9}$$

$$r_x(l) = r_s(l) + r_y(l) + r_v(l) \tag{10}$$

If the second and third modeling assumptions hold true, we have:

$$r_x(l) = r_y(l) \text{ for } l \neq 0, 1, \ldots, D\text{-}1 \tag{11}$$

The exclusion of the lags for $l \neq 0, 1, \ldots, D$-1 in **r** and **d** is critical, and we have arranged for that by forcing the filter and the predictor to form their estimates using the *delayed* data vector $\mathbf{x}(n\text{-}D)$. From (5), (8), and (11), we conclude that $\mathbf{d} = \mathbf{r}^f$ and therefore $\mathbf{c}_0 = \mathbf{a}_0$. Thus, the optimum NBI estimator $\mathbf{c}_0$ is equal to the D-step linear predictor $\mathbf{a}_0$, which can be determined exclusively from the input signal $x(n)$. Then, the signal with interference removed is:

$$x(n) - \hat{y}(n) = x(n) - a_0^H \mathbf{x}(n-D) = e^f(n) \tag{12}$$

which is identical to the D-step forward prediction error. This leads to the linear prediction NIC shown in Figure 1. For a full description of the analysis, we can see (Manolakis et al. 2000) [9].

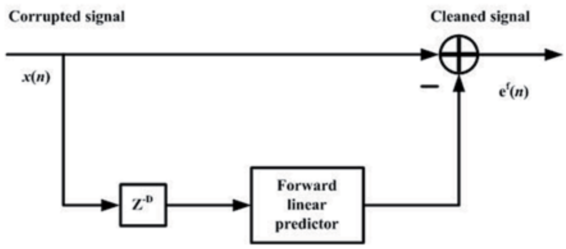

Fig. 1. Block diagram of linear prediction NBI canceller

3. Experiment

Figure 2 shows the experimental system used in this paper to verify the performance of the proposed method. The system includes a gearbox, a 4 kW three phase asynchronous motor for driving the gearbox, and a magnetic powder brake for loading. The motor rotating speed is controlled by an electromagnetic speed-adjustable motor, which allows the tested gear to operate under various speeds. The load is provided by the magnetic powder brake connected to the output shaft and the torque can be adjusted by a brake controller.

The data acquisition system is composed of acceleration transducers, PXI-1031 mainframe, PXI-4472B data acquisition cards, and LabVIEW software. The type of transducers is 3056B4 of Dytran Company. There are four transducers which are mounted in different places on gearbox. In order to acquire the speed and torque information, a speed and torque transducer is installed in the input shaft as illustrated in Figure 2. For this transducer, one revolution of input shaft will produce 60 impulses.

As shown in Figure 3, the gearbox has three shafts, which are mounted to the gearbox housing by rolling element bearings. Gear 1 on low speed (LS) shaft has 81 teeth and meshes with gear 3 with 18

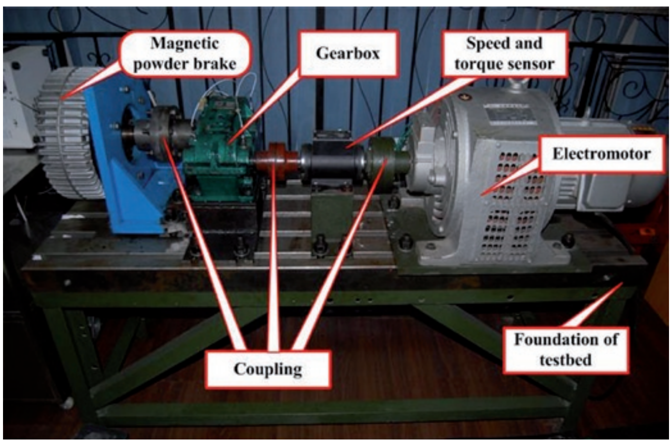

Fig. 2. Test-rig of gearbox

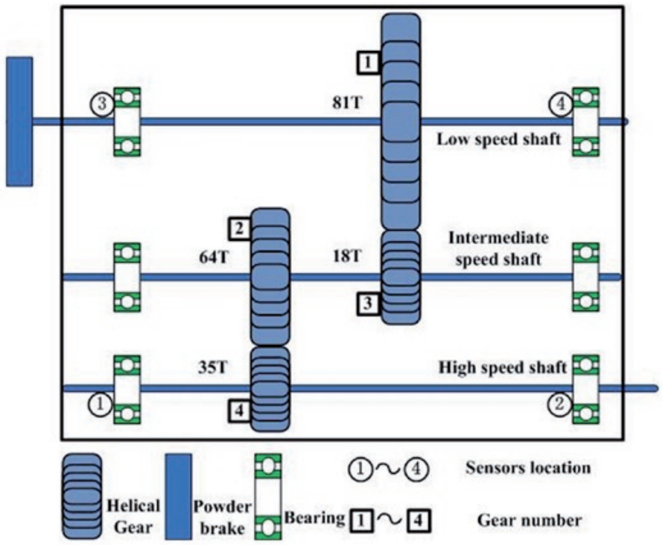

Fig. 3. Structure of gearbox and the transducers location

teeth. Gear 2 on Intermediate speed (IS) shaft has 64 teeth and meshes with gear 4, which is on the high speed (HS) shaft and has 35 teeth.

This experiment is a run-to-failure (RTF) test. It operated from normal to failure. When the vibration amplitude exceeds the 60 m/s^2, we define the gearbox failure. The whole process took 548 hours under approximate speed 1200 rpm and load 15 N•m. In this test, the sampling frequency was 20 KHz for 12 second. The sampling interval between two consecutive inspections is ten minutes. During the test, the gearbox was periodically inspected. It was found that the main fault mode was wear. Gear 2, 3, and 4 had slight wear. Gear 1 has serious wear and some teeth were broken. Then, the whole degradation process can be depicted as follows. When a normal gear operates some time, some pitting fault will appear on the gear face. With the time elapse, these pitting faults will extend to the spalling and lead to broken tooth finally. The degradation process of gear 1 can be depicted as Figure 4.

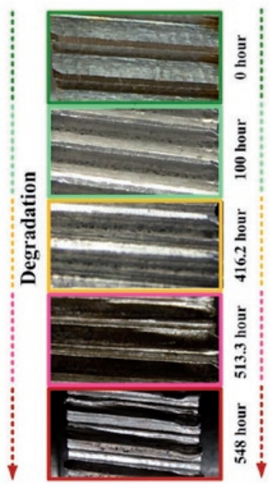

Fig. 4. Fault propagation over time

4. Data analysis and discussion

4.1. Degradation feature extraction

Because the rotating speed during the signal acquisition has small fluctuations, TS technology [3] must be used to mitigate the influence of varying speed. This was done by resampling the vibration data relative to a key-phasor [9]. Then, NIC is used to remove the narrowband signals out. Finally, sideband index (SI) is extracted from the NIC signals. SI is the average of the first order sidebands of the fundamental gear meshing frequency. It can be represented as Equation 13:

$$SI = (R_{I,-1}(x) + R_{I,+1}(x))/2 \tag{13}$$

In this analysis, the HS shaft is the synchronous shaft. In this paper, the parameters D and M of NIC are selected as 1 and 32 for all the data processing. For the RTF test described in Section 3, there are 3,288 inspection points in the gearbox life. From Figure 4, we can see that the gear had some incipient pitting fault in the face when it operated until 100 hours. In order to demonstrate the effectiveness of NIC technology, data collected at inspection point 601 (the first inspection point after 100 hours) was selected as the processing object. After time synchronous and NIC processing, results of time domain and frequency domain can be seen in Figure 6 and Figure 8.

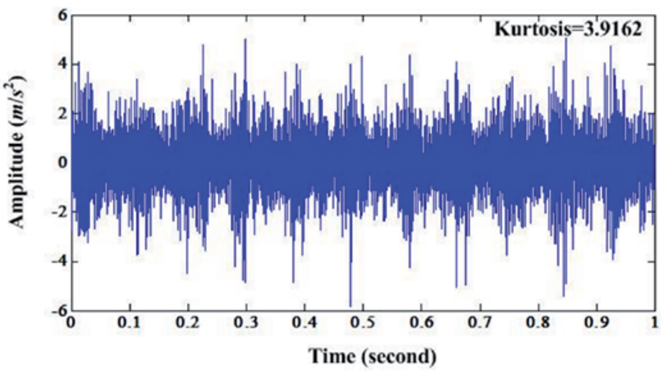

Fig. 5. Time domain signal of inspection point 601 without NIC processing

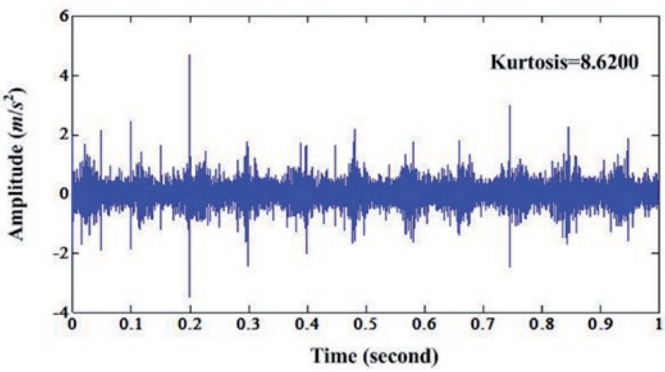

Fig. 6. Time domain signal of inspection point 601 after NIC processing

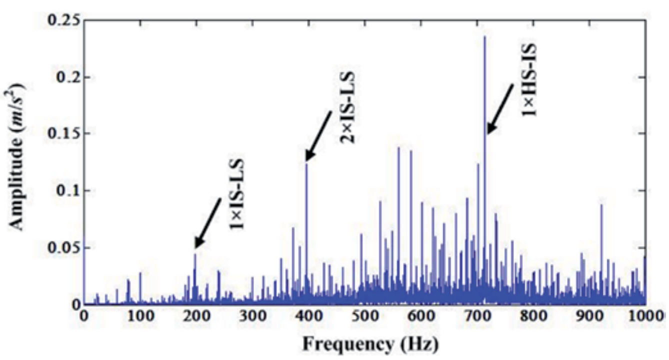

Fig. 7. Frequency domain information of inspection point 601 without NIC processing

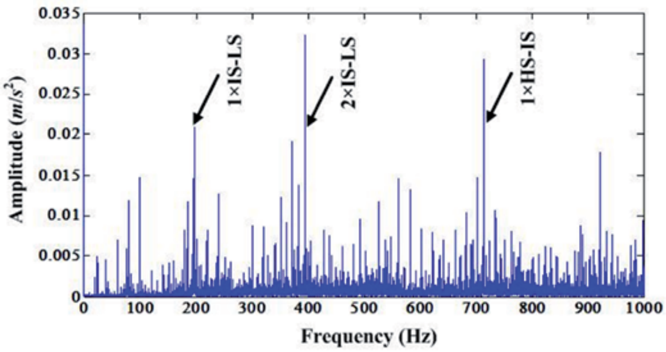

Fig. 8. Frequency domain information of inspection point 601 after NIC processing

Figure 5 is the time domain signal of inspection point 601 without NIC processing. Compared to the Figure 6, its kurtosis value is smaller. This denotes that NIC processing isolated the fault, which is impulsive in nature (e.g. higher kurotosis). From the view of frequency analysis, it is seen that the mesh tones of HS-IS (702.5764 Hz) are dominant in the frequency spectrum without NIC processing, as depicted in Figure 7. The main fault is found on gear 1. Mesh frequency of IS-LS (197.5996 Hz) and its harmonics should be dominant in the spectrum. Compared to Figure 7, Figure 8 shows that spectral energy of HS-IS (narrowband signal) is suppressed after NIC processing. This enabled the fault detection of gear 1 be more easily detected. Finally, the robust degradation feature SI can be extracted from the RTF data sets as illustrated in Figure 9.

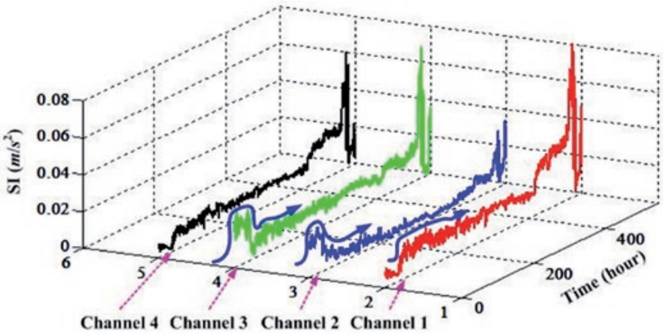

Fig. 9. Degradation feature SI extracted from NIC signal of four channels

From the Figure 9, we can see that degradation feature SI of channel four has the best performance. Its degradation trend is better than the features of other three channels. Degradation feature of channel 1increase after the gearbox operating a short time and it decrease gradually at the initial stage of gearbox's life. This is wear in, could possible affect the effectiveness of prognostic algorithms. Similarly, degradation features of channel 2 and channel 3 have high values at beginning and then enter into a relatively stationary process. These kinds of features will lead to ineffectiveness of the prognostic algorithms. In Figure 9, curves with arrow are used to denote the abnormal feature fluctuation.

4.2. Discussion

(1) In reference [9], degradation feature SI was extracted from time synchronous average (TSA) signals. We compared the SI extracted from TSA signals with the SI extracted from the NIC-TS signals. Here, the synchronous shaft is the LS shaft. SI extracted from TSA signals of four channels are depicted in Figure 10. Similar to Figure 9, degradation feature SI of channel four is the best. Figure 11 is the comparison of feature SI extracted from NIC-TS signals (showed in Figure 9) and TSA signals (showed in Figure 10) of channel four. It is showed

that SI extracted from NIC-TS signal is smoother than the SI extracted from TSA signals. SI extracted from TSA signals has large fluctuations at the early stage of gearbox's life.

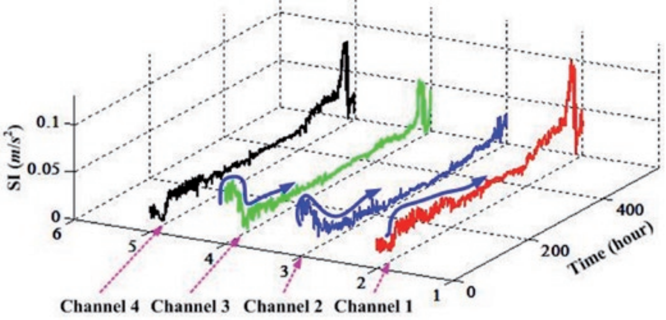

Fig. 10. Degradation feature SI extracted from TSA signal of four channels

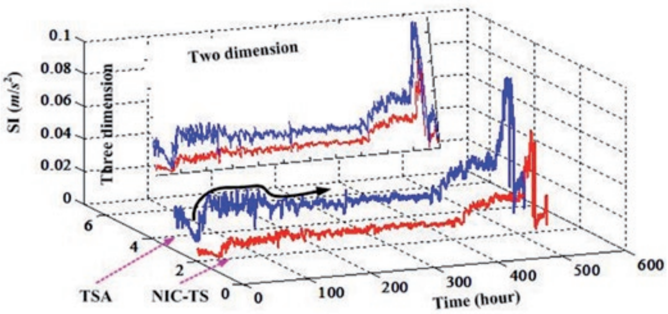

Fig. 11. Comparison of SI extracted from TSA and NIC-TS signals of channel four

(2) In section 4.1, the NIC was used to process the TS signal in which the HS shaft is the synchronous shaft. If the LS shaft is the synchronous shaft, the SIs based on the NIC-TSA processing and NIC-TS processing should be investigated. Figure 12 is the feature SI extracted from the NIC-TSA signals. It shows that all features SI of four channels have large fluctuations in the whole degradation process.

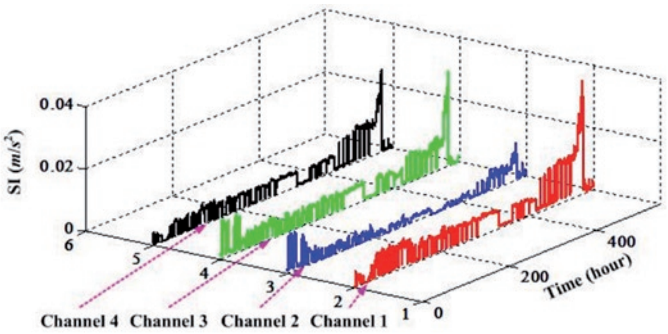

Fig. 12. SI extracted from NIC-TSA signals of four channels

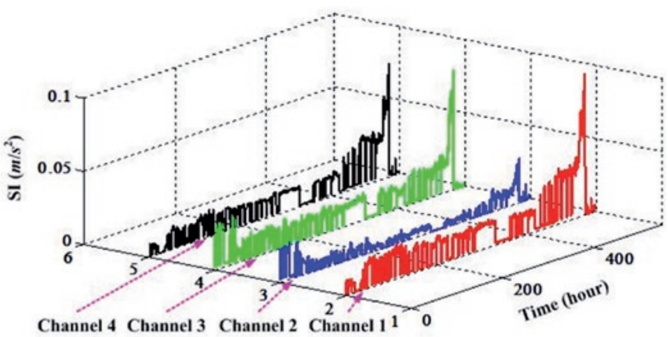

Fig. 13. SI extracted from NIC-TS signals of four channels

Figure 13 is the features SI extracted from the NIC-TS signals. It is very similar to Figure 12. Therefore, the degradation feature SI directly extracted from NIC-TS signal of HS shaft has the best performance.

From Figure 12 and Figure 13, it can be seen that all the features of four channels have large fluctuation when the gearbox degraded. Using LS shaft as the synchronous shaft, the TSA signal will have a very long length for one revolution. Really, there is nothing up there but noise which is due to the interpolation. So, this leads to the feature fluctuation.

(3) In this paper, the parameters *D* and *M* of NIC are selected by experience. The optimization of these two parameters can be investigated in future to enhance the NIC ability. Another problem is that the rotation speed and load are varying with time as depicted in Figure 14 and Figure 15. Even if the varying range is small, this will have certain influence to the trend of degradation feature. In real, taking wind turbine for example, its rotation speed and load are varying with wind speed. So, robust features which are not sensitive to speed and load varying need to be investigated in the future work.

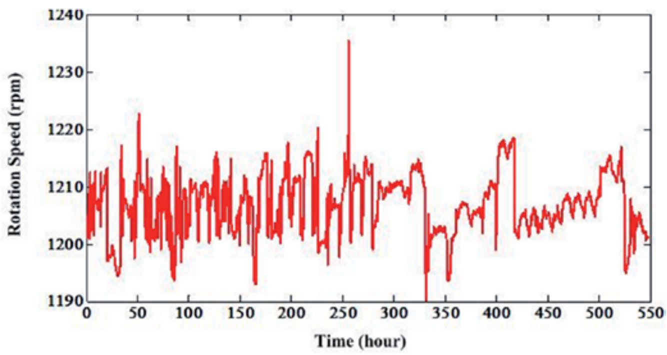

Fig. 14. Rotation speed of gearbox RTF data

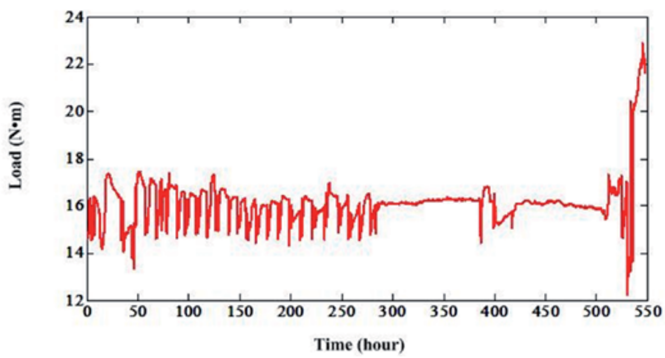

Fig. 15. Load of gearbox RTF data

5. Conclusion

This paper uses a new method NIC that can enhance the impulse signals produced by gear faults. NIC technology can suppress the interference of narrow band signal. Based on the TS signal of HS shaft, robust degradation feature can be extracted after NIC processing. Various results comparison from different view demonstrated the effectiveness of the proposed method.

References

1. Antolick LJ, Branning JS, Wade DR, and Dempsey PJ. Evaluation of gear condition indicator performance on rotorcraft fleet. 66th American helicopter society 2010.
2. Bechhoefer E, Li RY and He D. Quantification of condition indicator performance on a split torque gearbox. Journal of Intelligent Manufacturing 2012; 23(2): 213-220.
3. Bechhoefer E and Kingsley M. A review of time synchronous average algorithms. Annual Conference of the Prognostics and Health Management Society 2009.
4. Bechhoefer E, Van Hecke B and He D. Processing for Improved Spectral Analysis. Annual Conference of the Prognostics and Health Management Society 2013.
5. Brown ER, McCollom NN, Moore EE, and Hess A. Prognostics and Health Management: A Data-Driven Approach to Supporting the F-35 Lightning II. IEEE Aerospace Conference 2007.
6. Endo H and Randall RB. Enhancement of autogressive model based gear tooth fault detection technique by the use of minimum entropy deconvolution filter. Mechanical Systems and Signal Processing 2007; 21(2): 906-919.
7. Jardine AKS, Lin D, and Banjevic D. A review on machinery diagnostics and prognostics implementing condition-based maintenance. Mechanical Systems and Signal Processing 2006; 20(7): 1483-1510.
8. McDonald G L, Zhao Q, and Zuo MJ. Maximum correlated Kurtosis deconvolution and application on gear tooth chip fault detection. Mechanical Systems and Signal Processing 2012; 33: 237-255.
9. Manolakis D, Ingle V and Kogon S. Statistical and adaptive signal processing. 2005; New York, NY: McGraw-Hill.
10. Samuel PD and Pines DJ. A review of vibration-based techniques for helicopter transmission diagnostics. Journal of Sound and Vibration 2005; 282(1-2): 475-508.
11. Wang WY and Wong AK. Autoregressive model-based gear fault diagnosis. Journal of vibration and acoustics 2002; 24(2): 172-179.
12. Zhang XH, Kang JS, Zhao JS and Cao DC. Features for fault diagnosis and prognosis of gearbox. Chemical Engineering Transactions 2013; 33: 1027-1032.

Xinghui ZHANG
Jianshe KANG
Jianmin ZHAO
Mechanical Engineering College
Shijiazhuang, 050003, China
E-mails: dynamicbnt@gmail.com, jskang201206@126.com, Jm_zhao@hotmail.com

Eric BECHHOEFER
GPMS LLC
Cornwall, VT, USA
E-mail: eric@gpms-vt.com

Article citation info:
BUCHACZ A, PŁACZEK M, WRÓBEL A. Modelling of passive vibration damping using piezoelectric transducers – the mathematical model. Eksploatacja i Niezawodnosc – Maintenance and Reliability 2014; 16 (2): 301–306.

Andrzej BUCHACZ
Marek PŁACZEK
Andrzej WRÓBEL

MODELLING OF PASSIVE VIBRATION DAMPING USING PIEZOELECTRIC TRANSDUCERS – THE MATHEMATICAL MODEL

MODELOWANIE PASYWNEGO TŁUMIENIA DRGAŃ PRZY UŻYCIU PRZETWORNIKÓW PIEZOELEKTRYCZNYCH – MODEL MATEMATYCZNY*

A proposal of mathematical modelling of vibrating piezoelectric transducers using the electrical analogy is presented in this work. The developed mathematical model is used in analysis of vibrating piezoelectric plates with adjoined external passive electric elements and for designating of their characteristics. A substitute electric system of the piezoelectric transducer that is equal to a three-port system was introduced. A piezoelectric transformer created by connection of two plates was analysed. Substitute systems of both plates were introduced. All mechanical parameters of the analysed system were replaced by equivalent electrical parameters in obtained Mason's model.

Keywords: *piezoelectric transducers, piezoelectric transformer, vibration damping, passive electric circuits.*

W pracy przedstawiono propozycję modelowania matematycznego drgających przetworników piezoelektrycznych poprzez zastosowanie analogii elektrycznej. Opracowany model stosowany jest w analizie oraz wyznaczaniu charakterystyk drgających płytek piezoelektrycznych z dołączonymi, zewnętrznymi, biernymi elementami elektrycznymi. Wprowadzono układ zastępczy przetwornika piezoelektrycznego równoważny trójwrotnikowi elektrycznemu. W pracy analizowano połączenia dwóch płytek piezoelektrycznych działających jako transformator piezoelektryczny, wprowadzając układy zastępcze obu przetworników. Przy stosowaniu układów zastępczych w postaci obwodów elektrycznych wszystkie wielkości mechaniczne w otrzymanym układzie Masona zostały zastąpione równoważnymi wielkościami elektrycznymi.

Słowa kluczowe: *przetworniki piezoelektryczne, transformator piezoelektryczny, tłumienie drgań, modelowanie, pasywne obwody elektryczne.*

1. Introduction

Piezoelectric elements are increasingly used in modern technical means. The reason for the growth in popularity of this type of materials are, inter alia, high efficiency of conversion of electrical to mechanical energy or in the opposite direction and the possibility to produce a piezoelectric transducers of any shape, suitable for the application. One of the possible applications of piezoelectric transducers are systems with passive damping of mechanical vibrations with external electric circuits adjoined to the piezoelectric transducers [9–9, 18, 19].

In the Gliwice Research Centre works which aim is to develop a mathematical algorithms for analysis and determination of characteristics for both vibrating mechanical systems and mechatronic systems containing piezoelectric transducers used as vibration dampers or actuators are realized [1–14, 25, 26, 28]. Issues of synthesis of such kind of systems, so their design taking into account required characteristics, as well as computer-aided methods of synthesis and analysis are also considered [3–5, 10, 12, 16, 17].

Development of mathematical models of this type of systems with high detail representation of real systems is a very important issue due to the complexity of the phenomena occurring in them. The correct description of the system in the form of mathematical model already in the design phase is a important condition, necessary to obtain desired results, such as required characteristics of the system, as well as the maximum efficiency of its operation [7,21,22]. This work is therefore an introduction to the process of modelling of vibrating piezoelectric plates with passive electric circuits attached in order to damp vibrations. This paper proposes a description of the piezoelectric vibrating plate as a substitute electric circuit. Then the developed scheme was extended to describe two plates that interact with each other acting as a piezoelectric transformer. Using the electromechanical analogy, the dynamic flexibility of the system was determined and presented on chart. In further studies the created mathematical algorithm will be used to model and determine characteristics of systems with adjoined electric circuits. It will be also used to analyze the impact of the system's parameters on obtained characteristics.

2. The substitute scheme of the piezoelectric transducer

A mathematical model of longitudinally vibrating piezoelectric plate is considered in this work. The form of a single, free piezoelectric plate loaded by external forces F_1 and F_2 are presented in Fig. 1. Symbols u_1 and u_2 denote displacements of the transducer's surfaces and U denotes the electric voltage generated by the transducer as a result of its deformation [14].

Symbols a, b and d denote geometric dimensions of the considered system and Δd denotes the plate's thickness change.

A substitute electric system of the piezoelectric transducer that is equal to a three-port system was introduced. It is a system with three pairs of terminals corresponding to the mechanical and electri-

(*) Tekst artykułu w polskiej wersji językowej dostępny w elektronicznym wydaniu kwartalnika na stronie ***www.ein.org.pl***

cal inputs or outputs. A block diagram of this system together with the indication of the stiffness matrix is shown in Fig. 2 [24].

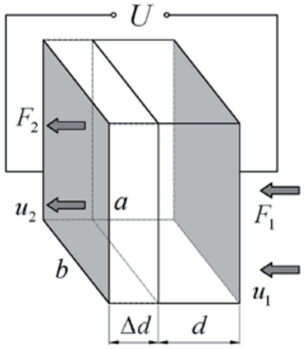

Fig. 1. The form of a single, free piezoelectric plate

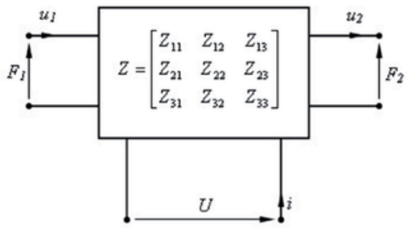

Fig. 2. A block diagram of a equivalent three-port system

Initially, in order to clarify the internal structure of the three-port system the value of a piezoelectric constant was assumed as zero. So, the system under consideration was not treated as piezoelectric and equations of forces acting on the plate can be described as [14]:

$$\begin{cases} F_1 = \dfrac{Z}{j\tan kd}\dot{u}_1 - \dfrac{Z}{j\sin kd}\dot{u}_2 \\ F_2 = \dfrac{Z}{j\sin kd}\dot{u}_1 - \dfrac{Z}{j\tan kd}\dot{u}_2 \end{cases}, \tag{1}$$

where:

$$k = \frac{\omega}{V}, \tag{2}$$

$$V = \sqrt{\frac{c}{\rho}}, \tag{3}$$

$$c = E + \frac{\varepsilon^2}{\varepsilon^S}, \tag{4}$$

$$Z = \rho V A, \tag{5}$$

In equations denotation was introduced: the symbol j denotes the imaginary unit, ε the relative deformation of the plate, ε^S the dielectric permittivity, ω a frequency of excitation, while symbols E, A and ρ denote the Young's modulus, the cross-section area and the density of the transducer [14].

The system of equations (1) describes dependences of the plate's surfaces movements on the applied forces. Using the electrical analogy a substitute electric circuit was introduced. It is a four port system of impedances connected in a star configuration. It is presented in Fig. 3.

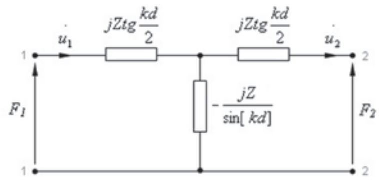

Fig. 3. A substitute electric circuit of the plate with the value of piezoelectric constant assumed as zero

Taking into account the non-zero value of the piezoelectric constant, the system of equations (1) can be supplemented by a relationship that describes the transformation of electrical energy into mechanical energy or in the opposite direction [14]:

$$hC_0\left(\dot{u}_1 - \dot{u}_2\right) = j\omega C_0 e_3 - i_3, \tag{6}$$

where:

$$h = \frac{\varepsilon}{\varepsilon^S}, \tag{7}$$

$$C_0 = \frac{\varepsilon^S A}{d}. \tag{8}$$

The left side of the equation (6) describes the current flowing in the longitudinal branch of the four port system after the transformation of mechanical values to electrical values. Using the transformation law, the considered system can be replaced by an ideal transformer with a ratio of:

$$r = hC_0. \tag{9}$$

The equivalent circuit of the piezoelectric plate that was created in this way is presented in Fig. 4.

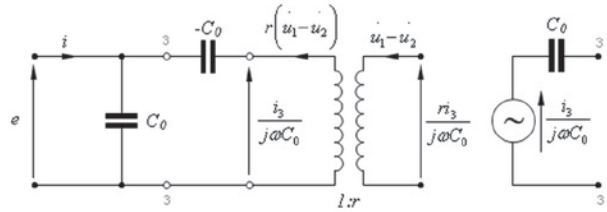

Fig. 4. A part of the electrical equivalent circuit of the piezoelectric plate

The transformation law is used for equivalent voltage, which in the Mason's equations are represented by an element [14]:

$$\frac{h}{j\omega} i = \frac{ri}{j\omega C_0}. \tag{10}$$

In the case of absence of piezoelectric coupling (r=0) there is not an electric current flow in the secondary winding of the transformer. So, the voltage of the electrical part can be described by the equation:

$$e = \frac{i}{j\omega C_0} \,. \tag{11}$$

In agreement with Thevenin theorem, the electrical current source was replaced by the voltage source and additional capacitance C_0 was introduced in parallel to the electrical input in the 3-3 node. The condition of equality of voltage on the electrical and mechanical part will be fulfilled in the case of joining a serial capacitor – C_0. The substitute Mason circuit of the piezoelectric plate that is powered by a parallel field is presented in Fig. 5. It represents mechanical and electrical parts.

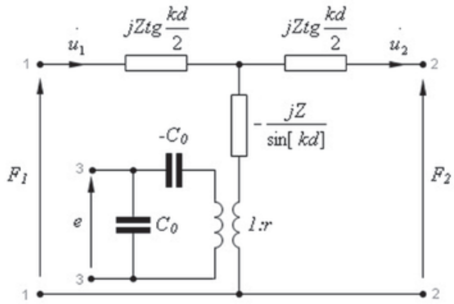

Fig. 5. The equivalent Mason circuit of piezoelectric plate

When using substitutive systems of piezoelectric transducers in the form of electrical circuits all mechanical values were replaced by an equivalent electrical values in the introduced Mason circuit:

$$e_1 = \frac{F_1}{r}\,,\quad e_2 = \frac{F_2}{r}\,, \tag{12}$$

$$i_1 = \dot{u}_1 r\,,\quad i_2 = \dot{u}_2 r\,, \tag{13}$$

$$Z_0 = \frac{Z}{r^2}\,, \tag{14}$$

$$r = \frac{eC_0}{\varepsilon^S}\,. \tag{15}$$

By substituting equations (12) to (15) in equations (1) and (6), the system can be described by equations:

$$e_1 = \frac{Z_0}{jtg[kd]} i_1 - \frac{Z_0}{j\sin[kd]} i_2 + \frac{1}{j\omega C_0} i_3\,, \tag{16}$$

$$e_2 = \frac{Z_0}{j\sin[kd]} i_1 - \frac{Z_0}{jtg[kd]} i_2 + \frac{1}{j\omega C_0} i_3\,, \tag{17}$$

$$e_3 = \frac{1}{j\omega C_0} i_1 - \frac{1}{j\omega C_0} i_2 + \frac{1}{j\omega C_0} i_3\,, \tag{18}$$

and a corresponding Mason circuit can be presented as shown in Fig. 6.

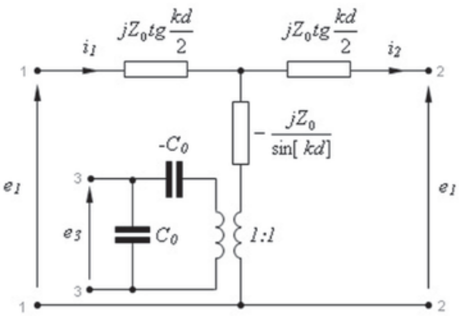

Fig. 6. The equivalent Mason circuit in electrical analogy of the piezoelectric transducer powered by the parallel field

The equivalent circuit of the piezoelectric transducer was transformed in such way that the forces F_1 and F_2 were replaced by electric voltages e_1 and e_2 and the values of displacement u_1 and u_2 by electrical currents i_1 and i_2. The ratio of turns of the primary winding to the number of turns of the secondary winding of the transformer is 1:1. Calculations carried out in the following part will therefore be conducted using the equivalent circuit shown in Fig. 6 and the corresponding equations. Note, however, that the arms 1-1 and 2-2 are representation of mechanical values.

3. The equivalent model of the piezoelectric transformer

The idea of creating a piezoelectric transformer appeared in the fifties of the twentieth century [15, 20, 23, 27]. Both, the direct and reverse piezoelectric effects are used in the piezoelectric transformer. By converting electrical energy into mechanical energy in the first piezoelectric plate of the transformer mechanical vibrations are being generated (the reverse piezoelectric effect). Vibrations are transmitted to the second piezoelectric plate and, as a result of mechanical deformation, electric charge is generated (simple piezoelectric effect). Operation of the piezoelectric transformer is illustrated in Fig. 7.

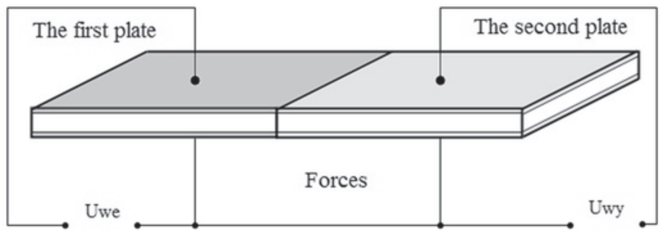

Fig. 7. Functional diagram of the piezoelectric transformer

In the presented case it was assumed that harmonic voltage is applied to the first piezoelectric plate of the transformer and causes vibration in the thickness direction of the plate. The second piezoelectric plate is used to recover and strengthening of the electric voltage. In the work [20] different types of piezoelectric transformers that transfer longitudinal vibrations are presented. Depending on the type of piezoelectric material used and the arrangement of electrodes the piezoelectric transformer is characterized by a specific gain value of the output voltage.

Modelling of the considered piezoelectric transformer by introduction of substitute, equivalent electrical circuits of each plate is presented in this paper. The first plate is subjected to external electric field and the other one to the forces generated by the first plate. Both plates are polarized in the direction of axis 3. Assumed equivalent circuit of a single piezoelectric plate is shown in Fig. 8 [23].

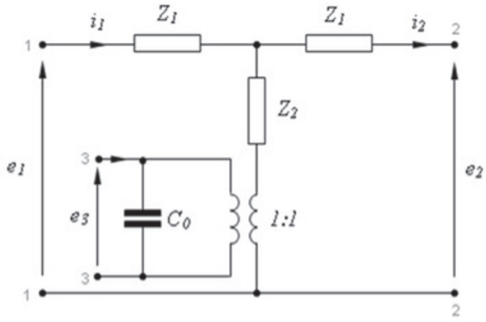

Fig. 8. Substitute electric circuit of a single, input piezoelectric plate of the transformer

Dependencies of impedances connected in a star configuration are described as:

$$Z_1 = Z_{1'} = jZ_0 tg\frac{[kd]}{2}, \tag{19}$$

$$Z_2 = Z_{2'} = \frac{Z_0}{j\sin[kd]}. \tag{20}$$

A diagram formed by connecting terminals of the pair of mechanical arms 2-2 is presented in Fig. 9. It is transformed model of the plate cooperating with the second piezoelectric transducer. In the place of the newly formed pair of arms 1-2 the second piezoelectric plate is coupled. The terminal 3-3 is powered by external input voltage U_{we} [23].

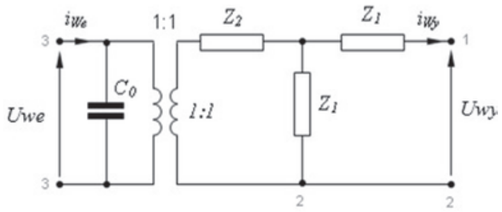

Fig. 9. The transformed substitute circuit of the input piezoelectric plate

In the case of the second piezoelectric plate its equivalent circuit is similar but supplemented by an additional capacitor C_0. An obtained equivalent circuit of the piezoelectric transformer is presented in Fig. 10.

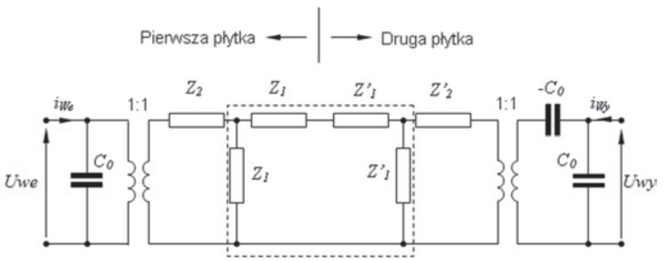

Fig. 10. The substitute circuit of the piezoelectric transformer transmitting longitudinal vibrations

The system consisting of the same type of piezoelectric plates was considered thus the piezoelectric transformer ratio, that is couplings between electrical and mechanical systems, is 1:1. The value of substitute impedance created from a connection of Z_1 and Z'_1 was determined:

$$Z_1{}'_1 = Z_1 + Z'_1 = 2jZ_0 tg\frac{[kd]}{2}, \tag{21}$$

and the connection of impedances Z_1, Z'_1 and $Z_1{}'_1$ was changed from the triangle configuration to the star configuration:

$$Z_A = \frac{Z_1 Z_1{}'_1}{Z_1 + Z'_1 + Z_1{}'_1} = \frac{\left(2jZ_0 tg\frac{[kd]}{2}\right)^2}{4jZ_0 tg\frac{[kd]}{2}} = \frac{j}{2} Z_0 tg\frac{[kd]}{2}, \tag{22}$$

$$Z_B = \frac{Z_1 Z_1'}{Z_1 + Z_1' + Z_1{}'_1} = \frac{\left(jZ_0 tg\frac{[kd]}{2}\right)^2}{4jZ_0 tg\frac{[kd]}{2}} = \frac{j}{4} Z_0 tg\frac{[kd]}{2}, \tag{23}$$

$$Z_C = \frac{Z_1' Z_1{}'_1}{Z_1 + Z_1' + Z_1{}'_1} = \frac{\left(2jZ_0 tg\frac{[kd]}{2}\right)^2}{4jZ_0 tg\frac{[kd]}{2}} = \frac{j}{2} Z_0 tg\frac{[kd]}{2}. \tag{24}$$

Obtained substitute circuit is presented in Fig. 11.

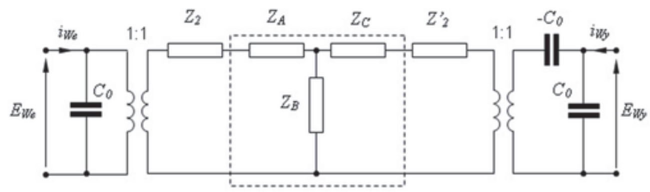

Fig. 11. Diagram of transformation of impedances connection from the triangle configuration to the star configuration

Further minimize of the number of system components was realized by combining elements respectively Z_2 together with Z_A and Z'_2 together with Z_C according to the equation:

$$Z_2 + Z_A = Z_C + Z_2' = \frac{Z_0}{j\sin[kd]} + \frac{jZ_0}{2} tg\frac{kd}{2}. \tag{25}$$

Using the trigonometric identity:

$$tg\frac{kd}{2} = \frac{1-\cos[kd]}{\sin[kd]}, \tag{26}$$

it was obtained:

$$Z_2 + Z_A = Z_C + Z_2' = \frac{Z_0}{j\sin[kd]} + \frac{jZ_0\left(1-\cos\left[kd\right]\right)}{2\sin\left[kd\right]} . \quad (27)$$

After transformations, equation (27) can be written in the form:

$$Z_2 + Z_A = Z_C + Z_{2'} = \frac{Z_0\left(1-\cos\left[kd\right]\right)}{2j\sin[kd]} . \quad (28)$$

Taking into account that:

$$tg\frac{kd}{2} = \frac{\sin\left[kd\right]}{1+\cos\left[kd\right]} , \quad (29)$$

it can be finally written down:

$$Z_2 + Z_A = Z_C + Z_2' = \frac{Z_0}{2j\cdot tg\frac{kd}{2}} . \quad (29)$$

The minimized form of the circuit is presented in Fig. 12.

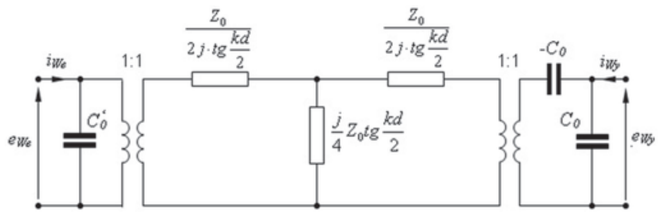

Fig. 12. Minimized circuit (containing a combination of resistors in a star configuration) of the piezoelectric transformer

Using electromechanical analogies the created system can be transformed to a resonant circuit composed of passive RLC components. This circuit is presented in Fig. 13.

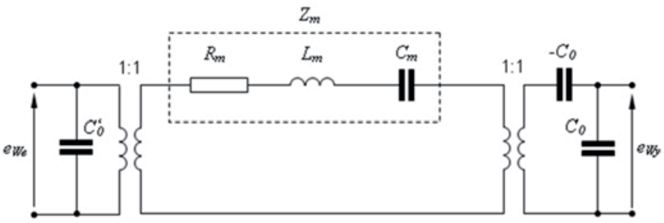

Fig. 13. Substitute scheme of the mechanical resonance system in the form of an electrical circuit

The obtained model is equivalent to a mechanical $R_mL_mC_m$ system [23]. The value of the first natural frequency can be described by the equation:

$$\omega_0 = \frac{\pi}{l}\sqrt{\frac{c}{\rho}} . \quad (30)$$

Values of the individual elements of passive resonant circuit were described by equations:

$$L_m = \frac{\pi Z_0}{4\omega_0} , \quad (31)$$

$$R_m = \frac{\pi Z_0}{4Q_m} , \quad (32)$$

$$C_m = \frac{1}{\omega_0{}^2 L_m} , \quad (33)$$

by symbol Q_m a quality constant was indicated [23].

Using equations (31) to (33) values of the individual elements of $R_mL_mC_m$ circuit were calculated. They were used to calculate the dynamic flexibility of the piezoelectric transformer without damping (in analogy of electrical admittance Y of the electric resonant circuit). The value of the Q_m constant was taken from [23] to be equal 2000. The obtained modulus of dynamic flexibility of the resonant system for the first natural frequency is shown in Fig. 14.

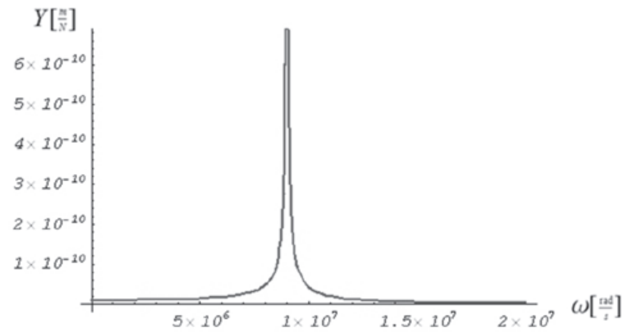

Fig. 14. Absolute value of the dynamic flexibility of mechanical resonant system

Fig. 14 shows designated course of absolute values of the dynamic flexibility of mechanical resonant system (the piezoelectric plate) obtained from the electrical analogy.

4. Conclusions

Presented algorithm can be used to develop an electrical equivalent circuit of a single piezoelectric plate and the piezoelectric transformer is an introduction to the process of modelling and testing of this type of vibrating systems that can be used to stabilize and damping of mechanical vibrations. In next works systems with vibrations damping will be considered. The damping will be introduced by connecting to the piezoelectric transducer passive electric circuits. The advantages of this type of passive vibration damping is primarily their low complexity and no need for an external power supply. This allows their applications in technical devices where is no possibility of access to the system during its operation or there is a need to reduce the complexity and energy consumption of the designed technical means.

Using the presented mathematical algorithm it is possible to realize modelling and testing of such systems, as well as analysis of the impact of their parameters on characteristics, including both parameters of the piezoelectric transducer as well as parameters of the external circuit. A necessary condition to realize a synthesis task, so designing of the system with required characteristics, is to develop a precise mathematical model of the designed system. Using this model it is possible to precise representation of the phenomena occurring in it.

Acknowledgements: *The work was carried out under the project number PBS2/A6/17/2013 agreement implemented under the Applied Research Program, funded by the National Centre for Research and Development.*

References

1. Białas K. Passive and Active Elements in Reduction of Vibrations of Torsional Systems. Solid State Phenomena 2010; 164: 260-264.
2. Białas K. Mechanical and electrical elements in reduction of vibrations. Journal of Vibroengineering 2012; 14(1): 123-128.
3. Buchacz A. Modelling, synthesis and analysis of bar systems characterized by a cascade structure represented by graphs. Mechanism and Machine Theory 1995; 30 (7): 969-986.
4. Buchacz A, Wojnarowski J. The modelling of vibrating bar systems with nonlinear changeable sections of robots by means of hypergraphs and structural numbers. Journal of the Tranklin Institute-Engineering and Applied Mathematics 1995; 332B (4): 443-467.
5. Buchacz A. The expansion of the synthesized structures of mechanical discrete systems represented by polar graphs. Journal of Materials Processing Technology 2005; 164: 1277-1280.
6. Buchacz A, Płaczek M. Damping of Mechanical Vibrations Using Piezoelements, Including Influence of Connection Layer's Properties on the Dynamic Characteristic. Solid State Phenomena 2009; 147-149: 869-875.
7. Buchacz A, Płaczek M. Development of Mathematical Model of a Mechatronic System, Solid State Phenomena 2010; 164: 319-322.
8. Buchacz A, Płaczek M. Selection of Parameters of External Electric Circuit for Control of Dynamic Flexibility of a Mechatronic System. Solid State Phenomena 2010; 164: 323-326.
9. Buchacz A, Płaczek M. The approximate Galerkin's method in the vibrating mechatronic system's investigation. Proceedings of The 14th International Conference Modern Technologies, Quality and Innovation ModTech 2010, Slanic Moldova, Romania 2010, pp. 147-150.
10. Buchacz A, Wróbel A. Computer-Aided Analysis of Piezoelectric Plates. Solid State Phenomena 2010; 164: 239-242.
11. Buchacz A, Płaczek M. The analysis of a composite beam with piezoelectric actuator based on the approximate method. Journal of Vibroengineering 2012; 14 (1): 111-116.
12. Buchacz A, Galeziowski D. Synthesis as a designing of mechatronic vibrating mixed systems. Journal of Vibroengineering 2012; 14 (2): 553 -559.
13. Buchacz A, Płaczek M., Wróbel A. Control of characteristics of mechatronic systems using piezoelectric materials. Journal of Theoretical and Applied Mechanics 2013; 51: 225-234.
14. Buchacz A, Wróbel A. Modeling and study of the piezoelectric effect influence on the characteristics of mechatronic systems. Silesian University of Technology Publishing House, Gliwice, 2010 (in Polish).
15. Crawford A. Piezoelectric Ceramic Transformers and Filters. Journal of the British Institution of Radio Engineers 1961; 21 (4): 353-360.
16. Dymarek A, Dzitkowski T. Modelling and synthesis of discrete – continuous subsystems of machines with damping. Journal of Materials Processing Technology 2005; 164-165: 1317-1326.
17. Dymarek A, Dzitkowski T. Searching for the values of damping elements with required frequency spectrum. Acta Mechanica et Automatica 2010; 4: 19-22.
18. Fleming A J, Behrens S, Reza Moheimani S O. Optimization and Implementation of Multimode Piezoelectric Shunt Damping Systems. Transactions on Mechatronics 2002; 7 (1): 87-94.
19. Hagood N W, von Flotow A. Damping of structural vibrations with piezoelectric materials and passive electric networks. Jurnal of Sound and Vibration 1991; 146 (2): 243-268.
20. Ho S T. Design of the Longitudinal Mode Piezoelectric Transformer. Proceedings of the International Conference on Power Electronics and Drive Systems, 2007, pp.: 1639 – 1644.
21. Jamroziak K, Kosobudzki M. Determining the torsional natural frequency of underframe of off-road vehicle with use of the procedure of operational modal analysis. Journal of Vibroengineering, 2012; 14 (2): 472-476.
22. Kulisiewicz M, Piesiak S, Bocian M. Identyfication of nonlinear damping using energy balance method with random pulse excitation. Journal of Vibration and Control 2001; 7 (5): 699-710.
23. Lin C. Design and analysis of piezoelectric transformer converters. Ph.D Dissertation, Virginia Polytechnic Institute, 1997.
24. Sherrit S, Leary S, Dolgin B, Bar-Cohen Y. Comparison of the Mason and KLM Equivalent Circuits for Piezoelectric Resonators in the Thickness Mode. Proceedings of the IEEE Ultrasonic Symposium 1999; 2 921-926.
25. Wróbel A. Kelvin Voigt's model of single piezoelectric plate. Journal of Vibroengineering 2012; 14 (2): 534-537.
26. Wróbel A. Model of piezoelectric including material damping, Proceedings of 16th International Conference ModTech 2012, ISSN 2069-6736, pp.1061-1064.
27. Zaitsu T, Ohnishi O, Inoue T, Shoyama M, Ninomiya T, Lee F C, Hua G C. Piezoelectric transformer operating in thickness extensional vibration and its application to switching converter. Proceedings of the Power Electronics Specialists Conference 1994; 1: 585-589.
28. Zolkiewski S. Damped Vibrations Problem Of Beams Fixed On The Rotational Disk. International Journal of Bifurcation and Chaos 2011; 21 (1): 3033-3041.

Andrzej BUCHACZ
Marek PŁACZEK
Andrzej WRÓBEL
Institute of Engineering Processes Automation and Integrated Manufacturing Systems
Faculty of Mechanical Engineering
Silesian University of Technology
Konarskiego 18A, 44-100 Gliwice, Poland
E-mails: andrzej.buchacz@polsl.pl, marek.placzek@polsl.pl, andrzej.wrobel@polsl.pl

Article citation info:
YANG Y, LU Z, LUO X, GE Z, QIAN Y. Mean failure mass and mean failure repair time: parameters linking reliability, maintainability and supportability. Eksploatacja i Niezawodnosc – Maintenance and Reliability 2014; 16 (2): 307–312.

Yongmin YANG
Zhimiao LU
Xu LUO
Zhexue GE
Yanling QIAN

MEAN FAILURE MASS AND MEAN FAILURE REPAIR TIME: PARAMETERS LINKING RELIABILITY, MAINTAINABILITY AND SUPPORTABILITY

ŚREDNIA MASA USZKODZENIA I ŚREDNI CZAS NAPRAWY USZKODZENIA: PARAMETRY ŁĄCZĄCE NIEZAWODNOŚĆ, OBSŁUGIWALNOŚĆ I UTRZYMYWALNOŚĆ

Up to now, no parameters linking reliability, maintainability and supportability directly are available in reliability engineering. Index such as availability can be used to check the compatibility of those RAM features only after individual index of every characteristic is obtained such as MTBF, MTTR, etc. Thus available methods to balance those three features are not efficient and direct during the product design phase. In this paper, concepts of mean failure mass and mean failure repair time are presented. By investigating the relationship of the failure probability and the mass of a product, a feature linking reliability and supportability is obtained. Similarly, by studying the relationship of the failure probability and the mean time to repair of a product, a feature linking reliability and maintainability is obtained. Based on above definitions, an approach of reliability, maintainability and supportability trade-off during design phase is achieved. Effectiveness of both of the new concepts is demonstrated by an example of balancing the maintainability and supportability of a subsystem of a space station.

Keywords: *mean failure mass, mean failure repair time, reliability, maintainability, LRU.*

Jak dotąd w inżynierii niezawodności nie istniały parametry łączące niezawodność, obsługiwalność i utrzymywalność. Wskaźniki takie jak gotowość mogą być stosowane w celu sprawdzenia zgodności tych cech RAM (Reliability, Availability, Maintainability – Niezawodność, Gotowość, Obsługiwalność) dopiero po uzyskaniu indywidualnego wskaźnika każdej charakterystyki, takich jak MTBF, MTTR, itp. W ten sposób dostępne metody równoważenia owych trzech cech nie są wystarczająco skuteczne i bezpośrednie w fazie projektowania produktu . Niniejszy artykuł przedstawia pojęcia średniej masy uszkodzenia i średniego czasu naprawy uszkodzenia. Badając zależność prawdopodobieństwa uszkodzenia i masy produktu, uzyskuje się cechę łączącą niezawodność i utrzymywalność. Podobnie, badając zależność prawdopodobieństwa uszkodzenia i średniego czasu naprawy produktu, uzyskuje się cechę łączącą niezawodność i obsługiwalność. Na bazie powyższych definicji osiągnięto kompromisowe podejście do niezawodności, obsługiwalności i utrzymywalności podczas fazy projektowania. Skuteczności obu nowych koncepcji dowodzi przykład równoważenia niezawodności i obsługiwalności podsystemu stacji kosmicznej.

Słowa kluczowe: *średnia masa uszkodzenia, średni czas naprawy uszkodzenia, niezawodność, obsługiwalność, LRU*

1. Introduction

Modern equipments or systems are becoming more dependent on system engineering methods to ensure the life cycle availability and reliability. RAM (reliability, availability and maintainability) features are more and more essential to systems such as atomic energy plants, space stations and aeroplanes [1, 2].

Assessment of RAM parameters, methodologies for RAM analysis and simulation or modeling for RAM are the major issues on RAM studies [3]. As an approach which affects the product design deeply, methodology for RAM analysis plays the most important role in the life cycle RAM work. By the view of applications, RAM analysis should be a synthesis way which will deal with reliability, availability and maintainability at the same time. Unfortunately the methods presented in literature are not able to analyze RAM features simultaneously. Many analysis methods deal with RAM feature individually [4–7]. Other methods perform analysis of reliability, maintainability and supportability in a serial way [1, 8]. The reason is that no direct parameters linking reliability, maintainability and supportability are available [9–11]. Index such as availability can be used to check the compatibility of those RAM features only after individual index of every characteristic is obtained such as MTBF, MTTR, etc.

Above situation leads to that methods used to balance RAM features are not efficient and direct during the product design phase. For some systems such as space station or expeditionary warships, support issue plays an important role for mission accomplishment. Spares supply is expensive and crucial herein. During the design phase, trade-off of reliability, maintainability and spare plan is much necessary. Indirect methods such as multidiscipline domain optimization (MDO) approach and RAM simulation have been employed for RAM trade-off [12–13]. As these methods are not able to point out what issues affect the RAM parameters and how to affect RAM parameters, direct analysis methods are needed for RAM features trade-off, so are the parameters which can link reliability, maintainability and supportability directly.

So far, existent RAM parameters are not able to link reliability, maintainability and supportability directly [9-10]. This paper aims to give two parameters. One directly links reliability and supportability, another directly links reliability and maintainability. As we know, supportability and maintainability are two concepts which depend on the usage and maintenance scenario. Failure-maintenance and failure-spare delivery schedule affect the product supportability and maintainability profoundly. Once the usage and maintenance scenario is confirmed, the failure-maintenance and failure-spare delivery relationships will express objective characteristics of the designed product. Naturally, there is a need to study the relationship of the failure probability and the mass of a product. Similarly, the relationship of the failure probability and the mean time to repair of a product is also an interesting target.

In this paper, concepts of mean failure mass and mean failure repair time are presented. Effectiveness of both of the new concepts is demonstrated by an example of balancing the maintainability and supportability of a subsystem of a space station.

2. The concept of mean failure mass

Failure of a product is its inherent property. When a failure occurs, some units (LRU and SRU, namely line replaceable unit and shop replaceable unit) in the product need to be maintained or to be replaced directly. For a matured product, a unit locates in a fixed location. For units in a product, a failure and a unit replacement relationship contains the product structural information and the maintenance information. Once the maintenance scenario is confirmed, the failure-replacement relationship of the unit is fixed.

For organizational-level maintenance or intermediate-level maintenance, failure of a LRU or a SRU can result in a replacement of another LRU or SRU. Hence, the following concept is presented.

Definition 1: suppose some failure of unit A will result in a replacement of unit *B*. Let the set of failures of unit *A* which will result in replacement of unit *B* be Ω. Under the given conditions and given time, the total failure probability of unit *A* in Ω is named $F_a(t)$. The mass of unit *B* is named M_b. Define the product of $F_a(t)$ and M_b as: mean failure mass of unit *B* brought by unit *A* which is expressed by $MFM_{a\text{-}b}$:

$$MFM_{a\text{-}b}\,(t)=F_a(t)\cdot M_b \tag{1}$$

Definition 2: suppose some failure of unit *A* will result in a replacement of itself. Let the set of failures of unit *A* which will result in replacement of itself be Ω. Under the given conditions and given time, the total failure probability of unit *A* in Ω is named $F_a(t)$. The mass of unit *A* is named M_a. Define the product of $F_a(t)$and M_a as: mean failure mass of unit *A* which is expressed by MFM_a:

$$MFM_a(t)=F_a(t)\cdot \mathrm{Ma} \tag{2}$$

By definition 1 and definition 2, it is obvious that MFM is a variable of time *t* with a dimension of mass (for instance, kilogram). It can be seen as how much mass has been lost by failure in average which in most cases can also be regarded as the delivery burden of spares. For example, suppose there are 100 LRU *A*s and 100 LRU *B*s in service. LRU *A* has a failure probability of 0.25 in 6 months and a mass of 10 kg. LRU *B* has a failure probability of 0.50 in 6 months and a mass of 6 kg. Calculation shows that in 6 months, 25 LRU *A*s and 50 LRU *B*s will fail. For LRU *A*, 25 spares with 250 kg are needed, meanwhile for LRU *B*, 50 spares with 300kg are needed. Under this circumstance, on the view of weight, LRU *B* has a greater support burden than LRU *A* with a ration of 300 to 250. Actually, by definition 2, this ratio can be obtained direct. By definition 2, MFM_a is the product of 0.25 and 10 kg, that is 2.5; MFM_b is the product of 0.5 and 6 kg, that is 3. MFM_b/MFM_a is exactly the ratio of 3/2.5 which means the ratio of support burden of spares weight of LRU *A* to LRU *B*. It can be seen mean failure mass can be a useful parameter in the case where the spares delivery is difficult and expensive such as accommodation of a Space Station.

3. The concept of mean failure repair time

As mentioned above, for a matured product, a unit locates in a fixed location. Once the maintenance scenario is confirmed, the failure-maintenance relationship is fixed. Under given conditions, the time consumed for a unit repair is of an objective value named as mean time to repair. If every failure results in an immediate repair, then next concept will be objective.

Definition 3: suppose some failure of unit *A* will result in a repair of unit *B*. Let the set of failures of unit *A* which will result in repair of unit *B* be Ω. Under the given conditions and given time, the total failure probability of unit *A* in Ω is named $F_a(t)$. The *MTTR* (mean time to repair) of unit *B* is named $MTTR_b$. Define the product of $F_a(t)$ and $MTTR_b$ as: mean failure repair time of unit *B* brought by unit *A* which is expressed by $MFRT_{a\text{-}b}$:

$$MFRT_{a\text{-}b}\,(t)=F_a(t)\cdot MTTR_b \tag{3}$$

Definition 4: suppose some failure of unit *A* will result in a repair of itself. Let the set of failures of unit *A* which will result in repair of itself be Ω. Under the given conditions and given time, the total failure probability of unit *A* in Ω is named $F_a(t)$. The *MTTR* (mean time to repair) of unit *A* is named $MTTR_a$. Define the product of $F_a(t)$ and $MTTR_a$ as: mean failure repair time of unit *A* which is expressed by $MFRT_a$:

$$MFRT_a\,(t)=F_a(t)\cdot MTTR_a \tag{4}$$

By definition 3 and definition 4, it is obvious that MFRT is a variable of time t with a dimension of time (for instance, hour). It can be seen as how much repair time has been spent by failure in average which in most cases can also be regarded as the maintenance burden. Example can be simply given similarly as section 2.

4. Applications

Definition 1 to 4 implies that the object is a unit. A unit is a replacement or repair target, so above definitions have no doubt in reality usage. But if the object is a module or a system which consists of several units, then the average support burden and average maintenance burden cannot be obtained from above definitions directly. Although definition 1 to 4 are not suitable to a module or a system, we can still borrow MFM and MFRT to express total spares delivery burden and total maintenance burden of a module or a system, which are the total spares mass need to be delivered and the total maintenance time need for every failure repair. Once MFM and MFRT can be calculated directly, RAM trade-off analysis can be easily accomplished.

4.1. Failure-replacement correlative matrix and failure-maintenance correlative matrix

A failure-replacement correlative matrix can be employed to express failure-replacement relationship of LRUs in a system:

Table1. Failure-replacement correlative matrix Σ

	unit 1	unit 2	…	unit n
failure of unit 1	m_{11}	m_{12}	…	m_{1n}
failure of unit 2	m_{21}	m_{22}	…	m_{2n}
…	…	…	…	…
failure of unit m	m_{n1}	m_{n2}	…	m_{nn}

If failure of unit *i* results in replacement of unit *j*, set m_{ij} as 1. If failure of unit *i* doesn't result in replacement of unit *j*, then set m_{ij} as

0. Note that matrix Σ depends on the structure of the system and LRU selection plan. Similarly, A failure-maintenance correlative matrix can be similarly defined as Φ. In most cases, Σ and Φ have the same expression, so we treat them as the same one. Once Σ is known, the MFM and MFRT of a system can be calculated by following equations:

$$MFM_s(t) = \left[F_1(t) \quad F_2(t) \quad \cdots \quad F_n(t)\right]\Sigma \begin{bmatrix} M_1 \\ M_2 \\ \cdots \\ M_n \end{bmatrix} = \mathrm{F\Sigma M}$$

$$MFRT_s(t) = \left[F_1(t) \quad F_2(t) \quad \cdots \quad F_n(t)\right]\Sigma \begin{bmatrix} MTTR_1 \\ MTTR_2 \\ \cdots \\ MTTR_n \end{bmatrix} = \boldsymbol{F\Sigma T} \qquad (6)$$

where F is a vector consists of failure probability of every unit. $\boldsymbol{M}$ is a vector consists of mass of every unit. $\boldsymbol{T}$ is a vector consists of MTTR of every unit. Obviously, when all the units of a system are independent in the view of failure-replacement and failure-maintenance, matrix Σ is diagonal:

$$\begin{aligned} MFM_s(t) &= \textstyle\sum_{i=1}^{n} MFM_i(t) \\ MFRT_s(t) &= \textstyle\sum_{i=1}^{n} MFRT_i(t) \end{aligned} \qquad (7)$$

Formula (5) to (7) are reasonable only if the failures of every unit are independent which means the elements of $\boldsymbol{F}$ are independent.

4.2. Corrective and preventive maintenance

Above concepts are induced from corrective maintenance where failure is the only reason for units replacement or repair. But actual cases are more complicated where preventive maintenance is also a major issue. As preventive maintenance is more regular, one can simply add its affect on corresponding parameters of corrective maintenance. Suppose during time t, the system support burden and maintenance burden resulting from failures are $\boldsymbol{F\Sigma M}$ and $\boldsymbol{F\Sigma T}$. We also suppose during time t, there are n times scheduled replacement for unit A. Suppose corrective repair doesn't affect scheduled preventive replacement and the time consumed of other preventive maintenances is negligible, then the total the system support burden and maintenance burden can be written as:

$$\begin{aligned} MFM_s(t) &= \boldsymbol{F\Sigma M} + nM_a \\ MFRT_s(t) &= \boldsymbol{F\Sigma T} + nMTTR_a \end{aligned} \qquad (8)$$

The ratio is reasonable which can be showed simply as follows. Suppose there are m unit A. Then for time t, mass of $m{\cdot}F_a(t){\cdot}M_a$ will be replaced for corrective maintenance. At the same time, for preventive maintenance every unit A will be replaced n times. Then mass of $m{\cdot}n{\cdot}M_a$ will be replaced for preventive maintenance. Total replaced mass is $m{\cdot}F_a(t){\cdot}M_a+ m{\cdot}n{\cdot}M_a$. It is obvious that for defined MFM, replaced mass for preventive maintenance can directly added as $n{\cdot}M_a$.

4.3. Trade-off analysis by MFM and MFRT.

When MFM and MFRT are achieved, trade-off analysis can be done efficiently. As MFM and MFRT are deeply dependent on the product structure and the LRU selection results, this trade-off can be used for LRU selection optimization. In general, a product structure can be expressed as a tree. Following is an example:

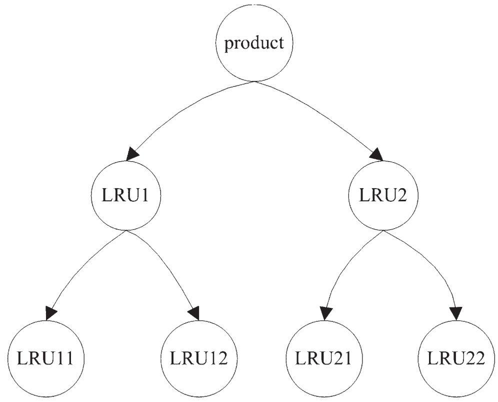

Fig. 1. A product structure tree

The LRU selection can be (1) LRU1 and LRU2, or (2) LRU11, LRU12, LRU21 and LRU22. Normally, selection (1) results in greater MFM, as spare defined as bigger item will lead to uneconomical spares delivery. Selection (1) also leads to a smaller MFRT, as maintenance for bigger item will consume smaller dismantlement time. At the same time, selection (2) results in smaller MFM and greater MFRT, as spares defined as smaller item will lead to economical spare delivery and consume greater replacement time.

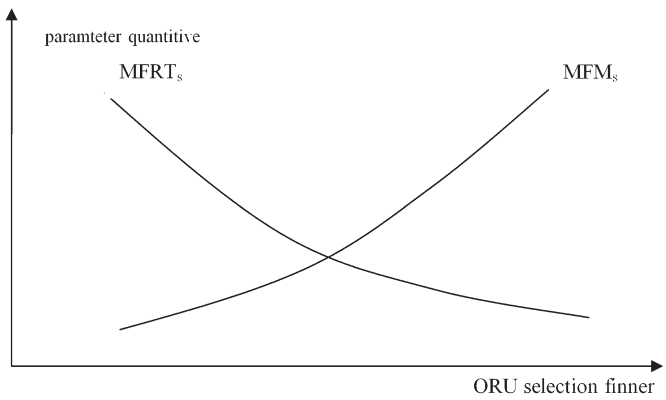

Fig. 2. ORU selection trade-off

Above figure shows that MFM and MFRT are contradictory with regard to different LRU selection level. By a unification ration, an optimization point can be found for the total cost function of MFM and MFRT.

5. Case study

MFM and MFRT represent the mean spares delivery burden and maintenance burden which are contradictory in some sense. As they both are relative to LRU selection plan, they are suitable for RAM trade-off in product design phase. Following is an example of LRU selection by RAM trade-off on CDRA (Carbon Dioxide Removal Assembly) of ECLSS (Environmental Control and Life Support Systems). Here the concept of ORU(Orbit Replaceable Unit) is employed instead of LRU.

In following study, 7 ORU selection plans are given. The first approach is to compute MFM and MFRT directly and employ a resulted synthetical objective function to carry on ORU selection. The first approach is called direct calculation method. In next step, a Monte Carlo method is used to simulate the failure occurence in a time range. Real spares mass delivered and maintenance time consumed are calculated by accumulation approach. The second way is called simulation

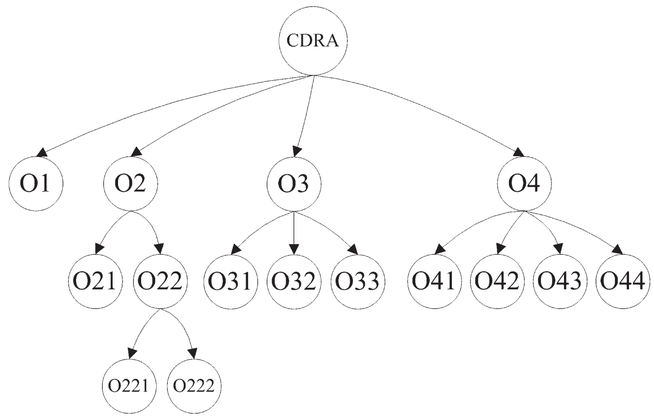

Fig. 3. Structural tree of CDRA

Table 2. Name of ORUs

O1	AIR I/O Selector Valve Module	O32	Open Loop Vent Valve
O2	Desiccant and Sorbent module	O33	AIR Save Pump
O21	Desiccant Bed	O4	AIR Blower and Precooler Module
O22	CO2 Sorbent Module	O41	Selector Valve 4
O221	CO2 Sorbent Bed	O42	AIR Blower
O222	Check Valve	O43	Precooler
O3	AIR Save Pump Module	O44	Selector Valve 5
O31	Selector Valve 3		

Table 4. ORU Selection Scheme

Selection	Number of ORU	ORU
1	5	01,021,022,03,04
2	6	01,021,0221,0222,03,04
3	7	01,021,022,031,032,033,04
4	8	01,021,0221,0222,031,032,033,04
5	9	01,021,0221,0222,03,041,042,043,044
6	10	01,021,022,031,032,033,041,042,043,044
7	11	01,021,0221,0222,031,032,033,041,042,043,044

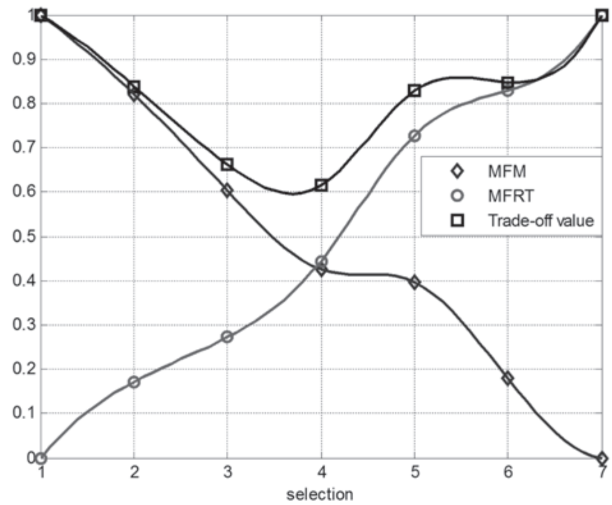

Fig. 4. plot of objective function of direct calculation method

Table 3. Basic data of ORUs

ORU or Module	Failure rate(1/y)	MTTR(h)	Mass(kg)	Maintenance plan
AIR I/O Selector Valve Module 1	0.0815	0.92	10	Corrective maintenance
Desiccant and Sorbent module 2	0.3879	1.23	52	Preventive maintenance
Desiccant Bed 21	0.2827	2.21	19	Preventive maintenance
CO2 Sorbent Module22	0.3052	1.26	26	Preventive maintenance
CO2 Sorbent Bed221	0.1594	1.90	24	Preventive maintenance
Check Valve222	0.1458	2.22	5	Corrective maintenance
AIR Save Pump Module3	0.4099	1.55	25	Corrective maintenance
Selector Valve 3 31	0.1730	2.58	4	Corrective maintenance
Open Loop Vent Valve 32	0.1601	2.63	4	Corrective maintenance
AIR Save Pump 33	0.0768	2.84	18	Corrective maintenance
AIR Blower and Precooler Module 4	0.7078	1.38	30	Corrective maintenance
Selector Valve 4 41	0.2230	3.38	4	Corrective maintenance
AIR Blower42	0.0733	2.92	20	Corrective maintenance
Precooler43	0.1885	2.96	4	Corrective maintenance
Selector Valve 5 44	0.2230	3.32	4	Corrective maintenance

method. Finally, the effectiveness of new definitions can be verified by comparison of above results obtained in different ways.

CDRA of ECLSS has 4 modules, the AIR I/O Selector Valve Module, Desiccant and Sorbent module, AIR Save Pump Module and AIR Blower and Precooler Module. The structure tree of CDRA is shown in Fig. 3, and the names of ORU in CDRA are given in Table 2. In addition, the basic reliability, mass and MTTR of ORUs are given in table 3. According to structure tree of CDRA, there are 7 ORU selection scheme as shown in table 4.

Some assumptions are given for MFM and MFRTcomputation:

(1) For simplicity, suppose the ORU's reliability is of exponential distribution.

(2) Failure and replacement of every unit doesn't affect each other.

The MFM and MFRT are computed as ORU selection indices by formulas (2), (4), (7), (8). For synthesis trade-off analysis, MFM and MFRT are normalized as :

$$x_i = \frac{X_i - X_{\min}}{X_{\max} - X_{\min}} \tag{9}$$

Where X_{min} is the minimum value of MFM or MFRT, X_{max} is the maximum value of MFM or MFRT. Let the synthetical objective function be:

$$\min\left\{\sqrt{MFM^2 + MFRT^2}\right\} \tag{10}$$

Results are shown in Table 5 and Fig. 4. The selection (4) is the optimal solution from the curve of trade-off value.

In another approach, Monte Carlo method is used to simulate failure occurance of the ORUs of CDRA in a time range. The real spares

Table 5. MFM and MFRT

Selection	Number of ORU	MFM(kg)	MFRT(h)	MFM (normalized)	MFRT (normalized)	Trade-off value
1	5	147.7801	10.1655	1	0	1
2	6	143.9708	12.8225	0.8212	0.1713	0.8389
3	7	139.3280	14.3858	0.6034	0.2721	0.6619
4	8	135.5187	17.0428	0.4246	0.4435	0.6140
5	9	134.9192	21.4509	0.3965	0.7278	0.8288
6	10	130.2764	23.0141	0.1787	0.8286	0.8476
7	11	126.4671	25.6712	0	1	1

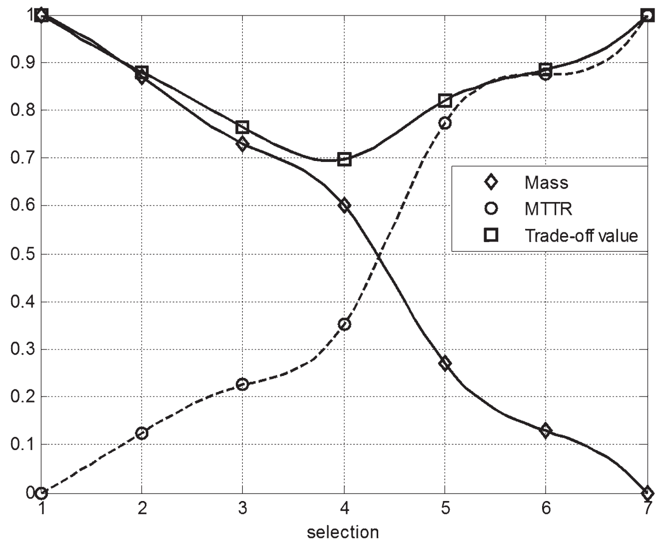

Fig. 5. Plot of objective function of simulation method

mass and maintenance time are achieved by accumulation computation. Here the ORU's failure rate is assumed to be of exponential distribution. The spares delivery burden and maintenance burden are achieved by employing Monte Carlo method and normalization method shown in Table 6 and Fig. 5.

The selection (4) is also the optimal solution by Monte Carlo simulation.

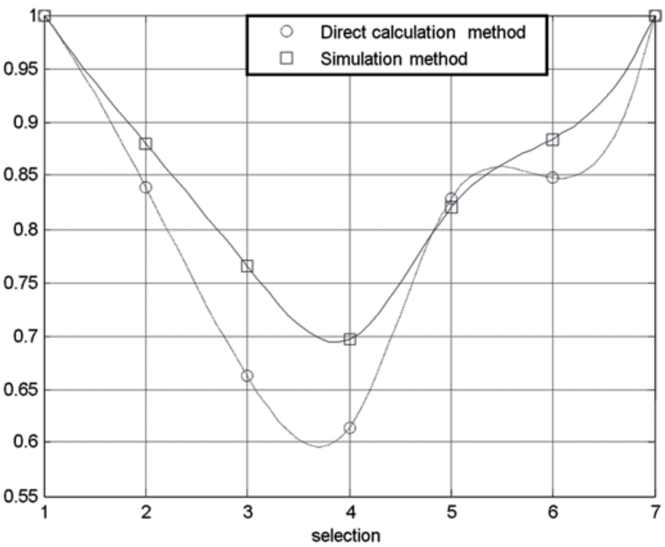

Fig. 6. Trade-off value of two methods

Finally, the results of two different trade-off ways are compared in Fig.6. The trade-off objective function value of direct calculation method and classical Monte Carlo simulation method shows the same tendency and the same optimal ORU selection point. This case study shows that the concepts of mean failure mass and mean failure repair time are much useful for RAM trade-off analysis.

6. Conclusions

Because of some restriction during the design phase of products, the traditional methods used to balance RAM are not efficient and direct. In this paper, an approach of reliability, maintainability and supportability trade-off during design phase is achieved using the concepts of mean failure mass and mean failure repair time both of which are firstly presented. The article uses the concepts of MFM and MFRT to express total spares delivery burden and total maintenance burden of a module or a system, which are the total spares mass need to be delivered and the total maintenance time needed for every failure repair. Once MFM and MFRT of a system can be calculated directly, the system RAM trade-off analysis can be easily accomplished. A case of a Carbon Dioxide Removal Assembly (CDRA) of space station showed that the concepts of MFM and MFRT are very useful for a simple calculation of the support and maintenance burden which leads to a direct trade-off of RMS. The trade-off results of direct computation and simulation are same which shows the new concepts and relative computation method are effective. From above paper, one can see that MFM and MFRT are the parameters linking reliability, maintainability and supportability.

Acknowledgement: *The research work is financed by the project of National Natural Science Foundation of China 51005238 .*

References

1. Eti MC, Ogaji SOT, Probert SD. Integrating reliability, availability, maintainability and supportability with risk analysis for improved operation of the Afam thermal power-station. Applied Energy 2007; 84(2): 202-221.
2. Gary JZ, Donald D. Maintainability Readiness Assessment (MRA). Proceedings of the 2008 Annual Reliability and Maintainability Symposium.Washington, DC, USA 2008; 488-490.
3. Saraswat S, Yadava GS. An overview on reliability, availability, maintainability and supportability (RAMS) engineering. International Journal of Quality & Reliability Management 2008; 3 (25): 330-344.
4. Bluvband Z. Availability Growth Aspects of Reliability Growth. Proceeding of Annual Reliability and Maintainability Symposium, IEEE 1990: 522-527.
5. Mi J. Interval Estimation of Availability of a Series System. IEEE Transaction on Reliability1991; 40 (5): 541-546.
6. Oliveto FE. An Algorithm to Partition the Operational Availability Parts of an Optimal Provisioning Strategy. IEEE Proceeding of Annual Reliability and Maintainability Symposium 1999; 310-316.
7. Carpaneto E, Mosso A, Ponta A, Roggero E. Comparison of Reliability and Availability Evaluation Techniques for Distribution Network Systems. IEEE Proceeding of reliability and maintainability symposium 2002; 563-568.
8. Sugatani A, Miyamoto Y, Murakami S, Koyano K, Ide R, Ishida H, Kuraya N, Yamada Y, Abe T, Niwa Y. Development of reliability and maintainability analysis system. SICE Annual Conference in Sapporo, Jappan 2004; 163-167.
9. Leon PMDe, Diaz VG, Martinez LB, Marquez AC. A practical method for the maintainability assessment in industrial devices using indicators and specific attributes. Reliability Engineering and System Safety 2012; 100: 84–92
10. Ebeling C E. An introduction to reliability and maintainability engineering [M]. Tata McGraw-Hill Education 2004.
11. Villemeur A. Reliability, Availability, Maintainability, and Safety Assessment: Assessment, hardware, software, and human factors[M]. Wiley 1992.
12. Rotab MR, Zohrul, Kabir, A.B.M. Availability Simulation of an Ammonia Plant. Reliability Engineering and System Safety 1995; 48: 217-227.
13. Bowles JB, Dobbins JG. High-Availability Transaction Processing: Practical Experience in Availability Modeling and Analysis. Proceeding of Annual Reliability and Maintainability Symposium, IEEE 1998; 268-213.

Yongmin YANG
Zhimiao LU
Xu LUO
Zhexue GE
Yanling QIAN
Laboratory of Science and Technology on Integrated Logistics Support
School of Mechatronics Engineering and Automation
National University of Defense Technology
De Ya Road., 109, Changsha, Hunan 410073, P. R. China
E-mails: yangyongmin@163.com, neorainbow@yeah.net,
luoxu2002@gmail.com, gzx@nudt.edu.cn, ylqian@nudt.edu.cn

Article citation info:
ŻYCZYŃSKA A. The heat consumption and heating costs after the insulation of building partitions of building complex supplied by the local oil boiler room. Eksploatacja i Niezawodnosc – Maintenance and Reliability 2014; 16 (2): 313–318.

Anna ŻYCZYŃSKA

THE HEAT CONSUMPTION AND HEATING COSTS AFTER THE INSULATION OF BUILDING PARTITIONS OF BUILDING COMPLEX SUPPLIED BY THE LOCAL OIL BOILER ROOM

ZUŻYCIE CIEPŁA I KOSZTY OGRZEWANIA PO DOCIEPLENIU PRZEGRÓD BUDOWLANYCH ZESPOŁU BUDYNKÓW ZASILANYCH Z LOKALNEJ KOTŁOWNI OLEJOWEJ*

The paper presents the indices of energy consumption obtained in operating conditions as well as the heating costs before and after the insulation of external partitions of eight multiple dwelling buildings supplied by the common heat source which is the local boiler room heated by light fuel oil. The heat distribution to the particular buildings is by the district heating network. In order to determine the average unitary indices of energy consumption aimed at heating of the whole building complex, the analysis of fuel consumption is carried out, with consideration of standard computational conditions. The analysis lasted for four years after the insulation of buildings, from 2008 to 2011; its results are compared to the ones obtained from the analysis conducted before the insulation, in 2006. The investment was realised in 2007. The obtained real energy consumption indices are compared to the current requirements of technical conditions. On the basis of the data referring to the operation of buildings, the decrease in the heat consumption due to the insulation of partitions, the variability of fuel price, and the costs of heat generation are estimated . Moreover, the decrease in the emission of pollutants into the atmosphere is defined, as well as the costs of heat generation, which would be incurred if there was no insulation of partitions, are estimated.

***Keywords**: heat-transfer coefficient, the insulation of building partitions, heat energy consumption in a building, heating costs.*

W artykule przedstawiono wskaźniki zużycia energii uzyskane w warunkach eksploatacyjnych i koszty ogrzewania przed i po dociepleniu przegród zewnętrznych grupy ośmiu budynków mieszkalnych wielorodzinnych zasilanych ze wspólnego źródła ciepła. Źródłem ciepła jest kotłownia lokalna opalana olejem opałowym lekkim, dystrybucja ciepła do poszczególnych budynków następuje poprzez osiedlową sieć ciepłowniczą. W celu określenia średnich jednostkowych wskaźników zużycia energii na cele grzewcze dla całego zespołu budynków przeprowadzono analizę zużycia paliwa uwzględniając standardowe warunki obliczeniowe. Analizą objęto okres czterech lat po dociepleniu budynków od 2008–2011 r. i odniesiono do stanu przed dociepleniem z 2006 r., inwestycja była realizowana w 2007 r. Uzyskane rzeczywiste wskaźniki zużycia energii porównano do obecnie obowiązujących wymagań warunków technicznych. Na podstawie danych z eksploatacji budynków przeanalizowano spadek zużycia ciepła z tytułu docieplenia przegród, zmienność cen paliwa i kosztów eksploatacyjnych ogrzewania, określono spadek emisji zanieczyszczeń do atmosfery, oszacowano koszty eksploatacyjne ogrzewania jakie zostałyby poniesione w przypadku braku docieplenia przegród budowlanych.

***Słowa kluczowe**: współczynnik przenikania ciepła, docieplenie przegród budowlanych, zużycie ciepła w budynku, koszty ogrzewania.*

1. Introduction

The sector of building industry is one of major consumers of heat energy in economy. For this reason, the energetic policy of particular countries aims at introducing the strategies which reduce the energy consumption in this sector. Energy that is essential to heat rooms has the biggest share in the structure of energy consumption in a building which is not equipped with air conditioning [2, 5, 13]. For various types of buildings, one analyses the possibility of saving the heat energy by enhancing the parameters of thermal insulation of a building structure, increasing the efficiency of heating systems, the appropriate choice of heat source as well as by energy management [1, 4], [6–8], [11–12]. The investments aimed at the decrease in the heat consumption in building engineering, have been realised for several years in Poland and many other countries. Such investments are financially supported by the European Union or national budget. The most significant outcomes of such ventures are heat savings which contribute to the decrease in fuel consumption, and consequently, results in the reduction of the emission of pollutants into the atmosphere, and the drop in the operating costs of heating. Financial support is conditioned upon the fulfilment of requirements referring to the heat insulation of building partitions. The heat energy savings calculated in various studies according to current algorithm based on the domestic regulations as well as European and Polish standards, are the approximate predictive quantities. It is possible to determine the true level of energy savings and its unitary indices of consumption which can be compared to the requirements, owing to the measurements of heat energy or fuel consumption, performed in the operating condition, for heating purposes in a building and subsequently, by the analysis of obtained results, simultaneously, allowing for the changes in outside

(*) Tekst artykułu w polskiej wersji językowej dostępny w elektronicznym wydaniu kwartalnika na stronie ***www.ein.org.pl***

temperature and the length of the heating season. In the case of the high indices while managing the property, the steps should be taken to introduce conscious energy management in a building. The energetic savings and the average real indices of energy consumption for heating purposes, obtained in the operating conditions, are examined in the article.

2. The Description of object

Among the analysed group of eight buildings, two types can be distinguished: three one-storey, two-family houses made in the traditional way; and five three-storey, twelve-family buildings of one- or two-staircase made in the industrial technology, known as 'żerańska brick'. The district was built in the years 1968-1978, whereas the existing single-function oil boiler room as well as two-wire heating network were built in 2003. The location of buildings (third climate zone) and the route of network are displayed in fig.1.

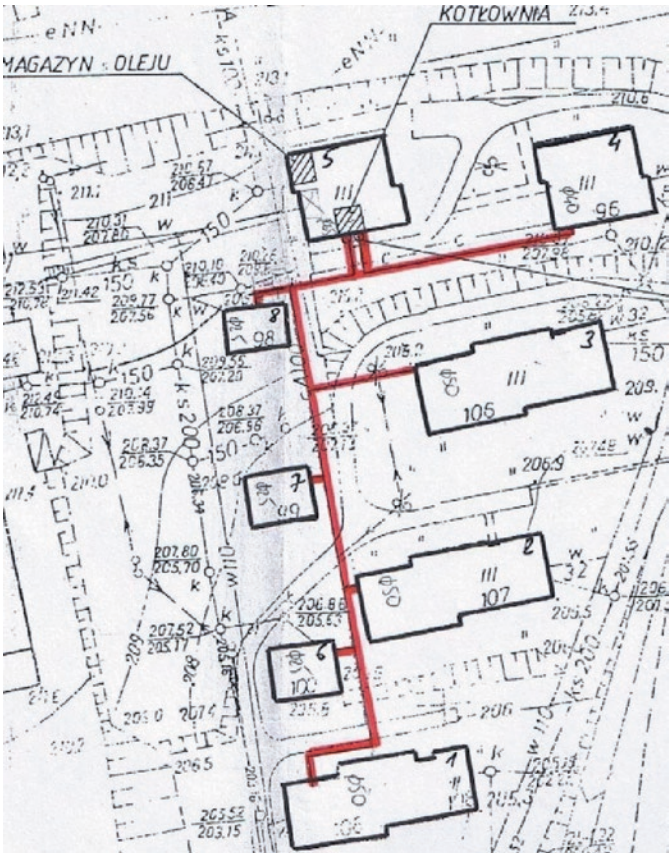

Fig. 1. The localization of dwelling-house complex together with the route of heating network

The total usable area which is heated amounts to 3745,5 m^2 where 66 apartments are located and is occupied by 246 people. The proprietor of the district is a homeowner association administered by a licensed property manager. The settlement of consumption costs is proportional to the heated usable area.

Before the insulation, building partitions in the objects were characterised by the following coefficients: heat transfer coefficients [15] expressed in [W/m^2K]: external walls – 1,15 or 1,12; ventilated slab roofs – 0,93 or 0,72; a roof – 1,43; the ceilings of cellars from 0,83; 1,00 to 1,01; floors on ground – 0,56 or 0,46; windows – 2,6 and 1,8 and the external doors – 2,5 or 1,8. The shape coefficient A/Ve (A – the sum total of the partitions area separating heated area from the external environment, not heated area and ground; Ve – cubic capacity of heating) of two-family buildings amounts to 1,01, whereas of the remaining ones to 0,53 or 0,54. The heating systems in buildings have not been modernised since their installation, at the end of 1970s'. The hydraulic regulation was realised by the orifices fixed at heaters and at the bottom of risers. However, the boiler room is equipped with the weather control panel which allows to regulate the system centrally. The generation of warm water takes place locally by electricity, in separate apartments. In 2007 the external walls, roofs and slab roofs in all buildings were insulated; the windows at staircases and external doors were replaced. The heating system stayed unchanged. The computational heat transfer coefficients of partitions after the insulation [15] expressed by [W/m^2K], amount to: external walls – 0,25; ventilated slab roofs – 0,22 or 0,21; a roof – 0,22; the ceilings of cellars - from 0,83 to 1,01; floors on ground - 0,56 or 0,46; staircase windows - 1,8 and external doors - 1,8. It should be stated that according to the administrator and users' information, before the insulation, the buildings were not sufficiently heated and the calculated temperatures of internal air were not achieved. Figure 2 shows the buildings before the commencement of investment; whereas figure 3 presents the already finished venture

3. The methodology of computations

The computations, conducted during the years 2008–2011, comprise the determination of the level of heat consumption for heating purposes; the emisson of pollutants; and the analysis of operating costs related to heating, and their comparison with the state from 2006. On the basis of the fuel supply documents, the consumption of light fuel oil for heating purposes could be analysed; and the unitary prices as well as the calorific value and density of light fuel oil could be assumed. The consumption of heat and the operating costs of heating were brought to the same level of reference. Thus, the values of corrective coefficient (φ), for the external computational conditions in a given year (assuming that internal temperature amounts to 20°C), were determined according to the dependence (1) and on the basis of the data concerning the length of the standard and real heating season; as well as the standard and measured average, monthly temperatures of outside air from the nearest weather station. The average index of the demand for the final energy and the non-renewable primary energy, was determined during the analysed period in every year. Owing to the fact that there is no individual measurement of heat consumption in buildings, the indices contain heat losses resulting from the generation and distribution of heat in the existing system. Subsequently, the obtained results are compared to the current requirements of technical conditions for dwelling buildings. The average, unitary prices of light fuel oil as well as the average unitary heating costs before and after the insulation are calculated in order to estimate the financial indices. The ecological effect is illustrated by the decrease in the emission of pollutants such as, carbon dioxide, carbon oxide, sulfur oxides, nitrogen oxides, dust and benzo-[a]-pyrene

The following dependencies are used in computations:

$$\phi = \frac{Sd_s}{Sd_r} \tag{1}$$

where:

- φ – the corrective coefficient for a given year
- Sd_r – the number of degree days for a given year
- Sd_s – the number of degree days for a meteorological station in a standard year (for the analysed case 3825,2 [day · K / year])

Fig.2 Buildings before the investment: two-family, one-staircase and two-staircase dwelling-house [15]

Fig.3 Buildings after the investment: two-family, one-staircase and two-staircase dwelling-houses [15]

$$Q_{co} = 0{,}001 \cdot \varphi \cdot V \cdot W_0 \cdot \rho \tag{2}$$

where:

Q_{co} – the heat energy consumption for heating purposes [GJ/ year]
V – the volume of oil used for heating purposes [dm^3/year]
W_o – the calorific value of oil (42,6 MJ/dm^3 is assumed)
ρ – the density of oil (0,85 kg/dm^3 is assumed)

$$EK_H = 100 \cdot \frac{Q_{co}}{A_f \cdot 3{,}6} \tag{3}$$

$$EK_H{}^* = EK_H \cdot \eta \tag{4}$$

$$EP_H = w_i \cdot EK_H \tag{5}$$

$$EP_H{}^* = w_i \cdot EK_H{}^* \tag{6}$$

$$EP_{HWT} = 55 + 90 \cdot A/V_e \tag{7}$$

$$EP_{HWT}{}' = 1{,}15 \cdot EP_{HWT} \tag{8}$$

where:

EK_H – the average index of the demand for the final energy to heat the district, together with the losses on the grounds of the generation in the local source and transmission by the district heating network [kWh/m^2·year]
$EK_H{}^*$ – the average index of the demand for the final energy to heat the district buildings, reduced in the losses due to the generation and transmission [kWh/m^2·year]
EP_H – the average index of the demand for the non-renewable primary energy to heat the district, together with the losses due to the generation in the local source and transmission by the district heating network [kWh/m^2·year] acc[9]
$EP_H{}^*$ – the average index of the demand for the non-renewable primary energy to heat the district buildings, reduced in losses due to the generation and transmission [kWh/ m^2·year]
EP_{HWT} – the average index of the demand for non-renewable primary energy to heat new buildings, determined according to the requirements of technical conditions [kWh/m^2·year] acc.[10]
$EP_{HWT}{}'$ – the average index of the demand for non-renewable primary energy to heat modernised buildings, determined according to the requirements of technical conditions [kWh/ m^2·year] acc.[10]
A/V_e – the coefficient of building shape (0,57 1/m is assumed as the average value weighted for the whole group of buildings)
A_f – the usable area of rooms of regulated temperature (in total 3745,5 m^2 for all the buildings)
w_i – the expenditure coefficient of non-renewable primary energy (1,1 is assumed acc. [9])
η – the efficiency of energy generation in a boiler room and transmission of the district heating network (by the application of [9], 0,85 is assumed as the product of values 0,89 and 0,95)

$$K_r = V \cdot C_j \tag{9}$$

$$K_r{}^* = \varphi \cdot V \cdot C_j \tag{10}$$

$$k_j = \frac{K_r{}^*}{A_f \cdot 12} \tag{11}$$

where:

K_r – the annual costs of the oil purchase [zl/year]
$K_r{}^*$ – the corrected annual costs of the oil purchase [zl/year]
k_j – the unitary cost of heating [zl/m^2·month]

C_j – the average gross price of fuel oil in a given year [zl/dm^3]

The ecological indices resulting from the fuel consumption are expressed by determining the emission of carbon dioxide (CO_2), carbon oxide (CO), sulfur dioxide (SO_2), nitrogen oxides (NO_x), dust (TSP=PM10) and benzo-[a]-pyrene, employing the dependency (12) as well as the assumptions included in [14]:

$$E = B \cdot W \tag{12}$$

$$B = 0{,}001 \cdot \varphi \cdot V \tag{13}$$

where:

E – substance emission [kg]
B – fuel consumption [m^3]
W – the index of sling load [kg/m^3]

4. The analysis of results

The computational results are achieved on the basis of the above dependencies, the source data concerning operation, made accessible by the property administrator, and the information included in building documentation in tables 1, 2, 3, 4 as well as in the diagrams (figs. 4 and 5).

4.1. The heat savings concerning heating

The achieved real level of heat consumption on heating, obtained during the years 2008-2011 (2007 is assumed to be temporal due to the investment realisation) is referred to 2006 and extends from 16,3% to 21,5% for particular year

Table1. The demand for heat

Lp.	Year	φ	V	φ·V	Q_{co}	q_j
-	-	-	dm^3/year	dm^3/year	GJ/year	GJ/m^2
1	2006	1,010	70713	71420	2586	0,690
2	2007	1,041	60779	63271	2291	0,612
3	2008	1,074	55151	59232	2145	0,573
4	2009	1,030	58025	59766	2164	0,578
5	2010	0,897	65164	58452	2117	0,565
6	2011	1,025	54684	56051	2030	0,542

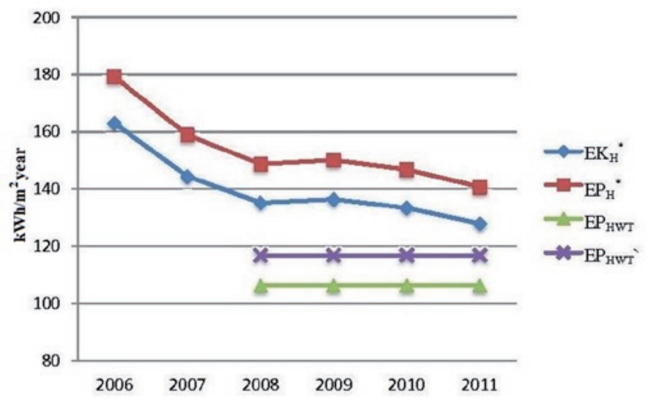

Fig. 4 The value of EK_H^* and EP_H^* in reference to EP_{HWT} and EP_{HWT}'

Nevertheless, the indices of the demand for energy which are displayed in fig.5 reach the following level:

– According to the requirements of technical conditions [10] for a 'new' building

EP_{HWT} = 106,3 kWh/m^{2}year

– According to the requirements of technical conditions [10] for a 'modernised' building

EP_{HWT}' = 116,9 kWh/m^{2}year

– The average index after thermomodernisation in the years 2008-2011, excluding 2007 of the realisation of investment, respectively

EK_H^* = 133,2 kWh/m^{2}year and **EP_H^* = 146,5 kWh/m^{2}year**

– The discrepancy between the real state and technical requirements:

ΔEP_H = 25,3 %

4.2. The operating costs

Table 2 contains the annual consumption costs incurred before and after the insulation of building partitions; the average unitary prices of fuel purchase; as well as the estimated unitary fees per month for 1m^2 of heated area. The annular costs of oil purchase (K_r^{**}) are shown in table 2, and the unitary heating costs (k_j^*) depicted in fig. 5, in the case of absence of insulation of external partitions (for each year, the level of heat energy consumption is assumed as in 2006; whereas the price of fuel purchase is assumed as the average value for a given year).).

Table 2. The operating costs

Lp.	Year	C_j	O_Z	K_r	K_r^*	K_r^{**}
-	-	zł/dm^3	zł/GJ	zł/year	zł/year	zł/year
1	2006	1,90	52,47	134188	135698	135698
2	2007	2,28	62,97	138648	144258	162838
3	2008	2,66	73,46	146933	157558	189977
4	2009	2,27	62,69	131640	135668	162123
5	2010	2,69	74,29	175032	157236	192120
6	2011	3,43	94,73	187557	192255	244971

Oz – the average cost of one GJ of heat energy for the group of buildings

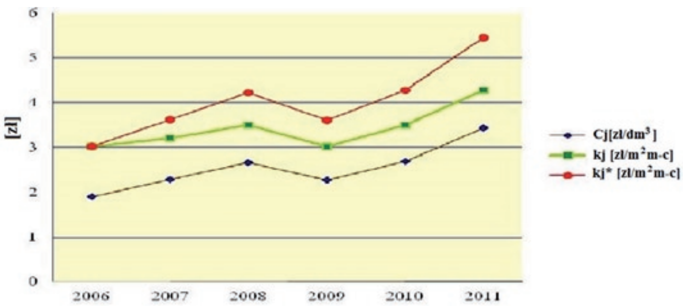

Fig. 5 The variability of unit costs of heating and prices of light fuel oil

4.3. The ecological effect

The emission of pollutants in the particular years of analysed period is shown in table 3, while its decrease with reference to 2006 is presented in table 4. The proportional drop in the emission of pollutants is designated as **ΔE**. The type of fuel has not been changed, hence the proportional decrease in the emission of every kind of pollutant is the same.

5. Summary

As a result of the insulation of external walls, roofs and slab roofs; as well as the replacement of external doors and windows at staircases, the real energy savings (achieved in the operating conditions) referred to the standard computational conditions of 2006 (before

Table 3. The emission of pollutants

Lp.	Year	B	SO_2	NOx	CO	CO_2	PM10	Benzo(a)piren
-	-	m^3/year	kg/year	kg/year	kg/year	kg/year	kg/year	kg/year
1	2006	71,42	364,2	142,8	40,7	192834	24,28	0,0186
2	2007	63,27	322,7	126,5	36,1	170832	21,51	0,0165
3	2008	59,23	302,1	118,5	33,8	159927	20,14	0,0154
4	2009	59,77	304,8	119,5	34,1	161368	20,32	0,0155
5	2010	58,45	298,1	116,9	33,3	157821	19,87	0,0152
6	2011	56,05	285,9	112,1	31,9	151335	19,06	0,0146

Table 4. The decrease in the emission of pollutants

Lp.	Rok	ΔE	ΔSO_2	ΔNOx	ΔCO	ΔCO_2	ΔPM10	ΔBenzo(a)piren
-	-	%	kg/year	kg/year	kg/year	kg/year	kg/year	kg/year
1	2007	11,4	41,5	16,3	4,6	22002	2,77	0,0021
2	2008	17,1	62,1	24,3	6,9	32907	4,14	0,0032
3	2009	16,3	59,4	23,3	6,6	31466	3,96	0,0031
4	2010	18,2	66,1	25,9	7,4	35013	4,41	0,0034
5	2011	21,5	78,3	30,7	8,8	41499	5,22	0,0040

the insulation) are within the range from 16,3 to 21,5% for particular years within the period of 2008 and 2011. The obtained decrease in the consumption of heat energy is lower than expected due to the lack of reliable hydraulic regulation of heating

The averaged for the whole group of buildings, the lowest value of final energy consumption index amounts to 127,9 kWh/m^{2}year in the operating conditions; whereas the value of non-renewable primary energy consumption index is 140,7 kWh/m^{2}year. In the case of averaged value, required for the buildings after the modernisation, amounting to 116,9 kWh/m^{2}year, the obtained value exceeds the required one of about 20,4%. Consequently, it is necessary to introduce subsequent activities so as to reduce the consumption of heat energy in the complex of buildings by raising the efficiency of use, consumption and transmission in the heating installation; as well as to provide the rational energy management by the users of buildings.

The decrease in the consumption of fuel takes place together with the decrease in the emission of pollutants which is characteristic of light fuel oil combustion, at the level equal to the level of energy saving

The energetic savings generate financial savings concerning the consumption costs of heating; nevertheless, the prices of fuel which rise constantly, reduce these effects substantially. In the discussed case, the unitary costs do not decrease despite the limitation on fuel consumption. Yet, from the analysis conducted before the insulation and after considering the rise in oil prices, the operating costs would be higher, for instance of about 27,3% in the last year. The increase in oil prices consumes the financial savings received from the reduction of heat consumption. The differences occurring between the obtained results for particular years show that the approach to the operation and usage of a building as well as its technical equipment exerts the impact on the real energetic and financial effects of thermomodernisation.

The improvement of heat insulation contributes to the freezing elimination in the fragments of buildings partitions and allows to achieve the inside temperature which provides comfort in heated rooms. The realised investment encompassing the whole complex of buildings simultaneously, increases substantially the aesthetic qualities and the market value of a property. These imponderable effects are also significant to the owners of properties.

Bibliography

1. Chengmin Ch, Yufeng Z, Lijun M. Assessment for central heating systems with different heat sources: A case study. Energy and Buildings 2012; 48:168–174.
2. Colmenar-Santos A, Terán de Lober L N, Borge-Diez D, Castro-Gil M. Solutions to reduce energy consumption in the management of large buildings. Energy and Buildings 2013; 56: 66–77.
3. Source data from the administrator of buildings concerning the parameters and quantity of light fuel oil consumption as well as the heating costs from 2006 to 2007.
4. Joelsson A, Gustavsson L. District heating and energy efficiency in detached houses of differing size and construction. Applied Energy 2009; 86: 126-134.
5. Leidl Ch M, Lubitz W D. Comparing domestic water heating technologies. Technology in Society 2009; 31: 244–256.
6. Mřrck O, Thomsen K E, Rose J. The EU CONCERTO project Class 1 – Demonstrating cost-effective low-energy buildings – Recent results with special focus on comparison of calculated and measured energy performance of Danish buildings. Applied Energy 2012; 97: 319–326.
7. Olesena B W, de Carli M. Calculation of the yearly energy performance of heating systems based on the ichele European Building Energy Directive and related CEN standards. Energy and Buildings 2011; 43:1040–1050.
8. Peeters L, Van der Veken J, Hens H, Helsen L, D'haeseleer W. Control of heating systems in residential buildings: Current practice. Energy and Buildings 2008; 40:1446–1455.

9. The Regulation of Infrastructure Minister from 6.11.2008 concerning the methodology for the computation of energetic characteristics of a building, a dwelling house or the part of a building being an independent technical – usable entity; as well as the method of devising the model certifiates of energy characteristics. (Dz.U. nr 201/2008 r., poz. 1240)
10. The Regulation of Infrastructure Minister from 6.11.2008 altering the regulation referring to the technical conditions to which buildings should correspond and their location. (Dz.U. nr 201/2008 r., poz. 1238).
11. Schuler A, Weber Ch, Fahl U. Energy consumption for space heating of West-German households: empirical evidence, scenario projections and policy implications. Energy Policy 2000; 28: 877–894.
12. Tolga Baltaa M, Dincerb I, Hepbaslia A. Performance and sustainability assessment of energy options for building HVAC applications. Energy and Buildings 2010; 42:1320–1328.
13. Tuominen P, Forsstr J, Honkatukia J. Economic effects of energy efficiency improvements in the Finnish building stock. Energy Policy 2013; 52:181–189.
14. The indices of the emission of pollutants from the fuel combustion. Boilers of the maximal power amounting to 5 MWt. Krajowy Administrator Systemu Handlu Uprawnieniami do Emisji. Krajowy Ośrodek Bilansowania i Zarządzania Emisjami. January, 2011.
15. Życzyńska A, Dyś G. Energy audits of discussed buildings performed in 2006.

Anna ŻYCZYŃSKA
Department of Historic Objects Conservation
Faculty of Building and Architectures
Lublin University of Technology
ul. Nadbystrzycka 40, 20-816 Lublin, Poland
E-mail: a.zyczynska@pollub.pl

Article citation info:
AU-YONG CP, ALI AS, AHMAD F. Prediction cost maintenance model of office building based on condition-based maintenance. Eksploatacja i Niezawodnosc – Maintenance and Reliability 2014; 16 (2): 319–324.

Cheong Peng AU-YONG
Azlan Shah ALI
Faizah AHMAD

PREDICTION COST MAINTENANCE MODEL OF OFFICE BUILDING BASED ON CONDITION-BASED MAINTENANCE

PREDYKCYJNO-KOSZTOWY MODEL KONSERWACJI BUDYNKU BIUROWEGO OPARTY O UTRZYMANIE ZALEŻNE OD BIEŻĄCEGO STANU TECHNICZNEGO (CBM)

Building maintenance costs are continuously increasing as a result of poor maintenance. Consequently, there is an urgent need to develop solutions to reduce the maintenance costs. Various studies demonstrated that the characteristics of condition-based maintenance are directly related to the cost performance. Thus, this paper seeks to establish the relationships between the characteristics of condition-based maintenance and the cost performance. The researcher then developed a regression model for maintenance planning and prediction. The study adopted a mix method approach that includes questionnaire survey, interview, and case study. The findings highlighted the reliability of maintenance data and information as the most significant characteristic of condition-based maintenance. Consequently, the study concluded that the planning and the application of the condition-based maintenance strategy should consider its significant characteristics and make reference to the resulting prediction model. Furthermore, the study recommended measures to improve the significant characteristics and the cost performance in practice.

***Keywords**: characteristics, condition-based maintenance, cost performance, office building, Malaysia.*

Koszty konserwacji budynków nieustannie rosną ze względu na nieodpowiednią konserwację. Z tej racji, niezbędne jest wypracowanie rozwiązań obniżających koszty konserwacji. Różne badania wykazały, iż charakterystyki utrzymania urządzeń zależnie od ich bieżącego stanu technicznego (condition-based maintenance, CBM) są bezpośrednio powiązane z wydajnością kosztu. Niniejszy artykuł stara się więc ustalić związek pomiędzy charakterystykami utrzymania budynków zależnie od ich bieżącego stanu technicznego a wydajnością kosztu. Następnie opracowano model regresji dla planowania konserwacji jak i predykcji. W badaniach użyto metody mieszanej łączącej badania kwestionariuszowe, wywiad oraz studium przypadku. Rezultaty podkreśliły, iż wiarygodność danych z konserwacji i informacji to najbardziej istotne charakterystyki CBM. W konsekwencji, wnioski z badań sugerują, iż planowanie i wdrożenie strategii utrzymania w zależności od bieżącego stanu technicznego powinno brać pod uwagę jej istotne charakterystyki i odwoływać się do wynikającego z niej modelu predykcji. Ponadto, praca zawiera zalecenia jakimi środkami można w praktyce poprawić istotne charakterystyki i wydajność kosztu.

***Słowa kluczowe**: charakterystyki, utrzymanie zależne od bieżącego stanu technicznego (CBM), wydajność kosztu, budynek biurowy, Malezja.*

1. Introduction

Building maintenance is the combination of technical and administrative actions to ensure the items and elements of a building are of an acceptable standard to perform their required functions. Generally, building maintenance is divided into planned maintenance and unplanned maintenance under BS3811 [25]. Planned maintenance is the predetermined tasks that are well organised and performed in advance so as to reduce or to prevent any damages to the components or items. It is subdivided into scheduled maintenance and condition-based maintenance. On the other hand, unplanned maintenance is carried out in the event of contingency maintenance without any predetermined plan after failure or damage was detected. It is subdivided into corrective maintenance and emergency maintenance [1].

Moreover, planned maintenance should be the major activity in building maintenance compared to unplanned maintenance. Otherwise, unplanned maintenance will result in frequent breakdown or downtime, and subsequently, high maintenance cost for repair and replacement works [7]. Thus, condition-based maintenance, as a strategy of planned maintenance, should be recommended to achieve the optimal maintenance expenditure.

This paper aims to establish the relationship between the characteristics and the performance through inferential analysis; then, to develop a regression model for prediction purpose. Taking into cognizance of the advantages and disadvantages of condition-based maintenance, this paper focuses on the characteristics of condition-based maintenance towards maintenance performance as shown in Figure 1.

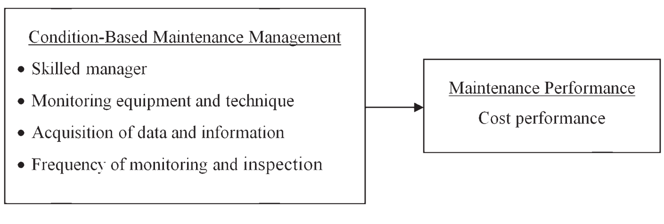

Fig. 1. Relationship between characteristics of condition-based maintenance and maintenance performance

2. High-Rise Office Building

In Malaysia, high-rise building is defined as building of more than 7 storeys (or the top floor of the building is more than 60 feet) [8]. This definition is in accordance with the Uniform Building By-Laws 1984. Despite the increasing concerns on the maintenance of buildings in Malaysia, there are few researches on the facilities and maintenance management of high rise office building.

Office buildings usually have their own maintenance management teams managed by the maintenance or the building managers to preserve the conditions of the buildings [30]. Generally, the services provided by the building managers in office buildings are cleaning, landscaping, general maintenance, lighting, heating, ventilating and air conditioning (HVAC), lift or escalator, mechanical and electrical, sanitary and plumbing, access, signage, parking and others [22]. These services are significant for office buildings as they provide functions, safety, health and comfort to the building users in daily activities.

However, building satisfaction surveys indicated that most building users were not satisfied with the building services [30]. The building users' dissatisfaction was mainly due to issues such as lack of maintenance staff, lack of expertise, lack of tools and technology, insufficient allocations and inappropriate maintenance strategies. These issues are more evident in medium-sized high-rise office building, which is equipped with more sophisticated systems, such as fire detection and protection systems, central heating, ventilating and air conditioning system, escalators and others [15].

Therefore, this study focuses on the issue related to the building users' dissatisfaction in high-rise office buildings through the examination of the characteristics of condition-based maintenance strategy towards maintenance performance.

3. Characteristics of Condition-Based Maintenance

Condition-based maintenance is defined as the maintenance initiated as a result of knowledge of the condition or significant deterioration of an item or component through continuous monitoring and routine inspection to minimise the total cost of repairs [11, 12, 17, 19, 25]. This maintenance strategy is aimed to minimise the total maintenance cost by collecting and gathering the condition data of the building systems, especially those critical components. However, the maintenance strategy might not be applicable to all building systems or assets in terms of the availability of such maintenance technology and cost effectiveness [17]. The characteristics of condition-based maintenance toward maintenance performance are stated below:

3.1. Skilled Manager

This maintenance strategy requires vigorous analysis on the data and information of systems condition and reliability, as well as financial maintenance data. Meanwhile, building managers must have proper understanding on the failure modes and rates, asset criticality, and other significant factors while implementing condition-based maintenance [11]. In order to perform condition-based maintenance effectively, there must be qualified maintenance personnel with related experience, skill and knowledge. High level of training is required for the supervisors and technicians to carry out the maintenance works include condition monitoring, routine inspection, as well as repair and replacement [6, 27]. In this circumstance, skilled manager should be able to provide or conduct training session for the maintenance personnel improve their skill and knowledge. Thus, satisfactory level of skill and knowledge of manager is required to ensure the success of the maintenance strategy.

3.2. Monitoring Equipment and Technique

According to Edward et al. [10], there is a wide range of techniques to examine the condition of specific items or assets, such as oil analysis, vibration monitoring, thermography and so on. Specific measuring and monitoring equipments are required by expertise to perform the maintenance tasks. The tools might be complicated and costly for an organisation [6]. Due to the technical complexity of building systems and the level of sophistication of monitoring tools increases, the maintenance management must be able to train and develop the skill of maintenance personnel for adaptation of new maintenance technology. Therefore, the criteria that should be taken into consideration for condition-based maintenance include:

- Availability of monitoring equipment and technique.
- Capability to adopt the monitoring technology.

3.3. Acquisition of Data and Information

Bevilacqua and Braglia [5] argued that the data and information acquisition systems are the necessary applications to perform condition-based maintenance. The documentation and record of information are essential to ensure the reliability of information about the conditions and remaining lifetime of system components. Ali [2] further explained that the conditions of buildings and systems must be considered to allocate adequate maintenance cost. Thus, the maintenance personnel should acquire the data and information regarding the conditions of building system components. In order to achieve the success of condition-based maintenance, the reliability of data and information regarding system conditions must be taken into consideration.

3.4. Frequency of Monitoring and Inspection

Condition-based maintenance can only be implemented with proper system monitoring and inspection. Tsang [28] found that the frequency of inspection must be determined, either the components are monitored continuously or inspection is performed with fixed interval, so that action can be taken in time to prevent the failures or breakdowns occur. The maintenance personnel need to identify an optimal frequency or interval of inspection to avoid over-inspection or under-inspection. Then, Hameed et al. [16] demonstrated that planning of appropriate maintenance activities prior to failure and maintenance cost is greatly influenced by the ability to monitor and inspect the condition of systems. Thus, it is necessary to identify the optimal frequency of monitoring and inspection, so that condition-based maintenance can improve the performance in term of cost-effectiveness.

4. Maintenance Performance

The development of performance measurement in management aims to improve the quality and service, as well as to meet cost parameters [4]. The measurement of maintenance performance is an assessment that helps to identify the strengths and weaknesses of the maintenance activities. In addition, the result of performance measurement indicates the effectiveness of the existing strategy. Consequently, the management team is able to plan and make appropriate decision for future maintenance strategy [13].

The measurement of performance can be obtained through the level of success or failure in terms of schedule, cost and functionality [18, 26]. Acknowledging that the rising maintenance cost is one of the major concerns of the industry and public, this study chose cost performance as the dependent variable. The cost or expenditure for building maintenance is often used in measuring the performance of buildings. The maintenance performance is calculated using the variance of actual expenditure and planned cost for building maintenance activities [2]. However, accuracy of planned cost reflects the credibility of maintenance performance. Therefore, it is vital for top management to identify the planned maintenance cost at the planning stage.

For the purpose of this study, a comparison between the actual and the planned cost was made to identify the level of maintenance performance. For example, maintenance performance of a building system is deemed below expectation when the actual expenditure for maintenance tasks exceeds the planned cost. In contrast, high performance level is achieved when the total expenditure is below the planned cost for maintenance works.

5. Research Methodology

This research adopted a mixed method approach that was adopted by Ali [3] and Nik Mat [23] to study maintenance-related topics. The approach comprises literature review, questionnaire survey, semi-structured interviews, and case study. This approach allows researchers to address more complicated research questions and achieve higher reliability and validity of the research [29]. The research was divided into stages and conducted sequentially. Firstly, the characteristics of condition-based maintenance were identified through literature reviews and subsequently; questionnaires were drafted.

Secondly, simple random sampling was adopted in the questionnaire survey to identify the relevant respondents who have been or were involved in office building maintenance management during the period of this research. This method ensures the sample accuracy by selecting the respondents at random and by considering all elements in the population[24]. Population criteria included building requirements, which were high-rise office buildings (7-storey and above) located in Klang Valley, Malaysia and must have been completed for more than two years. 338 (research population) sets of the questionnaire were sent out by post and 100 sets were returned, which gave a return rate of 30 percent. The respondents were maintenance management staff working in the office buildings (see Figure 2). Based on the data obtained during the survey, some of the respondents, included in the category of "others", were either managing directors of a property management firm, or mechanical and electrical engineers. 85 percent of the respondents were building manager, building supervisor and executive specialising in the planning and the execution of maintenance management activities. They are considerably expert in the planning and implementation of maintenance strategies, and thus able to provide accurate and reliable answers towards the questions.

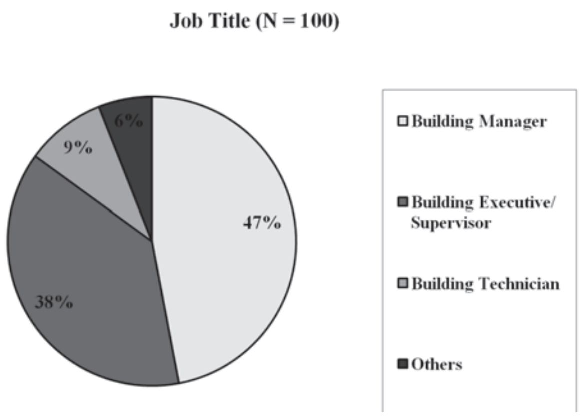

Fig. 2. Respondents' Profile

Subsequently, the survey result was converted and analysed through Statistical Package for Social Science (SPSS) software. Reliability analysis was conducted for the condition-based maintenance characteristics variables to enhance the reliability of the data. The purpose of this analysis was to check the consistency of the scale of data [20]. Cronbach's alpha test showed a coefficient of 0.888. A coefficient of more than 0.70 indicates good reliability.

A correlation test was suitable to measure the relationship between the characteristics of maintenance strategy [9]. It helped to indicate the influence of the maintenance characteristics on the maintenance expenditure. This was performed through the SPSS software. The Pearson product-moment correlation was employed for the analysis. The correlation test was calculated using the following formula:

$$r = \frac{\sum (x-\bar{x})\times(y-\bar{y})}{\sqrt{\sum (x-\bar{x})^2 \sum (y-\bar{y})^2}} \tag{1}$$

Where,

$(x-\bar{x})$ = the deviation of variable X from its mean;

$(y-\bar{y})$ = the deviation of variable Y from its mean.

The findings on the relationships between condition-based maintenance characteristics and cost performance were used as the basis for the prediction of maintenance performance. The predicted value of a dependent variable from the value of an independent variable is called regression [14]. In this study, there were more than one significant independent variables identified. Thus, a multiple linear regression was used to analyse the collective and the separate contributions of two or more independent variables to the variation of the dependent variable. The multiple linear regression is formulated as:

$$Y = \beta_0 + \beta_1 X_1 + \beta_2 X_2 + \ldots + \beta_k X_k + \varepsilon \tag{2}$$

Where,

Y is the dependent variable (Y = maintenance expenditure variance)

$X_1, X_2, \ldots, X_k$ are the independent variables (X_1 = skill and knowledge of manager; X_2 = availability of monitoring equipment and technique; X_3 = capability to adopt the monitoring technology...)

$Y = \beta_0 + \beta_1 X_1 + \beta_2 X_2 + \ldots + \beta_k X_k$ is the deterministic portion of the model

β_i determines the contribution of the independent variable X_i

ε is the random error

In order to validate the questionnaire results, building managers were interviewed at the third stage. In the interview sessions, the interviewees were required to answer the interview questions and to provide further explanation about the implementation of the maintenance strategy. Thus, the building manager with more than five years' experiences and expertise in office building maintenance was the minimum requirement as the interview respondent. The interviewees were selected from the questionnaire respondents who fulfil the requirement. 76 respondents who met the requirement were identified. However, only 15 of them agreed to participate in the interview session. Semi-structured interviews were conducted to obtain further details and understandings about the significant characteristics of condition-based maintenance determined through the correlation analysis. For example, one of the interview questions was *"Does the level of manager skill and knowledge significantly influence the cost performance? How does it influence the cost performance?"* This type of interview allows the researcher to explore and uncover the respondents' views in detail [21].

Then, a case study was carried out on a 27-storey office building located in Kuala Lumpur. The building is thirteen years old, with total floor area of 324,000 square feet, privately owned and managed under the in-house maintenance and management team. The purpose of the case study was to test the applicability of the developed regression model. Relevant information about the significant predictor was collected. The data was applied into the regression model for calculation of the ratio of maintenance expenditure variance. Consequently, the ratio was compared to the exact scenario of the office building.

6. Finding and Discussions

6.1. Relationship between Characteristics of Condition-Based Maintenance and Cost Performance

The findings revealed the relationship between characteristics of condition-based maintenance and cost performance as shown in Table 1. The dependent variable of this study was cost performance, which was determined by maintenance expenditure variance whilst the independent variables were the five variables discussed earlier. SPSS considers variables with the significance value of 0.05 or below to be significantly correlated. Four out of the identified five independent variables were determined to be significantly correlated to the maintenance expenditure variance. The variables are as follows:

- Skill and knowledge of manager
- Availability of monitoring equipment and technique
- Capability to adopt the monitoring technology
- Reliability of maintenance data and information

Table 1. Correlation between characteristics of condition-based maintenance and maintenance cost performance

Characteristic	Maintenance Expenditure Variance
Skilled Manager-Skill and Knowledge	-.276**
Equipment and Technique-Availability	-.350**
Equipment and Technique-Capability to Adopt	-.240*
Acquisition of Data-Reliability	-.394**
Monitoring and Inspection-Frequency	-.138

***. Correlation is significant at the 0.01 level (2-tailed)*

**. Correlation is significant at the 0.05 level (2-tailed)*

In condition-based maintenance, skilful and knowledgeable maintenance manager is needed for allocating appropriate manpower, providing training, monitoring the system conditions, as well as supervising the execution of inspection and maintenance works. The analysis result as shown in Table 1 stated that the level of manager skill and knowledge was significantly correlated to the maintenance expenditure variance. Condition-based maintenance is meant to prevent system failure by monitoring the system condition and restoring the system to its required standard before failure occurs. When a manager does not have sufficient skill and knowledge to adopt the condition-based maintenance effectively, defects and failures are likely to occur. Thus, additional maintenance cost will be required for the repair works. As a result, the exact maintenance expenditure varies from the planned maintenance expenditure. Meanwhile, the analysis result was supported by majority of the interviewees, who demonstrated that skilful manager is able to ensure the optimal workforce, tools and parts allocated for each maintenance task at minimal cost.

Additionally, the availability of condition monitoring technology may help to improve the maintenance outcome. It was found that the availability of equipment and technique significantly correlated to the maintenance expenditure variance (see Table 1). Since Tsang [28] mentioned that the availability of reliable monitoring and inspection technology is one of the factors to be concerned in condition-based maintenance, the selection of monitoring equipment and technique must be suitable for the monitoring and inspection of building systems. Furthermore, most of the interviewees noted that the condition of building system can be easily tracked and monitored by having appropriate equipment and technique. Therefore, the probability of system failure is minimised. The maintenance expenditure variance is prevented as well because emergency repair cost is reduced.

Meanwhile, specific monitoring and inspection tools and equipment require the expertise to operate and use them in condition-based maintenance. The capability to adopt equipment and technique was found to be significantly correlated to the maintenance expenditure variance (see Table 1). According to Carnero [6], it is complicated and costly for an organisation to acquire the condition monitoring tools and technology. If yet, the maintenance personnel are not capable to utilise those tools and technology, more maintenance issues may occur. Then, additional maintenance cost will be needed to solve the problems. Therefore, the exact maintenance expenditure varies from the planned one. In fact, the interview results proved that capable to adopt and utilise monitoring equipment and technique is compulsory for predicting and remedying system defects.

Furthermore, system condition data and information is one of the most important aspects to be considered in condition-based maintenance. In this maintenance strategy, the maintenance tasks such as replacement works are implemented when the parts are almost end of their lifetime by referring to the condition data. The reliability of data and information was found to be significantly correlated to the maintenance expenditure variance (see Table 1). The primary aim of condition-based maintenance is to prevent failure occurs by monitoring the condition of building systems. Basically, emergency repair cost will not be allocated in planning stage of this maintenance strategy. Some interviewees revealed that reliable condition data can indicate the need of maintenance accurately. This will help to enhance the quality of system operation, as well as utilise the resources and time. Oppositely, when the obtained system condition data is not reliable and accurate, the occurrence of sudden breakdown may not able to be avoided. As a result, additional maintenance expenditure is required for the repair work and it varies from the planned maintenance expenditure.

6.2. Regression Model of Maintenance Cost Performance

Since there were four characteristics found to be significantly correlated to the cost performance, the predictors of maintenance expenditure variance (MEV) included skill and knowledge of manager (SKM), availability of monitoring equipment and technique (AET), capability to adopt monitoring technology (CAT), as well as reliability of maintenance data and information (RDI). The regression model for the research was produced as follows (see also Table 2):

Model 1 (Enter Method)

$$MEV = 6.686 - 0.162\ SKM - 0.392\ AET + 0.272\ CAT - 0.513\ RDI \quad (3)$$

Coefficient of multiple regression, $R^2 = 0.186$ (18.6%)

However, the analysis result determined that three predictors were not significant with p-value of more than 0.05. So, another regression model that eliminated the non-significant predictors was developed as follows (see also Table 3). This model was determined appropriate and accurate to estimate the maintenance expenditure variance.

Model 2 (Stepwise Method)

$$MEV = 6.281 - 0.665\ RDI \quad (4)$$

Coefficient of multiple regression, $R^2 = 0.148$ (14.8%)

In order to ensure that the regression models were not violated, the validity of the regression models was checked. Data tabulated in Table 2 and Table 3 had proven that there was no problem of multicollinearity for Model 1 and Model 2 respectively. Whereby, the tolerance value should not be less than 0.1 and variance inflation factor, VIF should not be greater than 10.

Table 2. Coefficients[a] – enter method (characteristics of condition-based maintenance toward maintenance expenditure variance)

Model		Unstandardized Coefficients		Standardized Coefficients	t	Sig.	Collinearity Statistics	
		B	Std. Error	Beta			Tolerance	VIF
1	(Constant)	6.686	.743		8.999	.000		
	Skilled Manager-Skill and Knowledge	-.162	.240	-.083	-.675	.501	.572	1.748
	Equipment and Technique-Availability	-.392	.218	-.226	-1.800	.075	.544	1.838
	Equipment and Technique-Capability to Adopt	.272	.268	.137	1.014	.313	.472	2.121
	Acquisition of Data-Reliability	-.513	.222	-.297	-2.315	.023	.521	1.919

a. Dependent Variable: Maintenance Expenditure Variance

Table 3. Coefficients[a] – stepwise method (characteristics of condition-based maintenance toward maintenance expenditure variance)

Model		Unstandardized Coefficients		Standardized Coefficients	t	Sig.	Collinearity Statistics	
		B	Std. Error	Beta			Tolerance	VIF
1	(Constant)	6.281	.577		10.880	.000		
	Acquisition of Data-Reliability	-.665	.161	-.384	-4.121	.000	1.000	1.000

6.3. Testing the Applicability of the Regression Model in Practical

Since Model 2 was identified as the appropriate model to estimate the cost performance, case study on a selected office building was carried out to collect the data about the reliability of maintenance data and maintenance expenditure variance. Level of concern towards the reliability of maintenance data was reflected by the accuracy of maintenance data (see Table 4); while the maintenance expenditure variance was reflected by the ratio of actual maintenance expenditure to planned maintenance expenditure (see Table 5).

Table 4. Measurement units of the predictor

Accuracy of Maintenance Data, %	Level of Concern towards Reliability of Maintenance Data	Measurement Unit
20% and below	Very low degree	1
21 – 40%	Low degree	2
41 – 60%	Average	3
61 – 80%	High degree	4
81% and above	Very high degree	5

Table 5. Measurement units of the prediction

Maintenance Expenditure Variance (Ratio)	Measurement Unit
0 – 0.80	1
0.81 – 0.90	2
0.91 – 1.00	3
1.01 – 1.10	4
1.11 – 1.20	5
1.21 and above	6

In the case study, the management team of the building had a very high degree of concern towards the reliability of maintenance data. The management ensured 85% of the maintenance data was accurate, getting the measurement unit score of 5. Meanwhile, the actual and planned annual maintenance costs of the building were both 148,000 Malaysian Ringgit. Therefore, the ratio of the maintenance expenditure variance was 1.00, with the measurement unit score of 3.

The measurement unit score of the predictor was inserted in to the regression model for calculation as follows:

$$\begin{aligned} MEV &= 6.281 - 0.665\ RDI \\ &= 6.281 - 0.665\ (5) \\ &= 2.956 \approx 3 \end{aligned}$$

As a result, the prediction of maintenance expenditure variance that was calculated through the regression model matched to the exact scenario of the studied case. So, the applicability of the regression model in practical was validated and confirmed. The result also summarised that very high degree of concern towards the reliability of maintenance data is a must to eliminate the issue of over-budget.

7. Conclusion

The findings revealed that the characteristics of condition-based maintenance directly influenced the cost performance. Therefore, it is important to understand the influences of condition-based maintenance characteristics in the maintenance process, from planning to the outcome of maintenance. Skill and knowledge manager, availability of monitoring equipment and technique, capability to adopt monitoring technology, as well as reliability of maintenance data and information were highlighted as the characteristics that significantly influencing the maintenance performance. Model 2 developed from stepwise regression analysis highlighted reliability of maintenance data and information as the significant predictor in condition-based maintenance strategy. Using the prediction model, practitioners can predict the variance of maintenance expenditure from the level of concern towards the reliability of maintenance data. Thus, they may decide how much of concern towards the reliability of maintenance data is required in order to achieve optimal maintenance expenditure. Several measures were recommended to improve the maintenance characteristics. The measures include provision of training to maintenance personnel, effective communication between maintenance personnel and clients, planning of maintenance interval based on priority of building services and safety level to occupants, and the collaboration with the service providers. In conclusion, it is vital for the building maintenance practitioners to incorporate the identified significant characteristics and measures for improvement in planning and executing condition-based maintenance with optimum maintenance cost performance. Nevertheless, further research should be conducted on measures to improve the maintenance strategy and outcome.

***Acknowledgement**: The authors gratefully acknowledge the financial support of the University of Malaya Research Grant (UMRG), grant no. RP007A/13SUS established at the University of Malaya, Sustainability Science Research Cluster.*

References

1. Ahn S, Kim W. On Determination of the Preventive Maintenance Interval Guaranteeing System Availability under a Periodic Maintenance Policy. Structure and Infrastructure Engineering: Maintenance, Management, Life-Cycle Design and Performance 2011;7(4): 307-14.
2. Ali A S. Cost Decision Making in Building Maintenance Practice in Malaysia. Journal of Facilities Management 2009;7(4): 298-306.
3. Ali A S. Integrative Mechanisms in the Design Process of Building Refurbishment Projects [Unpublished Thesis]. Shah Alam: Universiti Teknologi MARA; 2008.
4. Amaratunga D, Baldry D. Moving from Performance Measurement to Performance Management. Facilities 2002; 20(5/6): 217-23.
5. Bevilacqua M, Braglia M. The Analytic Hierarchy Process Applied to Maintenance Strategy Selection. Reliability Engineering and System Safety 2000; 70:71-83.
6. Carnero M C. An Evaluation System of the Setting up of Predictive Maintenance Programmes. Reliability Engineering and System Safety 2006; 91: 945-63.
7. Chareonsuk C, Nagarur N, Tabycanon M T. A Multicriteria Approach to the Selection of Preventive Maintenance Intervals. International Journal of Production Economics 1997; 49: 55-64.
8. DBKL. Jawatankuasa Perancang Bandar 1986. Garis Panduan Bagi Kawalan Pembangunan. Kuala Lumpur: Dewan Bandaraya Kuala Lumpur; 1986.
9. Diamond I, Jefferies J. Beginning Statistics: An Introduction for Social Scientists. London: SAGE Publications Ltd; 2006.
10. Edward D J, Holt G D, Harris F C. Predictive Maintenance Techniques and Their Relevance to Construction Plant. Journal of Quality in Maintenance Engineering 1998; 4(1): 25-37.
11. Ellis B A. Condition Based Maintenance. The Jethro Project 2008: 1-5.
12. Flores-Colen I, De Brito J. A Systematic Approach for Maintenance Budgeting of Buildings Facades Based on Predictive and Preventive Strategies. Construction and Building Materials 2010; 24: 1718-29.
13. Frangopol D M, Liu M. Maintenance and Management of Civil Infrastructure based on Condition, Safety, Optimization, and Life-Cycle Cost. Structure and Infrastructure Engineering: Maintenance, Management, Life-Cycle Design and Performance 2007; 3(1): 29-41.
14. Graziano A M, Raulin M L. Research Methods: A Process of Inquiry. 7th ed. Boston: Pearson Education Inc; 2010.
15. Halim T, Muthusamy K, Chia S Y, Lam S W. A Systems Approach in the Evaluation and Comparison of Engineering Services Applied in Facilities Management. Facilities 2011; 29(3/4): 114-32.
16. Hameed Z, Ahn S H, Cho Y M. Practical Aspects of a Condition Monitoring System for a Wind Turbine with Emphasis on its Design, System Architecture, Testing and Installation. Renewable Energy 2010; 35: 879-94.
17. Horner R M, El-Haram M A, Munns A. Building Maintenance Strategy: A New Management Approach. International Journal of Quality in Maintenance 1997; 3(4): 273-80.
18. Johnson J. Choas: The Dollar Drain of IT Project Failures. Application Development Trend 1995; 2: 41-7.
19. Kelly A, Harris M J. Management of Industrial Maintenance. Butterworths, London 1978.
20. Leech N L, Barrett K C, Morgan G A. IBM SPSS for Intermediate Statistics: Use and Interpretation. 4th ed. New York: Taylor and Francis Group, LLC; 2011.
21. Marshall C, Rossman G B. Designing Qualitative Research. 4th ed. California: Sage Publication, Inc; 2006.
22. Myeda N E, Kamaruzzaman S N, Pitt M. Measuring the Performance of Office Buildings Maintenance Management in Malaysia. Journal of Facilities Management 2011; 9(3): 181-99.
23. Nik Mat N E M. Performance Measurement of Office Buildings Maintenance Management [Unpublished Dissertation]. Kuala Lumpur: University of Malaya; 2009.
24. Saris W E, Gallhofer I N. Design, Evaluation, and Analysis of Questionnaires for Survey Research. New Jersey: John Wiley & Sons Inc.; 2007.
25. Seeley I H. Building Maintenance. 2nd ed. New York: Palgrave; 1987.
26. Sidwell A C. Project Management: Dynamics and Performance. Journal of Construction Management and Economics 1990; 8: 159-78.
27. Swanson L. Linking Maintenance Strategies to Performance. International Journal of Production Economics 2001; 70: 237-44.
28. Tsang A H C. Condition-Based Maintenance: Tools and Decision Making Journal of Quality in Maintenance Engineering 1995; 1(3): 3-17.
29. Yin R K. Case Study Research: Design and Methods. 4th ed. Thousand Oaks, California: SAGE Publication, Inc; 2009.
30. Zawawi E M A, Kamaruzzaman S N. Personnel Characteristics of Maintenance Practice: A Case of High-Rise Office Buildings in Malaysia. Journal of Sustainable Development 2009; 2(1): 111-6.

Cheong Peng AU-YONG
Azlan Shah ALI
Faizah AHMAD
Faculty of Built Environment,
University of Malaya,
50603 Kuala Lumpur, Malaysia.
Emails: auyongcp@um.edu.my, asafab@um.edu.my, faiz@um.edu.my

Article citation info:
KOŁODZIEJ P, BORYGA M. Frequency analysis of coupling with adjustable torsional flexibility. Eksploatacja i Niezawodnosc – Maintenance and Reliability 2014; 16 (2): 325–329.

Paweł KOŁODZIEJ
Marek BORYGA

FREQUENCY ANALYSIS OF COUPLING WITH ADJUSTABLE TORSIONAL FLEXIBILITY

ANALIZA CZĘSTOŚCIOWA SPRZĘGŁA O REGULOWANEJ PODATNOŚCI SKRĘTNEJ*

The article presents the frequency analysis of a flexible coupling allowing changes of torsional flexibility. The authors derived a relationship for coupling flexibility considering geometric and material parameters. Coupling flexibility change is executed in such a manner that the quotient of extortion frequency and natural frequency of the system is higher than 1.4. Oscillation parameters for selected values of torsional flexibility were calculated for extortion frequencies approximating natural frequencies and after flexibility change.

***Keywords**: couplings flexibility, torsional stiffness, frequency analysis, amplitude characteristics.*

W pracy przedstawiono analizę częstościową sprzęgła podatnego umożliwiającego zmianę sztywności skrętnej. Wyprowadzono zależność na sztywność sprzęgła uwzględniając parametry geometryczne i materiałowe. Zmiana sztywności sprzęgła dokonuje się tak aby iloraz częstości wymuszenia i częstości drgań własnych układu był większy od 1,4. Obliczono parametry drgań dla wybranych wartości współczynnika sztywności skrętnej przy częstościach wymuszenia bliskich częstości drgań własnych oraz po zmianie sztywności.

***Słowa kluczowe**: sprzęgło podatne, sztywność skrętna, analiza częstościowa, charakterystyka amplitudowa.*

1. Introduction

The development of technology in machine design and exploitation extorts the necessity to choose the most favourable construction solutions and increasing exploitation velocity in production processes. Considering the results of the above-mentioned activities, one should conclude that the increase of movement velocity causes the increase of dynamic strains. Naming the relations with the term machine "dynamicity", one should consider the characteristics of its mechanical state, i.e. the values of oscillation amplitudes of the construction as a whole and its individual elements and sub-assemblies. High values of dynamic strains have negative impact on durability, reliability, precision of work, shape errors and positioning precision [1]. The oscillations during the work of driving systems strained with changeable moment depend on the amplitude value and the coercion frequency, mass inertia moments of the drive elements, torsional stiffness and damping.

Mechanical systems with changeable flexibility are used as elements of coupling constructions, shafts and vibration eliminators. An example of such a torsional vibration eliminator using a changeable flexibility of neoprene rings, playing a role of springs and dampers, is presented in the works by Slavick and Bollinger's [13]. Stiffness change results from axial relocation of countersunk screw causing the increase or decrease of pressure onto the rings. The range of neoprene flexibility changes allows adjusting the eliminator with a plate, weighting 20 kg, to resonance frequency of milling machine spindle used for device milling. In Kowal's publications [8–10] the changes of couplings or transmission shaft flexibility using cylindrical or disc push springs in packages are done with screw thread mechanisms. According to the author a coupling is a system effectively limiting dynamic strains during the set work and starting the drive system. Module construction made of disc springs allows building systems with different static characteristics. Filipowicz [2–5] and Filipowicz, Kuczaj [6, 11] presented new solutions of flexible systems and conducted theoretical and practical analysis of the double-acting couplings. The researchers concluded that the constructions allow obtaining torsion angles of a few degrees, transforming significant values of torque and easing momentary overloads. Moreover, they noticed that defining the most favourable characteristics of couplings (for the types of the machines) requires selecting the sets and systems of springs and threat mechanism parameters, what is possible as early as at designing stage.

The aim of the present work is to define the influence of torsional flexibility of the designed flexible coupling to the parameter of extorted normal oscillations. The contents of the article is the following. Chapter 2 presents the method of solving the equations of extorted, deadened vibrations. Chapter 3 explains how to adjust the torsional stiffness of coupling. Chapter 4 contains the description of coupling and calculating its torsional stiffness. In chapter 5 the results of analyses for ten selected values of torsional stiffness values are presented.

2. Equations of extorted vibrations and their solutions

Differential equation of extorted vibrations can be presented as illustrated in [14]:

$$\mathbf{B}\ddot{\mathbf{q}} + \mathbf{C}\dot{\mathbf{q}} + \mathbf{K}\mathbf{q} = \mathbf{H}\sin\omega t \tag{1}$$

where: $\mathbf{B}$, $\mathbf{C}$, $\mathbf{K}$ – inertia, damping and stiffness matrices respectively, $\mathbf{H}$ – vector, amplitude of extorting force, $\mathbf{q}$ – vector of generalised coordinates, ω – frequency of extorted vibrations [rad/s], t – time [s].

Filling the stationary solution to the vibration equation you obtain a system of algebraic equations in which the unknown is the vector of complex amplitudes $\overline{\mathbf{a}}$ of set extorted vibrations [14]:

(*) Tekst artykułu w polskiej wersji językowej dostępny w elektronicznym wydaniu kwartalnika na stronie ***www.ein.org.pl***

$$(\mathbf{K}-\omega^2\mathbf{B})\bar{\mathbf{a}}+i\omega\mathbf{C}\bar{\mathbf{a}}=\mathbf{H} \quad (2)$$

where: $i=\sqrt{-1}$ – imaginary unit.

In the case of flexible coupling, system of equations has a form of

$$\begin{bmatrix} J_s & 0 \\ 0 & J_m \end{bmatrix}\begin{bmatrix} \ddot{\theta}_1 \\ \ddot{\theta}_2 \end{bmatrix}+\begin{bmatrix} c & -c \\ -c & c \end{bmatrix}\begin{bmatrix} \dot{\theta}_1 \\ \dot{\theta}_2 \end{bmatrix}+\begin{bmatrix} k & -k \\ -k & k \end{bmatrix}\begin{bmatrix} \theta_1 \\ \theta_2 \end{bmatrix}=\begin{bmatrix} 0 \\ M \end{bmatrix}e^{i\omega t} \quad (3)$$

where: J_s – mass moment of inertia in the rotor and rotating elements of active part of coupling reduced to engine rotor axis [kg·m²], J_m – machine inertia moment reduced to the rotation axis of output shaft coupling [kg·m²], c – viscous damping coefficient [N·m·s/rad], k – torsional stiffness [N·m/rad], M – load torque coupling, [N·m], θ_1 – angle tilt of active part of coupling [rad], θ_2 – angle tilt of passive part of coupling [rad].

Using formula (2) and the transformations, one obtains:

$$\begin{bmatrix} k-J_s\omega^2+ic\omega & -(k+ic\omega) \\ -(k+ic\omega) & k-J_m\omega^2+ic\omega \end{bmatrix}\begin{bmatrix} \bar{a}_1 \\ \bar{a}_2 \end{bmatrix}=\begin{bmatrix} 0 \\ M \end{bmatrix} \quad (4)$$

Having solved the obtained expressions into real and imaginary parts, one obtains:

$$\bar{a}_1=A_1(\omega)+iB_1(\omega)=\frac{M(k\alpha-\beta)}{[\alpha^2+\beta(J_s+J_m)]\omega^2}+i\frac{M\gamma J_m}{\alpha^2+\beta(J_m+J_s)} \quad (5)$$

$$\bar{a}_2=A_2(\omega)+iB_2(\omega)=\frac{M(\delta\alpha-\beta)}{[\alpha^2+\beta(J_s+J_m)]\omega^2}+i\frac{M\gamma J_s}{\alpha^2+\beta(J_m+J_s)} \quad (6)$$

where: $\alpha=\omega^2 J_s J_m-k(J_s+J_m)$, $\beta=\omega^2c^2(J_s+J_m)$, $\gamma=\omega c J_s$, $\delta=k-\omega^2 J_s$.

The module of amplitude and the phase angle is calculated with the formulas [14]:

$$a_i(\omega)=\sqrt{[A_i(\omega)]^2+[B_i(\omega)]^2} \quad (7)$$

$$\phi_i(\omega)=arctg\frac{B_i(\omega)}{A_i(\omega)} \quad (8)$$

3. The selection of coupling torsional stiffness

Characteristic equation allows defining natural vibration frequencies ω_0. The equation has the form:

$$\det(\mathbf{K}-\omega_0^2\mathbf{B})=0 \quad (9)$$

In case of flexible coupling the equation has a form

$$\begin{bmatrix} k & -k \\ -k & k \end{bmatrix}-\omega_0^2\begin{bmatrix} J_s & 0 \\ 0 & J_m \end{bmatrix}=0 \quad (10)$$

The calculated roots of equation (10) are:

$$\omega_0=0 \text{ and } \omega_0=\sqrt{\frac{k(J_s+J_m)}{J_sJ_m}} \quad (11)$$

The coupling has positive effect on the dynamic properties of the system provided the following condition is satisfied [12]:

$$\frac{\omega}{\omega_0}>\sqrt{2} \quad (12)$$

The torsional stiffness k must be adjusted in such a manner to make the coupling work at supercritical conditions, passing through resonance in the initial period of starting-up, when the dynamic torque is not yet excessively high. Placing the calculated value of main oscillations (11) into the relation (12) and making transformations one obtains the relation for the required torsional stiffness k:

$$k<\frac{J_sJ_m\omega^2}{2(J_s+J_m)} \quad (13)$$

4. Torsional stiffness of a flexible coupling

4.1. Coupling description

The analysis of problems concerning the influence of flexible elements stiffness on the values of dynamic loads in drive systems, brings to a conclusion that it is an effective method of reducing negative interactions to use the devices whose construction allows obtaining an adaptable (within a certain range) value of torsional stiffness. Still, the flexibility would be changeable independently from drive movement parameters and external load. Considering the above information one should conclude that the task is satisfied by the coupling with in-built mechanism of fluent change of torsional stiffness [7], whose scheme of actions is presented in figure 1.

In the above figures the authors presented the rules governing the torsional flexibility coupling. Stiffness change of the system requires blocking the active length of flat spring connecting active and passive discs. The blockade is possible due to the linear movement of driving disc attached to an shaft spline. Maximum coupling flexibility is obtained for springs' active length is the highest (L_{max}) and minimum is the lowest (L_{min}).

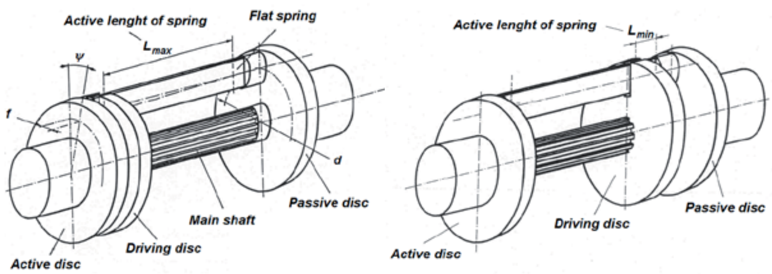

Fig. 1. The scheme of actions of flexible coupling

Figure 2 presents the construction of the designed coupling [7]. In the input shaft 10 brush runs 12 are attached to power drive 11 via toothed gear transmission (wheels 13 and 14) and lead-screw 15. The lead screw which can turn in active disc 16 and support plate is used to control the swashplate 18. Axial movement of the swashplate along the shaft spline 17 causes decrease of active length of flat springs 20 limiting the angle of turn between active 16 and passive 19 discs. Flat springs 20 are fixed in the covers 21, which can rotate in freely in discs 16 and 19.

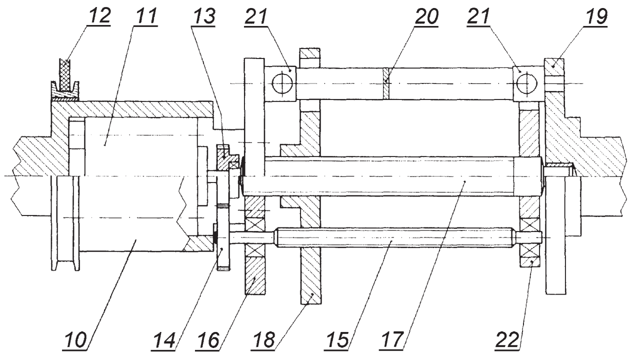

Fig. 2. Flexible coupling

4.2. Torsional stiffness calculations

Deflection of flat spring is:

$$f = \frac{FL^3}{3EJ_x} \tag{14}$$

where: F – load force onto the spring [N], L – active length of the spring [mm], E – Young's modulus [MPa], J_x – axial moment of inertia spring [mm^4].

The force acting on one spring can be calculated from the formula:

$$F = \frac{2M}{nd} \tag{15}$$

where: d – spring distribution diameter [mm], n – the number of springs.

For small angles it can be formed as:

$$f = \frac{d}{2} tg\psi \tag{16}$$

where: ψ – relative angle of coupling torsion of discs [rad]

Comparing the relations (14) and (16) and using formula (15) you obtain:

$$\frac{d}{2} tg\psi = \frac{2ML^3}{3ndEJ_x} \tag{17}$$

For small angles expressed in radians $tg\psi \approx \psi$ thus appropriate transformation of formula (17) for the right units, you can obtain the relation for torsional stiffness k:

$$k = \frac{M}{\psi} = \frac{3nd^2EJ_x}{4000L^3} \tag{18}$$

Figure 3 presents graph of the torsional stiffness coefficient of coupling k depending on active spring length L, wherein axis of k is logarithmic. The graph was obtained for the following coupling parameters: $n = 4$, $d = 100$ mm, $J_x = 5.625$ mm^4, $E = 2.1 \cdot 10^5$ MPa, $L = (5 \div 105)$ mm.

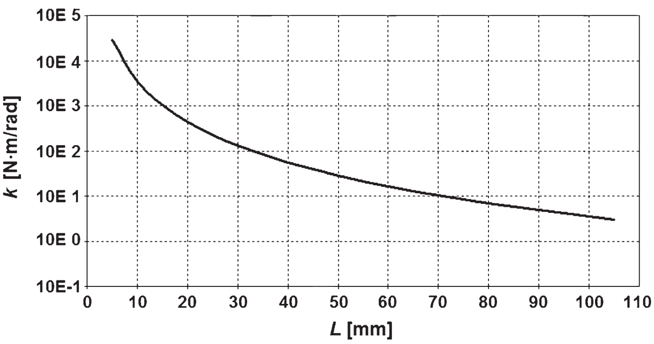

Fig. 3. Graph presenting torsional stiffness k with relation to active length of spring L

5. Results of the analysis

The calculations were made for ten selected values of torsional stiffness k within the regulation range. Column 1 in table 1 contains the frequencies of natural oscillation (ω_0) determined from the relations (11, 5, 6) and the values of angular transformations amplitudes of active (a_1) and passive (a_2) discs. The calculations employed the values of construction parameters of coupling presented in the previous chapter. Moreover, it was assumed that $J_s = 0.03$ kg·m^2, $J_m = 10$ kg·m^2, $c = 0.2$ N·m·s/rad and $M = 3.5$ N·m. Column 2 presents the values of torsional stiffness determining from the relation (13), with consideration for condition (12).

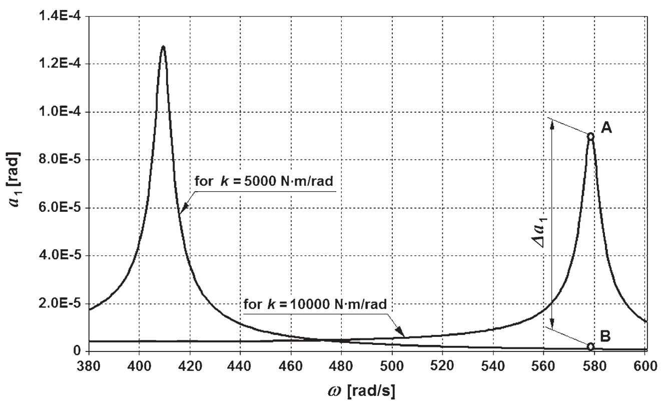

Fig. 4. The graph of amplitude a_1 in relation to extortion ω frequency for torsional stiffness k = 10000 N·m/rad and k = 5000 N·m/rad

Figures 4 and 5 present the results of simulations for a selected calculation case presented in table 1. Figure 4 presents a graph of amplitude a_1 with relation to extortion frequency ω . Initially, the system was near the resonance spot A (torsional stiffness $k = 10000$ N·m/rad whereas extortion frequency was $\omega = 578$ rad/s and was approximating the natural frequency ω_0). At that point, the value of amplitude was $a_1 = 9.017 \cdot 10^{-5}$ rad. The change of torsional stiffness from 10000 N·m/rad to $k = 5000$ N·m/rad caused system transformation to point

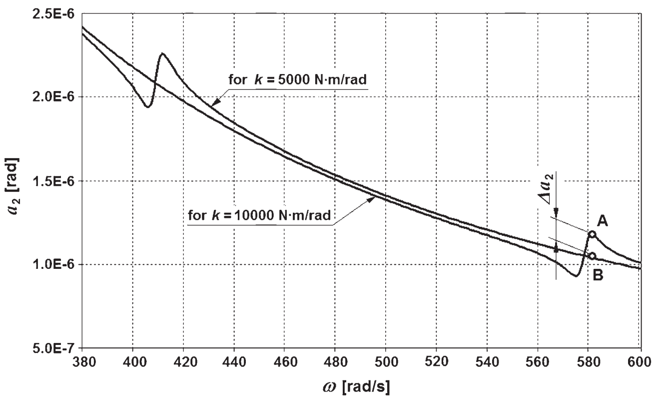

Fig. 4. Graph of amplitude a1 in relation to extortion ω frequency for torsional stiffness k = 10000 N·m/rad and k = 5000 N·m/rad

Table 1. The values of torsional stiffness k and amplitude of angular displacement of a_1 and a_2 coupling discs

1				2		
k	ω_0	a_1	a_2	k	a_1	a_2
[N·m/rad]	[rad/s]	[rad]	[rad]	[N·m/rad]	[rad]	[rad]
25000	914.239	$5.682 \cdot 10^{-5}$	$5.090 \cdot 10^{-7}$	12500	$4.181 \cdot 10^{-7}$ (0.74%)	$4.202 \cdot 10^{-7}$ (82.56%)
10000	578.215	$9.017 \cdot 10^{-5}$	$1.177 \cdot 10^{-6}$	5000	$1.046 \cdot 10^{-6}$ (1.16%)	$1.050 \cdot 10^{-6}$ (89.28%)
5000	408.860	$1.274 \cdot 10^{-4}$	$2.254 \cdot 10^{-6}$	2500	$2.023 \cdot 10^{-6}$ (1.59%)	$2.078 \cdot 10^{-6}$ (92.16%)
2500	289.107	$1.806 \cdot 10^{-4}$	$4.370 \cdot 10^{-6}$	1250	$4.015 \cdot 10^{-6}$ (2.22%)	$4.145 \cdot 10^{-6}$ (94.86%)
1250	204.430	$2.549 \cdot 10^{-4}$	$8.537 \cdot 10^{-6}$	625	$8.455 \cdot 10^{-6}$ (3,32%)	$8.435 \cdot 10^{-6}$ (98.80%)
630	144.553	$3.606 \cdot 10^{-4}$	$1.666 \cdot 10^{-5}$	312,5	$1.665 \cdot 10^{-5}$ (4.62%)	$1.669 \cdot 10^{-5}$ (100.21%)
315	102.623	$5.101 \cdot 10^{-4}$	$3.329 \cdot 10^{-5}$	157,5	$3.435 \cdot 10^{-5}$ (6.73%)	$3.374 \cdot 10^{-5}$ (101.34%)
160	73.139	$7.199 \cdot 10^{-4}$	$6.542 \cdot 10^{-5}$	80	$6.596 \cdot 10^{-5}$ (9.16%)	$6.586 \cdot 10^{-5}$ (100.66%)
80	51.717	$1.036 \cdot 10^{-3}$	$1.335 \cdot 10^{-4}$	40	$1.414 \cdot 10^{-4}$ (13.64%)	$1.349 \cdot 10^{-4}$ (101.03%)
60	31.670	$1.208 \cdot 10^{-3}$	$1.794 \cdot 10^{-4}$	30	$3.700 \cdot 10^{-4}$ (30.62%)	$1.816 \cdot 10^{-4}$ (101.21%)

B and decreasing the amplitude down to $a_1 = 1.046 \cdot 10^{-6}$ rad (over 86 times lower than in point A).

Figure 5 presents the graph of amplitude a_2 with relation to extortion frequency ω. In this case the decrease of a_2 is not as significant as for a_1. The decrease of torsional stiffness k = 10000 N·m/rad to k = 5000 N·m/rad caused a decrease of amplitude a_2 from z $1.177 \cdot 10^{-6}$ rad down to $1.050 \cdot 10^{-6}$ rad (points A and B).

6. Conclusions

On the basis of the discussions conducted in the framework of the present work, the following conclusions can be drawn:

- The presented construction solution of flexible coupling (with control system) may constitute a system for constant control and vibration compensation in mechanical systems.
- The change of torsional stiffness with relation to active spring length is strongly non-linear. For the assumed geometric and material parameters the torsional stiffness varies from 30.6 N·m/rad, in case of maximum spring length L_{max} = 105 mm up to 283500 N·m/rad for minimum active spring length L_{min} = 5 mm.
- Linear change of torsional stiffness k generates non-linear change of angular displacement of coupling active disc a_1. The amplitude a_1 decreases and ranges from 0.74% to 30.62% of a_1 amplitude before the change, wherein increase of over 10% applies the values of torsional stiffness k over 80 N·m/rad.
- The change of k has smaller influence on angular displacement of passive disc plate a_2. For k values more than 1250 N·m/rad amplitude a_2 decreases in the range of 82.56% to 98.80% of the amplitude value before the change and for k less than 630 N·m/rad, a_2 increase to 101%.

References

1. Cempel Cz. Minimalizacja drgań maszyn i ich elementów. w: Współczesne zagadnienia dynamiki maszyn. Wrocław: Ossolineum, 1976.
2. Filipowicz K. Determining of the static characteristics of a torsionally flexible metal coupling. Acta Montanistica Slovaca 2007; 12(4): 304-308.
3. Filipowicz K. Research of metal flexible torsional clutches applied in mining machines. Acta Montanistica Slovaca 2008; 13(2): 204-210.
4. Filipowicz K. Nowe rozwiązania układów napędowych maszyn z metalowymi sprzęgłami podatnymi skrętnie i sprzęgłami przeciążeniowymi. Przegląd Mechaniczny 2009; 2: 41-46.
5. Filipowicz K. Badania układów napędowych maszyn roboczych ze sprzęgłami podatnymi. Maszyny Górnicze 2010; 2: 3-12.
6. Filipowicz K, Kuczaj M. Kinematic and dynamic simulation of the functioning of torsionally flexible metal coupling. Transport Problems 2010; 5(3): 95-102.
7. Kołodziej P, Stępniewski A. Sprzęgło podatne. Patent nr PL 193910 B1 z marca 2007.
8. Kowal A. Sprzęgło metalowe o budowie modułowej umożliwiającej dobór podatności skrętnej. Technologia i Automatyzacja Montażu 2006; 2: 64-66.
9. Kowal A. Sprzęgło mechaniczne. Patenty nr PL 190945 B1 i PL 191092 B1 z lutego 2006.
10. Kowal A. Metalowe sprzęgło przeciążeniowe o dużej podatności skrętnej. Szybkobieżne Pojazdy Gąsienicowe 2007; 1(22): 105-112.
11. Kuczaj M, Filipowicz K. Computer finite element analysis of stress derived from particular unit sof torsionally flexible metal coupling. Transport Problems 2010; 5(4): 19-26.

12. Podstawy Konstrukcji Maszyn. Red. M. Dietrich. Wyd. 3. T. 3. Warszawa: WNT 1999.
13. Slavicek J, Bollinger J G. Design and application of a self-optimizing damper for increasing machine tool performance. Advances in Machine Tool Design and Research ; Proceedings of the Tenth International Machine Tool Design and Research Conference 1969: 71–81.
14. Wrotny L T. Dynamika układów mechanicznych. Repetytorium teoretyczne i zadania. Warszawa: Oficyna Wydawnicza Politechniki Warszawskiej, 1995.

Paweł KOŁODZIEJ
Marek BORYGA
The Department of Mechanical Engineering and Automation
The Faculty of Production Engineering, University of Life Sciences in Lublin
Doświadczalna 50A, 20-280 Lublin, Poland
e-mails: pawel.kolodziej@up.lublin.pl, marek.boryga@up.lublin.pl

Article citation info:
WALCZAK M, PIENIAK D, NIEWCZAS AM. Effect of recasting on the useful properties CoCrMoW alloy. Eksploatacja i Niezawodnosc – Maintenance and Reliability 2014; 16 (2): 330–336.

Mariusz WALCZAK
Daniel PIENIAK
Agata M. NIEWCZAS

EFFECT OF RECASTING ON THE USEFUL PROPERTIES CoCrMoW ALLOY

WPŁYW POWTÓRNEGO PRZETAPIANIA NA WŁAŚCIWOŚCI UŻYTKOWE STOPU CoCrMoW*

Recasting of the previously cast metal can change the chemical composition of the newly formed material, which ultimately could affect the properties of a dental alloy. The research used a dental alloy CoCrMoW trade name Remanium 2001. Three groups of dental alloy were prepared by mixing 50% fresh alloy to alloy remnants from previous castings. The specimens in the first casting group used 100% fresh alloy and served as control (R1). The second group consisted of equal amounts of fresh alloy and alloy remnants cast only once (R2). The third group contained 50% fresh alloy and alloy cast twice (R3). Microstructural analysis was performed and the chemical composition, XRD studies, hardness, and tribological test and the metal–ceramic bond strength was investigated according to ISO9693 standard. New material should be used in casting, and if previously casted material is used, it should be mixed with new material. The use of the recasting procedure can lower the costs of CoCrMoW castings and can be safely in dentistry.

***Keywords**: cobalt alloys, durability of prosthetic devices, recasting.*

Przetapianie uprzednio odlanego metalu może spowodować zmianę składu chemicznego nowopowstałego materiału, co w końcowym efekcie może oddziaływać na właściwości użytkowestopu stomatologicznego. Do badań zastosowano stop stomatologiczny CoCrMoW o nazwie handlowej Remanium 2001.Przygotowano 3 grupy stopu stomatologicznego przez zmieszanie 50% fabrycznie nowego stopu ze stopem po poprzednim przetopieniu. Grupę pierwszą odlano w 100% z nowego fabrycznie stopu jako grupę kontrolną (R1). Grupa druga (R2) została odlana z mieszaniny jednakowych ilości nowegostopu oraz stopu odlanego tylko raz. Grupa trzecia (R3) zawierała 50% świeżego stopu oraz stopu odlanego 2 razy.Wykonano analizę mikrostrukturalną oraz składu chemicznego, badania XRD, pomiary twardości, badania tribologiczne oraz badania przyczepności wg ISO 9693.Wykazano, że w odlewaniu należy używać nowego materiału a w przypadku wykorzystania materiału wcześniej używanego należy go wymieszać z materiałem nowym.Wykorzystanie procedury przetapiania może obniżyć koszty odlewów CoCrMoW oraz może być bezpieczne w stomatologii.

***Słowa kluczowe**: stopy kobaltu, trwałość aparatów protetycznych, powtórne przetapianie.*

1. Introduction

The recasting of previously casted alloy is a routine procedure used in dental laboratories in order to reduce the cost of permanent partial dentures.

The prosthetic "scrap" encompasses the residuals generated in frame dentures casting process e.g. originating from the runners, from casting cones and improperly completed melts e.g. withmisruns, shrinkage porosities and cracks and is frequently used as a part of charge for recasting [20]. The state of load occurring in oral cavity in course of mastication process is diversified and causes various level of stress concentration in hard tooth tissues and in dental fillings which may result in damages of denture fasteners or in ceramic phase separation from prosthetic apparatuses with permanent porcelain veneers [5, 21].

The addition of 50% recast material to a brand new alloy is allowed by greater part of dental alloys manufacturers. Some manufacturers established the condition that the addition of so called scrap can be recasted only once and must wholly originate from the same batch. However the use of additions in the form of repeatedly remelted materials is not allowed by other alloys manufacturers or no information concerning potential use of post-production scrap is not published by them.

In the opinion of Bauer et al. [4] the scrap produced in dentistry is extremely pure due to the fact that this metal is melted in controlled conditions without necessity to apply any chemical process used in industrial conditions. Dental alloys reuse seems promising in case of Ni–Cr [12] and Co–Cr alloys [1] as well as gold based alloys [17].

From references [4, 12, 13] it appears that the properties of recasted alloy may differ from the properties of a new alloy purchased from the manufacturer. The differences may be associated with its chemical composition [13], castability [12], as well as with mechanical properties [4]. However the opinions concerning mechanical properties are extremely divided. Some authors [1, 4] think that these properties can increase or decrease [11, 20] but the research carried out by Palaskar et al.[12] demonstrate that there is no statistically significant castability change as a result of alloys recasting. There are experimental studies described in literature [13] and reflecting changed chemical composition of final products under the influence of successive recasting processes and development of new phases determining the changes in alloy properties. The deterioration in the scope of corrosion properties [6] or even cytotoxicity [2] is also possible due to changed chemical composition in case of recasting.

(*) Tekst artykułu w polskiej wersji językowej dostępny w elektronicznym wydaniu kwartalnika na stronie ***www.ein.org.pl***

The process associated with remelted materials use may change the composition of metal oxide surface layer which may be of critical importance for metal ceramic bond [24].

Sufficient bond strength between porcelain and metal structure of applied biomaterial [19, 21] is an important factor determining the durability of metal ceramic apparatuses. The use of recycled alloys is not recommended by Ucar et al. [19] to avoid potential reduction of bond strength between porcelain and metal.

Therefore the purpose of the present study was to evaluate the effect of addition of remelted materials on some mechanical properties of CoCrMoW alloy i.e. hardness, tribological wear, metal ceramic bond strength as well as evaluation of microstructure and chemical composition of newly produced castings.

2. Material and methods

Remanium 2001 dental alloy (Dentaurum, Germany) with cobalt matrix and nominal Remanium 2001 (w/w) consisting of 63% Co, 23% Cr, 7.3% Mo, 4.3% W, 1.6% Si and Mn<1% and N<1% [27] has been used in tests. This alloy is used for casting of denture elements (among others crowns and bridges) with permanent ceramic veneers. Three groups of identical dental alloy have been prepared in order to simulate standard applications used in dental laboratories. The first group has been casted in 100% from new alloy as a control group (R1). The other groups have been made of 50% new alloy and 50% remnants from the previous group (Table 1). The second group (R2) has been casted as the mixture of equal amounts of the new alloy and the alloy after previous recasting. The alloy used in the third group (R3) has been prepared adding new alloy and 50% remnants from second group (R2).

The process associated with preparation of specimens made of CoCrMoW alloy was carried out in conditions existing in professional prosthetic dental laboratory in accordance with procedures applied for production of metal denture elements. The castings have been produced in investment casting process by means of vacuum – pressure casting machine Nautilius (Bego, Germany) and ceramic crucibles.

Tabele 1. Different recast alloy groups used in this study

Groups	Procedure
Never cast (R1)	Cast 100% new alloy
Cast once (R2)	Cast from 50% new alloy and 50% remnants from first group
Cast twice (R3)	Cast from 50% new alloy and 50% remnants from second group

The specimens used for testing: hardness, chemical composition analysis and tribological tests have been made as the discs with diameter of Ø 25 mm and thickness of 2 mm. The discs have been subjected to grinding by means of water abrasive papers with grain size of 220, 600 and 1200 correspondingly. After grinding the specimens were mechanically polished by means of diamond particles suspension 3 μm and oxides particles suspension 0.05μm as well as washed in acetone and dried thereafter.

The hardnessof tested materials was measured under the load of 98.07N on FV-700 Vickers hardness meter with automatic ARS 900 system manufactured by Future-Tech Corp. Fourty (40) hardness measurements have been performed for each group of specimens.

The analysis of chemical composition has been performed by means of Q4 Tasman 130 spark emission spectrometer (Bruker, Germany) in detail Co130 testing channel used to complete five (5) analyses (sparking sequences) for each specimen.

X-ray Diffraction device manufactured by Rigaku Ultima IV and equipped with CuKα has been used for XRD analysis in order to enable phase identification (mainly carbides identification) for the groups of CoCrMoW alloys under tests.

ICDD database was used for the interpretation of obtained results. The tests were carried out under accelerating voltage of 40 kV and current of 40mA. The scanning range 2θ was included between 35° and 55° at scanning speed of 0.2°min^{-1} and step of 0.02°. The scanning range has been selected on the basis data available in literature [10] in a manner enabling the identification of carbides types reinforcing the alloys under tests.

The wear tests were carried out by means of "ball-on-disc" tribotester manufactured by CSM Instruments, at temperature of 37ºC in artificial saliva environment (pH=5.3). The composition of artificial saliva has been prepared on the basis of PN-EN ISO 10271:2012 standard [26]. The balls with diameter of 6 mm and hardness of 2000HV (manufactured by CSM Instruments)made of Al_2O_3 have been used as counterpart (ball). The tests were carried out under the load of 10N with linear speed of 1.88 cm/s on the radius of 3 mm. The total test travel used to record friction coefficient variation was equal to 100 m. The reduction of specimen material volume occurred in the form of wear trace as a result of specimen - counterpart mating was used as the wear measure. Therefore Dektak 150 profile contact tester manufactured byVeeco Instruments has been used to measure the surface area ofspecimen wear profile along specimen circumference (in 12 locations). Tip radius of measuring needle was equal to 2 μm. The volumetric wear has been determined as the average value of specimen wear surface area multiplied by the circumference of the circle of wear trace produced in the ball-on-disc test.

The specimens for ceramic bond strength tests have been prepared in accordance with requirements included in PN-EN ISO 9693 [25] standard in the form of rectangular plates with dimensions of 25×3×0.5 mm. IPS d.SIGN dental porcelain (IvoclarVivadent, Schaan, Liechtenstein) with dimensions of 8×3×1 mm has been applied centrally onto the metal plates. The whole process associated with dental porcelain fusion to metal was carried out in conditions existing in professional prosthetic dental laboratory. Nine (9) specimens from each test group have been used for test. Three point bending test has been carried out by means of Zwick Z100 universal testing machine equipped with 500N measuring head. The distance between the supports was equal to 20 mm and the diameter of specimen supporting rollers was equal to 2 mm. The testing speed (traverse beam feed) was equal to 1.5 mm/min. The loss of bond strength was indicated by the value of force at which a load disturbance (reduction) was observed in deflection curve. Then the bond strength (τ_b) has been determined using the following formula [25]:

$$\tau_b = k \cdot F_{fail} \tag{1}$$

where: k – the factor depending on thickness of base metal and Young module, F_{fail} – the force causing the loss of metal-ceramic bond strength.

The microstructure of tested materials and their surface after tribological tests has been analysed by means of Phenom G2 pro desk top scanning microscope.

3. Tests results and discussion

The microstructure of tested cast alloys is characterized by typical coarse grained dendritic structure (Fig. 1). The microstructure of castings containing remelted material is similar to microstructure of brand new castings. There were no inclusions which could originate from charge contamination in the form of investment material. Furthermore diversified carbides shapes have been revealed in course of SEM analysis. The carbides phases are characterized by dual structure i.e. occurring in the form of blocky precipitations as well as lamellar precipitations ("pearlitic type"). In the opinion of some authors [15],

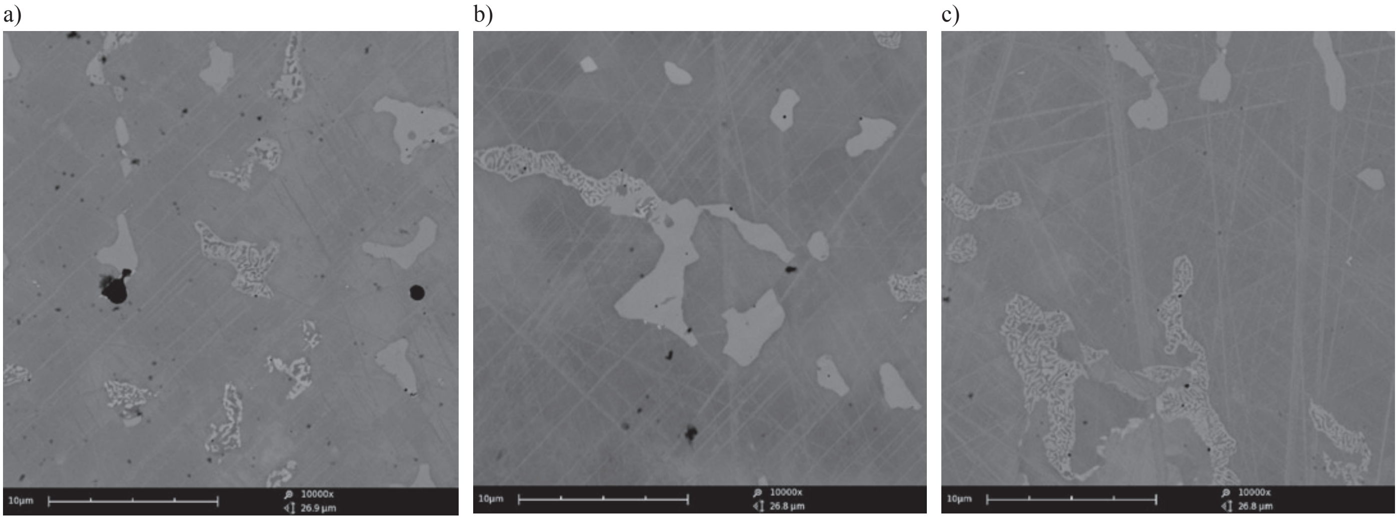

Fig. 1. SEM microstructure of castings: (a) control sample R1, (b) recasting R2, (c) recasting R3

the lamellar structure of carbides is caused by cooling rate variation between 8 and 16 ºC/min; 35 ºC/min [16] is the maximum cooling rate for the creation of eutectoid phase. Carbides precipitations may have decisive impact on increased reinforcement of an alloy and its reduced plasticity [20].

The average hardness achieved by a brand new alloy and recycled materials reaches a value similar to that declared by the manufacturer of 336HV10 (Fig. 2). There are no significant differences between R1 and R2 groups ($p=0.942$) demonstrated by non-parametric test for independent test by U Mann-Whitney (for $\alpha=0.05$) carried out by means of STATISTICA program. However the difference found between R1 and R3 group ($p<0.05$) as well as between R2 and R3 group ($p<0.05$) was significant.

Hardness results have been additionally analysed by means of Kruskal-Wallis test at assumed significance level $\alpha=0.05$. However no significant difference has been found between R1 and R2 groups but the difference found between R1 and R3 group ($p<0.05$) as well as between R2 and R3 group ($p<0.05$) was significant. Detected hardness differences are closely associated with changed chemical composition of remelted materials and particularly with percentage of carbon content contributing to the formation of hard carbides. The changes of chemical composition in tested materials are presented in table 2.

It should emphasized that there is information about elements concentrations under 1% indicated in manufacturer's data. The carbon content for R1 and R2 groups is similar and average hardness values are identical in the both groups (334HV10). However a change in carbon concentration has been denoted in remelted materials from R3 group which could be the explanation for hardness increase. However, the determining factor in the increase in the hardness of the alloy R3 is a large percentage of the hard carbide Cr_3C_2 (Fig. 3) as compared

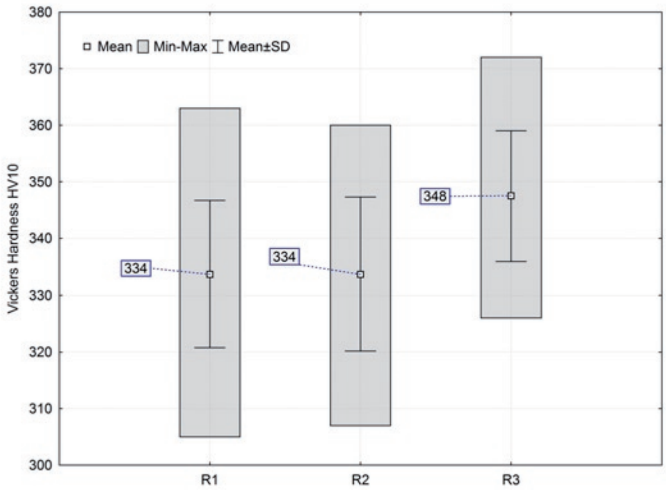

Fig. 2. The comparison of Vickers hardness of tested alloys groups

Table 2. Chemical composition of alloys under test [wt. %]

Groups	C	Si	Mn	P	S	Cr	Mo	Ni
R1	**0.059**	1.136	0.152	~0.014	<0.0020	22.86	8.426	0.058
Sd.	0.0076	0.013	0.0020	–	–	0.125	0.085	0.0025
R2	**0.060**	~1.221	0.153	~0.014	0.0029	22.84	~8.570	0.052
Sd.	0.0038	0.028	0.0022	–	0.0011	0.403	0.221	0.0026
R3	**0.073**	1.199	0.146	~0.014	0.0039	22.05	8.435	0.193
Sd.	0.017	0.047	0.014	–	0.0022	1.230	0.085	0.0029
Groups	W	Fe	Al	Cu	Nb	N	Ti	Co
R1	~4.299	<0.005	<0.005	0.0068	<0.005	0.192	0.0048	62.77
Sd.	0.034	–	–	0.0003	–	0.052	0.0003	0.111
R2	~4.320	<0.005	<0.005	0.0069	<0.005	0.203	0.0051	62.52
Sd.	–	–	0.021	0.0001	–	0.071	0.0002	0.150
R3	~4.315	<0.005	0.140	0.0068	<0.005	0.184	0.0047	63.23
Sd.	0.011	–	0.209	0.0002	–	0.057	0.0003	0.904

to the carbides present in the other study groups.The carbon content within 0.059÷0.073% indicates that materials under analysis belong to low carbon alloys group.

Figure 3 illustrates XRD pattern for the alloys groups under test indicating only the reflections from carbides without any reflections from matrix. The tests demonstrated the co-existence of carbides i.e. mainly $Cr_{23}C_6$, Cr_7C_3 and Cr_3C_2 in the alloys under test. Cr_7C_3 carbides percentage is the highest in R1 control group; $Cr_{23}C_6$, carbides prevail in R2 group and Cr_3C_2 in R3 group. Such circumstances are associated with changed chemical composition and carbides transformations occurring in course of alloy recasting processes. Additionally the presence of the following intermetallic phases has been detected in course of tests: $Cr_{0.7}Mo_{0.3}$ and Mo_6Co_7 – not marked on XRD pattern. However the authors of studies [9, 14] found that Cr_7C_3, Cr_3C_2 carbides may be produced in alloys with low chromium content but this opinion has been not confirmed in our tests (about 23% Cr). However Karaali et al. [8] emphasize that carbides i.e. MC, M_7C_3, $M_{23}C_6$ and M_6C may be produced in cobalt alloys for medical and dental applications but the carbon content occurring in said data is equal to 0.1÷0.35%C and CoC ralloys for dental applicationsshould be low carbon alloys.

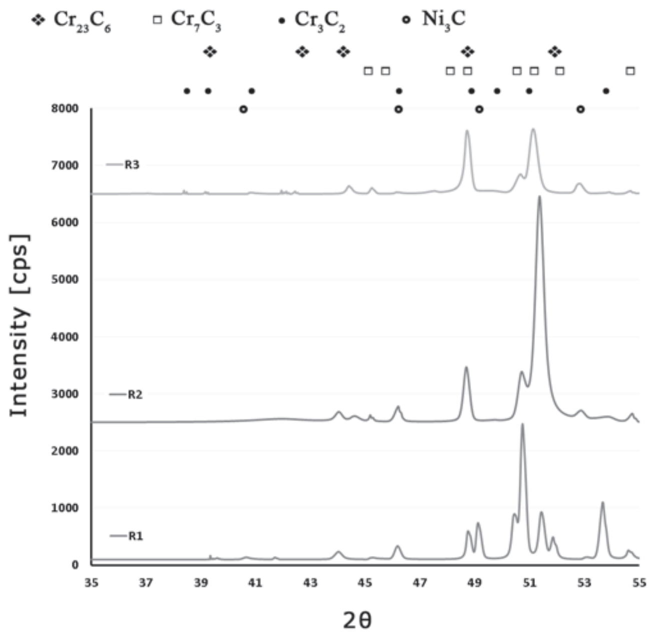

Fig. 3. XRD patterns of the as-cast R1, R2, R3 alloys

The results of tribological tests in artificial saliva demonstrated average friction coefficient on the level μ=0.32÷0.341 – similar for all materials groups under test (table 3).

Table 3. Summary of friction coefficients determined for tested materials mating with counterpart made of Al_2O_3

Groups	Average μ	Standard deviation
Never cast (R1)	0.320	0.021
Cast once (R2)	0.329	0.043
Cast twice (R3)	0.341	0.019

Figure 4 illustrates the changes of friction coefficient for mating surfaces CoCrMoW (specimen) – Al_2O_3 (counterpart) along the distance of 100 m. The top points of roughness profile are sheared off first, therefore the initial values of friction coefficients are higher. As a result of running – in of friction surface, the contact area between mating surfaces increases and the friction coefficient is reduced and stabilized. The stabilization of friction coefficients is practically observed in all cases under test after the distance of 20 m. The higher carbon content in an alloy and consequently increased hardness causes increased friction coefficient observed for R3 alloy.

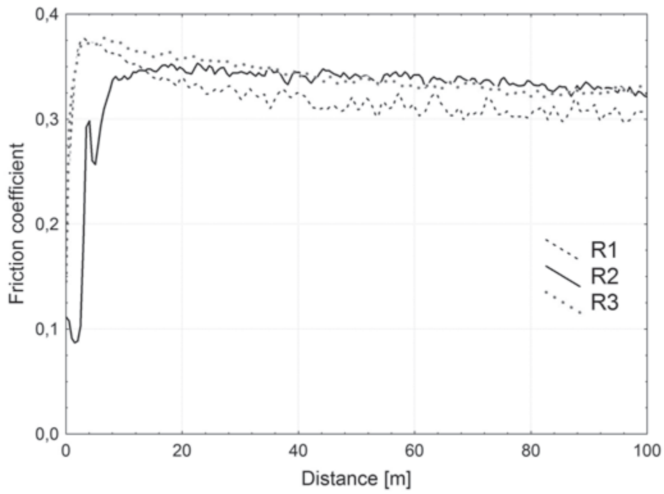

Fig. 4. The curve illustrating changes of friction coefficient vs. distance at the load of 10N

Hard carbides precipitations constitute a natural barrier for the counterpart material. The analysis of wear profiles (Fig. 5) and surface of paths –SEM pictures (Fig. 6) indicate to abrasive wear mechanism. The microcutting in the form of continuous cracks along wear traces and abrasion wear abrasion wear of relatively soft matrix are prevailing factor in this case. The wear process is intensified as a result of an additional impact of hard carbide phase loosely rolling between mating surfaces of specimen and counterpart with wearing surfaces. Such behaviour causes increased abrasive wear effect in alloys being tested. The scratches are caused by rolling carbides on the specimen mating surface or plastic deformation of matrix fragments leaving specific traces in the form chases. The chases are clearly visible on wear trace profile (Fig. 5). The authors of studies [3, 23] also confirm in their tests that the abrasive wear is the prevailing factor causing the destruction of the top layer of CoCrMo casting alloys.

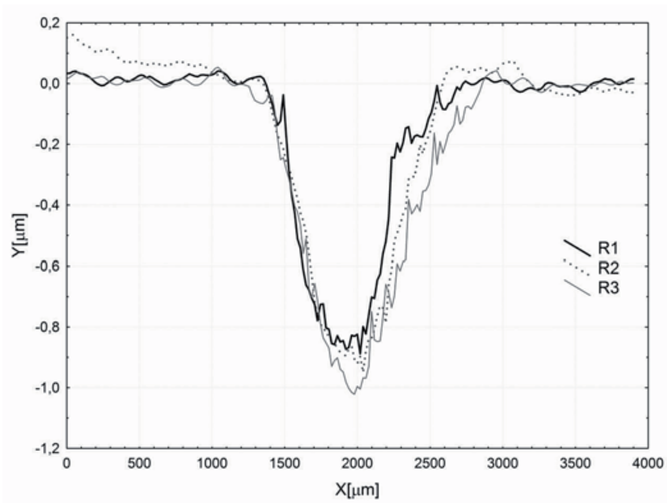

Fig. 5. Typical wear traces profiles

Figure 7 illustrates the results for volumetric wear for tested materials. When comparing the tested materials, it is possible to observe higher wear resistance of R1 control material by about 14% in relation to R2 alloy. However in case of addition of two times remelted

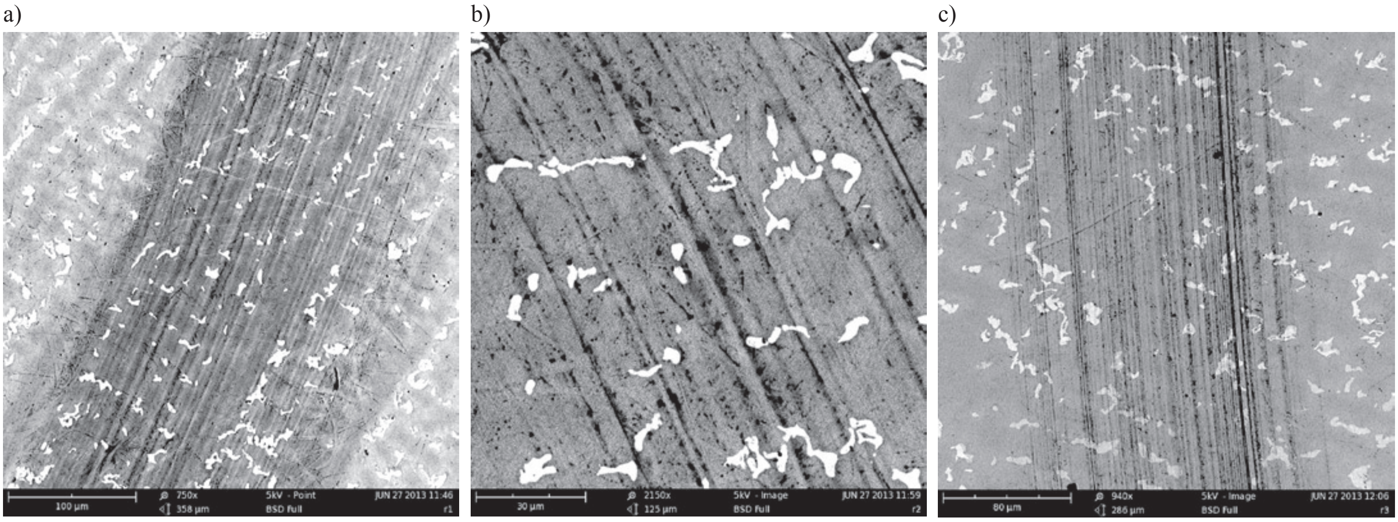

Fig. 6.SEM microstructure of wear trace: (a) R1, (b) R2 and (c) R3.

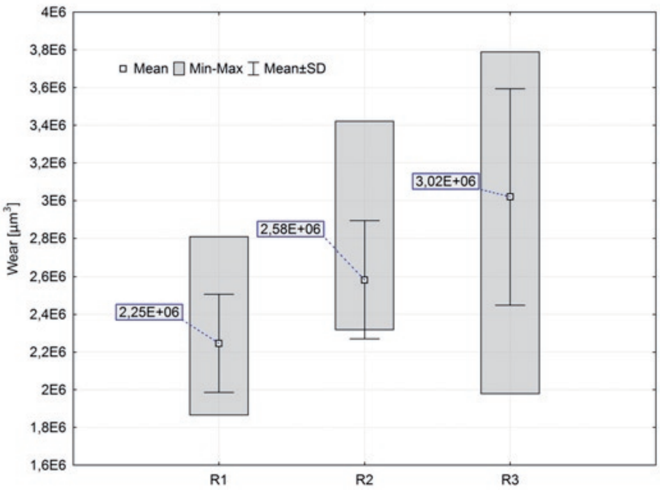

Fig. 7. Diagram illustrating volumetric wear for tested materials obtained for the distance of 100m

material to the fresh alloy (R3 specimen) its wear resistance will be reduced by about 34% in relation to R1 control specimen.

As described in literature [23], abrasive wear of cobalt alloys is determined by hard carbide particles or hard protrusion which are depressed by the counterpart and moved in relation to mating surfaces thereafter. From data available in literature [22] it appears that wear intensity in high carbon CoCrMo alloys is significantly lower than in low carbon alloys due to the fact that low carbon CoCrMo alloys are characterized by low volume percentage of carbides. The value of friction coefficient is affected by the environment (liquid medium) contacting and interacting with an active surface. For instance 0.36%NaCl environment increases the friction coefficient in high carbon cobalt casting alloys and its reduction in case of low carbon alloys [23]. However this trend is completely reversed in different medium (e.g. in 50% bovine serum or Dulbecco's Modified Eagle's Medium).

The values of friction coefficients obtained by the authors of the present article is similar to the data available in literature [23] obtained from tests performed for high carbon alloys (μ=0.19÷0.25) and for low carbon alloys (μ=0.27÷0.28) in various liquid media (but other than artificial saliva).

However the authors of the present article were unable to make any references in wider form because the scientific studies in the scope of tribological measurements for recast CoCrMo alloys in artificial saliva environment still remain to be realized. So called wear factor K considering the force and sliding distance applied in course of test is specified as a comparative wear measure by the authors engaged in the scope tribological wear research [18, 23]:

$$K = \frac{Wear\ volume}{Applied\ \ force \times sliding\ distance}[mm^3 N^{-1} m^{-1}] \qquad (2)$$

The table No 4 presented below contains the values of wear factors for all tested groups. Iijima et al. [7] emphasize the fact that the wear factor is an important feature characterizing the tribological properties of materials used for the production of prosthetic apparatuses. Furthermore they indicate to a serious problem occurring in the greater part of research studies in the scope of prosthetic dentistry i.e. the fact that the tribological properties are neglected by the scientists concentrating on the examination of strength and corrosion properties.

Significant differences between R1 and R2, R2 and R3 as well as R1 and R3 groups ($p<0.05$) have been demonstrated in course of statistical analysis of wear volume carried out in the form of U Mann-

Table 4. Summary of determined wear factors

Groups	Wear factor K [mm^{3}N^{-1}m^{-1}]	Standard deviation
Never cast (R1)	2.25×10^{-6}	0.26×10^{-6}
Cast once (R2)	2.58×10^{-6}	0.31×10^{-6}
Cast twice (R3)	3.02×10^{-6}	0.57×10^{-6}

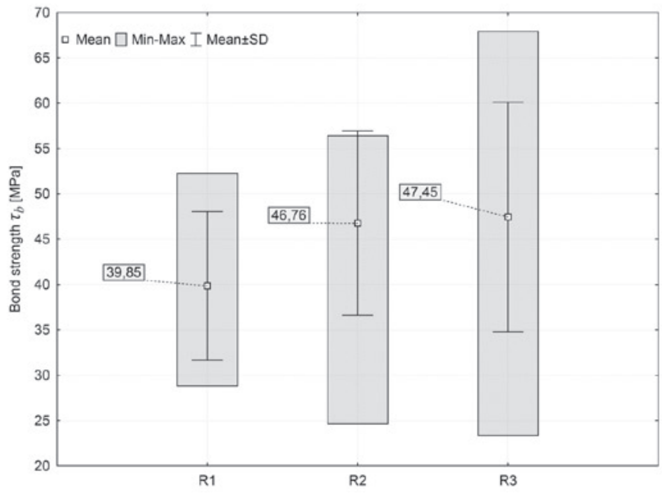

Fig. 8. The mean bond strength of metal-ceramic systems for different groups

a) b) c)

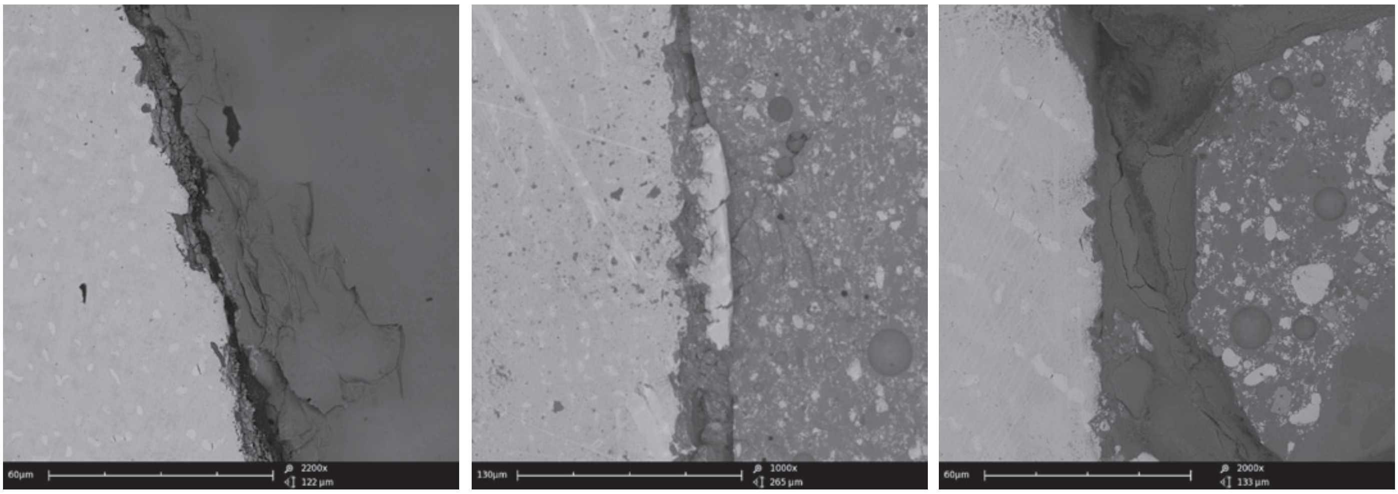

Fig. 9. SEM microphotograph of the cross-section of the metal-ceramic systems after debonding: (a) R1, (b) R2, (c) R3

Whitney test (for α=0.05). However the significant differences only between R1 and R3 groups (p<0.05) have been demonstrated by means of Kruskal-Wallis analysis. The differences demonstrated as a result of comparison between R1 and R2 groups were insignificant but *p* was close to *α* (p=0.06). The power of U Mann-Whitney test is the highest among non-parametric tests. In case of of Kruskal-Wallis test more prudence is necessary when drawing any substantive conclusions from performed tests due to greater probability of type I and II errors.

Figure 8 illustrates the variations of bond strength for metal-ceramic systems carried out in accordance of ISO 9693 procedures. This standard assumes the minimum strength on the level of τ_b =25 MPa in three point bending test. The mean strength values for metal-ceramic bond demonstrate that this minimum value has been achieved and even significantly exceeded in certain cases. Only in R2 and R3 specimens group with the addition of remelted alloy, one case of case has been recorded in each group when a specimen under test achieved the value τ_b<25MPa. The production of prosthetic apparatuses with permanent porcelain coat is a difficult process due to different nature of chemical bonds occurring in the both materials. This process in large part depends on manual skills of dental technician who should uniformly apply the dental porcelain onto metal substrate in a manner ensuring complete wetting of metal substrate and the thickness of individual ceramic layers being applied should be not excessive in order to avoid the weakening of metal-ceramic bond structure by pores occurring in course of porcelain firing process. Therefore the failure to achieve the minimum value of 25Ma for said two specimens could probably caused by excessive porosity in ceramic structure created in application phase but not by the addition of recast material.

In summary, no deterioration has been observed in metal–ceramic bond strength for alloys containing recast materials be even an insignificant growth. Comparing the results obtained for R2 group and for R1 control group, it can be observed that dental porcelain bond strength is 17% higher in R2 group. In case of comparison between R1 and R3 group the bond strength is increased in R3 alloy. However no statistically significant changes have been indicated by means of U Mann-Whitney test at significance level α=0.05 in all combinations of specimens under test (p>0.05). Such statistical result may be affected by a large dispersion in min-max values and insufficient size of sample (n=9); although the quantity of specimens used for tests was higher than that required in ISO 9693 standard (min. 6 pcs). However there is a significant difference between R1 and R3 group (p<0.01) at significance level α=0.1.

Figure 9 presents SEM microphotographs of the cross-section of the metal-ceramic systems after debonding for dental porcelain on metal substrate. The adhesive-cohesive fractures have been obtained in almost all tested groups of alloys on the metal substrate end. The cohesive fracture has been obtained in several cases (Fig. 9c) for R3 test group, with the fracture occurring within ceramic or metal oxides transitionlayer.

Ucar et al. [19] suggest that porcelain veneers on recast metals may result in changed composition of surface metal oxide and consequently in a critical impact on metal–ceramic bond strength. Their three point bending tests for NiCrMo demonstrated that use of recast base metal alloy with fresh alloy reduces the metal alloy–ceramic material bond strength but they did not achieve any statistically significant difference in metal–ceramic bond strength for alloys containing recast material.

4. Summary and conclusions

The alloys produced by the authors with the addition of recast materials meet the quality requirements applicable to prosthetic dental elements in the scope of their quality and durability and can be used in prosthetic dental laboratories. After applying remelting materials, in spite of small increase in hardness wear increased, preferably while affected the adhesion of dental porcelain. Hence, one can predict that such a material is certainly better suited to veneering than abrasion working elements.

On the basis ofits ownresearchfound thatthe production of durable prosthetic castings is possible provided that relevant procedure is adhered to, i.e. at least 50% of brand new must be used and remaining part of alloy may be casted once or twice. In the present study, the alloys with 50% addition of recast materials have been tested up to the second generation level only. Therefore the authors suggest the recasting of alloy addition to the level of determined number of generations as well as the testing of effect of increased number of recasting processes on the alloy properties. The recasting procedure may reduce the costs of CoCrMoW castings and may be safely used in dentistry.

References

1. Al–Ali AA, Evaluation of Macrohardness of Recasted Cobalt–Chromium Alloy. Al–Rafidain Dental Journal 2007; 7(1): 111–117.
2. Al-Hiyasa AS, Darmani H. The effects of recasting on the cytotoxicity of base metal alloys. The Journal of Prosthetic Dentistry 2005; 93: 158–163.
3. Balagna C, Spriano S, Faga MG. Characterization of Co–Cr–Mo alloys after a thermal treatment for high wear resistance. Materials Science

and Engineering C 2012; 32: 1868–1877.
4. Bauer J, Cella S, Pinto MM, Costa JF, Reis A, Loguercio AD. The use of recycled metal in dentistry: Evaluation of mechanical properties of titanium waste recasting. Resources, Conservation and Recycling 2010; 54: 1312-1316.
5. Beer K, Walczak M, Surowska B, Borowicz J. Wpływ powtórnego przetapiania na właściwości mechaniczne i mikrostrukturę odlewniczego stopu kobaltu. Inżynieria Materiałowa 2012; 5: 473-476.
6. Horasawa N, Marek M. The effect of recasting on corrosion of a silver-palladium alloy, „Dental Materials" 2004; 20: 352-357.
7. Iijima D, Yoneyama T, Doi H, Hamanaka H, Kurosaki N. Wear properties of Ti and Ti–6Al–7Nb castings for dental prostheses. Biomaterials 2003; 24: 1519–1524.
8. Karaali A, Mirouh K, Hamamda S, Guiraldenq P. Microstructural study of tungsten influence on Co–Cr alloys. Materials Science and Engineering A 2005; 390: 255–259.
9. Marciniak J, Kaczmarek M, Ziembowicz A. Biomaterials in stomatology. Editiorial Office of Silesian University of Technology, Gliwice 2008 (in Polish).
10. Mineta S, Namba S, Yoneda T, Ueda K, Narushima T. Carbide Formation and Dissolution in Biomedical Co-Cr-Mo Alloys with Different Carbon Contents during Solution Treatment. Metallurgical and Materials Transactions A, 2010; 41 (8): 2129-2138.
11. Ozyegin LS, Tuncer R, Avci E. Hardness, Behavior and Metal Surface Evaluation of Recasting Non-Precious Dental Alloys. Key Engineering Materials 2007; 330-332: 1425-1428.
12. Palaskar J, Nadgir DV, Shah I. Effect of Recasting of Nickel: Chromium Alloy on its Castability. The Journal of Indian Prosthodontic Society 2010; 10 (3): 160–164.
13. Peraire M, Martinez-Gomis J, Anglada JM, Bizar J, Salsench J, Gil FJ. Effects of Recasting on the Chemical Composition, Microstructure, Microhardness, and Ion Release of 3 Dental Casting Alloys and Titanium. The International Journal of Prosthodontics 2007; 20: 286-288.
14. Podrez-Radziszewska M, Haimann K, Dudziński W, Morawska-Sołtysik M. Characteristic of intermetallic phases in cast dental CoCrMo alloy. Archives of Foundry Engineering 2010; 3: 51-56.
15. Ramírez Vidaurri LE, Castro Román M, Herrera Trejo M, García López CV, Almanza Casas E. Cooling rate and carbon content effect on the fraction of secondary phases precipitate in as-cast microstructure of ASTM F75 alloy. Journal of Materials Processing Technology 2009; 209: 1681-1687.
16. Ramírez LE, Castro M, Méndez M, Lacaze J, Herrrera M, Lesoult G. Precipitation path of secondary phases during solidification of the CoCrMoC alloy. Scripta Materialia 2002; 47: 811-816.
17. Reisbick MH, Brantley WA. Mechanical property and microstructural variations for recast low-gold alloy. The International Journal of Prosthodontics 1995; 8 (4): 346-350.
18. Rieker CB, Schön R, Köttig P. Development and Validation of a Second-Generation Metal-on-Metal Bearing. Laboratory Studies and Analysis of Retrievals. The Journal of Arthroplasty 2004; 8: 5-11.
19. Ucar Y, Aksahin Z, Kurtoglu C. Metal ceramic bond after multiple casting of base metal alloy. The Journal of Prosthetic Dentistry 2009; 102: 165-171.
20. Walczak M, Beer K, Surowska B, Borowicz J. The issue of using remelted CoCrMo alloys in dental prosthetics. Archives of Civil and Mechanical Engineering 2012; 12: 171-177.
21. Walczak M, Bieniaś J, Surowska B, Multilayered system titanium – sol-gel coating – dental porcelain in dental prosthetics applications, Eksploatacja i Niezawodnosc – Maintenance and Reliability 2006; 3 (31): 35-40.
22. Yan Y, Neville A, Dowson D. Tribo-corrosion properties of cobalt-based medical implantalloys in simulated biological environments. Wear 2007; 263; 1105–1111.
23. Yan Y, Neville A, Dowson D, Williams S. Tribocorrosion in implants—assessing high carbon and low carbon Co–Cr–Mo alloys by in situ electrochemical measurements. Tribology International. 2006; 39: 1509–1517.
24. Yavuz T, Acar A, Akman S, Ozturk AN. Effect of Surface Treatment on Elemental Composition of Recast NiCr Alloy. Materials Sciences and Applications 2012; 3: 163-167.
25. PN-EN ISO 9693:2002, Metal-ceramic dental restorative systems.
26. PN-EN ISO 10271:2012. Dentistry– Corrosion test methods for metallic materials.
27. www.dentaurum.de - Website of Dentaurum Company; 29 July 2013.

Mariusz WALCZAK
Department of Materials Science
Lublin University of Technology
ul. Nadbystrzycka 36, 20-618 Lublin, Poland
Daniel PIENIAK
Applied Mechanics Section
Department of Fire Fighting Technique
Faculty of Fire Safety Engineering
Main School of Fire Service
ul. Słowackiego 52/54, 01-629 Warsaw, Poland
Agata M. NIEWCZAS
Department of Conservative Dentistry with Endodontics
Medical University of Lublin
ul. Karmelicka 7, 20-080 Lublin, Poland
E-mails: m.walczak@pollub.pl, danielp60@o2.pl, agata.niewczas@umlub.pl

Article citation info:
CHŁOPEK M, DZIK T, HRYNIEWICZ M. Determining the grip angle in a granulator with a flat matrix. Eksploatacja i Niezawodnosc – Maintenance and Reliability 2014; 16 (2): 337–340.

Michał CHŁOPEK
Tomasz DZIK
Marek HRYNIEWICZ

DETERMINING THE GRIP ANGLE IN A GRANULATOR WITH A FLAT MATRIX

WYZNACZANIE KĄTA CHWYTU W GRANULATORZE Z PŁASKĄ MATRYCĄ*

The article addresses the new concept of determining the grip angle in a roll – a flat matrix working arrangement. It was verified experimentally with the exemplary use of composite fuels. For this purpose, a methodology has been developed and the external and internal friction coefficients for several fuel blends have been determined. Knowing them enables one to determine the grip angle which has a significant influence on the efficiency of the granulator. Then, pressure granulation tests with selected blends were carried out. The test results and the calculations are presented in the article. The comparison of the experimental grip angle and the one determined on the basis of a theoretical equation testifies to the correspondence between the theory and the actual physical situation. The determined friction coefficients also determine the selection of an adequate diameter and width of the roller as well as the shape of its working surface. It is of essential importance for ensuring the correct operation of a press with a flat matrix.

***Keywords**: pressure granulation, composite fuels, grip angle, external and internal friction coefficient.*

W artykule zwrócono uwagę na nową koncepcję określania kąta chwytu w układzie roboczym rolka - płaska matryca. Poddano ją weryfikacji eksperymentalnej na przykładzie paliw kompozytowych. W tym celu opracowano metodykę i wyznaczono współczynniki tarcia zewnętrznego oraz wewnętrznego kilku mieszanek paliw. Ich znajomość umożliwia określenie kąta chwytu mającego istotny wpływ na wydajność granulatora. Następnie przeprowadzono próby granulacji ciśnieniowej wybranych mieszanek. Wyniki badań oraz obliczeń przedstawiono w artykule. Porównanie doświadczalnego kąta chwytu oraz wyznaczonego z równania teoretycznego świadczy o zbieżności teorii z rzeczywistą sytuacją fizyczną. Wyznaczone współczynniki tarcia determinują również dobór odpowiedniej średnicy i szerokości rolki, a także kształtu jej powierzchni roboczej. Ma to istotne znaczenie dla prawidłowej eksploatacji prasy z płaską matrycą.

***Słowa kluczowe**: granulacja ciśnieniowa, paliwa kompozytowe, kąt chwytu, współczynnik tarcia zewnętrznego i wewnętrznego.*

1. Introduction

Pressure granulation most often uses granulators with a ring matrix or a flat matrix [6,7] and structures combining the advantages of granulators and roll presses, which are used mainly to consolidate materials of mineral origin and post-production waste. A granulator with a flat matrix is a solution which offers great development potential. The key factors of structural nature which have an influence on the course of the pressure granulation process in a granulator with a flat matrix include the diameter, the roller width, the shape of its working surface, the matrix height and the geometry of the moulding forms [1, 2, 3, 12, 13]. The sources present experiments in the area of selecting some structural parameters of the working elements of the granulator obtained on a laboratory and industrial scale [1, 6, 8, 12]. These works focus on selecting the structural features of the matrix. The results of laboratory tests and operational tests have been found to provide a data base which is sufficient to make their proper selection.

To ensure a proper course of the pressure granulation process, it is important that the consolidated material is forced through the holes in the matrix, and most of all, that the condition of gripping the material being condensed in the roller-matrix arrangement is fulfilled. The issue of determining the grip angle in the working arrangement of the granulator has not been addressed in a complex way so far. Only one paper [6] presents considerations aimed at comparing the efficiency of a granulator with a flat matrix and a ring matrix, on the assumption that the grip angle is the same. Many more publications concern modelling of the process of condensing in a closed matrix [4, 14], a screw press [10, 11] and in a roll press in which material is consolidated in a way similar to that in a granulator with a flat matrix [5, 9]. There is, however, a shortage of knowledge about the phenomena which occur during the flow of material in the roll-flat matrix zone [7, 15]. Therefore, the geometrical dimensions of the roll, which have a significant influence on the course of the press operation, are selected in an experimental way, with the use of the trial and error method. This way of proceeding is time-consuming, expensive and does not enable determining the influence of the change of the feed properties on the granulation process. This inspired undertaking relevant own research. It was carried out with the exemplary use of composite fuels because the development of their production technology is innovative both in the field of science and technique [16].

2. Objective of the paper

The issue of fundamental importance for the proper operation of a granulator with a flat matrix is introducing a proper amount of material into the roller-flat matrix zone, its stable flow and forcing through the holes of the matrix. The grip angle [6] is of great importance here, similar to the case of a roll press [9]. A theoretical analysis has been carried out and used to develop a concept of determining the material grip angle in a granulator with a flat matrix [2]. Its innovative nature

(*) Tekst artykułu w polskiej wersji językowej dostępny w elektronicznym wydaniu kwartalnika na stronie ***www.ein.org.pl***

required that its correctness had to be checked. The objective of the research studies, the results of which are presented in the present article, was to verify experimentally the hypothesis on determining the grip angle in the working arrangement of the granulator on the basis of the knowledge of external and internal friction coefficients. This required building proper laboratory stations, developing a methodology and carrying out tests as well as carrying out pressure granulation trial tests with the exemplary use of composite fuels.

3. Determining the grip angle in a press working arrangement

A new concept of determining the material grip angle in the roller – matrix working arrangement has been presented in the paper [2]. It considers conditions of balance of an elementary section of the volume of material between the roller and the matrix. It has been assumed that the indispensable condition of a correct condensation process is to eliminate internal skids of material which may occur within the compaction zone. Focus was laid on its beginning, that is, the place where the working surface of the roller comes in contact with the material. The scheme of the material compaction arrangement in the roller – flat matrix zone is presented in Fig. 1.

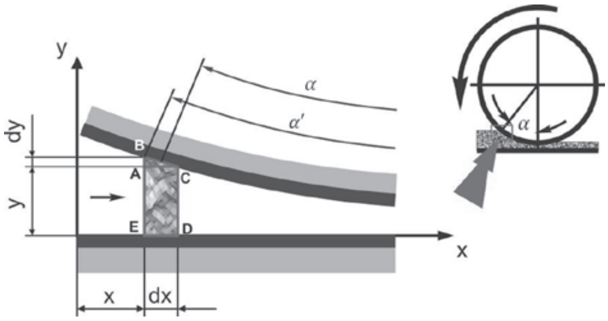

Fig. 1. Scheme of the material condensation arrangement in the roller – flat matrix zone [2]

The result of theoretical considerations is the dependence (1) determining the grip angle value α' which is presented below:

$$\alpha' \leq \arctan\left(\frac{1}{2}(\xi - \mu)\right) \tag{1}$$

Where: ξ– internal friction coefficient,
μ – external friction coefficient.

The considerations show that the grip angle in the working arrangement of the granulator can be determined theoretically if the internal and external friction coefficients are known. It is of essential importance for the correct selection of geometrical structural parameters of the roller and the shape of its working surface. Considering the theoretical nature of the considerations, it was decided that the presented hypothesis needed to be verified. It required laboratory tests to be carried out.

4. Experimental determination of external and internal friction coefficients

The external and internal friction coefficients of the feed were determined on the station presented in Fig. 2. It consists of a support structure on which a rotational base unit and an arm with a discharge trough are set. Before starting the measurements, the station is levelled with the use of adjustment screws. The trough is inclined to the level at an angle which makes it possible for the feed to freely slide down the trough. It is fed in a continuous manner while simultaneously reducing the inclination angle.

The external friction coefficient of the feed – steel frictional couple is the tangent of the angle at which the trough is inclined to the level at which the feed no longer continues to move. Then, such a position of the trough is determined which makes the feed pour down along the axis of the rotating base unit. It lasts until a regular cone is formed. Its height and mass are used to determine the internal friction method and the bulk density of the feed. Three trial tests were carried out for each case. The internal friction coefficient tests were carried out at the test station in which no consolidation of the material being condensed occurs because it features no cohesion at the moment when the roller grips the material. Table 1 contains results of measurements of the external friction coefficient, the internal friction coefficient and the bulk density of lignite, straw, miscanthus, plastifier and their blends under gravitational pressure. The presented results constitute an average of three measurements.

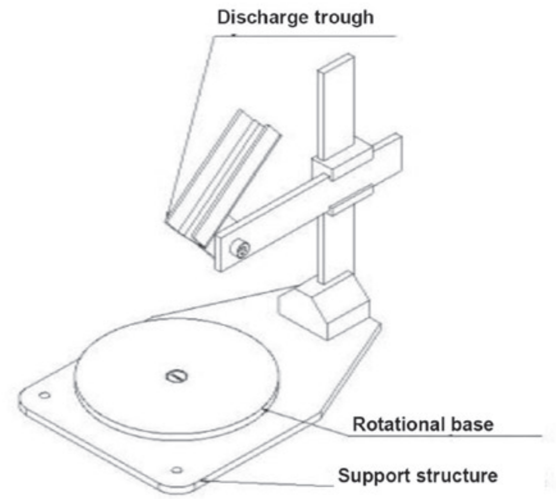

Fig. 2. Scheme of a test station designed to determine the external friction coefficient, the internal friction coefficient and the bulk density of fuel blends

Table 1. Friction coefficient and bulk density measurement results

Name	Internal friction coefficient	External friction coefficient	Bulk density [kg/m^3]
Lignite	0.74	0.34	650
Straw	1.23	0.32	110
Miscanthus	1.12	0.29	210
M1	0.98	0.32	371
M2	0.95	0.31	381
M3	0.92	0.36	401
M4	0.88	0.34	448
M5	0.8	0.31	542
WB 45 plastifier	0.78	0.39	1020

The tests proved that the highest internal friction coefficient is shown by grinded <3 mm plant biomass in the form of straw and miscanthus. It falls within the range from 1.12 to 1.23. However, the lowest external friction coefficient among the tested materials is 0.74 and it is shown by the <3 mm lignite whereas the WB45 plastifier features a slightly higher value. As expected, the blends had the friction coefficient dependent on the content of components. A higher content of lignite results in a reduced internal friction coefficient. Compositions of individual blends marked as M1 to M5 and their moistures are provided in table 2.

5. Composite fuel pressure granulation laboratory research tests

The tests of the pressure granulation of blends containing miscanthus, lignite and plastifier were carried out with the use of a laboratory granulator with a flat matrix, presented in Fig. 3. It is equipped with a matrix which is 25 mm thick and has a diameter of 120 mm. It has 36 cylindrical holes with a diameter of 8 mm which are disposed in a ring with an internal diameter of 52 mm and the external diameter of 100 mm. In the top part of the hole, there are conical 2.5 mm deep undercuts with a 60° flare angle. The granulator is equipped with two condensing rollers which are 40 mm thick and have a diameter of 64 mm. On the cylindrical surface of the rolls, there are 30 prismatic cuts with a width and depth of 3 mm. The rotational speed of the matrix is 300 rpm. The granulator is powered with a three-phase motor with the power output of 2.2 kW. The distance of the rollers from the matrix is set to be 0.1 mm. Before carrying out the measurements, the matrix and the rollers were heated up to the temperature of approximately 70°C by means of a mixture consisting of bran-water-oil-corundum powder.

The initial preparation of components of the blends consisted in drying lignite and miscanthus, then grinding them to a grain size below 3 mm. Immediately before starting the tests, the blend compositions, which are specified in table 2, were prepared. After blending the components exactly, the moisture of the blends, their bulk density, external and internal friction coefficients were measured. Then, the blend granulation tests were performed during which the weight of the obtained granules, their quality and the process duration were determined. The data obtained in the experimental research was used to calculate the experimental grip angle on the basis of the measurement of the granulator efficiency and the density of fuel blends which underwent pressure granulation. However, the theoretical grip angle was obtained from the dependence (1), using the experimentally determined external and internal friction coefficients. The results of the tests and calculations are presented in table 2. They point at a regularity which consists in that the experimental grip angle is bigger than the theoretical one. The average difference between them is 6.21 %. Fig. 4 shows selected results of tests and calculations in the form of a dependence of the experimental and theoretical grip angle on the granulator efficiency, obtained in the course of the composite fuel blend consolidation tests.

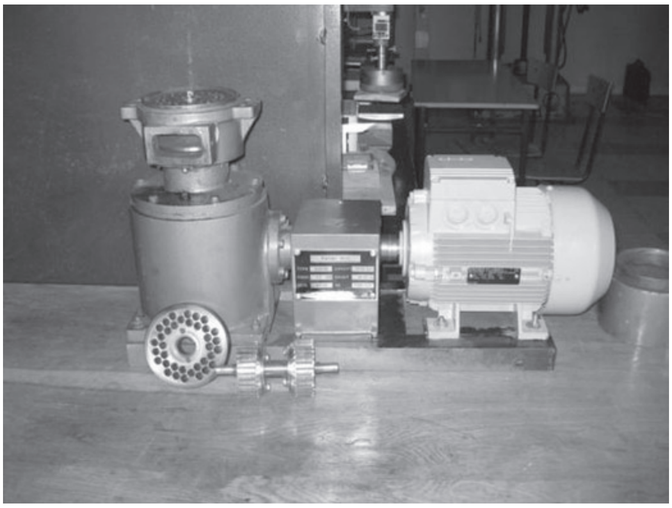

Fig. 3. Laboratory granulator

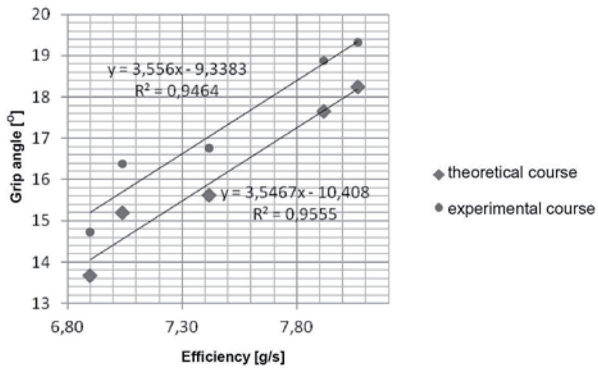

Fig.4. Dependence of the experimental and theoretical grip angle on the laboratory granulator efficiency obtained in subsequent trial tests.

In both cases, this is a linear dependence and the correlation coefficient is high. Furthermore, both straight lines have a similar gradient. The difference between the initial ordinates, calculated from regression equations, amounts to 1.0697, which, in reference to the experimental grip angle value, gives an error level of 7.0%, at its lowest value and 5.5% at the highest one. Their average calculated difference within the examined range is 6.29%. This confirms the observed regularity.

Table 2. Pressure granulation test results and grip angle value calculations

Blend number	M1		M2		M3		M4		M5	
Name	**Um**	**W [%]**	**Um**	**W [%]**	**Um**	**W [%]**	**Um**	**W [%]**	**Um**	**W [%]**
Miscanthus	0.68	13.00	0.60	13.00	0.55	13.00	0.50	13.00	0.45	13.00
Carbon	0.27	35.00	0.35	35.00	0.40	35.00	0.45	35.00	0.50	35.00
WB 45 plastifier	0.05	10.00	0.05	10.00	0.05	10.00	0.05	10.00	0.05	10.00
Blend moisture [%]	19.00		21.00		22.00		23.00		24.00	
Initial density [kg/m^3]	371		381		401		448		542	
Blend mass [g]	500.00		950.00		890.00		450.00		950.00	
Pelleting duration [s]	62.00		120.00		120.00		64.00		138.00	
Efficiency Qm [g/s]	8.06		7.91		7.41		7.04		6.90	
Remarks	Bad quality		Good quality		Good quality		Best quality		Granulate too wet	
Experimental grip angle α_{rz} [°]	**19.32**		**18.87**		**16.77**		**16.38**		**14.73**	
Measured internal friction coefficient ξ	0.98		0.95		0.92		0.88		0.8	
Measured external friction coefficient μ	0.32		0.31		0.36		0.34		0.31	
Theoretical grip angle α_{obl} [°]	**18.24**		**17.66**		**15.62**		**15.18**		**13.67**	

Markings used in the table: U_m– mass content of the component, W- moisture of the component.

Considering the presented research test results, it can be ascertained that there is conformity between theory and practice. However, explaining the reasons why the experimental grip angle value is higher in comparison to the theoretical one requires undertaking further research works.

6. Summary

Great interest in the pressure granulation of fine-grained materials, especially biomass and solid fuel blends, inspired research which aimed at developing a method of selecting the components of the granulator working arrangement. In the paper [2], the authors presented their own concept of a solution to the problem in which the determination of the grip angle in the roller - flat matrix working arrangement plays an important part. A hypothesis was formulated about the possibility of determining it on the basis of the knowledge of the external and internal friction coefficients of the feed. Continuing the research, the results of which are presented in the present article, the verification of this theory was carried out. It was found through an analysis of test and calculation results that there are no grounds to reject the hypothesis concerning the possibility of determining the grip angle on the basis of the knowledge of the external and internal friction coefficients. It is of significant importance for determining the operational efficiency of the granulator and allows for forecasting its decline caused by the reduction of the operating roller diameter due to its wear. The knowledge of the grip angle also allows one to determine the material condensation resistance torque correctly and therefore the demand for energy needed to perform the process already at the machine construction stage. It enables matching the granulator drive properly, which ensures durability of this arrangement.

The undertaken work will be continued for blends containing other components. This should enable explaining the reasons for the occurrence of the observed regularity which consists in that the experimental grip angle is bigger than the theoretical one. Research is also planned to discover phenomena which occur in the roller – flat matrix zone. In this case, it will be necessary to determine the changeability of friction coefficients and the side pressure versus regular pressure.

The paper has been carried out at AGH University of Science and Technology as part of the project entitled "CoalGas" – KIC "Work Package 5, agreement no 7.7.130.7006

References

1. Chłopek M, Hryniewicz M, Dzik T. Dobór cech konstrukcyjnych układu roboczego granulatora z płaską matrycą. [*English translation: Selection of structural features of a working arrangement of a granulator with a flat matrix*.] Materiały XXV Konferencji Naukowej nt. "Problemy rozwoju maszyn roboczych" (płyta CD) [*English translation: Proceedings of the 25th Scientific Conference entitled "Issues for the development of working machines*" (CD)]. Zakopane 2012.
2. Chłopek M, Dzik T, Hryniewicz M. The method for selection of the working system components for a pellet Press with flat die. Chemik 2012; 66: 491-500.
3. Colovic R, Vukmirovic D, Matulaitis R, Bliznikas S, Uchockis V, Juškiene V, Levic J. Effect of die channel press way length on physical quality of pelleted cattle Feed. Food and Feed Research 2010; 1: 1-6
4. Cunningham J, Sinka I, Zavaliangos A. Analysis of Tablet Compaction. I. Characterization of Mechanical Behaviour of Powder and Powder/Tooling Friction. Journal of Pharmaceutical Sciences; 93(8): 2022-2039
5. Cunningham J. Experimental Studies and Modelling of the Roller Compaction of Pharmaceutical Powders. Ph.D. thesis, Philadelphia: Drexel University 2005.
6. Hejft R. Ciśnieniowa Aglomeracja materiałów roślinnych. [*English translation: Pressure agglomeration of plant materials*.] Radom: ITE, 2002.
7. Hejft R, Obidziński S. Konstrukcje matryc w granulatorach z układem roboczym "matryca płaska-rolki zagęszczające" [*English translation: Designs of matrices in granulators with a "flat matrix - condensing roller" working arrangement*]. Chemik 2012; 66: 479-484.
8. Holm J, Henriksen U, Wand K, Hustad J, Posselt D. Experimental Verification of Novel Pellet Model Using a Single Pelleter Unit. Energy & Fuels 2007; 21: 2446-2449
9. Hryniewicz M. Metoda doboru pras walcowych oraz opracowania założeń do ich modernizacji lub konstrukcji. [*English translation: A method of selecting roll presses and making assumptions for their modernisation or construction*]. Krakow: Published by AGH, 1997.
10. Krizan P, Soos L, Matus M. Optimalisation of briquetting machine pressing chamber geometry. The Journal of Faculty of Technical Sciences 2010; 2: 19-24.
11. Michelangelli O, Yamanoi M, Gaspar-Cunha A, Covas J. Modelling pellet flow in single extrusion with DEM. Proceedings of the Institution of Mechanical Engineers, Part E: Journal of Process Mechanical Engineering 2011; 225(4): 255-268.
12. Obidziński S. Wpływ czasu docierania matrycy pierścieniowej na obciążenia w układzie roboczym granulatora w procesie granulowania pasz. [*English translation: Influence of the ring matrix wear-in time on the loads in the fodder granulation process*.] Inżynieria Rolnicza 2006; 7: 343-349.
13. Obidziński S. Influence of selected parameters of a pellet mill on the quality of the final product. Polish Journal of Food and Nutrion Sciences 2007; 57(2(A)): 121-124.
14. Sinka I. Modelling Powder Compaction. KONA Powder and Particle Journal 2006; 25: 4-22.
15. Sridhar I, Fleck N. Yield Behaviour of Cold Compacted Composite Powders. Acta Materialia 2000; 48: 3341-3352.
16. Taulbee D, Patil D, Honaker R, Parekh B. Briquetting of Coal Fines and Sawdust Part I: Binder and Briquetting Parameters- Evaluations. International Journal of Coal Preparation and Utilization 2009; 29: 1-22.

Michał CHŁOPEK
Tomasz DZIK
Marek HRYNIEWICZ
AGH University of Science and Technology
Faculty of Mechanical Engineering and Robotics
al. Mickiewicza 30, 30-059 Krakow, Poland
E-mails: mchlopek@agh.edu.pl, tdzik@.agh.edu.pl, mhryniew@agh.edu.pl

Article citation info:
WALKOWIAK T. Simulation based availability assessment of services provided by web applications with realistic repair time. Eksploatacja i Niezawodnosc – Maintenance and Reliability 2014; 16 (2): 341–346.

Tomasz WALKOWIAK

SIMULATION BASED AVAILABILITY ASSESSMENT OF SERVICES PROVIDED BY WEB APPLICATIONS WITH REALISTIC REPAIR TIME

SYMULACYJNA OCENA GOTOWOŚCI USŁUG SYSTEMÓW INTERNETOWYCH Z REALISTYCZNYM MODELEM CZASU ODNOWY*

Paper presents a numerical method for determining changes of availability of services provided by web applications in time. It takes into account the reliability and functional aspects. The reliability analysis allows determining the probability that the system is operational at a given time. The analysis includes the structure of a computer system, random times to failures (hardware or software – related to security breaches) and the detailed repair time model. The repair time model takes into account working hours of administrators and a time associated with delivering components to exchange. Functional analysis allows the determination of the probability that the user will be served in less than a specified time limit. It is based on modelling the interaction between a user and a server as a sequence of tasks on one or more hosts. It takes into account the variability of workload over a week and web application parameters such as the choreography of service, allocation of tasks on hosts and technical parameters of hosts and tasks. The described method was the basis for development of a Monte-Carlo simulator that allows variability of service availability over a week to be calculated. The paper contains the numerical results of the sample analysis.

Keywords: *web application, availability, reliability, Monte-Carlo simulation.*

W artykule przedstawiono metodę numerycznego wyznaczania zmian gotowości usług internetowych w czasie. Bierze ona pod uwagę aspekty niezawodnościowe i funkcjonalne systemu komputerowego świadczącego usługi. Analiza niezawodnościowa pozwala na wyznaczenie prawdopodobieństwa, że system będzie zdatny w danym momencie. Uwzględnia ona strukturę systemu komputerowego, losowe czasy do uszkodzeń (sprzętowych jak i oprogramowania związanych z naruszeniami zabezpieczeń) oraz szczegółowy model odnowy biorący pod uwagę godziny pracy administratorów oraz czas związany z dostarczeniem elementów do wymiany. Analiza funkcjonalna pozwala na wyznaczanie prawdopodobieństwa, że użytkownik zostanie obsłużony w czasie mniejszym niż zadany. Oparta jest ona na modelowaniu procesu realizacji usługi jako sekwencji zadań wykonywanych na jednym lub kilku komputerach. Bierze ona pod uwagę zmienność intensywności napływu użytkowników w ciągu tygodnia oraz parametry takie jak: sekwencję zadań, alokację zadań na komputerach oraz parametry techniczne komputerów i zadań. Opisana metoda była podstawą do stworzenia aplikacji komputerowej wyznaczającej techniką symulacji Monte-Carlo zmienność gotowości systemu w ciągu tygodnia. Artykuł zawiera numeryczne rezultaty przykładowej analizy.

Słowa kluczowe: *usługa internetowa, gotowość, niezawodność, symulacja Monte-Carlo.*

1. Introduction

Services provided on Internet are nowadays the basis of many enterprises.Their correct and uninterrupted operation is an important aspect of business success. Users of services provided by web applications can very easily move to another portal. Therefore, essentials are methods that allowassessing the service availability. Especially important is to investigate the influence of various parameters related to the configuration and maintenance of the web application on service availability.

Availability in case of repairable systems, to which web systems belong to, is understood as the probability that the system is operating at a specified time. Therefore to define availability of web application we need to understand what it means that service is operating. We will follow definition from [29]: "the system is operational when required tasks are performed correctly within the defined time limits". It includes two important aspects analysed in this paper.

In the first, this is the reliability aspect. The system must operate. It cannot be failed. Secondly, the functional aspect must be considered. The user who will be waiting for a response for longer than a few seconds will treat service as failed, and possibly will look for another website with similar functionality.

There are a large number of studies examining the reliability of websites or web applications. However, in most cases the reliability analysis is based on Markov processes [3] and the analysed system is modelled as a simple serial one [18]. In this paper, we propose to focus on the more realistic modelling of how repairs of computer systems are carried out. It will take into account working hours and weekends of system administrator. Analysis of the functional aspect is based on the commonly used solution in the analysis of complex technical systems: modelling and simulation [4]. Modelling is focussed on a process of execution of a user request that is described as a sequence of tasks realised on technical services provided by the system [26]. The computer simulation is responsible for calculation of service availability. It is based on a time event simulation with Monte Carlo analysis [8]. The simulator allows to calculate the probability that the user will receive an answer in a time less than the given threshold under given workload.

(*) Tekst artykułu w polskiej wersji językowej dostępny w elektronicznym wydaniu kwartalnika na stronie ***www.ein.org.pl***

2. State of art and related works

Reliability analysis of complex technical systems (to which web systems belong to) is a subject of researches for many years. It is described in a number of good textbooks, for example in a book by Barlow and Proshan [3]. The problem of repair time modelling is most often solved by the use of the exponential distribution [1, 3, 18]. This is due to popularity of Markov processes in reliability analysis. In relatively fewer cases researches are using other distributions for repair time modelling. For example, in [13, 14] authors assume that the repair time could be described by the geometric process(proposed by Lama in [16]). Moreover, most often it is assumed [1, 3] that the repair time begins immediately after the failure. However, the other scenario is also analysed in the literature [7, 30]. It assumes that the time from the component's failure to the completion of the repair is composed of two different periods: waiting and real repair. The waiting period is modelled as a random variable independent of the lifetime of the component. There are also works [14] that apply a mix approach, in which the repair time with a certain probability consists of the waiting and the real repair time or only of the real repair time.

The analytical approaches (mentioned above) have significant limitations [21] which includes the limited distributions (mostly exponential), narrow applicability (only to a special class of systems) and poor compliance with reality. To overcome these limitations the simulation approach is applied [4]. The use of computer simulation [5], in particular the Monte-Carlo simulation [8], to analyse the reliability of complex systems is also described by many researches, for example in the monograph [15] or in papers [6, 21].

Methods of availability analysis of web systems that are described in the literature are based on the analytical models [9, 12] or on real system monitoring [2, 11, 22]. In contrast, the method described in this paper is based on the use of computer simulation. The simulation is used for determining the user response time as a function of the user request rate (chapter 5).

The response time can be determined experimentally by performing load tests of real systems (using tools as: Funkload, Apache JMeter, Rational Performance Tester or Developer Tools from Microsoft), estimated by analytical models[19, 25] (in most cases based on queuing networks [17]) or by simulation techniques [24] (also very often based on queuing models).

3. Service availability

One of the quality metrics used for web systems is availability, defined as the probability that a user will be properly serviced by a system at a specific time, i.e.:

$$A(t) = \Pr(U_t)\ , \tag{1}$$

where U_t is an event that system provides correct responses.

Let S_t be an event that the computer system on which the web application is deployed is operational (there are no failures). Using an equation for conditional probabilities the service availability could be calculated as:

$$A(t) = \Pr(U_t \mid S_t)\Pr(S_t) + \Pr(U_t \mid \overline{S_t})\Pr(\overline{S_t})\ . \tag{2}$$

In case of analysed class of systems a user will benot correctly serviced if the computer system is failed. Therefore, $\Pr(U_t \mid \overline{S_t})$ =0. It simplifies the above equation to:

$$A(t) = \Pr(U_t \mid S_t) \cdot \Pr(S_t)\ . \tag{3}$$

The above equation is the basis of a numerical method that allows to calculate the value of the service availability. For readability, we will introduce names for individual factors of the product (3). Let $\Pr(S_t)$ be calledthe system availability, which is understood as the probability that the computer system, on which the web application is deployed is operational, is not failed. Let's $\Pr(U_t \mid S_t)$ call the functional availability defined as the probability that the user will receive an answer in a time less than a given threshold (t_{max}) under assumption that computer system is operational. Therefore, the functional availability is given by the equation:

$$\Pr(U_t \mid S_t) = \Pr(responsetime(T) < t_{\max} \mid T = t \wedge S_t)\ . \tag{4}$$

4. Reliability model

The paper considers a very wide class of web systems. In general some business services are accessed by the user using web interactions. The service responses are dynamically computed by the service components, which also interact with each other using the client-server protocols. On the low level the system consists of interconnected hosts with installed software (technical services) responsible for providing business service. In the considered approach to web system modelling, the hosts are the basic components of the system infrastructure. Thus, all the failures are attributed to them (of course they origin from hardware or software components faults).

There are numerous sources of failures in web systems. These encompass hardware malfunctions (transient and persistent), software bugs, human mistakes, viruses, exploitation of software vulnerabilities, malware proliferation, drainage type attacks on system and its infrastructure (such as ping flooding, DOS). We propose to model all of them from the point of view of resulting failure.

The most common source of host failures are caused by some exploitation of security vulnerability, often a proliferation of bogus service requests that lock up all the server resources. This is a common consequence of insufficient security metrics (for example caused by wrong firewall rules or a lack of antivirus software, etc.). It may result in inoperational host failure or in a lost in performance. In the first case the host cannot process services that are located on it, these in turn do not produce any responses to queries from the services located on other hosts. In the second case the host can operate, but it cannot provide the full computational resources, causing some services to fail or increasing their response time above the acceptable limits.

A web system from the point of reliabilityis a repairable system. The reliability analysis requires to model failures occurrence, their results and the repair time. For simplicity, we will assume that a failure of any host (caused by hardware or software component fault) will result in a web systemfailure [18].

Moreover, we propose to model system failures by a set of independent host failures.The occurrence of a host failure is described by a random process. Where, the time to failure is modelled by the exponential distribution (like in the Markov model). In case ofa repair time we propose to model it in details taking into consideration repairman working hours and a time required to replace the failed component or a time needed to react on a software failure.

Let's assume that the system administrator works five days a week in selected hours. And only during these hours any failure could be discovered and any repair operation could be started (for example software reinstallation). Moreover, a time required to deliver new equipment by courier will be taken into consideration. We assume that the system component to be replaced will be available on the next working day at a given hour.

Let's divide host failures into two groups: failures that require delivery of a new component and ones that don't (like failures connected with software or cases when required component is available onsite). Let's mark the probability of the first type failures as *pf*.

Taking into account all these assumptions we could distinguish following elements of period from the component's failure to the completion of the repair (withsystem administrator working hours from 8 am to 5 pm with one hour lunch break):

- time to failure discovery– equal to zero if a failure happens during working hours, in other cases it is a time to next working period: the finish of lunch break (2 pm) or next day (8 am), for example if a failure will occur just after 5 pm on Friday, it will be equal to 63 hours.
- failure analysis time – a time needed to discover a failure reason, we propose to model it by a random variable with a truncated normal distribution, if the failure analysis overlaps with not working hours, it is enlarged by a time to next working period (1 hour in case of overlapping witch lunch time, 15 hours during working days evenings and nights or even 63 hours in case of Friday afternoon);
- delivery time – with a probability of 1-*pf* it is equal to zero (it allows to model an operating system or software component failure), in other cases equal to a time to next working day (it models the delivery of a new system component by courier);
- component replacement time –time required to replace a failed hardware component or to reinstall failed software component, it is modelled by a random variable with the truncated normal distribution plus extra value in case of overlapping with not working hours(like in the case of failure analysis time).

Presented reliability model includes random values with exponential, truncated normal and discrete distributions. Therefore, it is hard to calculate the system availability by analytical methods (like Markov or semi-Markov chains). But it could be done using the numerical approach, strictly speaking by Monte-Carlo simulation [8]. Therefore, authors developed the reliability simulator. It was implemented in C++ within the Scalable Simulation Framework (SSF) [20]. SSF is an object–oriented API, a collection of class interfaces with prototype implementations. For the purpose of simulating reliability states the Parallel Real-time Immersive Modeling Environment (PRIME) [20] implementation of SSF was used. The main reason of using SSF was the fact that it was also used by authors for the development of the functional simulator of web system described in the next chapter.

Operation of the simulator is based on repetition of the failure and repair process simulation. Following simulations differ in the values of random variables occurring in the analysed system. Knowing the distribution of these variables (input data for simulation), one can get information about the behaviour of the system in the most probable cases. By observing changes of some metric values, the information about their distributions and any other statistics could be easily gathered. A single simulation last for a fixed length (in the analysed case a multiplication of seven days).

The reliability model contains some arbitrary assumptions, such as working hours of administrator or a number of shifts. The used method allows changing the assumptions and thus different scenarios could be also simulated. However, it could require changes in the source code of the simulator. Sample numerical results are presented in chapter 6.

5. Functional model

5.1. Response time prediction

As it was presented in chapter 3, the service availability depends on the system reliability (described in the previous chapter) and on the web system performance measured by the user response time. To calculate the user response time we need to analyse the process of user request execution. It is performed from the point of view of business service realised by web system [10].

The user initiates the communication requesting some tasks on a host, it could require a request to another host or hosts, after the task execution a host responds to requesting server, and finally the user receives the respond. Requests and responses of each task give a sequence of a user task execution, according to a given choreography. It could be described as a sequence of requests:

$$choreography(u) = \left(c(task_{b_1}), c(task_{b_2}), ..., c(task_{b_n})\right), \quad (5)$$

where $c(task_{b_i})$ represents a request ($\Rightarrow$) to $task_{b_i}$ or a response ($\Leftarrow$) from a given task. Some tasks after completing the calculation returnreply to the sender. Other tasks before sending the response can call other tasks. It is important to mention that each task is deployed on one of hosts and it cannot be changed during running of the system.

Based on the above model (a detailed description can be found in [26]) the response time is equal to the time required for communication between hosts, on which tasks are deployed and the time required to perform each of tasks. For following choreography:

$$\begin{aligned} &choregraphy(u) = \\ &u \Rightarrow task_1 \Rightarrow task_2 \Leftarrow task_1 \Rightarrow task_3 \Leftarrow task_1 \Leftarrow u \end{aligned} \quad (6)$$

the user response time could be calculated as a sum:

$$\begin{aligned} resoponsetime(u) = delay(h_0,h_1) + pt\left(task_1\right) + delay(h_1,h_2) + pt\left(task_2\right) + \\ delay(h_2,h_1) + delay(h_1,h_3) + pt\left(task_3\right) + delay(h_3,h_1) + delay(h_1,h_0) \end{aligned}, \quad (7)$$

where $delay(h_0,h_1)$ is a time of transmitting a request from host h_i to h_j, and *pt*(*task*) is a task processing time (on a host on which the task is deployed). For contemporary web systems not associated with media broadcasting the time of transmitting a request can be modelled by a random variable with a truncated normal distribution [26].

The processing time of each task depends on the type of task (its computational complexity), the type of a host (its performance) and of its load (number of other requests being handled concurrently). The last of these parameters is not a constant value over time. It depends on the workload (number of users) and its changes. Processing time is difficult to be determined in an analytical way, that is why the computer simulator based on the Monte- Carlo technique [8] was developed [27]. It was implemented, as the simulator discussed in the previous chapter, in the Prime SSF [20]environment. For a given choreography (for example described in WS-CDL), deployment of tasks to hosts, configuration of hosts (processor performance and number of cores), technical service parameters (types and configuration of web servers), computational complexity of each task, and model of a user (like a number of users) the developed software allows to determine the user response time.

5.2. Functional availability

Mentioned simulator software allows to determinate in a numerical way the probability that the user will receive an answer in a time less than a given threshold in a function of workload (described by intensity of user requests):

$$Af(\lambda) = \Pr(responsetime < t_{\max} \mid workload = \lambda)\ . \quad (8)$$

This metric is a numerical representation of client's perception of particular business service quality. It measures the probability that the user will not resign from active interaction with the service due too long service response time.

If we know how the intensity of user requests varies over a time ($workload(t)$) we could calculate the functional availability as:

$$\Pr(U_t \mid S_t) = Af(workload(t)) \; . \tag{9}$$

The values of the workload function depend on the type of offered service. For example, websites used by students have the greatest influx of users in the period just before exams and mostly at night. In the sample analysed in the next section, it is assumed that the workload is periodic with a period equal to one week. Daily and weekly variability is often observed in public services. This can be noticed analysing the variability of traffic over the networks of large Internet service providers.

6. Availability analysis of a case system

6.1. System availability

All the simulation results that illustrate the presented method were computed using a real-life example of the case-study web system. The system consists of six hosts. There were five hosts with business components communicating according to selected choreography and one router with a firewall. Since, today's computer devices are characterised by high reliability parameters, the intensity of failures was set to one year per year. The repair model parameters were set as follows:

- mean failure analysis time – 3 hours,
- mean component replacement time – 1 hour,
- probability of hardware failure *pf* (requiring a component to be delivered by courier) – 0.2,
- working hours of administrator – 8 am to 17 pm, with one hour break for lunch,
- standard deviation of truncated normal distributions – 20% of its mean values.

The achieved results for simulating 1,000 weeks 50,000 times are presented in Fig. 1. The changes of system availability during a week could be noticed. The lowest value is achieved on Monday. It agrees with authors experience, that Monday is a day that there isthe most work to be done by system administrator. It is caused by the fact that the administrator is not working during weekends and failures that occurred during that time are maintained on the next working day.

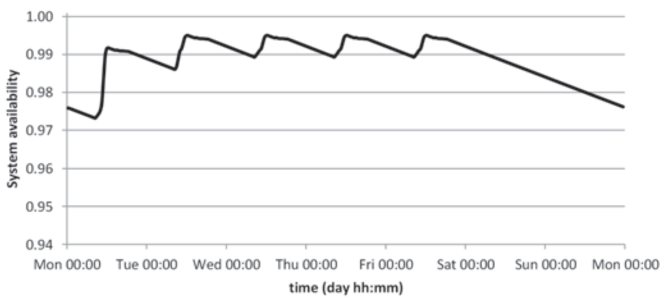

Fig. 1. System availability changes over a weekachieved by computer simulation of the case system

6.2. Functional availability

Another factor contributing to the service availability is the functional availability, defined as the probability that the user will obtain a response in time less than the given limit, assuming that the computer system running the service is not failed. As already mentioned the analysed system consists of six hosts and performs selected choreography. The time limit was set to 12 seconds. The results obtained from simulation, i.e. functional availability in a function of the user request rate, are shown in Fig. 2. Assuming weekly workload variations shown in Fig. 3, the functional availability in a function of time is presented in Fig. 4.

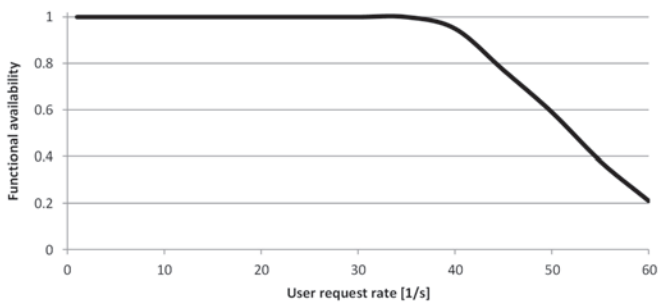

Fig. 2. Functional availability in a function of user request rate

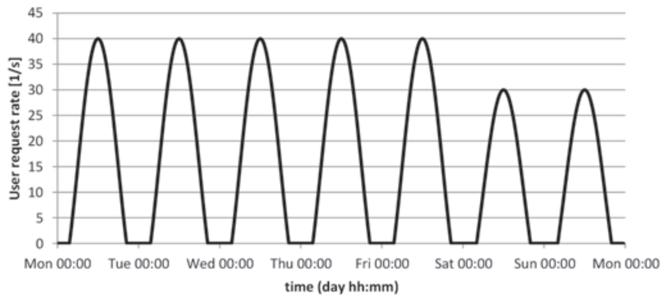

Fig. 3. Assumed changes in workload over a week

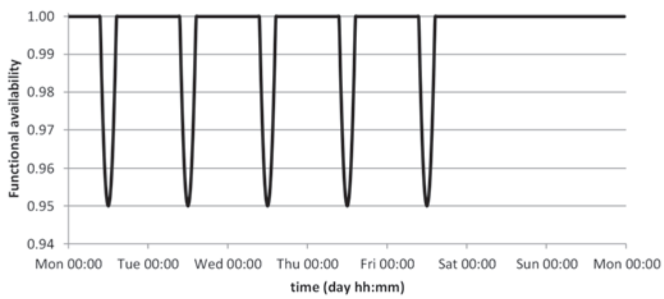

Fig. 4. Functional availability changes over a week for thecase system

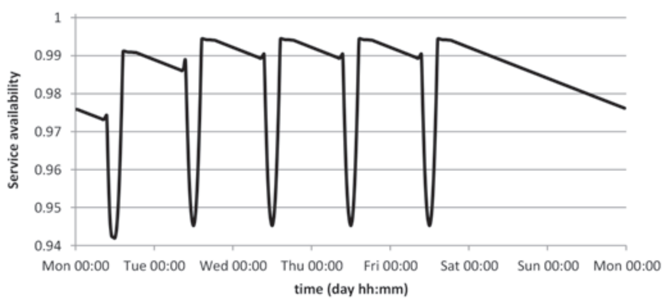

Fig. 5. Service availability changes over a week for thecase system

6.3. Service availability

According to equation (3) the product of the system (Fig. 1) and functional (Fig. 4) availability gives the services availability (Fig. 5) for the case web system. The daily variations of service availability are results of the diurnal variation in the workload and administrators working hours. In addition, there is a noticeable decline of availability in the weekend reaching its minimum on Monday around noon. The minimum value on Monday is linked to the accumulation of failures from Saturday and Sunday and daily maximum of the user request rate.

7. Final remarks

7.1. Conclusions

This paper presented a method for determining changes of availability of service provided by web applications in time (over a week). The method considers reliability and functional aspects. The reliability analysis takes into account the structure of the system (number of hosts), random failure occurrence (modelled by exponential distributions), failure analysis time (modelled by truncated Gaussian distribution), component replacement time (next working day) and working hours of system repairman (administrator).

Functional analysis allows to determinate the probability that the user will receive an answer in a time less than the given threshold. Functional model parameters include the web system choreography (interaction between tasks), system structure (number of hosts, host performance, task allocation on hosts and task execution time) and workload (changes in the user request rate over a week).

Numerical calculations were performed using the simulator developed by authors. The use of Monte-Carlo simulation allowed a flexible functional and reliability model of web system to be created. However, the presented approach has some significant drawbacks. Firstly, the simulation time associated with multiple repetitions (the basic principle of Monte-Carlo simulation) in case of the functional simulator could be large. Secondly, changes in the structure of the model (but not in its parameters) may require changes in the source code of the simulator.

The presented approach provides an easy way to explore the impact of changes in the system maintenance (such as working hours of administrators) or changes in functional parameters of the system (e.g. other allocation of tasks, increased level of security or performance of hosts) on the significant from the point of view of user's parameter: the service availability.

7.2. Future work

The presented method includes some assumptions that limit its applicability. First of all, the web system is modelled as a serial reliability system, i.e. a failure of any system component (hosts) results in a failure of the system. It is not true for web systems that useload balancing techniques or systems deployed in computing cloud. In such cases the failure of one of hosts (hardware or software) results in degradation of system performance not in a failure of the whole system.

The second assumption is to model failure results as an inoperation of a single host. However, some of security breaches, like viruses or malware, could result in degradation of hosts performance. So the web system is able to answer to user requests, only response time in longer. It is possible to extend the proposed two–state (operational – failed) reliability model to a multistate one. Each state will be described by a state of each system component (host). Whereas, each component could be in one of three states: operational, degraded performance and failed. The state probability for each of *N*-states (let mark them as S_i) could be calculated by a simple extension to simulator described in chapter 4. Using simulator described in chapter 5, it is possible to calculate functional availability ($\Pr(responsetime(T) < t_{\max} \mid T = t \wedge S_i)$) in each of states and finally the functional availability of service as:

$$A(t) = \sum_{i=1}^{N} \Pr(responsetime(T) < t_{\max} \mid T = t \wedge S_i) \cdot \Pr(S_i, t) \qquad (10)$$

The main problem of this solution is a number of states. For n independent elements, which could be failed, it gives 2^{2n} states [28]. So for the case system analysed in this paper it gives 4096 states. For each of states a time consuming functional simulation has to be performed (chapter 5). The problem could be solved by limiting the sum in (10) to the most probable states and skipping less probable states.

Another area of future work concerns the application of the proposed method in the analysis of websites deployed in computing cloud. In such case, the hardware failures playa much smaller role. This is due to the use of virtualization techniques and migration of virtual machines in the cloud in case of failures. However, the most frequently occurring software failures caused by security breaches and the process of recovery of the system after such failures can be modelled in the same way as described in this work.

The presented work was supported by the Polish National Science Centre under grant number N N516 475940.

References

1. Aven T, Uwe J. Stochastic Models in Reliability. New York: Springer, 1999.
2. Banerjee S, Srikanth H, Cukic B. Log-based reliability analysis of Software as a Service (SaaS). Proceedings of the 21st International Symposium on Software Reliability Engineering 2010; 1: 239-248.
3. Barlow R, Proschan F. Mathematical Theory of Reliability. Philadelphia: Society for Industrial and Applied Mathematics, 1996.
4. Birta L, Arbez G. Modelling and Simulation: Exploring Dynamic System Behaviour. London: Springer, 2007.
5. Clymer J. Simulation-based engineering of complex systems. Wiley Series in Systems Engineering and Management, Wiley-Interscience, 2009.
6. Faulin J, Juan A, Serrat C, Bargueño V. Predicting availability functions in time-dependent complex systems with SAEDES simulation algorithms. Reliability Engineering & System Safety 2008; 93(11): 1761-1771.
7. FinkelsteinM. A scale model of general repair, Microelectron. Reliab 1993; 33(1): 41-44.
8. Fishman G. Monte Carlo: Concepts, Algorithms, and Applications, Springer-Verlag, 1996.
9. Gokhale SS, Jijun L. Performance and Availability Analysis of an E-Commerce Site. Computer Software and Applications Conference, 2006; 1: 495-502.
10. Gold N, Knight C, Mohan A, Munro M. Understanding service-oriented software. IEEE Software 2004; 21: 71-77.
11. Goseva-Popstojanova K, Singh AD, Mazimdar S, LiF. Empirical characterization of session-based workload and reliability for Web servers. Empirical Software Engineering; 11(1): 71-117.
12. Janevski N, Goseva-Popstojanova K. Session Reliability of Web Systems Under Heavy-Tailed Workloads: An Approach based on Design and Analysis of Experiments. IEEE Transactions on Software Engineering 2013; 99(PrePrints): 1.

13. Jia J, Wu S. A replacement policy for a repairable system with its repairman having multiple vacations. Computers & Industrial Engineering, 2009; 57(1): 156-160.
14. Jishen J,ShaominW. Optimizing replacement policy for a cold-standby system with waiting repair times. Applied Mathematics and Computation Journal 2009; 133–141.
15. Juan AA, Faulin J, Ramirez-Marquez J E, MartorellAlsina S S. Simulation Methods for Reliability and Availability of Complex Systems, Springer 2012.
16. LamY. A note on the optimal replacement problem, Adv. Appl. Prob. 1998; 20(2): 479-482.
17. Lavenberg S. A perspective on queueing models of computer performance. Performance Evaluation 1989; 10:53-76.
18. Lipinski Z. State Model of Service Reliability. International Conference on Dependability of Computer Systems. IEEE Computer Society 2006; 35-42.
19. Liu X, Jin H, Sha L, Zhu X.Adaptive control of multi-tiered Web application using queueing predictor. Proc. IEEE/IFIP Netw. Operations Management Symp. (NOMS2006) 2006; 106-114.
20. Liu J. Parallel Real-time Immersive Modelling Environment (PRIME), Scalable Simulation Framework (SSF), User's manual, Colorado School of Mines Department of Mathematical and Computer Sciences. [Available online: http://prime.mines.edu/], 2006.
21. Malinowski J. A simulation model for complex repairable systems with inter-component dependencies and three types of component failures. Advances in Safety, Reliability and Risk Management - Proceedings of the European Safety and Reliability Conference, ESREL 2011, 2012; 128.
22. Merzbacher M, Patterson D. Measuring end-user availability on the Web: practical experience. Proceedings of the International Conference on Dependable Systems and Networks, 2002; 473 – 477.
23. Michalska K, Walkowiak T. Simulation approach to performance analysis information systems with load balancer. Information systems architecture and technology: advances in Web-Age Information Systems,Wrocław: Oficyna Wydawnicza Politechniki Wrocławskiej 2009; 269-278.
24. Rahmawan H, Gondokaryono YS. The simulation of static load balancing algorithms. International Conference on Electrical Engineering and Informatics 2009; 640-645.
25. Urgaonkar B, Pacificiy G, Shenoy P, Spreitzery M, Tantawi A. An analytical model for multitier internet services and its applications. Proc. of the ACM SIGMETRICS'05 Conference on measurement and modeling of computer systems, 2005; 291-302.
26. Walkowiak T. Information systems performance analysis using task-level simulator.International Conference on Dependability of Computer Systems. IEEE Computer Society Press, 2009; 218-225.
27. Walkowiak T. Simulation approach to Web system dependability analysis. Summer Safety and Reliability Seminars, SSARS 2011; 1: 197-204.
28. Walkowiak T, Michalska K. Functional based reliability analysis of Web based information systems. Dependable computer systems / Wojciech Zamojski [et al.] (eds.). Berlin ; Heidelberg: Springer, 2011; 257-269.
29. Zamojski W. Redundancja sprzętowa współczesnych systemów technicznych. Nadmiarowość w inżynieri i niezawodności. XXXII Zimowa Szkoła Niezawodności, Szczyrk. Radom: Instytut Technologii Eksploatacji 2004; 398-411.
30. ZhangY L, Wu S. Reliability analysis for a k/n(F) system with repairable repair-equipment, Appl. Math. Model. 2009; 33(7): 3052-3067.

Tomasz WALKOWIAK
Institute of Computer Engineering, Control and Robotics
Wrocław University of Technology
Wybrzeże Wyspiańskiego 27, 50-370, Wrocław, Poland
E-mail: Tomasz.Walkowiak@pwr.wroc.pl

INFORMATION FOR AUTHORS

Terms and Conditions of Publication:

- The quarterly „Maintenance and Reliability" publishes original papers written in Polish with an English translation.
- Translation into English is done by the Authors after they have received information from the Editorial Office about the outcome of the review process and have introduced the necessary modifications in accordance with the suggestions of the referees!
- Acceptance of papers for publication is based on two independent reviews commissioned by the Editor.

Fees:

- Pursuant to a resolution of the Board of PNTTE, as of 2009 the publication fee for one text is 600 zloty + VAT.
- Coloured graphical elements in the submitted text require agreement from the Editor and are charged extra.

Technical requirements:

- After receiving positive reviews and after acceptance of the paper for publication, the text must be submitted in a Microsoft Word document format.
- Drawings and photos should be additionally submitted in the form of graphical files in the *.tif, *.jpg or *.cdr (v. X3) formats.
- A manuscript should include (in accordance with the enclosed correct manuscript format: *.pdf, *.doc):
- names of authors, title, abstract, and key words that should complement the title and abstract (in Polish and in English)
- the text in Polish and in English with a clear division into sections (please, do not divide words in the text);
- tables, drawings, graphs, and photos included in the text should have descriptive two-language captions,
- if this can be avoided, no formulae and symbols should be inserted into text paragraphs by means of a formula editor
- references (written in accordance with the required reference format)
- author data – first names and surnames along with scientific titles, affiliation, address, phone number, fax, and e-mail address
- The Editor reserves the right to abridge and adjust the manuscripts.
- All submissions should be accompanied by a submission form.

Editor contact info: (Submissions should be sent to the Editor's address)

Editorial Office of „Eksploatacja i Niezawodność - Maintenance and Reliability"
Nadbystrzycka 36, 20-618 Lublin, Poland
e-mail: office@ein.org.pl

INFORMATION FOR SUBSCRIBERS

Fees

Yearly subscription fee (four issues) is 100 zloty and includes delivery costs.
Subscribers receive any additional special issues published during their year of subscription free of charge.

Orders

Subscription orders along with authorization to issue a VAT invoice without receiver's signature should be sent to the Editor's address.

Note

In accordance with the requirements of citation databases, proper citation of publications appearing in our Quarterly should include the full name of the journal in Polish and English without Polish diacritical marks, i.e.,

Eksploatacja i Niezawodnosc – Maintenance and Reliability.